

HOST STELLAR POPULATION PROPERTIES AND THE OBSERVATIONAL  
SELECTION FUNCTION OF TYPE IA SUPERNOVAE

by

ELSA M. JOHNSON

A DISSERTATION

Presented to the Department of Physics  
and the Graduate School of the University of Oregon  
in partial fulfillment of the requirements  
for the degree of  
Doctor of Philosophy

September 2010

**University of Oregon Graduate School**

**Confirmation of Approval and Acceptance of Dissertation prepared by:**

Elsa Johnson

Title:

"Host Stellar Population Properties and the Observational Selection Function of Type Ia Supernovae"

This dissertation has been accepted and approved in partial fulfillment of the requirements for the Doctor of Philosophy degree in the Department of Physics by:

Raymond Frey, Chairperson, Physics  
James Imamura, Member, Physics  
Gregory Bothun, Member, Physics  
Stephen Hsu, Member, Physics  
James Isenberg, Outside Member, Mathematics

and Richard Linton, Vice President for Research and Graduate Studies/Dean of the Graduate School for the University of Oregon.

September 4, 2010

Original approval signatures are on file with the Graduate School and the University of Oregon Libraries.

© 2010 Elsa M. Johnson

## An Abstract of the Dissertation of

Elsa M. Johnson for the degree of Doctor of Philosophy  
in the Department of Physics to be taken September 2010

Title: HOST STELLAR POPULATION PROPERTIES AND THE OBSERVATIONAL  
SELECTION FUNCTION OF TYPE IA SUPERNOVAE

Approved: \_\_\_\_\_  
Dr. Gregory Bothun

Supernovae Ia are viable standard candles for measuring cosmological distances because of their enormous light output and similar intrinsic brightness. However, dispersion in intrinsic brightness casts doubt on the overall reliability of supernovae as cosmological distance indicators. Moreover, as shown in this thesis, the dependence of peak brightness on host galaxy properties significantly contributes to this dispersion. As a result, there is good reason to doubt that the nearby sample of supernovae Ia is identical to the distant samples, which occur in host galaxies that are billions of years younger. This study explores the validity of supernovae Ia as standard candles by examining regions of nearby galaxies that hosted supernovae and modeling their observational selection function. The approach is two-fold. First, photometry is performed on the stellar population environment of supernovae to characterize that region as a function of supernova type. Then, the observational selection function is simulated to determine the true supernovae production rate of the  $z < 0.1$  redshift limit. We find that, on average, type Ia events occur

in redder and older populations; underluminous supernovae Ia occur in regions that seem to be preferentially dusty, whereas normal Ia coming from the same galaxy type occur in a wide range of extinction environments. Furthermore, redder peak colors correspond to redder underlying population colors. This finding implies that dust extinction effects can cause systematic errors in the luminosity calibration of Ia events. Finally, a single supernova rate does not adequately describe all supernovae Ia within  $z < 0.1$ . A rate of 0.25 SNU describes the population up to  $z < 0.03$ , and a much smaller rate, 0.1 SNU or less, describes supernovae past this distance. This finding indicates that observed supernova rates per galaxy remain biased by sample selection effects and that the intrinsic rate is likely uncertain by a factor of 2 to 3.

## CURRICULUM VITAE

NAME OF AUTHOR: Elsa M. Johnson

### GRADUATE AND UNDERGRADUATE SCHOOLS ATTENDED:

University of Oregon, Eugene  
University of California at Irvine  
Oregon State University

### DEGREES AWARDED:

Doctor of Philosophy, Physics, 2010, University of Oregon  
Master of Science, Physics, 1999, University of California at Irvine  
Bachelor of Science, Physics, 1993, Oregon State University

### AREAS OF SPECIAL INTEREST:

Observational Cosmology

### PROFESSIONAL EXPERIENCE:

Astronomy Instructor, University of Oregon, 2010  
Graduate Research Assistant, University of Oregon, 2001-2010  
Teaching Assistant, University of Oregon, 2001-2010  
Contractor at Los Alamos National Lab, Weirich & Associates, 2000  
Graduate Research Assistant, Los Alamos National Lab, 1998-1999  
Teaching Assistant, University of California at Irvine, 1996-1997

Summer Astronomy Intern, University of Wyoming, 1993

GRANTS, AWARDS AND HONORS:

Oregon Center for Optics Proposal Contest Grant, Physics Department at  
University of Oregon, 2009

PUBLICATIONS:

Johnson, E.; Imamura, J.; Steiman-Cameron, T., *The Publications of the  
Astronomical Society of the Pacific* **2006**, 118, 797-804

## ACKNOWLEDGMENTS

I would like to thank my advisor, Professor Greg Bothun for the opportunity to work on an interesting research project and his support throughout my graduate career. Thanks to Professor Ray Frey for chairing my committee and feedback on this dissertation.

Many, many thanks to friends and family who have supported me and kept me sane throughout this process. A special thanks goes out to my parents, Thomas and Linda Johnson who have always encouraged me to pursue my dreams, my sister Katie Schmit and especially Stephen Deskovic, my best friend. I couldn't have made it this far without his love, support and sense of humor.



For Mom, Dad and Steve

## TABLE OF CONTENTS

Chapter	Page
I. INTRODUCTION .....	1
II. SUPERNOVA TAXONOMY .....	9
2.1. Overview .....	9
2.2. Types of Supernovae .....	10
2.2.1. Type II SNe .....	10
2.2.2. Type II Subtypes .....	10
2.2.3. Type Ib, Ic and Ib/c .....	11
2.2.4. Type Ia .....	11
2.2.5. Type Ia Subtypes.....	12
2.2.6. Other Ia Oddities.....	13
III. SUPERNOVA COSMOLOGY .....	15
3.1. Distance Modulus .....	15
3.2. Supernova Ia Light Curves .....	17
3.2.1. Light Curve Fitting Techniques .....	19
3.3. Accuracy Issues in Supernova Cosmology .....	20
IV. DEMOGRAPHY .....	23
4.1. Local Supernova Sample .....	23
4.2. Observational Effects .....	26
4.3. Sample and Observer Statistics .....	28
4.4. Galaxy Type .....	34
4.5. Radial Distribution of SNe .....	36
4.6. Merging, Interacting and Other Multiple Systems .....	40
4.7. Prolific Galaxies .....	41
4.8. Summary .....	42

Chapter	Page
V. PHOTOMETRY .....	45
5.1. Background .....	45
5.2. Dust .....	46
5.2.1. Dust Estimation Techniques .....	47
5.3. Data Analysis .....	50
5.3.1. Data Sets .....	50
5.3.1.1. Sloan Digital Sky Survey .....	50
5.3.1.2. The Two Micron All Sky Survey .....	53
5.3.2. Grid Photometry .....	54
5.3.2.1. Color Analysis .....	57
5.3.2.2. Surface Brightness Analysis .....	246
5.3.2.3. Dust in pCMDs .....	250
5.3.3. Aperture Photometry .....	254
5.3.3.1. Average Aperture Colors .....	255
5.3.3.2. Host Galaxies with Multiple SNe .....	258
5.3.3.3. Amount of Flux .....	258
5.3.3.4. Color vs. Radius .....	268
5.3.3.5. Color-Color Plots .....	269
5.3.4. Environment Colors and Supernova Peak Colors .....	270
5.3.4.1. Template Color-Color Plots .....	270
5.3.4.2. Template Supernova Colors .....	279
5.4. Discussion .....	281
VI. SELECTION FUNCTION .....	287
6.1. Monte Carlo Simulations .....	287
6.1.1. Target Galaxy Selection .....	289
6.1.2. Selection Functions .....	290
6.1.3. Host Galaxy Dust .....	291
6.2. Simulations .....	293
6.2.1. Prior Work .....	293
6.2.2. Galaxy List .....	294

Chapter	Page
6.2.3. Light Curves .....	297
6.2.4. Supernova Search Routines .....	298
6.2.4.1. Magnitude and Distance Limited Surveys .....	298
6.2.5. Sky Coverage Algorithm .....	299
6.2.6. Observatory Details .....	302
6.2.6.1. Professional CCD Searches .....	302
6.2.6.2. Amateur Observers .....	308
6.2.6.3. Photographic Searches/Surveys .....	311
6.3. Results .....	314
6.3.1. Preliminaries .....	314
6.3.2. Magnitudes .....	315
6.3.3. Discussion .....	315
6.3.4. Improvements .....	316
VII. DISCUSSION AND FUTURE WORK .....	330
7.1. Implications of Supernova Ia Dependency on Stellar Environment .....	330
7.2. Supernova Ia Rate .....	331
7.3. Future Work .....	334
BIBLIOGRAPHY .....	337

## LIST OF FIGURES

Figure	Page
3.1. The Hubble diagram using data adapted from Amanullah et al. 2010 (A10). The line corresponds to a $\Lambda$ CDM ( $\Omega_M, \Omega_E, \omega$ ) = (0.25, 0.75, -1) model cosmology. ....	18
3.2. A Hubble residual diagram of unweighted data adapted from Amanullah et al. (2010) subtracted from the $\Lambda$ CDM model plotted with $\Lambda = 0$ , $\Omega_M = 1$ , 0.25 cosmologies. Data and corresponding errors are averaged in bins of $\Delta z = 0.05$ for $z < 1$ and $\Delta z = 0.2$ for $z > 1$ . ....	18
3.3. A Hubble residual diagram of unweighted data adapted from Amanullah et al. (2010) subtracted from the $\Lambda$ CDM model plotted with $\Lambda = 0$ , 0.25 universe and the standard $\Lambda$ CDM universe. Data and corresponding errors are averaged in bins of $\Delta z = 0.05$ for $z < 1$ and $\Delta z = 0.2$ for $z > 1$ . ....	19
3.4. An example of UBVRI Ia light curves of SN 2005cf adapted from Pastorello et al. (2007). The U, B, V, R, I light curves have been offset by -1, 0, 1, 2, 3 magnitudes, respectively for clarity. ....	22
4.1. The discovery magnitude vs. redshift of all supernovae detected from 1885-2009. Points within the bottom left quadrant of the graph ( $m < 20$ and $z < 0.1$ ) are the data selected for the local sample. ....	25
4.2. Supernovae detected per year from 1930-2009 for all SNe types (top) and just SNe Ia (bottom). ....	29
4.3. The number of SNe per discovery magnitude divided into Ia, II and Ib/c SN types from 1885-2009. ....	30
4.4. The number of SNe per discovery magnitude for all galaxies and RC3 galaxies from 1885-2009. In the bottom plot only SNe Ia discovery magnitudes are binned. ....	31

Figure	Page
4.5. The average discovery magnitude per year. The gaps in data correspond to no reports of SNe for those years. The thin gap in the 1940's was due to WWII. The average discovery magnitude from 1950 to was unusually dim because the few discoveries made during this time were actually found later on photographic plates. Aside from this discrepancy, there is a sharp increase in dim magnitudes around 1990 when CCDs became available to astronomers. ....	32
4.6. The discovery magnitude vs redshift for all Ia types and for core-collapse SNe. The plot demonstrates the larger number of Ia at redshifts greater than $cz > 15,000 \text{ km/s}$ . This is primarily due to searches focusing on SNe Ia for cosmology. It also indicates a selection effect against core-collapse SNe. ....	37
4.7. The distribution of supernovae per equal mass bin, where bin "1" corresponds to the central portion of the galaxy and bin 10 is outside the optical radius for sample A events. ....	38
4.8. Diameter and diameter ratios of galaxies with only one recorded supernova event (non-prolific) and those with at least 2 supernovae (prolific) in the last 100 years. All data are taken from sample A. ....	43
4.9. The number and redshift distribution of RC3 galaxies (filled boxes) in comparison to the entire (known) number of galaxies out to $z=0.1$ . ....	44
5.1. SN 1961h $u-g$ , $g-i$ , $i-z$ spatial plots. ....	58
5.2. SN 1996aa $u-g$ , $g-i$ , $i-z$ spatial plots. ....	58
5.3. SN 1939a $u-g$ , $g-i$ , $i-z$ spatial plots. ....	58
5.4. SN 1994d $u-g$ , $g-i$ , $i-z$ spatial plots. ....	58
5.5. SN 1996bk $u-g$ , $g-i$ , $i-z$ spatial plots. ....	59
5.6. SN 1999dg $u-g$ , $g-i$ , $i-z$ spatial plots. ....	59
5.7. SN 2003gs $u-g$ , $g-i$ , $i-z$ spatial plots. ....	59

Figure	Page
5.8. SN 2001a <i>u-g, g-i, i-z</i> spatial plots.....	59
5.9. SN 2007gi <i>u-g, g-i, i-z</i> spatial plots. ....	60
5.10. SN 2007ax <i>u-g, g-i, i-z</i> spatial plots.....	60
5.11. SN 2006n <i>u-g, g-i, i-z</i> spatial plots. ....	60
5.12. SN 2003jz <i>u-g, g-i, i-z</i> spatial plots.....	60
5.13. SN 2001n <i>u-g, g-i, i-z</i> spatial plots. ....	61
5.14. SN 1970j <i>u-g, g-i, i-z</i> spatial plots. ....	61
5.15. SN 1957b <i>u-g, g-i, i-z</i> spatial plots. ....	61
5.16. SN 1991bg <i>u-g, g-i, i-z</i> spatial plots. ....	61
5.17. SN 1991bi <i>u-g, g-i, i-z</i> spatial plots. ....	62
5.18. SN 1997cn <i>u-g, g-i, i-z</i> spatial plots.....	62
5.19. SN 2001cg <i>u-g, g-i, i-z</i> spatial plots.....	62
5.20. SN 2004w <i>u-g, g-i, i-z</i> spatial plots.....	62
5.21. SN 2004br <i>u-g, g-i, i-z</i> spatial plots. ....	63
5.22. SN 2002hl <i>u-g, g-i, i-z</i> spatial plots. ....	63
5.23. SN 1998d <i>u-g, g-i, i-z</i> spatial plots. ....	63
5.24. SN 1968e <i>u-g, g-i, i-z</i> spatial plots.....	63
5.25. SN 2001f <i>u-g, g-i, i-z</i> spatial plots. ....	64
5.26. SN 2004dt <i>u-g, g-i, i-z</i> spatial plots. ....	64
5.27. SN 2006dy <i>u-g, g-i, i-z</i> spatial plots. ....	64
5.28. SN 1999ej <i>u-g, g-i, i-z</i> spatial plots.....	64

Figure	Page
5.29. SN 2006ej <i>u-g, g-i, i-z</i> spatial plots.....	65
5.30. SN 2003y <i>u-g, g-i, i-z</i> spatial plots. ....	65
5.31. SN 1960r <i>u-g, g-i, i-z</i> spatial plots. ....	65
5.32. SN 1983g <i>u-g, g-i, i-z</i> spatial plots. ....	65
5.33. SN 2003cg <i>u-g, g-i, i-z</i> spatial plots.....	66
5.34. SN 2002bo <i>u-g, g-i, i-z</i> spatial plots. ....	66
5.35. SN 2002cv <i>u-g, g-i, i-z</i> spatial plots.....	66
5.36. SN 1991bc <i>u-g, g-i, i-z</i> spatial plots.....	66
5.37. SN 1991t <i>u-g, g-i, i-z</i> spatial plots. ....	67
5.38. SN 2004bd <i>u-g, g-i, i-z</i> spatial plots. ....	67
5.39. SN 1996ai <i>u-g, g-i, i-z</i> spatial plots.....	67
5.40. SN 2007ss <i>u-g, g-i, i-z</i> spatial plots. ....	67
5.41. SN 1997y <i>u-g, g-i, i-z</i> spatial plots. ....	68
5.42. SN 2005bc <i>u-g, g-i, i-z</i> spatial plots.....	68
5.43. SN 1969c <i>u-g, g-i, i-z</i> spatial plots.....	68
5.44. SN 2001en <i>u-g, g-i, i-z</i> spatial plots.....	68
5.45. SN 1987n <i>u-g, g-i, i-z</i> spatial plots. ....	69
5.46. SN 1998bu <i>u-g, g-i, i-z</i> spatial plots. ....	69
5.47. SN 1989m <i>u-g, g-i, i-z</i> spatial plots. ....	69
5.48. SN 1963i <i>u-g, g-i, i-z</i> spatial plots. ....	69
5.49. SN 1993z <i>u-g, g-i, i-z</i> spatial plots.....	70



Figure	Page
5.50. SN 1956a <i>u-g, g-i, i-z</i> spatial plots.....	70
5.51. SN 1999by <i>u-g, g-i, i-z</i> spatial plots. ....	70
5.52. SN 2007n <i>u-g, g-i, i-z</i> spatial plots. ....	70
5.53. SN 1991ak <i>u-g, g-i, i-z</i> spatial plots.....	71
5.54. SN 2001dp <i>u-g, g-i, i-z</i> spatial plots. ....	71
5.55. SN 1971g <i>u-g, g-i, i-z</i> spatial plots. ....	71
5.56. SN 1963j <i>u-g, g-i, i-z</i> spatial plots. ....	71
5.57. SN 1963p <i>u-g, g-i, i-z</i> spatial plots. ....	72
5.58. SN 1983w <i>u-g, g-i, i-z</i> spatial plots.....	72
5.59. SN 1982b <i>u-g, g-i, i-z</i> spatial plots. ....	72
5.60. SN 1974g <i>u-g, g-i, i-z</i> spatial plots. ....	72
5.61. SN 1989b <i>u-g, g-i, i-z</i> spatial plots. ....	73
5.62. SN 1992g <i>u-g, g-i, i-z</i> spatial plots. ....	73
5.63. SN 1995al <i>u-g, g-i, i-z</i> spatial plots.....	73
5.64. SN 1998aq <i>u-g, g-i, i-z</i> spatial plots.....	73
5.65. SN 2002jo <i>u-g, g-i, i-z</i> spatial plots. ....	74
5.66. SN 1998dk <i>u-g, g-i, i-z</i> spatial plots. ....	74
5.67. SN 1971l <i>u-g, g-i, i-z</i> spatial plots. ....	74
5.68. SN 2006x <i>u-g, g-i, i-z</i> spatial plots. ....	74
5.69. SN 1995bd <i>u-g, g-i, i-z</i> spatial plots. ....	75
5.70. SN 2003im <i>u-g, g-i, i-z</i> spatial plots. ....	75

Figure	Page
5.71. SN 1957a <i>u-g, g-i, i-z</i> spatial plots.....	75
5.72. SN 2003dt <i>u-g, g-i, i-z</i> spatial plots. ....	75
5.73. SN 1999x <i>u-g, g-i, i-z</i> spatial plots. ....	76
5.74. SN 2002ha <i>u-g, g-i, i-z</i> spatial plots.....	76
5.75. SN 1997bp <i>u-g, g-i, i-z</i> spatial plots. ....	76
5.76. SN 2001bg <i>u-g, g-i, i-z</i> spatial plots. ....	76
5.77. SN 1998es <i>u-g, g-i, i-z</i> spatial plots. ....	77
5.78. SN 1999dq <i>u-g, g-i, i-z</i> spatial plots. ....	77
5.79. SN 1999bh <i>u-g, g-i, i-z</i> spatial plots. ....	77
5.80. SN 2001fe <i>u-g, g-i, i-z</i> spatial plots. ....	77
5.81. SN 2001er <i>u-g, g-i, i-z</i> spatial plots. ....	78
5.82. SN 2004fw <i>u-g, g-i, i-z</i> spatial plots. ....	78
5.83. SN 1999aa <i>u-g, g-i, i-z</i> spatial plots.....	78
5.84. SN 2006ou <i>u-g, g-i, i-z</i> spatial plots. ....	78
5.85. SN 1999cc <i>u-g, g-i, i-z</i> spatial plots.....	79
5.86. SN 2000ce <i>u-g, g-i, i-z</i> spatial plots.....	79
5.87. SN 2003ag <i>u-g, g-i, i-z</i> spatial plots.....	79
5.88. SN 2000cv <i>u-g, g-i, i-z</i> spatial plots.....	79
5.89. SN 2001ed <i>u-g, g-i, i-z</i> spatial plots.....	80
5.90. SN 1954b <i>u-g, g-i, i-z</i> spatial plots. ....	80
5.91. SN 2003af <i>u-g, g-i, i-z</i> spatial plots. ....	80

Figure	Page
5.92. SN 1991aa <i>u-g, g-i, i-z</i> spatial plots.....	80
5.93. SN 1960f <i>u-g, g-i, i-z</i> spatial plots.....	81
5.94. SN 2004ey <i>u-g, g-i, i-z</i> spatial plots.....	81
5.95. SN 1987d <i>u-g, g-i, i-z</i> spatial plots.....	81
5.96. SN 1999gd <i>u-g, g-i, i-z</i> spatial plots.....	81
5.97. SN 1992p <i>u-g, g-i, i-z</i> spatial plots.....	82
5.98. SN 1998ab <i>u-g, g-i, i-z</i> spatial plots.....	82
5.99. SN 2004bk <i>u-g, g-i, i-z</i> spatial plots.....	82
5.100. SN 2006ac <i>u-g, g-i, i-z</i> spatial plots.....	82
5.101. SN 2002i <i>u-g, g-i, i-z</i> spatial plots.....	83
5.102. SN 2004p <i>u-g, g-i, i-z</i> spatial plots.....	83
5.103. SN 2005bg <i>u-g, g-i, i-z</i> spatial plots.....	83
5.104. SN 2005s <i>u-g, g-i, i-z</i> spatial plots.....	83
5.105. SN 2007s <i>u-g, g-i, i-z</i> spatial plots.....	84
5.106. SN 1999dk <i>u-g, g-i, i-z</i> spatial plots.....	84
5.107. SN 1961f <i>u-g, g-i, i-z</i> spatial plots.....	84
5.108. SN 1967h <i>u-g, g-i, i-z</i> spatial plots.....	84
5.109. SN 1986i <i>u-g, g-i, i-z</i> spatial plots.....	85
5.110. SN 1999gn <i>u-g, g-i, i-z</i> spatial plots.....	85
5.111. SN 1999gi <i>u-g, g-i, i-z</i> spatial plots.....	85
5.112. SN 1961i <i>u-g, g-i, i-z</i> spatial plots.....	85

Figure	Page
5.113. SN 2006ov <i>u-g, g-i, i-z</i> spatial plots.....	86
5.114. SN 1970a <i>u-g, g-i, i-z</i> spatial plots.....	86
5.115. SN 1996cb <i>u-g, g-i, i-z</i> spatial plots.....	86
5.116. SN 2003ie <i>u-g, g-i, i-z</i> spatial plots.....	86
5.117. SN 2005ay <i>u-g, g-i, i-z</i> spatial plots.....	87
5.118. SN 1995v <i>u-g, g-i, i-z</i> spatial plots. ....	87
5.119. SN 1996an <i>u-g, g-i, i-z</i> spatial plots.....	87
5.120. SN 1987k <i>u-g, g-i, i-z</i> spatial plots. ....	87
5.121. SN 2000db <i>u-g, g-i, i-z</i> spatial plots. ....	88
5.122. SN 1999br <i>u-g, g-i, i-z</i> spatial plots. ....	88
5.123. SN 2002ce <i>u-g, g-i, i-z</i> spatial plots.....	88
5.124. SN 2000ez <i>u-g, g-i, i-z</i> spatial plots.....	88
5.125. SN 2001ae <i>u-g, g-i, i-z</i> spatial plots.....	89
5.126. SN 2002hm <i>u-g, g-i, i-z</i> spatial plots. ....	89
5.127. SN 1995ah <i>u-g, g-i, i-z</i> spatial plots.....	89
5.128. SN 1999gk <i>u-g, g-i, i-z</i> spatial plots. ....	89
5.129. SN 1999cd <i>u-g, g-i, i-z</i> spatial plots.....	90
5.130. SN 1965l <i>u-g, g-i, i-z</i> spatial plots. ....	90
5.131. SN 2001j <i>u-g, g-i, i-z</i> spatial plots. ....	90
5.132. SN 2005dp <i>u-g, g-i, i-z</i> spatial plots. ....	90
5.133. SN 1989n <i>u-g, g-i, i-z</i> spatial plots. ....	91

Figure	Page
5.134. SN 1999an <i>u-g, g-i, i-z</i> spatial plots.....	91
5.135. SN 1999bg <i>u-g, g-i, i-z</i> spatial plots. ....	91
5.136. SN 2004bn <i>u-g, g-i, i-z</i> spatial plots. ....	91
5.137. SN 2005au <i>u-g, g-i, i-z</i> spatial plots.....	92
5.138. SN 2001hg <i>u-g, g-i, i-z</i> spatial plots. ....	92
5.139. SN 1996cc <i>u-g, g-i, i-z</i> spatial plots.....	92
5.140. SN 2004g <i>u-g, g-i, i-z</i> spatial plots. ....	92
5.141. SN 1985l <i>u-g, g-i, i-z</i> spatial plots. ....	93
5.142. SN 1998dl <i>u-g, g-i, i-z</i> spatial plots. ....	93
5.143. SN 1985h <i>u-g, g-i, i-z</i> spatial plots. ....	93
5.144. SN 1926a <i>u-g, g-i, i-z</i> spatial plots.....	93
5.145. SN 1999d <i>u-g, g-i, i-z</i> spatial plots. ....	94
5.146. SN 1999a <i>u-g, g-i, i-z</i> spatial plots.....	94
5.147. SN 2004cm <i>u-g, g-i, i-z</i> spatial plots.....	94
5.148. SN 2005ci <i>u-g, g-i, i-z</i> spatial plots.....	94
5.149. SN 1971s <i>u-g, g-i, i-z</i> spatial plots.....	95
5.150. SN 2003bl <i>u-g, g-i, i-z</i> spatial plots. ....	95
5.151. SN 1998ar <i>u-g, g-i, i-z</i> spatial plots. ....	95
5.152. SN 1946b <i>u-g, g-i, i-z</i> spatial plots. ....	95
5.153. SN 1992c <i>u-g, g-i, i-z</i> spatial plots.....	96
5.154. SN 2006dl <i>u-g, g-i, i-z</i> spatial plots. ....	96

Figure	Page
5.155. SN 2003aq <i>u-g, g-i, i-z</i> spatial plots.....	96
5.156. SN 2005gm <i>u-g, g-i, i-z</i> spatial plots. ....	96
5.157. SN 2005en <i>u-g, g-i, i-z</i> spatial plots.....	97
5.158. SN 2005h <i>u-g, g-i, i-z</i> spatial plots. ....	97
5.159. SN 2005z <i>u-g, g-i, i-z</i> spatial plots.....	97
5.160. SN 2001fv <i>u-g, g-i, i-z</i> spatial plots. ....	97
5.161. SN 2003z <i>u-g, g-i, i-z</i> spatial plots.....	98
5.162. SN 2004am <i>u-g, g-i, i-z</i> spatial plots.....	98
5.163. SN 1965h <i>u-g, g-i, i-z</i> spatial plots. ....	98
5.164. SN 2003bk <i>u-g, g-i, i-z</i> spatial plots. ....	98
5.165. SN 2003j <i>u-g, g-i, i-z</i> spatial plots. ....	99
5.166. SN 1969b <i>u-g, g-i, i-z</i> spatial plots. ....	99
5.167. SN 1999ev <i>u-g, g-i, i-z</i> spatial plots.....	99
5.168. SN 1954c <i>u-g, g-i, i-z</i> spatial plots.....	99
5.169. SN 2006by <i>u-g, g-i, i-z</i> spatial plots. ....	100
5.170. SN 1937a <i>u-g, g-i, i-z</i> spatial plots.....	100
5.171. SN 1984e <i>u-g, g-i, i-z</i> spatial plots.....	100
5.172. SN 1940b <i>u-g, g-i, i-z</i> spatial plots. ....	100
5.173. SN 1985g <i>u-g, g-i, i-z</i> spatial plots. ....	101
5.174. SN 1964f <i>u-g, g-i, i-z</i> spatial plots. ....	101
5.175. SN 1920a <i>u-g, g-i, i-z</i> spatial plots.....	101

Figure	Page
5.176. SN 2004fc <i>u-g, g-i, i-z</i> spatial plots. ....	101
5.177. SN 1988e <i>u-g, g-i, i-z</i> spatial plots.....	102
5.178. SN 1988a <i>u-g, g-i, i-z</i> spatial plots.....	102
5.179. SN 1985b <i>u-g, g-i, i-z</i> spatial plots. ....	102
5.180. SN 1990e <i>u-g, g-i, i-z</i> spatial plots.....	102
5.181. SN 2006ee <i>u-g, g-i, i-z</i> spatial plots.....	103
5.182. SN 2001cm <i>u-g, g-i, i-z</i> spatial plots.....	103
5.183. SN 1978h <i>u-g, g-i, i-z</i> spatial plots. ....	103
5.184. SN 1996b <i>u-g, g-i, i-z</i> spatial plots. ....	103
5.185. SN 1990h <i>u-g, g-i, i-z</i> spatial plots. ....	104
5.186. SN 1998s <i>u-g, g-i, i-z</i> spatial plots.....	104
5.187. SN 2005ip <i>u-g, g-i, i-z</i> spatial plots. ....	104
5.188. SN 2001h <i>u-g, g-i, i-z</i> spatial plots. ....	104
5.189. SN 2000i <i>u-g, g-i, i-z</i> spatial plots. ....	105
5.190. SN 1997bn <i>u-g, g-i, i-z</i> spatial plots. ....	105
5.191. SN 2002ca <i>u-g, g-i, i-z</i> spatial plots.....	105
5.192. SN 2004dg <i>u-g, g-i, i-z</i> spatial plots. ....	105
5.193. SN 2001ab <i>u-g, g-i, i-z</i> spatial plots.....	106
5.194. SN 2004t <i>u-g, g-i, i-z</i> spatial plots. ....	106
5.195. SN 2006gs <i>u-g, g-i, i-z</i> spatial plots.....	106
5.196. SN 1999ge <i>u-g, g-i, i-z</i> spatial plots.....	106

Figure	Page
5.197. SN 1991g <i>u-g, g-i, i-z</i> spatial plots. ....	107
5.198. SN 1992bt <i>u-g, g-i, i-z</i> spatial plots. ....	107
5.199. SN 2005bb <i>u-g, g-i, i-z</i> spatial plots. ....	107
5.200. SN 1993g <i>u-g, g-i, i-z</i> spatial plots. ....	107
5.201. SN 1997co <i>u-g, g-i, i-z</i> spatial plots.....	108
5.202. SN 2000au <i>u-g, g-i, i-z</i> spatial plots.....	108
5.203. SN 2005aa <i>u-g, g-i, i-z</i> spatial plots. ....	108
5.204. SN 2005i <i>u-g, g-i, i-z</i> spatial plots. ....	108
5.205. SN 2006bp <i>u-g, g-i, i-z</i> spatial plots. ....	109
5.206. SN 2001q <i>u-g, g-i, i-z</i> spatial plots. ....	109
5.207. SN 2000l <i>u-g, g-i, i-z</i> spatial plots. ....	109
5.208. SN 1991n <i>u-g, g-i, i-z</i> spatial plots. ....	109
5.209. SN 1998t <i>u-g, g-i, i-z</i> spatial plots. ....	110
5.210. SN 2005u <i>u-g, g-i, i-z</i> spatial plots. ....	110
5.211. SN 2000de <i>u-g, g-i, i-z</i> spatial plots.....	110
5.212. SN 1985f <i>u-g, g-i, i-z</i> spatial plots. ....	110
5.213. SN 2005kl <i>u-g, g-i, i-z</i> spatial plots. ....	111
5.214. SN 1997x <i>u-g, g-i, i-z</i> spatial plots. ....	111
5.215. SN 2001ch <i>u-g, g-i, i-z</i> spatial plots.....	111
5.216. SN 2005bh <i>u-g, g-i, i-z</i> spatial plots. ....	111
5.217. SN 1991a <i>u-g, g-i, i-z</i> spatial plots.....	112



Figure	Page
5.218. SN 2003l <i>u-g, g-i, i-z</i> spatial plots. ....	112
5.219. SN 2005az <i>u-g, g-i, i-z</i> spatial plots. ....	112
5.220. SN 2005la <i>u-g, g-i, i-z</i> spatial plots. ....	112
5.221. SN 1996aq <i>u-g, g-i, i-z</i> spatial plots. ....	113
5.222. SN 1997dq <i>u-g, g-i, i-z</i> spatial plots. ....	113
5.223. SN 2002ji <i>u-g, g-i, i-z</i> spatial plots. ....	113
5.224. SN 1999bc <i>u-g, g-i, i-z</i> spatial plots. ....	113
5.225. SN 2003i <i>u-g, g-i, i-z</i> spatial plots. ....	114
5.226. SN 2003aa <i>u-g, g-i, i-z</i> spatial plots. ....	114
5.227. SN 2006lv <i>u-g, g-i, i-z</i> spatial plots. ....	114
5.228. SN 2008d <i>u-g, g-i, i-z</i> spatial plots. ....	114
5.229. SN 2004aw <i>u-g, g-i, i-z</i> spatial plots. ....	115
5.230. SN 2006jc <i>u-g, g-i, i-z</i> spatial plots. ....	115
5.231. SN 2004gj <i>u-g, g-i, i-z</i> spatial plots. ....	115
5.232. SN 2004bs <i>u-g, g-i, i-z</i> spatial plots. ....	115
5.233. SN 2006fo <i>u-g, g-i, i-z</i> spatial plots. ....	116
5.234. SN 2000dv <i>u-g, g-i, i-z</i> spatial plots. ....	116
5.235. SN 2007rz <i>u-g, g-i, i-z</i> spatial plots. ....	116
5.236. SN 1988l <i>u-g, g-i, i-z</i> spatial plots. ....	116
5.237. SN 1997ef <i>u-g, g-i, i-z</i> spatial plots. ....	117
5.238. SN 1999di <i>u-g, g-i, i-z</i> spatial plots. ....	117

Figure	Page
5.239. SN 2006bf <i>u-g, g-i, i-z</i> spatial plots. ....	117
5.240. SN 2005hl <i>u-g, g-i, i-z</i> spatial plots. ....	117
5.241. SN 1976b <i>u-g, g-i, i-z</i> spatial plots. ....	118
5.242. SN 1990b <i>u-g, g-i, i-z</i> spatial plots. ....	118
5.243. SN 2001ci <i>u-g, g-i, i-z</i> spatial plots.....	118
5.244. SN 2004gn <i>u-g, g-i, i-z</i> spatial plots. ....	118
5.245. SN 1999bu <i>u-g, g-i, i-z</i> spatial plots. ....	119
5.246. SN 2004c <i>u-g, g-i, i-z</i> spatial plots.....	119
5.247. SN 1983i <i>u-g, g-i, i-z</i> spatial plots. ....	119
5.248. SN 1964l <i>u-g, g-i, i-z</i> spatial plots. ....	119
5.249. SN 2000ew <i>u-g, g-i, i-z</i> spatial plots.....	120
5.250. SN 2004cc <i>u-g, g-i, i-z</i> spatial plots.....	120
5.251. SN 2004bm <i>u-g, g-i, i-z</i> spatial plots. ....	120
5.252. SN 1995f <i>u-g, g-i, i-z</i> spatial plots. ....	120
5.253. SN 2000ds <i>u-g, g-i, i-z</i> spatial plots.....	121
5.254. SN 1997ei <i>u-g, g-i, i-z</i> spatial plots.....	121
5.255. SN 1999eh <i>u-g, g-i, i-z</i> spatial plots.....	121
5.256. SN 2000cr <i>u-g, g-i, i-z</i> spatial plots. ....	121
5.257. SN 2002bl <i>u-g, g-i, i-z</i> spatial plots. ....	122
5.258. SN 2002hn <i>u-g, g-i, i-z</i> spatial plots. ....	122
5.259. SN 2002ho <i>u-g, g-i, i-z</i> spatial plots. ....	122

Figure	Page
5.260. SN 2007uy <i>u-g, g-i, i-z</i> spatial plots. ....	122
5.261. SN 2005eo <i>u-g, g-i, i-z</i> spatial plots.....	123
5.262. SN 2004gk <i>u-g, g-i, i-z</i> spatial plots. ....	123
5.263. SN 2004gv <i>u-g, g-i, i-z</i> spatial plots. ....	123
5.264. SN 1998cc <i>u-g, g-i, i-z</i> spatial plots.....	123
5.265. SN 2005aj <i>u-g, g-i, i-z</i> spatial plots.....	124
5.266. SN 2006dk <i>u-g, g-i, i-z</i> spatial plots. ....	124
5.267. SN 2005o <i>u-g, g-i, i-z</i> spatial plots. ....	124
5.268. SN 2006lc <i>u-g, g-i, i-z</i> spatial plots.....	124
5.269. SN 1994y <i>u-g, g-i, i-z</i> spatial plots. ....	125
5.270. SN 2002ea <i>u-g, g-i, i-z</i> spatial plots.....	125
5.271. SN 1996ae <i>u-g, g-i, i-z</i> spatial plots.....	125
5.272. SN 1997bs <i>u-g, g-i, i-z</i> spatial plots.....	125
5.273. SN 1997eg <i>u-g, g-i, i-z</i> spatial plots.....	126
5.274. SN 1999bw <i>u-g, g-i, i-z</i> spatial plots.....	126
5.275. SN 1994ak <i>u-g, g-i, i-z</i> spatial plots.....	126
5.276. SN 2006aa <i>u-g, g-i, i-z</i> spatial plots.....	126
5.277. SN 1999gb <i>u-g, g-i, i-z</i> spatial plots. ....	127
5.278. SN 2004f <i>u-g, g-i, i-z</i> spatial plots. ....	127
5.279. SN 2006am <i>u-g, g-i, i-z</i> spatial plots.....	127
5.280. SN 2006m <i>u-g, g-i, i-z</i> spatial plots. ....	127

Figure	Page
5.281. SN 1972q $u-g$ , $g-i$ , $i-z$ spatial plots. ....	128
5.282. SN 1982f $u-g$ , $g-i$ , $i-z$ spatial plots. ....	128
5.283. SN 1989c $u-g$ , $g-i$ , $i-z$ spatial plots. ....	128
5.284. SN 1998bv $u-g$ , $g-i$ , $i-z$ spatial plots. ....	128
5.285. SN 2004df $u-g$ , $g-i$ , $i-z$ spatial plots. ....	129
5.286. SN 1994w $u-g$ , $g-i$ , $i-z$ spatial plots. ....	129
5.287. SN 1973r $u-g$ , $g-i$ , $i-z$ spatial plots. ....	129
5.288. SN 2001dc $u-g$ , $g-i$ , $i-z$ spatial plots. ....	129
5.289. SN 2001x $u-g$ , $g-i$ , $i-z$ spatial plots. ....	130
5.290. SN 1970g $u-g$ , $g-i$ , $i-z$ spatial plots. ....	130
5.291. SN 1961u $u-g$ , $g-i$ , $i-z$ spatial plots. ....	130
5.292. SN 1979c $u-g$ , $g-i$ , $i-z$ spatial plots. ....	130
5.293. SN 1936a $u-g$ , $g-i$ , $i-z$ spatial plots. ....	131
5.294. SN 1983e $u-g$ , $g-i$ , $i-z$ spatial plots. ....	131
5.295. SN 1961h $u,u-g$ , $g,g-i$ , and $i,i-z$ pseudo color-magnitude plots. ....	132
5.296. SN 1996aa $u,u-g$ , $g,g-i$ , and $i,i-z$ pseudo color-magnitude plots. ....	132
5.297. SN 1939a $u,u-g$ , $g,g-i$ , and $i,i-z$ pseudo color-magnitude plots. ....	132
5.298. SN 1994d $u,u-g$ , $g,g-i$ , and $i,i-z$ pseudo color-magnitude plots. ....	133
5.299. SN 1996bk $u,u-g$ , $g,g-i$ , and $i,i-z$ pseudo color-magnitude plots. ....	133
5.300. SN 1999dg $u,u-g$ , $g,g-i$ , and $i,i-z$ pseudo color-magnitude plots. ....	133
5.301. SN 2003gs $u,u-g$ , $g,g-i$ , and $i,i-z$ pseudo color-magnitude plots. ....	134

Figure	Page
5.302. SN 2001a <i>u,u-g, g,g-i, and i,i-z</i> pseudo color-magnitude plots. ....	134
5.303. SN 2007gi <i>u,u-g, g,g-i, and i,i-z</i> pseudo color-magnitude plots. ....	134
5.304. SN 2007ax <i>u,u-g, g,g-i, and i,i-z</i> pseudo color-magnitude plots. ....	135
5.305. SN 2006n <i>u,u-g, g,g-i, and i,i-z</i> pseudo color-magnitude plots. ....	135
5.306. SN 2003jz <i>u,u-g, g,g-i, and i,i-z</i> pseudo color-magnitude plots. ....	135
5.307. SN 2001n <i>u,u-g, g,g-i, and i,i-z</i> pseudo color-magnitude plots. ....	136
5.308. SN 1970j <i>u,u-g, g,g-i, and i,i-z</i> pseudo color-magnitude plots. ....	136
5.309. SN 1957b <i>u,u-g, g,g-i, and i,i-z</i> pseudo color-magnitude plots. ....	136
5.310. SN 1991bg <i>u,u-g, g,g-i, and i,i-z</i> pseudo color-magnitude plots. ....	137
5.311. SN 1991bi <i>u,u-g, g,g-i, and i,i-z</i> pseudo color-magnitude plots. ....	137
5.312. SN 1997cn <i>u,u-g, g,g-i, and i,i-z</i> pseudo color-magnitude plots. ....	137
5.313. SN 2001cg <i>u,u-g, g,g-i, and i,i-z</i> pseudo color-magnitude plots. ....	138
5.314. SN 2004w <i>u,u-g, g,g-i, and i,i-z</i> pseudo color-magnitude plots. ....	138
5.315. SN 2004br <i>u,u-g, g,g-i, and i,i-z</i> pseudo color-magnitude plots. ....	138
5.316. SN 2002hl <i>u,u-g, g,g-i, and i,i-z</i> pseudo color-magnitude plots. ....	139
5.317. SN 1998d <i>u,u-g, g,g-i, and i,i-z</i> pseudo color-magnitude plots. ....	139
5.318. SN 1968e <i>u,u-g, g,g-i, and i,i-z</i> pseudo color-magnitude plots. ....	139
5.319. SN 2001f <i>u,u-g, g,g-i, and i,i-z</i> pseudo color-magnitude plots. ....	140
5.320. SN 2004dt <i>u,u-g, g,g-i, and i,i-z</i> pseudo color-magnitude plots. ....	140
5.321. SN 2006dy <i>u,u-g, g,g-i, and i,i-z</i> pseudo color-magnitude plots. ....	140
5.322. SN 1999ej <i>u,u-g, g,g-i, and i,i-z</i> pseudo color-magnitude plots. ....	141

Figure	Page
5.323. SN 2006ej $u,u-g$ , $g,g-i$ , and $i,i-z$ pseudo color-magnitude plots. ....	141
5.324. SN 2003y $u,u-g$ , $g,g-i$ , and $i,i-z$ pseudo color-magnitude plots. ....	141
5.325. SN 1960r $u,u-g$ , $g,g-i$ , and $i,i-z$ pseudo color-magnitude plots. ....	142
5.326. SN 1983g $u,u-g$ , $g,g-i$ , and $i,i-z$ pseudo color-magnitude plots. ....	142
5.327. SN 2003cg $u,u-g$ , $g,g-i$ , and $i,i-z$ pseudo color-magnitude plots. ....	142
5.328. SN 2002bo $u,u-g$ , $g,g-i$ , and $i,i-z$ pseudo color-magnitude plots. ....	143
5.329. SN 2002cv $u,u-g$ , $g,g-i$ , and $i,i-z$ pseudo color-magnitude plots. ....	143
5.330. SN 1991bc $u,u-g$ , $g,g-i$ , and $i,i-z$ pseudo color-magnitude plots. ....	143
5.331. SN 1991t $u,u-g$ , $g,g-i$ , and $i,i-z$ pseudo color-magnitude plots. ....	144
5.332. SN 2004bd $u,u-g$ , $g,g-i$ , and $i,i-z$ pseudo color-magnitude plots. ....	144
5.333. SN 1996ai $u,u-g$ , $g,g-i$ , and $i,i-z$ pseudo color-magnitude plots. ....	144
5.334. SN 2007ss $u,u-g$ , $g,g-i$ , and $i,i-z$ pseudo color-magnitude plots. ....	145
5.335. SN 1997y $u,u-g$ , $g,g-i$ , and $i,i-z$ pseudo color-magnitude plots. ....	145
5.336. SN 2005bc $u,u-g$ , $g,g-i$ , and $i,i-z$ pseudo color-magnitude plots. ....	145
5.337. SN 1969c $u,u-g$ , $g,g-i$ , and $i,i-z$ pseudo color-magnitude plots. ....	146
5.338. SN 2001en $u,u-g$ , $g,g-i$ , and $i,i-z$ pseudo color-magnitude plots. ....	146
5.339. SN 1987n $u,u-g$ , $g,g-i$ , and $i,i-z$ pseudo color-magnitude plots. ....	146
5.340. SN 1998bu $u,u-g$ , $g,g-i$ , and $i,i-z$ pseudo color-magnitude plots. ....	147
5.341. SN 1989m $u,u-g$ , $g,g-i$ , and $i,i-z$ pseudo color-magnitude plots. ....	147
5.342. SN 1963i $u,u-g$ , $g,g-i$ , and $i,i-z$ pseudo color-magnitude plots. ....	147
5.343. SN 1993z $u,u-g$ , $g,g-i$ , and $i,i-z$ pseudo color-magnitude plots. ....	148

Figure	Page
5.344. SN 1956a <i>u,u-g</i> , <i>g,g-i</i> , and <i>i,i-z</i> pseudo color-magnitude plots. ....	148
5.345. SN 1999by <i>u,u-g</i> , <i>g,g-i</i> , and <i>i,i-z</i> pseudo color-magnitude plots. ....	148
5.346. SN 2007n <i>u,u-g</i> , <i>g,g-i</i> , and <i>i,i-z</i> pseudo color-magnitude plots. ....	149
5.347. SN 1991ak <i>u,u-g</i> , <i>g,g-i</i> , and <i>i,i-z</i> pseudo color-magnitude plots. ....	149
5.348. SN 2001dp <i>u,u-g</i> , <i>g,g-i</i> , and <i>i,i-z</i> pseudo color-magnitude plots. ....	149
5.349. SN 1971g <i>u,u-g</i> , <i>g,g-i</i> , and <i>i,i-z</i> pseudo color-magnitude plots. ....	150
5.350. SN 1963j <i>u,u-g</i> , <i>g,g-i</i> , and <i>i,i-z</i> pseudo color-magnitude plots. ....	150
5.351. SN 1963p <i>u,u-g</i> , <i>g,g-i</i> , and <i>i,i-z</i> pseudo color-magnitude plots. ....	150
5.352. SN 1983w <i>u,u-g</i> , <i>g,g-i</i> , and <i>i,i-z</i> pseudo color-magnitude plots. ....	151
5.353. SN 1982b <i>u,u-g</i> , <i>g,g-i</i> , and <i>i,i-z</i> pseudo color-magnitude plots. ....	151
5.354. SN 1974g <i>u,u-g</i> , <i>g,g-i</i> , and <i>i,i-z</i> pseudo color-magnitude plots. ....	151
5.355. SN 1989b <i>u,u-g</i> , <i>g,g-i</i> , and <i>i,i-z</i> pseudo color-magnitude plots. ....	152
5.356. SN 1992g <i>u,u-g</i> , <i>g,g-i</i> , and <i>i,i-z</i> pseudo color-magnitude plots. ....	152
5.357. SN 1995al <i>u,u-g</i> , <i>g,g-i</i> , and <i>i,i-z</i> pseudo color-magnitude plots. ....	152
5.358. SN 1998aq <i>u,u-g</i> , <i>g,g-i</i> , and <i>i,i-z</i> pseudo color-magnitude plots. ....	153
5.359. SN 2002jo <i>u,u-g</i> , <i>g,g-i</i> , and <i>i,i-z</i> pseudo color-magnitude plots. ....	153
5.360. SN 1998dk <i>u,u-g</i> , <i>g,g-i</i> , and <i>i,i-z</i> pseudo color-magnitude plots. ....	153
5.361. SN 1971l <i>u,u-g</i> , <i>g,g-i</i> , and <i>i,i-z</i> pseudo color-magnitude plots. ....	154
5.362. SN 2006x <i>u,u-g</i> , <i>g,g-i</i> , and <i>i,i-z</i> pseudo color-magnitude plots. ....	154
5.363. SN 1995bd <i>u,u-g</i> , <i>g,g-i</i> , and <i>i,i-z</i> pseudo color-magnitude plots. ....	154
5.364. SN 2003im <i>u,u-g</i> , <i>g,g-i</i> , and <i>i,i-z</i> pseudo color-magnitude plots. ....	155

Figure	Page
5.365. SN 1957a $u,u-g$ , $g,g-i$ , and $i,i-z$ pseudo color-magnitude plots. ....	155
5.366. SN 2003dt $u,u-g$ , $g,g-i$ , and $i,i-z$ pseudo color-magnitude plots. ....	155
5.367. SN 1999x $u,u-g$ , $g,g-i$ , and $i,i-z$ pseudo color-magnitude plots. ....	156
5.368. SN 2002ha $u,u-g$ , $g,g-i$ , and $i,i-z$ pseudo color-magnitude plots. ....	156
5.369. SN 1997bp $u,u-g$ , $g,g-i$ , and $i,i-z$ pseudo color-magnitude plots. ....	156
5.370. SN 2001bg $u,u-g$ , $g,g-i$ , and $i,i-z$ pseudo color-magnitude plots. ....	157
5.371. SN 1998es $u,u-g$ , $g,g-i$ , and $i,i-z$ pseudo color-magnitude plots. ....	157
5.372. SN 1999dq $u,u-g$ , $g,g-i$ , and $i,i-z$ pseudo color-magnitude plots. ....	157
5.373. SN 1999bh $u,u-g$ , $g,g-i$ , and $i,i-z$ pseudo color-magnitude plots. ....	158
5.374. SN 2001fe $u,u-g$ , $g,g-i$ , and $i,i-z$ pseudo color-magnitude plots. ....	158
5.375. SN 2001er $u,u-g$ , $g,g-i$ , and $i,i-z$ pseudo color-magnitude plots. ....	158
5.376. SN 2004fw $u,u-g$ , $g,g-i$ , and $i,i-z$ pseudo color-magnitude plots. ....	159
5.377. SN 1999aa $u,u-g$ , $g,g-i$ , and $i,i-z$ pseudo color-magnitude plots. ....	159
5.378. SN 2006ou $u,u-g$ , $g,g-i$ , and $i,i-z$ pseudo color-magnitude plots. ....	159
5.379. SN 1999cc $u,u-g$ , $g,g-i$ , and $i,i-z$ pseudo color-magnitude plots. ....	160
5.380. SN 2000ce $u,u-g$ , $g,g-i$ , and $i,i-z$ pseudo color-magnitude plots. ....	160
5.381. SN 2003ag $u,u-g$ , $g,g-i$ , and $i,i-z$ pseudo color-magnitude plots. ....	160
5.382. SN 2000cv $u,u-g$ , $g,g-i$ , and $i,i-z$ pseudo color-magnitude plots. ....	161
5.383. SN 2001ed $u,u-g$ , $g,g-i$ , and $i,i-z$ pseudo color-magnitude plots. ....	161
5.384. SN 1954b $u,u-g$ , $g,g-i$ , and $i,i-z$ pseudo color-magnitude plots. ....	161
5.385. SN 2003af $u,u-g$ , $g,g-i$ , and $i,i-z$ pseudo color-magnitude plots. ....	162



Figure	Page
5.386. SN 1991aa $u,u-g$ , $g,g-i$ , and $i,i-z$ pseudo color-magnitude plots.....	162
5.387. SN 1960f $u,u-g$ , $g,g-i$ , and $i,i-z$ pseudo color-magnitude plots.....	162
5.388. SN 2004ey $u,u-g$ , $g,g-i$ , and $i,i-z$ pseudo color-magnitude plots. ....	163
5.389. SN 1987d $u,u-g$ , $g,g-i$ , and $i,i-z$ pseudo color-magnitude plots. ....	163
5.390. SN 1999gd $u,u-g$ , $g,g-i$ , and $i,i-z$ pseudo color-magnitude plots. ....	163
5.391. SN 1992p $u,u-g$ , $g,g-i$ , and $i,i-z$ pseudo color-magnitude plots. ....	164
5.392. SN 1998ab $u,u-g$ , $g,g-i$ , and $i,i-z$ pseudo color-magnitude plots. ....	164
5.393. SN 2004bk $u,u-g$ , $g,g-i$ , and $i,i-z$ pseudo color-magnitude plots. ....	164
5.394. SN 2006ac $u,u-g$ , $g,g-i$ , and $i,i-z$ pseudo color-magnitude plots.....	165
5.395. SN 2002i $u,u-g$ , $g,g-i$ , and $i,i-z$ pseudo color-magnitude plots. ....	165
5.396. SN 2004p $u,u-g$ , $g,g-i$ , and $i,i-z$ pseudo color-magnitude plots. ....	165
5.397. SN 2005bg $u,u-g$ , $g,g-i$ , and $i,i-z$ pseudo color-magnitude plots. ....	166
5.398. SN 2005s $u,u-g$ , $g,g-i$ , and $i,i-z$ pseudo color-magnitude plots.....	166
5.399. SN 2007s $u,u-g$ , $g,g-i$ , and $i,i-z$ pseudo color-magnitude plots.....	166
5.400. SN 1999dk $u,u-g$ , $g,g-i$ , and $i,i-z$ pseudo color-magnitude plots. ....	167
5.401. SN 1961f $u,u-g$ , $g,g-i$ , and $i,i-z$ pseudo color-magnitude plots.....	167
5.402. SN 1967h $u,u-g$ , $g,g-i$ , and $i,i-z$ pseudo color-magnitude plots. ....	167
5.403. SN 1986i $u,u-g$ , $g,g-i$ , and $i,i-z$ pseudo color-magnitude plots. ....	168
5.404. SN 1999gn $u,u-g$ , $g,g-i$ , and $i,i-z$ pseudo color-magnitude plots. ....	168
5.405. SN 1999gi $u,u-g$ , $g,g-i$ , and $i,i-z$ pseudo color-magnitude plots. ....	168
5.406. SN 1961i $u,u-g$ , $g,g-i$ , and $i,i-z$ pseudo color-magnitude plots. ....	169

Figure	Page
5.407. SN 2006ov <i>u,u-g</i> , <i>g,g-i</i> , and <i>i,i-z</i> pseudo color-magnitude plots. ....	169
5.408. SN 1970a <i>u,u-g</i> , <i>g,g-i</i> , and <i>i,i-z</i> pseudo color-magnitude plots. ....	169
5.409. SN 1996cb <i>u,u-g</i> , <i>g,g-i</i> , and <i>i,i-z</i> pseudo color-magnitude plots. ....	170
5.410. SN 2003ie <i>u,u-g</i> , <i>g,g-i</i> , and <i>i,i-z</i> pseudo color-magnitude plots. ....	170
5.411. SN 2005ay <i>u,u-g</i> , <i>g,g-i</i> , and <i>i,i-z</i> pseudo color-magnitude plots. ....	170
5.412. SN 1995v <i>u,u-g</i> , <i>g,g-i</i> , and <i>i,i-z</i> pseudo color-magnitude plots. ....	171
5.413. SN 1996an <i>u,u-g</i> , <i>g,g-i</i> , and <i>i,i-z</i> pseudo color-magnitude plots. ....	171
5.414. SN 1987k <i>u,u-g</i> , <i>g,g-i</i> , and <i>i,i-z</i> pseudo color-magnitude plots. ....	171
5.415. SN 2000db <i>u,u-g</i> , <i>g,g-i</i> , and <i>i,i-z</i> pseudo color-magnitude plots. ....	172
5.416. SN 1999br <i>u,u-g</i> , <i>g,g-i</i> , and <i>i,i-z</i> pseudo color-magnitude plots. ....	172
5.417. SN 2002ce <i>u,u-g</i> , <i>g,g-i</i> , and <i>i,i-z</i> pseudo color-magnitude plots. ....	172
5.418. SN 2000ez <i>u,u-g</i> , <i>g,g-i</i> , and <i>i,i-z</i> pseudo color-magnitude plots. ....	173
5.419. SN 2001ae <i>u,u-g</i> , <i>g,g-i</i> , and <i>i,i-z</i> pseudo color-magnitude plots. ....	173
5.420. SN 2002hm <i>u,u-g</i> , <i>g,g-i</i> , and <i>i,i-z</i> pseudo color-magnitude plots. ....	173
5.421. SN 1995ah <i>u,u-g</i> , <i>g,g-i</i> , and <i>i,i-z</i> pseudo color-magnitude plots. ....	174
5.422. SN 1999gk <i>u,u-g</i> , <i>g,g-i</i> , and <i>i,i-z</i> pseudo color-magnitude plots. ....	174
5.423. SN 1999cd <i>u,u-g</i> , <i>g,g-i</i> , and <i>i,i-z</i> pseudo color-magnitude plots. ....	174
5.424. SN 1965l <i>u,u-g</i> , <i>g,g-i</i> , and <i>i,i-z</i> pseudo color-magnitude plots. ....	175
5.425. SN 2001j <i>u,u-g</i> , <i>g,g-i</i> , and <i>i,i-z</i> pseudo color-magnitude plots. ....	175
5.426. SN 2005dp <i>u,u-g</i> , <i>g,g-i</i> , and <i>i,i-z</i> pseudo color-magnitude plots. ....	175
5.427. SN 1989n <i>u,u-g</i> , <i>g,g-i</i> , and <i>i,i-z</i> pseudo color-magnitude plots. ....	176

Figure	Page
5.428. SN 1999an $u,u-g$ , $g,g-i$ , and $i,i-z$ pseudo color-magnitude plots. ....	176
5.429. SN 1999bg $u,u-g$ , $g,g-i$ , and $i,i-z$ pseudo color-magnitude plots. ....	176
5.430. SN 2004bn $u,u-g$ , $g,g-i$ , and $i,i-z$ pseudo color-magnitude plots. ....	177
5.431. SN 2005au $u,u-g$ , $g,g-i$ , and $i,i-z$ pseudo color-magnitude plots. ....	177
5.432. SN 2001hg $u,u-g$ , $g,g-i$ , and $i,i-z$ pseudo color-magnitude plots. ....	177
5.433. SN 1996cc $u,u-g$ , $g,g-i$ , and $i,i-z$ pseudo color-magnitude plots.....	178
5.434. SN 2004g $u,u-g$ , $g,g-i$ , and $i,i-z$ pseudo color-magnitude plots. ....	178
5.435. SN 1985l $u,u-g$ , $g,g-i$ , and $i,i-z$ pseudo color-magnitude plots. ....	178
5.436. SN 1998dl $u,u-g$ , $g,g-i$ , and $i,i-z$ pseudo color-magnitude plots. ....	179
5.437. SN 1985h $u,u-g$ , $g,g-i$ , and $i,i-z$ pseudo color-magnitude plots. ....	179
5.438. SN 1926a $u,u-g$ , $g,g-i$ , and $i,i-z$ pseudo color-magnitude plots. ....	179
5.439. SN 1999d $u,u-g$ , $g,g-i$ , and $i,i-z$ pseudo color-magnitude plots. ....	180
5.440. SN 1999a $u,u-g$ , $g,g-i$ , and $i,i-z$ pseudo color-magnitude plots. ....	180
5.441. SN 2004cm $u,u-g$ , $g,g-i$ , and $i,i-z$ pseudo color-magnitude plots. ....	180
5.442. SN 2005ci $u,u-g$ , $g,g-i$ , and $i,i-z$ pseudo color-magnitude plots. ....	181
5.443. SN 1971s $u,u-g$ , $g,g-i$ , and $i,i-z$ pseudo color-magnitude plots.....	181
5.444. SN 2003bl $u,u-g$ , $g,g-i$ , and $i,i-z$ pseudo color-magnitude plots. ....	181
5.445. SN 1998ar $u,u-g$ , $g,g-i$ , and $i,i-z$ pseudo color-magnitude plots. ....	182
5.446. SN 1946b $u,u-g$ , $g,g-i$ , and $i,i-z$ pseudo color-magnitude plots. ....	182
5.447. SN 1992c $u,u-g$ , $g,g-i$ , and $i,i-z$ pseudo color-magnitude plots. ....	182
5.448. SN 2006dl $u,u-g$ , $g,g-i$ , and $i,i-z$ pseudo color-magnitude plots. ....	183

Figure	Page
5.449. SN 2003aq $u,u-g$ , $g,g-i$ , and $i,i-z$ pseudo color-magnitude plots. ....	183
5.450. SN 2005gm $u,u-g$ , $g,g-i$ , and $i,i-z$ pseudo color-magnitude plots. ....	183
5.451. SN 2005en $u,u-g$ , $g,g-i$ , and $i,i-z$ pseudo color-magnitude plots. ....	184
5.452. SN 2005h $u,u-g$ , $g,g-i$ , and $i,i-z$ pseudo color-magnitude plots. ....	184
5.453. SN 2005z $u,u-g$ , $g,g-i$ , and $i,i-z$ pseudo color-magnitude plots. ....	184
5.454. SN 2001fv $u,u-g$ , $g,g-i$ , and $i,i-z$ pseudo color-magnitude plots. ....	185
5.455. SN 2003z $u,u-g$ , $g,g-i$ , and $i,i-z$ pseudo color-magnitude plots. ....	185
5.456. SN 2004am $u,u-g$ , $g,g-i$ , and $i,i-z$ pseudo color-magnitude plots. ....	185
5.457. SN 1965h $u,u-g$ , $g,g-i$ , and $i,i-z$ pseudo color-magnitude plots. ....	186
5.458. SN 2003bk $u,u-g$ , $g,g-i$ , and $i,i-z$ pseudo color-magnitude plots. ....	186
5.459. SN 2003j $u,u-g$ , $g,g-i$ , and $i,i-z$ pseudo color-magnitude plots. ....	186
5.460. SN 1969b $u,u-g$ , $g,g-i$ , and $i,i-z$ pseudo color-magnitude plots. ....	187
5.461. SN 1999ev $u,u-g$ , $g,g-i$ , and $i,i-z$ pseudo color-magnitude plots. ....	187
5.462. SN 1954c $u,u-g$ , $g,g-i$ , and $i,i-z$ pseudo color-magnitude plots. ....	187
5.463. SN 2006by $u,u-g$ , $g,g-i$ , and $i,i-z$ pseudo color-magnitude plots. ....	188
5.464. SN 1937a $u,u-g$ , $g,g-i$ , and $i,i-z$ pseudo color-magnitude plots. ....	188
5.465. SN 1984e $u,u-g$ , $g,g-i$ , and $i,i-z$ pseudo color-magnitude plots. ....	188
5.466. SN 1940b $u,u-g$ , $g,g-i$ , and $i,i-z$ pseudo color-magnitude plots. ....	189
5.467. SN 1985g $u,u-g$ , $g,g-i$ , and $i,i-z$ pseudo color-magnitude plots. ....	189
5.468. SN 1964f $u,u-g$ , $g,g-i$ , and $i,i-z$ pseudo color-magnitude plots. ....	189
5.469. SN 1920a $u,u-g$ , $g,g-i$ , and $i,i-z$ pseudo color-magnitude plots. ....	190

Figure	Page
5.470. SN 2004fc <i>u,u-g, g,g-i, and i,i-z</i> pseudo color-magnitude plots. ....	190
5.471. SN 1988e <i>u,u-g, g,g-i, and i,i-z</i> pseudo color-magnitude plots. ....	190
5.472. SN 1988a <i>u,u-g, g,g-i, and i,i-z</i> pseudo color-magnitude plots. ....	191
5.473. SN 1985b <i>u,u-g, g,g-i, and i,i-z</i> pseudo color-magnitude plots. ....	191
5.474. SN 1990e <i>u,u-g, g,g-i, and i,i-z</i> pseudo color-magnitude plots. ....	191
5.475. SN 2006ee <i>u,u-g, g,g-i, and i,i-z</i> pseudo color-magnitude plots.....	192
5.476. SN 2001cm <i>u,u-g, g,g-i, and i,i-z</i> pseudo color-magnitude plots. ....	192
5.477. SN 1978h <i>u,u-g, g,g-i, and i,i-z</i> pseudo color-magnitude plots. ....	192
5.478. SN 1996b <i>u,u-g, g,g-i, and i,i-z</i> pseudo color-magnitude plots. ....	193
5.479. SN 1990h <i>u,u-g, g,g-i, and i,i-z</i> pseudo color-magnitude plots. ....	193
5.480. SN 1998s <i>u,u-g, g,g-i, and i,i-z</i> pseudo color-magnitude plots.....	193
5.481. SN 2005ip <i>u,u-g, g,g-i, and i,i-z</i> pseudo color-magnitude plots. ....	194
5.482. SN 2001h <i>u,u-g, g,g-i, and i,i-z</i> pseudo color-magnitude plots. ....	194
5.483. SN 2000i <i>u,u-g, g,g-i, and i,i-z</i> pseudo color-magnitude plots. ....	194
5.484. SN 1997bn <i>u,u-g, g,g-i, and i,i-z</i> pseudo color-magnitude plots. ....	195
5.485. SN 2002ca <i>u,u-g, g,g-i, and i,i-z</i> pseudo color-magnitude plots.....	195
5.486. SN 2004dg <i>u,u-g, g,g-i, and i,i-z</i> pseudo color-magnitude plots. ....	195
5.487. SN 2001ab <i>u,u-g, g,g-i, and i,i-z</i> pseudo color-magnitude plots. ....	196
5.488. SN 2004t <i>u,u-g, g,g-i, and i,i-z</i> pseudo color-magnitude plots. ....	196
5.489. SN 2006gs <i>u,u-g, g,g-i, and i,i-z</i> pseudo color-magnitude plots.....	196
5.490. SN 1999ge <i>u,u-g, g,g-i, and i,i-z</i> pseudo color-magnitude plots. ....	197

Figure	Page
5.491. SN 1991g $u,u-g$ , $g,g-i$ , and $i,i-z$ pseudo color-magnitude plots. ....	197
5.492. SN 1992bt $u,u-g$ , $g,g-i$ , and $i,i-z$ pseudo color-magnitude plots. ....	197
5.493. SN 2005bb $u,u-g$ , $g,g-i$ , and $i,i-z$ pseudo color-magnitude plots. ....	198
5.494. SN 1993g $u,u-g$ , $g,g-i$ , and $i,i-z$ pseudo color-magnitude plots. ....	198
5.495. SN 1997co $u,u-g$ , $g,g-i$ , and $i,i-z$ pseudo color-magnitude plots. ....	198
5.496. SN 2000au $u,u-g$ , $g,g-i$ , and $i,i-z$ pseudo color-magnitude plots. ....	199
5.497. SN 2005aa $u,u-g$ , $g,g-i$ , and $i,i-z$ pseudo color-magnitude plots. ....	199
5.498. SN 2005i $u,u-g$ , $g,g-i$ , and $i,i-z$ pseudo color-magnitude plots. ....	199
5.499. SN 2006bp $u,u-g$ , $g,g-i$ , and $i,i-z$ pseudo color-magnitude plots. ....	200
5.500. SN 2001q $u,u-g$ , $g,g-i$ , and $i,i-z$ pseudo color-magnitude plots. ....	200
5.501. SN 2000l $u,u-g$ , $g,g-i$ , and $i,i-z$ pseudo color-magnitude plots. ....	200
5.502. SN 1991n $u,u-g$ , $g,g-i$ , and $i,i-z$ pseudo color-magnitude plots. ....	201
5.503. SN 1998t $u,u-g$ , $g,g-i$ , and $i,i-z$ pseudo color-magnitude plots. ....	201
5.504. SN 2005u $u,u-g$ , $g,g-i$ , and $i,i-z$ pseudo color-magnitude plots. ....	201
5.505. SN 2000de $u,u-g$ , $g,g-i$ , and $i,i-z$ pseudo color-magnitude plots. ....	202
5.506. SN 1985f $u,u-g$ , $g,g-i$ , and $i,i-z$ pseudo color-magnitude plots. ....	202
5.507. SN 2005kl $u,u-g$ , $g,g-i$ , and $i,i-z$ pseudo color-magnitude plots. ....	202
5.508. SN 1997x $u,u-g$ , $g,g-i$ , and $i,i-z$ pseudo color-magnitude plots. ....	203
5.509. SN 2001ch $u,u-g$ , $g,g-i$ , and $i,i-z$ pseudo color-magnitude plots. ....	203
5.510. SN 2005bh $u,u-g$ , $g,g-i$ , and $i,i-z$ pseudo color-magnitude plots. ....	203
5.511. SN 1991a $u,u-g$ , $g,g-i$ , and $i,i-z$ pseudo color-magnitude plots. ....	204

Figure	Page
5.512. SN 2003l <i>u,u-g, g,g-i, and i,i-z</i> pseudo color-magnitude plots. ....	204
5.513. SN 2005az <i>u,u-g, g,g-i, and i,i-z</i> pseudo color-magnitude plots. ....	204
5.514. SN 2005la <i>u,u-g, g,g-i, and i,i-z</i> pseudo color-magnitude plots. ....	205
5.515. SN 1996aq <i>u,u-g, g,g-i, and i,i-z</i> pseudo color-magnitude plots. ....	205
5.516. SN 1997dq <i>u,u-g, g,g-i, and i,i-z</i> pseudo color-magnitude plots. ....	205
5.517. SN 2002ji <i>u,u-g, g,g-i, and i,i-z</i> pseudo color-magnitude plots. ....	206
5.518. SN 1999bc <i>u,u-g, g,g-i, and i,i-z</i> pseudo color-magnitude plots. ....	206
5.519. SN 2003i <i>u,u-g, g,g-i, and i,i-z</i> pseudo color-magnitude plots. ....	206
5.520. SN 2003aa <i>u,u-g, g,g-i, and i,i-z</i> pseudo color-magnitude plots. ....	207
5.521. SN 2006lv <i>u,u-g, g,g-i, and i,i-z</i> pseudo color-magnitude plots. ....	207
5.522. SN 2008d <i>u,u-g, g,g-i, and i,i-z</i> pseudo color-magnitude plots. ....	207
5.523. SN 2004aw <i>u,u-g, g,g-i, and i,i-z</i> pseudo color-magnitude plots. ....	208
5.524. SN 2006jc <i>u,u-g, g,g-i, and i,i-z</i> pseudo color-magnitude plots. ....	208
5.525. SN 2004gj <i>u,u-g, g,g-i, and i,i-z</i> pseudo color-magnitude plots. ....	208
5.526. SN 2004bs <i>u,u-g, g,g-i, and i,i-z</i> pseudo color-magnitude plots. ....	209
5.527. SN 2006fo <i>u,u-g, g,g-i, and i,i-z</i> pseudo color-magnitude plots. ....	209
5.528. SN 2000dv <i>u,u-g, g,g-i, and i,i-z</i> pseudo color-magnitude plots. ....	209
5.529. SN 2007rz <i>u,u-g, g,g-i, and i,i-z</i> pseudo color-magnitude plots. ....	210
5.530. SN 1988l <i>u,u-g, g,g-i, and i,i-z</i> pseudo color-magnitude plots. ....	210
5.531. SN 1997ef <i>u,u-g, g,g-i, and i,i-z</i> pseudo color-magnitude plots. ....	210
5.532. SN 1999di <i>u,u-g, g,g-i, and i,i-z</i> pseudo color-magnitude plots. ....	211

Figure	Page
5.533. SN 2006bf <i>u,u-g, g,g-i, and i,i-z</i> pseudo color-magnitude plots.....	211
5.534. SN 2005hl <i>u,u-g, g,g-i, and i,i-z</i> pseudo color-magnitude plots. ....	211
5.535. SN 1976b <i>u,u-g, g,g-i, and i,i-z</i> pseudo color-magnitude plots. ....	212
5.536. SN 1990b <i>u,u-g, g,g-i, and i,i-z</i> pseudo color-magnitude plots. ....	212
5.537. SN 2001ci <i>u,u-g, g,g-i, and i,i-z</i> pseudo color-magnitude plots. ....	212
5.538. SN 2004gn <i>u,u-g, g,g-i, and i,i-z</i> pseudo color-magnitude plots. ....	213
5.539. SN 1999bu <i>u,u-g, g,g-i, and i,i-z</i> pseudo color-magnitude plots. ....	213
5.540. SN 2004c <i>u,u-g, g,g-i, and i,i-z</i> pseudo color-magnitude plots. ....	213
5.541. SN 1983i <i>u,u-g, g,g-i, and i,i-z</i> pseudo color-magnitude plots. ....	214
5.542. SN 1964l <i>u,u-g, g,g-i, and i,i-z</i> pseudo color-magnitude plots. ....	214
5.543. SN 2000ew <i>u,u-g, g,g-i, and i,i-z</i> pseudo color-magnitude plots.....	214
5.544. SN 2004cc <i>u,u-g, g,g-i, and i,i-z</i> pseudo color-magnitude plots.....	215
5.545. SN 2004bm <i>u,u-g, g,g-i, and i,i-z</i> pseudo color-magnitude plots. ....	215
5.546. SN 1995f <i>u,u-g, g,g-i, and i,i-z</i> pseudo color-magnitude plots.....	215
5.547. SN 2000ds <i>u,u-g, g,g-i, and i,i-z</i> pseudo color-magnitude plots.....	216
5.548. SN 1997ei <i>u,u-g, g,g-i, and i,i-z</i> pseudo color-magnitude plots. ....	216
5.549. SN 1999eh <i>u,u-g, g,g-i, and i,i-z</i> pseudo color-magnitude plots. ....	216
5.550. SN 2000cr <i>u,u-g, g,g-i, and i,i-z</i> pseudo color-magnitude plots. ....	217
5.551. SN 2002bl <i>u,u-g, g,g-i, and i,i-z</i> pseudo color-magnitude plots. ....	217
5.552. SN 2002hn <i>u,u-g, g,g-i, and i,i-z</i> pseudo color-magnitude plots. ....	217
5.553. SN 2002ho <i>u,u-g, g,g-i, and i,i-z</i> pseudo color-magnitude plots. ....	218



Figure	Page
5.554. SN 2007uy <i>u,u-g, g,g-i, and i,i-z</i> pseudo color-magnitude plots. ....	218
5.555. SN 2005eo <i>u,u-g, g,g-i, and i,i-z</i> pseudo color-magnitude plots. ....	218
5.556. SN 2004gk <i>u,u-g, g,g-i, and i,i-z</i> pseudo color-magnitude plots. ....	219
5.557. SN 2004gv <i>u,u-g, g,g-i, and i,i-z</i> pseudo color-magnitude plots. ....	219
5.558. SN 1998cc <i>u,u-g, g,g-i, and i,i-z</i> pseudo color-magnitude plots.....	219
5.559. SN 2005aj <i>u,u-g, g,g-i, and i,i-z</i> pseudo color-magnitude plots. ....	220
5.560. SN 2006dk <i>u,u-g, g,g-i, and i,i-z</i> pseudo color-magnitude plots. ....	220
5.561. SN 2005o <i>u,u-g, g,g-i, and i,i-z</i> pseudo color-magnitude plots. ....	220
5.562. SN 2006lc <i>u,u-g, g,g-i, and i,i-z</i> pseudo color-magnitude plots. ....	221
5.563. SN 1994y <i>u,u-g, g,g-i, and i,i-z</i> pseudo color-magnitude plots. ....	221
5.564. SN 2002ea <i>u,u-g, g,g-i, and i,i-z</i> pseudo color-magnitude plots.....	221
5.565. SN 1996ae <i>u,u-g, g,g-i, and i,i-z</i> pseudo color-magnitude plots.....	222
5.566. SN 1997bs <i>u,u-g, g,g-i, and i,i-z</i> pseudo color-magnitude plots.....	222
5.567. SN 1997eg <i>u,u-g, g,g-i, and i,i-z</i> pseudo color-magnitude plots. ....	222
5.568. SN 1999bw <i>u,u-g, g,g-i, and i,i-z</i> pseudo color-magnitude plots. ....	223
5.569. SN 1994ak <i>u,u-g, g,g-i, and i,i-z</i> pseudo color-magnitude plots. ....	223
5.570. SN 2006aa <i>u,u-g, g,g-i, and i,i-z</i> pseudo color-magnitude plots.....	223
5.571. SN 1999gb <i>u,u-g, g,g-i, and i,i-z</i> pseudo color-magnitude plots. ....	224
5.572. SN 2004f <i>u,u-g, g,g-i, and i,i-z</i> pseudo color-magnitude plots.....	224
5.573. SN 2006am <i>u,u-g, g,g-i, and i,i-z</i> pseudo color-magnitude plots. ....	224
5.574. SN 2006m <i>u,u-g, g,g-i, and i,i-z</i> pseudo color-magnitude plots. ....	225

Figure	Page
5.575. SN 1972q $u,u-g$ , $g,g-i$ , and $i,i-z$ pseudo color-magnitude plots. ....	225
5.576. SN 1982f $u,u-g$ , $g,g-i$ , and $i,i-z$ pseudo color-magnitude plots. ....	225
5.577. SN 1989c $u,u-g$ , $g,g-i$ , and $i,i-z$ pseudo color-magnitude plots. ....	226
5.578. SN 1998bv $u,u-g$ , $g,g-i$ , and $i,i-z$ pseudo color-magnitude plots. ....	226
5.579. SN 2004df $u,u-g$ , $g,g-i$ , and $i,i-z$ pseudo color-magnitude plots. ....	226
5.580. SN 1994w $u,u-g$ , $g,g-i$ , and $i,i-z$ pseudo color-magnitude plots. ....	227
5.581. SN 1973r $u,u-g$ , $g,g-i$ , and $i,i-z$ pseudo color-magnitude plots. ....	227
5.582. SN 2001dc $u,u-g$ , $g,g-i$ , and $i,i-z$ pseudo color-magnitude plots. ....	227
5.583. SN 2001x $u,u-g$ , $g,g-i$ , and $i,i-z$ pseudo color-magnitude plots. ....	228
5.584. SN 1970g $u,u-g$ , $g,g-i$ , and $i,i-z$ pseudo color-magnitude plots. ....	228
5.585. SN 1961u $u,u-g$ , $g,g-i$ , and $i,i-z$ pseudo color-magnitude plots. ....	228
5.586. SN 1979c $u,u-g$ , $g,g-i$ , and $i,i-z$ pseudo color-magnitude plots. ....	229
5.587. SN 1936a $u,u-g$ , $g,g-i$ , and $i,i-z$ pseudo color-magnitude plots. ....	229
5.588. SN 1983e $u,u-g$ , $g,g-i$ , and $i,i-z$ pseudo color-magnitude plots. ....	229
5.589. The $u-g$ color plotted as a function of radial distance (in units of scale length) from the host galaxy center. All points are from galaxies with inclinations less than 38 degrees from face on. ....	271
5.590. The $g-i$ color plotted as a function of radial distance (in units of scale length) from the host galaxy center. All points are from galaxies with inclinations less than 38 degrees from face on. ....	272
5.591. The $i-z$ color plotted as a function of radial distance (in units of scale length) from the host galaxy center. All points are from galaxies with inclinations less than 38 degrees from face on. ....	273

Figure	Page
5.592. The $u$ -Ks color plotted as a function of radial distance (in units of scale length) from the host galaxy center. All points are from galaxies with inclinations less than 38 degrees from face on.....	274
5.593. The $u$ - $g$ ; $g$ - $r$ color-color plots for type Ia and subtypes, II, Ib/c and all other core collapse SNe. The diagonal line in each plot indicates the reddening vector. ....	275
5.594. The $g$ - $r$ ; $r$ - $i$ color-color plots for type Ia and subtypes, II, Ib/c and all other core collapse SNe. The diagonal line in each plot indicates the reddening vector. ....	276
5.595. The $r$ - $i$ ; $i$ - $z$ color-color plots for type Ia and subtypes, II, Ib/c and all other core collapse SNe. The diagonal line in each plot indicates the reddening vector. ....	277
5.596. The $u$ - $r$ ; $r$ -Ks color-color plots for type Ia and subtypes, II, Ib/c and all other core collapse SNe. The diagonal line in each plot indicates the reddening vector. ....	278
5.597. The color-color plots for all Ia and Ia subtypes used as light curve templates in supernova cosmology. The diagonal line in each plot indicates the reddening vector. ....	280
5.598. The environment $g$ - $r$ color vs supernova peak color for template Ia SNe. ....	282
5.599. The environment $g$ - $r$ color vs supernova peak color for template Ia SNe. Here the elliptical galaxies are distinguished from the spiral galaxies. ....	283
5.600. The environment color-SN peak color plots for template SNe Ia. ....	284
6.1 Redshift distributions for all simulated CCD catalog/distance limited searches (solid line) for a rate of $R=0.2$ . SNU. The plots on the left are for 100% duty cycle ( $\epsilon$ ) and the plot on the right correspond to 50% duty cycle. The rows correspond to $A_V = 0, 1, 2$ amounts of extinction from top to bottom. The dashed line is the observed Ia from the same observers. ....	317

Figure	Page
6.2. Redshift distributions for all simulated CCD catalog/distance limited searches (solid line) for a rate of $R=0.25$ . SNu. The plots on the left are for 100% duty cycle (e) and the plot on the right correspond to 50% duty cycle. The rows correspond to $A_V=0,1,2$ amounts of extinction from top to bottom. The dashed line is the observed Ia from the same observers. ....	318
6.3. Redshift distributions for all simulated CCD catalog/distance limited searches (solid line) for a rate of $R=0.3$ . SNu. The plots on the left are for 100% duty cycle (e) and the plot on the right correspond to 50% duty cycle. The rows correspond to $A_V=0,1,2$ amounts of extinction from top to bottom. The dashed line is the observed Ia from the same observers. ....	319
6.4. Redshift distributions for all simulated CCD magnitude limited searches (solid line). The plots on the left are 100% duty cycle and the plot on the right correspond to 50% duty cycle. The rows correspond to $A_V=0,1,2$ amounts of extinction from top to bottom for a rate $R=0.1$ . SNu. The dashed line is the observed Ia from the same observer.....	320
6.5. Redshift distributions for all simulated CCD magnitude limited searches (solid line). The plots on the left are 100% duty cycle and the plot on the right correspond to 50% duty cycle. The rows correspond to $A_V=0,1,2$ amounts of extinction from top to bottom for a rate $R=0.15$ . SNu. The dashed line is the observed Ia from the same observer.....	321
6.6. Redshift distributions for all simulated photographic searches (solid line). The plots on the left are 100% duty cycle and the plot on the right correspond to 50% duty cycle. The rows correspond to $A_V=0,1,2$ amounts of extinction from top to bottom for a rate $R=0.25$ . SNu. The dashed line is the observed Ia from the same observer. ....	322
6.7. Redshift distributions for all simulated photographic searches (solid line). The plots on the left are 100% duty cycle and the plot on the right correspond to 50% duty cycle. The rows correspond to $A_V=0,1,2$ amounts of extinction from top to bottom for a rate $R=0.30$ . SNu. The dashed line is the observed Ia from the same observer. ....	323
6.8. The ratio of the observed number of SNe Ia to the simulated SNe for the CCD catalog group for a rate of $R=0.2$ . ....	324

Figure	Page
6.9. The ratio of the observed number of SNe Ia to the simulated SNe for the CCD catalog group for a rate of $R=0.25$ . .....	325
6.10. The ratio of the observed number of SNe Ia to the simulated SNe for the CCD catalog group for a rate of $R=0.30$ . .....	326
6.11. The magnitude distribution of the observed (dashed line) and simulated (solid) Ia population for $R=0.25$ . .....	327
6.12. The magnitude distribution of the observed (dashed line) and simulated (solid) Ia population for $R=0.30$ . .....	328
6.13. Distribution of simulated (solid line) LOSS magnitudes and observed magnitudes for $A_V=0,1,2$ (top to bottom plots) for 100% efficiencies. ....	329
7.1. The observational white dwarf mass distribution function adapted from Koester et al. (2009). Mass is in units of solar mass. ....	335
7.2. A Hubble residual diagram of unweighted data adapted from Amanullah et al. (2010) subtracted from the $\Lambda$ CDM model plotted with $\omega = -1/3, -0.9, -1, -1.1$ cosmologies. Data and corresponding errors are averaged in bins of $\Delta z = 0.05$ for $z < 1$ and $\Delta z=0.2$ for $z > 1$ . .....	335

## LIST OF TABLES

Table	Page
4.1. List of columns in supernova database. The first column refers to information about the SN host galaxy: distance (redshift), size (diameters), sky coordinates (RA and Dec) and brightness (apparent magnitude). Morphological type means the shape of the galaxy, such as spiral, elliptical or irregular. Merger/pair indicates if a host is two interacting galaxies and multiple SNe means that the galaxy has had more than one recorded SNe. In the second column, type means SNe type, RA and Dec are the SNe sky coordinates, discovery magnitude is the apparent brightness of the SNe upon discovery – not to be confused with the peak apparent brightness. Distance to galaxy center is the distance estimate of the SNe to the host center. If the SNe is used in cosmological studies, this is also indicated (at $z < 0.1$ , there are approximately 250. SNe). The observer properties includes the name of the group(s) or individual(s) credited with the discovery, geocentric coordinates, discovery telescope mirror diameter, which recording medium (photographic or CCD) imaged the SN, any filters used on the telescope, whether the discoverer was part of a professional astronomy search or an amateur observer, and the number of independent discovery groups per supernova. ....	26
4.2. Number of SNe in samples A and B for all galaxies and just RC3 galaxies. N. and S. Celestial sphere refers to all SNe with declinations greater and less than 0, respectively. ....	33
4.3. Statistics of Sample B. Both discoveries means SNe independently found by both professional and amateur observers. Unknown obs. refers to incomplete or missing information about the discovery observatory. ....	33
4.4. Number of SN Ia in redshift bins of $cz=3000\text{km/s}$ per galaxy morphological type for sample A. Subtypes have not been included. ....	35
4.5. Number of SN II in redshift bins of $cz=3000\text{km/s}$ per galaxy morphological type for sample A. Subtypes have not been included. ....	35
4.6. Number of SN Ib/c in redshift bins of $cz=3000\text{km/s}$ per galaxy morphological type for sample A. ....	36

Table	Page
4.7. Average discovery supernova magnitude per SN type. Types listed as “Other Ia pec” are 2002cx-like, 1999aa-like, etc. types (see chapter II). .....	40
4.8. Number of SNe per type in interacting or merged systems in sample A. ....	41
4.9. Number of galaxies with multiple SNe. The first column describes the number of possible SNe in the sample (there were no galaxies with just 7 or 8. SNe). Column 2 gives the number of occurrences of galaxies with the amounts of SNe in column 1. Columns 3 though 4 give the number of galaxies with 1 or more type Ia and the last column describes galaxies with only non Ia (e.g. NGC 6946; set discussion in text). ....	42
5.1. All SNe with at least one color from SDSS. SNe listed have both spatial and pCMD plots. The column ‘cz’ refers to the host galaxy redshift and ‘SN mag.’ is the discovery magnitude of the supernova. The last two columns are the figure numbers for the spatial and pCMD plots, respectively, in this chapter. ....	230
5.2. Fraction of SNe per structure per type. ....	237
5.3. The <i>u-g</i> colors for each structure divided by SN type. ....	239
5.4. The <i>g-i</i> colors for each structure divided by SN type. ....	239
5.5. The <i>i-z</i> colors for each structure divided by SN type. ....	240
5.6. Percentages of center grid bluer than the whole 4x4 kpc region. ....	244
5.7. Percentage of structure bluer than entire 4x4kpc region for type Ia. ....	245
5.8. Percentage of structure bluer than entire 4x4kpc region for type II. ....	246
5.9. Percentage of structure bluer than entire 4x4kpc region for type Ib/c. ....	246
5.10. The average <i>u</i> surface brightness for each SN type and structure. ....	248
5.11. The average <i>g</i> surface brightness for each SN type and structure. ....	248

Table	Page
5.12. The average $i$ surface brightness for each SN type and structure. ....	248
5.13. Percentages of center grid brighter than the whole 4x4 kpc region. ....	249
5.14. Percentages of Ia center grids brighter than the whole 4x4 kpc region. ....	249
5.15. Percentages of II center grids brighter than the whole 4x4 kpc region. ....	250
5.16. Percentages of Ib/c center grids brighter than the whole 4x4 kpc region. ....	250
5.17. Fitted slopes of linear structures in pCMDs. The slope and error are estimated from linear regression using the grids nearest the supernova event. The column 'MW Dust' refers to slopes with dust similar to the Milky Way. ....	252
5.18. Visible supernovae on SDSS images in this sample. The discovery date is the date the SNe was reported. The image date is the date of the SDSS image. Two of the SDSS images have SNe visible before the reported discovery. ....	254
5.19. Average color of each band per SN type. ....	255
5.20. The $u-g$ colors for SNe type and host galaxy type. F07 is data from Fukugita et al., 2007. Errors were calculated for the entire galaxy type. ....	256
5.21. The $g-r$ colors for SNe type and host galaxy type. F07 is data from Fukugita et al., 2007. Errors were calculated for the entire galaxy type. ....	257
5.22. The $r-i$ colors for SNe type and host galaxy type. F07 is data from Fukugita et al., 2007. Errors were calculated for the entire galaxy type. ....	257



Table	Page
5.23. The <i>i-z</i> colors for SNe type and host galaxy type. F07 is data from Fukugita et al., 2007. Errors were calculated for the entire galaxy type and not subdivided by SN type. ....	257
5.24. The environment colors of all SNe occurring in galaxies with more than one SNe. The first three columns describe the attributes of the host galaxy including redshift and major and minor diameters. The next three columns list the SNe occurring in each galaxy, type and distance from the center of the galaxy in units of fractional radius. The rest of the columns are the colors for each SNe environment. ....	259
5.25. Percentage of grids with non-zero fluxes by color and percentage of grids with numbers of non-zero flux for SDSS bands. ....	268

# CHAPTER I

## INTRODUCTION

Supernovae Ia (SNe Ia) are some of the most powerful events in the Universe. The luminosity of these stellar explosions can outshine that of their host galaxy and sometimes indicate the presence of a distant galaxy that is otherwise invisible even to the largest of telescopes. A SN Ia is theorized to come from a white dwarf, an unburned carbon-oxygen (C/O) stellar core remnant supported only by electron degeneracy against gravitational collapse. Chandrasekhar (1931) calculated that a non-rotating white dwarf star reaches a maximum mass of approximately 1.4 times that of the sun before the degeneracy pressure is overcome. This limit is reached either through the accretion of material from a companion star or the collision of the white dwarf and another star. Once near or past this threshold, the white dwarf can no longer support its mass and explodes, utterly destroying the star. The explosive event, now considered a SN Ia, is seen for days and usually months. The concept that all SNe Ia must originate from white dwarf progenitors reaching the same critical mass of  $1.4 M_{\odot}^1$  leads to the statement that the intrinsic brightness of these objects must be the same for all SNe Ia.

Due to their similarity in brightness and powerful luminosity, astronomers have long courted SNe Ia as a viable tool to measure vast cosmological distances (Zwicky 1939; Wilson 1939) - even before they were separated into types and subtypes (e.g., Zwicky et al. 1961; Branch et al. 1977). It wasn't until Phillips (1993) discovered an

---

<sup>1</sup>  $M_{\odot}$  = 1 solar mass

empirical trend between the width and decay rate of the SN Ia light curve<sup>2</sup> and the peak blue luminosity, that the use of SNe Ia as distance indicators gained a huge amount of momentum. Based on this peak-decay rate relationship, Riess et al. (1998) and Perlmutter et al. (1999) independently determined a positive cosmological constant and an accelerating Universe.

However, using a simple white dwarf mass function, von Hippel et al. (1997) demonstrated that SN Ia peak brightness can span 1.8 magnitudes depending on the stellar population age. The model is based on the principle that massive ( $M_{\text{star}} > M_{\odot}$ ) stars<sup>3</sup> evolve faster than smaller stars ( $M_{\text{star}} < M_{\odot}$ ) and potentially<sup>4</sup> produce large C/O cores. Less massive stars not only form smaller C/O cores, but also take a much longer time to reach the white dwarf state. The larger the C/O mass, the more fuel to create  $^{56}\text{Ni}$  during the SN explosion that eventually decays into  $^{56}\text{Co}$  and  $^{56}\text{Fe}$ . The abundance and decay of  $^{56}\text{Ni}$  determines the peak brightness and shape of the SN light curve. Therefore older progenitors tend to produce much less  $^{56}\text{Ni}$  in comparison to white dwarfs from a younger stellar population and result in dimmer SN events. The von Hippel et al. (1997) model was able to derive a range in peak brightness that was similar to the scatter found in the Phillips (1993) observational data using a white dwarf mass function similar to the one in the local solar neighborhood. The model demonstrated that SNe Ia produce too large of a scatter in peak brightness to be used as standard candles. Not only does the scatter in the uncorrected SN magnitude span the observed range of all cosmological models, but the luminosity is heavily age dependent, implying that SNe produced at large

---

<sup>2</sup> Light curve refers to the behavior of the SN brightness as a function of time

<sup>3</sup> This assumes that the massive star is not large enough or suffers enough mass loss to not fuse anything heavier than  $^4\text{He}$ .

<sup>4</sup> Determining the final white dwarf masses from the initial mass function of a stellar population is a very complex and somewhat unknown process. A massive star doesn't always become a large white dwarf because mass loss and other internal stellar physics. But large white dwarfs can only come from massive stars as opposed to smaller solar mass main sequence stars, which cannot.

redshifts<sup>5</sup> have different intrinsic brightnesses than nearby SNe. For example, at redshifts of  $z \sim 1.5$  the age of the Universe was approximately four billion years old (assuming a standard cosmology). One billion year old galaxies at this distance have white dwarf populations created from main sequence stars larger than  $\sim 2M_{\odot}$  because stars smaller than this haven't left the main sequence. Statistically, there is a much higher probability that these white dwarfs are more massive than that average mass of nearby ( $z < 0.1$ ) white dwarfs, creating an age dependent population of SN Ia progenitors. The trouble with an evolving progenitor population is that the data can't be calibrated because the distant SN Ia population will mimic a specific cosmology, indeterminate from the actual cosmology. These findings were potentially crippling to a budding branch of cosmology and as a result, the von Hippel et al. (1997) paper was delayed in publication by 2 years, because the referees were applying for funding to explore SNe Ia as standard candles (Bothun, personal communication).

Regardless of the age-dependent inaccuracies of SNe as distance indicators, numerous cosmology groups and supernova search teams emerged in the last 15 years in support of supernovae Ia as "standardizable" candles with better data and more sophisticated data analysis techniques (e.g. SALT; Guy et al., 2005; MCLS2K2; Jha et al., 2007) to extract the peak SN Ia brightness. Considerations for sources of scatter such as age, metallicity (metal abundance) and dust are adjusted empirically rather than based on a physical model of the supernova. Theoretically, large metal abundances in progenitors are suspected of inhibiting the production of  $^{56}\text{Ni}$ , creating dimmer SNe. Dust surrounding the supernova extinguishes and reddens the SN light to some varying amount. All three effects are estimated from residuals of the supernova light curve to the particular fitting routine, reducing the peak magnitude scatter to values as low as  $\sim 0.12$  mag (Bailey et al., 2009). But these smaller values in error arise from eliminating dusty outliers and intrinsically dim SNe that don't fit the standard template SNe (e.g. Reindl et al., 2005; Wang et al., 2006; Riess et al., 2007; Amanullah et al., 2010).

---

<sup>5</sup> Redshift here is due to the effect due to an expanding universe and is interchangeably expressed as  $cz$  (units km/s) or  $z$  (unitless). It is also another way of expressing cosmological distances.

Presently, cosmologists are focusing their efforts on reducing the scatter even further in the SN peak magnitudes. This is critical if SNe are to be useful in determining a cosmological model because SN data used independently can only statistically eliminate one cosmological model, a matter dominated universe (for the latest analysis see: Genovese et al., 2009). Used in conjunction with data from the Wilkinson Microwave Anisotropy Probe (WMAP; Bennett et al., 2003) and baryonic acoustic oscillations (BAO; Eisenstein et al., 2005), the SN data supports a standard dark energy universe. But, if SN data are to stand alone without relying on the WMAP and BAO results, then there needs to be a significant reduction in the scatter beyond using the current empirical techniques. More importantly, it yet remains to be proven that SNe at large distances are similar to nearby SNe. This requires a greater understanding of the intrinsic and extrinsic factors of the supernova that effect the light output, namely an accurate model of the SN, knowledge of the progenitor stellar population age, metallicity and an accurate estimation of the surrounding host galaxy dust. Furthermore, a thorough understanding of the observer biases may illuminate systematic errors in the SN data, possibly demonstrating if most SNe are discovered or missed in specific host galaxy environments.

Until a few years ago, the importance of understanding the exact nature of the progenitor was not as large of a concern as it is today because it was expected that the scatter would substantially decrease with more SN data, but this has not been the case even with over 550 SNe Ia used as distance markers (Amanullah et al., 2010). Although it is largely agreed upon that a white dwarf undergoes a thermonuclear explosion, no one knows details such as the companion stellar type, the kind of explosion (carbon deflagration, detonation or a combination), the abundance of metal in the progenitor or how the progenitor builds enough mass to reach the Chandrasekhar limit (collision or accretion). And to add to the confusion, it's unclear as to which property (age, dust, metals) causes the scatter in the peak SN brightness. Current efforts approach the problem through SN explosion models and analysis of the host galaxy properties in an attempt to connect these to the SN light output. The host galaxy properties are either the average metal abundance, age of the stars, total galaxy mass or dust. It is unclear if these

large average properties can sensibly be compared to the local SN population that spawned the progenitor, although recent evidence indicates a connection between host galaxy luminosity, mass, metallicity and supernova brightness (Gallagher et al., 2008; Kelly et al., 2009). In fact it's assumed that distant galaxies are metal-poor and in comparison to local populations and will produce dimmer SNe (Sullivan et al., 2010). But contrary to these findings are that metal poor progenitors produce brighter SNe (Howell et al., 2009). Riess (2000) dismissed age and evolution of the SN population as a smaller effect on peak SN brightness in comparison to the variation of metallicity and host galaxy morphological type of nearby galaxies. But Ivanov et al. (2000) found that metals are not a significant factor in the overall peak brightness of a supernova, suggesting that age must be responsible for the range in brightness. Howell et al. (2009) further supports an age dependent peak luminosity with their observational data, except this is based on the average age of the galaxy. If progenitor age is a strong factor in peak brightness and galaxies at far redshifts are metal poor, then a redshift dependent stellar evolution effect cannot be ignored.

The above discussion only describes the intrinsic properties of SNe that can effect the peak brightness. The other cause for scatter is dust from the host galaxy and from the supernova. Dust remains a very elusive property; there is no consensus if dust reddens light the same way as it does in the Milky Way (e.g. Wang et al. 2006; Reindl et al. 2005). Current techniques to estimate dust extinction in SN light curves requires a priori assumptions about the intrinsic brightness of the supernova and the radial position of the supernova within the host galaxy. SNe outside or near the optical radius of the host galaxy are assumed to be essentially dust free, but this is still no guarantee that SN light is not effected by dust. There is evidence of circumstellar dust from the progenitor, present around some SNe Ia with time dependent characteristics (Blondin et al., 2009).

Adding to these uncertainties is the fact that a progenitor has never been imaged with sufficient resolution prior to an observed explosion. There is also an emerging number of "super-Chandrasekhar" mass SNe Ia (Howell et al., 2006; Yuan et al., 2010; Scalzo et al., 2010), where the luminosity produced can only be modeled by a progenitor

with a mass exceeding the Chandrasekhar limit. Recently, Gilfanov and Bogàn (2010) reported that 95% of SN Ia progenitors from elliptical host galaxies are caused from merging white dwarfs as opposed to accretion. The observational evidence comes from the lack of X-rays that should be present due to the accretion process. This is a cause for concern because the masses of the merging white dwarfs could, in all possibility, exceed the Chandrasekhar limit, defeating the idea of a similar intrinsic brightness. Within the local universe<sup>6</sup> approximately 10% of SNe Ia used as standard candles are from elliptical hosts (Amanullah et al., 2010; Jha et al., 2007; Wang et al. 2006), and because these objects are used in templates to estimate peak brightnesses of other SNe, they can give incorrect estimates of distance. Even if all progenitors explode at the Chandrasekhar limit, there is evidence that the explosion physics doesn't emit the same amount of light in similar SNe Ia. Kasen et al. (2009) replicated the observed SN luminosity - light curve shape relationship, the basis of all empirical adjustments to the peak luminosity, in their progenitor models. They found that asymmetries arise in the explosion, which are responsible for the scatter about the calibrated peak luminosities. Furthermore, Kasen et al. (2009) state that the scatter produced has the potential of overestimating distances by approximately 2% at large redshifts.

Therefore, it is crucial to know as much about the intrinsic and extrinsic characteristics of local SNe and whether it is possible to "standardize" them to a sufficient degree before we can be certain of conclusions drawn about distant SNe and the measurements they make of dark energy. Finding correlations between the SNe and the global host galaxy properties does not guarantee that the average stellar population is at all similar the particular progenitor environment and stellar neighbors. Nor is it clear if SNe at high redshifts are undoubtedly the same as the nearby sample ( $z < 0.1$ ). The next 10 years of observational cosmology will consist of at least one space based telescope designed to detect supernovae at redshifts of  $z \sim 1$  (Albrecht et al., 2009). With large money resources devoted to supernova cosmology, we must closely examine the nature of these events, all the while asking if SNe Ia are truly capable of determining properties

---

<sup>6</sup> For this work, the local universe is defined as all distances within  $z < 0.1$  or about 410Mpc ( $H_0 = 73 \text{ km/s/Mpc}$ ).

of the Universe or is the data merely a reflection of assumptions derived from a non-representative sample.

The first step in exploring this problem is to have a complete statistical description of the entire low redshift ( $z < 0.1$ ) sample of extragalactic supernovae by examining where most of these objects are found in galaxies, the type of galaxy, where on earth are the discoveries made, etc. The statistics can indicate if there is an environment that favors a specific type of supernova, as well as describe the observational biases in the sample. The next step is to study the local underlying stellar population where SNe have occurred. Through photometry, the ratios of colors indicate properties such as age, metal abundance and dust. We can see if these events come from a specific kind of stellar population and if there is any correlation with the stellar population and the peak brightness or colors of the SNe Ia. Photometry will be of portions of galactic regions near the supernova event rather than all of host galaxy light.

After a complete physical description of the local Ia population, the next step is examining how properties of SNe Ia are effected by observations. Observational biases can introduce several systematic errors into the data. For example, with recent results connecting bright galaxies to bright supernovae (Sullivan et al., 2010), there is a possibility of over selecting bright galaxies for SN observations and missing a substantial portion of SNe coming from dimmer, more plentiful galaxies. By characterizing the biases, a SN Ia rate can be determined for the nearby population of stars, putting an estimate onto how many SNe we should be capable of detecting at large distances. If the distant sample is significantly different than the nearby population either from selection effects, a redshift dependent stellar population or dust, then the cosmological results based on the data are wrong.

This thesis work approaches the first step by creating a database of all historical SNe, host galaxies properties and discoverer information. The database will be used for statistics on the population and serve as a reference for all parts of the analysis. The next step will be done by performing photometry on available online sky images of specific sites of supernovae events from the last 115 years. This sample extends to all known



types of SNe. The regions are divided into various sizes and compared against one another, looking for any “typical” stellar population that hosts SNe based on type and subtype. The colors of the stellar environment are then compared to the Ia peak colors for a sub sample of SNe Ia. The last step is modeling the observational selection function of these events for the last 70 years. The simulations will include information based on actual observatories and conditions of both professional and amateur supernova discoveries. Events are simulated via Monte Carlo techniques from a database of known nearby galaxies using various rates.

The rest of this research is organized as follows: chapter II will review each type and subtype of supernova. Chapter III will summarize how SNe Ia are used as cosmological probes, light curve fitting techniques and accuracy issues in supernova cosmology. Chapter IV will describe the local supernova population and chapter V will discuss the photometric analysis. Chapter VI will explain and show the results of the observational selection function and rate and chapter VII will be a summary and discussion of all results with future work to follow.

## CHAPTER II

### SUPERNOVA TAXONOMY

#### 2.1. Overview

Supernovae were originally divided into only two categories based on whether or not there was hydrogen (type II) or no hydrogen (type I) in their spectra. Later, type I evolved into Ia, Ib and Ic when it was discovered that types Ib and Ic do not have silicon features in their spectra, unlike type Ia. Today this classification has expanded to at least seven subtypes and it steadily grows as more supernovae are discovered. In particular, the category 'Ia' has divided into several subtypes grouped by features in their spectra and peak brightness. In many cases these SNe, such as SN 1991aa, are a mixture of two categories in that their spectral features resemble one type of supernova and then evolve to resemble another kind of supernova at later times. It is unclear if some of these subtypes are physically distinct from each other or they are similar, but obscured by dust or other environmental variables. With the possibility of a double degenerate progenitor, the paradigm of explosions only at the Chandrasekhar limit is not necessarily true anymore. The diversity of brightness produced by such events will add to the growing list of SN categories.

## 2.2. Types of Supernovae

### 2.2.1. Type II SNe

Type II is the general category for a collapse of a degenerate stellar core in a massive ( $M \sim 8M_{\odot}$ ) star. Hydrogen lines in the spectrum are assumed to be from the outer envelope of the star. The peak optical luminosity spans a large range and is usually less than Ia,

### 2.2.2. Type II Subtypes

Type II<sub>n</sub> are believed to be massive core collapse supernova surrounded by circumstellar material. Their spectra indicate many narrow (hence the “n”) hydrogen lines coming from an interaction of the explosion and the surrounding material. It isn’t clear where these spectral lines originate because they could be either from photo-ionized pre-shock circumstellar gas or from the collision of the explosion shock material and the circumstellar material (Smith et al., 2009 and references therein). Spectra do largely vary and seem to indicate non spherical geometry with the explosion and surrounding material (Hoffman et al., 2008). The progenitors are believed to be luminous blue variables – large, short-lived stars with a high mass loss rate.

Type II<sub>b</sub> are a cross between II and Ib types that show weak hydrogen lines initially in the spectrum, but then evolve and show strong helium lines with diminished or no hydrogen features. Type IIP is named after a “plateau” feature in the light curve after peak brightness. Models suggest (Smartt et al, 2009) that masses of the progenitor range from 8-168 $M_{\odot}$ . These objects have been considered possible distance indicators. Their intrinsic brightness is standardized through expanding photosphere method (Schmidt Kirshner and Eastman, 1992) based on the P Cygni profiles (spectra indicative of expanding photosphere) of Fe II (Hamuy and Pinto 2002; Olivares 2009). The simplified description of this technique is that as the SN IIP expands from the explosion and enters the plateau phase, the temperature remains roughly constant and from this, the peak brightness can be derived. Due to larger errors in the calibration technique, results are less than promising (D’Andrea et al., 2010).

Type IIL is spectroscopically similar to type IIP but light curve decays linearly after peak brightness. Recently, it has been theorized that magnetars possibly power the light curve for some IIL (Kasen and Bildsten, 2009). However evidence may also point to a black hole. (Patnaude, Loeb and Jones, 2009).

### 2.2.3. Type Ib, Ic and Ib/c

Like type II, type Ib are also from a core collapse of a massive star, however there is no hydrogen in the spectra but strong He I lines indicating that the outer hydrogen envelope is stripped away, probably due to high stellar winds. Spectra show strong O, Mg, and Ca lines. Long duration gamma ray bursts are usually associated with these events. Type Ic is very similar to type Ib, but the helium envelope is also stripped away as shown by the lack of helium lines in the spectra. Type Ib/c<sup>7</sup> are an intermediate type between Ib and Ic and have weak He lines in the spectra. The progenitors are believed to be Wolf Rayet stars (Gaskell et al., 1986), massive stars with winds that evolved from O spectral type stars. Long gamma ray bursts are also associated with these events and are usually located in the brightest areas of galaxies (Kelly et al., 2008). Of the nearby Ib, Ic and Ib/c events, no one has detected a progenitor out of 10 possible sites, which is somewhat surprising since these events are associated with most massive of stars. The probability that a massive progenitor cannot be detected in pre explosion images is an unlikely occurrence and other means of explosion – such as interacting binaries has been suggested (Smartt 2009). Type Ibn, as the name suggests, is a type Ib SN with narrow He lines. Excesses in infrared light indicate circumstellar material around the event. There are four known events classified as Ibn.

### 2.2.4. Type Ia

Type Ia is the detonation of a  $\sim 1.4M_{\odot}$  C/O white dwarf. The mass is either reached through accretion from a companion star, or collision with another white dwarf. There is

---

<sup>7</sup> From this point on, all Ib, Ic and Ibc will be collectively referred to as Ib/c for the rest of the dissertation.

no hydrogen or helium in the spectrum, but SiII and SII lines are present with Fe lines in the post maximum spectrum. The optical and infrared light curve is powered by the beta decay of  $^{56}\text{Ni}$  into  $^{56}\text{Co}$  and then  $^{56}\text{Fe}$ .

SNe Ia are found in older stellar populations and younger star forming galaxies. Their rate appears bimodal, consisting of a young prompt component and an older delayed component (Mannucci et al., 2006). Although both collision and accretion scenarios exist, the most common SNe Ia model is accretion from a main sequence or evolved companion (not necessarily a white dwarf) with explosion dynamics consisting of carbon deflagration in the core followed by detonation (Khokhlov 1991). This model recreates most of the light curve. However, Gilfanov and Bogàn (2010) hypothesized that the lack of X-ray data that should be present in an accretion process, implies that most of the progenitors in dustless elliptical galaxies are white dwarf-white dwarf (double degenerate) mergers. The lack of X-rays in spirals could mean that the dust is obscuring the x-rays, but because ellipticals are assumed dust free, any x-rays from accretion should be detected. Unfortunately, no model has adequately described the process of a merging event with light curves and abundances mimicking the observed light curve. In any case, the observational evidence is not providing a conclusive answer to the type of progenitor.

### 2.2.5. Type Ia Subtypes

Under luminous Ia have a peak brightness approximately 2 magnitudes dimmer than “normal” SNe Ia. Most dim SNe Ia appear in older stellar populations, found in elliptical and S0/a galaxies. These objects are sometimes collectively known as “91bg” events, named after the first known under luminous event, 1991bg. Recently, these objects have been modeled as double degenerate, sub Chandrasekhar mass Ia (Pakmor et al., 2010). Although, this model doesn’t mimic the light curves accurately, it does provide a plausible scenario. The light curve decays much faster than the normal Ia but too fast for to be useful in the template fits.

Over luminous Ia, like under luminous Ia are known by the first detected event, 1991T. 91T type events are intrinsically brighter events than normal Ia by about one

magnitude. The post maximum spectra resemble normal Ia events (Foley et al., 2009). It is unclear if these objects are considered to be super Chandrasekhar mass progenitors or part of a continuum of larger-than-average white dwarfs. Recent models by Meng et al. (2010) suggest that 91T Ia are the same as normal Ia, Both emit a beam of polarized light coming from the interaction of the explosion and companion. In the case of 91T events, this beam is within our viewing angle and pointed away for normal SNe Ia.

### 2.2.6. Other Ia Oddities

#### *Super Chandrasekhar Mass Ia Events*

Recent discoveries of SN Ia with luminosities brighter than 91T-type Ia further support the double degenerate merger scenario. Super Chandrasekhar mass events have estimated white dwarf masses exceeding  $1.4M_{\odot}$  based on the  $^{56}\text{Ni}$  decay light curve. In the case of 2007if, the mass is estimated at  $2.4M_{\odot}$  (Scalzo et al., 2010). Four have so far been discovered and all since 2003.

#### *1999aa-like Events*

Spectra indicate 1999aa events are a cross between normal and 91T types.

#### *2002ic-like Events*

SN 2002ic appeared as a type Ia with strong H emission indicating possible circumstellar matter (Hamuy et al. 2003).

#### *2002cx events*

SN 2002cx was originally classified as Ia because the pre-maximum spectra resembled 1991T events, yet it was under luminous. The expansion velocity of the shock is  $\frac{1}{2}$  that of normal SNe Ia (Li et al., 2003) and spectral SII and SiII peaks are very weak which is unusual for SNe Ia (Branch et al., 2004). In particular, SN 2008ha (Puckett et al., 2008) is extremely dim with an absolute luminosity  $1/100^{\text{th}}$  of a normal Ia (Foley et al., 2009). These events have been suggested to be the collapse of an oxygen-neon core of an  $\sim 8M_{\odot}$ .

star or Wolf Rayet star ( $\sim 30M_{\odot}$ ) (Valenti et al., 2009). For more information on unusual types, see Pastorello (2009), who provides a more complete summary of each new category.

## CHAPTER III

### SUPERNOVA COSMOLOGY

#### 3.1. Distance Modulus

Before discussing the data analysis portion of this dissertation, it is important to understand how supernova Ia are used in cosmology, which particular cosmological parameters SNe Ia are measuring and the limits on the SNe Ia peak magnitude dispersion required to measure the cosmological quantities. SNe Ia are used as distance indicators by assuming a known intrinsic brightness from which the distance is determined from the flux-luminosity relationship:

$$F = \frac{L}{4\pi d_l^2} \quad (3.1)$$

Where  $F$  is flux,  $L$  is luminosity and  $d_l$  is the luminosity distance to the object. In practice, the flux is measured in a the system of magnitudes:

$$m = -2.5 \log(F) \quad (3.2)$$

$$= 2.5 \log\left(\frac{L}{4\pi d_l^2}\right) \quad (3.3)$$



Here, small  $m$  refers to the apparent magnitude, the quantity measured at the detector. In order to compute the distance from  $m$ , the absolute magnitude is defined as the flux at 10 parsecs from the object (SN)

$$M = -2.5 \log(F_{10pc}) \quad (3.4)$$

$$= 2.5 \log\left(\frac{L}{4\pi(10pc)^2}\right) \quad (3.5)$$

Taking the difference between the absolute and apparent magnitudes gives the distance modulus  $m-M$ ,

$$m - M = 5 \log(d_L) - 5 \quad (3.6)$$

or

$$m - M = 5 \log(d_L) + 25 \quad (3.7)$$

where  $d_L$  in equation (3.7) is measured in Mpc. Measuring  $m-M$  is relatively straightforward, but to determine cosmological quantities such as the matter energy density,  $\Omega_M$ <sup>8</sup>, and dark energy density  $\Omega_E$ , requires solving the Friedmann-Lemaitre-Roberston-Walker metric. Assuming a flat Universe this is:

$$d_L = c \frac{(1+z)}{H_0} \int_0^z \frac{dz'}{H(z')} \quad (3.8)$$

where

$$H(z) = \left[ \Omega_M (1+z)^3 + \Omega_E \exp\left(3 \int_0^z dz' \frac{1+\omega(z')}{1+z'}\right) \right]^{-1/2} \quad (3.9)$$

---

<sup>8</sup> Here  $\Omega = \rho/\rho_c$  where  $\rho_c$  is the critical density.

The dark energy equation of state is given as  $\omega$ , the ratio of pressure to density,  $\omega = P/\rho$ . If dark energy can be described as a scalar field that responds only to gravitational potential, then  $\omega = -1$  and dark energy is considered a cosmological constant. But if there is a time varying component to the field, then dark energy changes with redshift. The distinction or determination of the behavior of dark energy, whether it is constant or varying with time, is the current task of supernova distance indicators at high redshifts.

Figure 3.1 shows the most current Hubble diagram using the SCPUnion2 data set from Amanullah et al. (2010) plotted with a  $\{\Omega_M = 0.25; \Omega_E = 0.75; \omega = -1\}$  universe (Wright, 2006), also known as a flat concordance  $\Lambda$ CDM model. The data appear to fit the cosmology within about a half a magnitude. Now, taking the data from Amanullah et al. (2010), subtracting it from the  $\Lambda$ CDM model and then binning it into redshifts of size  $\Delta z = 0.05$  for  $z < 1$  and  $\Delta z = 0.2$  for  $z > 1$  gives figures 3.2 and 3.3. Figure 3.2 plots the binned residual data against two matter dominated, zero dark energy models  $\{\Omega_M = 1; \Omega_E = 0\}$  and  $\{\Omega_M = 0.25; \Omega_E = 0\}$ . Clearly, the mass dominated universes do not fit the data as well as the  $\Lambda$ CDM model although some error bars overlap with the  $\{\Omega_M = 0.25; \Omega_E = 0\}$ . Figure 3.3 directly compares the Amanullah et al. (2010) data with the  $\Lambda$ CDM and  $\{\Omega_M = 0.25; \Omega_E = 0\}$ , demonstrating the difference of the two cosmologies. At distances past  $z > 0.9$ , the data fall between both models and the  $\Lambda$ CDM model is a less convincing fit to the data. But predominately, the  $\Lambda$ CDM universe is the best fit to the data in comparison to the other models.

## 3.2. Supernova Ia Light Curves

In order to determine the peak brightness of SNe Ia, measurements of the magnitude must be made for several days and months starting at times prior to peak brightness. Once the light curve is measured for several days, the peak apparent magnitude is extrapolated from the peak on the curve. Finding the absolute luminosity is not as straightforward. If all SNe Ia had the same luminosities, then finding the value of the distance modulus would be trivial, but in reality this is not the case. SNe Ia are treated as “calibrateable”,

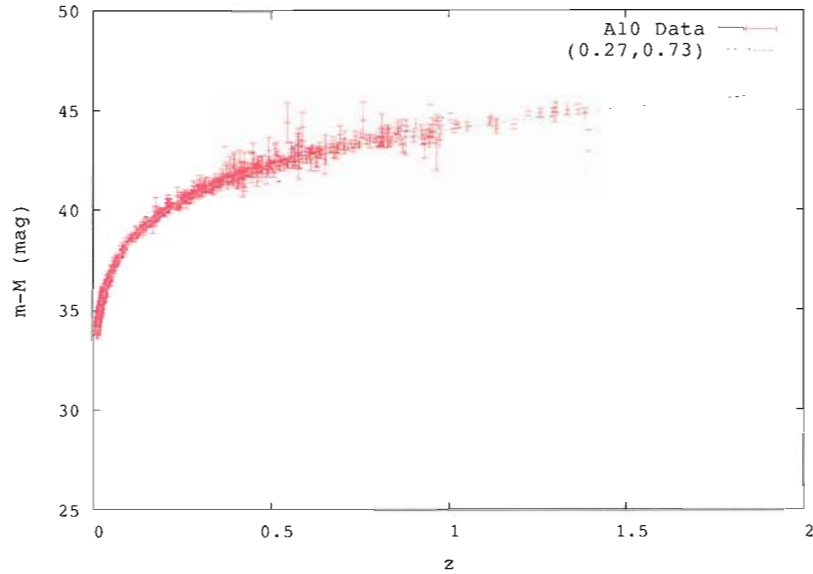


Figure 3.1. The Hubble diagram using data from Amanullah et al. 2010 (A10). The line corresponds to a  $\Lambda$ CDM  $(\Omega_M, \Omega_E, \omega) = (0.25, 0.75, -1)$  model cosmology.

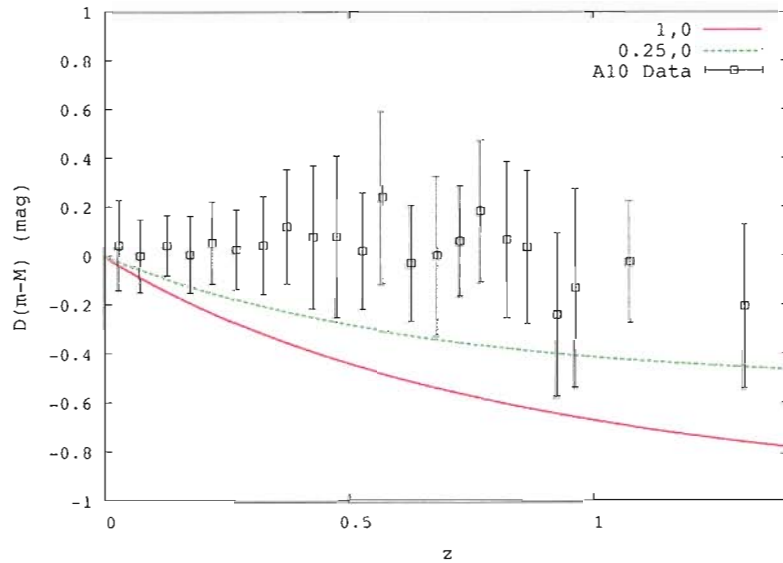


Figure 3.2. A Hubble residual diagram of unweighted data adapted from Amanullah et al. (2010) subtracted from the  $\Lambda$ CDM model plotted with  $\Lambda = 0$ ,  $\Omega_M = 1$ ,  $0.25$  cosmologies. Data and corresponding errors are averaged in bins of  $\Delta z = 0.05$  for  $z < 1$  and  $\Delta z = 0.2$  for  $z > 1$ .

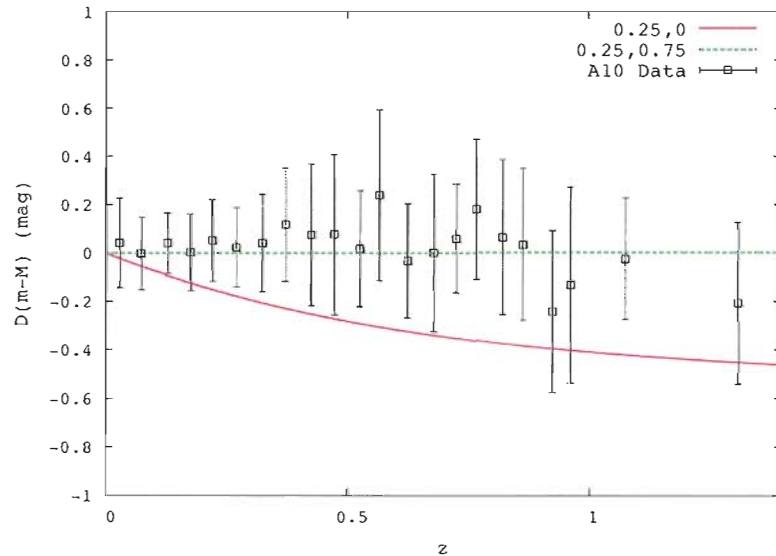


Figure 3.3. A Hubble residual diagram of unweighted data adapted from Amanullah et al. (2010) subtracted from the  $\Lambda$ CDM model plotted with  $\Lambda = 0, 0.25$  universe and the standard  $\Lambda$ CDM universe. Data and corresponding errors are averaged in bins of  $\Delta z = 0.05$  for  $z < 1$  and  $\Delta z = 0.2$  for  $z > 1$ .

meaning that they have different intrinsic luminosities related by empirically derived parameters. In practice, a characteristic of the shape of the light curve (depending on the particular fitting technique) is used to parameterize the absolute magnitude. Ideal or template Ia shapes are based on nearby SNe with complete light curve coverage and independently known distances to their host galaxies. Figure 3.4 shows an example of a normal Ia light curve based on SN 2005cf data from Pastorello et al. (2007). Each curve has been offset by 1 magnitude for clarity. Notice the shorter rise to the peak magnitude compared to the long decay tail.

### 3.2.1. Light Curve Fitting Techniques

The history of the absolute luminosity-light curve shape relationship begins with Phillips (1993) who related the decline rate of the light curve to the peak luminosity via the parameter  $\Delta m_{15}$ , a measurement of the B band magnitude 15 days after peak brightness.

The latest version of the  $\Delta m_{15}$  method was presented in Wang et al. (2006) and uses a color parameter called  $\Delta c_{12}$  to determine the amount of extinction in the light curve. Perlmutter et al. (1997) introduced the stretch parameter, where the amount of stretch required to increase or decrease the width of the measured light curve to match a template, was proportional to the absolute magnitude. The stretch parameter has since been folded into the latest light curve fitters, such as SALT2 (Guy et al., 2007) that relies on other information such as color and spectral energy distribution. Riess et al. (1995) used the shape of the light curve shape (LCS) and defined a parameter  $\Delta$  that describes the fit of a measured light curve to template light curves. MLCS2k2 (Jha et al., 2007) is the updated version of LCS, which uses dust extinction estimators and K-corrections in their fit. Wang et al. (2003) discovered a connection with the colors of the light curves and developed the technique CMAGIC. Bailey (2009) uses spectral flux ratios and so far, has had the most successful fits where dispersion in the peak magnitudes is reduced to 0.12.

All of these methods, except for the spectral flux ratios, are based on ideal supernovae, meaning that 91bg-types, 91T-types and highly reddened SNe Ia are not used in creating the SN templates and fit routines. The most uncertain parameter in these fits is the host galaxy extinction. All current fit routines estimate a new extinction law,  $R_V$  based on their SN sample which currently is not the same as  $R_V=3.1$  law derived for the Milky Way by Cardelli et al. (1989). Estimates for  $R_V$  vary from 1~2 (e.g. Wang et al., 2009; Kessler et al., 2009; Folatelli et al., 2010) depending on the data sample and the fits technique.

### 3.3. Accuracy Issues in Supernova Cosmology

From the discussion in both this chapter and previous chapters, there can be several arguments against supernovae Ia being accurate enough to measure the equation of state based on the unknown effects of intrinsic and extrinsic parameters of these objects. Most of these uncertainties come from the lack of knowing the exact nature of the progenitor and if it is at all probable that one progenitor can describe all SNe Ia. Added to the

complication of unknown progenitor is that if the double degenerate scenario is possible, then the idea of similar C/O mass in all progenitors is no longer valid. The fitting techniques mentioned above only approach a diverse SN Ia population from an empirical standpoint, meaning that even with numerous data, such as spectra and light curve shape, we still don't know what an "ideal" Ia spectra or light curve resembles. Panagia (2009) finds that spectra from Ia do not always correlate with the photometric qualities, and the range in SN Ia luminosity can vary by a factor of 10.

The issues with Ia progenitors are further compounded by intervening dust, which remains the most difficult quantity to measure or estimate independent of the supernova data. Dust cannot be expected to be similar from galaxy to galaxy. However, estimating the amount of extinction and reddening based on the light curve fitter is not acceptable since it is based on assumptions of the peak brightness of SNe Ia and of the light curve shape.

Observational bias such as the Malmquist bias is prevalent in all astronomy and so far, there has not been a way to verify if the sample of Ia chosen for cosmology is complete in describing all SNe Ia. With a small sample size of 22 SN Ia light curves at distances of  $z > 1$ , these objects hardly form a representative sample of SNe at high redshifts. Yet, these supernovae are the most critical data because SNe at  $z > 1$  can constrain the choice of cosmological models better than at smaller redshift regimes. Doing accurate photometry on dim objects at these distances requires a lot of time on large telescopes. Discovery of distant SNe requires a dedicated telescope capable of limiting magnitudes larger than 25mag, which usually requires long exposure times. It takes months of observations to create a light curve. One can argue that eventually enough data will be taken to adequately measure the equation of state to a significant precision. But with Malmquist and evolution biases in the data there will be offsets and scatter in the distant supernova population potentially exceeding magnitude differences between cosmological models (e.g. Sullivan et al., 2010) and even worse, these effects can imitate different cosmologies. Only by analyzing and understanding factors that effect SN properties from a physical and not empirical standpoint, can there be any

confidence in applying calibrations to the data and indicate if standardizing supernovae Ia to the precision required is even a possibility.

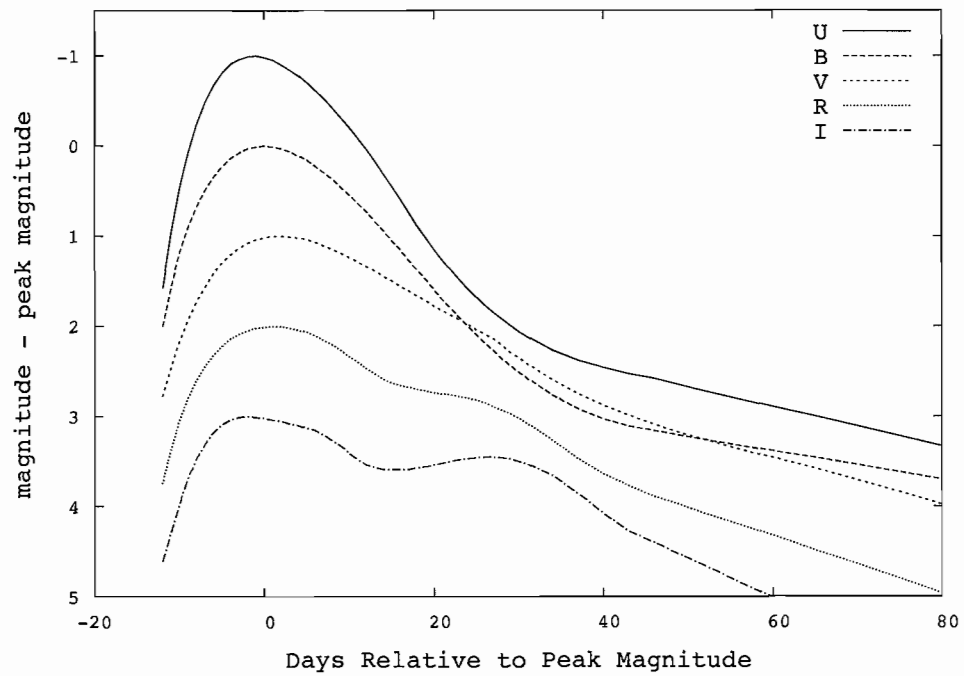


Figure 3.4. An example of UBVRI Ia light curves of SN 2005cf adapted from Pastorello et al. (2007). The U, B, V, R, I light curves have been offset by -1, 0, 1, 2, 3 magnitudes, respectively for clarity.

## CHAPTER IV

### DEMOGRAPHY

#### 4.1. Local Supernova Sample

In order to characterize the observed supernova population, it is important to define a sample that is complete to a specific distance or magnitude so that all SNe events are potentially observable by most ground based telescopes. By establishing an appropriate size or brightness limit, there is a higher probability of separating the intrinsic traits of the SNe from the observational selection effects as compared to a distant population. For this study, a local sample is defined as events occurring with apparent magnitudes brighter or equal to 20. These magnitudes correspond to roughly to a distance of  $z < 0.1$  (see figure 4.1) for detecting supernova. At this distance, cosmological effects are insignificant. And there is the added benefit that a majority of the host galaxies are visible and more than likely catalogued, making comparisons the SNe properties to the host galaxies feasible.

Supernova discoveries are reported to the Central Bureau of Astronomical Telegrams (CBAT<sup>9</sup>) for official confirmation and designation. CBAT is responsible for distributing information of the newly found SN to other astronomers for follow up observations and giving credit to the discoverer. Until recently, all supernovae were reported to CBAT, but now with many faint, distant discoveries ( $m > 21$ ), research groups aren't always reporting their findings to CBAT, but rather cataloguing and publishing their findings under designations specific to their supernova search team (e.g. Hicken et al. 2009; Drake et al, 2009). It is difficult to get independent confirmation of these dim objects because only large telescopes can observe them. With hundreds of faint SNe

---

<sup>9</sup> <http://www.cfa.harvard.edu/iau/cbat.html>



discovered yearly, it is unlikely that most telescopes can observe all of them before the SNe fade. Additionally, not all dim SNe are catalogued by the discovery teams. Since most large collaborations are targeting distant SNe Ia before their peak brightness, events outside these criteria (e.g. any type a month past peak brightness) are sometimes ignored. Therefore it is safe to say that the number of reported distant SNe is incomplete and largely biased towards Ia discoveries.

The International Astronomical Union (IAU) provides a continually updated list<sup>10</sup> of discovered SNe since 1885 (as of this writing, over 5000 events have been reported). The database for these demography studies was constructed using the IAU SN list as a basis. The list contains the SN name, coordinate information, SN type, discovery magnitude, date of discovery, discoverer and host galaxy name if it's from the Messier, NGC, IC, UGC or MCG catalogs. If the SN occurs in a galaxy not listed in one of these catalogs, it is labeled as anonymous. Information was added to the database pertaining to the host galaxy properties, SNe characteristics and discovery telescope information using NED<sup>11</sup> database and IAU circulars. If the galaxy was labeled anonymous, every effort was made to find the name and relevant information of the host galaxy. Table 4.1 lists out the columns for each supernova entry.

Data was collected until April 2008, giving a total sample size of 3103 SNe equal to or brighter than 20<sup>th</sup> magnitude. The 3103 sample was further reduced to 2526 SNe, as 508 currently do not have published host galaxy redshifts and 70 have redshifts greater than  $z=0.1$ . This sample of 2526 will be referred to as sample A and will be used to describe the statistics for this chapter unless otherwise indicated.

---

<sup>10</sup> <http://www.cfa.harvard.edu/iau/lists/Supernovae.html>

<sup>11</sup> The NASA/IPAC Extragalactic Database (NED) is operated by the Jet Propulsion Laboratory, California Institute of Technology, under contract with the National Aeronautics and Space Administration.

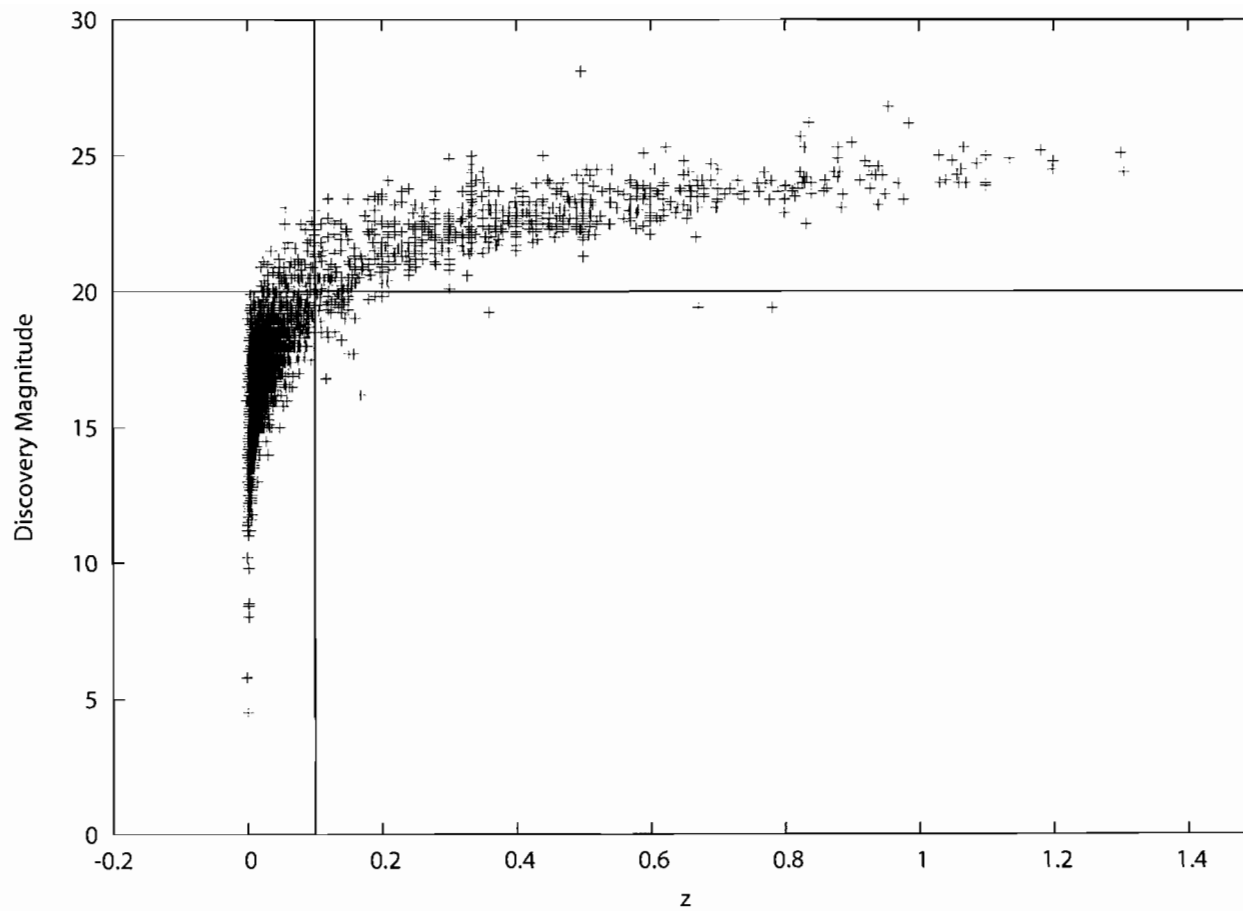


Figure 4.1. The discovery magnitude vs. redshift of all supernovae detected from 1885-2009. Points within the bottom left quadrant of the graph ( $m < 20$  and  $z < 0.1$ ) are the data selected for the local sample.

Table 4.1. List of columns in supernova database. The first column refers to information about the SN host galaxy: distance (redshift), size (diameters), sky coordinates (RA and Dec) and brightness (apparent magnitude). Morphological type means the shape of the galaxy, such as spiral, elliptical or irregular. Merger/pair indicates if a host is two interacting galaxies and multiple SNe means that the galaxy has had more than one recorded SNe. In the second column, type means SNe type, RA and Dec are the SNe sky coordinates, discovery magnitude is the apparent brightness of the SNe upon discovery – not to be confused with the peak apparent brightness. Distance to galaxy center is the distance estimate of the SNe to the host center. If the SNe is used in cosmological studies, this is also indicated (at  $z < 0.1$ , there are approximately 250 SNe). The observer properties includes the name of the group(s) or individual(s) credited with the discovery, geocentric coordinates, discovery telescope mirror diameter, which recording medium (photographic or CCD) imaged the SN, any filters used on the telescope, whether the discoverer was part of a professional astronomy search or an amateur observer, and the number of independent discovery groups per supernova.

Host Galaxy Properties	SN Properties	Observer Properties
Galaxy name	Type	Name of discovery group
Redshift	RA, Dec	Latitude and longitude of observatory
Major and minor diameters	Discovery magnitude	Telescope diameter
RA, Dec	Distance to center of galaxy	CCD or photograph
Apparent magnitude	Used in SN cosmology?	Discovery filter
Morphological type	Discovery date	Amateur or professional discovery
Merger/pair information		Number of independent discoverers
RC3* galaxy?		
Multiple SNe host?		

\*Here, RC3 refers to the Third Reference Catalogue of Bright Galaxies (de Vaucouleur et al., 1995).

## 4.2. Observational Effects

The first step in characterizing sample A is separating out the observational selection effects from the intrinsic traits of the supernova populations. Perhaps the largest selection effect is seen in figure 4.2. Here, the number of discoveries in local sample and the total number of reported SNe through CBAT is plotted per year, along with just the Ia population for all magnitudes and those from sample A. It is clear from both plots that there is a large increase in discoveries starting around 1995. Out of 5000 discoveries officially reported, 4000 occurred in the last 15 years. This is due to the increased use and availability of CCDs for both professional and amateur observers occurring in the mid

1990s coupled with the utilization of SNe Ia as standard candles (Phillips, 1993). With the realization of an accelerating Universe from two independent supernova groups, Hi-Z (Riess et al., 1998) and Supernova Cosmology Project (SCP) (Perlmutter et al., 1997), the number of professional and dedicated supernova searches exploded. CCDs also allow for many of these searches to be automated, increasing the number of images and therefore discoveries per night. Interestingly, in 2004 there is a significant dip in discoveries (over 100) from the previous year. The number of large professional supernova search teams went from five in 2003 to three in 2004 and also that year, the Lick Observatory Supernova Search (LOSS) reduced their search list of galaxies from 14,000 to 7500. Also note in Fig 4.2, the sharp decline in discoveries from 2007 (584 SNe) to 2008 (281 SNe) because dim SNe are no longer consistently reported. In sample A, the frequency of SNe per year (past 2000) fluctuates between 200-300 per year.

Figure 4.3 shows histograms of all SNe discovery magnitudes, separated into Ia and Ia subtypes, types II and Ib/c for the entire sample (including SNe at  $z > 0.1$ ) through 2009. The bimodal distribution for Ia reflects the two types of supernova searches – distance limited and magnitude limited. Distance limited searches correspond to the larger peak centered at 18<sup>th</sup> magnitude; these are the most common type of survey that consists of scanning catalogued galaxies for SNe. Magnitude limited searches result in objects with dimmer discovery magnitudes (peak centered at 22<sup>nd</sup> magnitude). These are typically deep searches targeting random patches in the sky – usually only done by large observatories where the limiting magnitude of the telescope is  $> 20$ . Notice that there isn't a similar double peak distribution for type II and Ib/c SNe, indicating that dimmer core collapsed SNe aren't detected in the magnitude limited searches. It is unclear why this is the case, other than speculating that these magnitude limited searches for SNe are targeting Ia objects and dim core-collapsed SNe go unreported.

Figure 4.4 shows a similar plot of discovery magnitude distributions for just sample A. Galaxies from the Third Reference Catalogue of Bright Galaxies (hereafter RC3; de Vaucouleurs et al., 1995), shown in gray, are distinguished from the rest of the sample. The RC3 catalogue is singled out because it contains the nearest and brightest

galaxies, typically selected for supernova observations. The SN discovery magnitude peaks around 17.5 and quickly drops off by  $m=20$ . This behavior could mean that either all SNe are detected in nearby RC3 galaxies and very few events (currently) are discovered before fading or, more than likely, this is due to the difference between magnitude and distance limited searches. Large observatories are only focused on specific patches in the sky and not nearby galaxies, whereas smaller observatories (professional and amateur) are only going to detect events less than 20<sup>th</sup> magnitude. Therefore events missed in nearby galaxies that have faded passed 20<sup>th</sup> magnitude will more than likely not be detected.

Figure 4.5 shows how the average discovery magnitude has increased significantly, particularly in the 1990s by about 1.5 magnitudes, which is a reflection of the invention of CCDs. The dimmer magnitudes seen in the 1950's are from Palomar Sky Survey Plates (Abell, 1959) reexamined by Zwicky in the early 70's. These objects are near the detection limits of the photographic survey (20<sup>th</sup>~21<sup>st</sup> magnitude) and 12 SNe are not associated with any known host galaxy. If these are indeed real events, it may indicate how easily dim SNe go unnoticed. The average magnitude does dip in 2007, which means that large observatories were focusing on deeper searches, leaving most of the brighter SNe to be discovered by amateurs and other catalogue based searches.

### 4.3. Sample and Observer Statistics

Details about each observatory, such as the coordinates, telescope diameter, search technique, were recorded in the database for each supernova until the beginning of 2007 making 2319 events. This will be referred to as sample B and the statistics from this group were used in the selection function simulation (see chapter VI). As mentioned before ~80% of all discoveries have occurred in the last 15 years. This constitutes ~69% of sample B supernovae with 82% of these discoveries occurring in the Northern hemisphere. Predominately, most events detected are from galaxies in the north celestial hemisphere (67% of sample), whereas 60% of RC3 galaxies have declinations greater

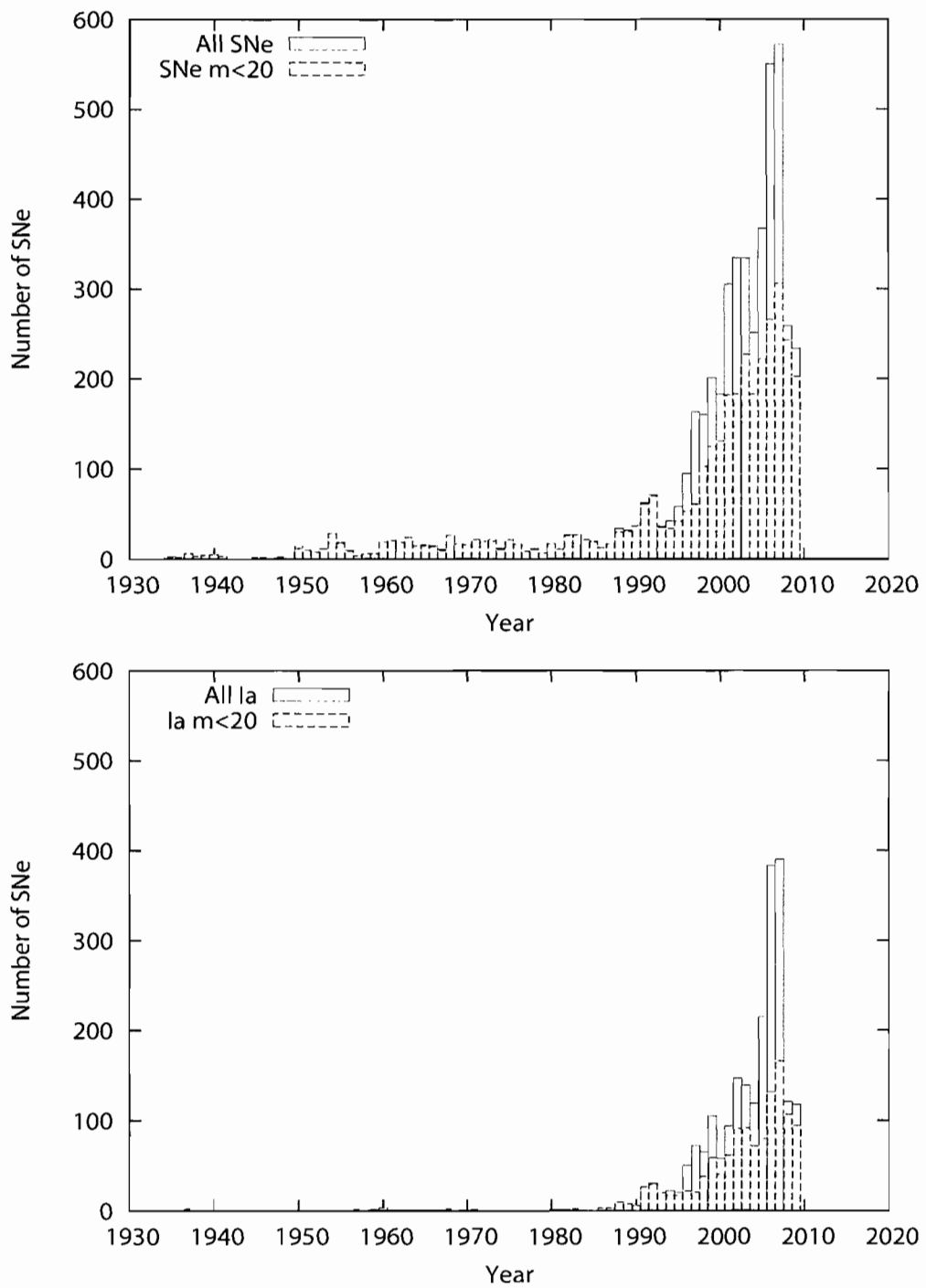


Figure 4.2. Supernovae detected per year from 1930-2009 for all SNe types (top) and just SNe Ia (bottom).

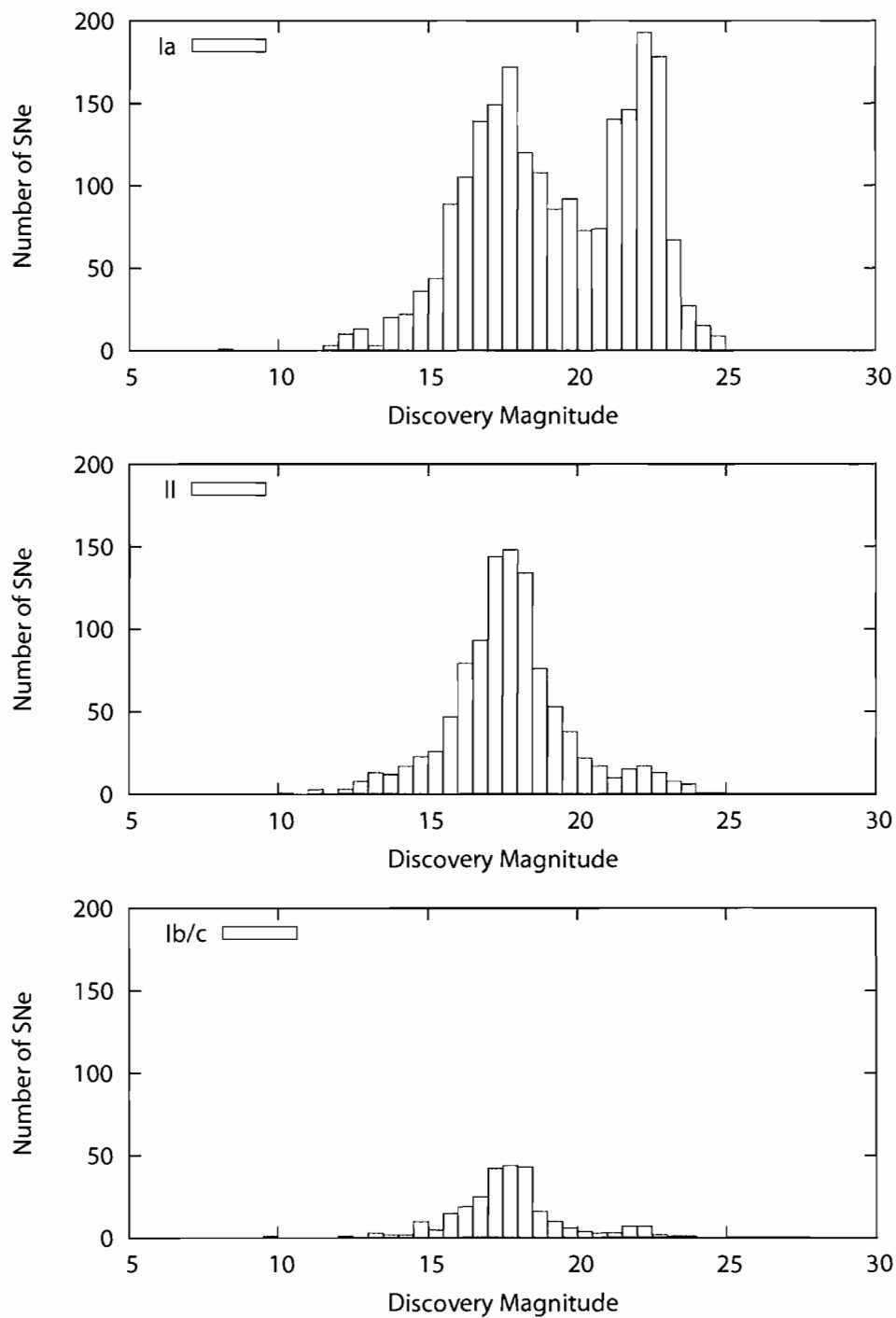


Figure 4.3. The number of SNe per discovery magnitude divided into Ia, II and Ib/c SN types from 1885-2009.

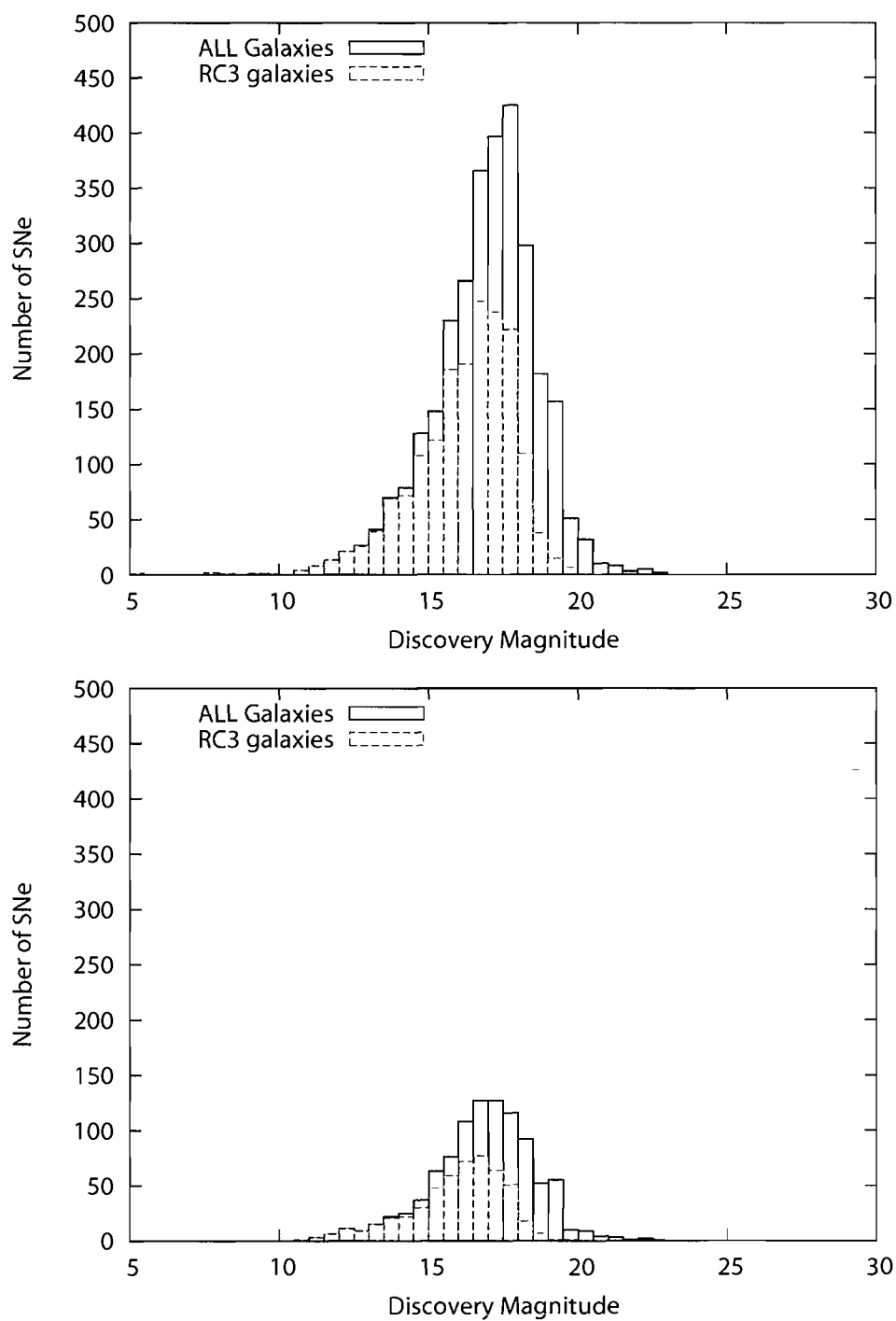


Figure 4.4. The number of SNe per discovery magnitude for all galaxies and RC3 galaxies from 1885-2009. In the bottom plot only SNe Ia discovery magnitudes are binned.



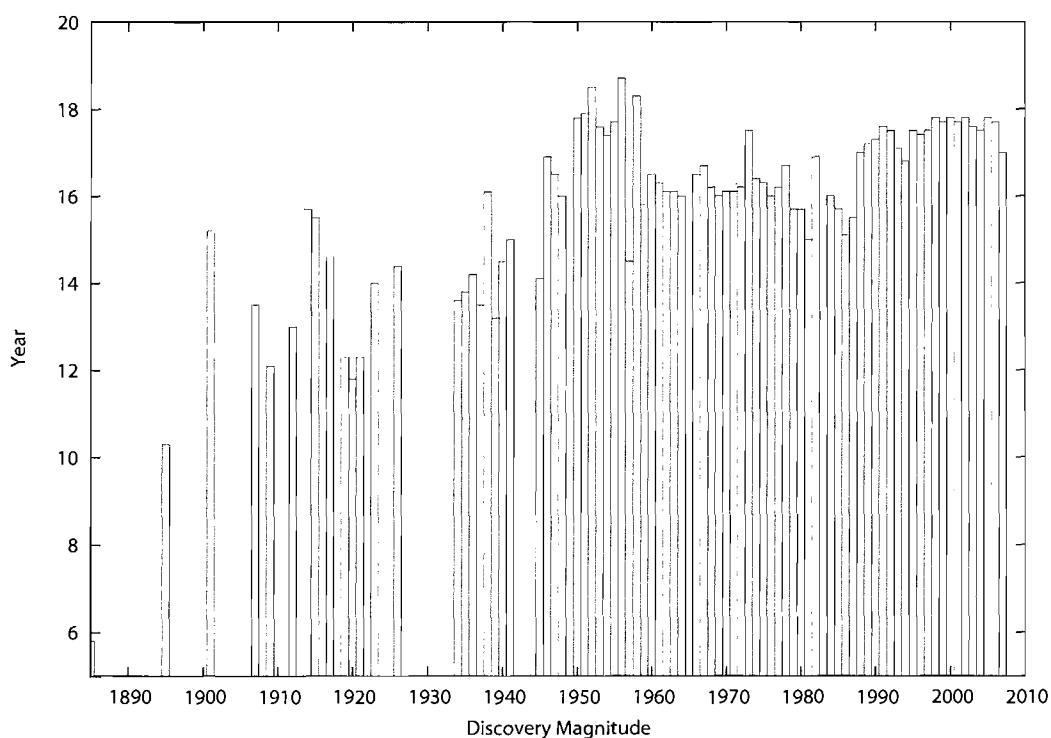


Figure 4.5. The average discovery magnitude per year. The gaps in data correspond to no reports of SNe for those years. The thin gap in the 1940's was due to WWII. The average discovery magnitude from 1950 to was unusually dim because the few discoveries made during this time were actually found later on photographic plates. Aside from this discrepancy, there is a sharp increase in dim magnitudes around 1990 when CCDs became available to astronomers.

than zero. Clearly events are biased towards galaxies in the northern hemisphere.

Numbers of SNe for each sample are shown in table 4.2.

Table 4.2. Number of SNe in samples A and B for all galaxies and just RC3 galaxies. N. and S. Celestial sphere refers to all SNe with declinations greater and less than 0, respectively.

	Sample A	Sample A RC3	Sample B	Sample B RC3
All SNe	2526	1754	2319	1599
All Ia	922	571	831	516
non Ia	1168	941	1070	841
unknown SNe	436	242	418	242
N. Celestial sphere	1682	-	1552	-
S. Celestial sphere	844	-	767	-

A quarter of discoveries come from amateur searches (table 4.3) with over 80% of these amateur discoveries coming from RC3 host galaxies. Approximately 3% of Sample B SNe have more than one reported discoverer and both amateurs and professionals found about half of these. Table 4.3 summarizes these observational quantities and those for just Ia types for all and just RC3 galaxies. Most of the discoveries are from observatories located in the northern hemisphere and 70% of these discoveries are from RC3 galaxies. For SNe Ia, 62% of sample B come from RC3 galaxies. These statistics will be referred to again in chapter VI. Almost half of the amateur discoveries are type Ia and for professional discoverers, SNe Ia constitute 1/3 of their discoveries. The reason for this discrepancy is due to the large number of unknown SNe discovered in large photographic searches such as POSSI altering the professional statistic.

Table 4.3. Statistics of Sample B. Both discoveries means SNe independently found by both professional and amateur observers. Unknown obs. refers to incomplete or missing information about the discovery observatory.

	All SNe	All Ia	All RC3 SNe	All RC3 Ia
Total SNe	2319	831	1599	516
Discovered at latitudes>0	1840	674	1290	436
Professional discoveries	1670	560	1063	299
Amateur discoveries	586	249	478	196
Both discoveries	37	17	36	17
Unknown obs.	26	5	22	4

#### 4.4. Galaxy Type

Demography based on host galaxy type (spiral, elliptical or irregular) and supernova type has been studied several times (e.g. van den Bergh et al., 2002, 2003 & 2005; Williams et al., 2003; Tsvetkov, 2004; Yasuda and Fukugita, 2009) with the conclusion that SNe Ia occur in all types of galaxies and at all radii, and core-collapse (CC) SNe occur inside the host galaxy radius in mostly Sa to Sd spirals and irregular galaxies. This conclusion is true of sample A, but also it is important to point out that a study of this kind is only relevant to events in host galaxies at distances of  $z < 0.05$ . There are two reasons for this, the lack of detailed catalogued information on galaxies past  $z < 0.05$  and the brighter intrinsic luminosity of SNe Ia compared to CC SNe. The first reason can be explained in tables 4.4-4.6, which show the number of each main type of SNe in 5 main morphological types in redshift bins of  $cz = 3000\text{km/s}$ . As distance increases, the galaxy type becomes increasingly unknown. It becomes difficult to categorize galaxies at far redshifts because of the small apparent diameters and resolution of most images. There are over 500,000 known galaxies due to recent redshift surveys such as 2dFGRS (Colless et al., 2001) and there hasn't been enough time to morphologically type each galaxy, although SDSS and their Galaxy Zoo project (Lintott et al., 2008) is enlisting help from the public to remedy this situation. Galaxy classification has not been reliably automated by a computer routine and relies on human decision and is therefore prone to bias (Hakobyan et al., 2008). For example, note the number of core-collapse events occurring in E/S0 galaxies. These classifications are suspect since several of these galaxies are actually merger remnants, spirals or irregulars (Hakobyan et al., 2008). Limiting the misclassification error means reducing the sample A to events  $z < 0.05$ . The second reason why studies based on SN type and host galaxy morphology are limited to close events is that SNe Ia are, on average, intrinsically brighter by about 2-3 orders of magnitude than core-collapse SNe. Meaning that the limiting distance is  $z \sim 0.06-0.07$  for core-collapse SNe and not  $z = 0.1$ , as it is for normal Ia. Plotting the discovery magnitude vs. redshift separately for SNe Ia and CC SNe populations (fig. 4.6) shows the trend of decreasing CC SNe at higher redshift, with an increase in SNe Ia discovered at higher redshifts.

However the number of CC SNe drops significantly at  $z \sim 0.05$ , so results past this point aren't very telling other than CC SNe are observational selected against. This is true of sample A and the entire sample of SNe collected by IAU (fig 4.3).

Table 4.4. Number of SN Ia in redshift bins of  $cz=3000\text{km/s}$  per galaxy morphological type for sample A. Subtypes have not been included.

$cz$ (km/s)	E/S0	Sa-b	Sc-Ir	Spiral	Unknown
-1500	0	0	0	0	0
1500	21	111	8	2	5
4500	37	150	17	16	12
7500	38	96	26	16	33
10500	21	51	12	24	35
13500	9	12	2	10	19
16500	5	12	1	5	29
19500	4	4	1	4	18
22500	4	1	0	0	19
25500	1	0	0	0	19
28500	0	0	0	0	11

Table 4.5. Number of SN II in redshift bins of  $cz=3000\text{km/s}$  per galaxy morphological type for sample A. Subtypes have not been included.

$cz$ (km/s)	E/S0	Sa-b	Sc-Ir	Spiral	Unknown
-1500	0	1	1	0	0
1500	2	215	27	8	6
4500	9	180	37	30	19
7500	1	93	25	19	37
10500	1	31	7	18	25
13500	1	5	2	5	14
16500	0	1	0	3	5
19500	0	0	1	0	9
22500	0	0	0	0	9
25500	0	0	0	0	0
28500	0	0	0	0	1

Table 4.6. Number of SN Ib/c in redshift bins of  $cz=3000\text{km/s}$  per galaxy morphological type for sample A.

cz (km/s)	E/S0	Sa-b	Sc-Ir	Spiral	Unknown
-1500	0	0	1	0	0
1500	3	58	5	0	1
4500	6	59	11	7	3
7500	4	20	14	7	6
10500	0	5	0	1	5
13500	0	0	0	0	3
16500	0	0	0	1	0
19500	0	0	0	0	1
22500	0	0	0	0	0
25500	0	0	1	0	1
28500	0	0	0	0	0

#### 4.5. Radial Distribution of SNe

The location of a supernova within its host galaxy may give an indication of a preferred environment for the progenitor, such as whether or not a supernova typically occurs in regions of heavy star formation. Type Ia appear to occur at all radii of the host galaxy including outside the visible radius ( $< 25\text{mag/arcsec}^2$ ) where as types II and Ib/c SNe are usually within the galaxy radius, particularly near HII regions. Figure 4.7 shows the radial distribution of SNe divided into type II, Ib/c and Ia, and including all subtypes. These statistics are based on sample A galaxies with inclinations greater than 45 degrees. Each galaxy is divided into 10 concentric rings of equal mass about the galactic center. The reason for dividing the galaxies into equal mass is to check if the number of SNe occurring is directly proportional the amount of stellar mass. If this is the case, then all the bins should have the same numbers of SNe in them. These rings of constant mass are estimated by assuming that all morphological types of galaxies have an exponential brightness profile of the form  $\sim e^{-r/\alpha}$ , where  $\alpha$  is the scale length of each galaxy. If the central surface brightness of the galaxy is assumed to be  $21.6\text{ mag/arcsec}^2$ , then the brightness fades to  $25\text{mag/arcsec}^2$  at 3 scale lengths, the visible radius of the galaxy. In order to get the bin limits, the profile is integrated and divided into 10 rings where bin 1 corresponds to the galaxy center.

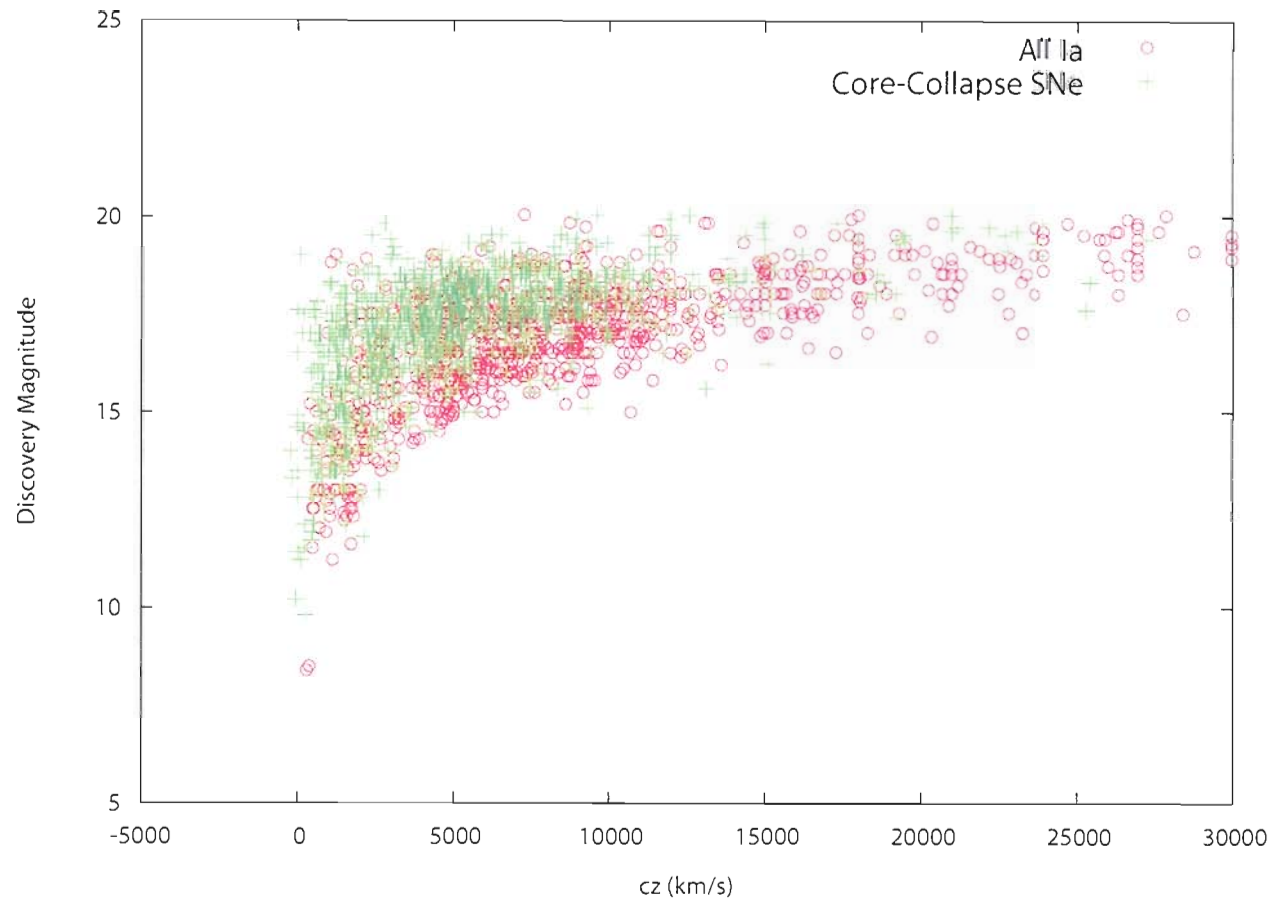


Figure 4.6. The discovery magnitude vs redshift for all Ia types and for core-collapse SNe. The plot demonstrates the larger number of Ia at redshifts greater than  $cz > 15,000 \text{ km/s}$ . This is primarily due to searches focusing on SNe Ia for cosmology. It also indicates a selection effect against core-collapse SNe.

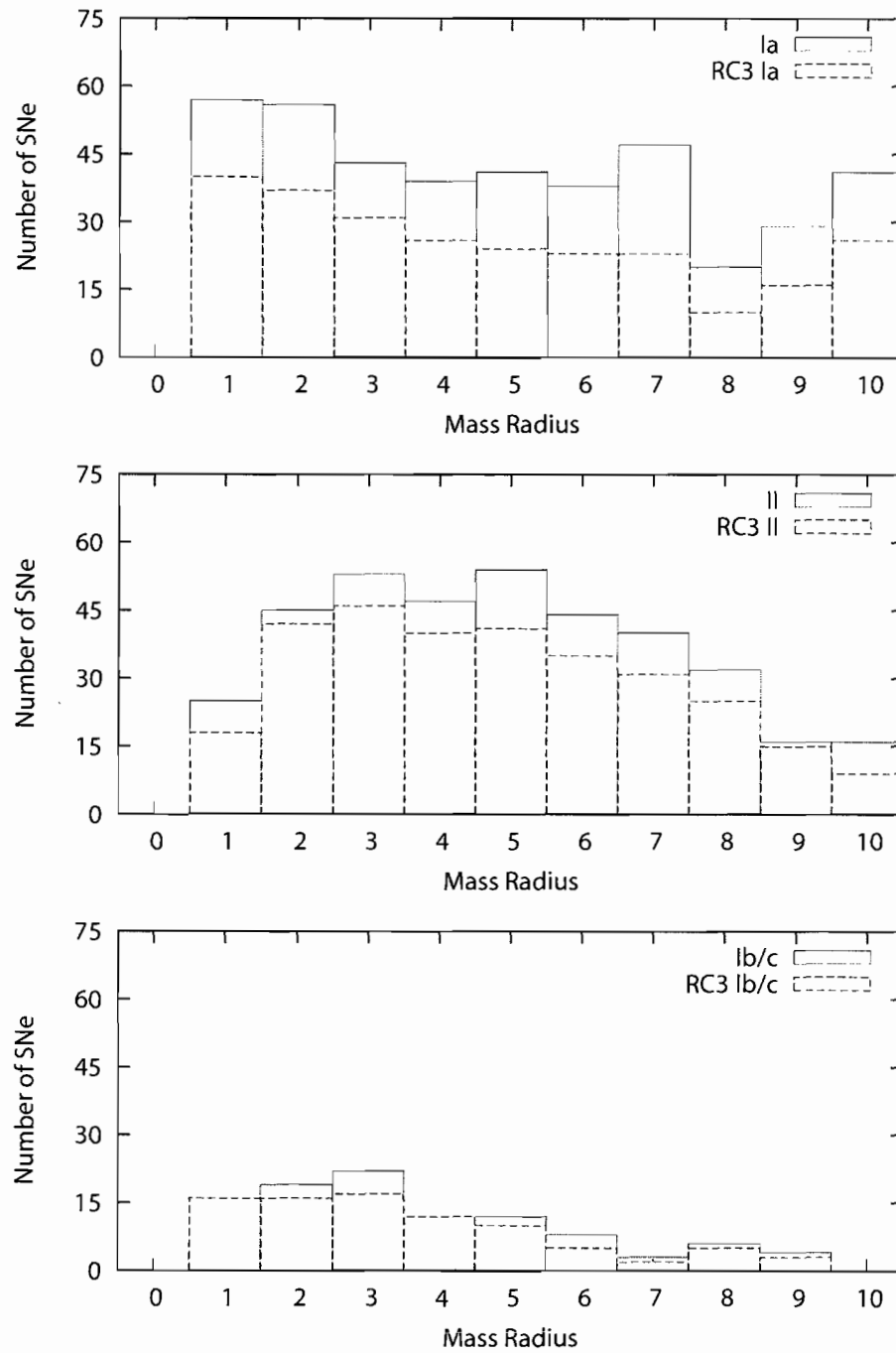


Figure 4.7. The distribution of supernovae per equal mass bin, where bin “1” corresponds to the central portion of the galaxy and bin 10 is outside the optical radius for sample A events.

SNe Ia are distributed throughout their host galaxies indicating that type Ia have no preferred environment, although the numbers do decline at greater radii, it is not clear if this is due to the inclination cut off (45 degrees) or a real phenomena. What is clear is that more SNe Ia appear towards the outside portions of the galaxies than in the 7<sup>th</sup> and 8<sup>th</sup> bin meaning that there is a selection effect taking place. SNe Ia are easier to detect outside the galaxy than towards the edges of the galaxy. Type Ib/c are mostly found within the first two scale lengths (through bin 5) of the galaxy, particularly in the first scale length. Bartunov et al. (1992) and van den Berg (1997) first noticed that Ib/c are more centrally concentrated than other core-collapse SNe in their host galaxies. Hakobyan (2008), and Anderson and James (2009) show that half of SNe Ib/c events occur within a fractional radius of  $r/R \sim 0.34$ , or at 1 scale length. For type II, the average fractional galactic radius is  $r/R = 0.58$ , in agreement with Anderson and James (2009). Notice in fig 4.7 the deficit of type II near the central cores of galaxies. The different distributions of type II and Ib/c at galactic centers could be a selection effect because type II are dimmer than Ia and are theorized to come from smaller progenitors ( $8-16M_{\odot}$ ) than Ib/c ( $>20M_{\odot}$ ). But Hakobyan (2008) and Anderson and James (2009) attribute this effect to a dependence of core-collapse SNe type on metallicity. Type Ib/c are more likely to occur in the centers of galaxies because of the high abundance of metals whereas type II are hindered because increased metallicity increases the minimum mass for type II progenitors (Eldridge and Tout, 2004). The numbers of SNe II also significantly decline towards the outer portions of the galaxy, a reflection of the radial distribution of active star formation (Petrosian et al., 2005).

Since this work is mainly concerned with selection effects, an examination of the SNe discovery magnitude and fractional radius will show any dependence on detection ability and central surface brightness of the galaxy. Keep in mind, that this is the discovery magnitude and has no bearing on the SN peak magnitude. Table 4.7 shows the average SNe discovery magnitudes divided by types and subtypes and binned into 1, 2 and 3 scale lengths, for galaxies with inclinations less than 45 degrees. Older, photographic SNe magnitudes were not included in this analysis. Type Ia and Ib/c SNe



discovered within 1 scale length of the host galaxy are on average brighter than found elsewhere. However, SNe II discovered between 1 and 2 scale lengths of the galaxy are brighter than ones found near the center of the host galaxy. All three types have the same discovery magnitude ( $\sim 17.2$ ) between 1 and 2 scale lengths, but SNe II are typically dimmer by about 0.3 than the other types for the central and outer regions. This means that more type II will be missed in galactic centers than type Ia and Ib/c. For type Ib/c the average discovery magnitude between 1 and 2 scale lengths is brighter than Ib/c found outside the visible edge of the galaxy. This more than likely is due to low number statistics since there are only 10 SNe Ib/c found past three scale lengths. All subtypes of Ia, including those that aren't 91T or 91bg have brighter discovery magnitudes than Ia. This is probably due to the fact that these SNe were discovered before or near peak magnitude, which facilitated typing them as peculiar. Past peak maximum, there was probably no distinction between peculiar types and normal Ia.

Table 4.7. Average discovery supernova magnitude per SN type. Types listed as “Other Ia pec” are 2002cx-like, 1999aa-like, etc. types (see chapter II).

Scale length	Ia	II	Ib/c	II <sub>n</sub>	II <sub>b</sub>	II <sub>P</sub>	II <sub>L</sub>	Ia 91bg	Ia 91T	Other Ia pec
1	17.07	17.33	16.93	16.88	n/a	16.53	18.40	15.94	15.47	16.48
2	17.12	17.16	17.22	17.48	17.10	17.35	n/a	18.80	16.10	17.60
3	17.27	17.55	17.07	17.33	18.02	17.30	n/a	17.53	16.08	17.32

#### 4.6. Merging, Interacting and Other Multiple Systems

Statistics based on the number of SNe in multiple interacting systems is somewhat lacking. Like morphology, the catalog listings are either incomplete or incorrect. This discrepancy was discovered when comparing identical galaxies in various galaxy catalogs. The statistics listed in table 4.8 are a conglomeration of different catalogs and interacting, merged and multiple systems are lumped together in one statistic. Future research will require each galaxy to be visually inspected for indication of a merged or multiple galaxy system.

Table 4.8. Number of SNe per type in interacting or merged systems in sample A.

Type	N
Ia	110
II	116
Ib/c	47
IIIn	20
IIb	6
IIP	12
III	4
Ia pec	8
Unknown	88
Total SNe	411

#### 4.7. Prolific Galaxies

Prolific galaxies are galaxies that have produced multiple SNe. In sample A, there are 169 galaxies that have produced 400 SNe. All but 13 galaxies are in the RC3. The biggest producer is NGC 6946, which has had 9 SNe (all core-collapse) from 1917 – 2008. NGC 6946 is a small starburst galaxy near the galactic plane and lies about 7 Mpc away. The next largest producer is NGC 5236 with 6 SNe, one of these being type Ia. The largest producer of Ia is NGC 1316, having four; two were in the 1980s, located midway between the center and edge of the galaxy and two were in 2006 close to the galactic center. NGC 1316 is a Sab peculiar type galaxy, approximately 20 Mpc away. Other galaxies are not this extreme, in fact most have had only 2 SNe. All three examples demonstrate how a few galaxies can alter the statistics of an entire sample by being dominate SN producers. Table 4.9 summarizes the basic statistics for this prolific sample and specifies the number of SNe Ia and Ia subtypes occurring in these galaxies.

Table 4.9. Number of galaxies with multiple SNe. The first column describes the number of possible SNe in the sample (there were no galaxies with just 7 or 8 SNe). Column 2 gives the number of occurrences of galaxies with the amounts of SNe in column 1. Columns 3 through 4 give the number of galaxies with 1 or more type Ia and the last column describes galaxies with only non Ia (e.g. NGC 6946; see discussion in text).

No. of SNe per Galaxy	all SNe	1 Ia	2 Ia	3 Ia	4 Ia	only non Ia
9	1	0	0	0	0	1
6	1	1	0	0	0	0
5	3	1	0	0	0	2
4	8	2	1	2	1	2
3	26	10	0	0	0	16
2	130	53	14	0	0	63

Figure 4.8 compares the major diameter and the ratio of minor to major diameter, an indicator of inclination, to the redshift for galaxies with only one SNe and those with several SNe. The number of prolific galaxies is biased toward the closest ones ( $z < 0.07$ ), but not necessarily galaxies with the largest, apparent diameters. As all plots show, the distributions are very similar in size and ratio.

#### 4.8. Summary

The demography section serves as a statistical foundation and description for the simulations and photometry that follow. But there are several important points to emphasize:

- Over half of the total SNe and SNe population of local events ( $z < 0.1$ ) come from galaxies in the RC3 catalog. There are 23,000 galaxies listed in this catalog in comparison to approximately 500,000 galaxies that are within this distance, but not in the RC3. Figure 4.9 demonstrates this large difference between the two groups of galaxies as a function of redshift.
- More discoveries have been detected in positive declinations in the sky.
- Galaxies capable of producing more than one SN Ia in a 100-year span exist.

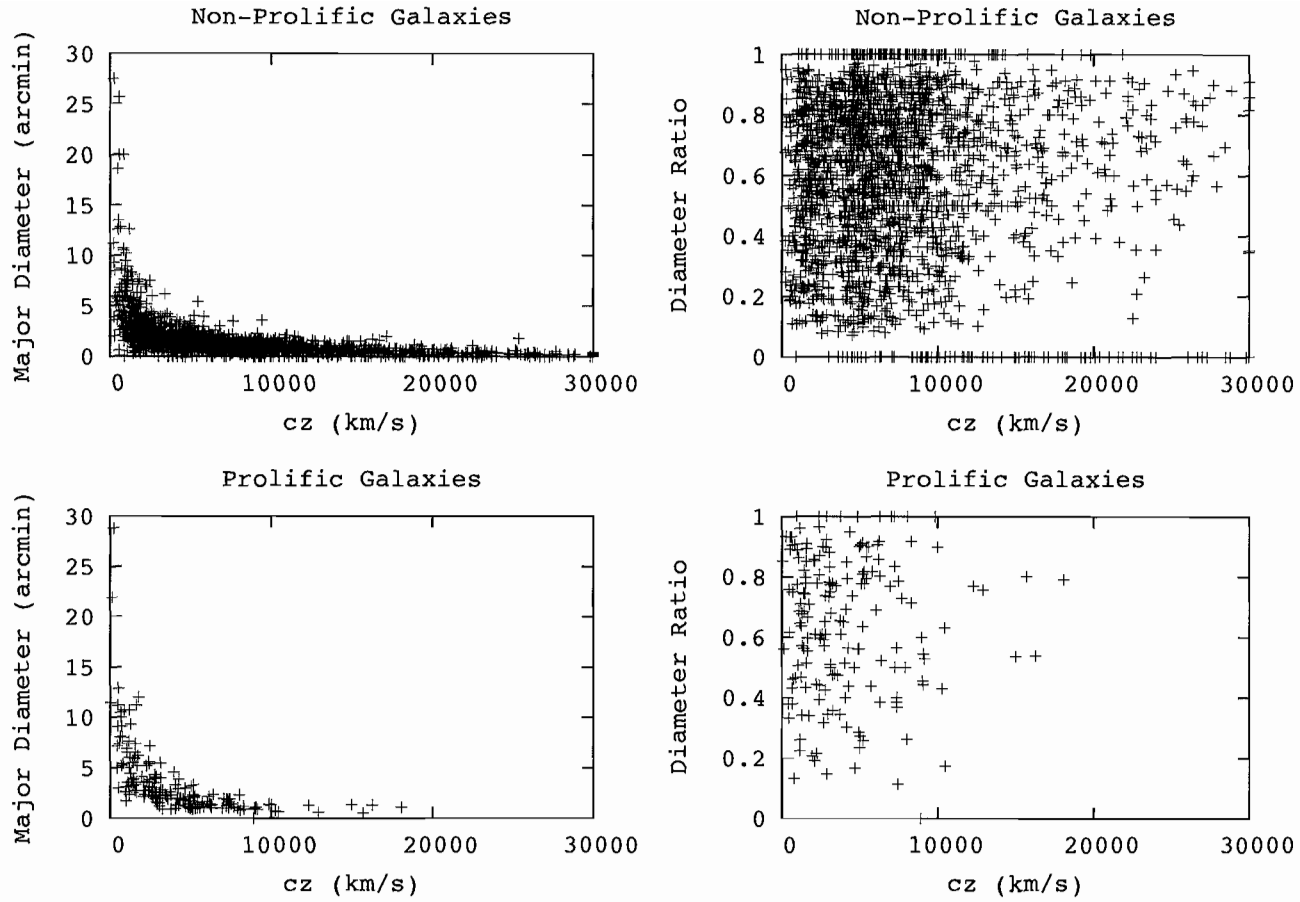


Figure 4.8. Diameter and diameter ratios of galaxies with only one recorded supernova event (non-prolific) and those with at least 2 supernovae (prolific) in the last 100 years. All data are taken from sample A.

- Type II SNe do not frequently occur in the center of galaxies. This could be a selection effect, since SNe II are dimmer than Ia and difficult to detect against the bright galactic center. Or, SN II are not frequently produced in the center of galaxies, because the metal rich environment favors Ib/c events instead. In the photometry section (chapter V), metallicity and type II production will be further explored and tested.
- SNe Ia appear to be distributed the most uniformly as a function of stellar mass, except there are more galaxies outside the optical radius than at the edge of the galaxy.
- Galaxy morphological statistics only appear to be complete up to  $z \sim 0.03$ .

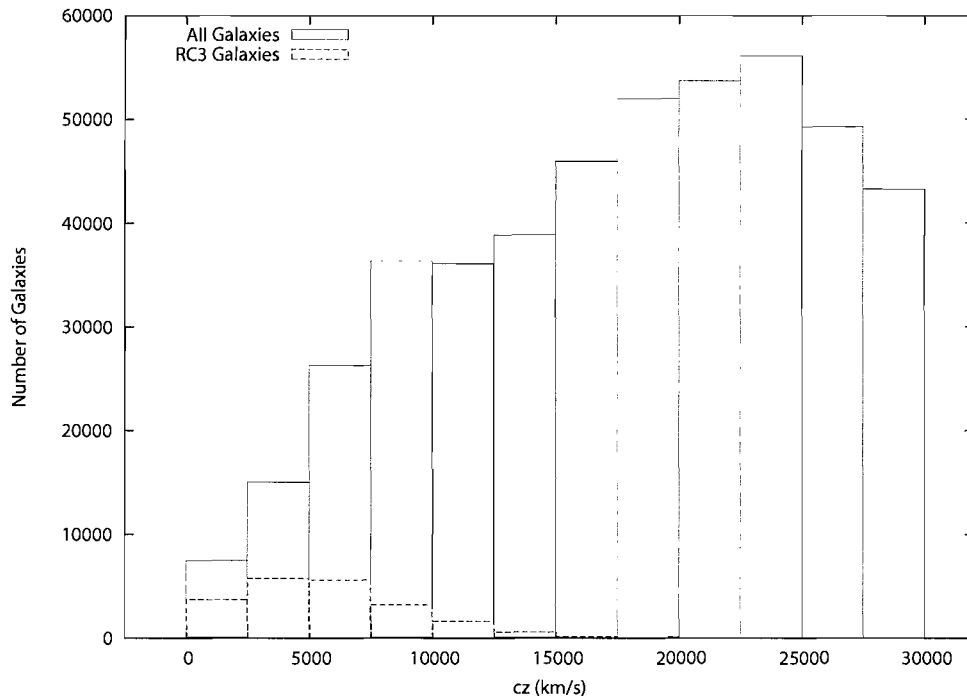


Figure 4.9. The number and redshift distribution of RC3 galaxies (filled boxes) in comparison to the entire (known) number of galaxies out to  $z=0.1$ .

## CHAPTER V

### PHOTOMETRY

#### 5.1. Background

The underlying local stellar population colors of a supernova provide clues to the properties of the progenitor and overall behavior of the light curve. As the previous section indicated, there are specific environments for particular types of SNe. The colors indicate the age and metal abundance of the stars, which in turn reflect properties of the progenitor and the amount of dust present in the region. Photometry of SN local stellar populations, let alone host galaxies has been extremely limited. van Dyk et al. (1999) examined Hubble Space Telescope images taken prior to a SN event, in an effort to find the progenitors prior to the explosion. They found three core-collapse progenitors out of a possible 27 and made color magnitude diagrams of the stellar background within the supernova region. Williams et al. (2003) examined the broadband colors of 18 high redshift ( $z > 0.4$ ) host galaxies in order to find a correlation with the peak supernova Ia brightness, yielding null results.

Core-collapse SNe show an obvious connection between environment and type. Kelly et al. (2008) demonstrated that type Ic trace the brightest regions of stellar populations. Recent studies of host galaxy luminosity and mass indicate a correlation between host mass and peak brightness of SN Ia events (Sullivan et al., 2010; Kelly et al., 2010). Residuals in the Hubble diagram from fits to cosmological models show a trend of brighter supernova with larger, more luminous hosts, for SNe with similar light curve shapes.

Beyond these studies, correlations between the host galaxy properties and the supernova are done with spectral energy distributions (SED) of the host. SEDs are a novel way of modeling a galactic stellar formation, evolution and dust and deriving properties such as metal abundances as well as mass. Presently, there are contradictory findings of a connection between host galaxy metallicity and Ia residuals from the Hubble diagram (Gallagher et al., 2008; Howell et al., 2009). Neill et al. (2009) found that the brighter SNe Ia come from galaxies with active star formation by comparing the SNe Ia  $^{56}\text{Ni}$  abundance (derived from the light curve) and SED derived host galaxy metallicity. There was also a slight trend noticed between age of the stellar population and the peak brightness of the SNe Ia in regions presumed free from host galaxy dust extinction. SEDs are quite complex and sophisticated, but are not necessarily indicative of the specific age and properties of the local population of stars that spawned the SNe. Stellar populations and properties vary from the bulge to the disk stars to regions of active star formation in the arms. The limitation of looking at all of the host galaxy light is that individual stellar populations are averaged together and information is lost.

## 5.2. Dust

Before discussing the analysis techniques of this chapter, it's important to explain how dust is currently estimated for type Ia host galaxies. Dust reddens and dims the supernova magnitudes and colors (e.g. 1996ai, 2002bo). It remains the most widely varying and unknown of all SN properties and therefore deserves its own discussion.

There are two possible sources of dust: (1) from the host stellar population environment, and (2) circumstellar dust from the supernova explosion. The first kind is independent of the supernova event, occurring in the local environment. The other type of dust comes from the progenitor in the form of ejecta surrounding explosion and the changing optical depth, varies the peak magnitude. Galactic dust is presumed to decrease with radius and as a result, several template light curves were derived from events in the outer portions of spiral galaxies and E/S0 galaxies. There are problems with this assumption supported by the following evidence:

- The second kind of dust doesn't guarantee any region to be dust-free. SN 2002ic is the first known Ia event with circumstellar material detected around it, followed by 2005gj and 2006x. These SNe occurred within the host galaxy radius, but presently, there is no physical reason why they couldn't occur outside the galaxy.
- Recent models of dust grain distributions post supernova explosion shock, indicate smaller grains are vaporized and larger grains remain mostly intact (Borkowski et al. 2006, Silvia et al. 2010), making the extinguishing properties less wavelength dependent or evacuating a usually dusty region (for a region of predominately smaller dust grain sizes).

### 5.2.1. Dust Estimation Techniques

There are three quantities to understand when describing the effects of dust. They are reddening  $E(B-V)$ , extinction  $A_V$  and  $R_V$ , the reddening law  $R_V$  where  $R_V = A_V/E(B-V)$ . Reddening can be defined as the difference of measured color to intrinsic color or  $E(B-V) = (B-V)_0 - (B-V)_{\text{meas}}$ . The extinction describes how many magnitudes of absorption occur in a wavelength (usually V). The reddening law describes how much extinction occurs for the excess in color. The reddening law is not necessarily the same for all galaxies. For example, the reddening law for the Milky Way is  $R_V = 3.1$  (Schlegel et al., 1998), whereas for Small Magellanic Cloud, it is  $R_V = 2.72$  (Prévot et al., 1984; Bouchet et al., 1985). Dust grain distributions are a function of the active star formation and star formation histories. The variation and uncertainty of the dust properties makes the separation of intrinsic (metallicity, age) and extrinsic (dust) effects much more challenging. Light curve fitting techniques have evolved to estimating extinction due to dust and the reddening laws for the best fit to the Hubble plot (fig 3.1). Some of these techniques will now be discussed.

Lira (1995) found that all SNe Ia light curves evolve similarly to one another after about month past peak brightness. Utilizing this observation, Phillips et al. (1999) formulated a time dependent relation of the intrinsic (B-V) color at these late times, which could further calibrate SNe as standard candles and estimate host galaxy dust. By



collecting a sample of unreddened SNe (SNe absent of Na I / Ca II absorption lines and coming from E/S0 galaxies or outside spiral galaxies), a baseline B-V color was derived and applied to all SNe. Any deviation from the intrinsic color was considered dust. In some cases there were bluer B-V colors, but this meant that the intrinsic color needed to be re-evaluated. Most modern techniques now use a similar method.

Wang et al. (2006) builds upon Phillips et al. (1999) by introducing the parameter  $\Delta c_{12}$ , which is the B-V color 12 days after the peak value suggesting that this is much more stable than the peak color. These colors are derived from unreddened SNe using the same criteria as Phillips et al. (1999) above. Wang et al. (2006) shows that this parameter is tightly correlated to the decline rate parameter,  $\Delta m_{15}$  (Phillips, 1993; Hamuy et al., 1996a) which is the main quantity used to determine the intrinsic peak magnitudes (see chapter III). Host galaxy reddening is then determined by applying this relationship to a SN, where any difference between the measured  $\Delta m_{15}$  and  $\Delta c_{12}$  and the empirically derived correlation is dust. However, Wang et al. (2006) states that this assumes SNe from E/S0 galaxies are free from reddening, an assumption that might not necessarily be true according to their findings, or that metallicity must play a factor in the intrinsic brightness. In order to eliminate oddballs, only data points that had  $E(B-V) < 0.06$  in the tail of the light curve (defined as 90 days past peak) were kept. The authors used the same time dependent B-V color equation derived in Phillips et al. (1999) to estimate the reddening. The dust laws derived from their analysis are different from the Milky Way and suggest that the difference might be due to two different origins of dust – interstellar and circumstellar. The reddening law derived from 73 SNe in Wang et al. (2006) works with all data except for six SNe (1999ej, 2002cx, 2003du, 1999cl, 1996ai, and 1997br) of which two (1999ej, and 2002cx) were not included in deriving the dust law because both SNe are too faint and one is spectroscopically peculiar.

Reindl et al. (2005) does a similar analysis except using the B-V color 35 days after maximum. They also derive the intrinsic  $(B-V)_0$  and  $(V-I)_0$  peak colors of unreddened SNe (again, same criteria as Phillips et al. 1999) and use these to determine the amount of dust in SNe. Reindl et al. (2005) finds a different reddening law from 62 SNe and omits

the significant outliers from the fits (six data points). Their reddening law is similar to Wang et al. (2006) concluding that the dust in the observed supernova galaxies is not the same as dust in the Milky Way.

Nobili and Goobar (2008) combine spectra with stretch parameterization to estimate the peak magnitudes and determine reddening. From here, they derived a much smaller reddening law that doesn't fit the entire sample of data, particularly the redder data points. The authors conclude that other processes are occurring such as intrinsic differences in the progenitor, light echoes (Wang, 2005) or possibly a different dust law for circumstellar dust is required.

Bailey et al. (2009) use flux ratios of spectra with a combination of light curve fitters to determine absolute peak magnitudes and extinction. Noting dust features in the spectra, the authors use UV lines to determine the amount of extinction. Most of the redder spectra in their sample seem to correlate well with the observations of extrinsic dust appearing as Na I and Ca II absorption lines. Their technique works well on all 58 data points in the sample ( $z < 0.1$ ) except for SN 1999cl where the Na I lines vary in time. Using flux ratios in this manner has had the most success reducing the dispersion in the peak SNe Ia magnitudes to 0.12.

All techniques discussed above, with the exception of the flux ratios, rely on an indirect approach to the empirical fits of the light curves and not on a physical model. In an effort to directly determine the dust and other stellar population characteristics of SNe, the second component of the analysis will measure the underlying SN stellar population colors and compare the environments to traits of the SN population. Instinctually, if there is a correlation between host galaxy properties and SN event, there should be an even tighter correlation between the local stellar population and SN. Similar colors would indicate supernovae come from a stellar population of the same age, metallicity or dust extinction. Two approaches are taken to measure the local SN region colors: grid photometry (Bothun, 1986) and circular aperture photometry. Both methods are discussed in further detail below. Both techniques can only be used in regions where there is a significant amount of flux from the galaxy. Therefore, this sample is biased against SNe

events that occurred near faint stellar populations and well outside the visible radius of the galaxy.

### 5.3. Data Analysis

With a potential sample size of over 3000 SN regions of which 1000 are type Ia, this analysis requires images taken in the same filter system and ideally, from the same telescope. Fortunately in the last ten years, large sky coverage surveys such as Sloan Digital Sky Survey (SDSS; York et al., 2000) and the Two Micron All Sky Survey (2MASS; Skrutskie et al., 2006) have come online and provide images readily available for the public with resolutions of 1"/pixel and smaller. Each area of sky covered is imaged in either 5 (SDSS) or 3 (2MASS) filter bands. Higher resolution images ( $\sim 0.1''/\text{pixel}$ ) from Hubble Space Telescope (HST) are also available but not all data are taken with the same filter set because HST is not a survey instrument. Thus, SDSS and 2MASS images are the optimal choice for this particular analysis. However, further studies would require HST resolution and will be pursued in the future.

#### 5.3.1. Data Sets

##### 5.3.1.1. Sloan Digital Sky Survey

Sloan Digital Sky Legacy Survey (SDSS)<sup>12</sup> was an imaging and spectroscopic survey that covered 8400 deg<sup>2</sup> in five filters  $u$  (3551Å),  $g$  (4686Å),  $r$  (6165Å),  $i$  (7481Å) and  $z$

---

<sup>12</sup>Funding for the SDSS and SDSS-II has been provided by the Alfred P. Sloan Foundation, the Participating Institutions, the National Science Foundation, the U.S. Department of Energy, the National Aeronautics and Space Administration, the Japanese Monbukagakusho, the Max Planck Society, and the Higher Education Funding Council for England. The SDSS Web Site is <http://www.sdss.org/>. The SDSS is managed by the Astrophysical Research Consortium for the Participating Institutions. The Participating Institutions are the American Museum of Natural History, Astrophysical Institute Potsdam, University of Basel, University of Cambridge, Case Western Reserve University, University of Chicago, Drexel University, Fermilab, the Institute for Advanced Study, the Japan Participation Group, Johns Hopkins University, the Joint Institute for Nuclear Astrophysics, the Kavli Institute for Particle Astrophysics and Cosmology, the Korean Scientist Group, the Chinese Academy of Sciences (LAMOST), Los Alamos National Laboratory, the Max-Planck-Institute for Astronomy (MPIA), the Max-Planck-Institute for Astrophysics (MPA), New Mexico State University, Ohio State University, University of

(8931Å). Based at Apache Point Observatory in New Mexico, at an altitude of 2797m, the survey was conducted in two parts, SDSS-I (2000-2005) and SDSS-II (2005-2008). The detector of the 2.5m telescope consists of 6 columns of 5, 2048x2048 pixel CCD cameras with a resolution of 0.397 arcsec/pixel, totaling a 3 degree field of view. Each row corresponds to one filter in  $u, g, r, i$  or  $z$  with a limiting magnitude of 22.3, 23.3, 23.1, 22.3, 20.8, respectively. The regions covered by the survey were the 7500 square degrees of the North Galactic Cap and 740 square degrees of the South Galactic Cap. SDSS provides corrected images, meaning that the data have been flat-fielded, bias-subtracted and removed of bright saturated sources by an automated processing pipeline. Further details of the telescope and camera can be found in York et al. (2000), Gunn et al. (2006) and Gunn et al. (1998).

Photometry is performed on  $u, g, r, i, z$  band images from the SDSS Seventh Data Release (Abazajian et al. 2009). Galaxy images chosen have redshifts less than 10,000km/s and have hosted any type event from 1895 to the beginning of 2008. As SDSS released more data to the public, only host galaxies of Ia and Ia Pec type events were selected with the same redshift criteria. This amounts to a total of 503 supernova regions of which 152 are type Ia and Ia Pec, 26 are type I and 325 are all other types.

SDSS uses asinh magnitudes (Lupton et al., 1999) for objects in the SDSS catalog. These magnitudes are ideally suited for areas of low flux such as regions outside the  $25\text{mag}/\text{arcsec}^2$  optical radius of a galaxy, where supernovae can occur. For these low flux regions, the magnitudes approach “zero-flux” (between 24-25 mag for SDSS  $ugriz$  filters) magnitude instead of giving non-numerical results as would the traditional Pogson<sup>13</sup> system. For objects with a flux at least ten times greater than the zero-flux point, the asinh magnitude system is within 1% of the Pogson magnitudes. Thus, the asinh system is adopted here.

---

Pittsburgh, University of Portsmouth, Princeton University, the United States Naval Observatory, and the University of Washington.

<sup>13</sup> Pogson magnitudes are defined as:  $m_1 - m_2 = -2.5 \log(L_1/L_2)$  where  $L_1$  and  $L_2$  are the luminosities of two objects.

Apparent magnitudes are calculated as

$$m_{sdss} = -1.0857 \left[ \operatorname{asinh} \left( \frac{1}{2b} \frac{f}{f_0} \right) + \ln b \right] \quad (5.1)$$

where

$$\frac{f}{f_0} = \left( \frac{\text{flux}}{\text{exposuretime}} \right) 10^{(zp-ec \times \text{airmass})}, \quad (5.2)$$

$zp$  is the zeropoint, and  $ec$  is the extinction coefficient, both provided in the SDSS tsfield file. Flux is the sky subtracted object counts and  $b$  is a softening parameter. The softening parameter is roughly equal to the noise error in the sky background. See Lupton et al. (1999) for details on the derivation. The asinh magnitudes are very close to the AB magnitudes (Oke and Gunn, 1983), but the  $u$  and  $z$  bands require small additional terms of -0.04 and 0.02, respectively, to correct for offsets from the AB system.

Errors in the magnitude are found by

$$m_{err} = 1.0857 \frac{f}{f_0} (error) \frac{1}{2b} \left( 1 + \frac{f}{2bf_0} \right)^{-1/2} \quad (5.3)$$

where

$$\frac{f}{f_0} (error) = \left( \frac{\text{flux error}}{\text{exposure time}} \right) 10^{(zp-ec \times \text{airmass})} \quad (5.4)$$

$$\text{flux error} = \left( \frac{\text{sky} + \text{object counts}}{\text{gain}} \right) + n \times (\text{dark variance} + \text{sky count error}) \quad (5.5)$$

and  $n$  is the number of pixels in the aperture. The gain, dark variance, zeropoint, airmass and extinction coefficient were all found in the tsfield information file. The sky counts

and sky error were determined using the IRAF<sup>14</sup> IMEXAMINE tool. Finally, galactic extinction is subtracted from each value using Schlegel et al. (1998).

### 5.3.1.2. The Two Micron All Sky Survey

The Two Micron All Sky Survey (2MASS<sup>15</sup>) was a ground based infrared survey that imaged the entire night sky in J(1.25 $\mu$ ), H(1.65 $\mu$ ) and K<sub>S</sub>(2.17 $\mu$ ) from 1997 to 2001. It consisted of two 1.3m telescopes based in Arizona and Chile and produced 512x1024 images with resolutions of 1"/pixel.

Images from 2MASS are downloaded of the same 503 SNe locations as SDSS corresponding in K<sub>S</sub> band. Magnitudes are calculated using

$$m_{2MASS} = zp - 2.5 \log(flux) \quad (5.6)$$

where the flux is background subtracted and  $zp$  is the zeropoint for the K<sub>S</sub> band. Exposure time is already accounted for in each pixel in the 2MASS processing pipeline.

Errors in magnitudes are found by

$$m_{err} = \frac{flux}{\left( \frac{flux}{4 * G} + area * (3.4 * \sigma)^2 + (0.024 * area * \sigma)^2 \right)^{1/2}} \quad (5.7)$$

Area is the number of pixels of the aperture,  $\sigma$  is the sky count error and  $g$  is the gain.

Like the SDSS images, sky background level and sky count errors are determined with

---

<sup>14</sup> IRAF is distributed by the National Optical Astronomy Observatory, which is operated by the Association of Universities for Research in Astronomy, Inc., under cooperative agreement with the NSF.

<sup>15</sup> This publication makes use of data products from the Two Micron All Sky Survey, which is a joint project of the University of Massachusetts and the Infrared Processing and Analysis Center/California Institute of Technology, funded by the National Aeronautics and Space Administration and the National Science Foundation.

IMEXAMINE in IRAF. All final magnitudes were corrected for galaxy extinction. Since SDSS uses AB magnitudes and 2MASS filter are based on the Vega system, the 2MASS data was converted to the AB system by adding a factor of 1.84 to the  $K_S$  band magnitudes. A detection in  $K_S$  is anything with a signal to noise greater than 5.

### 5.3.2. Grid Photometry

In order to examine varying stellar populations across host galaxies, we use grid photometry, a technique first demonstrated by Bothun (1986) to analyze irregular galaxy NGC 4449. A galaxy is divided into grids where the flux is measured in each grid rather than using isophotes, which average over a larger area in the azimuthal direction of the galaxy. This technique allows for greater isolation of individual stellar populations. However, it is unrealistic to assume that only one stellar population is contained in its entirety in one grid, since grids are distributed evenly across a region regardless of the galactic structure. Possibly, due to the lack of greater resolution for defining the stellar populations to a higher degree, grid photometry has evolved to pixel maps (e.g. Eskridge et al., 2003; Lanyon-Foster et al., 2007). Instead of a grid, flux is evaluated in 1 pixel. This method is ideal for more distant galaxies and lower resolution images, because it can isolate stellar populations to a higher degree. However, due to the unknown uncertainties in supernova position, grids are a better option than individual pixels since the pixel containing the supernova location may be in error. Grids also have the advantage over pixels because noisy pixels are averaged out. Therefore, grids are sufficient for our purposes.

A square approximately 4 x 4 kpc in size, is centered about each supernova event on SDSS *u g r i z* images. The square is then further divided into overlapping grids of size 6 x 6 or 7 x 7 pixels, corresponding to areas ranging from 40 pc to 1.3 kpc in size for a Hubble constant of  $H_0=73 \text{ km s}^{-1} \text{ Mpc}^{-1}$ . Due to their proximity, and therefore large number of grids, M81 and IC 3311 have grids of 15 x 15 pixels. Over half of the regions have grids less than or equal to 0.5kpc. SN positions are converted from equatorial coordinates to pixel image coordinates using the algorithms in Pier et al. (2003). Each

environment was checked individually for positional accuracy using ALADIN (Bonnarel et al., 2000) through the NED database. The fluxes are extracted using the POLYPHOT task from IRAF and the magnitudes are calculated in Fortran code written specific to this analysis.

The final choice of the colors was based on a combination of the amount of flux available in each filter and specific bands that provide information on metal abundance and stellar age. Ideally,  $u-z$  would be the broadest and best color for analysis, however, there is a lower signal to noise ratio (S/N) in both filters. The  $g-i$  color has the largest wavelength baseline with good S/N and provides the greatest amount of contrast for examining the regional structure. Still with a significant number of regions having flux in one or both wavelengths, the  $u$  and  $z$  filters are utilized. The  $u-g$  color is an indicator for stellar age and the  $i-z$  color is sensitive to metal abundance.

Figures 5.1 to 5.294 contain the spatial maps of each region plotted in colors  $u-g$ ,  $g-i$  and  $i-z$ , where the x and y axes correspond to the image coordinates (the x and y axes are not labeled). In the spatial maps, only grids brighter than  $5\sigma$  above sky background are plotted. Here,  $\sigma$  corresponds to the error calculated for each particular grid. The data is divided into levels and color-coded such that each level spans a  $3\sigma_c$  range in values. Here,  $\sigma_c$  is the error for each color band. For example, all grids between  $0.7 < g-i < 0.9$  are dark green. The error is the same for all SNe regions, even though  $\sigma$  varies for each grid and galaxy. This was done by setting  $\sigma_c$  to the largest error in each color in all data sets and only considering data that make the sky background cutoff. The errors are 0.12, 0.07 and 0.06, in magnitude, for  $u-g$ ,  $g-i$  and  $i-z$ , respectively. The slight color variations within each level were left in giving a better sense of the galactic structure near the supernova.

Unknown types and type I were eventually omitted from the data because a lot of the analysis presented relies on the exact category of SN. For space considerations, SNe in areas where there is no flux in any color band in the center grid are not displayed as well, even if there was color in the surrounding region. As a result, there are a remaining



294 SNe regions (106 Ia, 102 II, 61 Ib/c and 25 II subtypes) with non zero flux in at least two bands.

Following the spatial plots are the pseudo-color magnitude diagrams (pCMD) of each corresponding SN (figures 295-588). In every pCMD, the grid centered at the supernova location is indicated by either a circle, cross or star. The circle means that both color bands are above the detection limit, the cross means that only one band is above detection limit and a star indicates that both colors are below the flux limit. As with the spatial plots, only SNe are plotted with flux in the center grid of at least one color band and only known SNe are plotted. Neighboring grids (1-4 rings of grids) surrounding the center grid are shown in cyan in an attempt to clarify which, if any, structures are nearest to the supernova, such as dust, effects due to inclination, etc. It is important to keep in mind that these grids are a combination of star colors and dust (hence, why they are “pseudo” CMDs) meaning that these colors can’t be directly compared to standard CMDs that contain colors and magnitudes of individually resolved stars. The regions in both the spatial plots and CMDs are grouped by SN type starting with Ia and Ia subtypes, then type II, Ib/c, II<sub>n</sub>, II<sub>P</sub>, and II<sub>L</sub>. Type II<sub>b</sub> was integrated with type Ib/c. Within these categories, the regions were grouped by similar colors using both the pCMDs and spatial plots. This was based on examination of the entire 4 x 4 kpc region rather than the specific colors at the site of SN event. Some regions couldn’t be easily grouped. For convenience, table 5.1 lists out the SN regions in alphanumeric order with the corresponding figure number for all plots and type. An asterisk by some SNe Ia, indicates supernovae used in cosmological studies for light curve templates.

In order to determine or confirm structural information (spiral arms, inter arm, bulge, disk etc), the *g* band images were utilized as well (not included in this document). The *g* band images were particularly necessary for regions with less than 225 grids, as the resolution in the spatial maps was low. In the end, 7 pieces of information are studied for each supernova environment. All three types of plots work together; the spatial maps show color variation, age and metallicity of the 4x4 kpc region; the pCMDs provide information on the amount of flux in each band and discern between areas of low flux,

such as blue faint disks, with bright blue regions of young stars. The pCMDs also indicate if the region is truly dusty or within an older population of stars. The  $g$  band images are useful not only for structural information of the sample, provide information about the low signal to noise regions.

### 5.3.2.1. Color Analysis

#### *Ia types*

A cursory examination of the spatial plots shows that the colors in the Ia regions are much redder than the core collapsed regions (redder areas are plotted as black, red, orange, yellow and bluer areas are plotted as cyan, purple, pink and magenta – or lighter if this is a black and white copy). The redder colors correspond to about 30 Ia and Ia subtype regions ( $\sim 28\%$  of this sample) that have elliptical or S0 galaxy colors (e.g. 1961h). Note that not all of these regions with E/S0 galaxy colors are E/S0 galaxies (e.g. 1994d). By contrast, the core-collapsed regions tend to be riddled with very blue star forming regions (e.g. 1991n, 1996an). There are commonalities between the different types, both Ia and core collapsed occur in dusty regions (e.g. 2002bo, 2004am & 2004cc), arms (e.g. 1998bu, 1990e, 1983i) and in some cases, Ia occur in very blue high flux regions (2001ed) and core collapsed SNe are found in E/S0 hosts (2000ds, 2006ee). This prompts the question: are all structures such as arms and disks hosting different SNe, similar to one another or is the type of SN produced correlated with the color of the structure? In order to answer this and explore other properties of SN host regions, the analysis will go as follows. First, the structural location (arm, bulge, disk etc) is examined, along with the relative colors of these structures as a function of SN type. Then the structure color (central grid) will be compared to the total average colors of the region by SN type, followed by a similar analysis but instead, comparing the relative amounts of flux in  $u$ ,  $g$  and  $i$  for each structure to the average brightness for the region. The slopes of the dust and other linear-like portions in the pCMDs are measured followed by a discussion about still-visible SNe in the SDSS image.

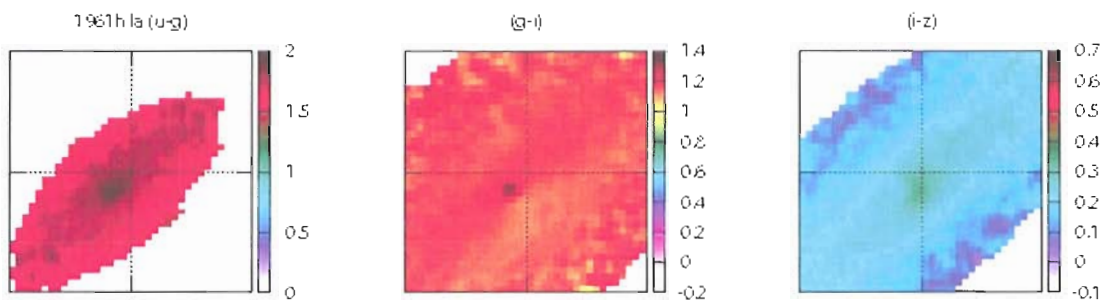


Figure 5.1. SN 1961h  $u-g$ ,  $g-i$ ,  $i-z$  spatial plots.

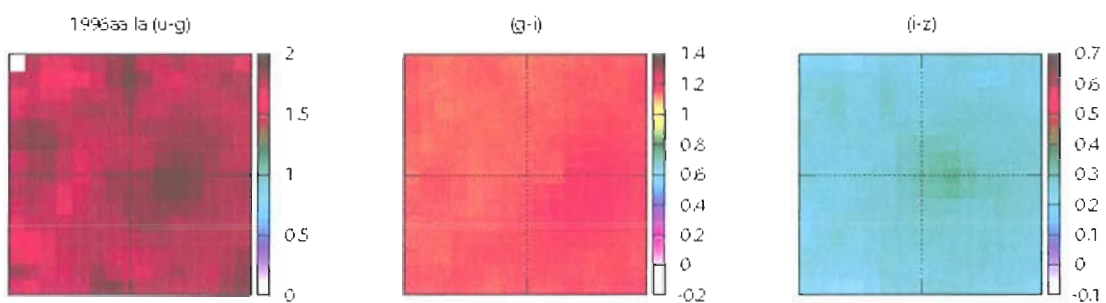


Figure 5.2. SN 1996aa  $u-g$ ,  $g-i$ ,  $i-z$  spatial plots.

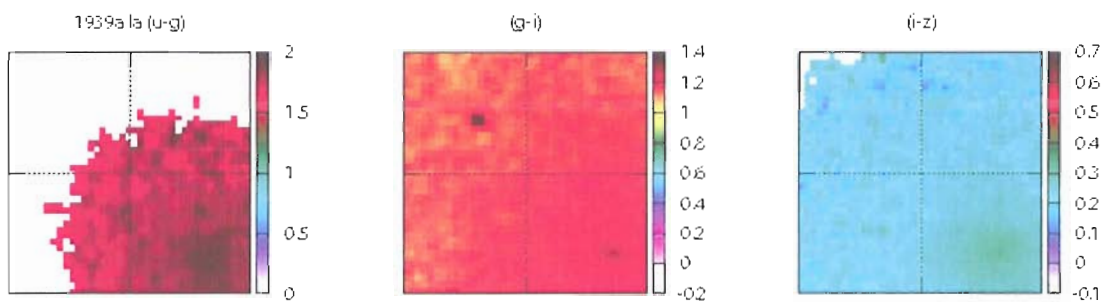


Figure 5.3. SN 1939a  $u-g$ ,  $g-i$ ,  $i-z$  spatial plots.

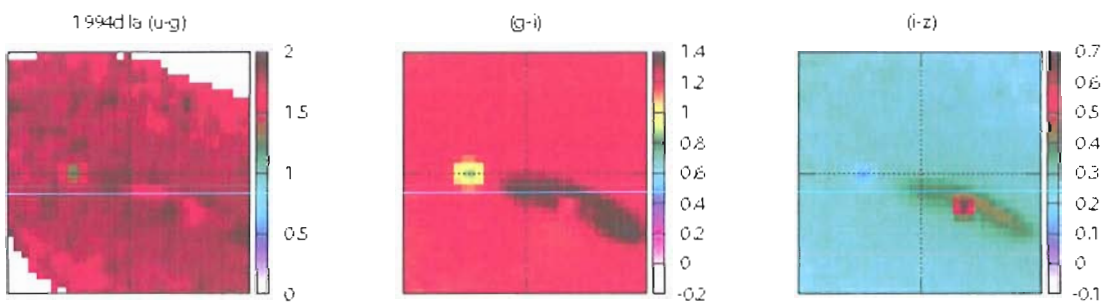


Figure 5.4. SN 1994d  $u-g$ ,  $g-i$ ,  $i-z$  spatial plots.

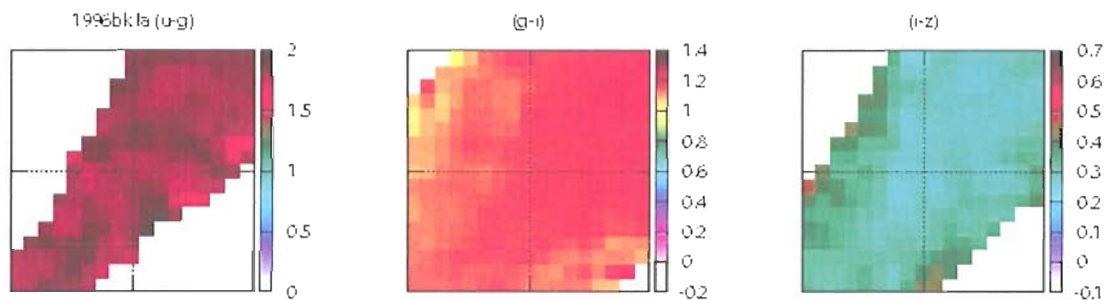


Figure 5.5. SN 1996bk  $u-g$ ,  $g-i$ ,  $i-z$  spatial plots.

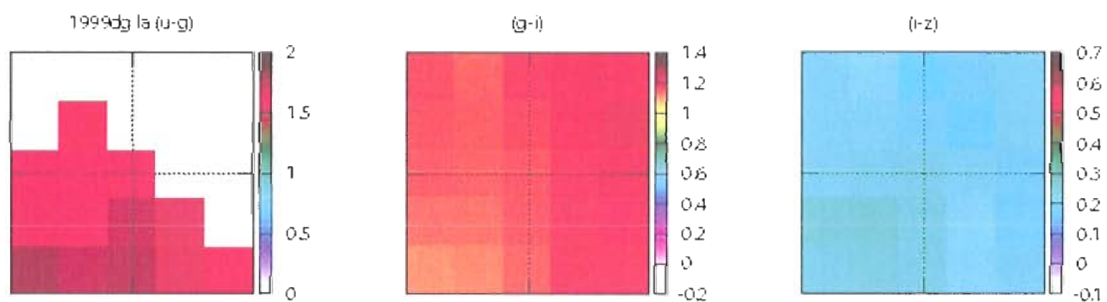


Figure 5.6. SN 1999dg  $u-g$ ,  $g-i$ ,  $i-z$  spatial plots.

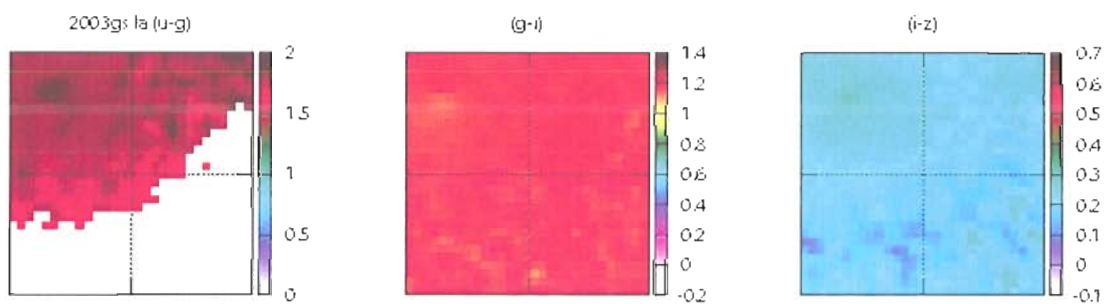


Figure 5.7. SN 2003gs  $u-g$ ,  $g-i$ ,  $i-z$  spatial plots.

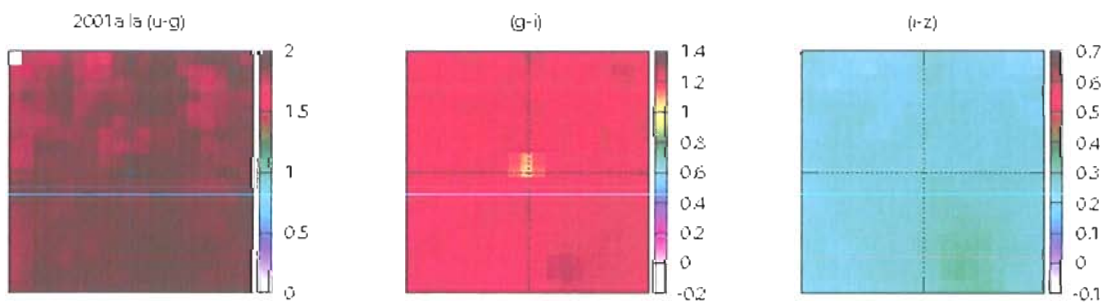


Figure 5.8. SN 2001a  $u-g$ ,  $g-i$ ,  $i-z$  spatial plots.

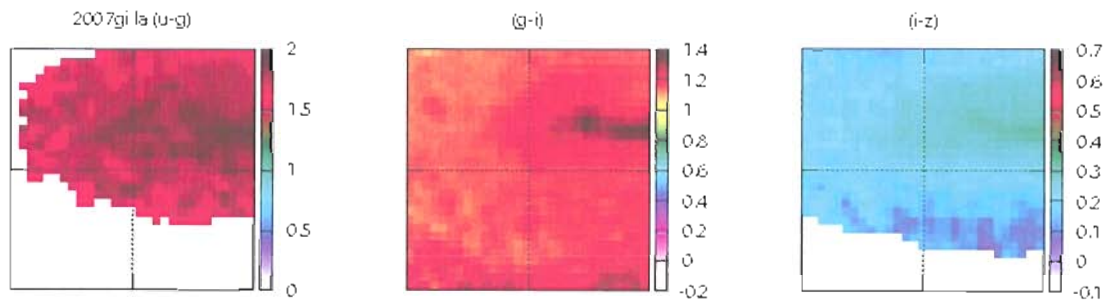


Figure 5.9. SN 2007gi  $u-g$ ,  $g-i$ ,  $i-z$  spatial plots.

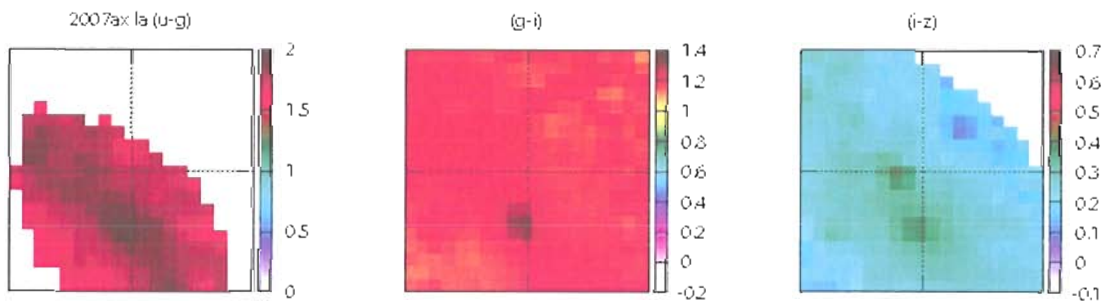


Figure 5.10. SN 2007ax  $u-g$ ,  $g-i$ ,  $i-z$  spatial plots.

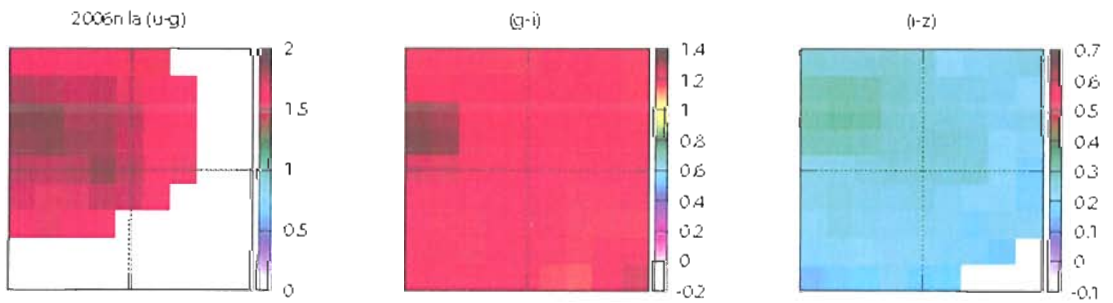


Figure 5.11. SN 2006n  $u-g$ ,  $g-i$ ,  $i-z$  spatial plots.

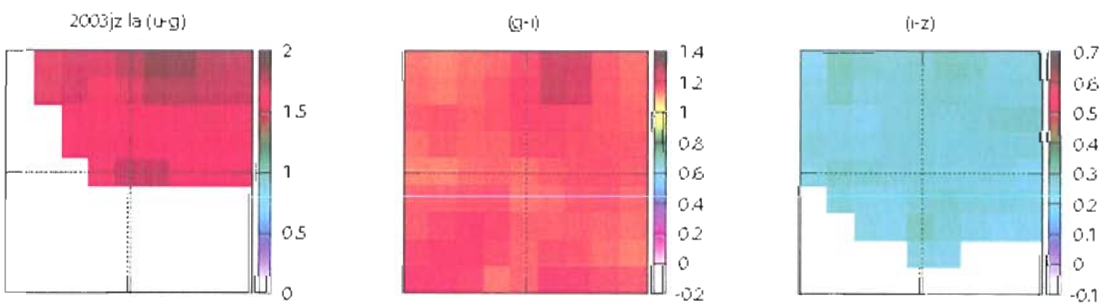


Figure 5.12. SN 2003jz  $u-g$ ,  $g-i$ ,  $i-z$  spatial plots.

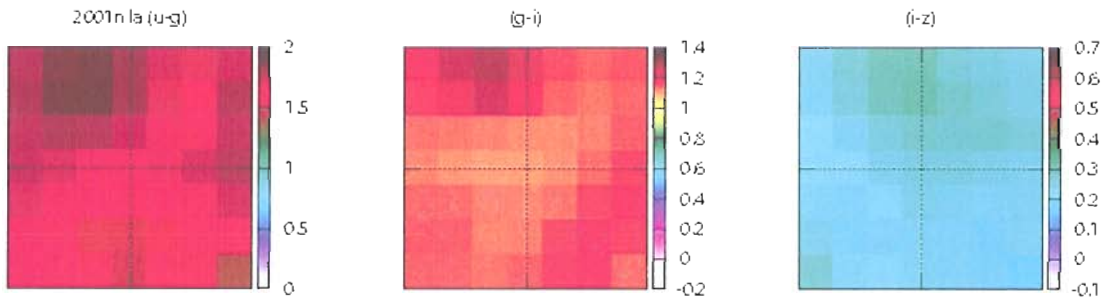


Figure 5.13. SN 2001n  $u-g$ ,  $g-i$ ,  $i-z$  spatial plots.

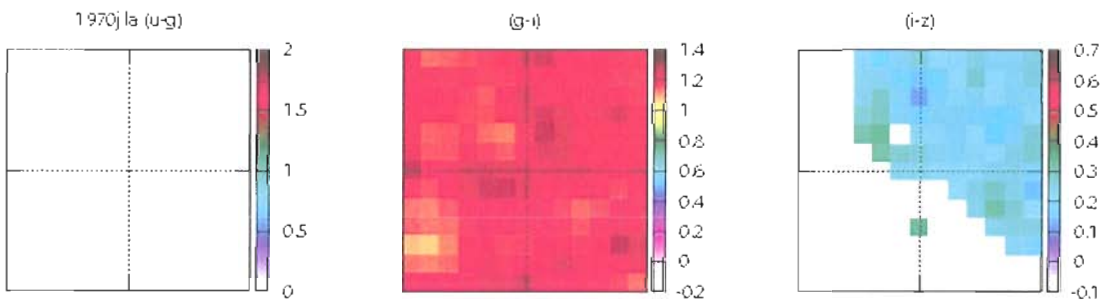


Figure 5.14. SN 1970j  $u-g$ ,  $g-i$ ,  $i-z$  spatial plots.

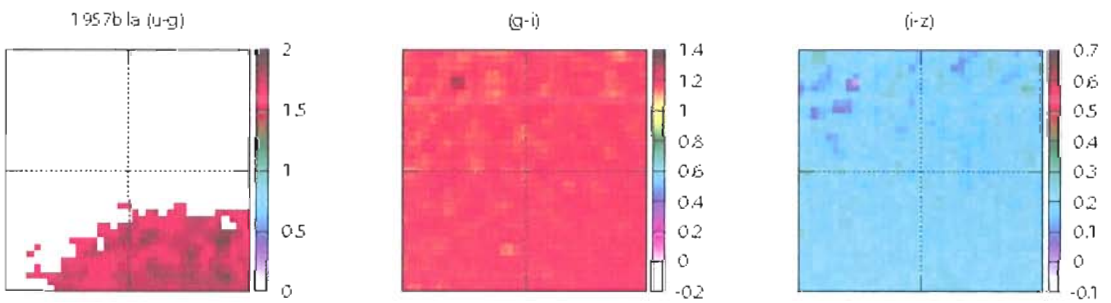


Figure 5.15. SN 1957b  $u-g$ ,  $g-i$ ,  $i-z$  spatial plots.

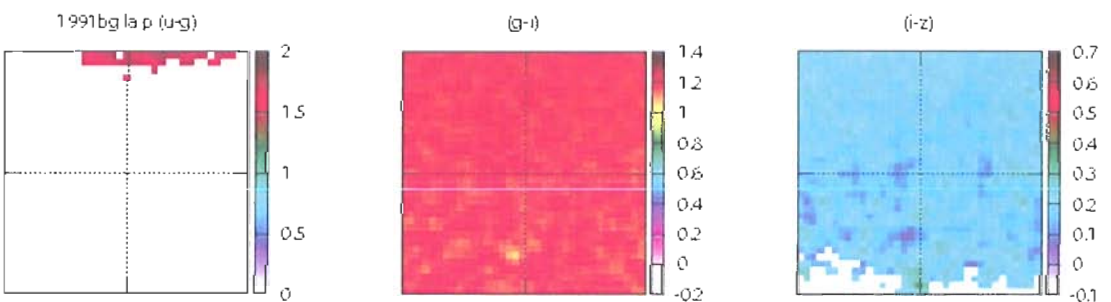


Figure 5.16. SN 1991bg  $u-g$ ,  $g-i$ ,  $i-z$  spatial plots.

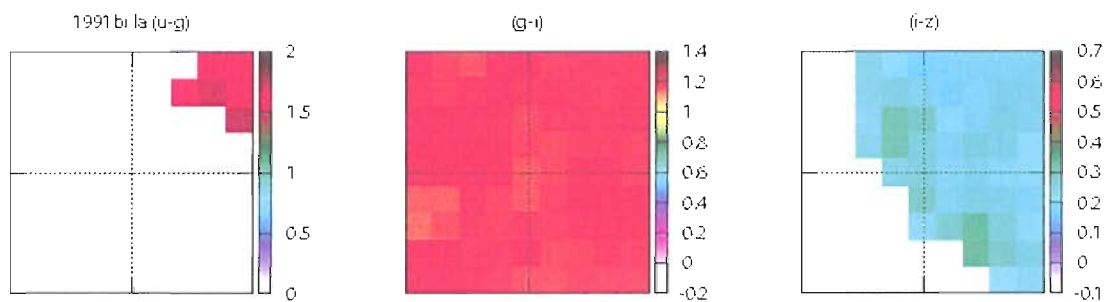


Figure 5.17. SN 1991bi  $u-g$ ,  $g-i$ ,  $i-z$  spatial plots.

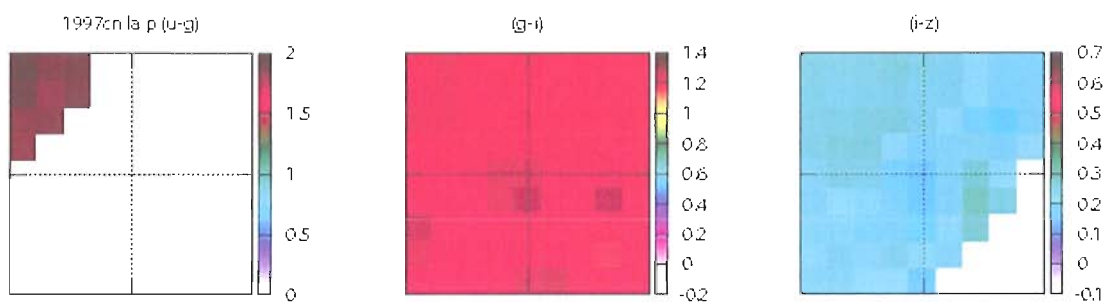


Figure 5.18. SN 1997cn  $u-g$ ,  $g-i$ ,  $i-z$  spatial plots.

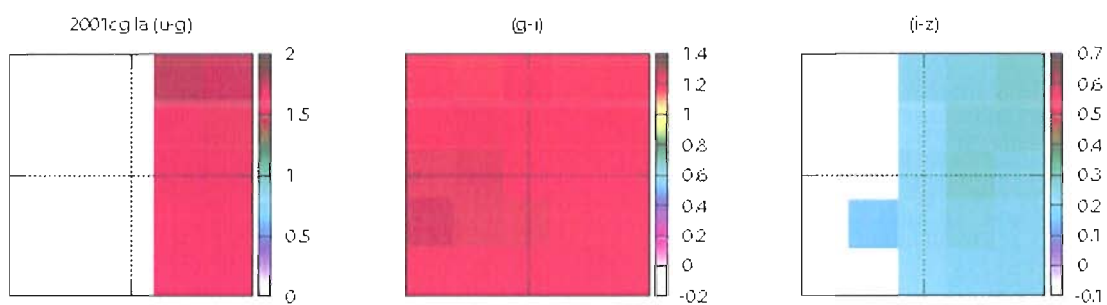


Figure 5.19. SN 2001cg  $u-g$ ,  $g-i$ ,  $i-z$  spatial plots.

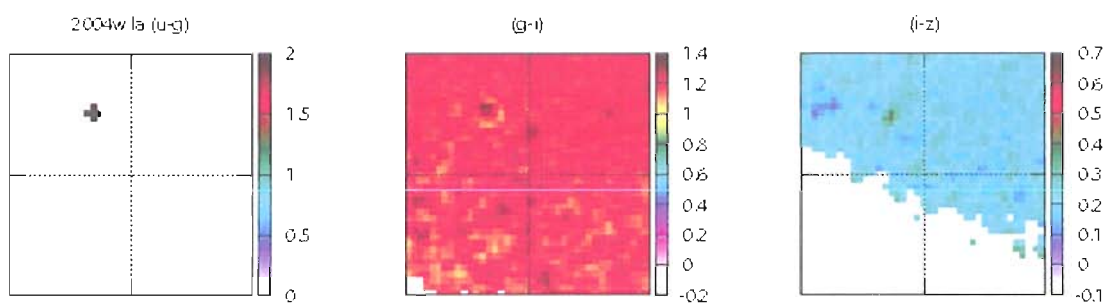


Figure 5.20. SN 2004w  $u-g$ ,  $g-i$ ,  $i-z$  spatial plots.

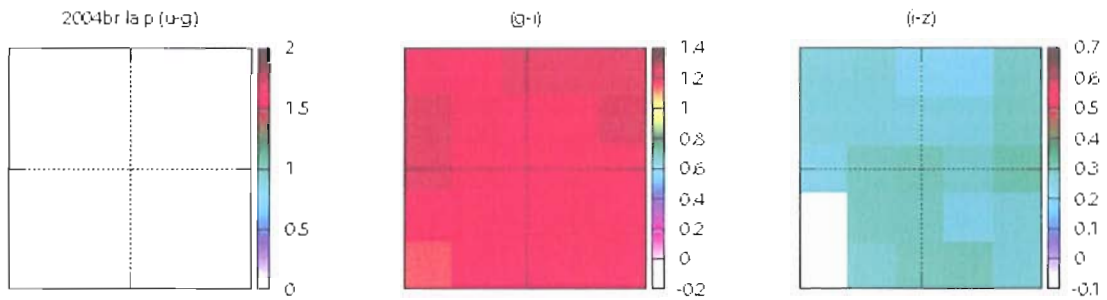


Figure 5.21. SN 2004br  $u-g$ ,  $g-i$ ,  $i-z$  spatial plots.

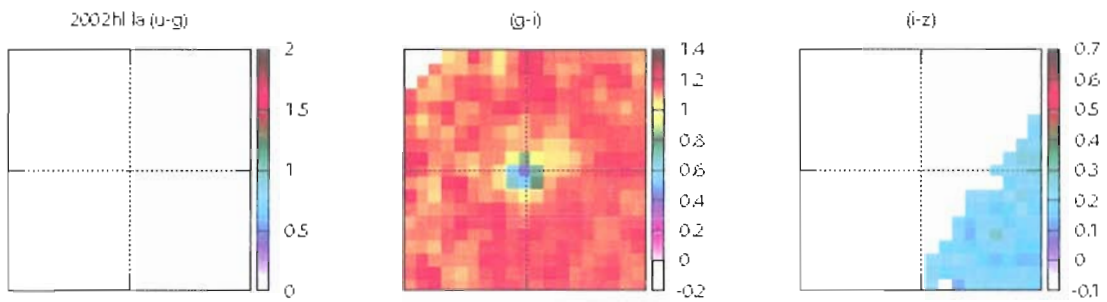


Figure 5.22. SN 2002hl  $u-g$ ,  $g-i$ ,  $i-z$  spatial plots.

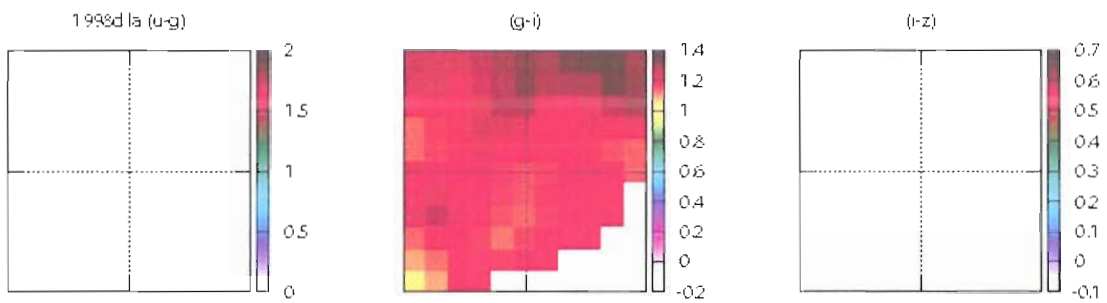


Figure 5.23. SN 1998d  $u-g$ ,  $g-i$ ,  $i-z$  spatial plots.

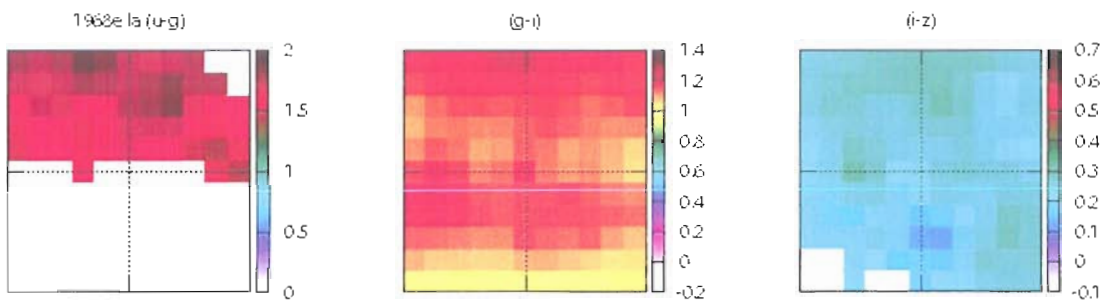
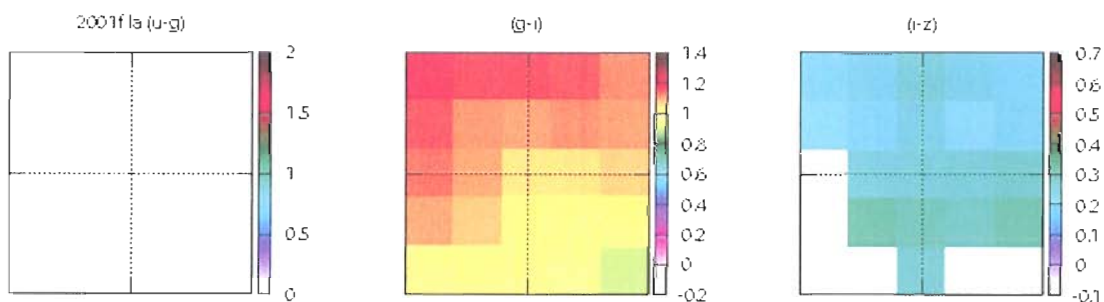
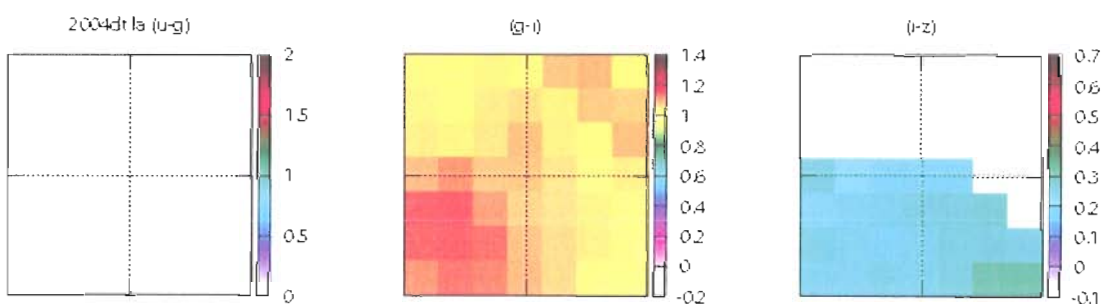
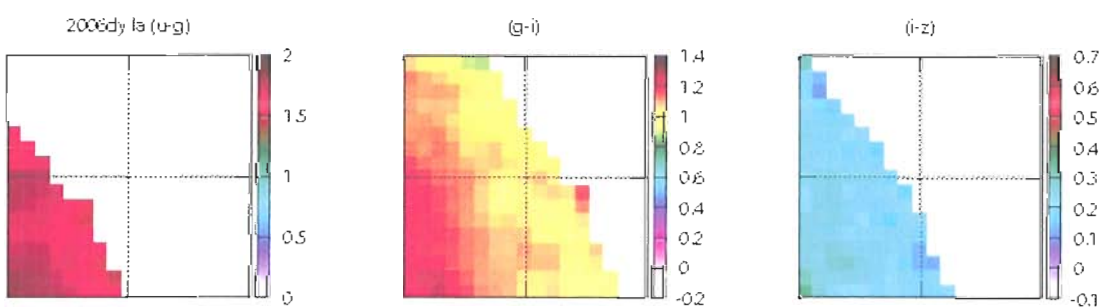
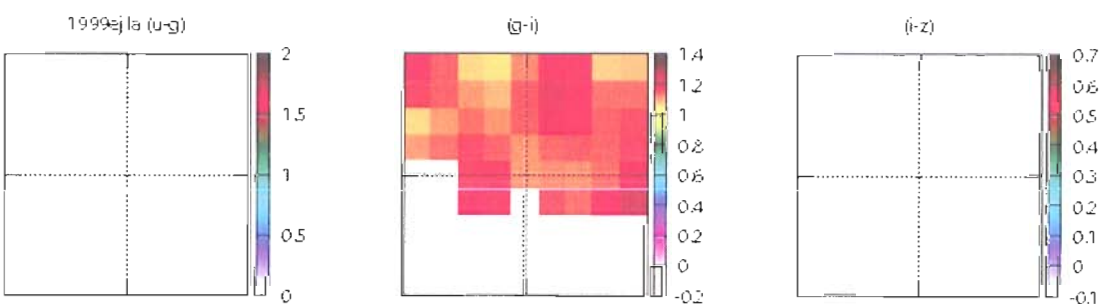


Figure 5.24. SN 1968e  $u-g$ ,  $g-i$ ,  $i-z$  spatial plots.



Figure 5.25. SN 2001f  $u-g$ ,  $g-i$ ,  $i-z$  spatial plots.Figure 5.26. SN 2004dt  $u-g$ ,  $g-i$ ,  $i-z$  spatial plots.Figure 5.27. SN 2006dy  $u-g$ ,  $g-i$ ,  $i-z$  spatial plots.Figure 5.28. SN 1999ej  $u-g$ ,  $g-i$ ,  $i-z$  spatial plots.

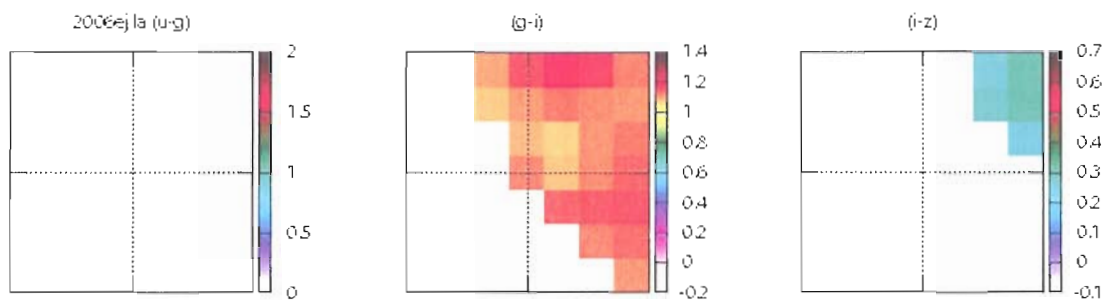


Figure 5.29. SN 2006ej  $u-g$ ,  $g-i$ ,  $i-z$  spatial plots.

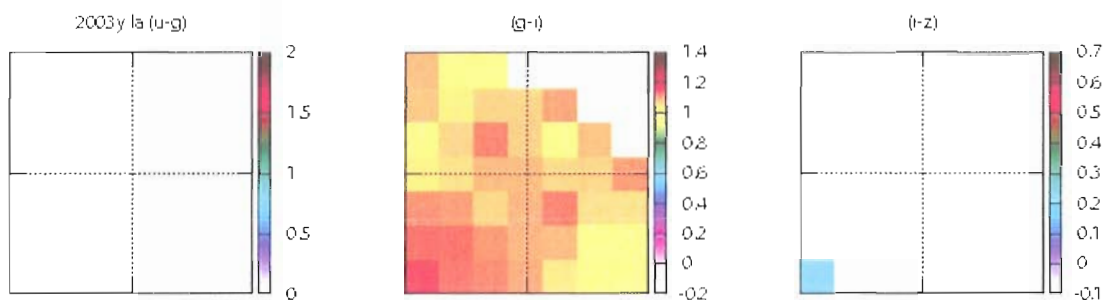


Figure 5.30. SN 2003y  $u-g$ ,  $g-i$ ,  $i-z$  spatial plots.

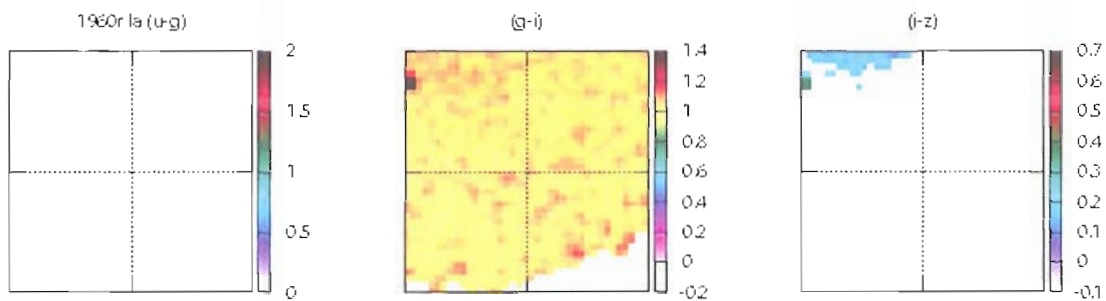


Figure 5.31. SN 1960r  $u-g$ ,  $g-i$ ,  $i-z$  spatial plots.

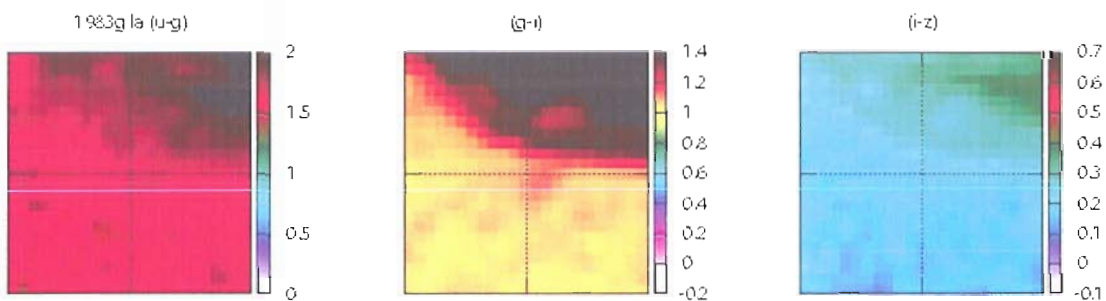


Figure 5.32. SN 1983g  $u-g$ ,  $g-i$ ,  $i-z$  spatial plots.

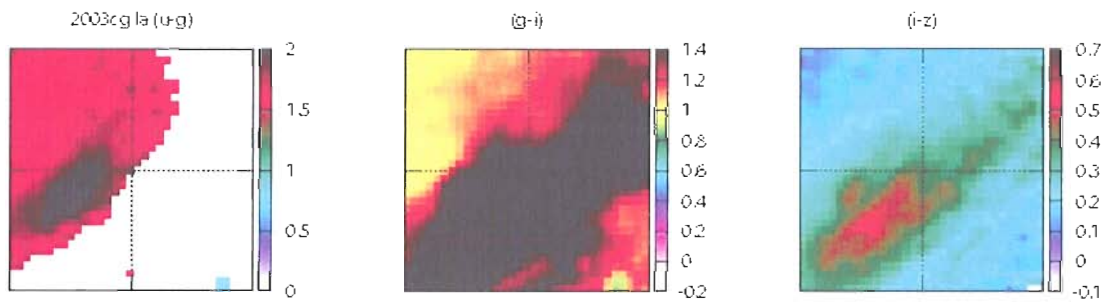


Figure 5.33. SN 2003cg  $u-g$ ,  $g-i$ ,  $i-z$  spatial plots.

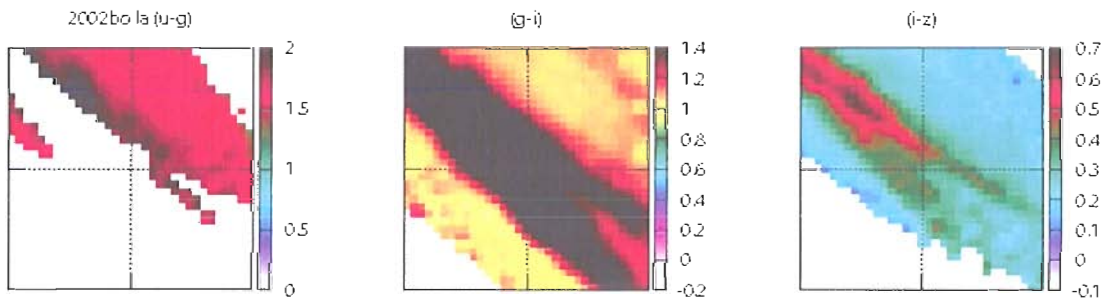


Figure 5.34. SN 2002bo  $u-g$ ,  $g-i$ ,  $i-z$  spatial plots.

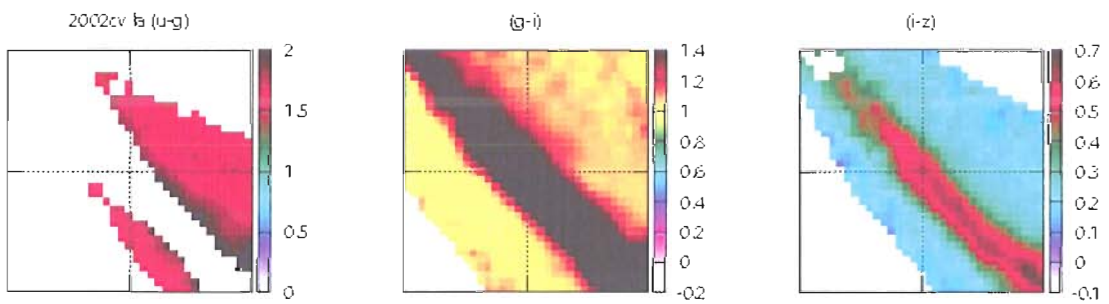


Figure 5.35. SN 2002cv  $u-g$ ,  $g-i$ ,  $i-z$  spatial plots.

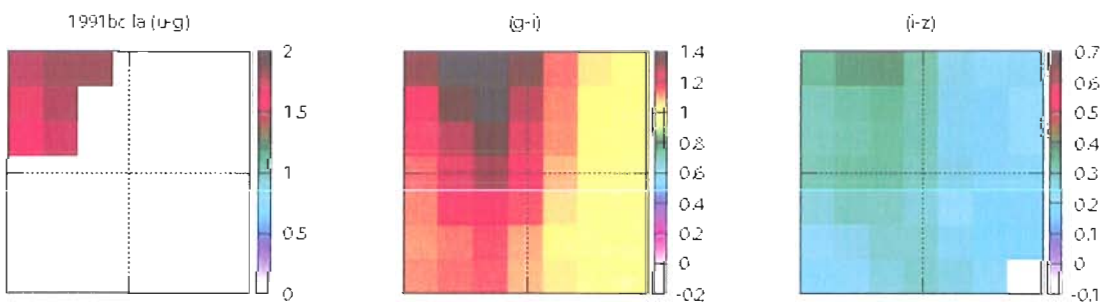


Figure 5.36. SN 1991bc  $u-g$ ,  $g-i$ ,  $i-z$  spatial plots.

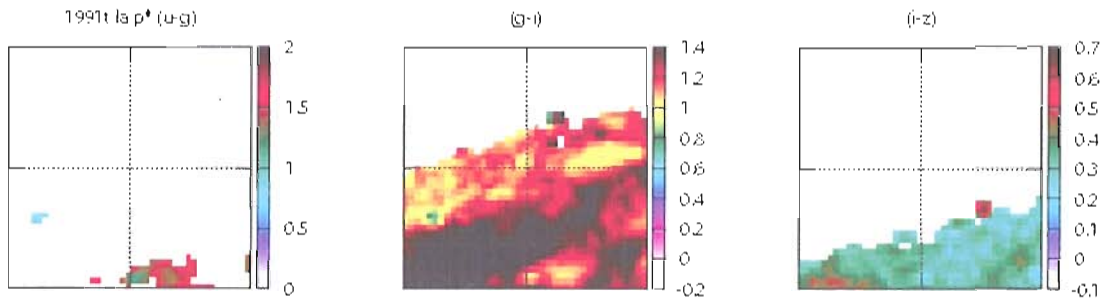


Figure 5.37. SN 1991t  $u-g$ ,  $g-i$ ,  $i-z$  spatial plots.

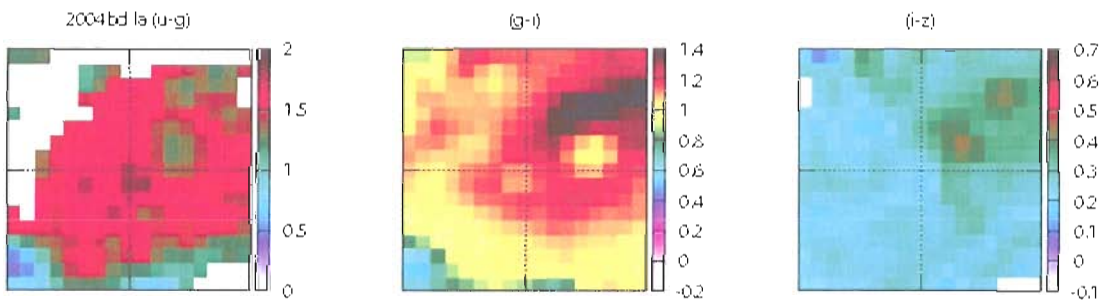


Figure 5.38. SN 2004bd  $u-g$ ,  $g-i$ ,  $i-z$  spatial plots.

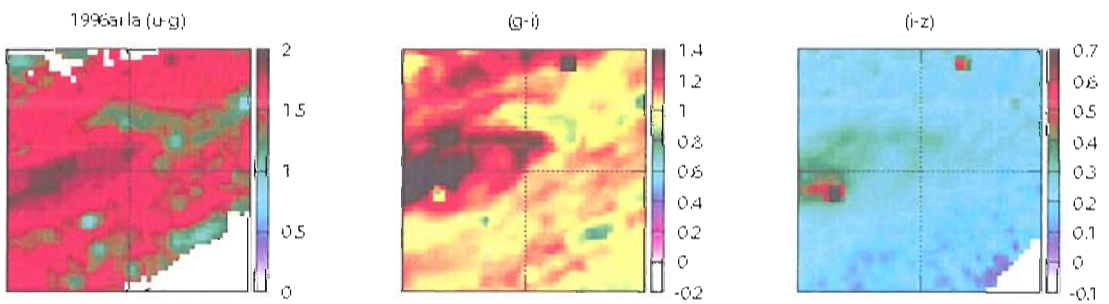


Figure 5.39. SN 1996ai  $u-g$ ,  $g-i$ ,  $i-z$  spatial plots.

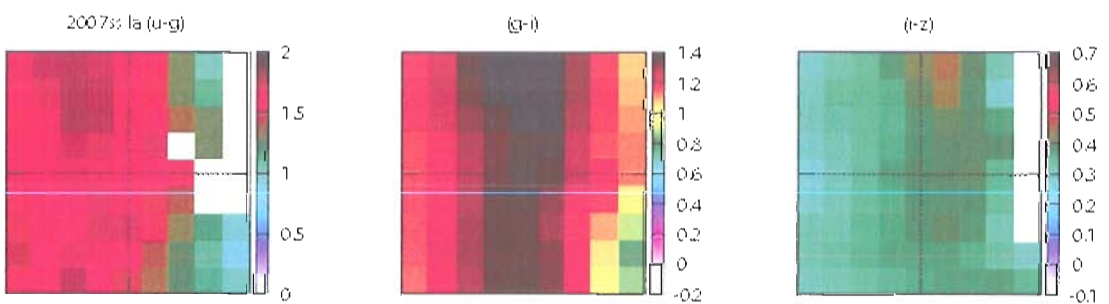


Figure 5.40. SN 2007ss  $u-g$ ,  $g-i$ ,  $i-z$  spatial plots.

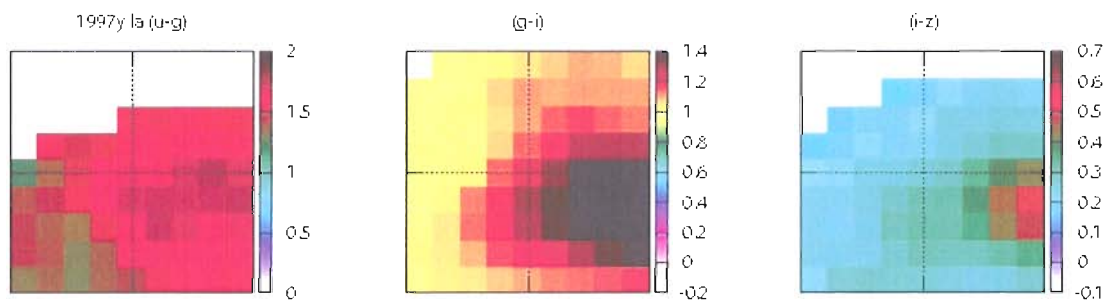


Figure 5.41. SN 1997y  $u-g$ ,  $g-i$ ,  $i-z$  spatial plots.

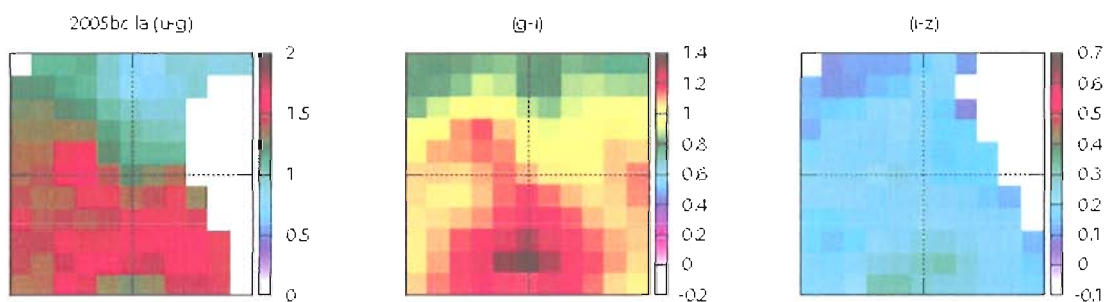


Figure 5.42. SN 2005bc  $u-g$ ,  $g-i$ ,  $i-z$  spatial plots.

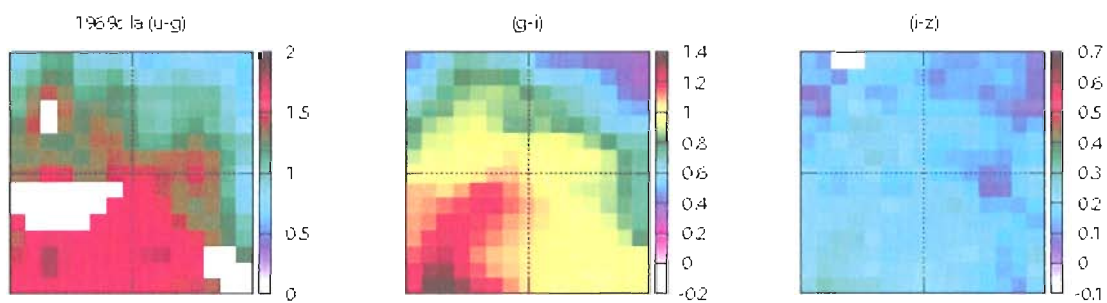


Figure 5.43. SN 1969c  $u-g$ ,  $g-i$ ,  $i-z$  spatial plots.

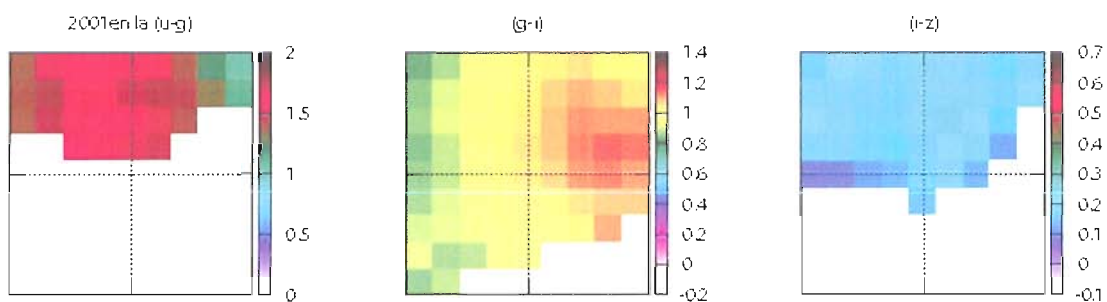


Figure 5.44. SN 2001en  $u-g$ ,  $g-i$ ,  $i-z$  spatial plots.

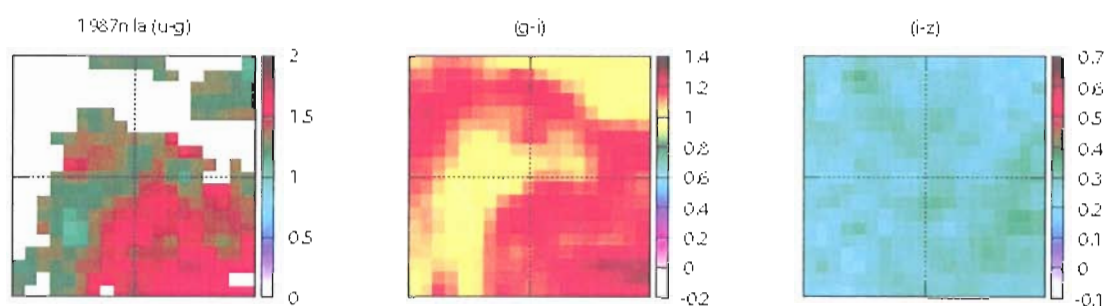


Figure 5.45. SN 1987n  $u-g$ ,  $g-i$ ,  $i-z$  spatial plots.

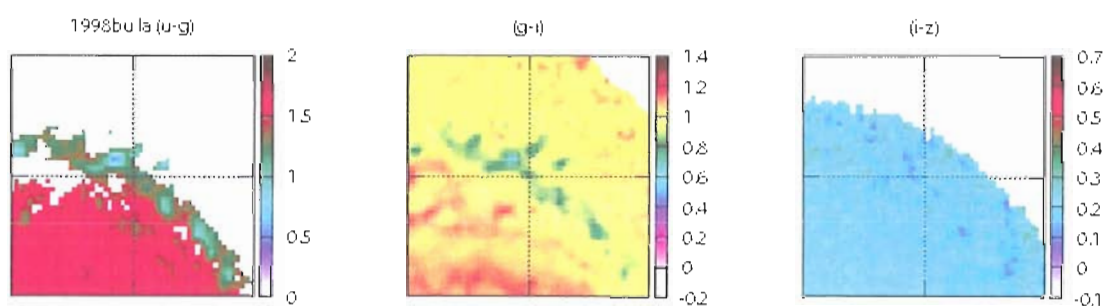


Figure 5.46. SN 1998bu  $u-g$ ,  $g-i$ ,  $i-z$  spatial plots.

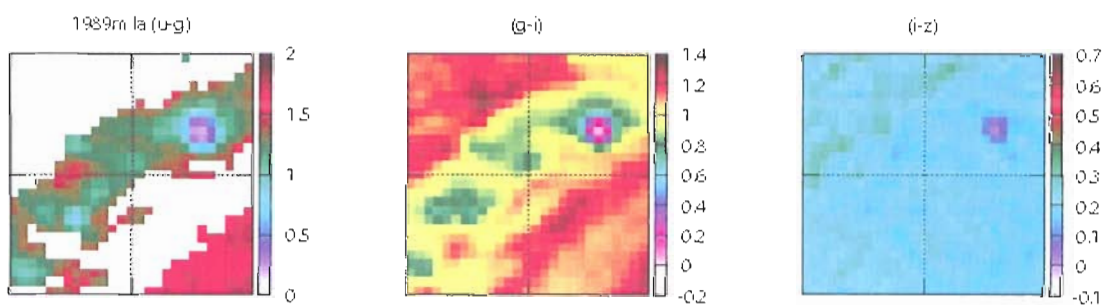


Figure 5.47. SN 1989m  $u-g$ ,  $g-i$ ,  $i-z$  spatial plots.

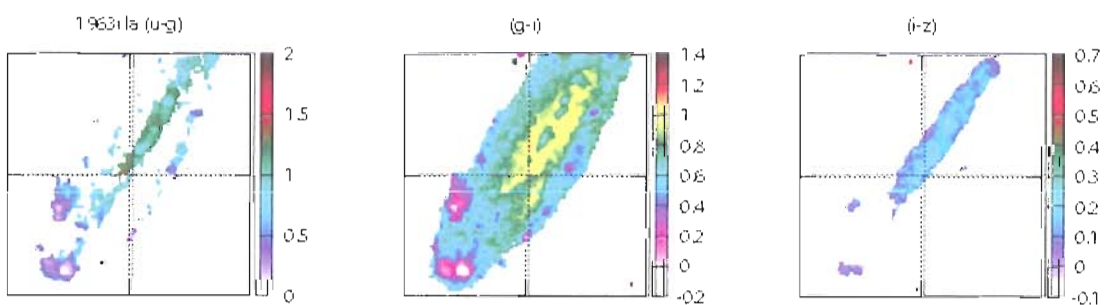


Figure 5.48. SN 1963i  $u-g$ ,  $g-i$ ,  $i-z$  spatial plots.

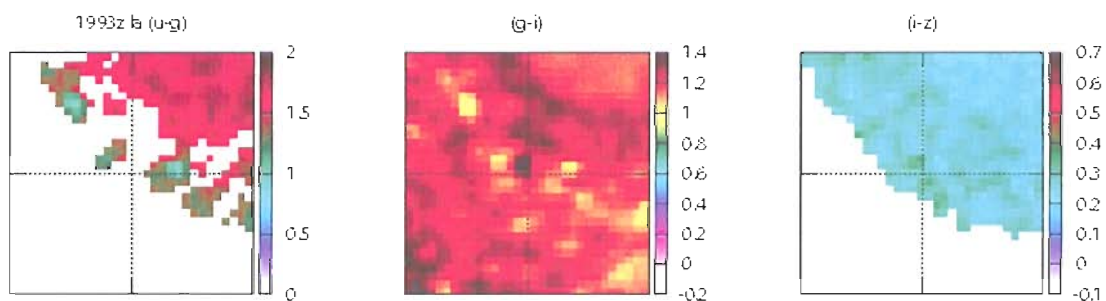


Figure 5.49. SN 1993z  $u-g$ ,  $g-i$ ,  $i-z$  spatial plots.

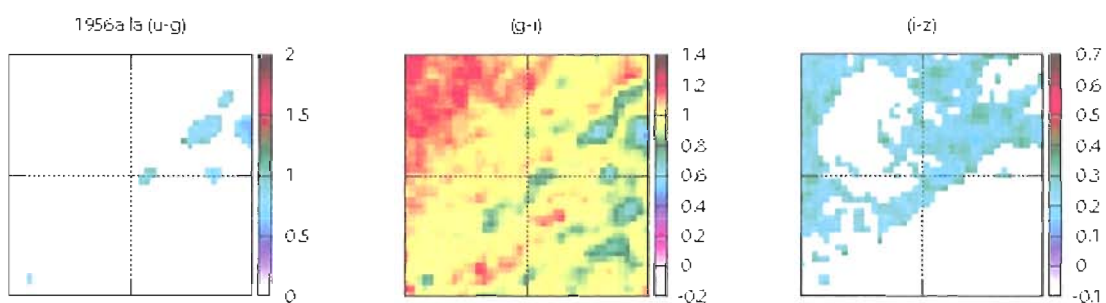


Figure 5.50. SN 1956a  $u-g$ ,  $g-i$ ,  $i-z$  spatial plots.

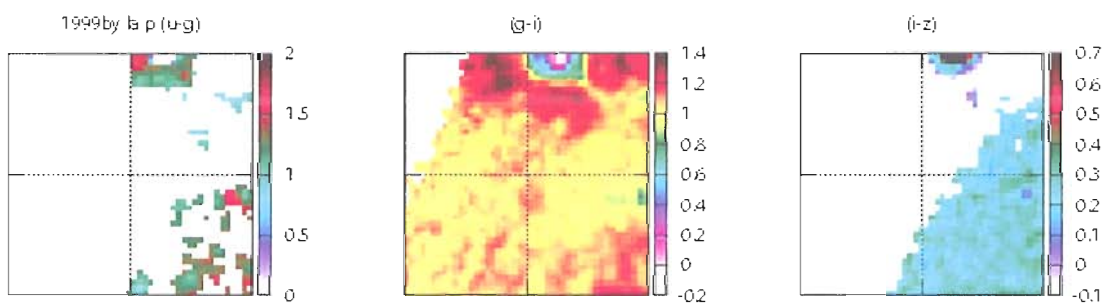


Figure 5.51. SN 1999by  $u-g$ ,  $g-i$ ,  $i-z$  spatial plots.

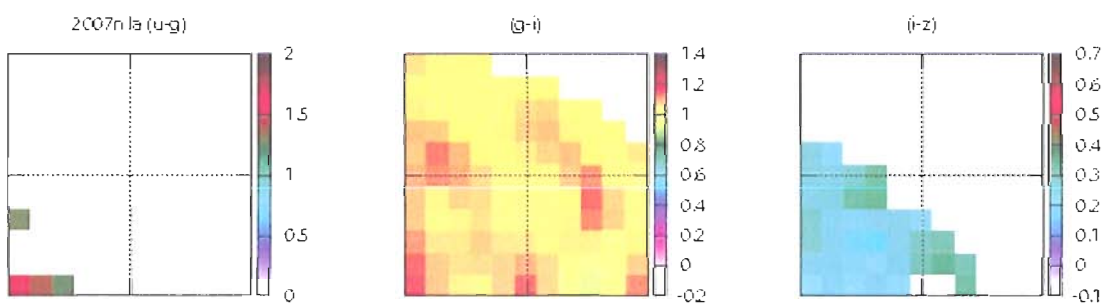


Figure 5.52. SN 2007n  $u-g$ ,  $g-i$ ,  $i-z$  spatial plots.

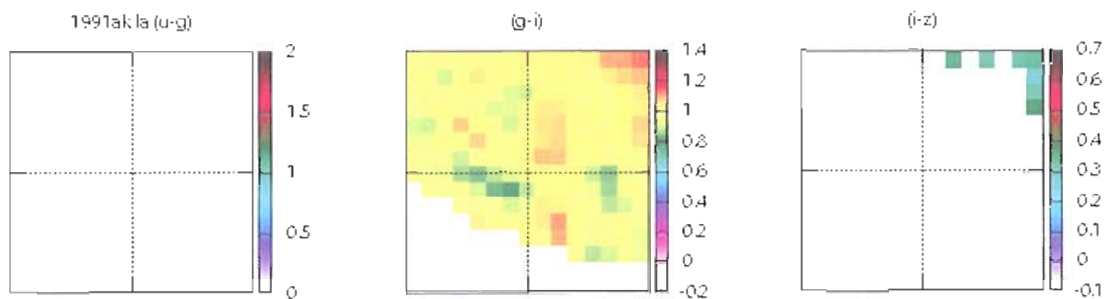


Figure 5.53. SN 1991ak  $u-g$ ,  $g-i$ ,  $i-z$  spatial plots.

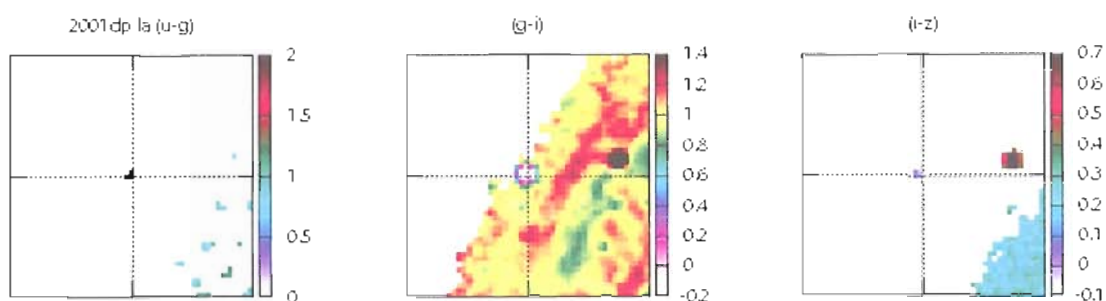


Figure 5.54. SN 2001dp  $u-g$ ,  $g-i$ ,  $i-z$  spatial plots.

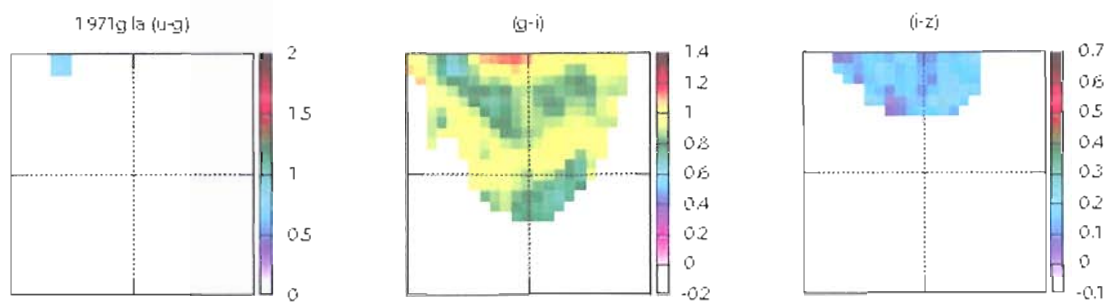


Figure 5.55. SN 1971g  $u-g$ ,  $g-i$ ,  $i-z$  spatial plots.

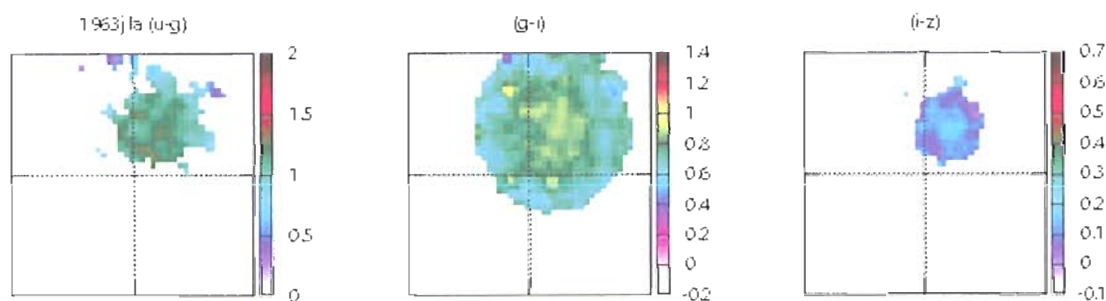


Figure 5.56. SN 1963j  $u-g$ ,  $g-i$ ,  $i-z$  spatial plots.



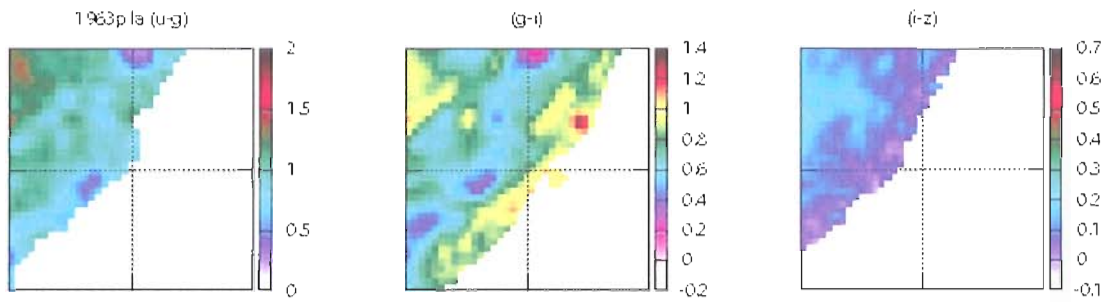


Figure 5.57. SN 1963p  $u-g$ ,  $g-i$ ,  $i-z$  spatial plots.

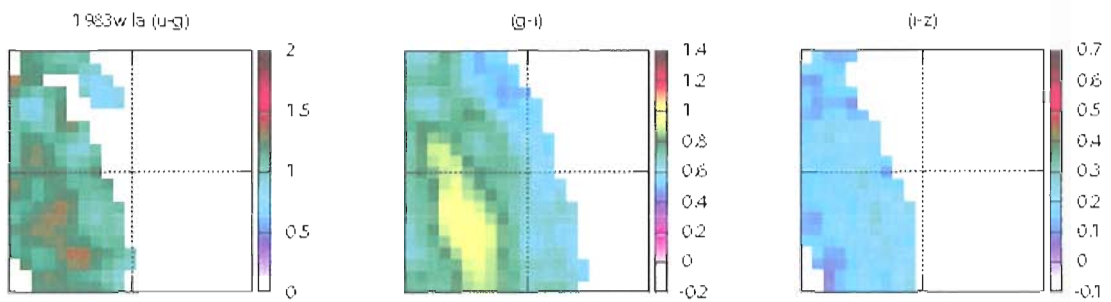


Figure 5.58. SN 1983w  $u-g$ ,  $g-i$ ,  $i-z$  spatial plots.

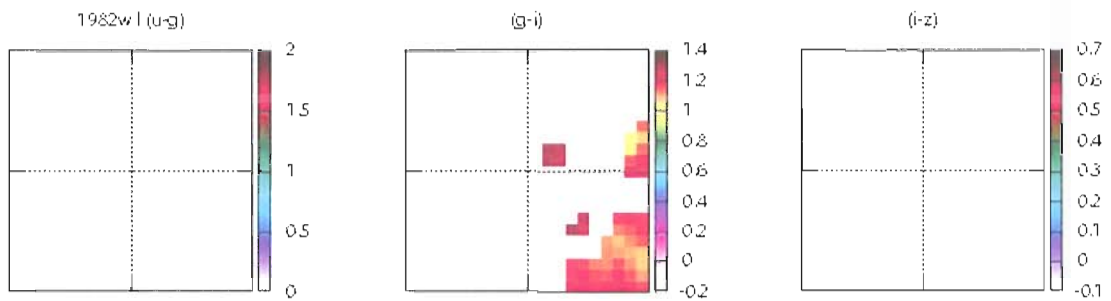


Figure 5.59. SN 1982w  $u-g$ ,  $g-i$ ,  $i-z$  spatial plots.

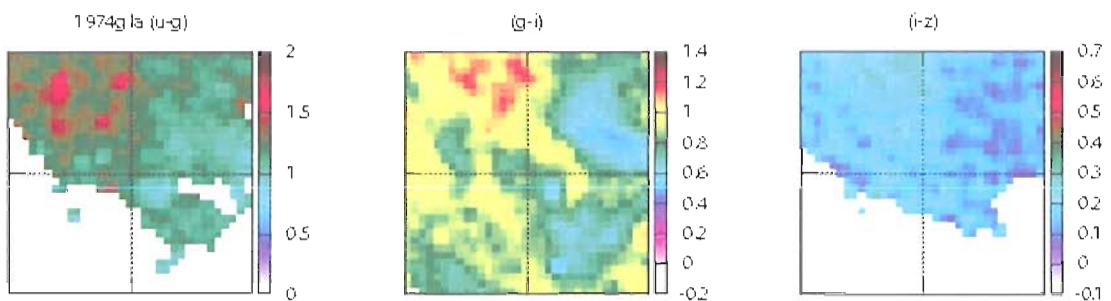
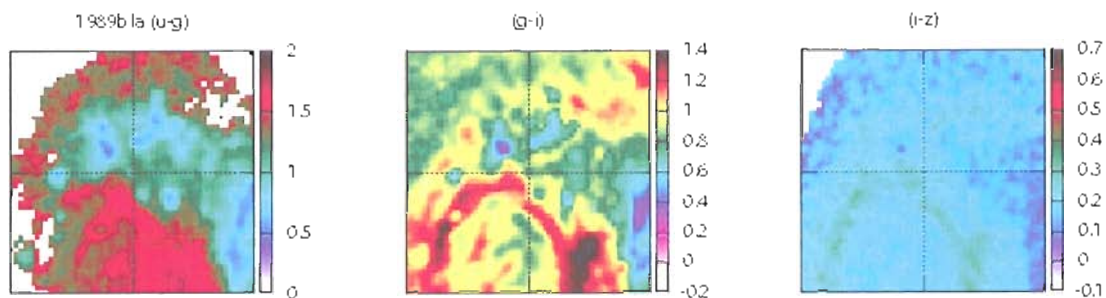
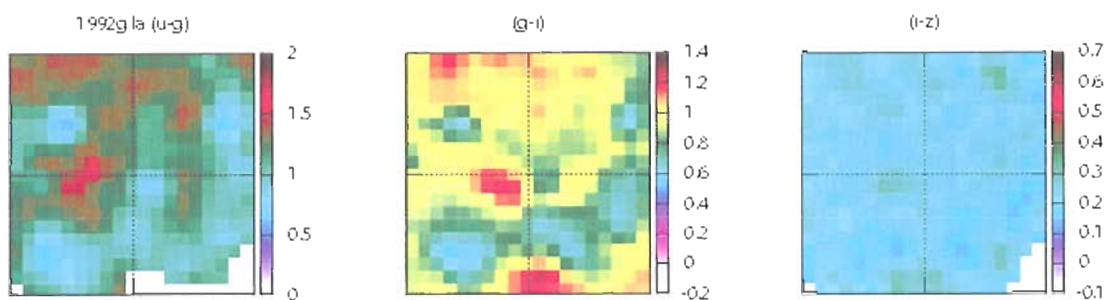
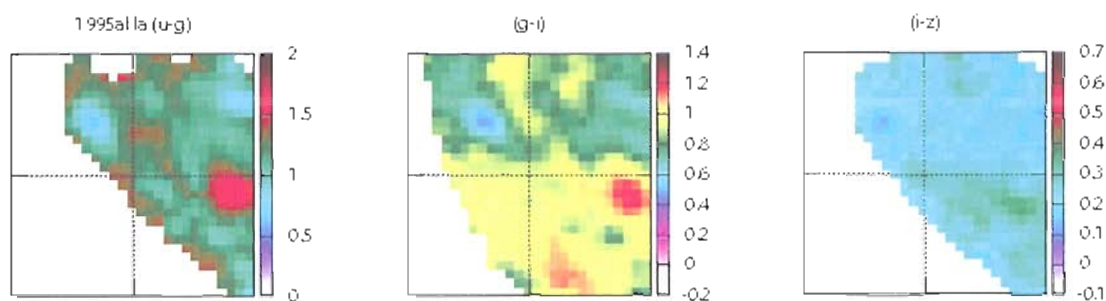
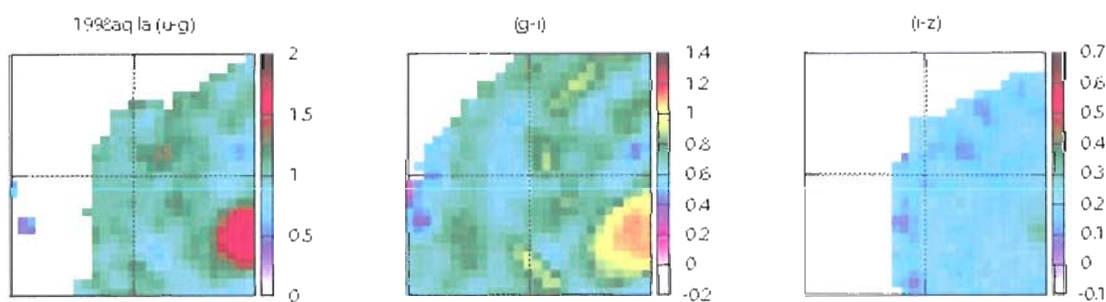


Figure 5.60. SN 1974g  $u-g$ ,  $g-i$ ,  $i-z$  spatial plots.

Figure 5.61. SN 1989b  $u-g$ ,  $g-i$ ,  $i-z$  spatial plots.Figure 5.62. SN 1992g  $u-g$ ,  $g-i$ ,  $i-z$  spatial plots.Figure 5.63. SN 1995al  $u-g$ ,  $g-i$ ,  $i-z$  spatial plots.Figure 5.64. SN 1998aq  $u-g$ ,  $g-i$ ,  $i-z$  spatial plots.

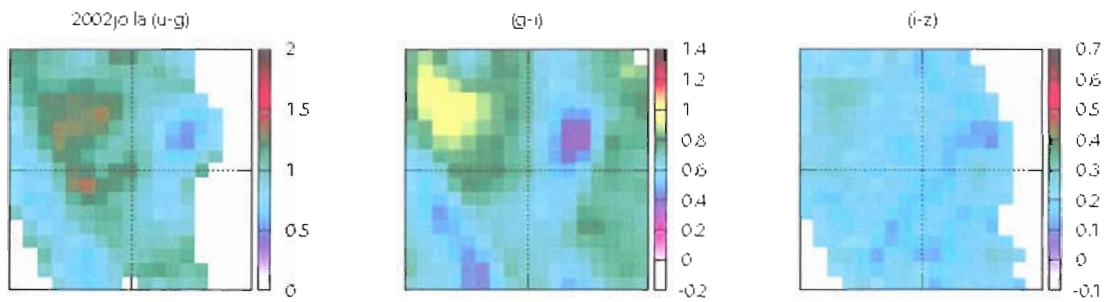


Figure 5.65. SN 2002jo  $u-g$ ,  $g-i$ ,  $i-z$  spatial plots.

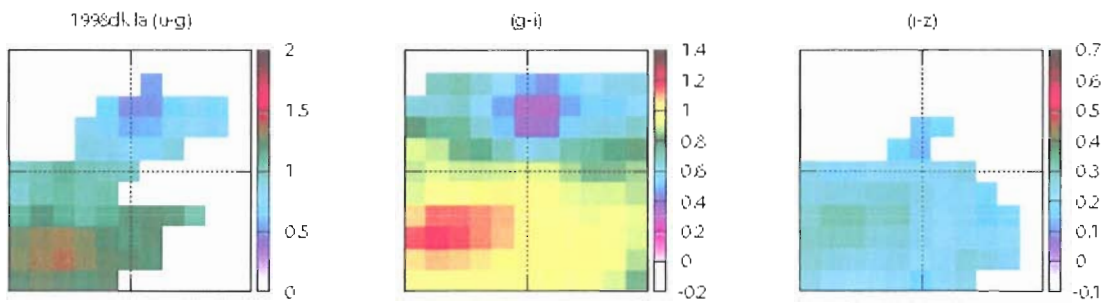


Figure 5.66. SN 1998dk  $u-g$ ,  $g-i$ ,  $i-z$  spatial plots.

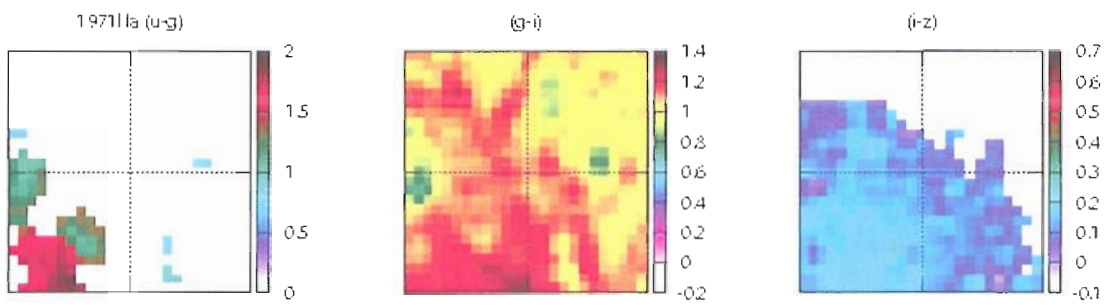


Figure 5.67. SN 1971Ia  $u-g$ ,  $g-i$ ,  $i-z$  spatial plots.

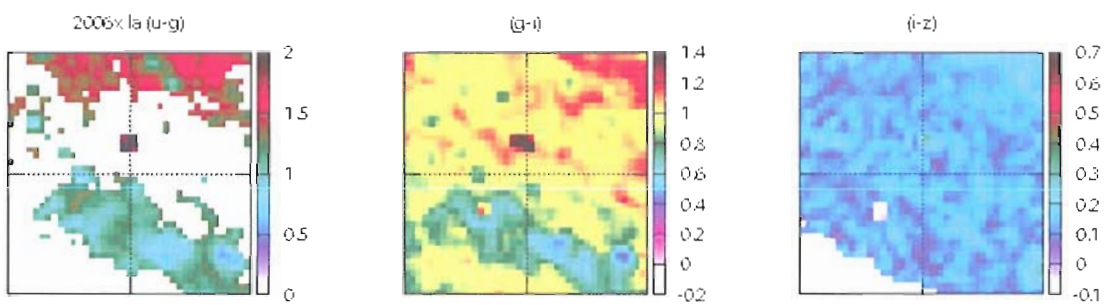


Figure 5.68. SN 2006x  $u-g$ ,  $g-i$ ,  $i-z$  spatial plots.

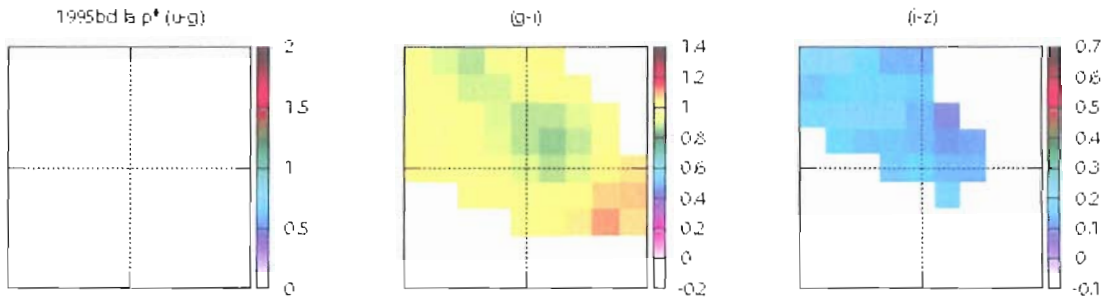


Figure 5.69. SN 1995bd  $u-g$ ,  $g-i$ ,  $i-z$  spatial plots.

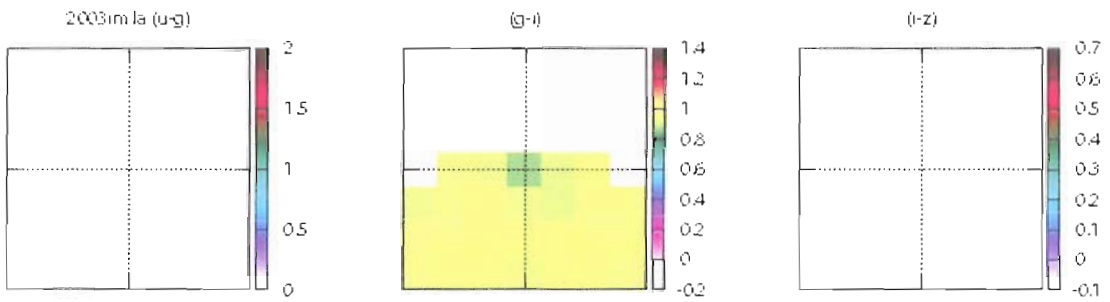


Figure 5.70. SN 2003im  $u-g$ ,  $g-i$ ,  $i-z$  spatial plots.

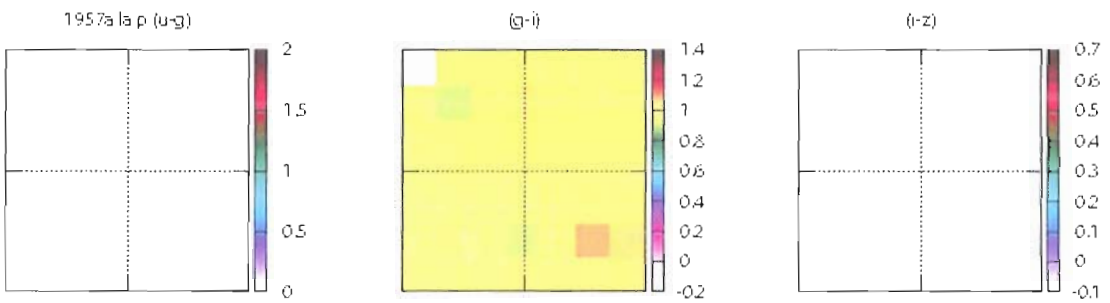


Figure 5.71. SN 1957a  $u-g$ ,  $g-i$ ,  $i-z$  spatial plots.

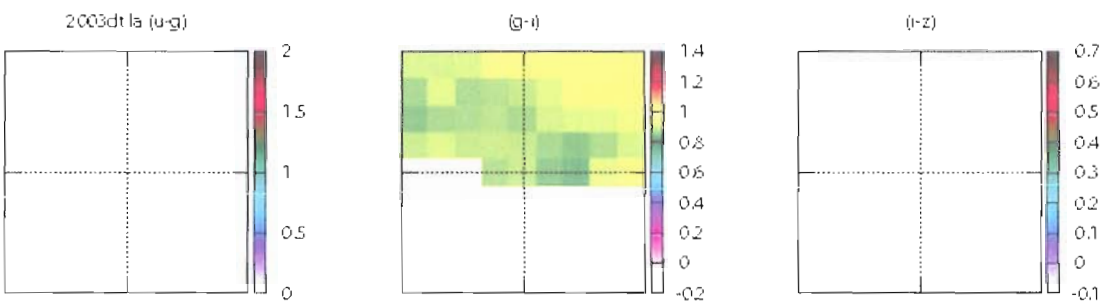


Figure 5.72. SN 2003dt  $u-g$ ,  $g-i$ ,  $i-z$  spatial plots.

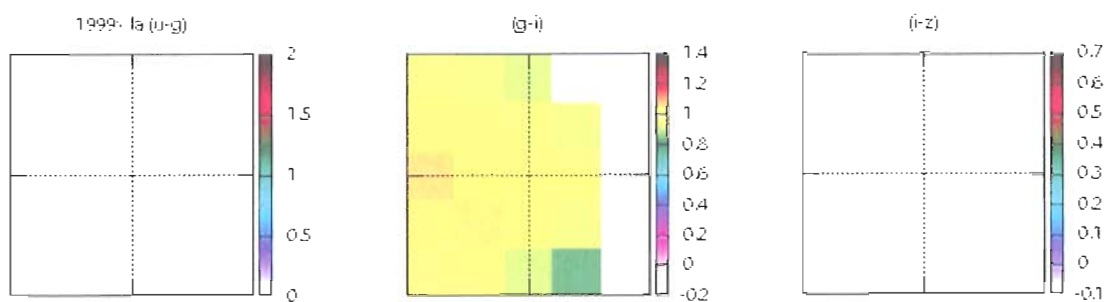


Figure 5.73. SN 1999x  $u-g$ ,  $g-i$ ,  $i-z$  spatial plots.

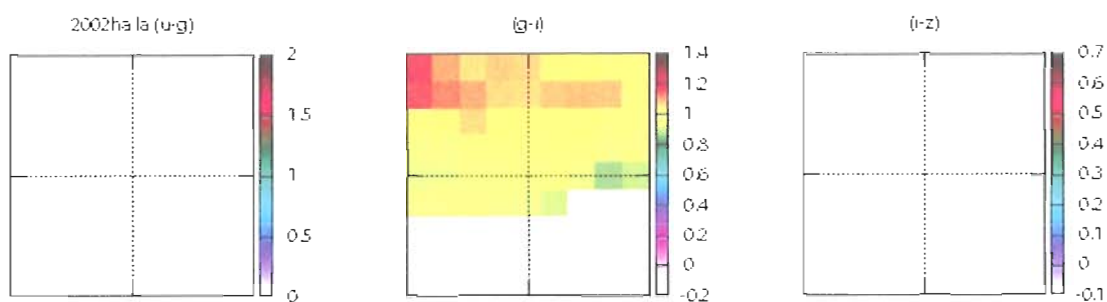


Figure 5.74. SN 2002ha  $u-g$ ,  $g-i$ ,  $i-z$  spatial plots.

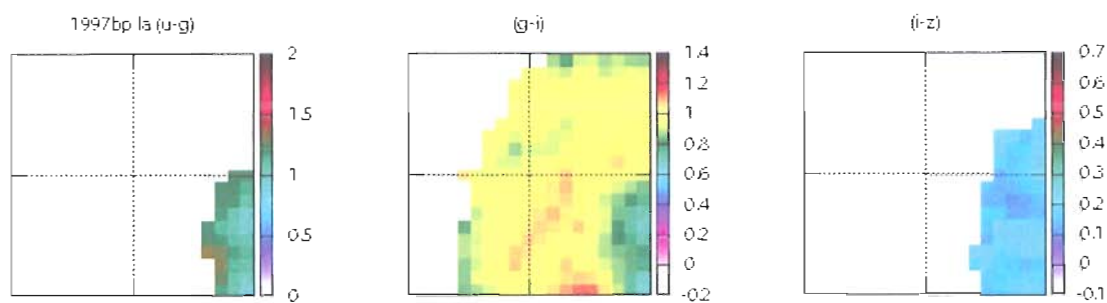


Figure 5.75. SN 1997bp  $u-g$ ,  $g-i$ ,  $i-z$  spatial plots.

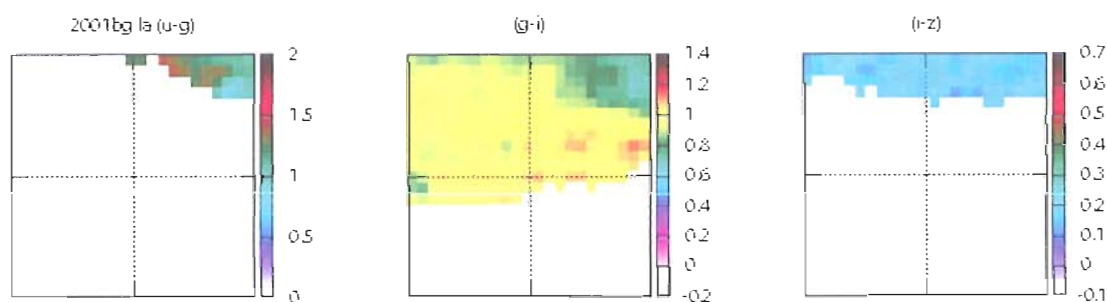


Figure 5.76. SN 2001bg  $u-g$ ,  $g-i$ ,  $i-z$  spatial plots.

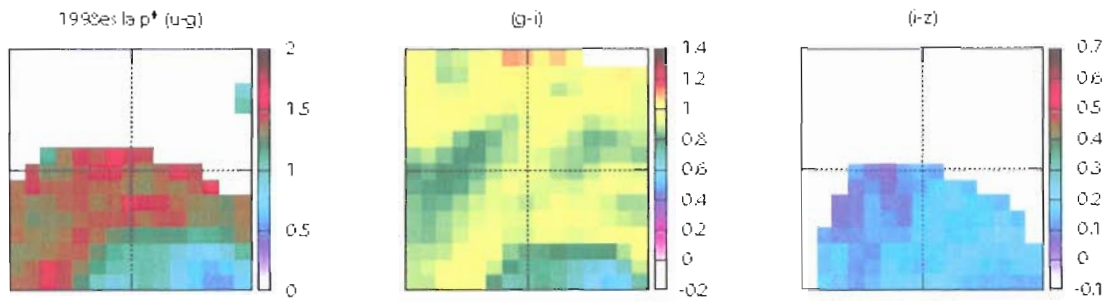


Figure 5.77. SN 1998es  $u-g$ ,  $g-i$ ,  $i-z$  spatial plots.

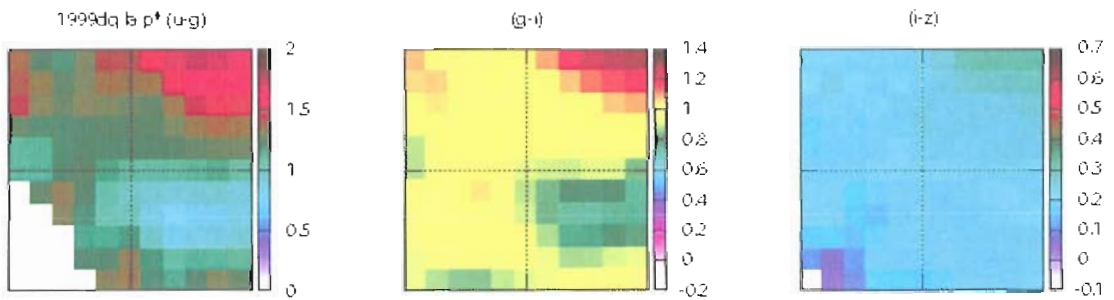


Figure 5.78. SN 1999dq  $u-g$ ,  $g-i$ ,  $i-z$  spatial plots.

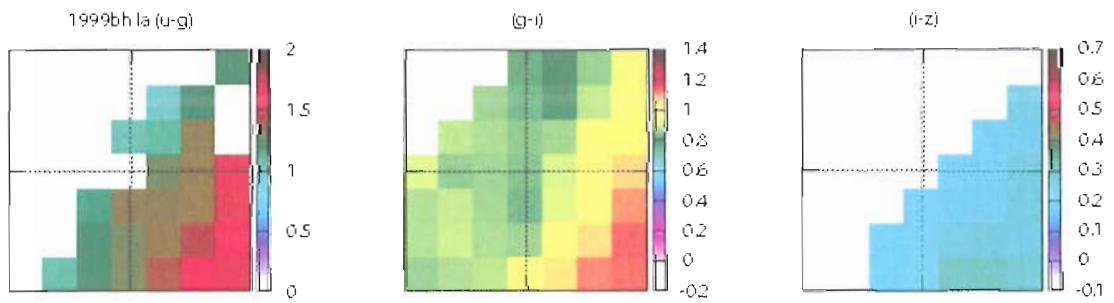


Figure 5.79. SN 1999bh  $u-g$ ,  $g-i$ ,  $i-z$  spatial plots.

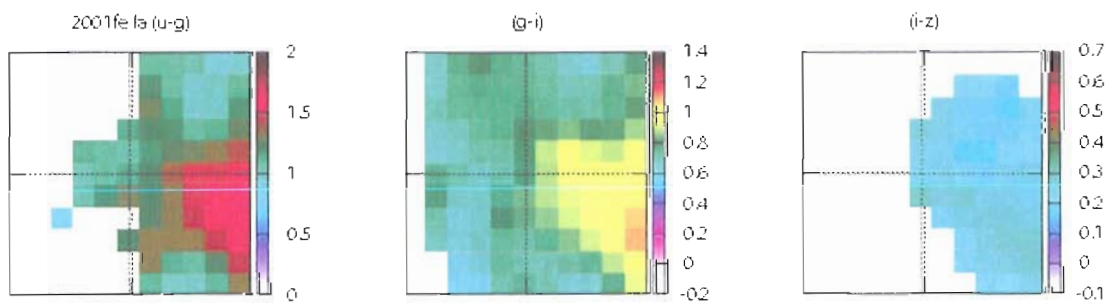
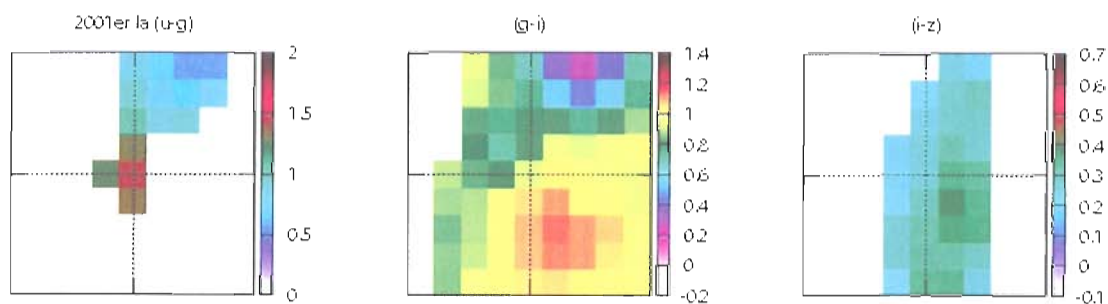
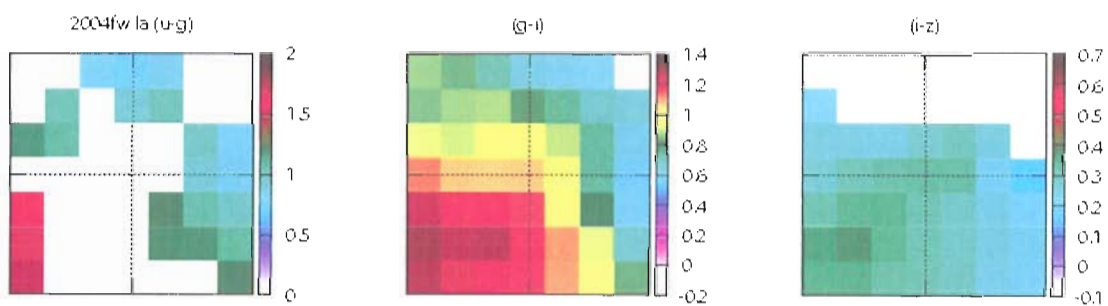
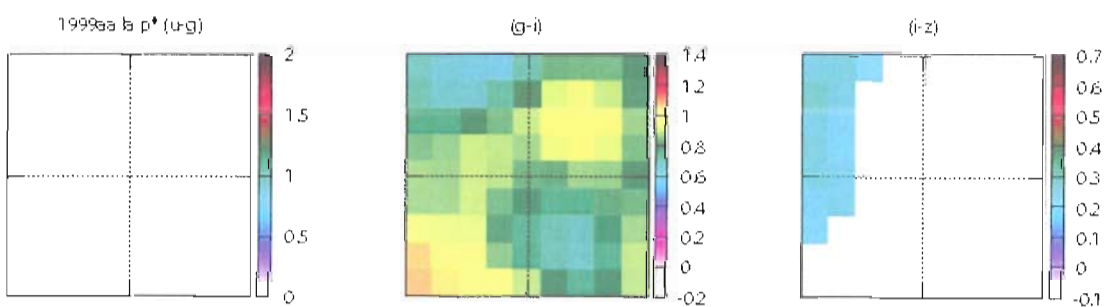
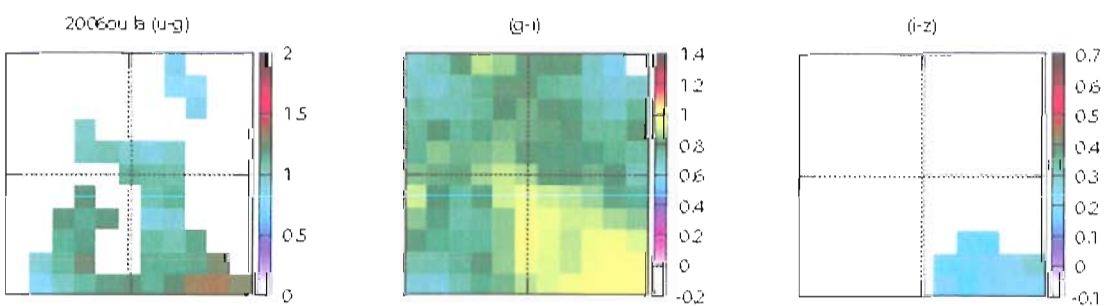


Figure 5.80. SN 2001fe  $u-g$ ,  $g-i$ ,  $i-z$  spatial plots.

Figure 5.81. SN 2001er  $u-g$ ,  $g-i$ ,  $i-z$  spatial plots.Figure 5.82. SN 2004fw  $u-g$ ,  $g-i$ ,  $i-z$  spatial plots.Figure 5.83. SN 1999aa  $u-g$ ,  $g-i$ ,  $i-z$  spatial plots.Figure 5.84. SN 2006ou  $u-g$ ,  $g-i$ ,  $i-z$  spatial plots.

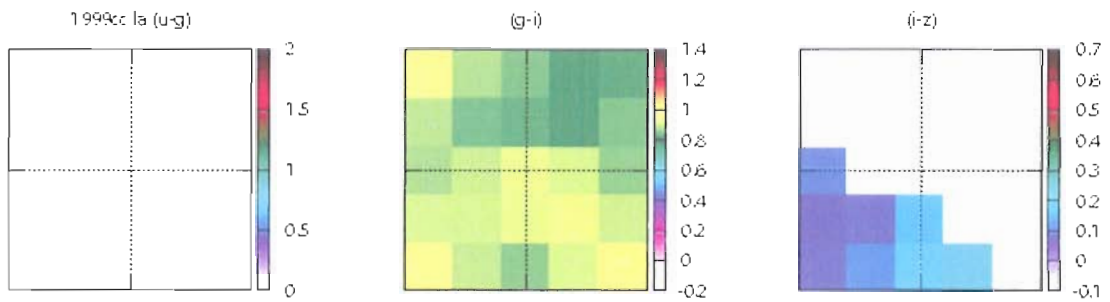


Figure 5.85. SN 1999cc  $u-g$ ,  $g-i$ ,  $i-z$  spatial plots.

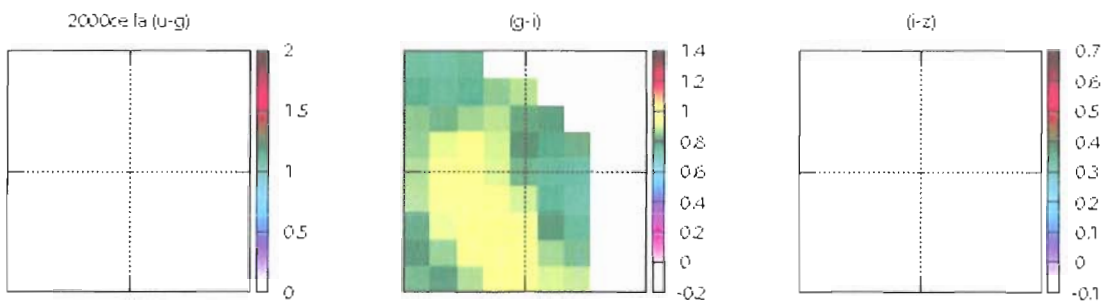


Figure 5.86. SN 2000ce  $u-g$ ,  $g-i$ ,  $i-z$  spatial plots.

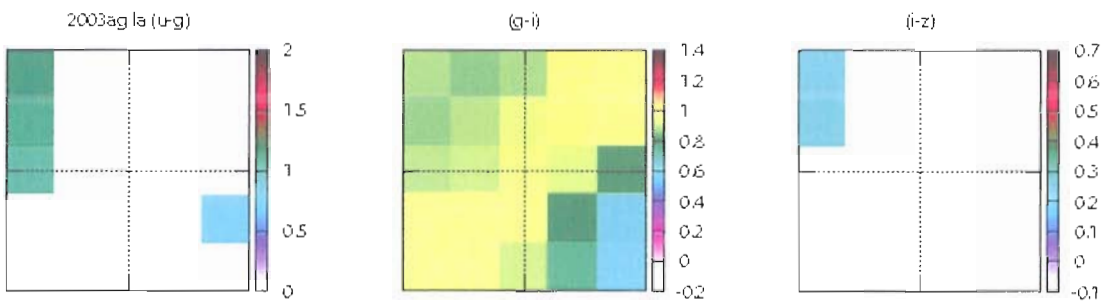


Figure 5.87. SN 2003ag  $u-g$ ,  $g-i$ ,  $i-z$  spatial plots.

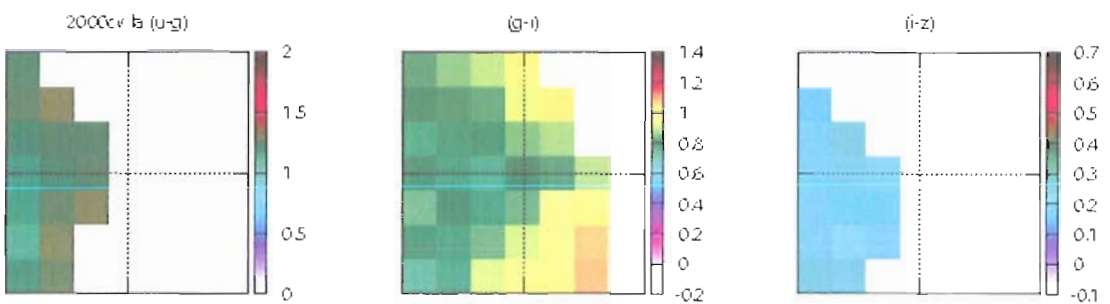


Figure 5.88. SN 2000cv  $u-g$ ,  $g-i$ ,  $i-z$  spatial plots.



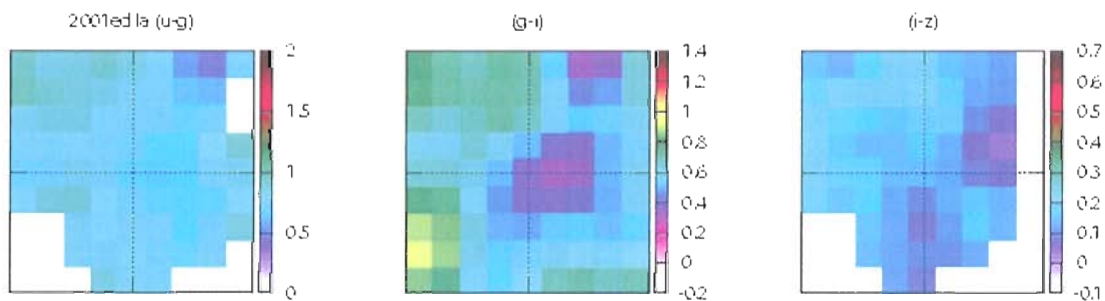


Figure 5.89. SN 2001ed  $u-g$ ,  $g-i$ ,  $i-z$  spatial plots.

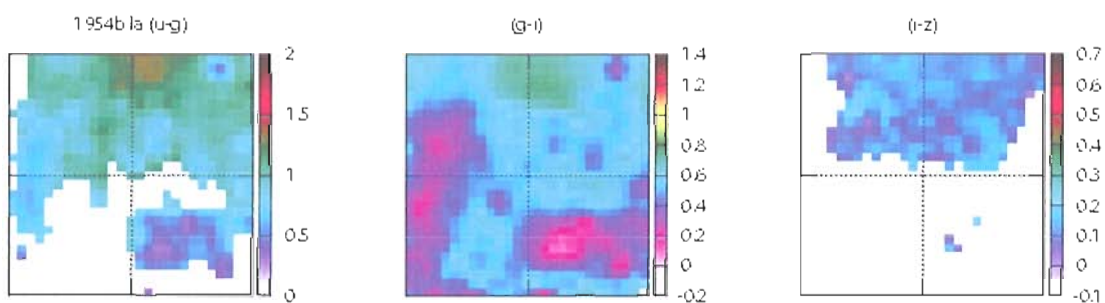


Figure 5.90. SN 1954b  $u-g$ ,  $g-i$ ,  $i-z$  spatial plots.

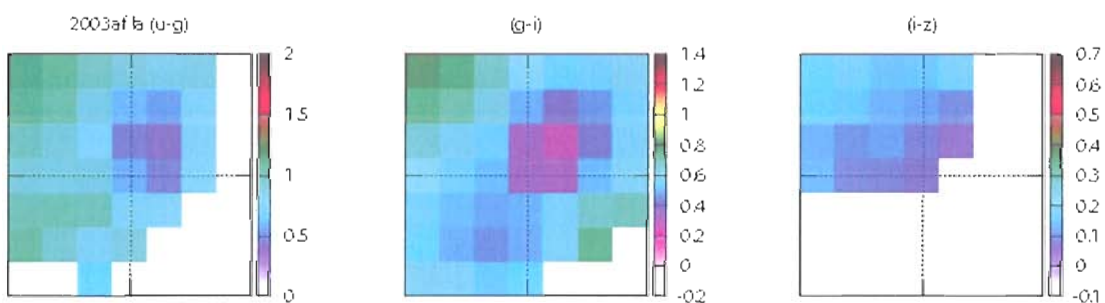


Figure 5.91. SN 2003af  $u-g$ ,  $g-i$ ,  $i-z$  spatial plots.

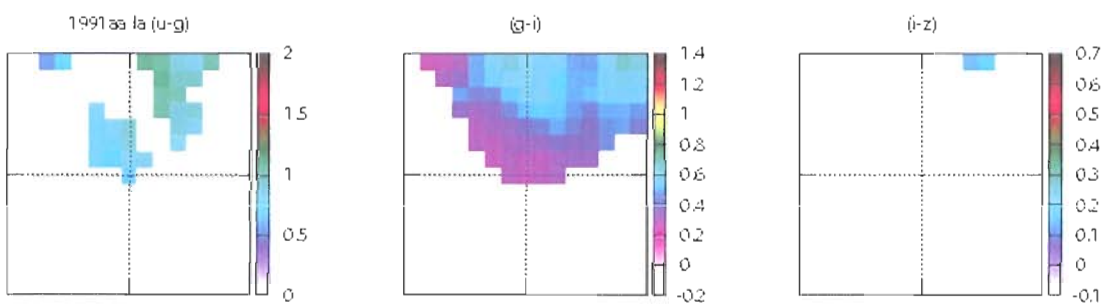


Figure 5.92. SN 1991aa  $u-g$ ,  $g-i$ ,  $i-z$  spatial plots.

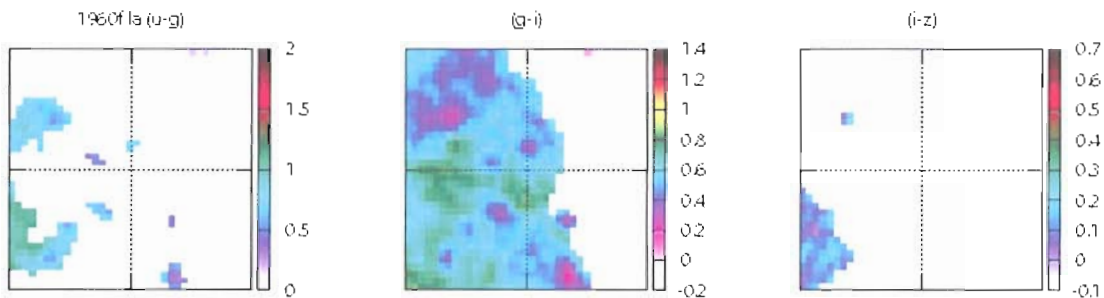


Figure 5.93. SN 1960f  $u-g$ ,  $g-i$ ,  $i-z$  spatial plots.

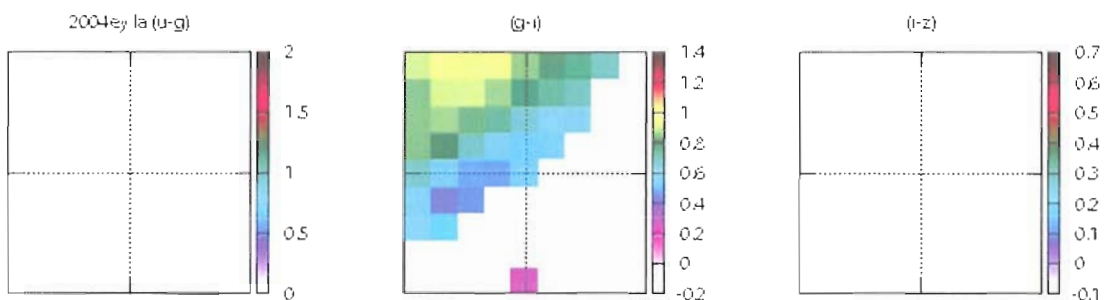


Figure 5.94. SN 2004ey  $u-g$ ,  $g-i$ ,  $i-z$  spatial plots.

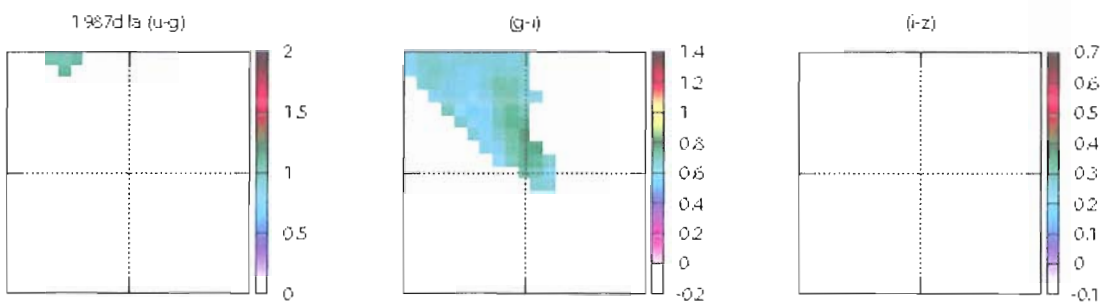


Figure 5.95. SN 1987d  $u-g$ ,  $g-i$ ,  $i-z$  spatial plots.

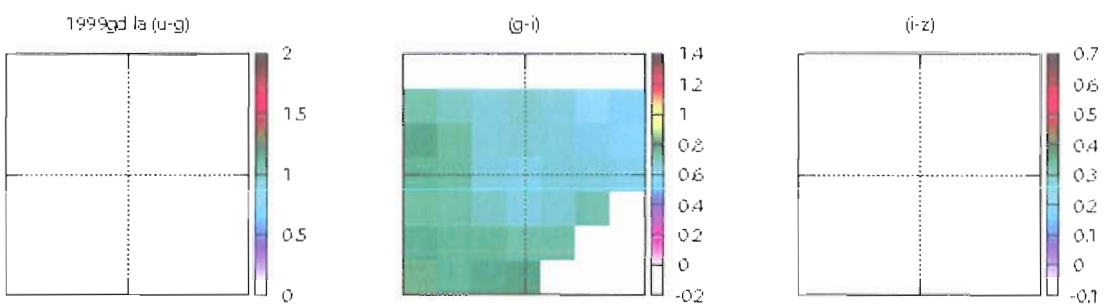


Figure 5.96. SN 1999gd  $u-g$ ,  $g-i$ ,  $i-z$  spatial plots.

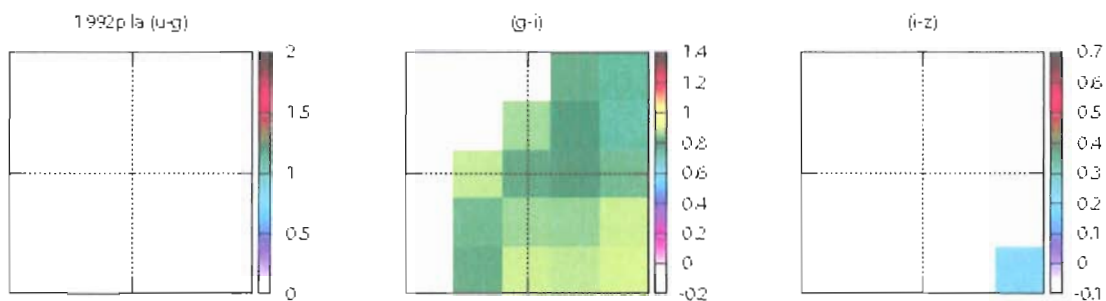


Figure 5.97. SN 1992p  $u-g$ ,  $g-i$ ,  $i-z$  spatial plots.

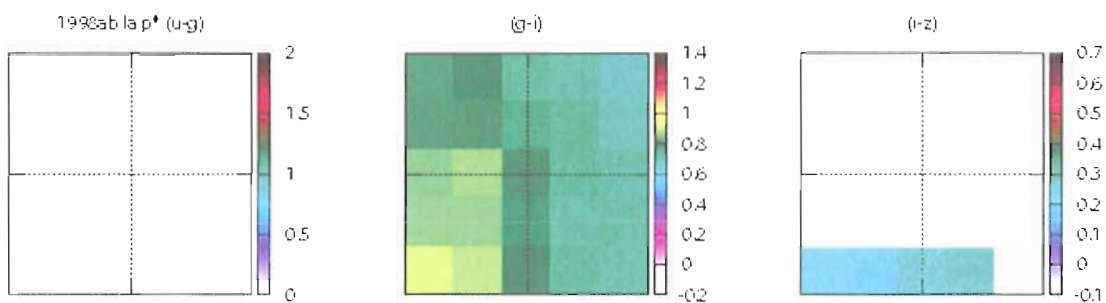


Figure 5.98. SN 1998ab  $u-g$ ,  $g-i$ ,  $i-z$  spatial plots.

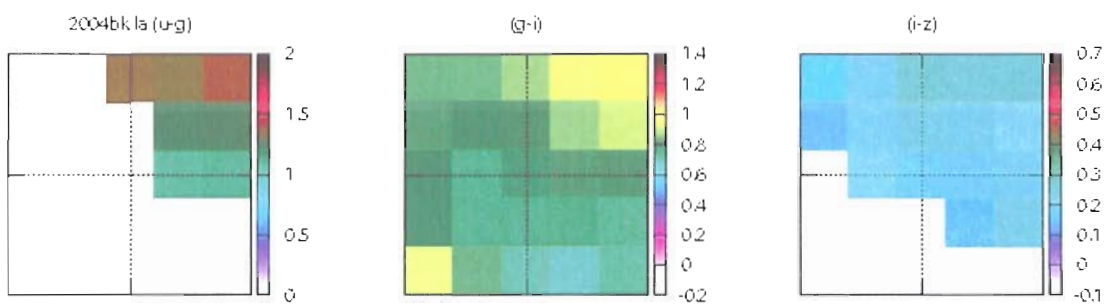


Figure 5.99. SN 2004bk  $u-g$ ,  $g-i$ ,  $i-z$  spatial plots.

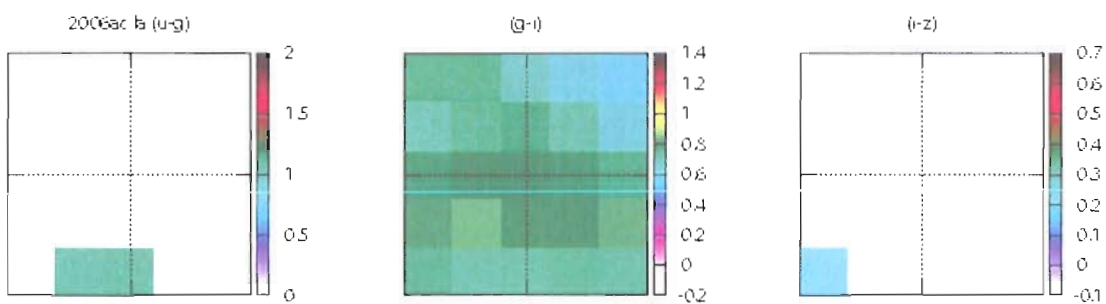


Figure 5.100. SN 2006ac  $u-g$ ,  $g-i$ ,  $i-z$  spatial plots.

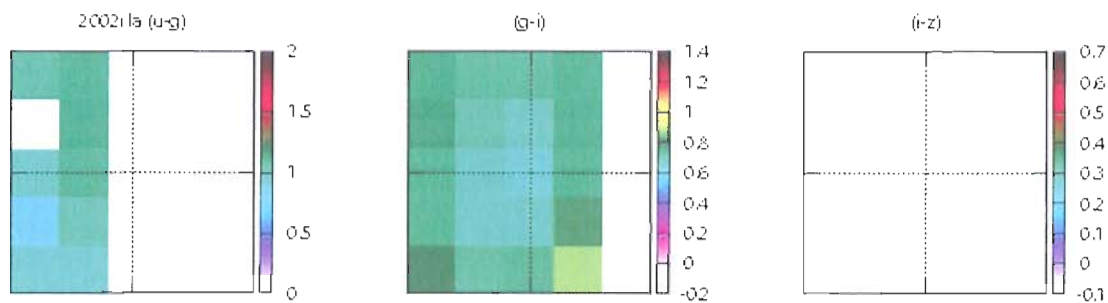


Figure 5.101. SN 2002i  $u-g$ ,  $g-i$ ,  $i-z$  spatial plots.

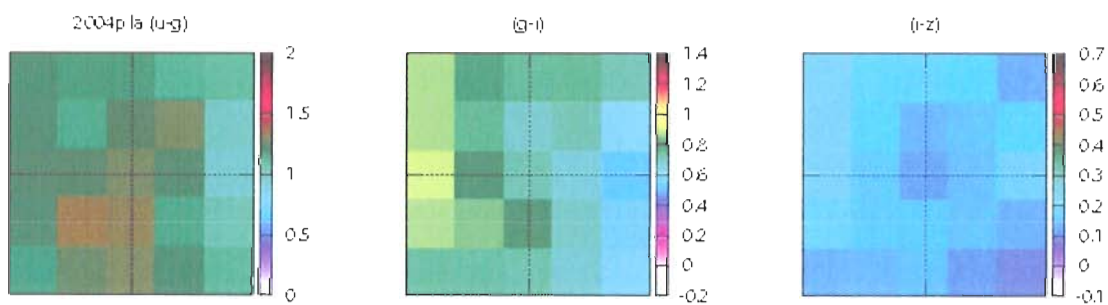


Figure 5.102. SN 2004p  $u-g$ ,  $g-i$ ,  $i-z$  spatial plots.

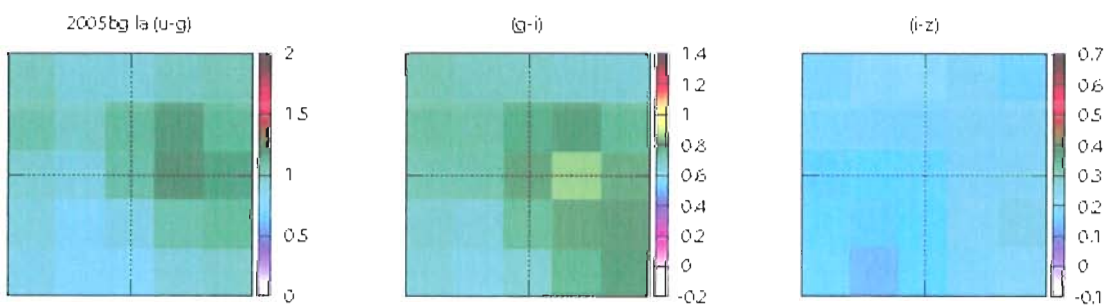


Figure 5.103. SN 2005bg  $u-g$ ,  $g-i$ ,  $i-z$  spatial plots.

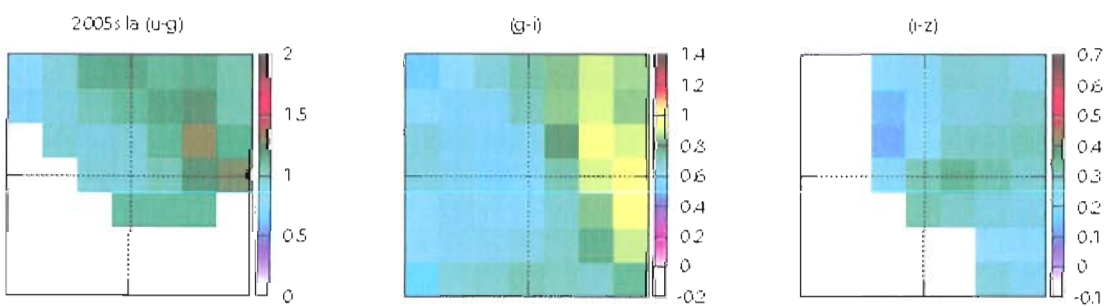


Figure 5.104. SN 2005s  $u-g$ ,  $g-i$ ,  $i-z$  spatial plots.

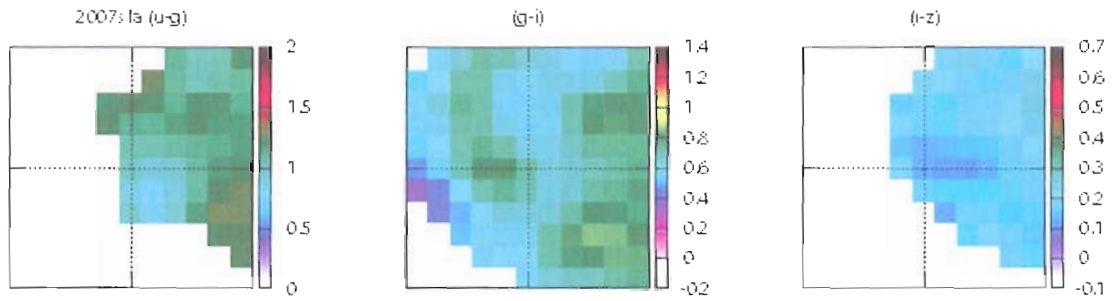


Figure 5.105. SN 2007s  $u-g$ ,  $g-i$ ,  $i-z$  spatial plots.

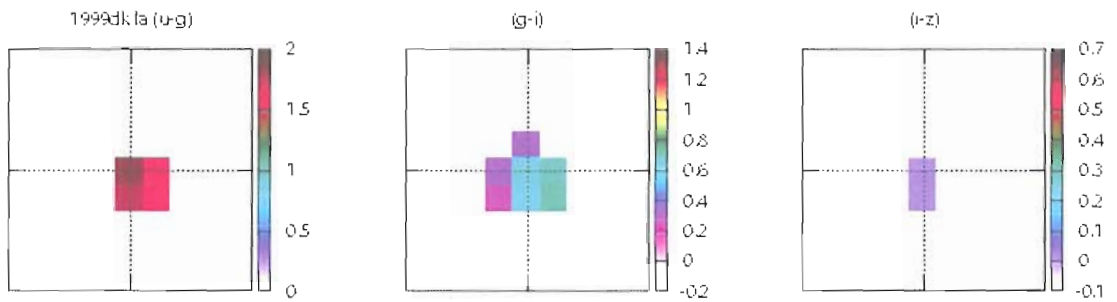


Figure 5.106. SN 1999dk  $u-g$ ,  $g-i$ ,  $i-z$  spatial plots.

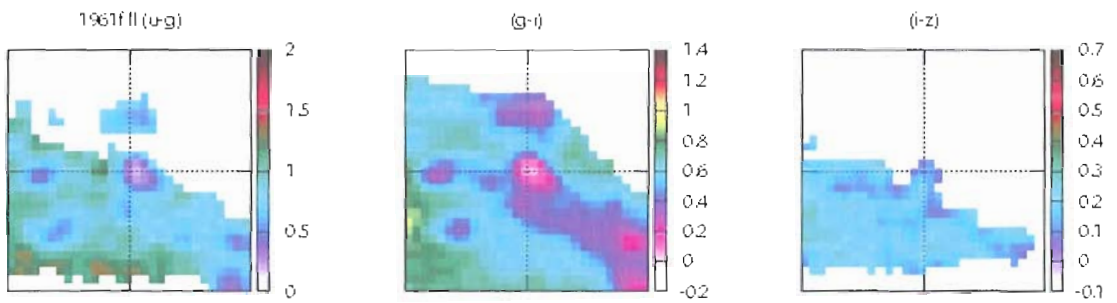


Figure 5.107. SN 1961f  $u-g$ ,  $g-i$ ,  $i-z$  spatial plots.

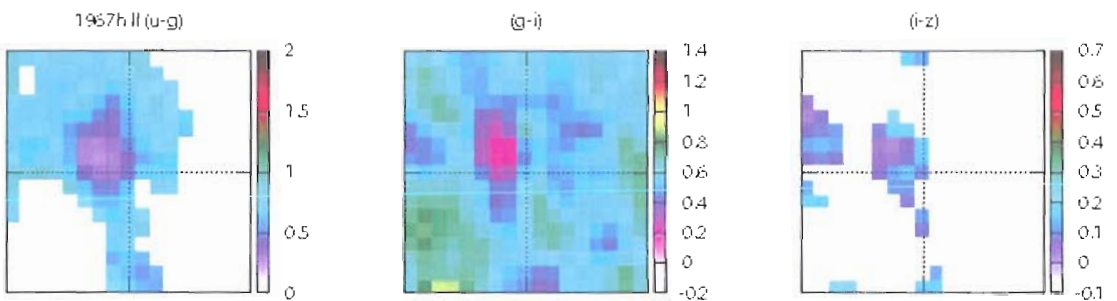


Figure 5.108. SN 1967h  $u-g$ ,  $g-i$ ,  $i-z$  spatial plots.

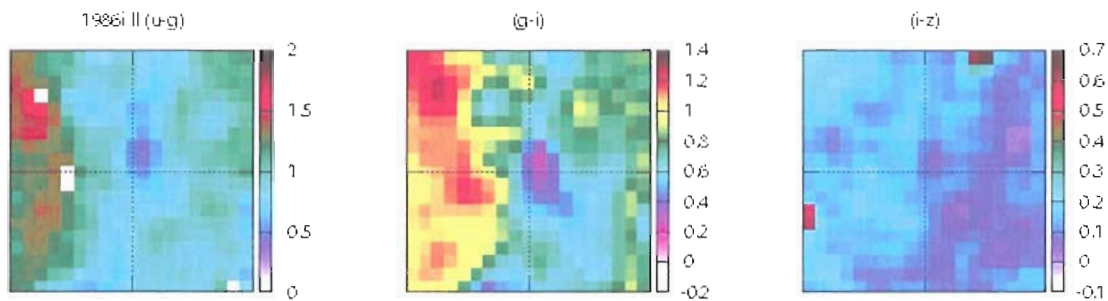


Figure 5.109. SN 1986i  $u-g$ ,  $g-i$ ,  $i-z$  spatial plots.

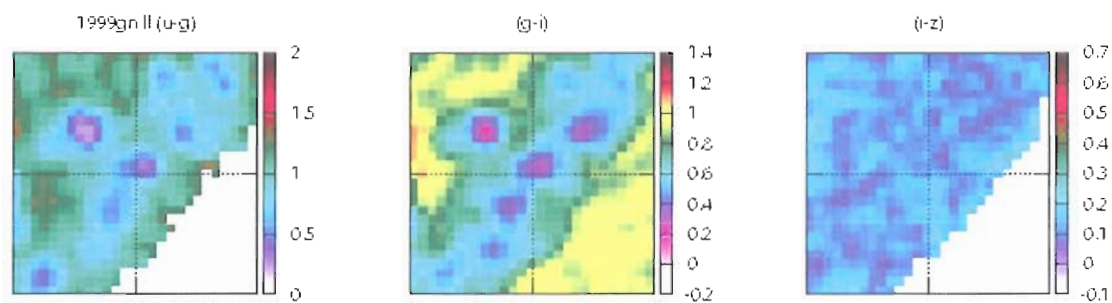


Figure 5.110. SN 1999gn  $u-g$ ,  $g-i$ ,  $i-z$  spatial plots.

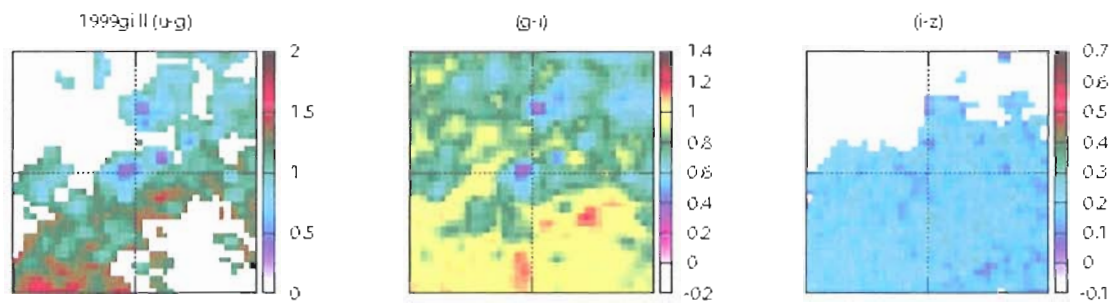


Figure 5.111. SN 1999gi  $u-g$ ,  $g-i$ ,  $i-z$  spatial plots.

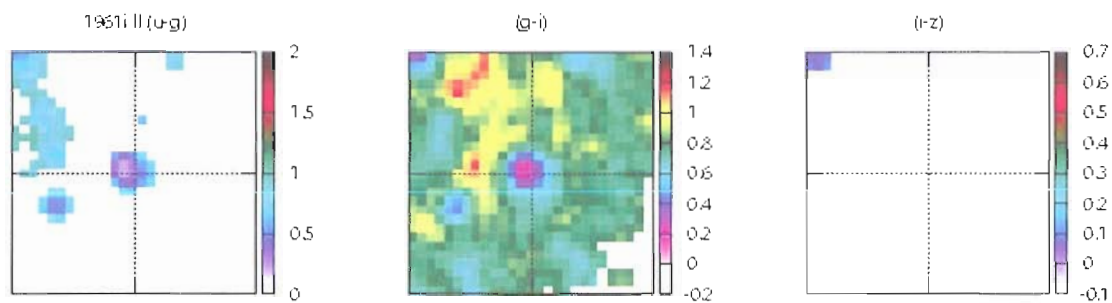


Figure 5.112. SN 1961i  $u-g$ ,  $g-i$ ,  $i-z$  spatial plots.

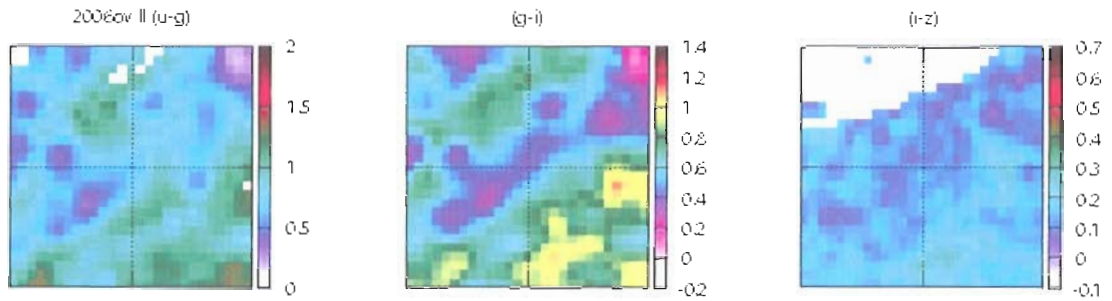


Figure 5.113. SN 2006ov  $u-g$ ,  $g-i$ ,  $i-z$  spatial plots.

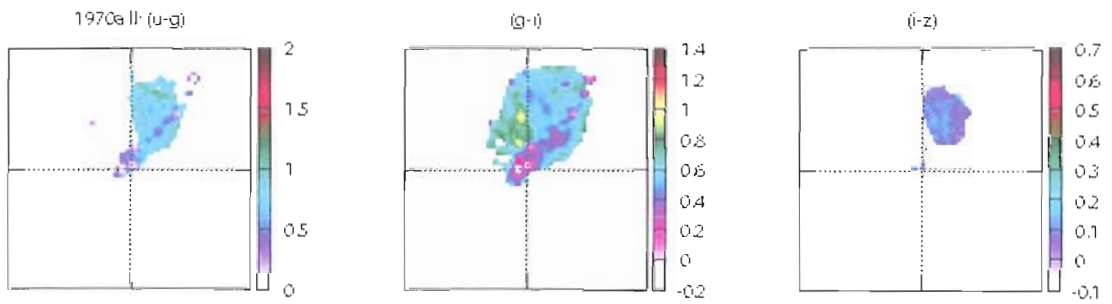


Figure 5.114. SN 1970a  $u-g$ ,  $g-i$ ,  $i-z$  spatial plots.

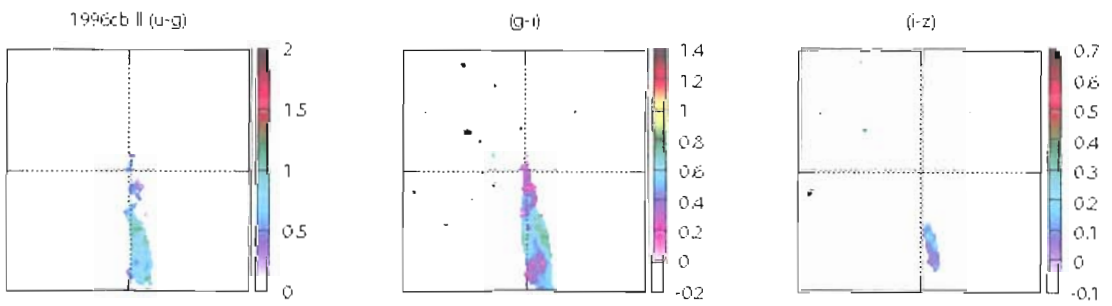


Figure 5.115. SN 1996cb  $u-g$ ,  $g-i$ ,  $i-z$  spatial plots.

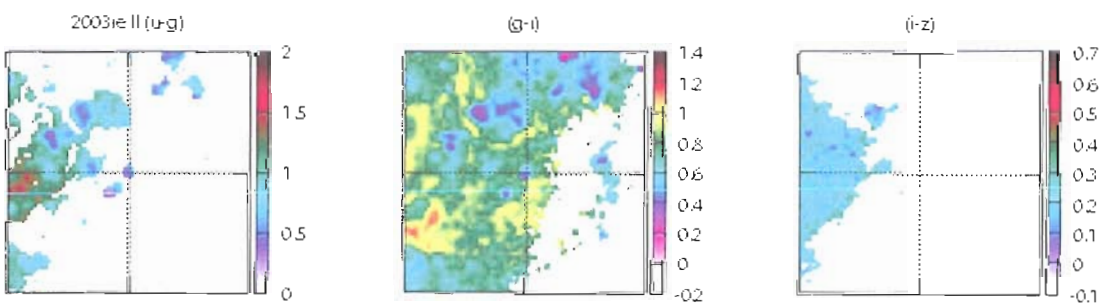


Figure 5.116. SN 2003ie  $u-g$ ,  $g-i$ ,  $i-z$  spatial plots.

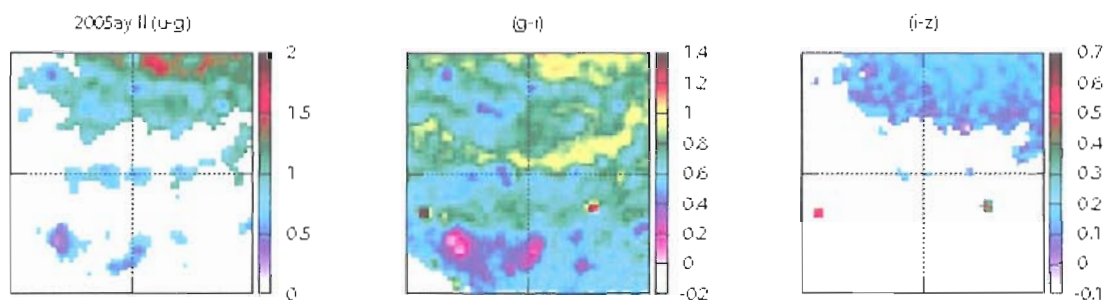


Figure 5.117. SN 2005ay  $u-g$ ,  $g-i$ ,  $i-z$  spatial plots.

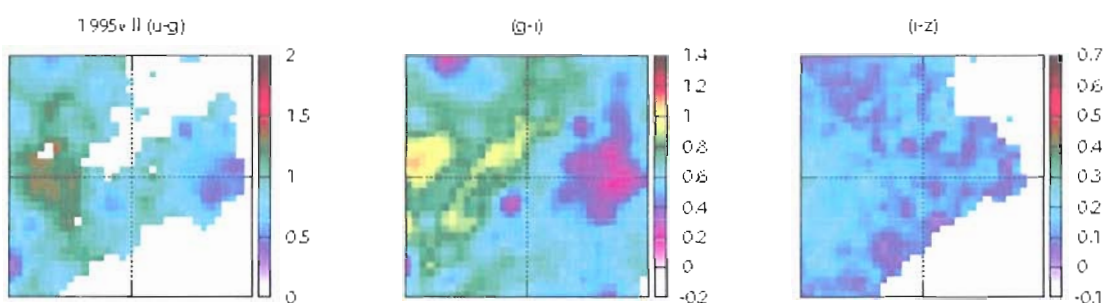


Figure 5.118. SN 1995v  $u-g$ ,  $g-i$ ,  $i-z$  spatial plots.

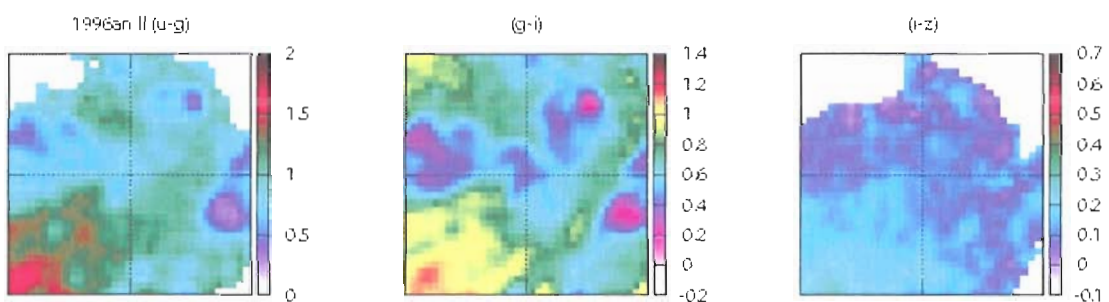


Figure 5.119. SN 1996an  $u-g$ ,  $g-i$ ,  $i-z$  spatial plots.

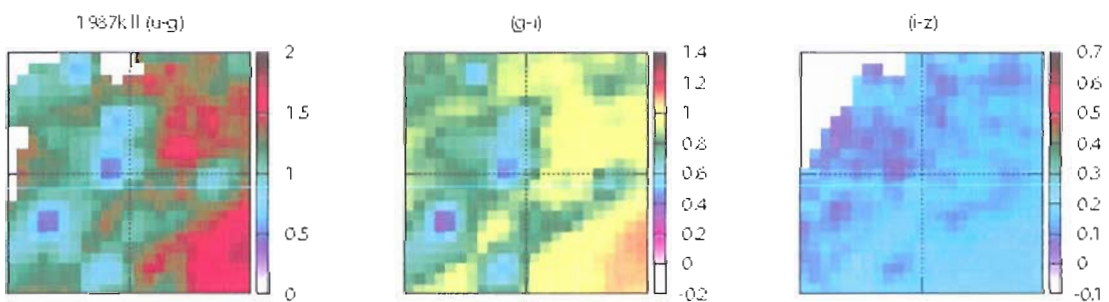


Figure 5.120. SN 1987k  $u-g$ ,  $g-i$ ,  $i-z$  spatial plots.



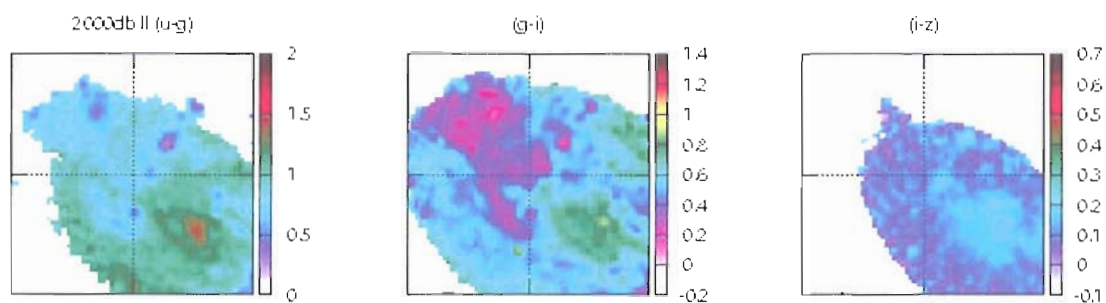


Figure 5.121. SN 2000db  $u-g$ ,  $g-i$ ,  $i-z$  spatial plots.

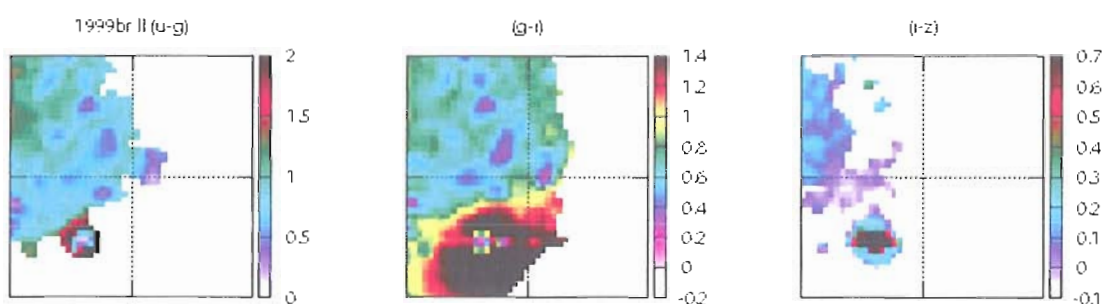


Figure 5.122. SN 1999br  $u-g$ ,  $g-i$ ,  $i-z$  spatial plots.

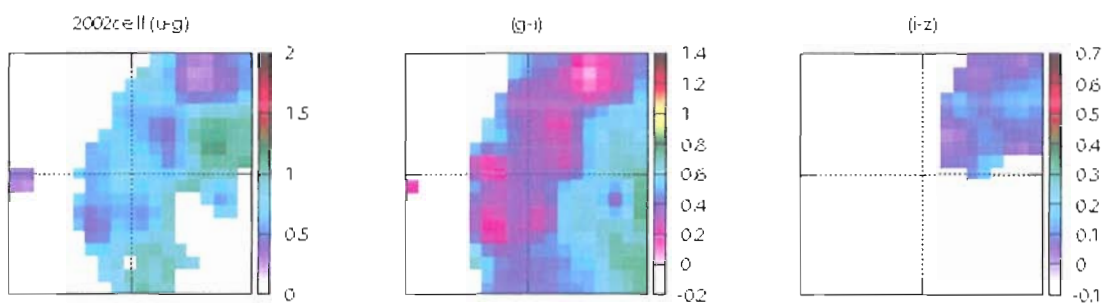


Figure 5.123. SN 2002ce  $u-g$ ,  $g-i$ ,  $i-z$  spatial plots.

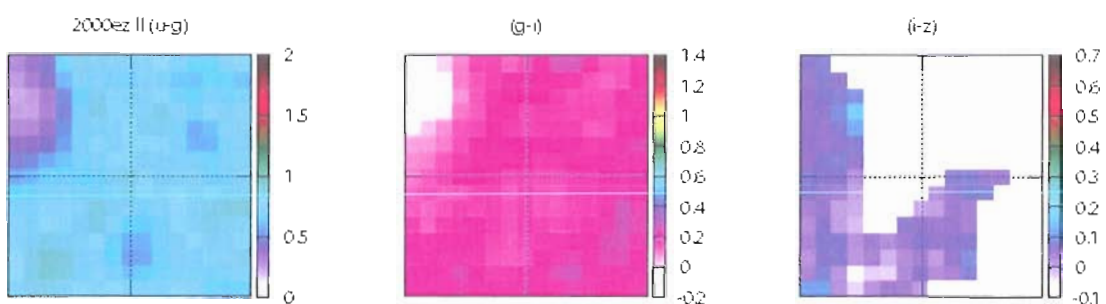


Figure 5.124. SN 2000ez  $u-g$ ,  $g-i$ ,  $i-z$  spatial plots.

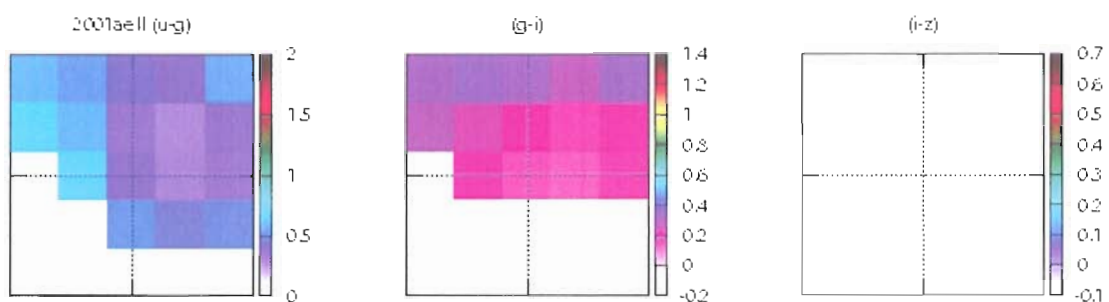


Figure 5.125. SN 2001ae  $u-g$ ,  $g-i$ ,  $i-z$  spatial plots.

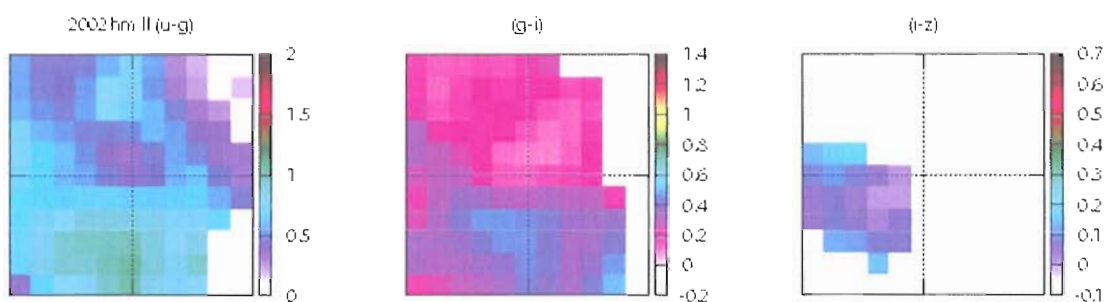


Figure 5.126. SN 2002hm  $u-g$ ,  $g-i$ ,  $i-z$  spatial plots.

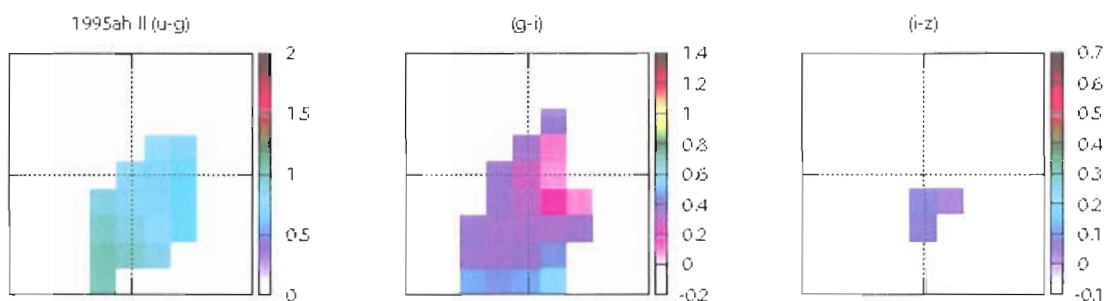


Figure 5.127. SN 1995ah  $u-g$ ,  $g-i$ ,  $i-z$  spatial plots.

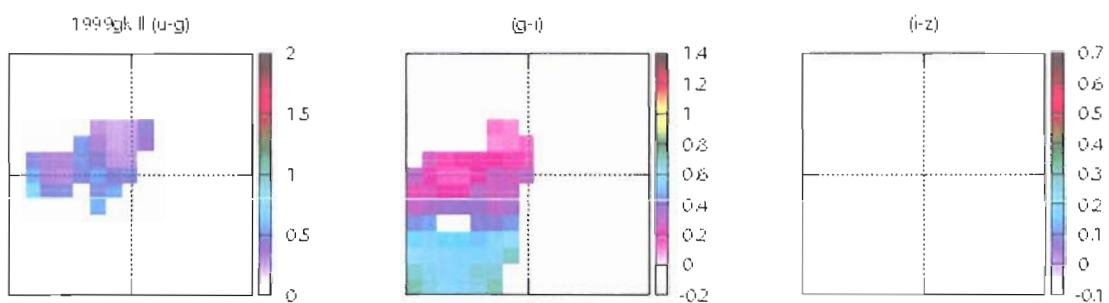


Figure 5.128. SN 1999gk  $u-g$ ,  $g-i$ ,  $i-z$  spatial plots.

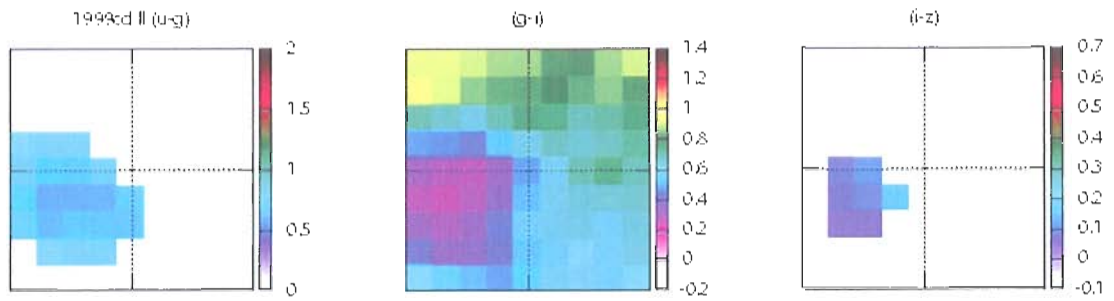


Figure 5.129. SN 1999cd  $u-g$ ,  $g-i$ ,  $i-z$  spatial plots.

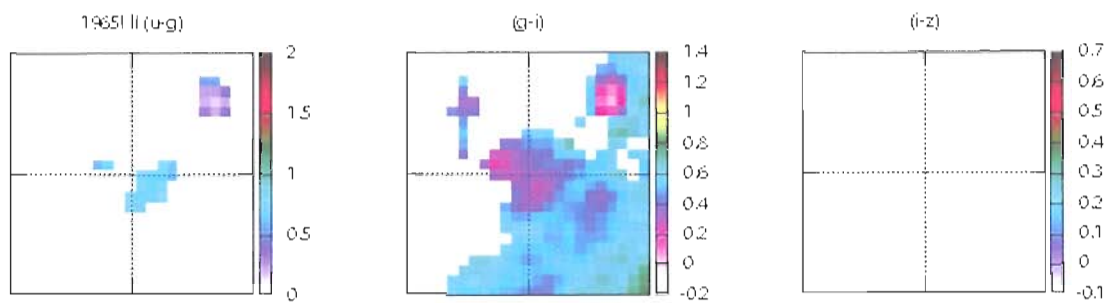


Figure 5.130. SN 1965I  $u-g$ ,  $g-i$ ,  $i-z$  spatial plots.

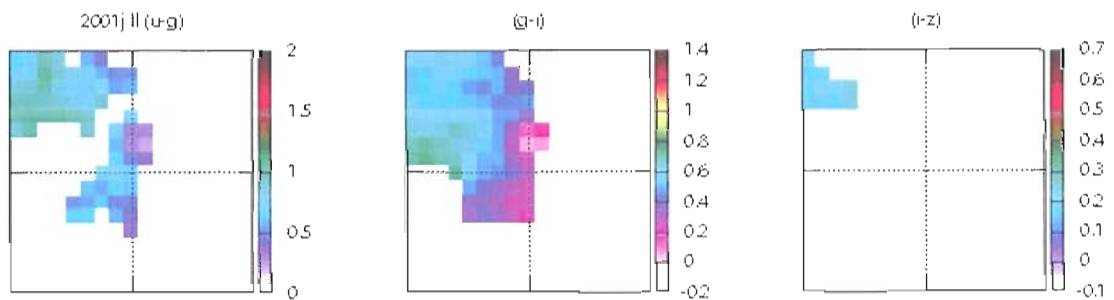


Figure 5.131. SN 2001j  $u-g$ ,  $g-i$ ,  $i-z$  spatial plots.

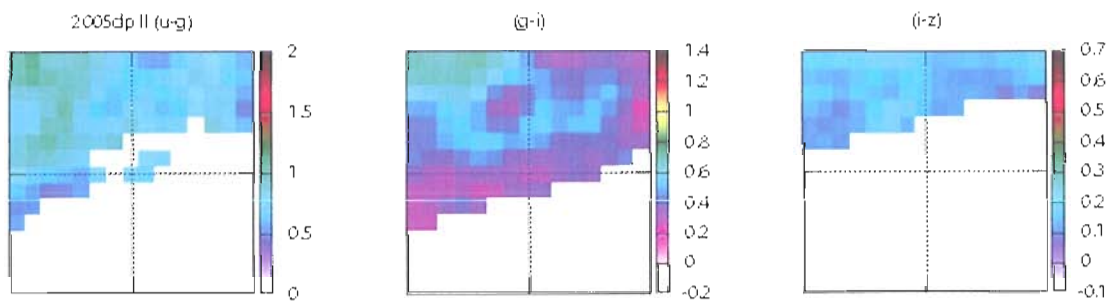


Figure 5.132. SN 2005dp  $u-g$ ,  $g-i$ ,  $i-z$  spatial plots.

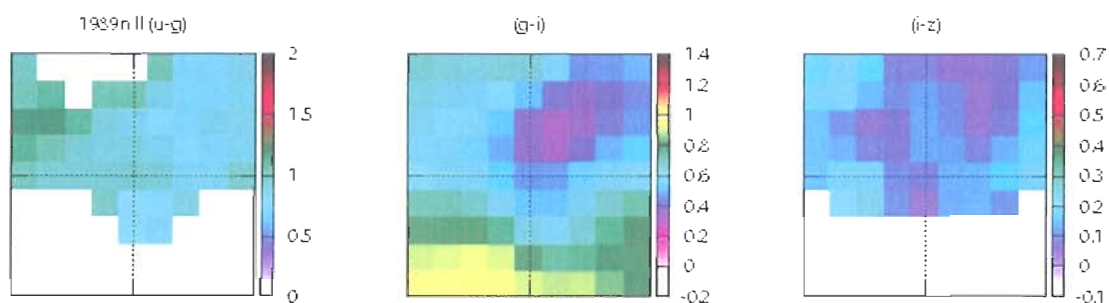


Figure 5.133. SN 1989n  $u-g$ ,  $g-i$ ,  $i-z$  spatial plots.

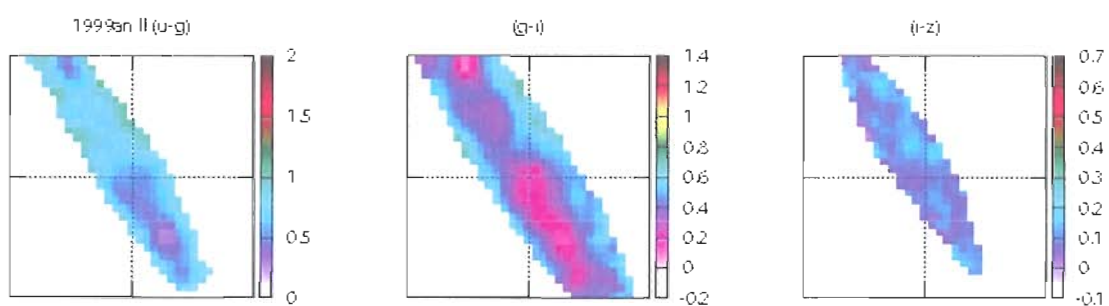


Figure 5.134. SN 1999an  $u-g$ ,  $g-i$ ,  $i-z$  spatial plots.

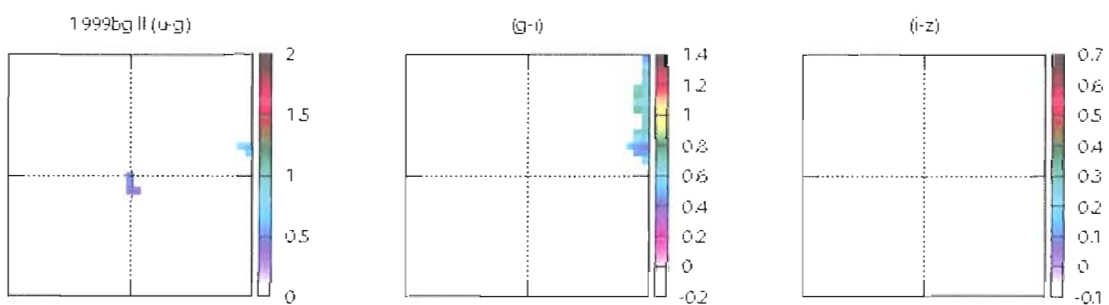


Figure 5.135. SN 1999bg  $u-g$ ,  $g-i$ ,  $i-z$  spatial plots.

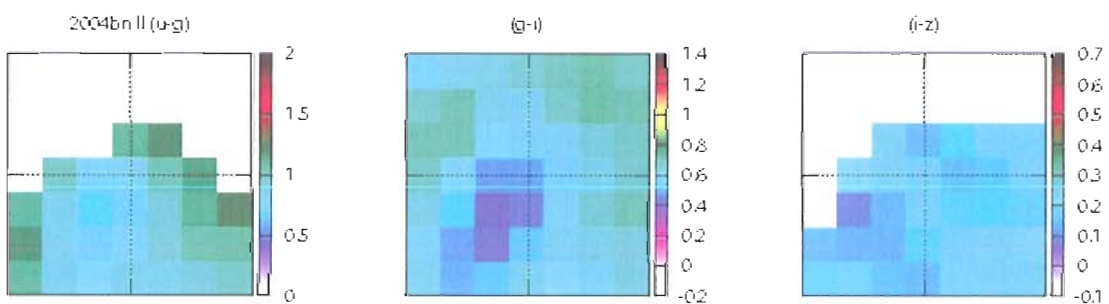


Figure 5.136. SN 2004bn  $u-g$ ,  $g-i$ ,  $i-z$  spatial plots.

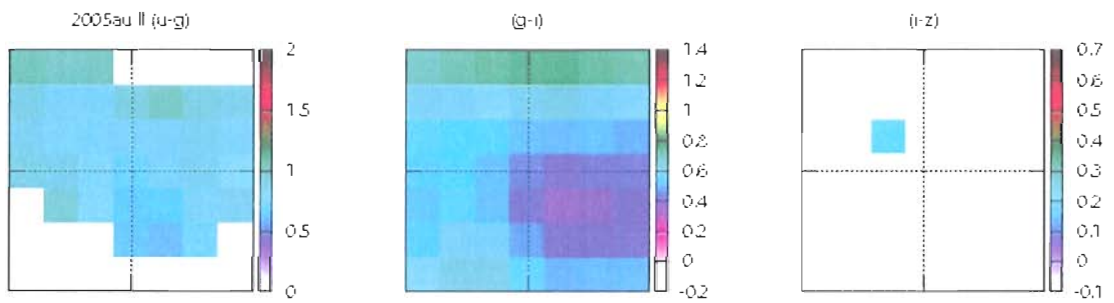


Figure 5.137. SN 2005au  $u-g$ ,  $g-i$ ,  $i-z$  spatial plots.

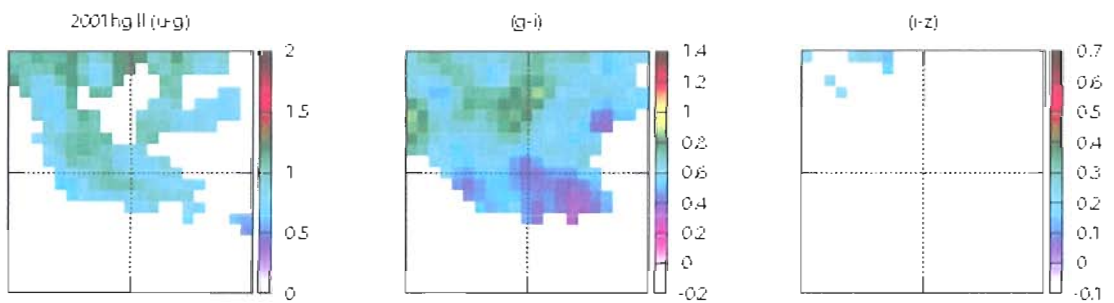


Figure 5.138. SN 2001hg  $u-g$ ,  $g-i$ ,  $i-z$  spatial plots.

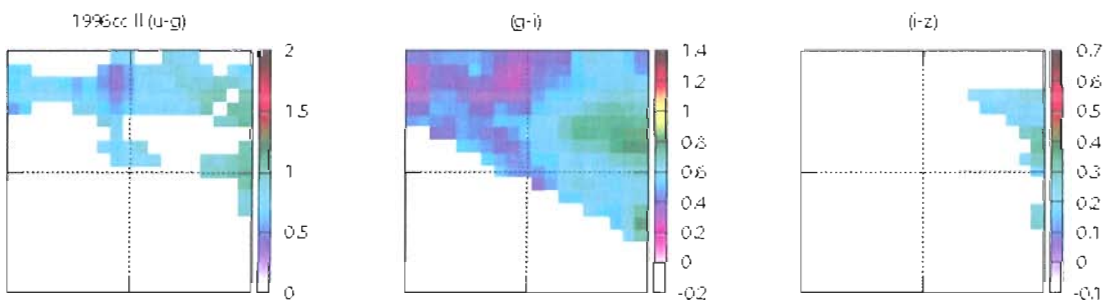


Figure 5.139. SN 1996cc  $u-g$ ,  $g-i$ ,  $i-z$  spatial plots.

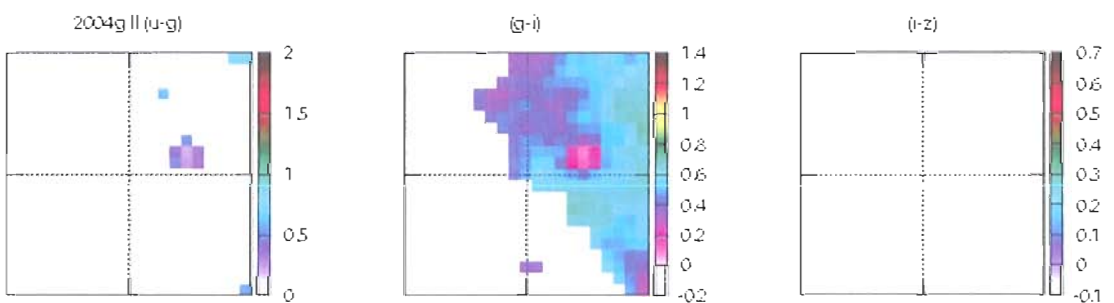


Figure 5.140. SN 2004g  $u-g$ ,  $g-i$ ,  $i-z$  spatial plots.

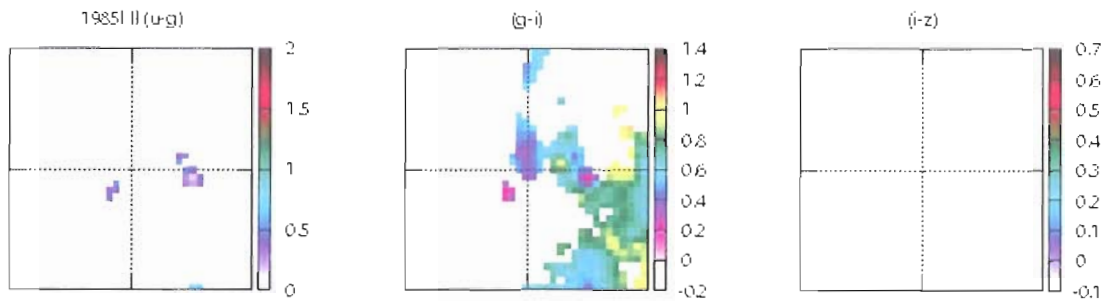


Figure 5.141. SN 1985l  $u-g$ ,  $g-i$ ,  $i-z$  spatial plots.

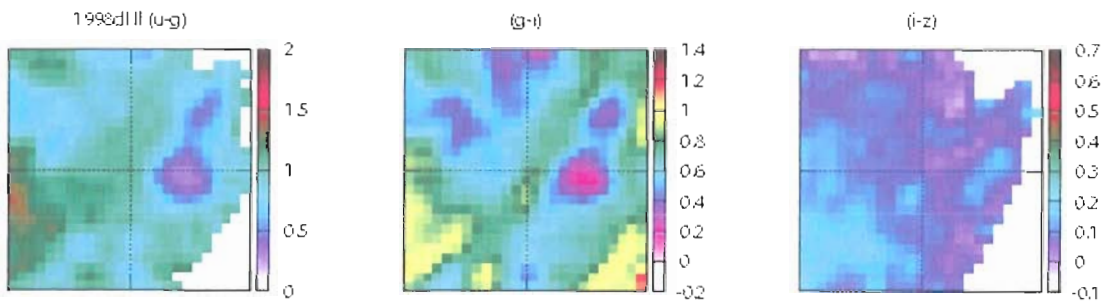


Figure 5.142. SN 1998dl  $u-g$ ,  $g-i$ ,  $i-z$  spatial plots.

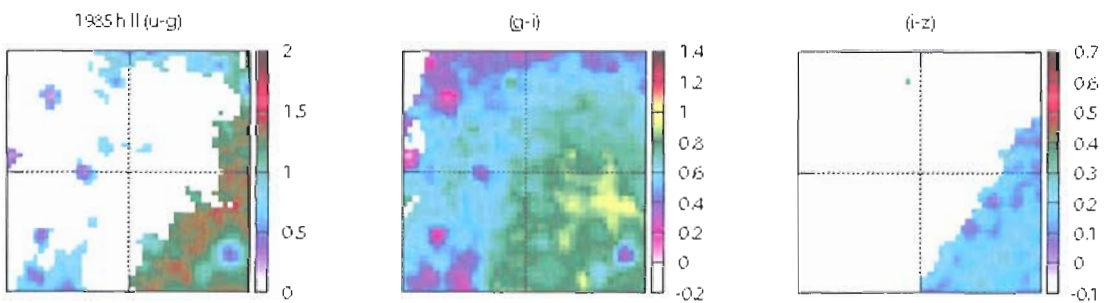


Figure 5.143. SN 1985h  $u-g$ ,  $g-i$ ,  $i-z$  spatial plots.

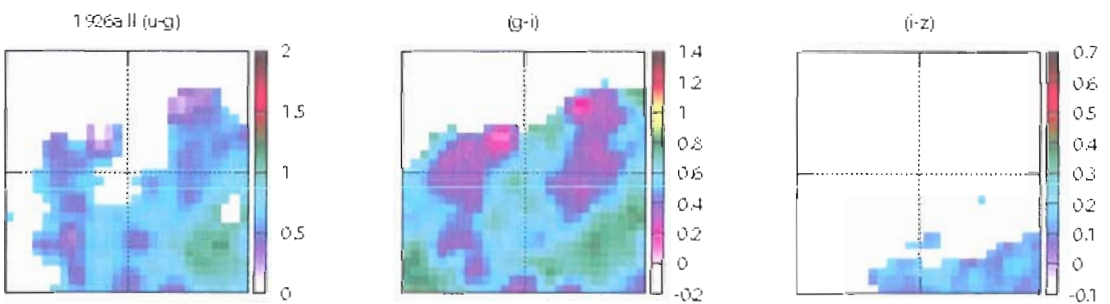


Figure 5.144. SN 1926a  $u-g$ ,  $g-i$ ,  $i-z$  spatial plots.

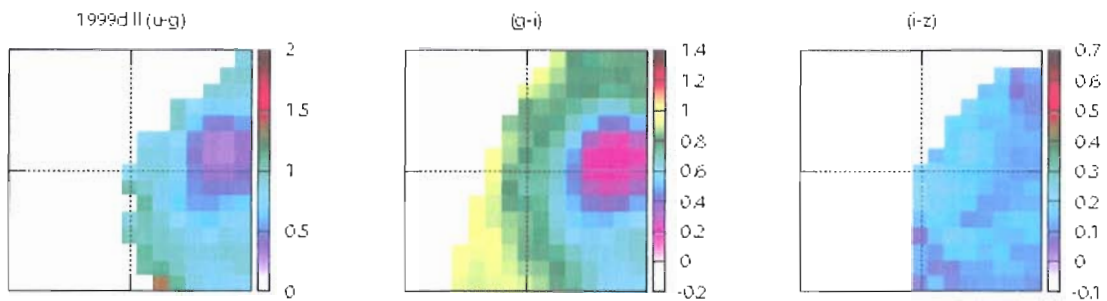


Figure 5.145. SN 1999d  $u-g$ ,  $g-i$ ,  $i-z$  spatial plots.

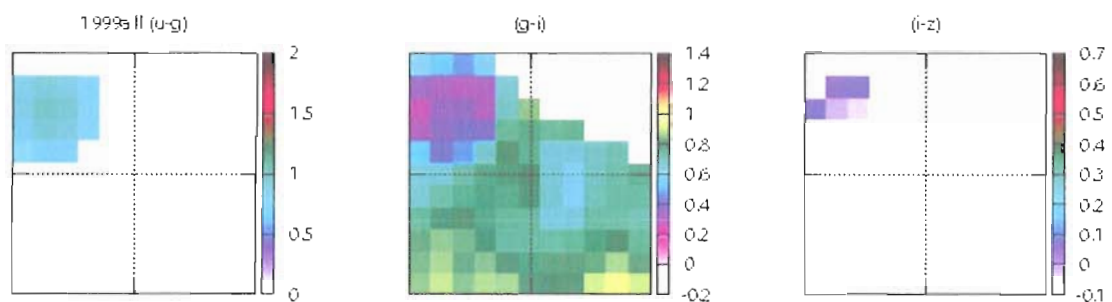


Figure 5.146. SN 1999a  $u-g$ ,  $g-i$ ,  $i-z$  spatial plots.

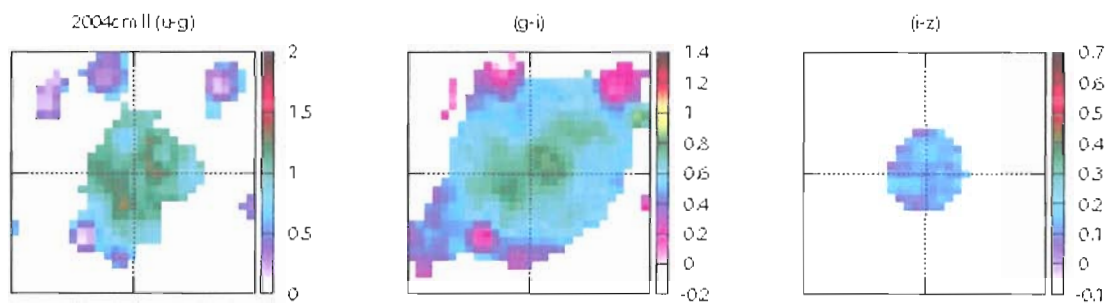


Figure 5.147. SN 2004cm  $u-g$ ,  $g-i$ ,  $i-z$  spatial plots.

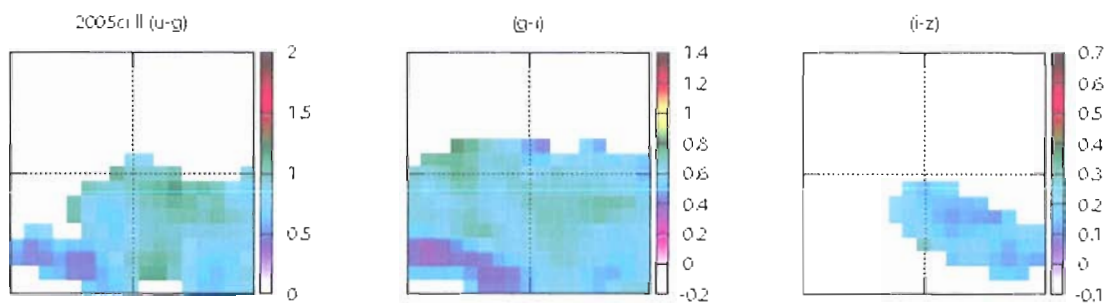
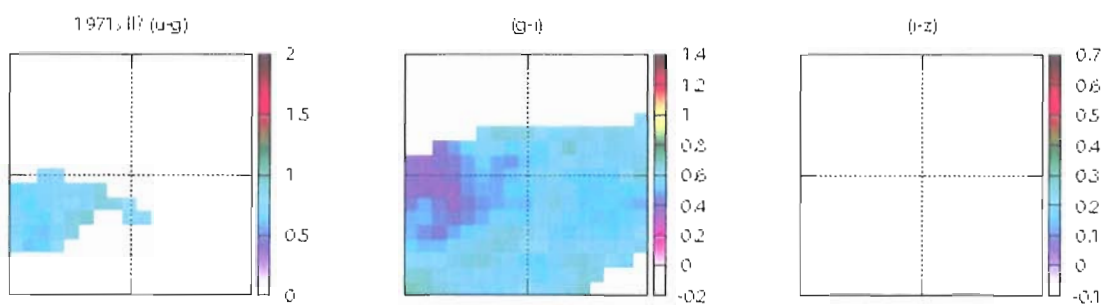
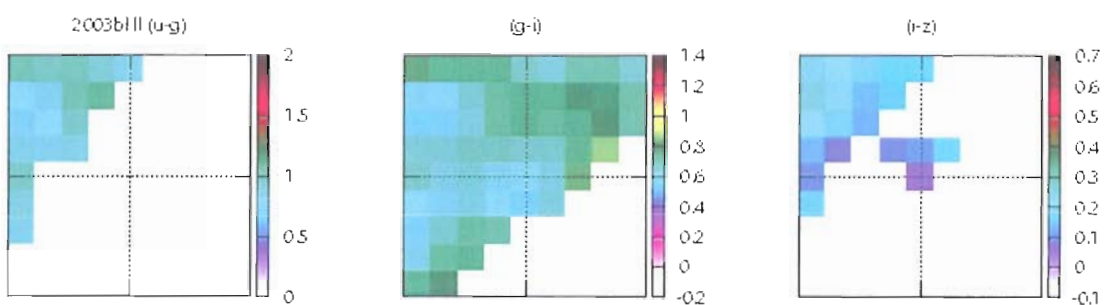
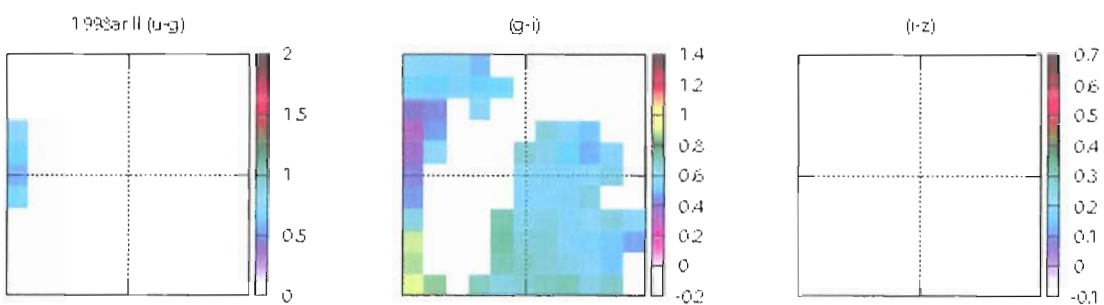
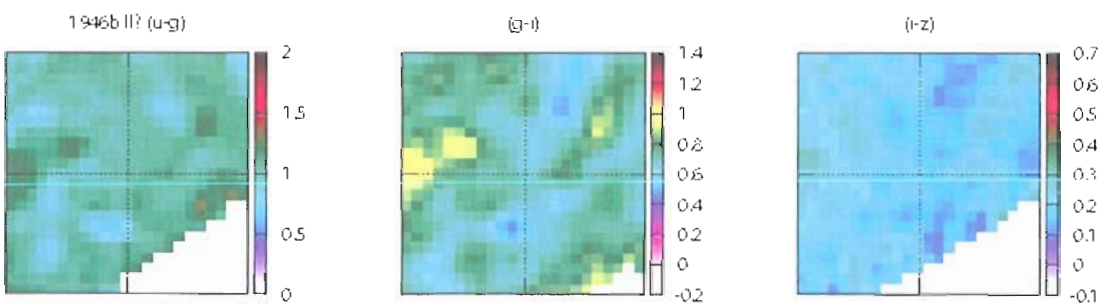


Figure 5.148. SN 2005ci  $u-g$ ,  $g-i$ ,  $i-z$  spatial plots.

Figure 5.149. SN 1971s  $u-g$ ,  $g-i$ ,  $i-z$  spatial plots.Figure 5.150. SN 2003bl  $u-g$ ,  $g-i$ ,  $i-z$  spatial plots.Figure 5.151. SN 1998ar  $u-g$ ,  $g-i$ ,  $i-z$  spatial plots.Figure 5.152. SN 1946b  $u-g$ ,  $g-i$ ,  $i-z$  spatial plots.



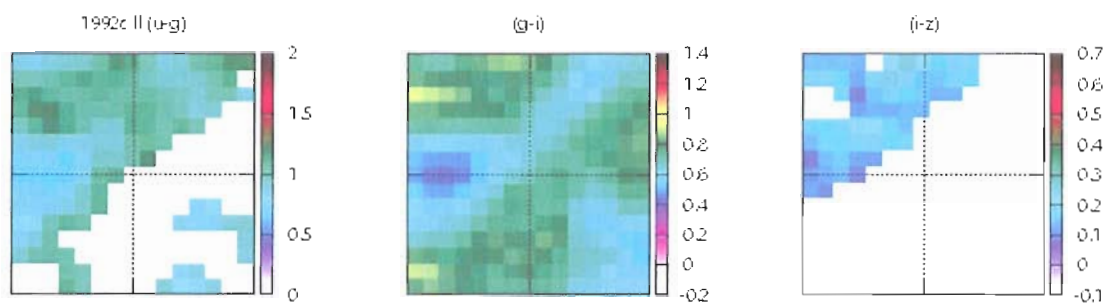


Figure 5.153. SN 1992c  $u-g$ ,  $g-i$ ,  $i-z$  spatial plots.

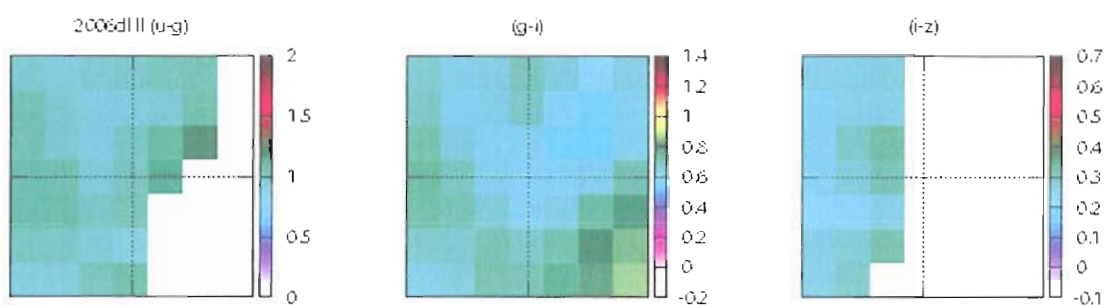


Figure 5.154. SN 2006dl  $u-g$ ,  $g-i$ ,  $i-z$  spatial plots.

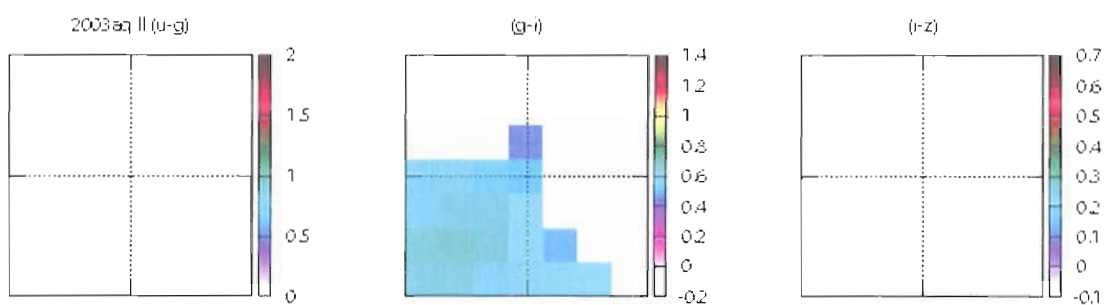


Figure 5.155. SN 2003aq  $u-g$ ,  $g-i$ ,  $i-z$  spatial plots.

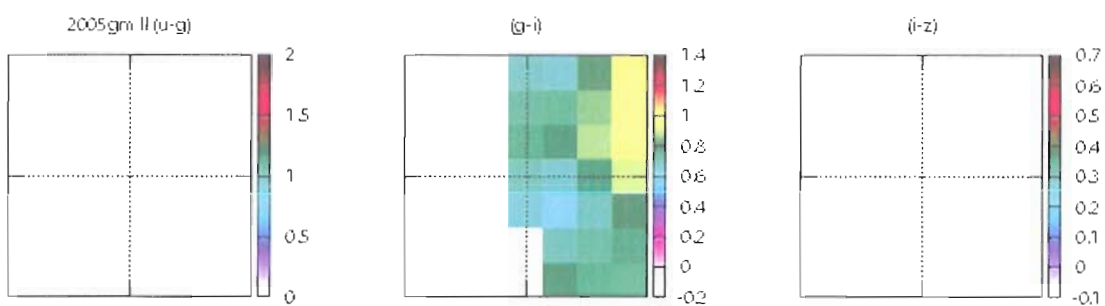


Figure 5.156. SN 2005gm  $u-g$ ,  $g-i$ ,  $i-z$  spatial plots.

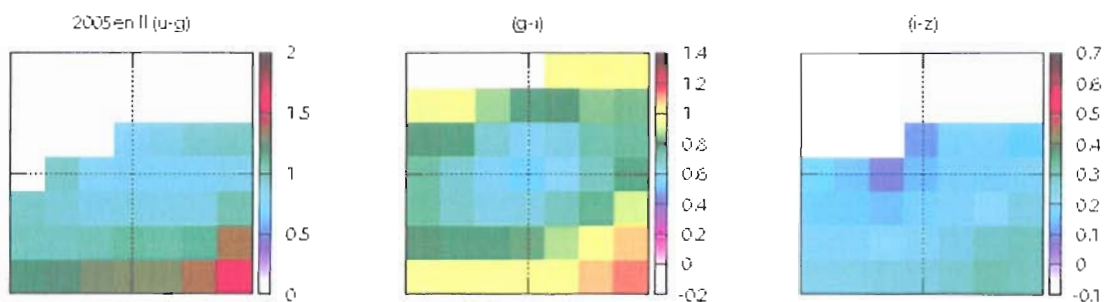


Figure 5.157. SN 2005en  $u-g$ ,  $g-i$ ,  $i-z$  spatial plots.

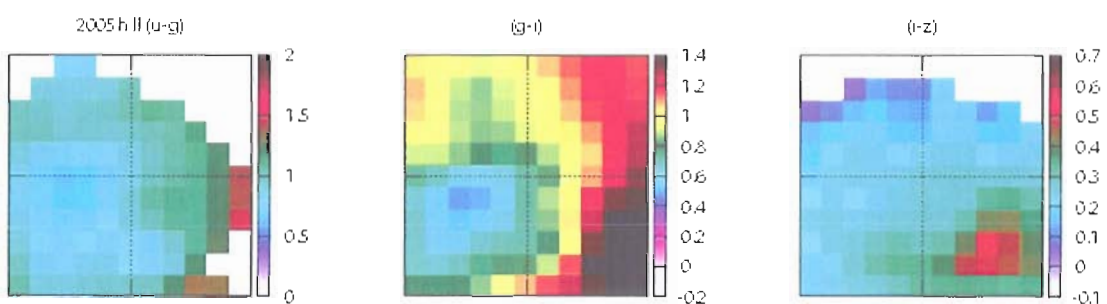


Figure 5.158. SN 2005h  $u-g$ ,  $g-i$ ,  $i-z$  spatial plots.

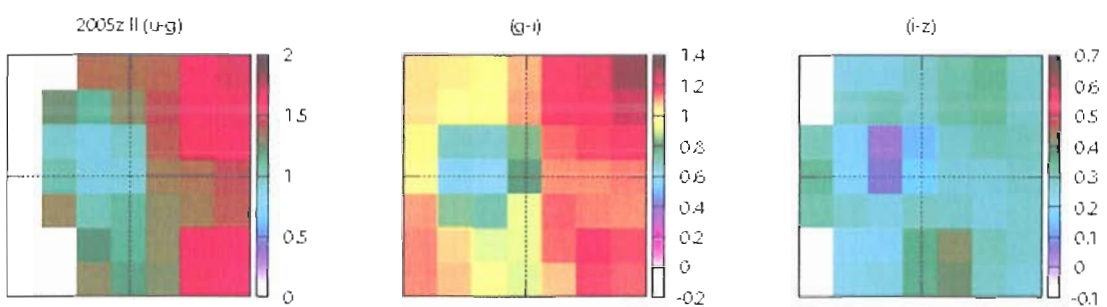


Figure 5.159. SN 2005z  $u-g$ ,  $g-i$ ,  $i-z$  spatial plots.

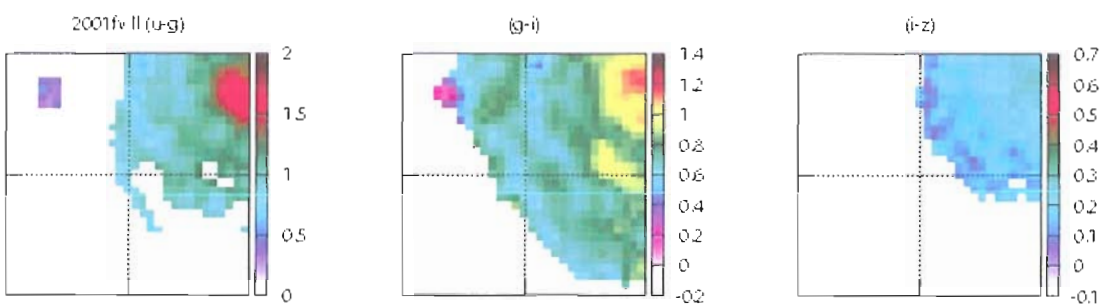


Figure 5.160. SN 2001fv  $u-g$ ,  $g-i$ ,  $i-z$  spatial plots.

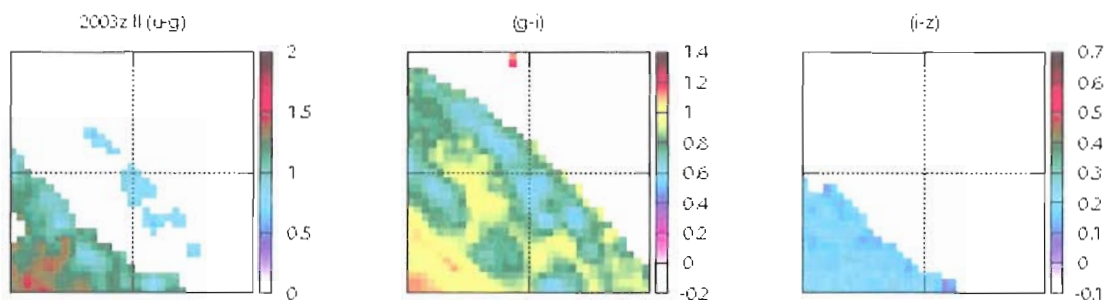


Figure 5.161. SN 2003z  $u-g$ ,  $g-i$ ,  $i-z$  spatial plots.

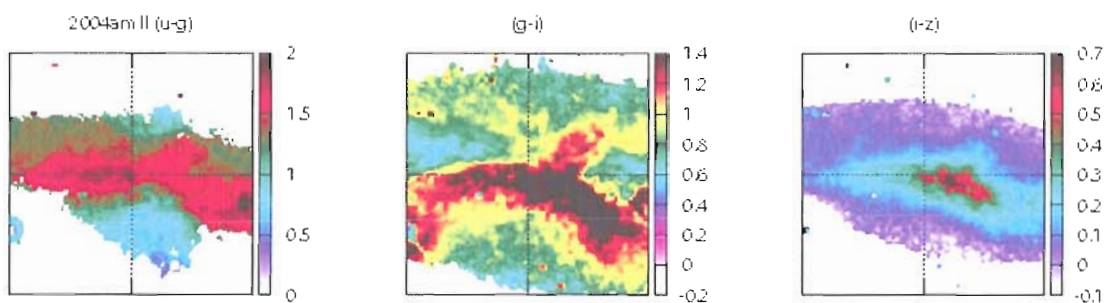


Figure 5.162. SN 2004am  $u-g$ ,  $g-i$ ,  $i-z$  spatial plots.

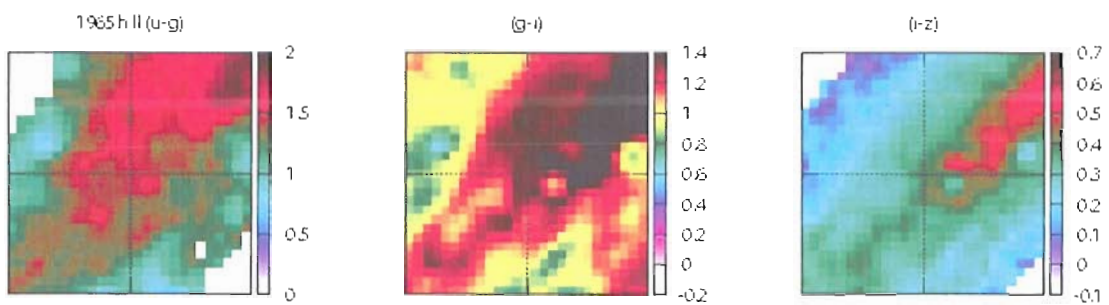


Figure 5.163. SN 1965h  $u-g$ ,  $g-i$ ,  $i-z$  spatial plots.

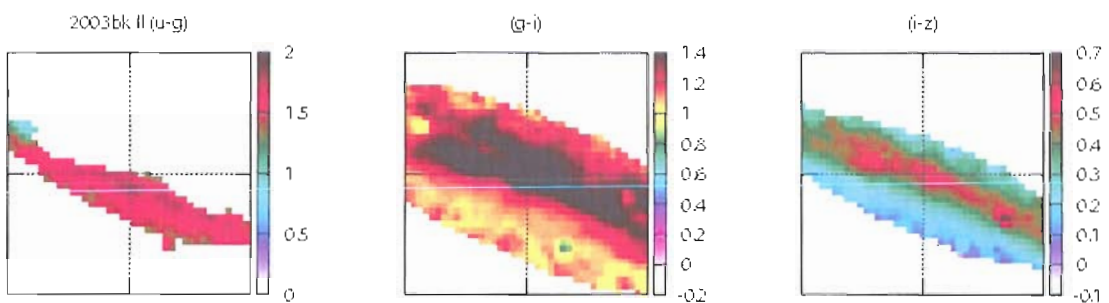
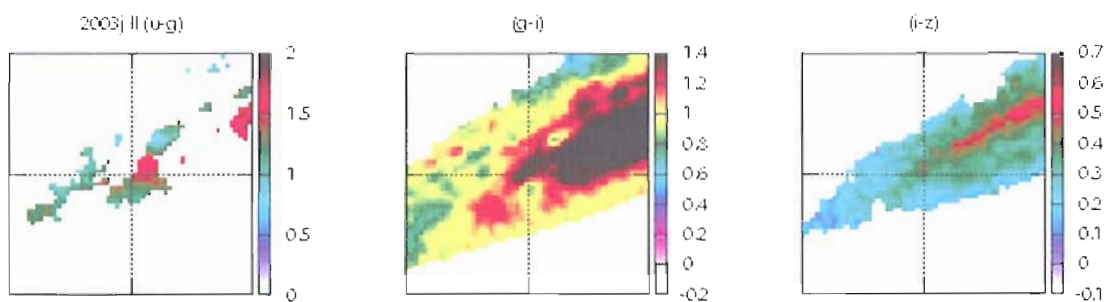
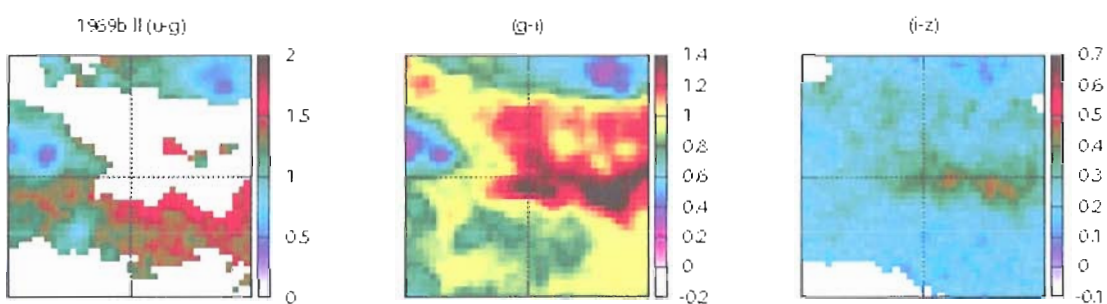
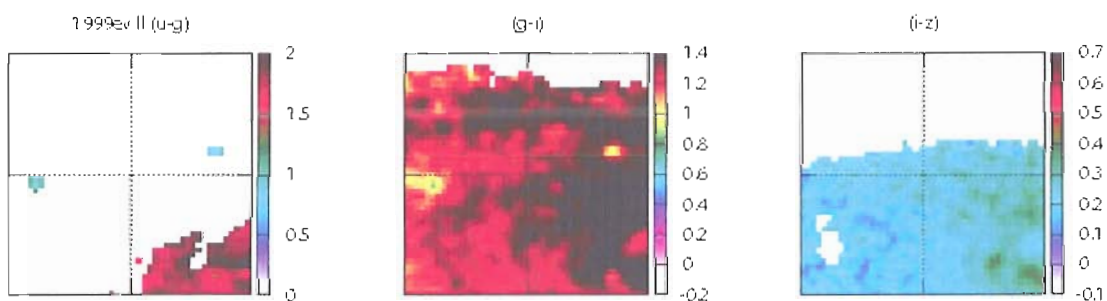
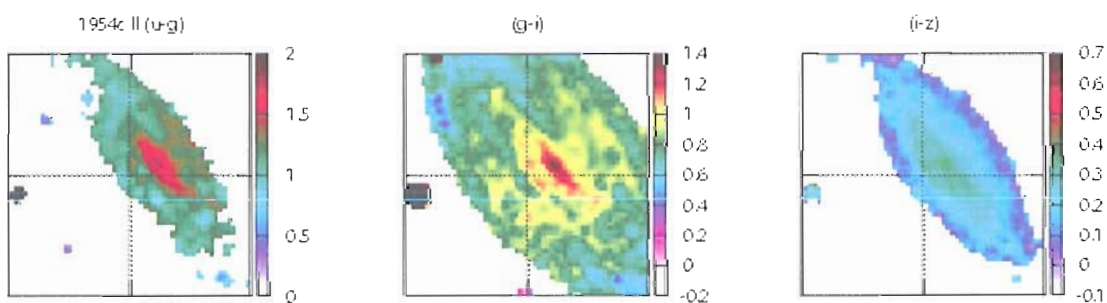


Figure 5.164. SN 2003bk  $u-g$ ,  $g-i$ ,  $i-z$  spatial plots.

Figure 5.165. SN 2003j  $u-g$ ,  $g-i$ ,  $i-z$  spatial plots.Figure 5.166. SN 1969b  $u-g$ ,  $g-i$ ,  $i-z$  spatial plots.Figure 5.167. SN 1999ev  $u-g$ ,  $g-i$ ,  $i-z$  spatial plots.Figure 5.168. SN 1954c  $u-g$ ,  $g-i$ ,  $i-z$  spatial plots.

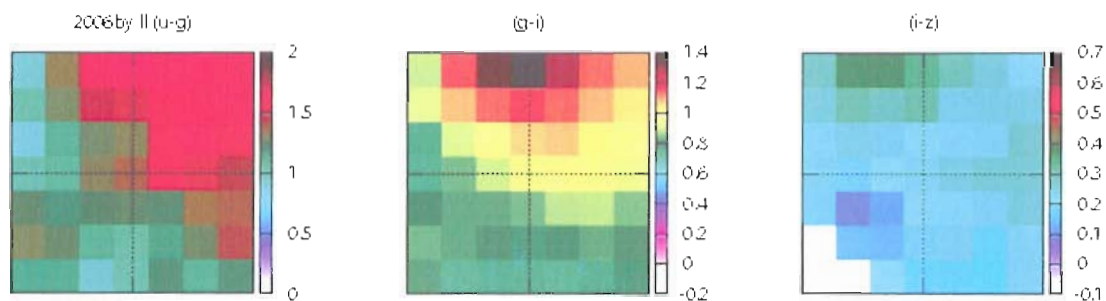


Figure 5.169. SN 2006by  $u-g$ ,  $g-i$ ,  $i-z$  spatial plots.

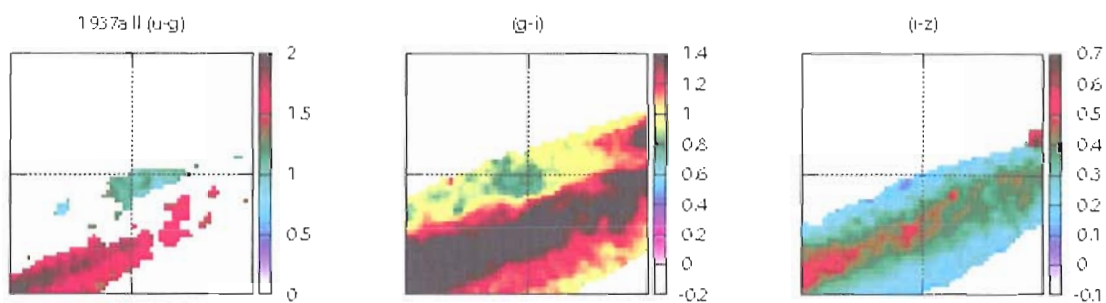


Figure 5.170. SN 1937a  $u-g$ ,  $g-i$ ,  $i-z$  spatial plots.

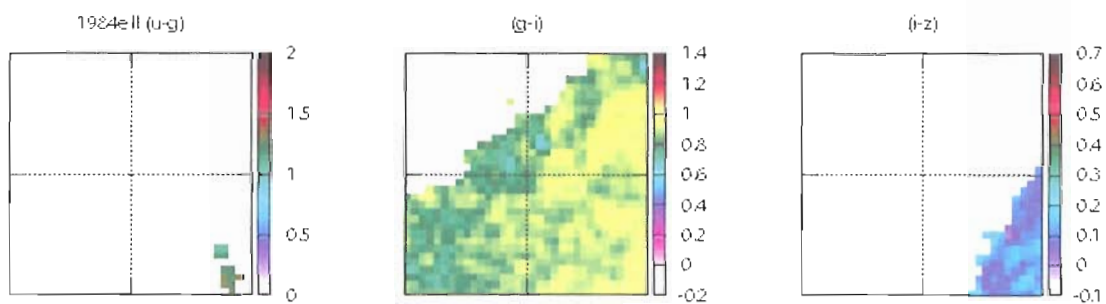


Figure 5.171. SN 1984e  $u-g$ ,  $g-i$ ,  $i-z$  spatial plots.

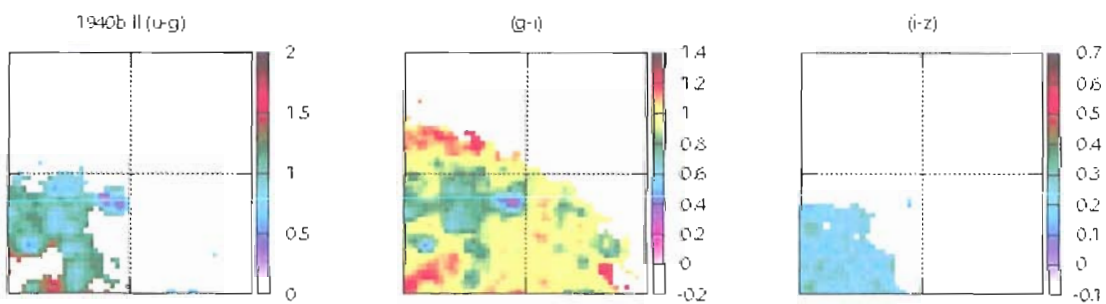


Figure 5.172. SN 1940b  $u-g$ ,  $g-i$ ,  $i-z$  spatial plots.

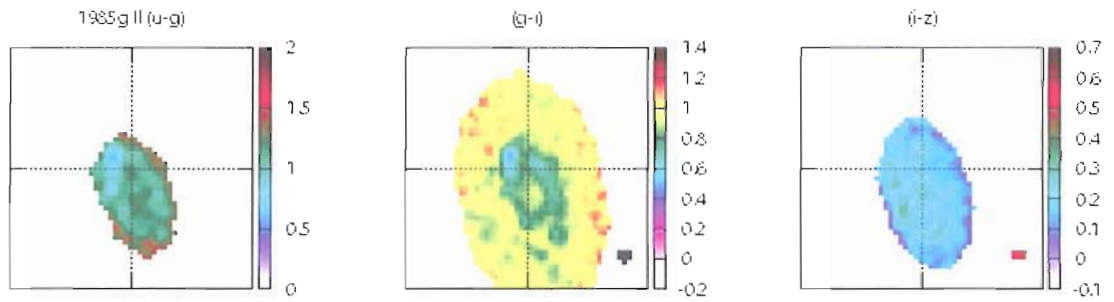


Figure 5.173. SN 1985g  $u-g$ ,  $g-i$ ,  $i-z$  spatial plots.

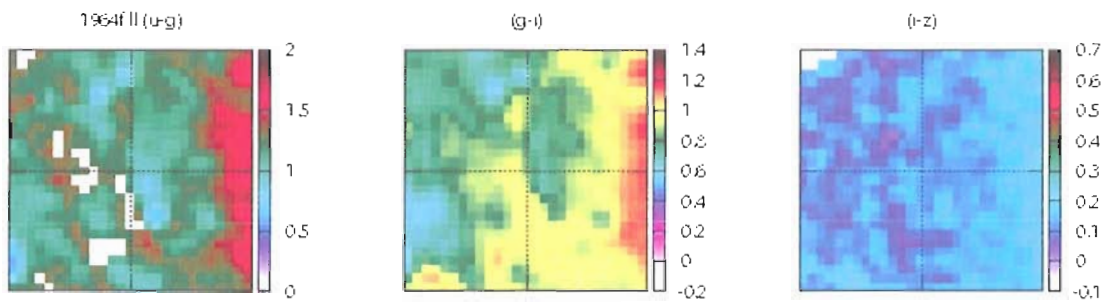


Figure 5.174. SN 1964f  $u-g$ ,  $g-i$ ,  $i-z$  spatial plots.

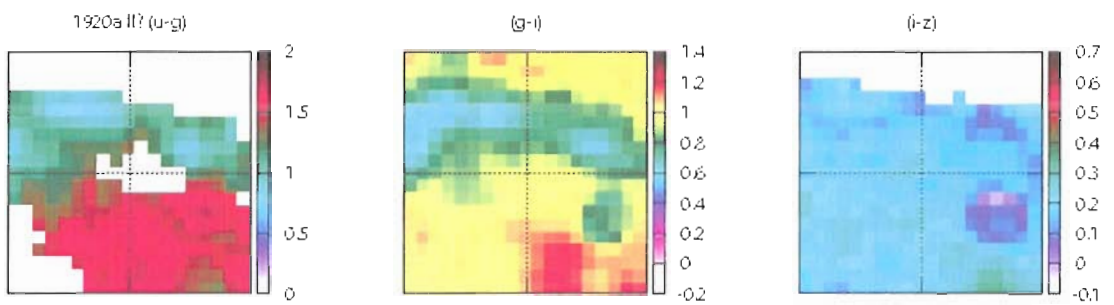


Figure 5.175. SN 1920a  $u-g$ ,  $g-i$ ,  $i-z$  spatial plots.

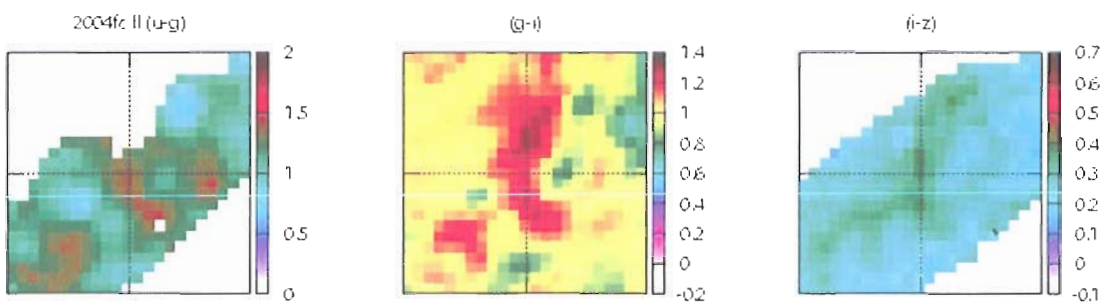


Figure 5.176. SN 2004fc  $u-g$ ,  $g-i$ ,  $i-z$  spatial plots.

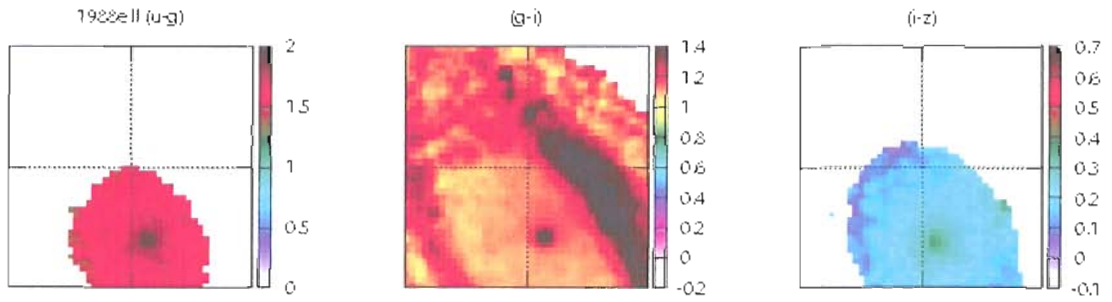


Figure 5.177. SN 1988e  $u-g$ ,  $g-i$ ,  $i-z$  spatial plots.

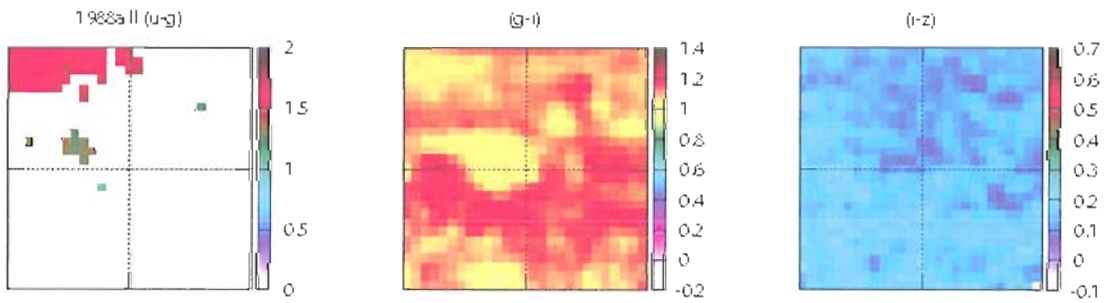


Figure 5.178. SN 1988a  $u-g$ ,  $g-i$ ,  $i-z$  spatial plots.

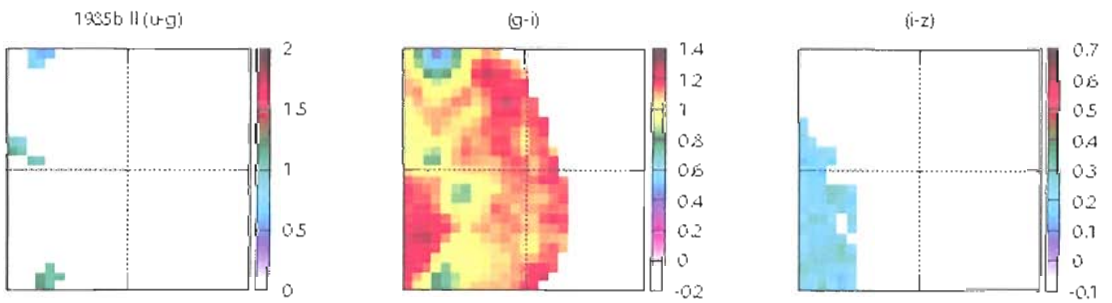


Figure 5.179. SN 1985b  $u-g$ ,  $g-i$ ,  $i-z$  spatial plots.

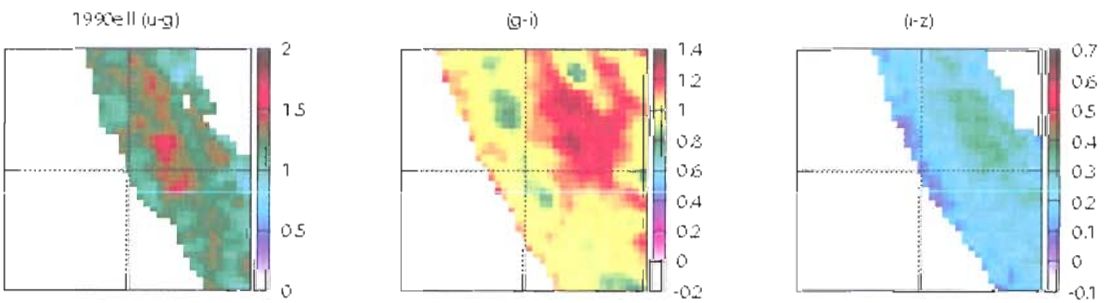
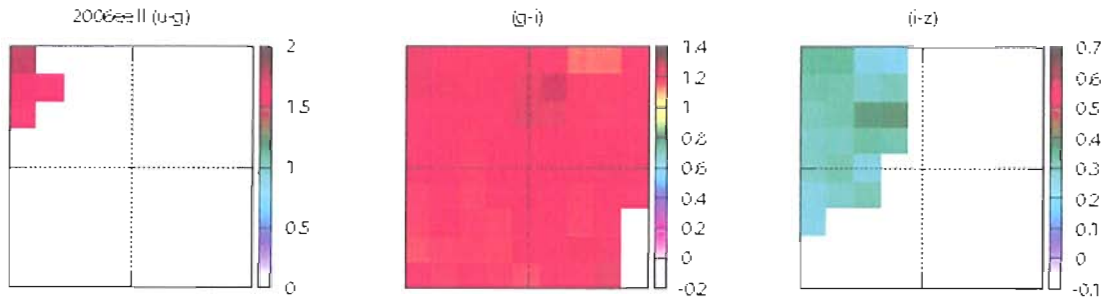
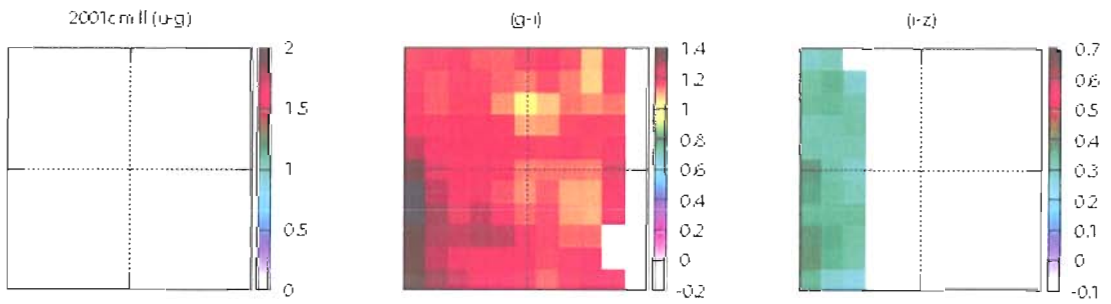
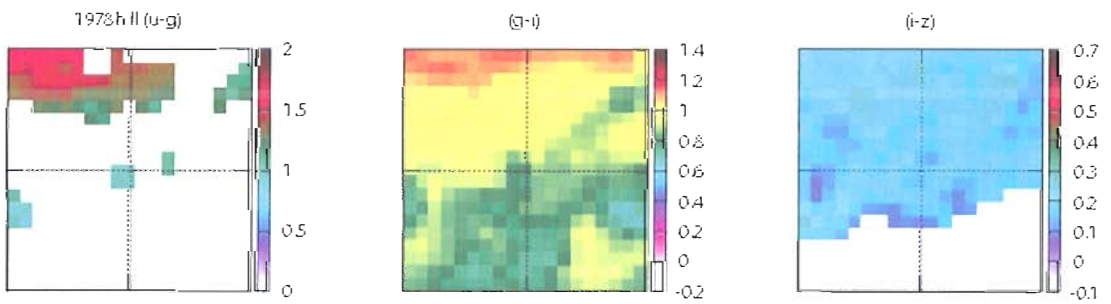
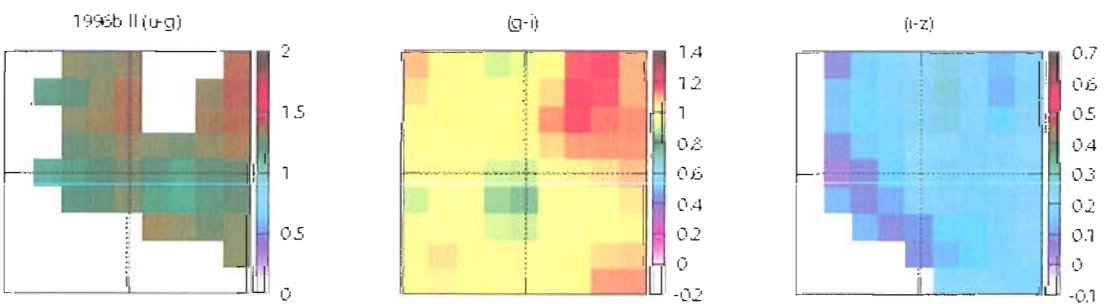
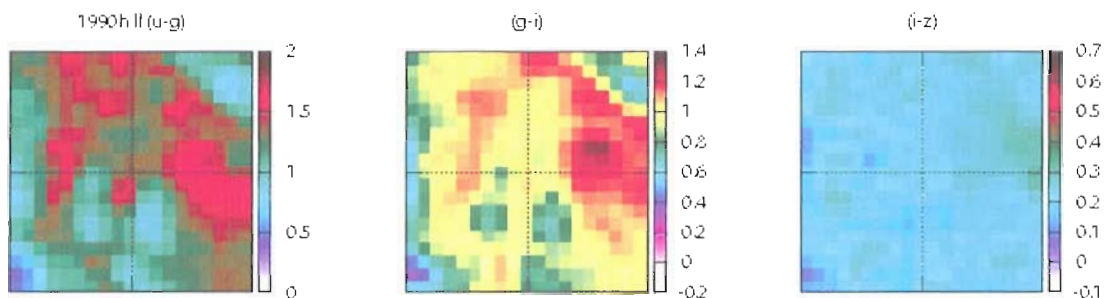
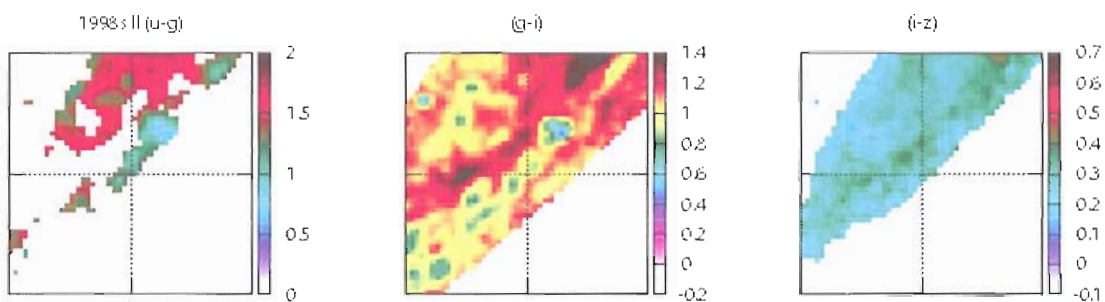
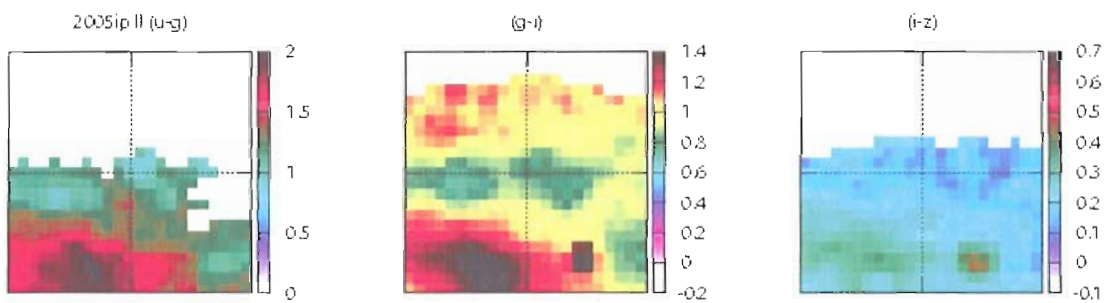
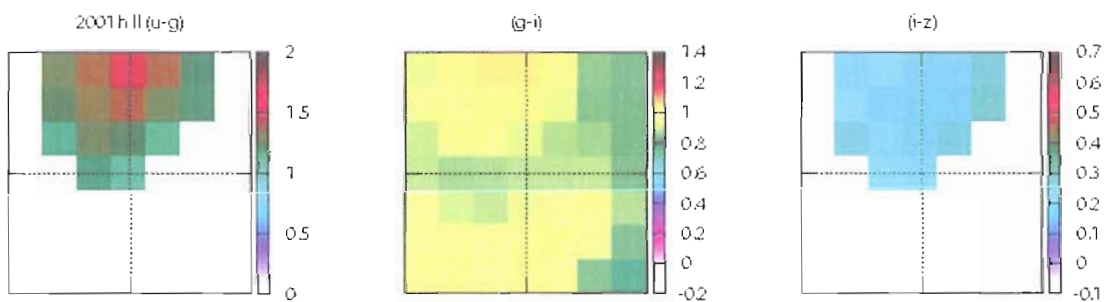


Figure 5.180. SN 1990e  $u-g$ ,  $g-i$ ,  $i-z$  spatial plots.

Figure 5.181. SN 2006ee  $u-g$ ,  $g-i$ ,  $i-z$  spatial plots.Figure 5.182. SN 2001cm  $u-g$ ,  $g-i$ ,  $i-z$  spatial plots.Figure 5.183. SN 1978h  $u-g$ ,  $g-i$ ,  $i-z$  spatial plots.Figure 5.184. SN 1996b  $u-g$ ,  $g-i$ ,  $i-z$  spatial plots.



Figure 5.185. SN 1990h  $u-g$ ,  $g-i$ ,  $i-z$  spatial plots.Figure 5.186. SN 1998s  $u-g$ ,  $g-i$ ,  $i-z$  spatial plots.Figure 5.187. SN 2005ip  $u-g$ ,  $g-i$ ,  $i-z$  spatial plots.Figure 5.188. SN 2001h  $u-g$ ,  $g-i$ ,  $i-z$  spatial plots.

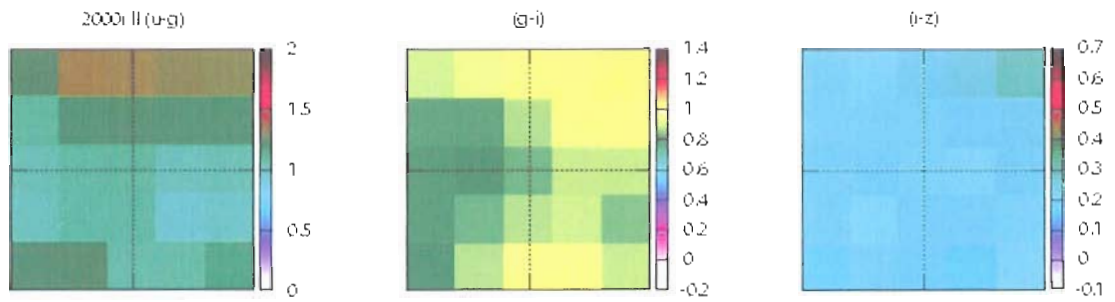


Figure 5.189. SN 2000i  $u-g$ ,  $g-i$ ,  $i-z$  spatial plots.

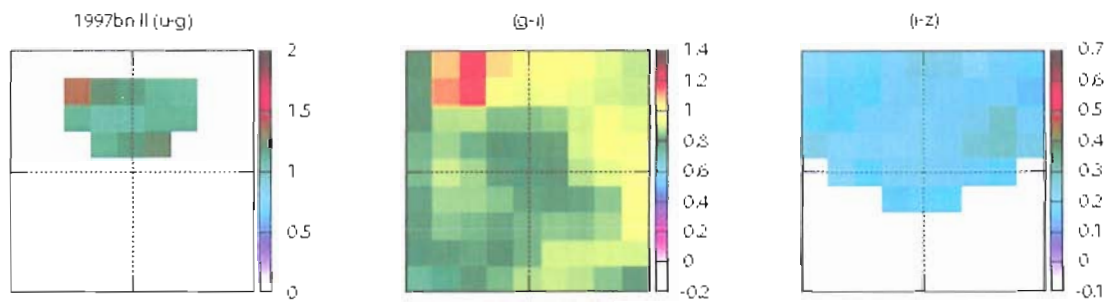


Figure 5.190. SN 1997bn  $u-g$ ,  $g-i$ ,  $i-z$  spatial plots.

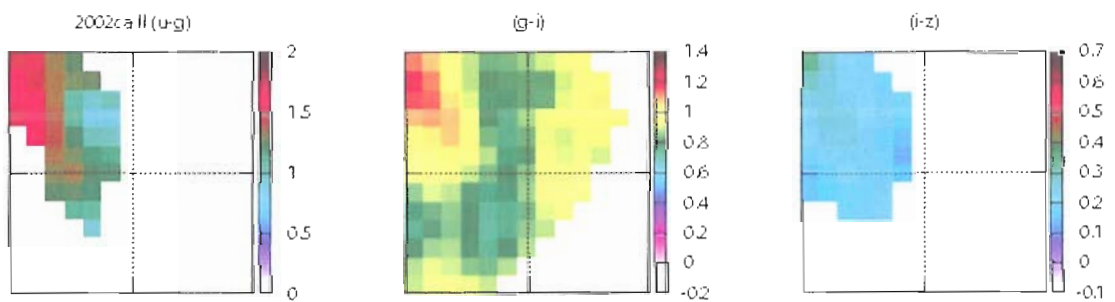


Figure 5.191. SN 2002ca  $u-g$ ,  $g-i$ ,  $i-z$  spatial plots.

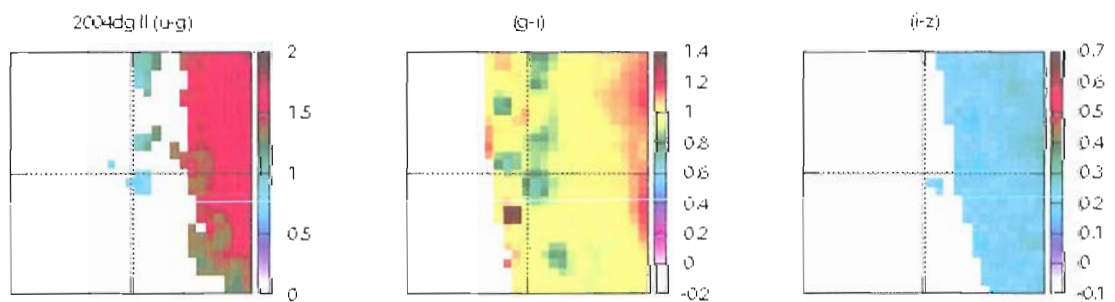
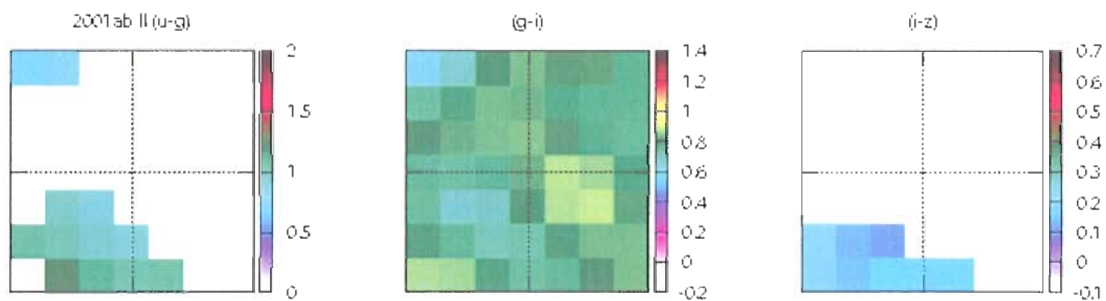
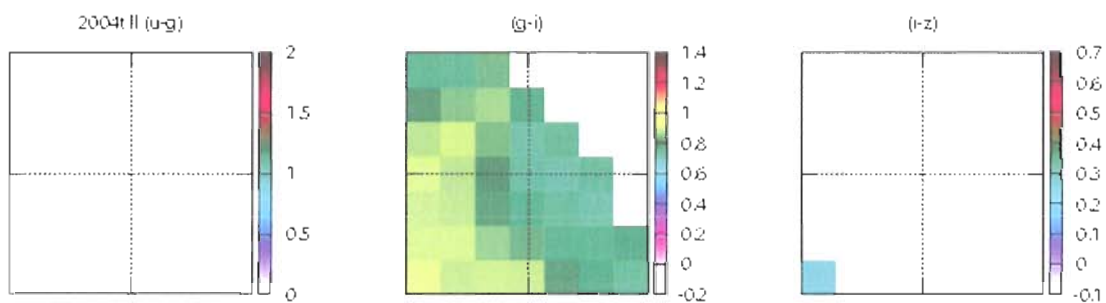
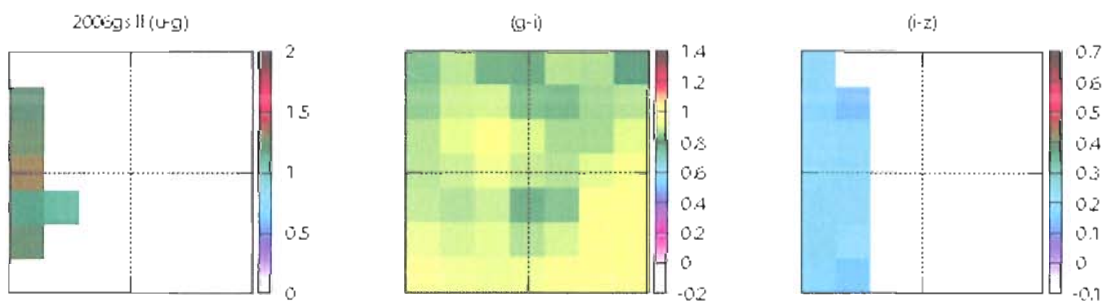
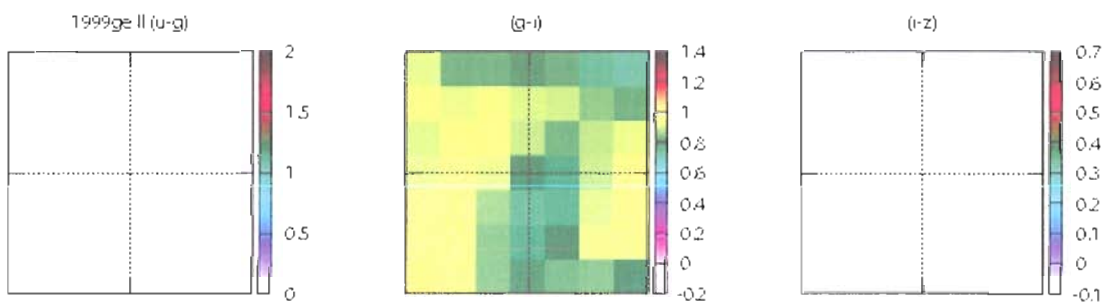
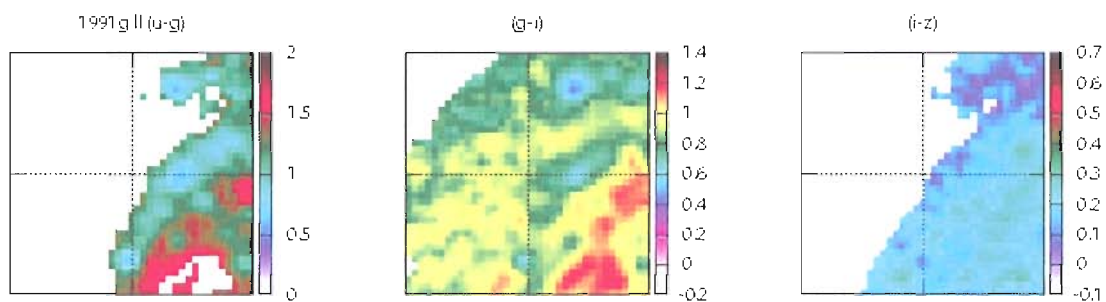
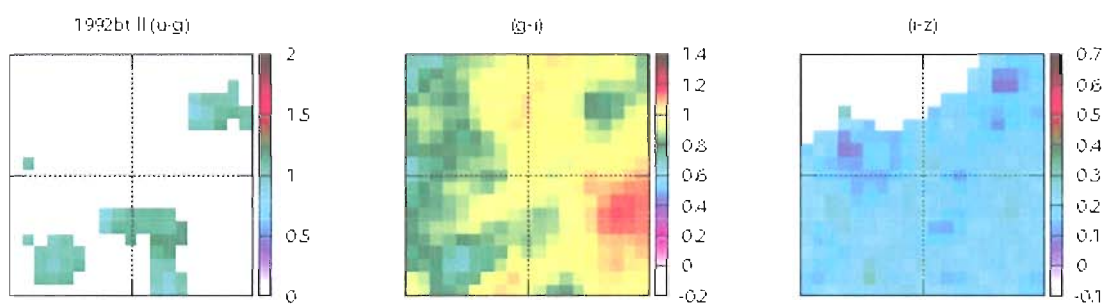
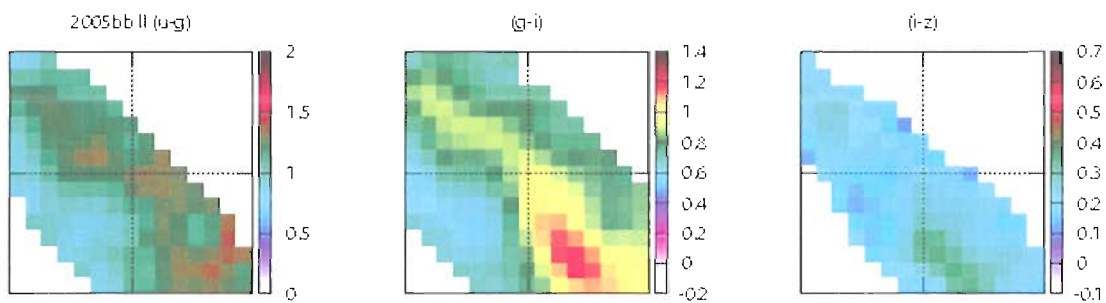
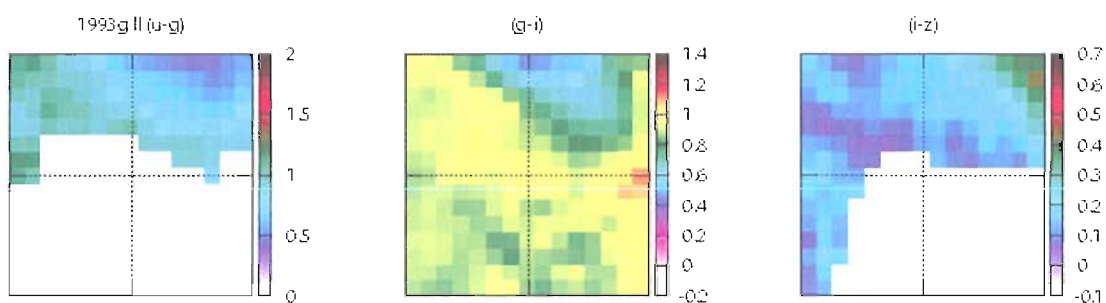
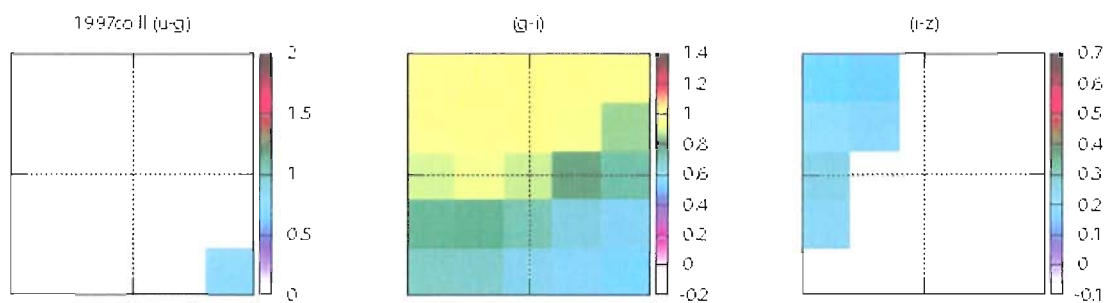
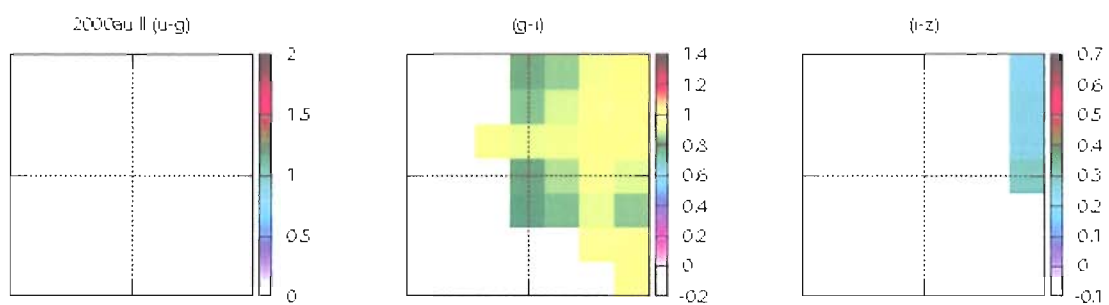
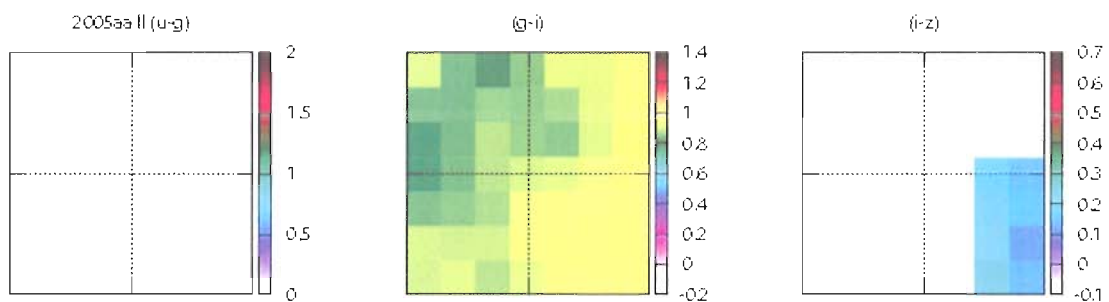
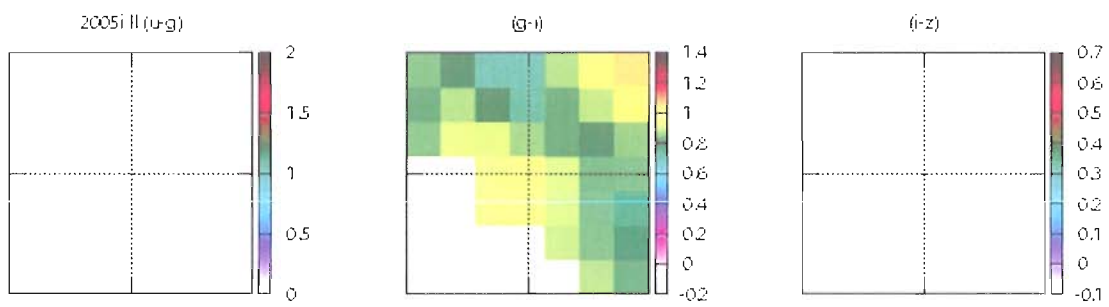
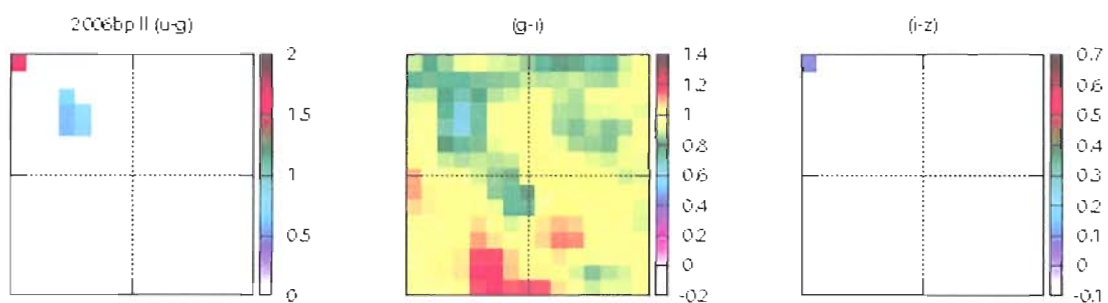
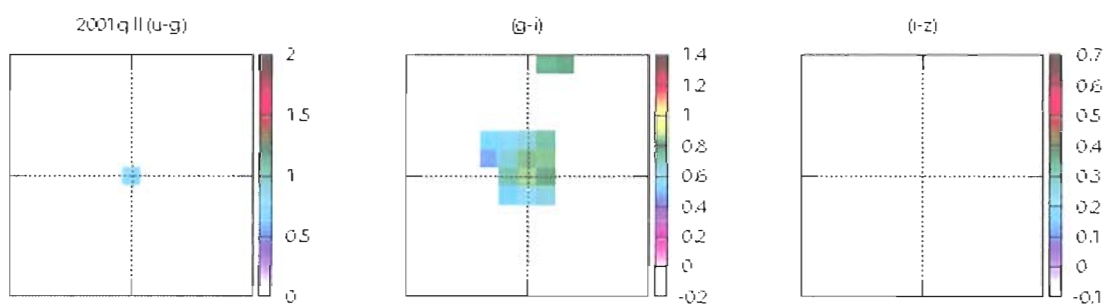
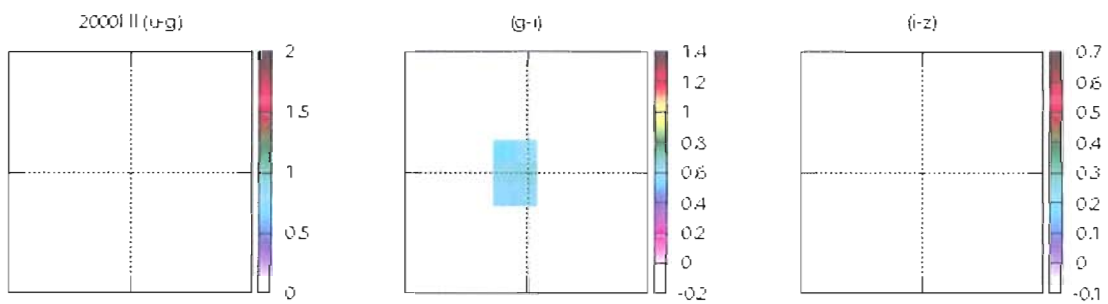
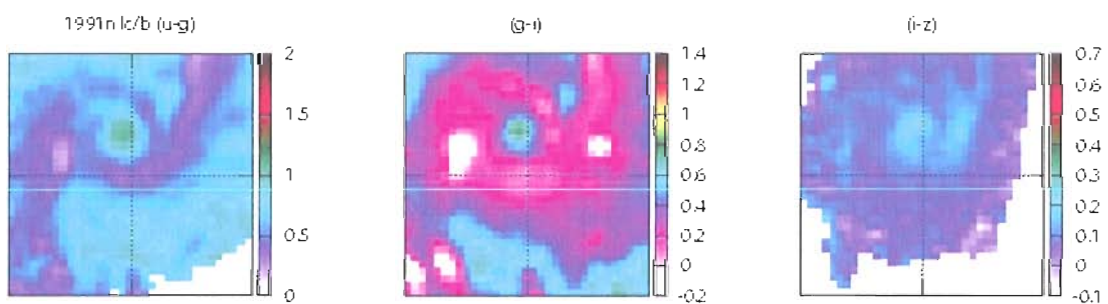


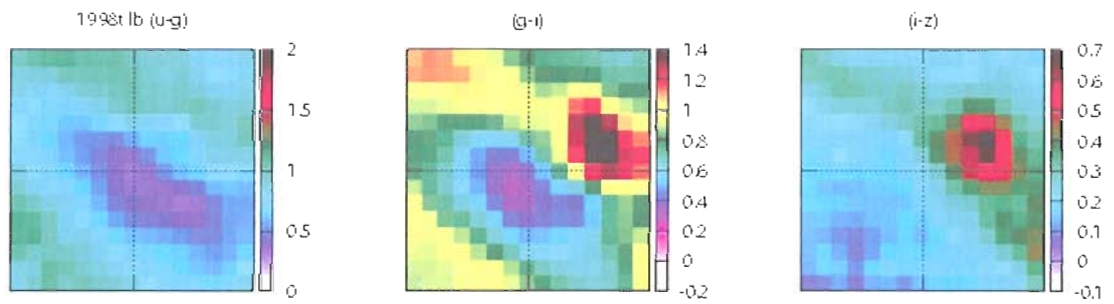
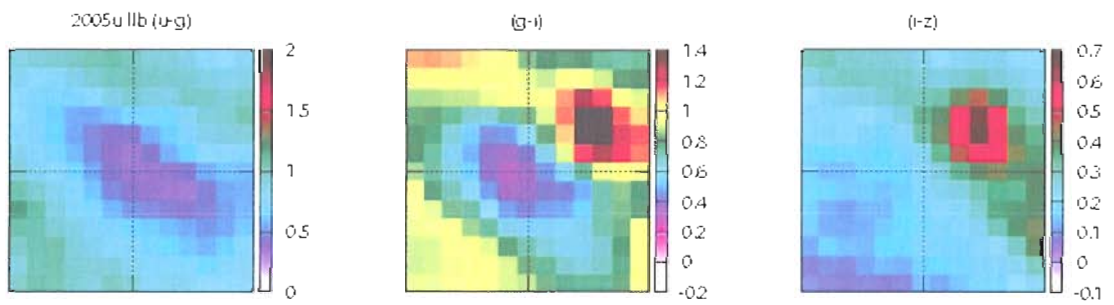
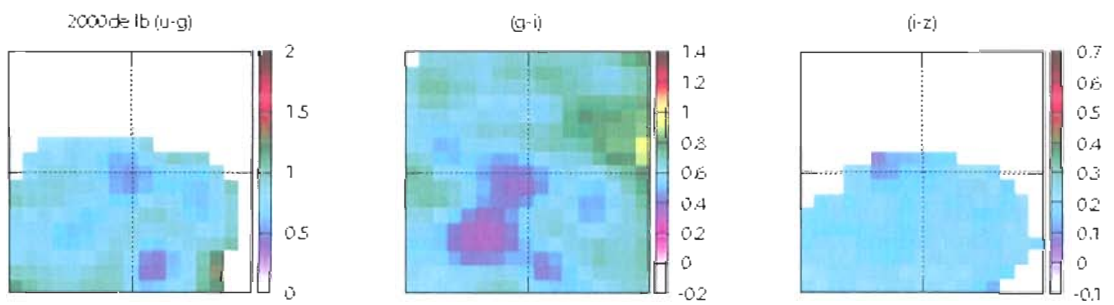
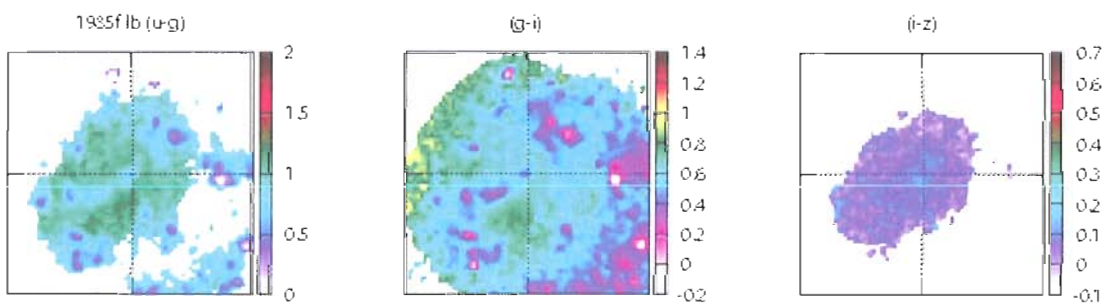
Figure 5.192. SN 2004dg  $u-g$ ,  $g-i$ ,  $i-z$  spatial plots.

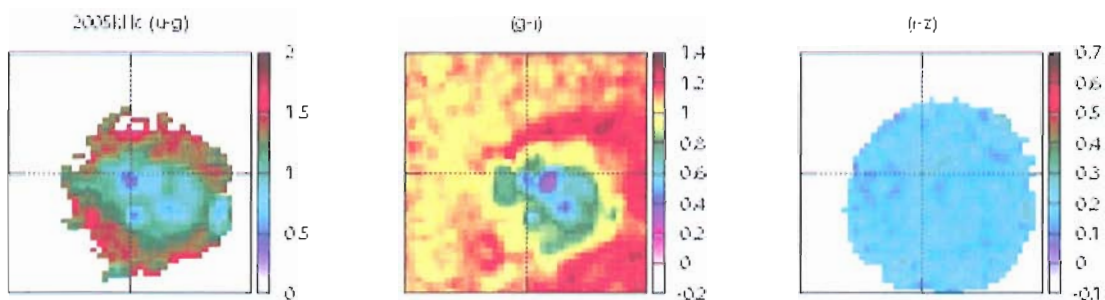
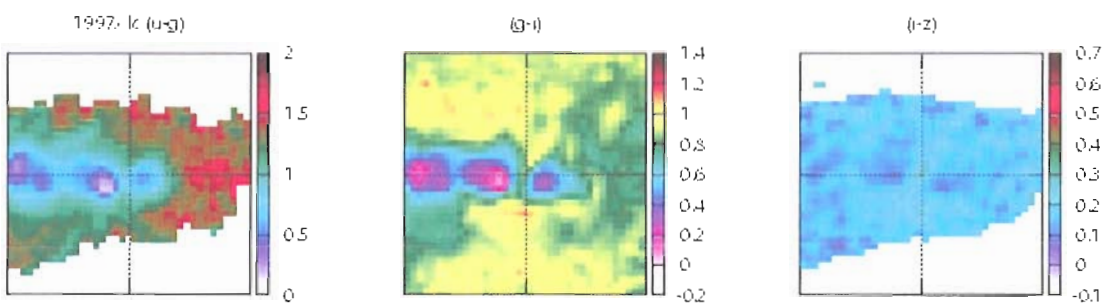
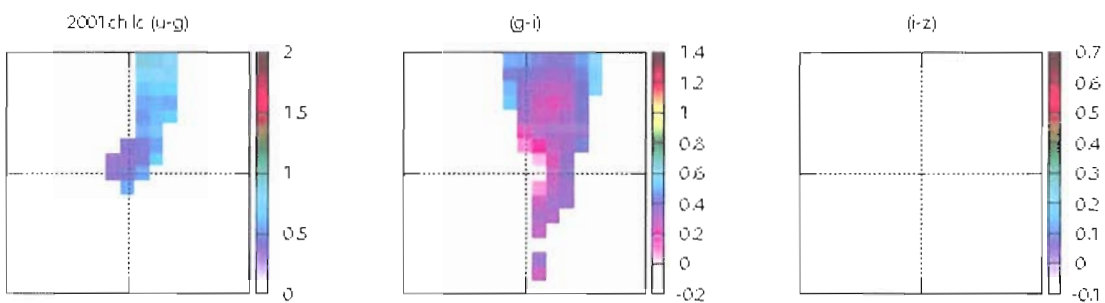
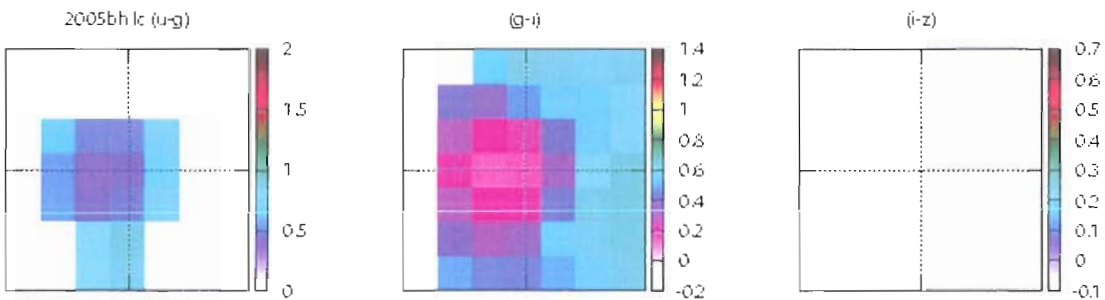
Figure 5.193. SN 2001ab  $u-g$ ,  $g-i$ ,  $i-z$  spatial plots.Figure 5.194. SN 2004t  $u-g$ ,  $g-i$ ,  $i-z$  spatial plots.Figure 5.195. SN 2006gs  $u-g$ ,  $g-i$ ,  $i-z$  spatial plots.Figure 5.196. SN 1999ge  $u-g$ ,  $g-i$ ,  $i-z$  spatial plots.

Figure 5.197. SN 1991g  $u-g$ ,  $g-i$ ,  $i-z$  spatial plots.Figure 5.198. SN 1992bt  $u-g$ ,  $g-i$ ,  $i-z$  spatial plots.Figure 5.199. SN 2005bb  $u-g$ ,  $g-i$ ,  $i-z$  spatial plots.Figure 5.200. SN 1993g  $u-g$ ,  $g-i$ ,  $i-z$  spatial plots.

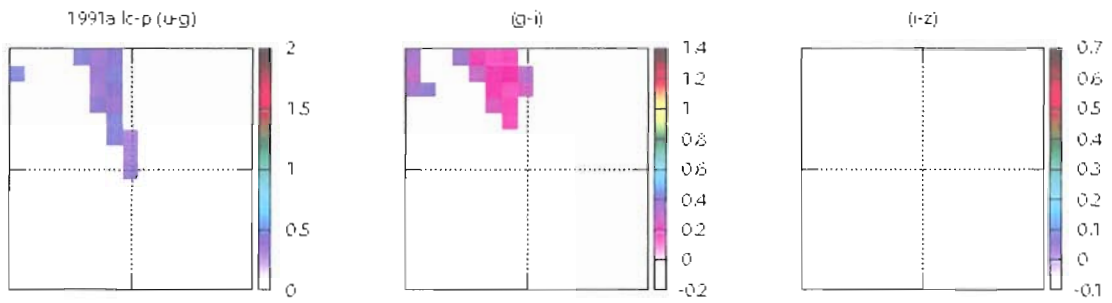
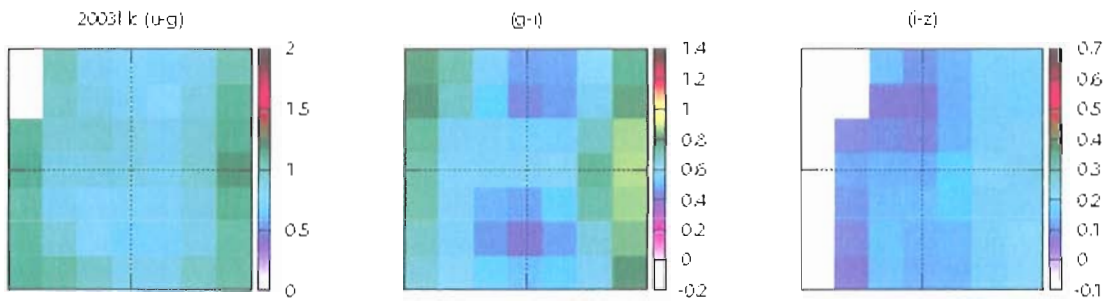
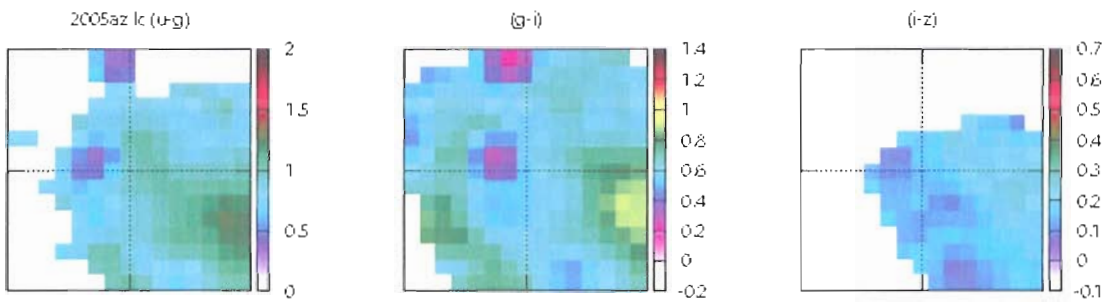
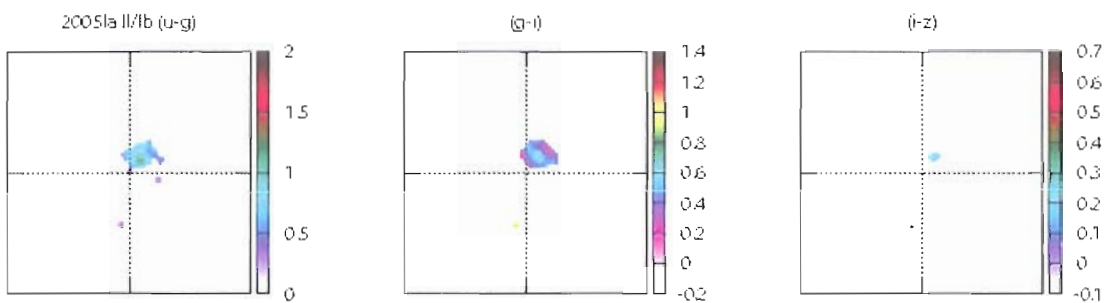
Figure 5.201. SN 1997co  $u-g$ ,  $g-i$ ,  $i-z$  spatial plots.Figure 5.202. SN 2000au  $u-g$ ,  $g-i$ ,  $i-z$  spatial plots.Figure 5.203. SN 2005aa  $u-g$ ,  $g-i$ ,  $i-z$  spatial plots.Figure 5.204. SN 2005i  $u-g$ ,  $g-i$ ,  $i-z$  spatial plots.

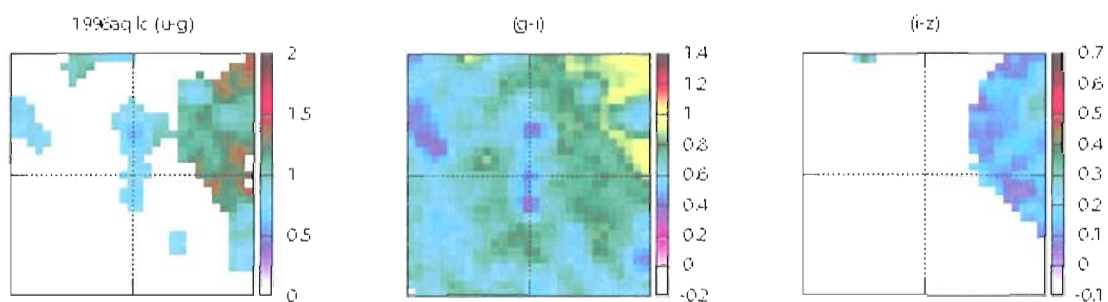
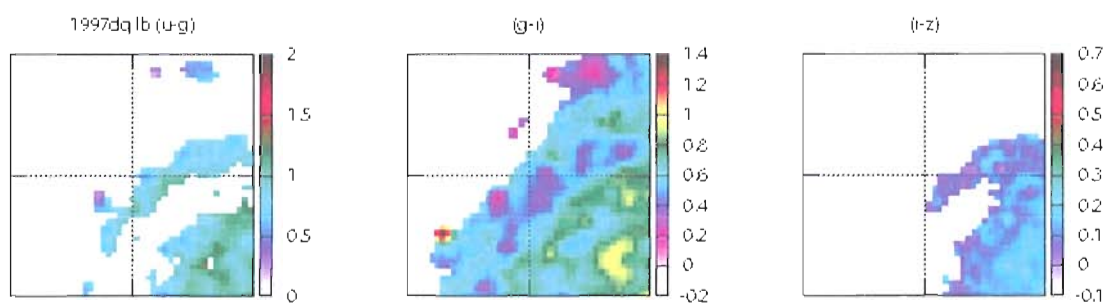
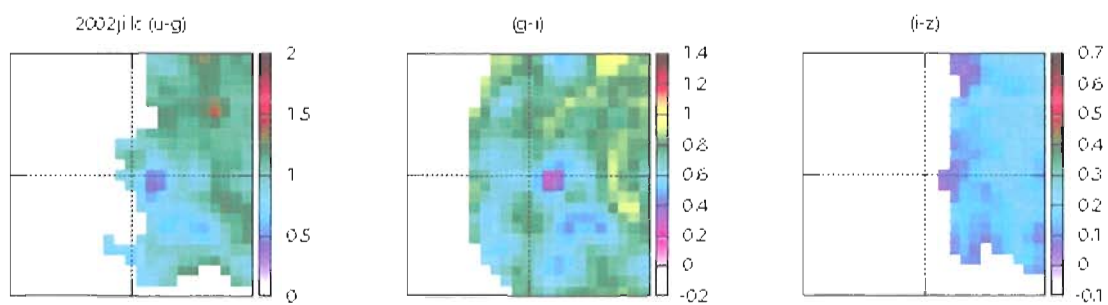
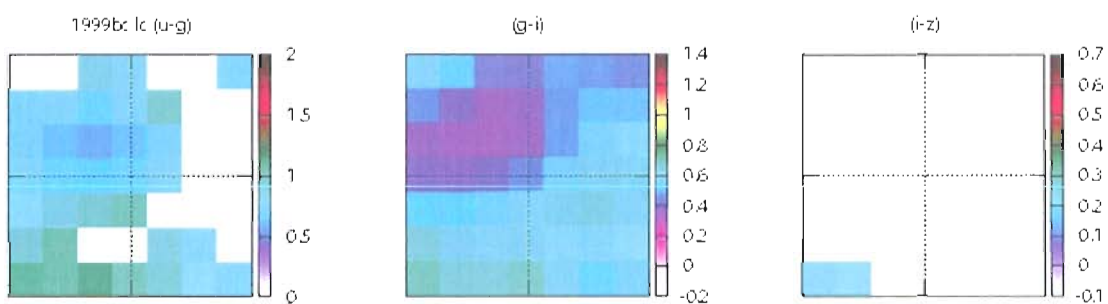
Figure 5.205. SN 2006bp  $u-g$ ,  $g-i$ ,  $i-z$  spatial plots.Figure 5.206. SN 2001q  $u-g$ ,  $g-i$ ,  $i-z$  spatial plots.Figure 5.207. SN 2000I  $u-g$ ,  $g-i$ ,  $i-z$  spatial plots.Figure 5.208. SN 1991n  $u-g$ ,  $g-i$ ,  $i-z$  spatial plots.

Figure 5.209. SN 1998t  $u-g$ ,  $g-i$ ,  $i-z$  spatial plots.Figure 5.210. SN 2005u  $u-g$ ,  $g-i$ ,  $i-z$  spatial plots.Figure 5.211. SN 2000de  $u-g$ ,  $g-i$ ,  $i-z$  spatial plots.Figure 5.212. SN 1985f  $u-g$ ,  $g-i$ ,  $i-z$  spatial plots.

Figure 5.213. SN 2005kl  $u-g$ ,  $g-i$ ,  $i-z$  spatial plots.Figure 5.214. SN 1997x  $u-g$ ,  $g-i$ ,  $i-z$  spatial plots.Figure 5.215. SN 2001ch  $u-g$ ,  $g-i$ ,  $i-z$  spatial plots.Figure 5.216. SN 2005bh  $u-g$ ,  $g-i$ ,  $i-z$  spatial plots.



Figure 5.217. SN 1991a  $u-g$ ,  $g-i$ ,  $i-z$  spatial plots.Figure 5.218. SN 2003l  $u-g$ ,  $g-i$ ,  $i-z$  spatial plots.Figure 5.219. SN 2005az  $u-g$ ,  $g-i$ ,  $i-z$  spatial plots.Figure 5.220. SN 2005la  $u-g$ ,  $g-i$ ,  $i-z$  spatial plots.

Figure 5.221. SN 1996aq  $u-g$ ,  $g-i$ ,  $i-z$  spatial plots.Figure 5.222. SN 1997dq  $u-g$ ,  $g-i$ ,  $i-z$  spatial plots.Figure 5.223. SN 2002ji  $u-g$ ,  $g-i$ ,  $i-z$  spatial plots.Figure 5.224. SN 1999bc  $u-g$ ,  $g-i$ ,  $i-z$  spatial plots.

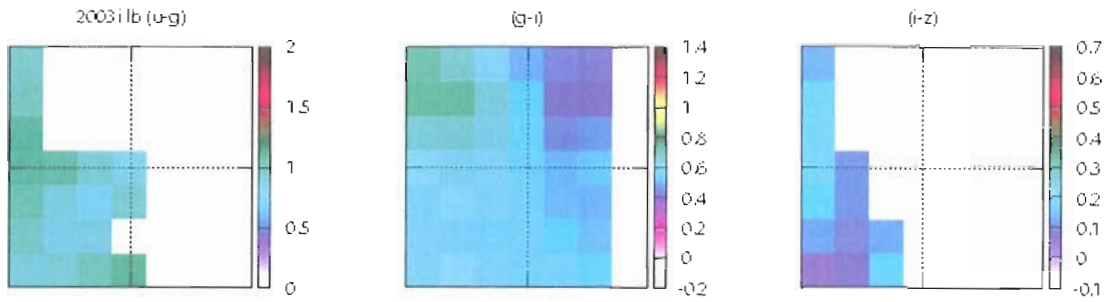


Figure 5.225. SN 2003i  $u-g$ ,  $g-i$ ,  $i-z$  spatial plots.

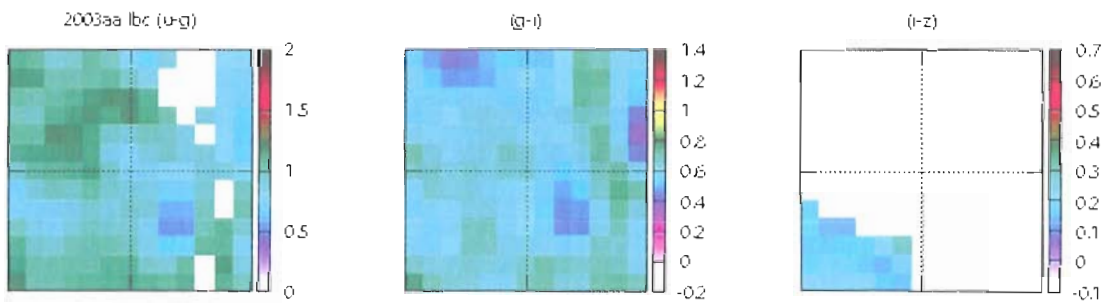


Figure 5.226. SN 2003aa  $u-g$ ,  $g-i$ ,  $i-z$  spatial plots.

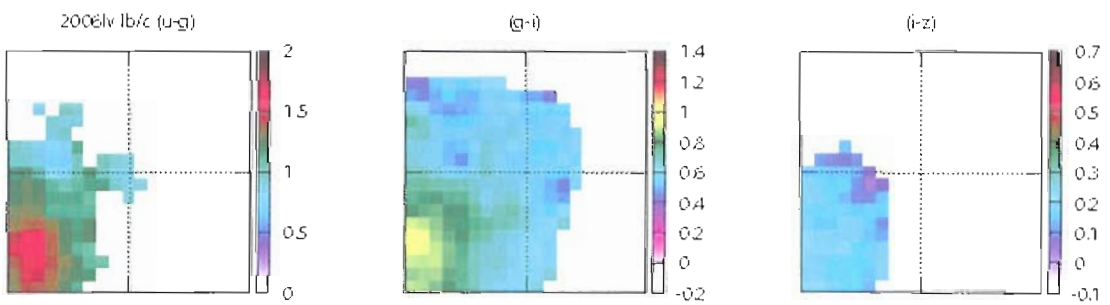


Figure 5.227. SN 2006lv  $u-g$ ,  $g-i$ ,  $i-z$  spatial plots.

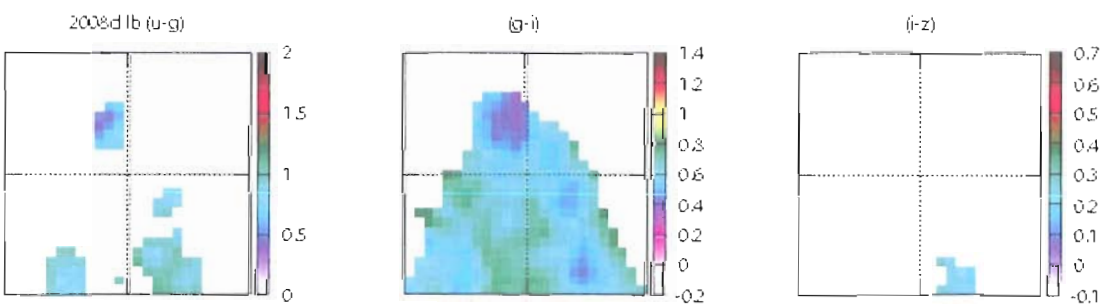


Figure 5.228. SN 2008d  $u-g$ ,  $g-i$ ,  $i-z$  spatial plots.

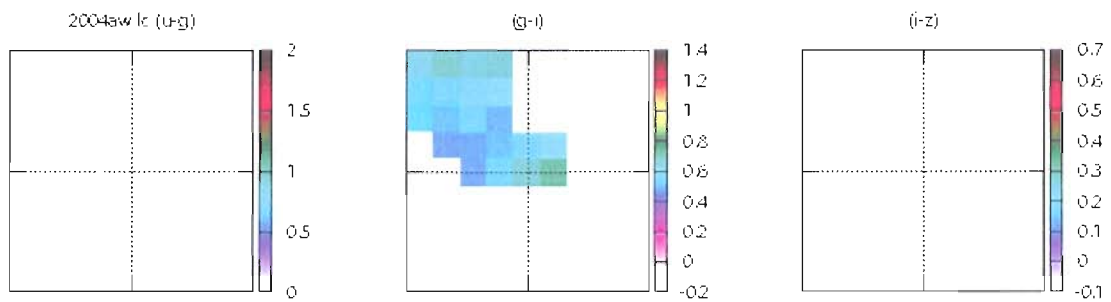


Figure 5.229. SN 2004aw  $u-g$ ,  $g-i$ ,  $i-z$  spatial plots.

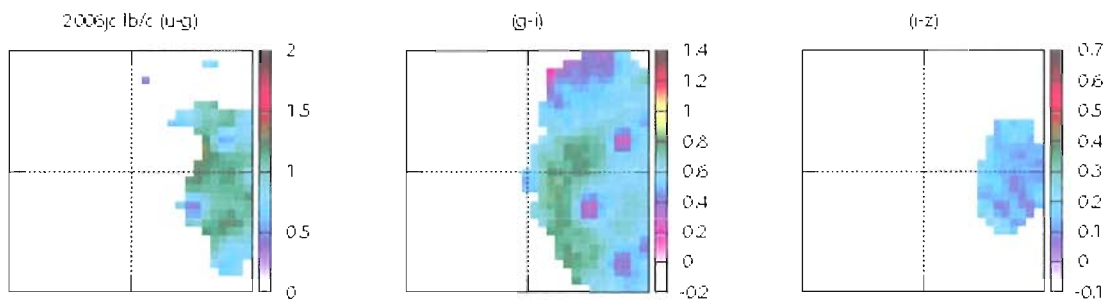


Figure 5.230. SN 2006jc  $u-g$ ,  $g-i$ ,  $i-z$  spatial plots.

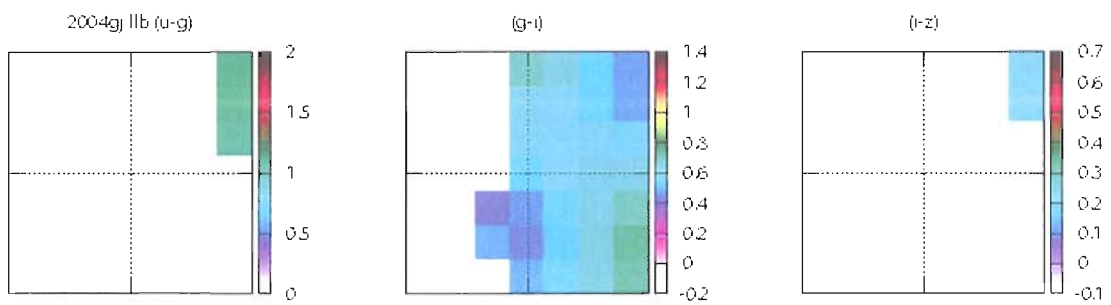


Figure 5.231. SN 2004gj  $u-g$ ,  $g-i$ ,  $i-z$  spatial plots.

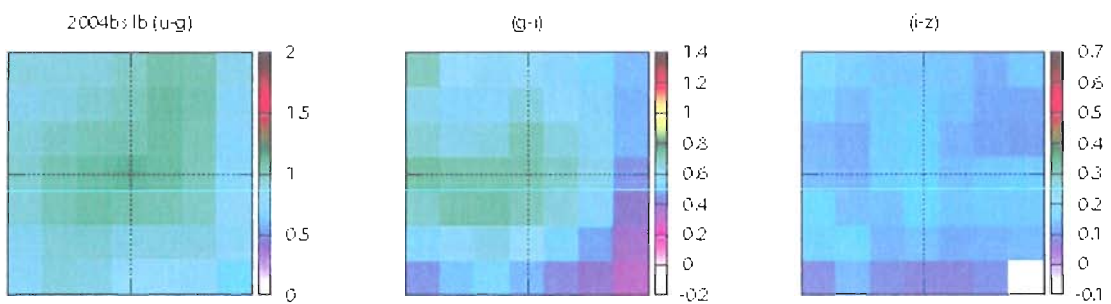


Figure 5.232. SN 2004bs  $u-g$ ,  $g-i$ ,  $i-z$  spatial plots.

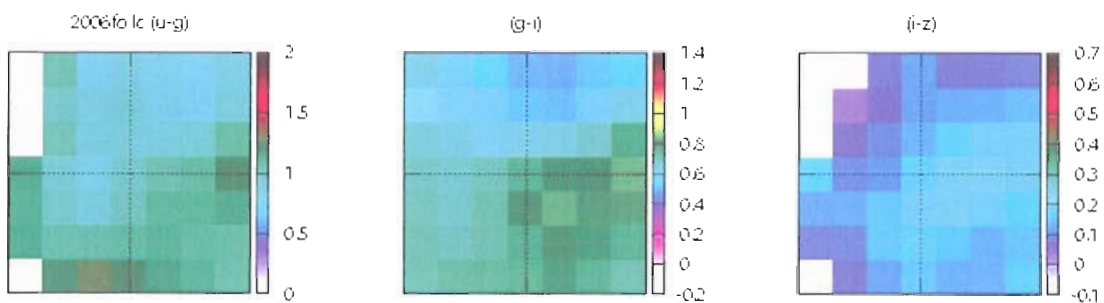


Figure 5.233. SN 2006fo  $u-g$ ,  $g-i$ ,  $i-z$  spatial plots.

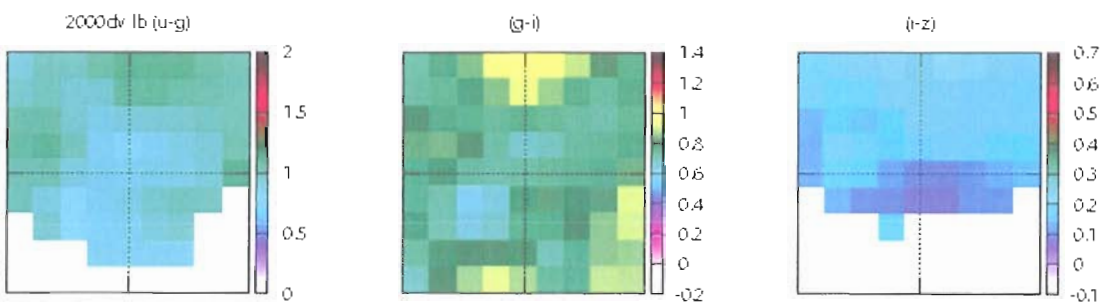


Figure 5.234. SN 2000dv  $u-g$ ,  $g-i$ ,  $i-z$  spatial plots.

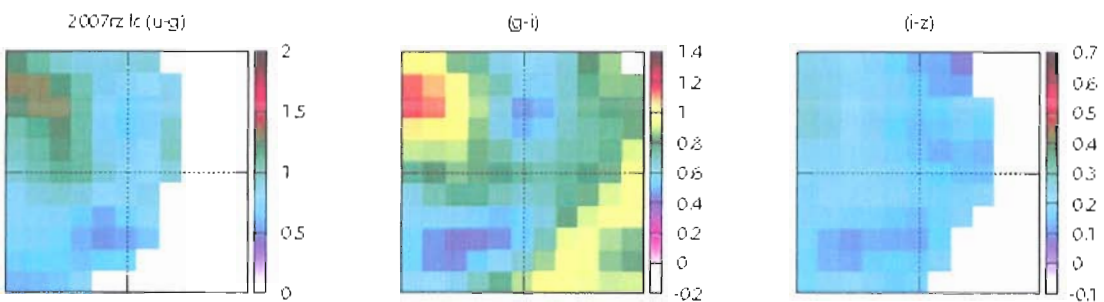


Figure 5.235. SN 2007rz  $u-g$ ,  $g-i$ ,  $i-z$  spatial plots.

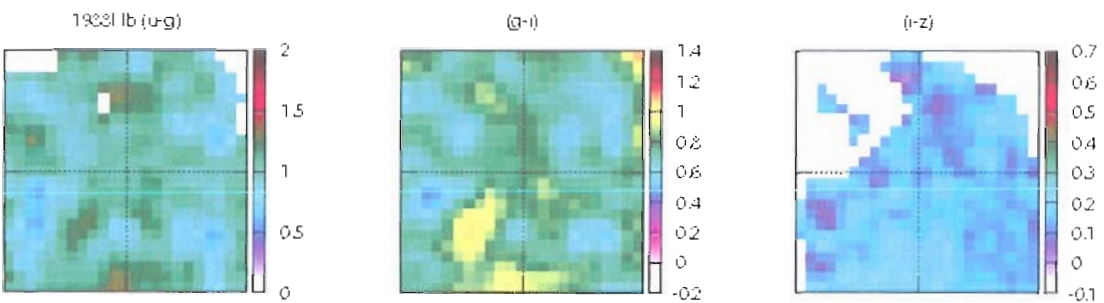


Figure 5.236. SN 1988l  $u-g$ ,  $g-i$ ,  $i-z$  spatial plots.

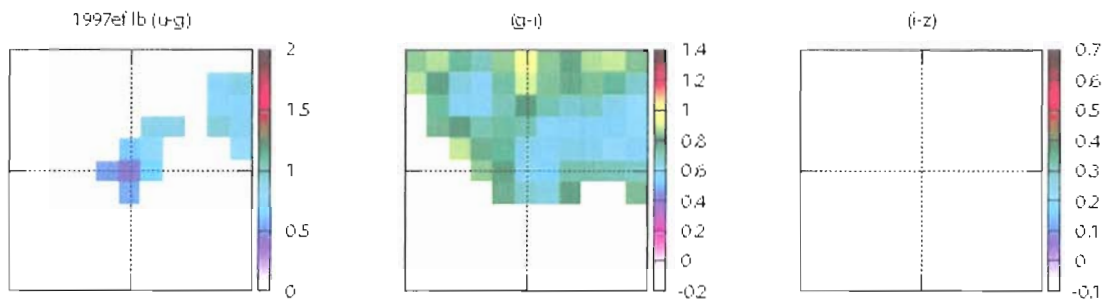


Figure 5.237. SN 1997ef  $u-g$ ,  $g-i$ ,  $i-z$  spatial plots.

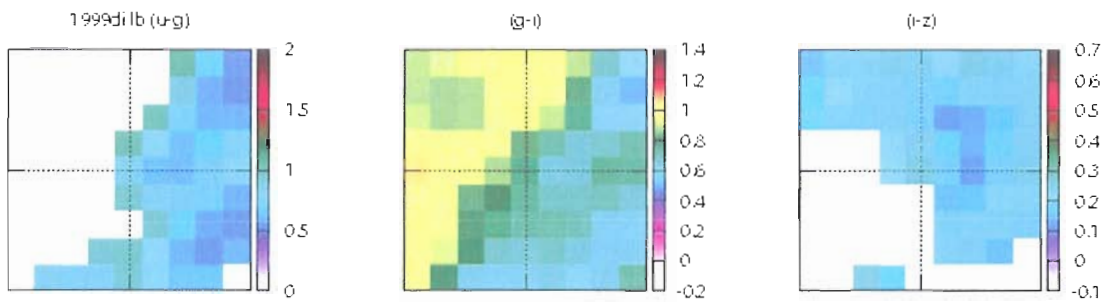


Figure 5.238. SN 1999di  $u-g$ ,  $g-i$ ,  $i-z$  spatial plots.

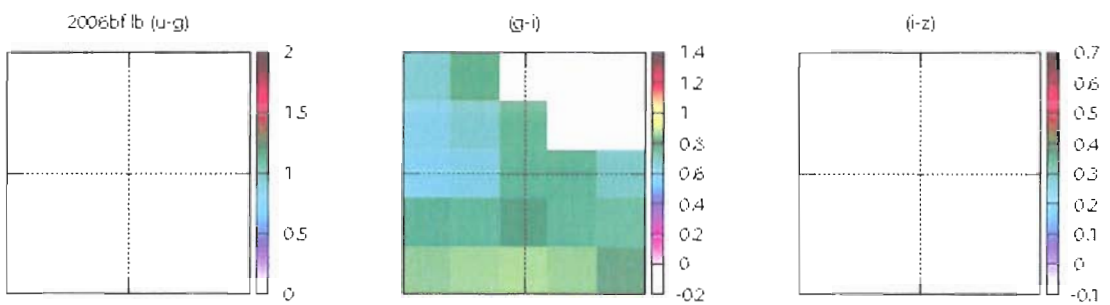


Figure 5.239. SN 2006bf  $u-g$ ,  $g-i$ ,  $i-z$  spatial plots.

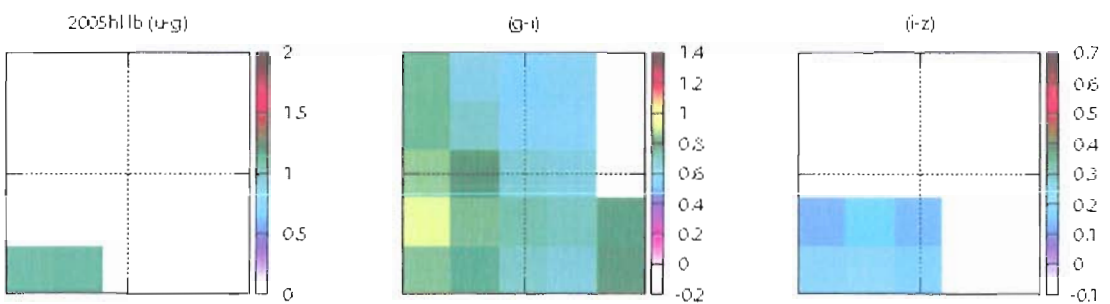
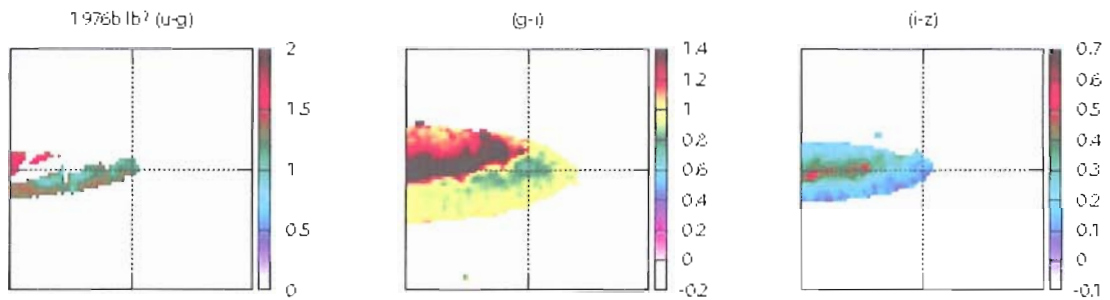
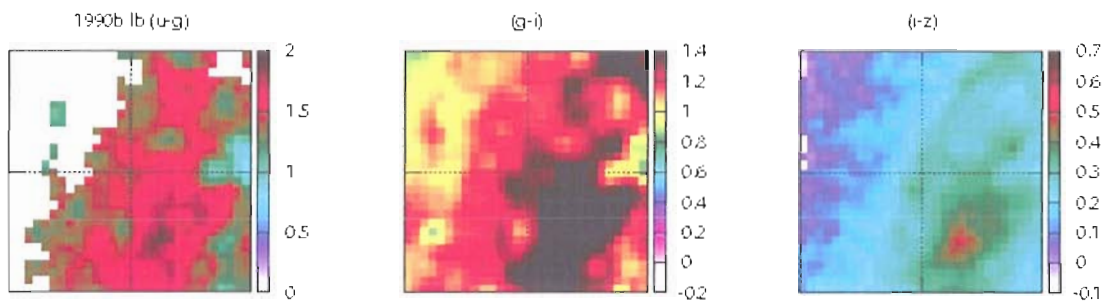
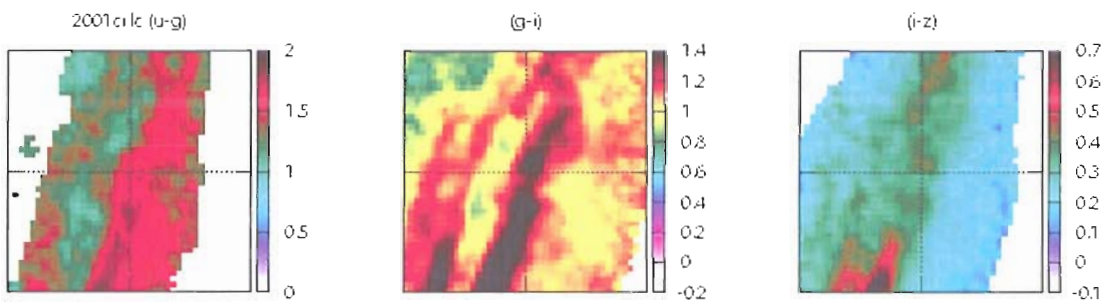
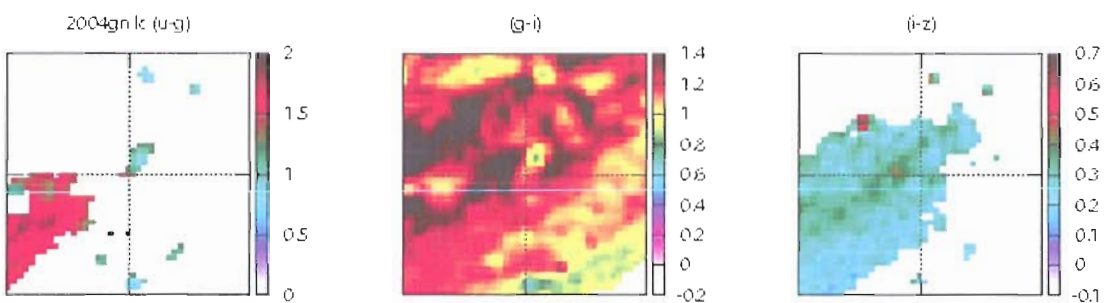
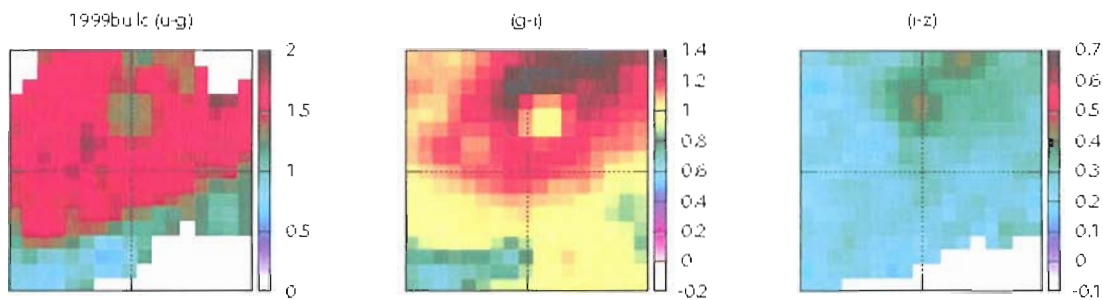
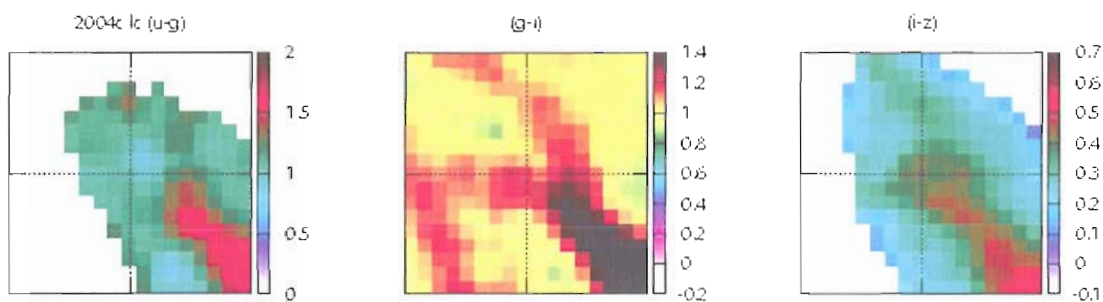
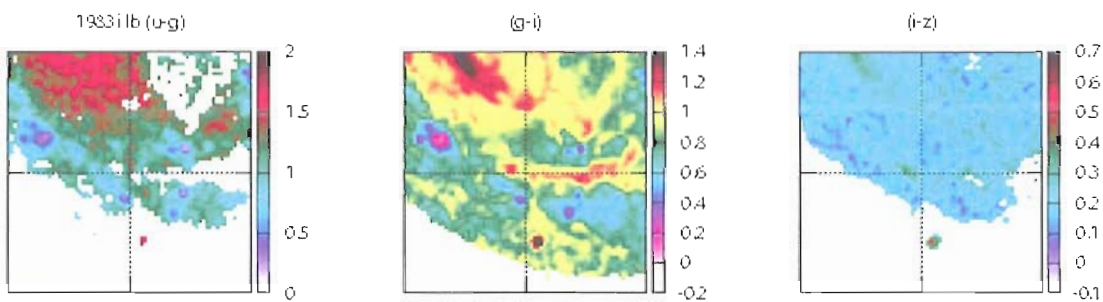
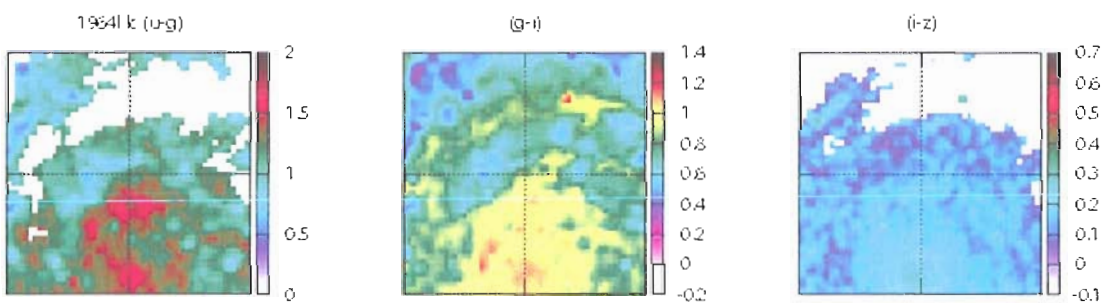


Figure 5.240. SN 2005hl  $u-g$ ,  $g-i$ ,  $i-z$  spatial plots.

Figure 5.241. SN 1976b  $u-g$ ,  $g-i$ ,  $i-z$  spatial plots.Figure 5.242. SN 1990b  $u-g$ ,  $g-i$ ,  $i-z$  spatial plots.Figure 5.243. SN 2001ci  $u-g$ ,  $g-i$ ,  $i-z$  spatial plots.Figure 5.244. SN 2004gn  $u-g$ ,  $g-i$ ,  $i-z$  spatial plots.

Figure 5.245. SN 1999bu  $u-g$ ,  $g-i$ ,  $i-z$  spatial plots.Figure 5.246. SN 2004c  $u-g$ ,  $g-i$ ,  $i-z$  spatial plots.Figure 5.247. SN 1983i  $u-g$ ,  $g-i$ ,  $i-z$  spatial plots.Figure 5.248. SN 1964l  $u-g$ ,  $g-i$ ,  $i-z$  spatial plots.



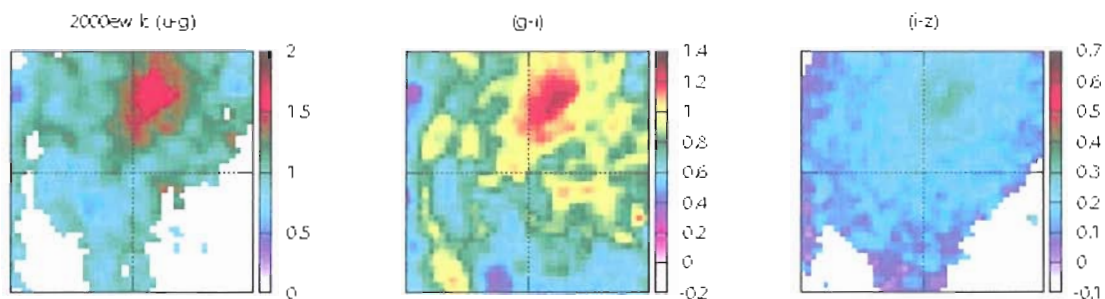


Figure 5.249. SN 2000ew  $u-g$ ,  $g-i$ ,  $i-z$  spatial plots.

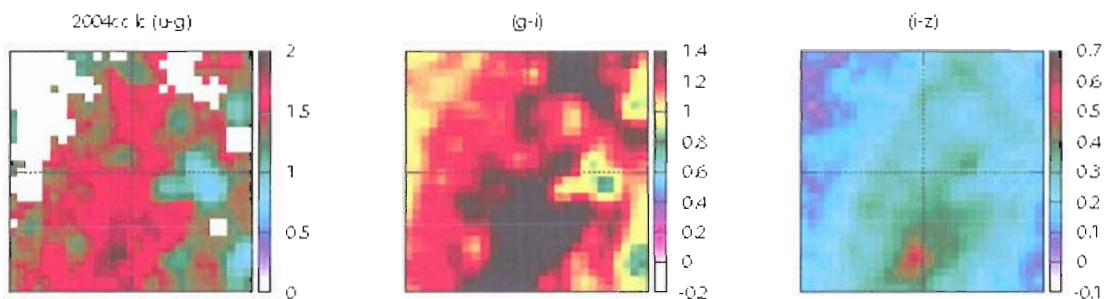


Figure 5.250. SN 2004cc  $u-g$ ,  $g-i$ ,  $i-z$  spatial plots.

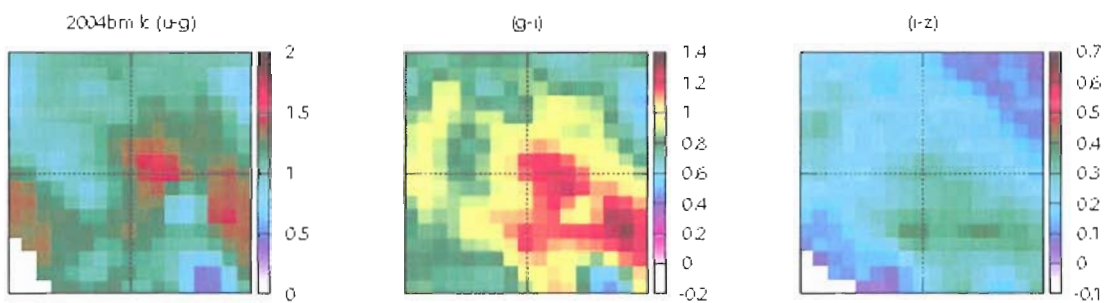


Figure 5.251. SN 2004bm  $u-g$ ,  $g-i$ ,  $i-z$  spatial plots.

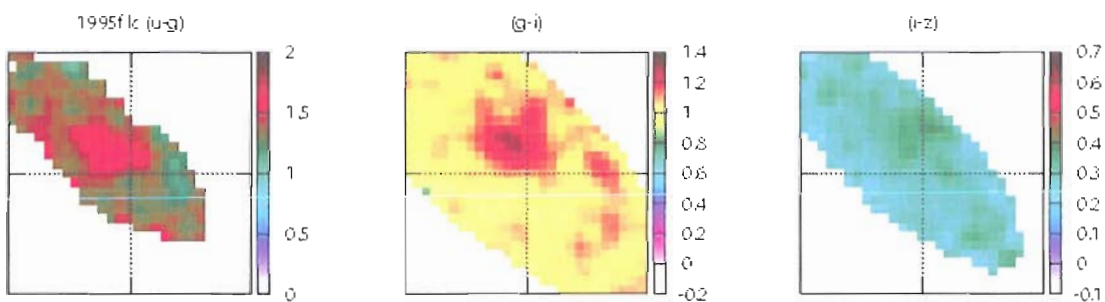
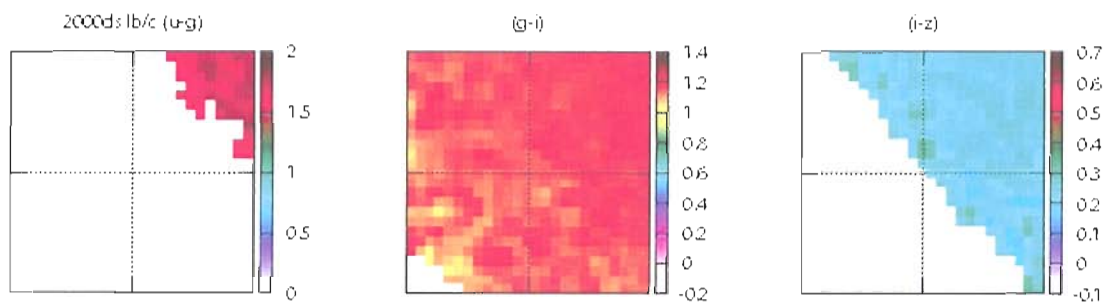
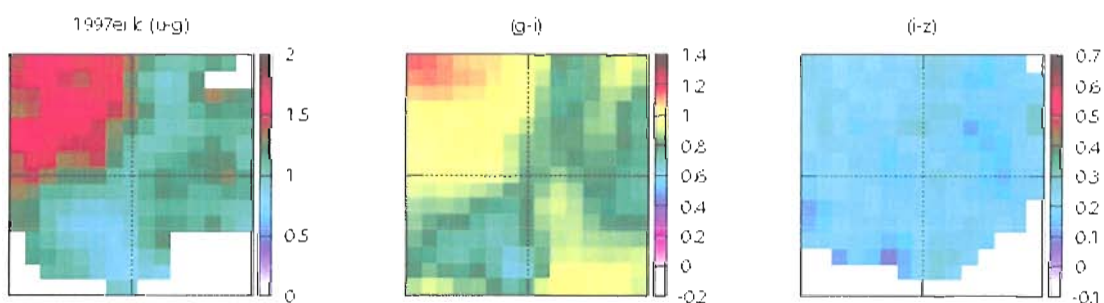
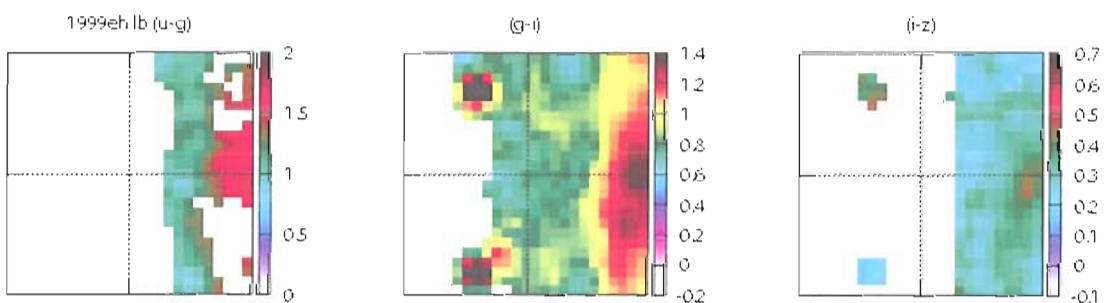
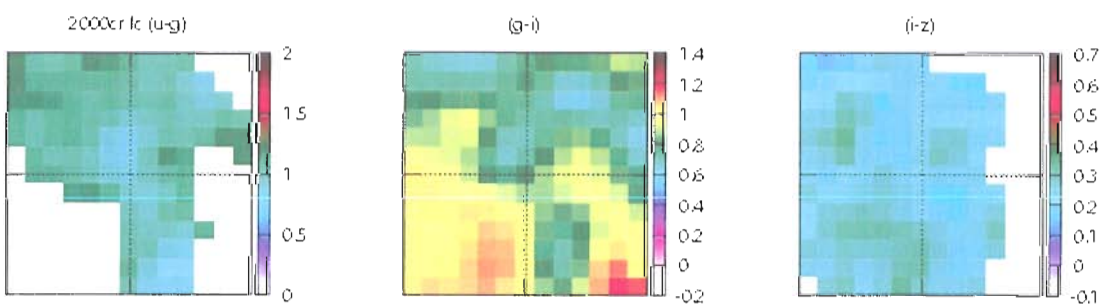


Figure 5.252. SN 1995f  $u-g$ ,  $g-i$ ,  $i-z$  spatial plots.

Figure 5.253. SN 2000ds  $u-g$ ,  $g-i$ ,  $i-z$  spatial plots.Figure 5.254. SN 1997ei  $u-g$ ,  $g-i$ ,  $i-z$  spatial plots.Figure 5.255. SN 1999eh  $u-g$ ,  $g-i$ ,  $i-z$  spatial plots.Figure 5.256. SN 2000cr  $u-g$ ,  $g-i$ ,  $i-z$  spatial plots.

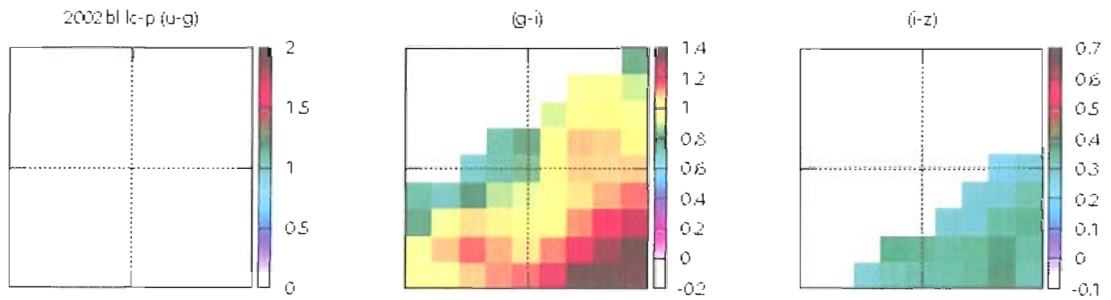


Figure 5.257. SN 2002bl  $u-g$ ,  $g-i$ ,  $i-z$  spatial plots.

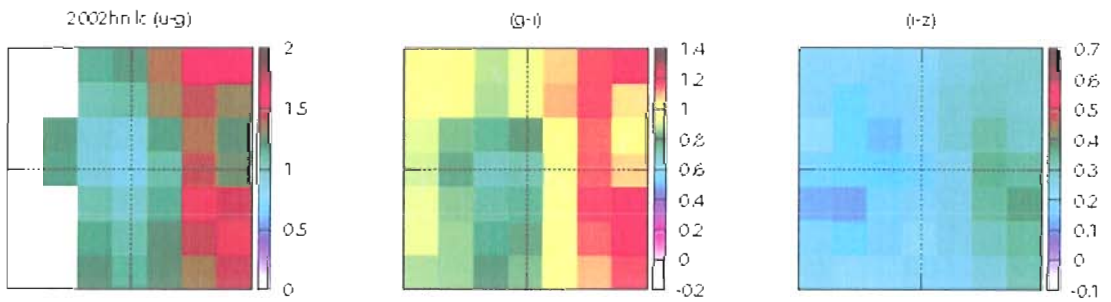


Figure 5.258. SN 2002hn  $u-g$ ,  $g-i$ ,  $i-z$  spatial plots.

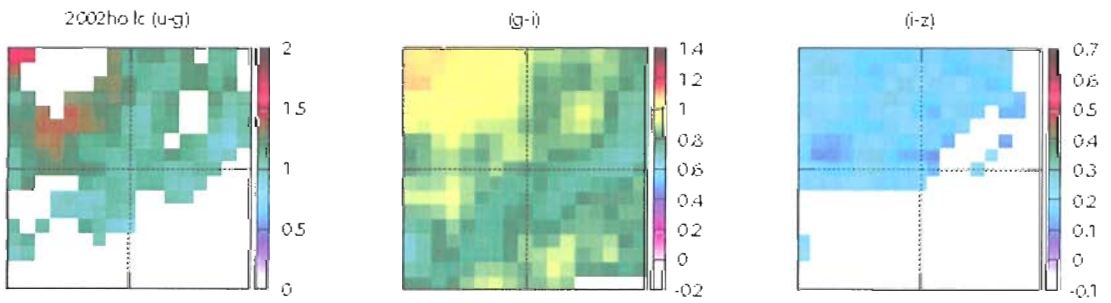


Figure 5.259. SN 2002ho  $u-g$ ,  $g-i$ ,  $i-z$  spatial plots.

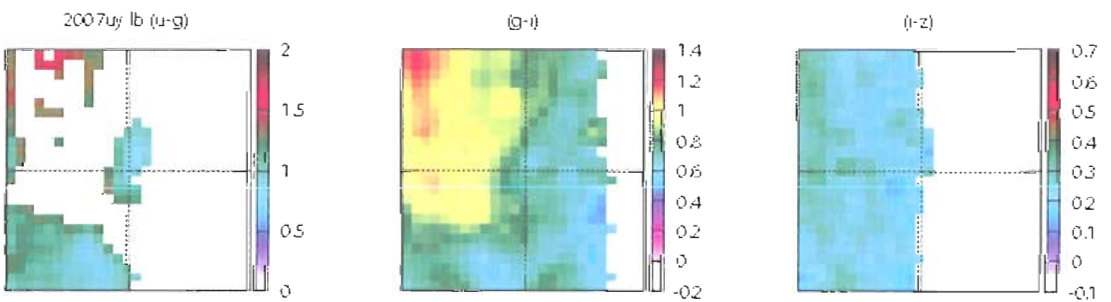


Figure 5.260. SN 2007uy  $u-g$ ,  $g-i$ ,  $i-z$  spatial plots.

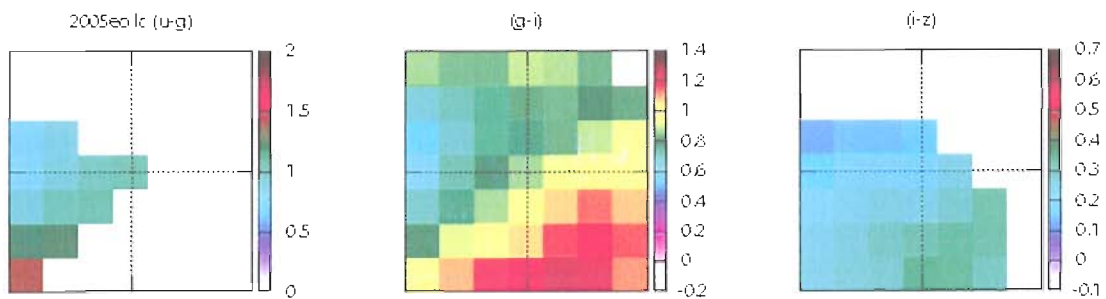


Figure 5.261. SN 2005eo  $u-g$ ,  $g-i$ ,  $i-z$  spatial plots.

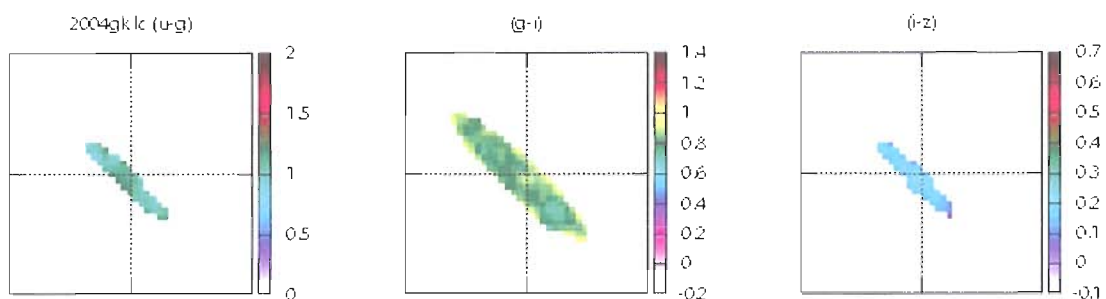


Figure 5.262. SN 2004gk  $u-g$ ,  $g-i$ ,  $i-z$  spatial plots.

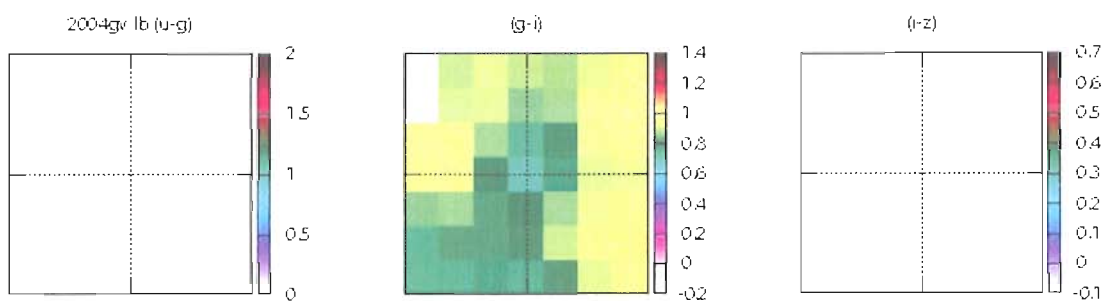


Figure 5.263. SN 2004gv  $u-g$ ,  $g-i$ ,  $i-z$  spatial plots.

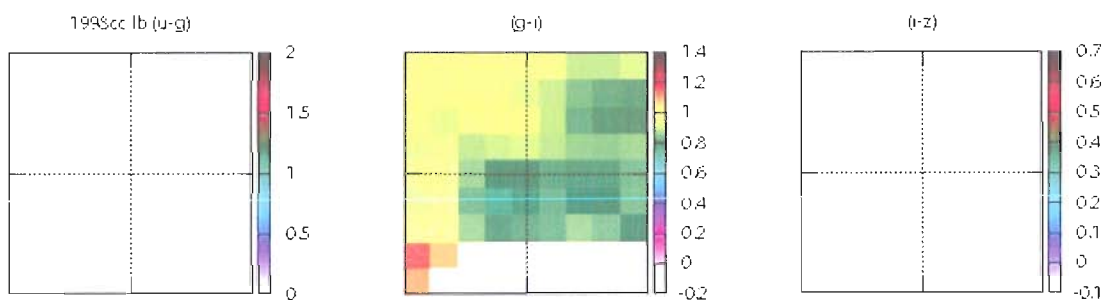
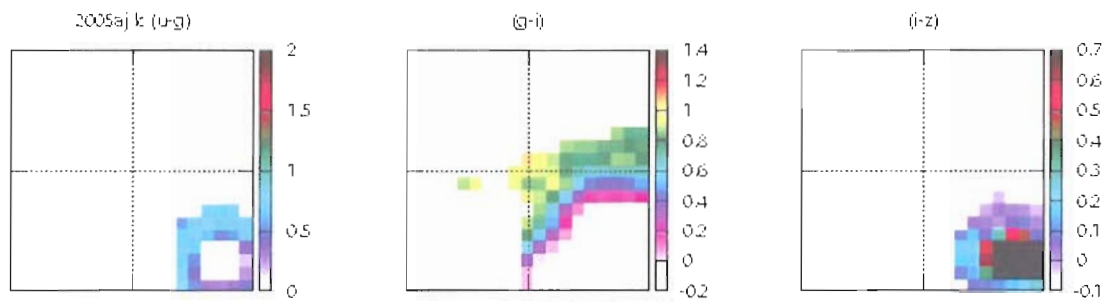
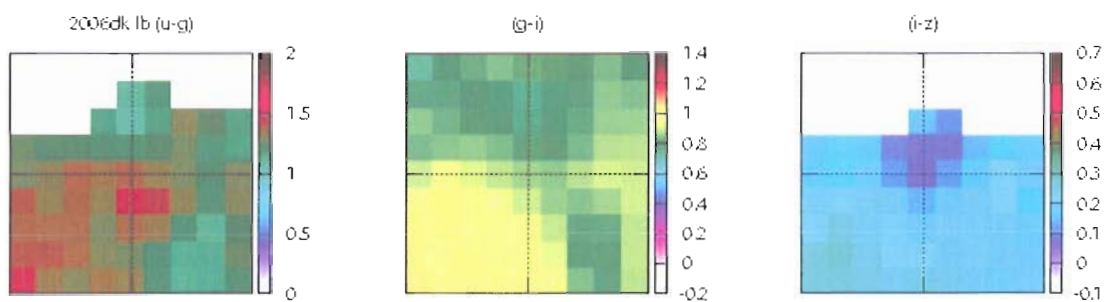
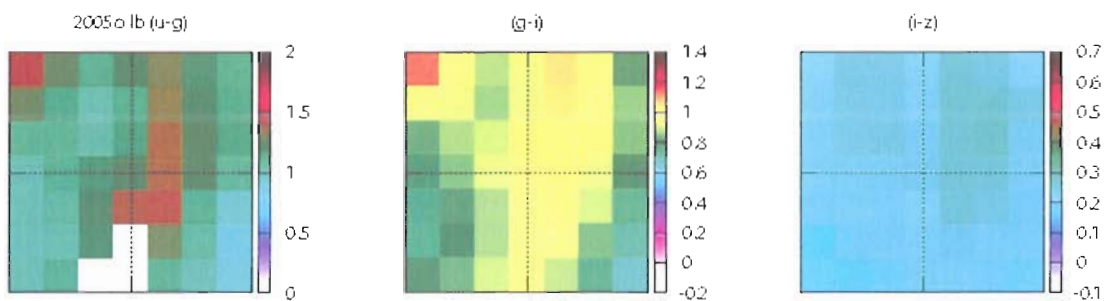
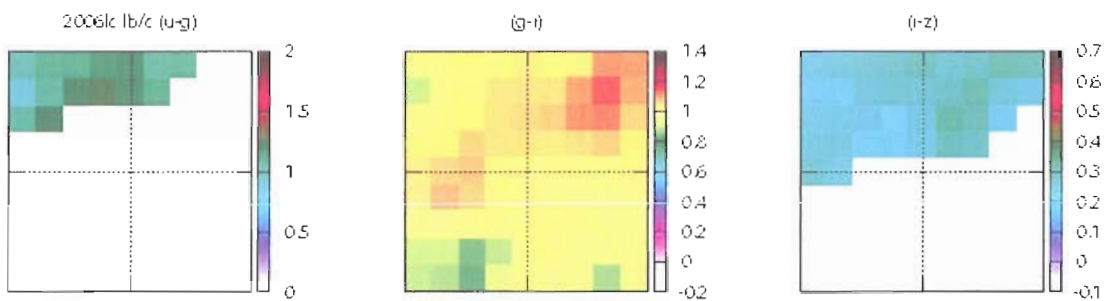
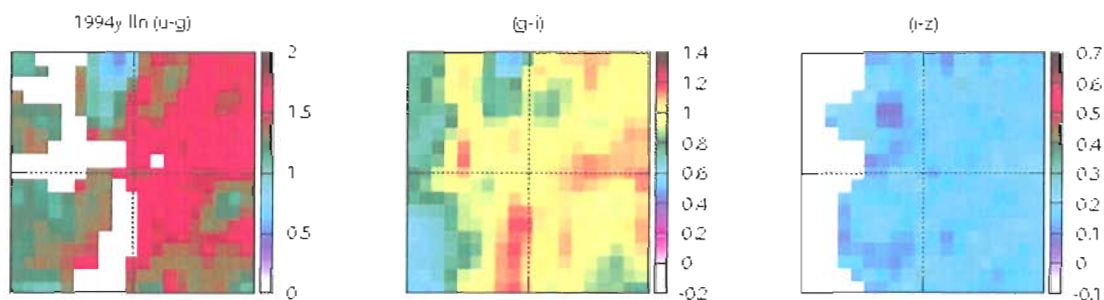
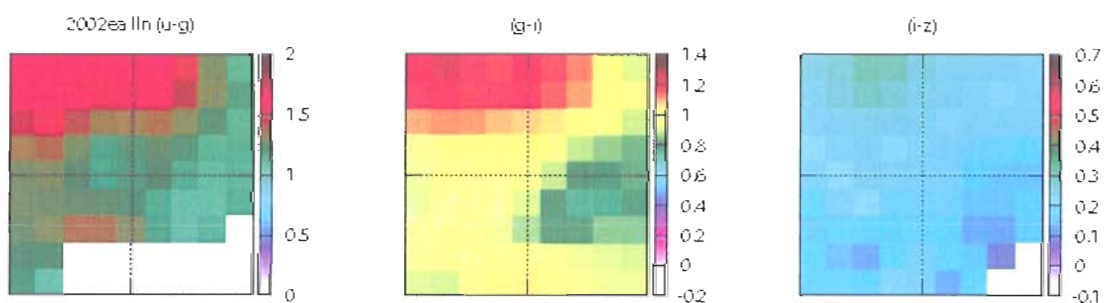
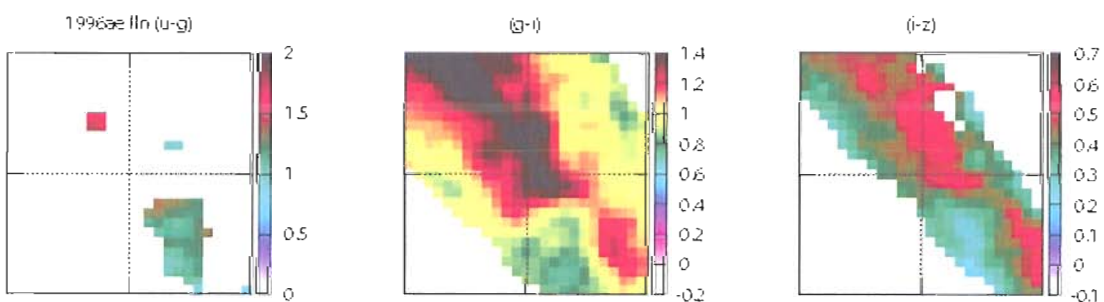
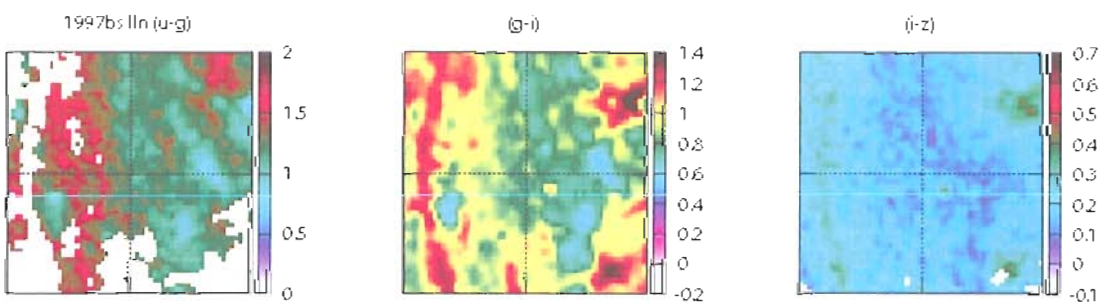


Figure 5.264. SN 1998cc  $u-g$ ,  $g-i$ ,  $i-z$  spatial plots.

Figure 5.265. SN 2005aj  $u-g$ ,  $g-i$ ,  $i-z$  spatial plots.Figure 5.266. SN 2006dk  $u-g$ ,  $g-i$ ,  $i-z$  spatial plots.Figure 5.267. SN 2005o  $u-g$ ,  $g-i$ ,  $i-z$  spatial plots.Figure 5.268. SN 2006lc  $u-g$ ,  $g-i$ ,  $i-z$  spatial plots.

Figure 5.269. SN 1994y  $u-g$ ,  $g-i$ ,  $i-z$  spatial plots.Figure 5.270. SN 2002ea  $u-g$ ,  $g-i$ ,  $i-z$  spatial plots.Figure 5.271. SN 1996ae  $u-g$ ,  $g-i$ ,  $i-z$  spatial plots.Figure 5.272. SN 1997bs  $u-g$ ,  $g-i$ ,  $i-z$  spatial plots.

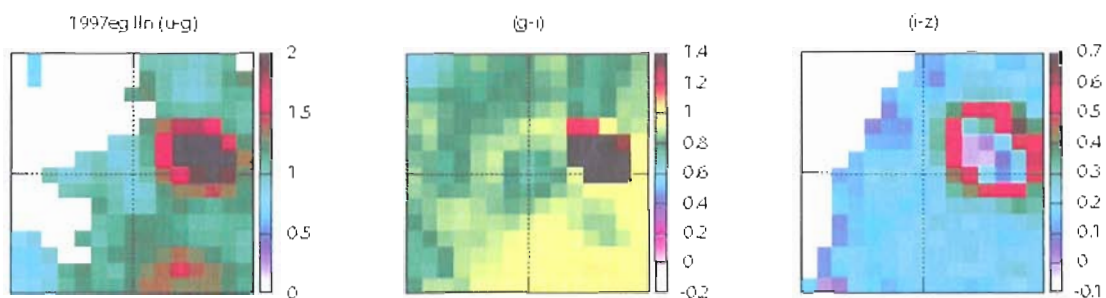


Figure 5.273. SN 1997eg  $u-g$ ,  $g-i$ ,  $i-z$  spatial plots.

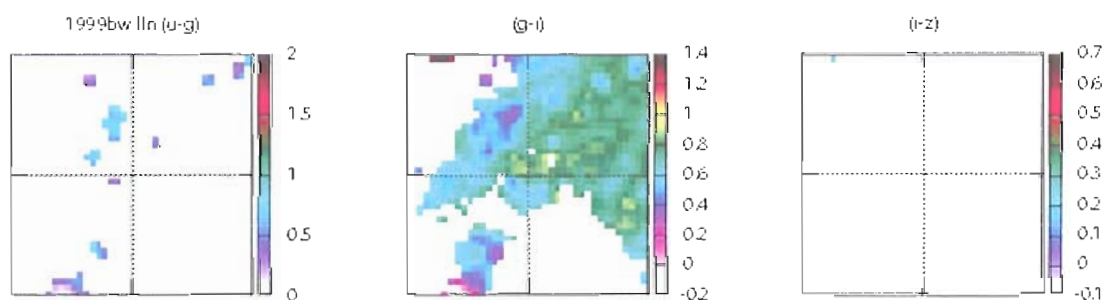


Figure 5.274. SN 1999bw  $u-g$ ,  $g-i$ ,  $i-z$  spatial plots.

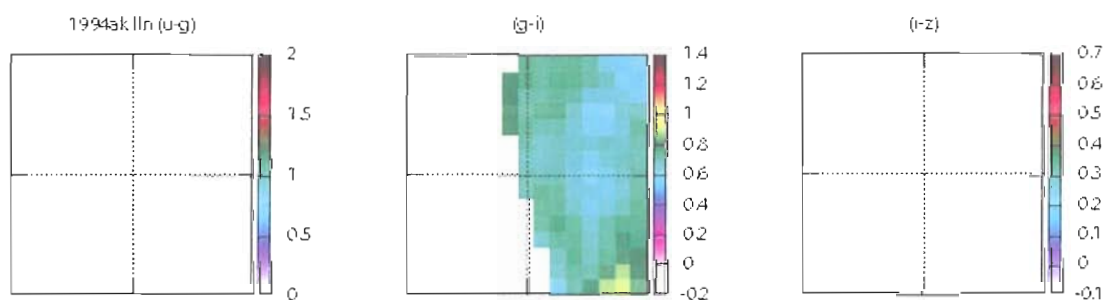


Figure 5.275. SN 1994ak  $u-g$ ,  $g-i$ ,  $i-z$  spatial plots.

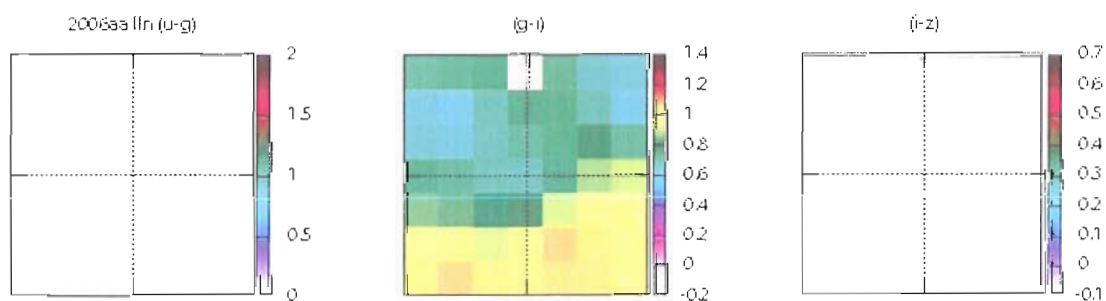


Figure 5.276. SN 2006aa  $u-g$ ,  $g-i$ ,  $i-z$  spatial plots.

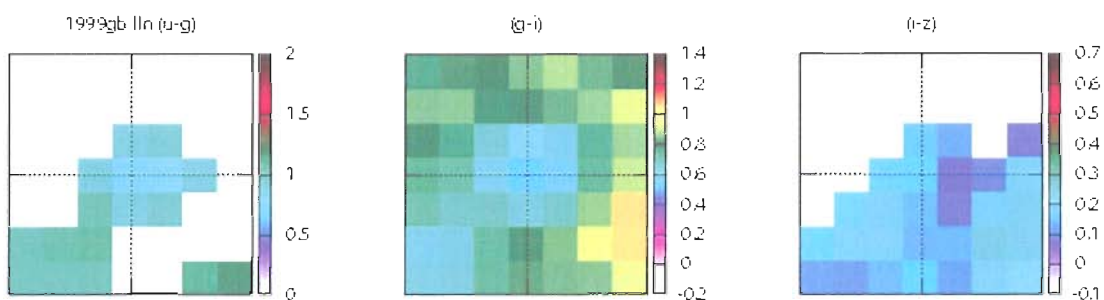


Figure 5.277. SN 1999gb  $u-g$ ,  $g-i$ ,  $i-z$  spatial plots.

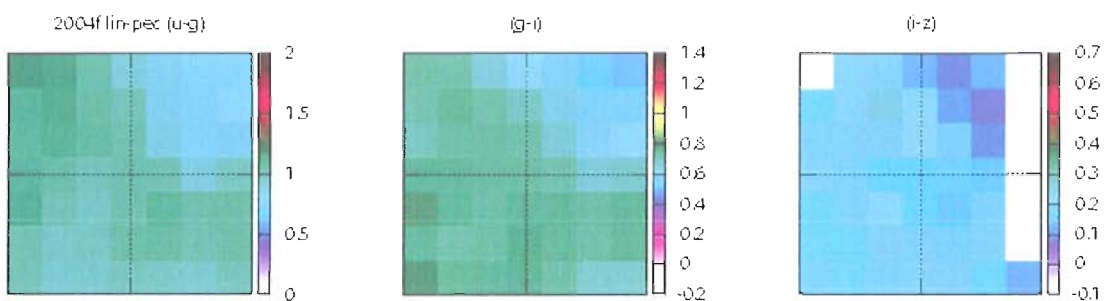


Figure 5.278. SN 2004f  $u-g$ ,  $g-i$ ,  $i-z$  spatial plots.

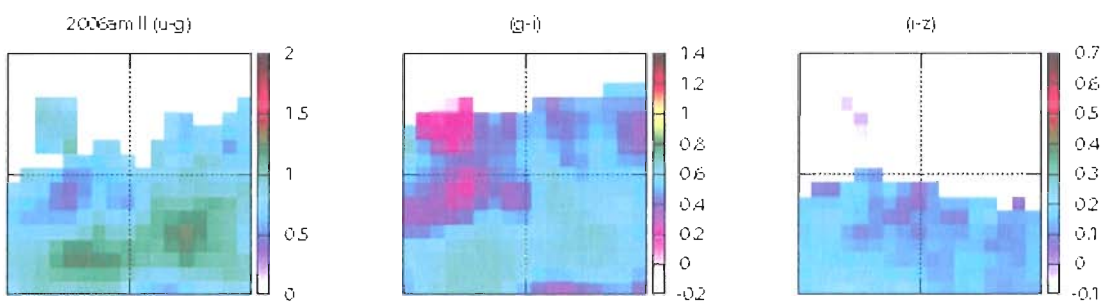


Figure 5.279. SN 2006am  $u-g$ ,  $g-i$ ,  $i-z$  spatial plots.

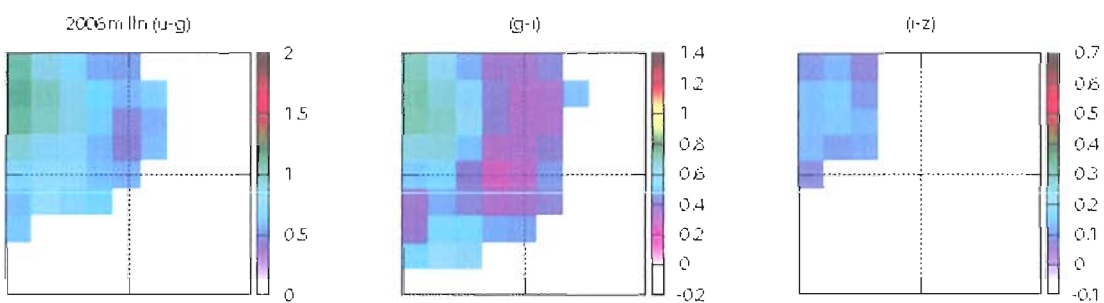
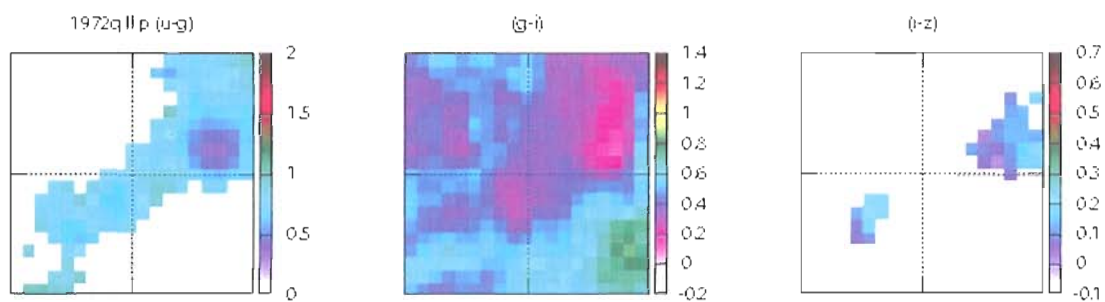
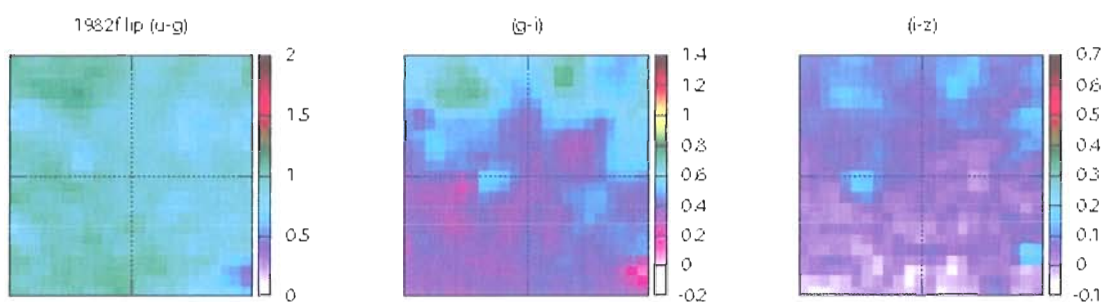
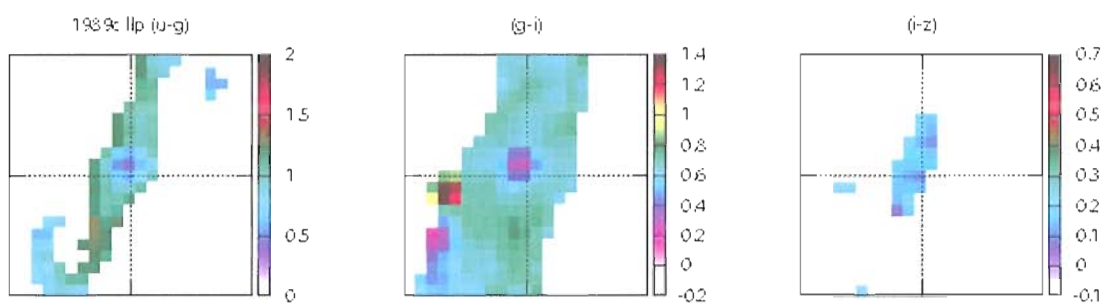
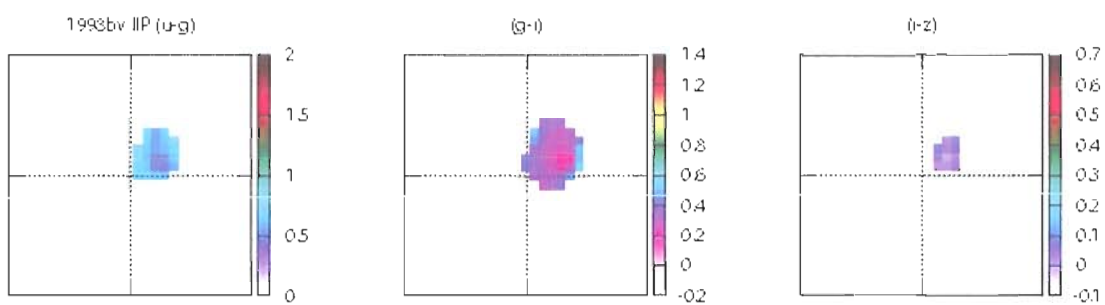
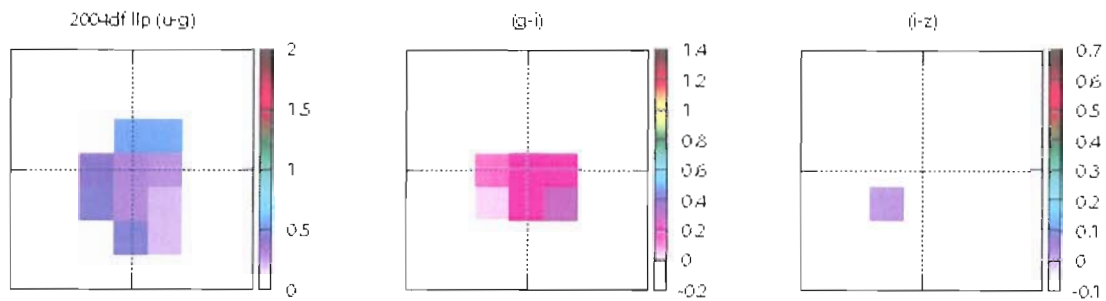
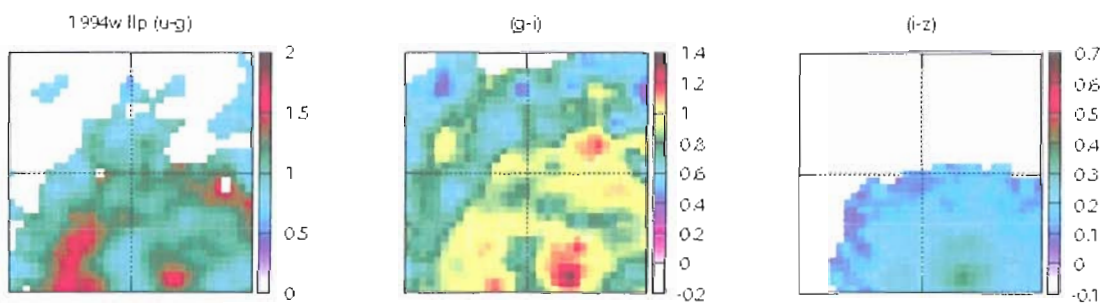
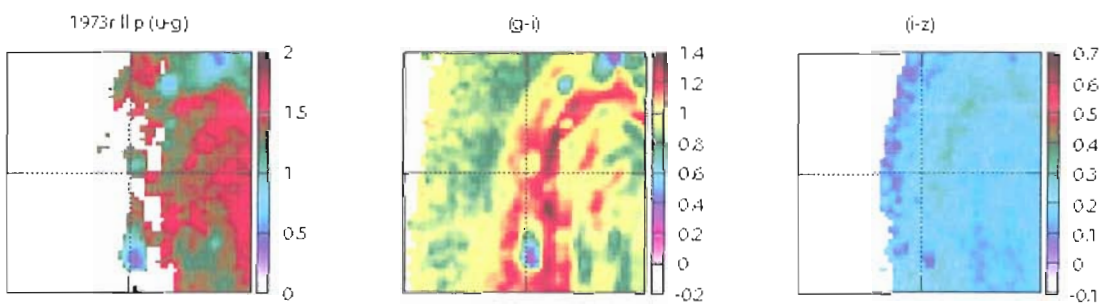
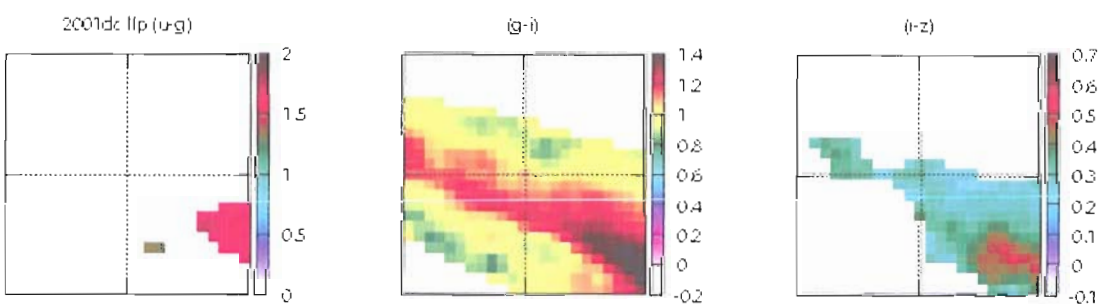
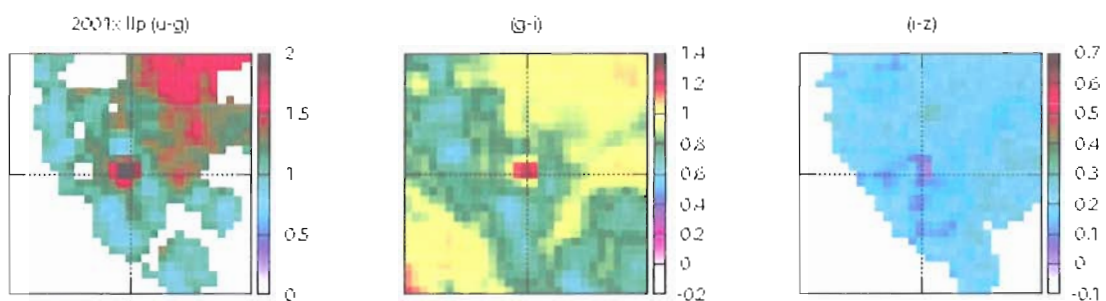
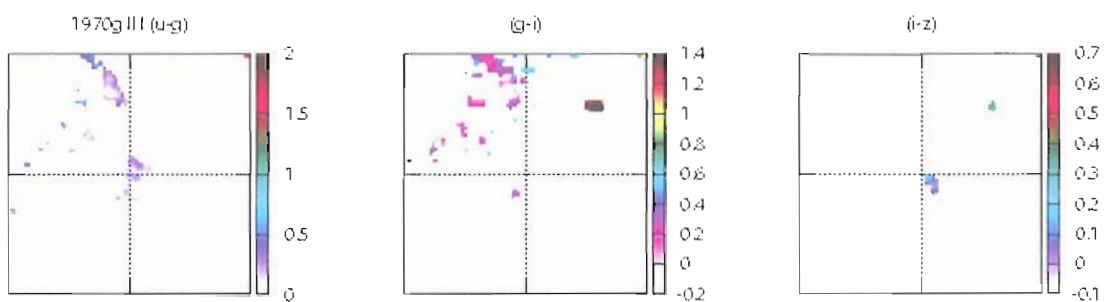
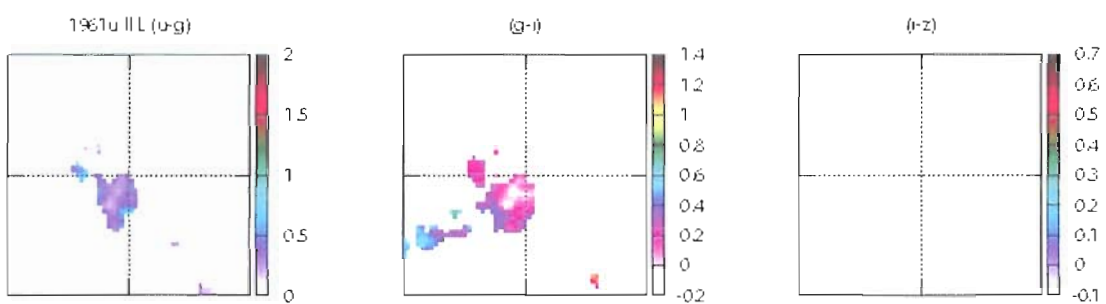
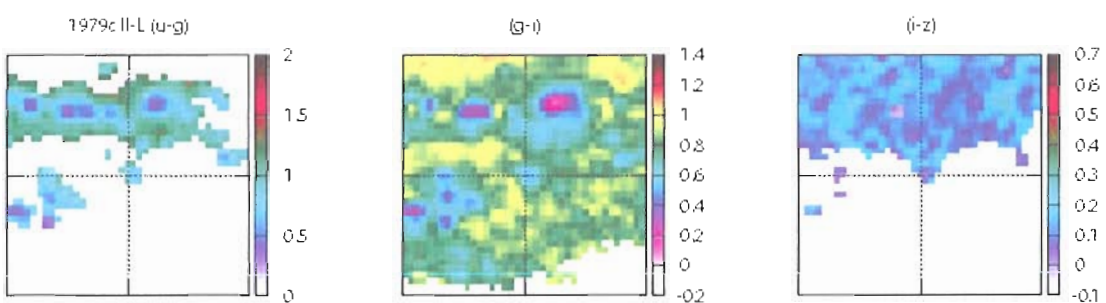


Figure 5.280. SN 2006m  $u-g$ ,  $g-i$ ,  $i-z$  spatial plots.



Figure 5.281. SN 1972q  $u-g$ ,  $g-i$ ,  $i-z$  spatial plots.Figure 5.282. SN 1982f  $u-g$ ,  $g-i$ ,  $i-z$  spatial plots.Figure 5.283. SN 1989c  $u-g$ ,  $g-i$ ,  $i-z$  spatial plots.Figure 5.284. SN 1998bv  $u-g$ ,  $g-i$ ,  $i-z$  spatial plots.

Figure 5.285. SN 2004df  $u-g$ ,  $g-i$ ,  $i-z$  spatial plots.Figure 5.286. SN 1994w  $u-g$ ,  $g-i$ ,  $i-z$  spatial plots.Figure 5.287. SN 1973r  $u-g$ ,  $g-i$ ,  $i-z$  spatial plots.Figure 5.288. SN 2001dc  $u-g$ ,  $g-i$ ,  $i-z$  spatial plots.

Figure 5.289. SN 2001x  $u-g$ ,  $g-i$ ,  $i-z$  spatial plots.Figure 5.290. SN 1970g  $u-g$ ,  $g-i$ ,  $i-z$  spatial plots.Figure 5.291. SN 1961u  $u-g$ ,  $g-i$ ,  $i-z$  spatial plots.Figure 5.292. SN 1979c  $u-g$ ,  $g-i$ ,  $i-z$  spatial plots.

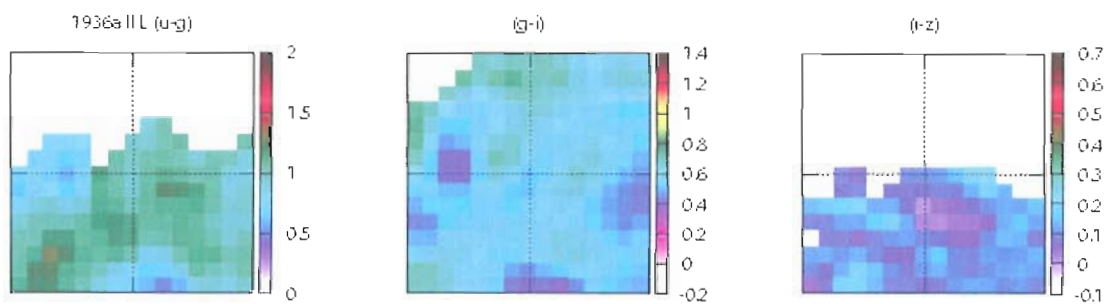


Figure 5.293. SN 1936a  $u-g$ ,  $g-i$ ,  $i-z$  spatial plots.

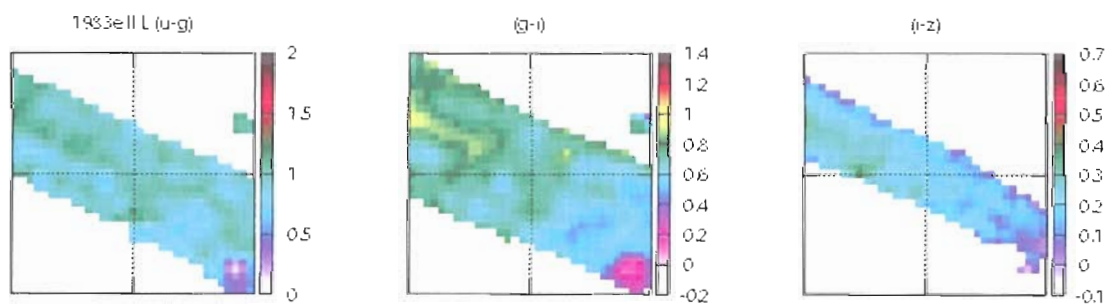


Figure 5.294. SN 1983e  $u-g$ ,  $g-i$ ,  $i-z$  spatial plots.

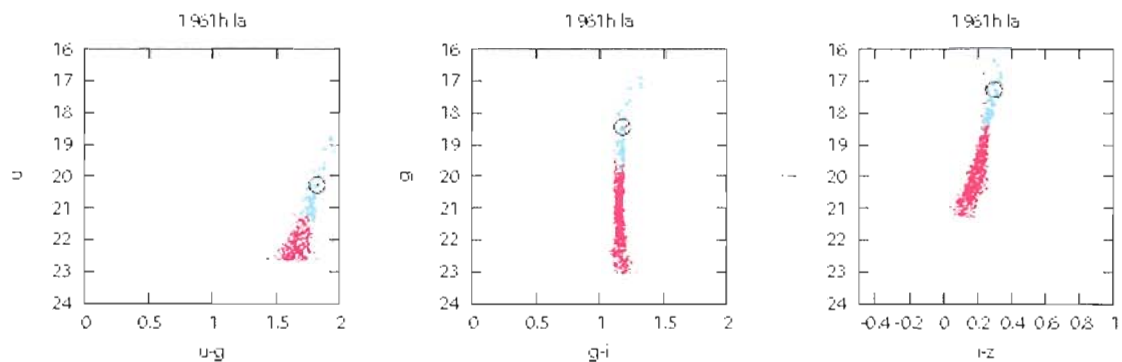


Figure 5.295. SN 1961h  $u,u-g$ ,  $g,g-i$ , and  $i,i-z$  pseudo color-magnitude plots.

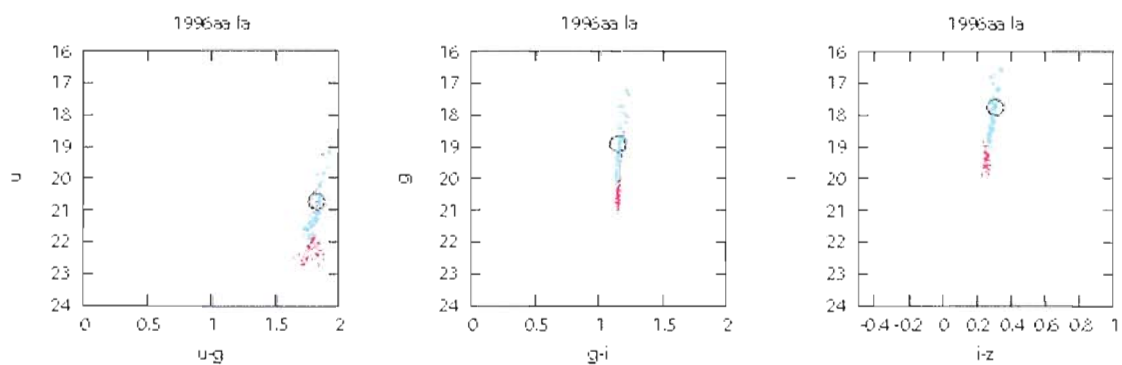


Figure 5.296. SN 1996aa  $u,u-g$ ,  $g,g-i$ , and  $i,i-z$  pseudo color-magnitude plots.

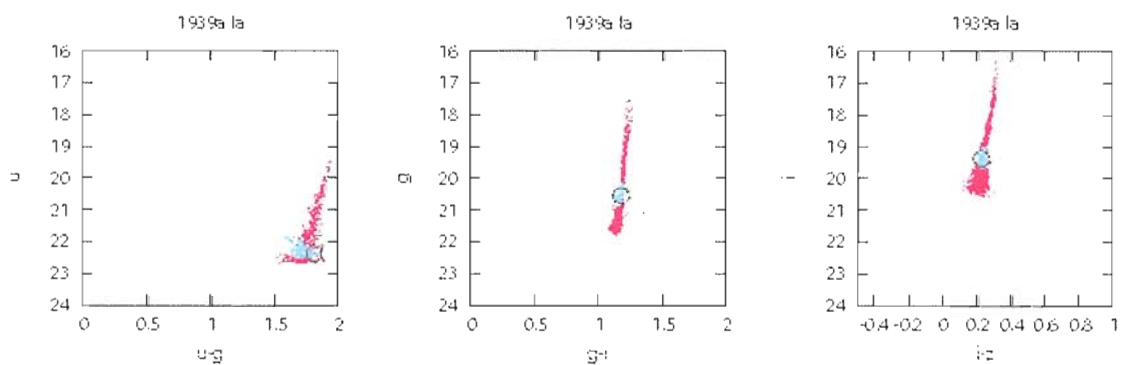


Figure 5.297. SN 1939a  $u,u-g$ ,  $g,g-i$ , and  $i,i-z$  pseudo color-magnitude plots.

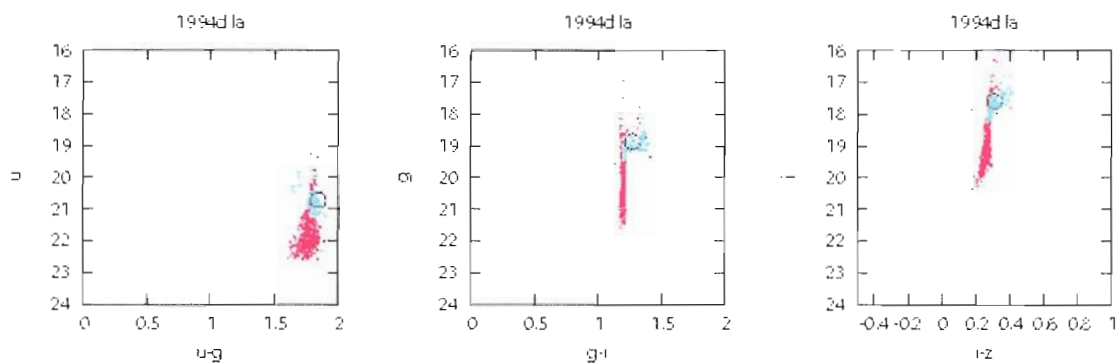


Figure 5.298. SN 1994d  $u,u-g$ ,  $g,g-i$ , and  $i,i-z$  pseudo color-magnitude plots.

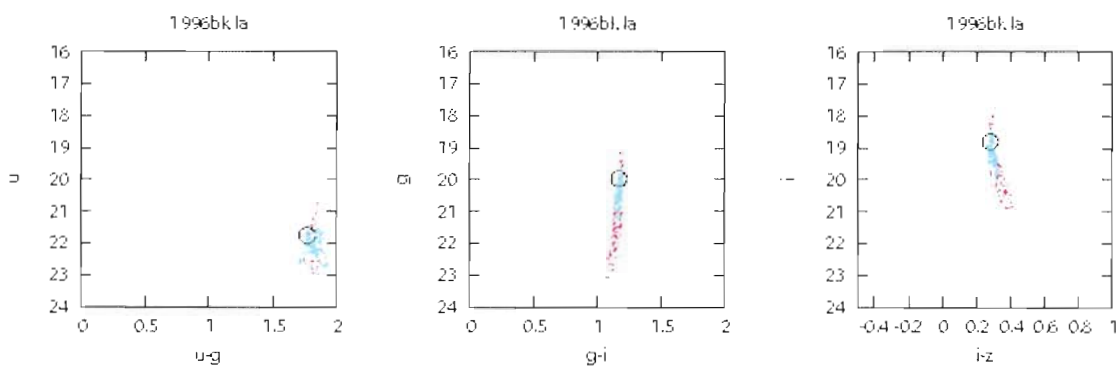


Figure 5.299. SN 1996bk  $u,u-g$ ,  $g,g-i$ , and  $i,i-z$  pseudo color-magnitude plots.

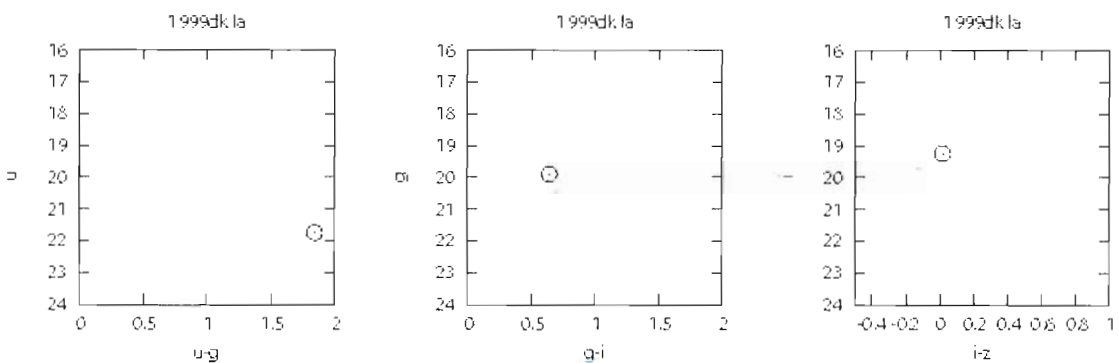


Figure 5.300. SN 1999dk  $u,u-g$ ,  $g,g-i$ , and  $i,i-z$  pseudo color-magnitude plots.

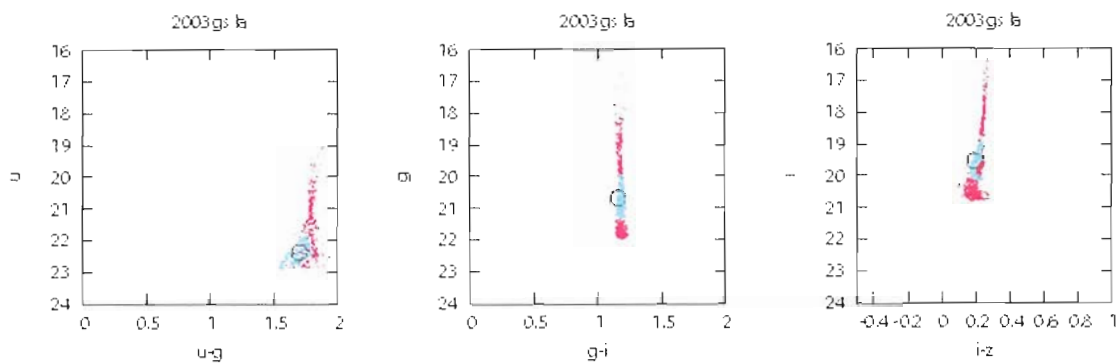


Figure 5.301. SN 2003gs  $u,u-g$ ,  $g,g-i$ , and  $i,i-z$  pseudo color-magnitude plots.

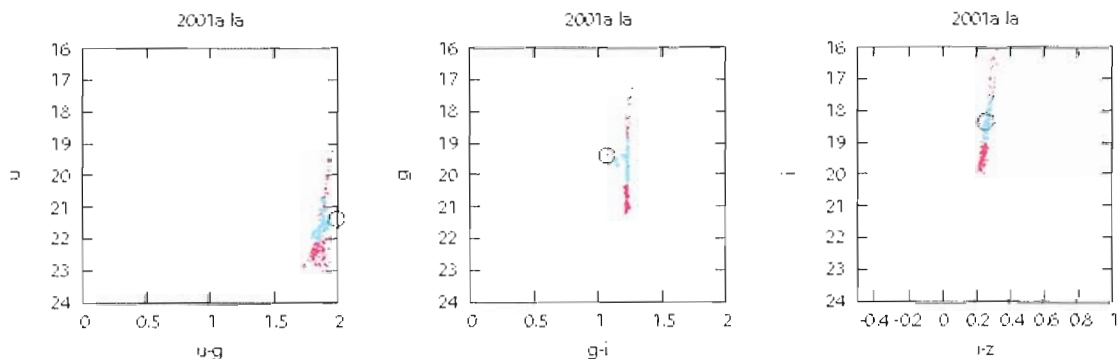


Figure 5.302. SN 2001a  $u,u-g$ ,  $g,g-i$ , and  $i,i-z$  pseudo color-magnitude plots.

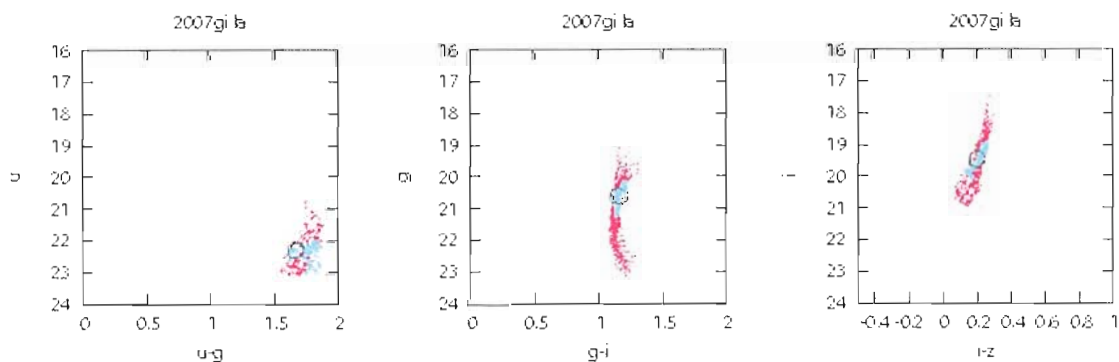


Figure 5.303. SN 2007gi  $u,u-g$ ,  $g,g-i$ , and  $i,i-z$  pseudo color-magnitude plots.

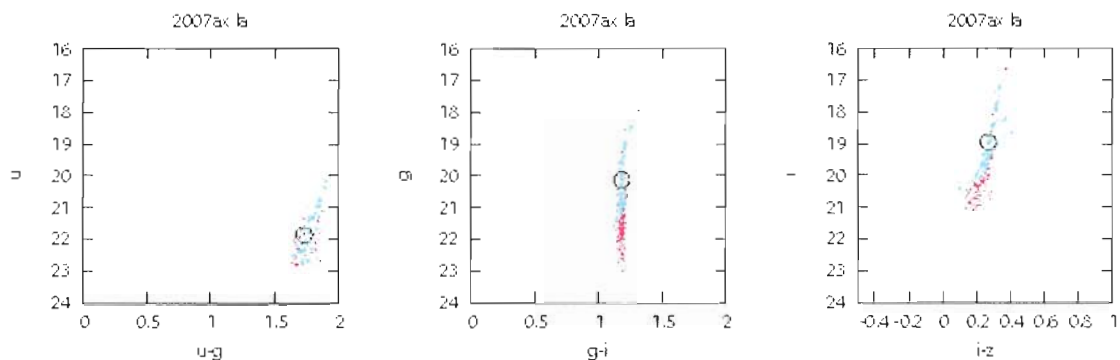


Figure 5.304. SN 2007ax  $u,u-g$ ,  $g,g-i$ , and  $i,i-z$  pseudo color-magnitude plots.

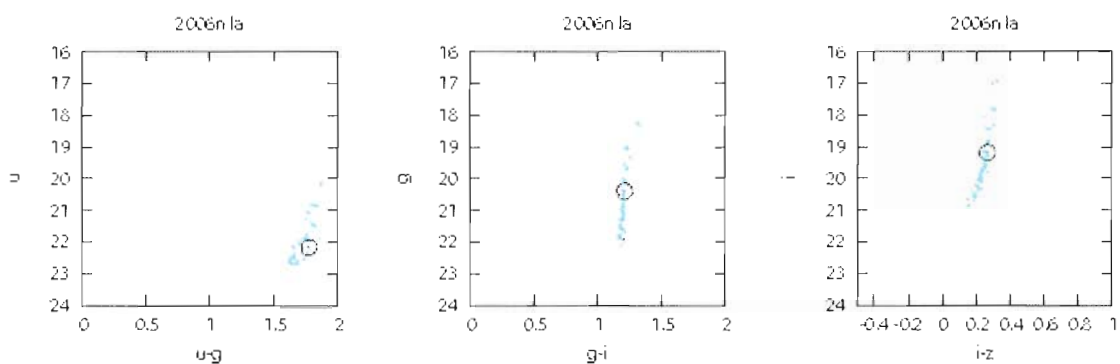


Figure 5.305. SN 2006n  $u,u-g$ ,  $g,g-i$ , and  $i,i-z$  pseudo color-magnitude plots.

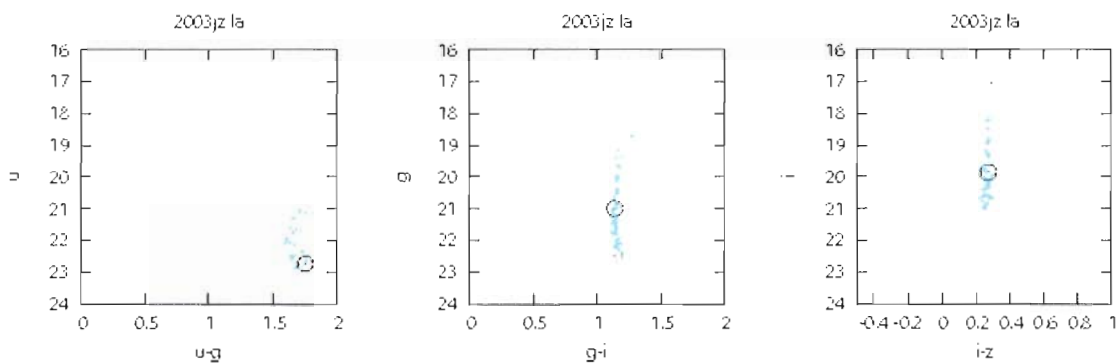


Figure 5.306. SN 2003jz  $u,u-g$ ,  $g,g-i$ , and  $i,i-z$  pseudo color-magnitude plots.



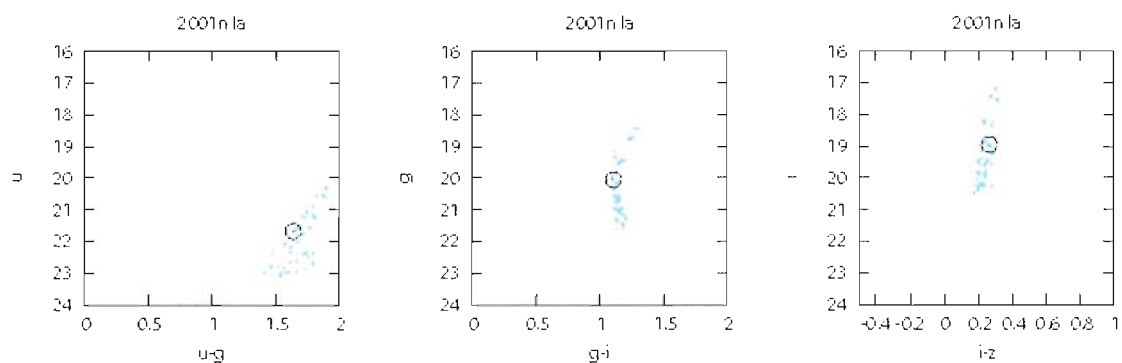


Figure 5.307. SN 2001n  $u,u-g$ ,  $g,g-i$ , and  $i,i-z$  pseudo color-magnitude plots.

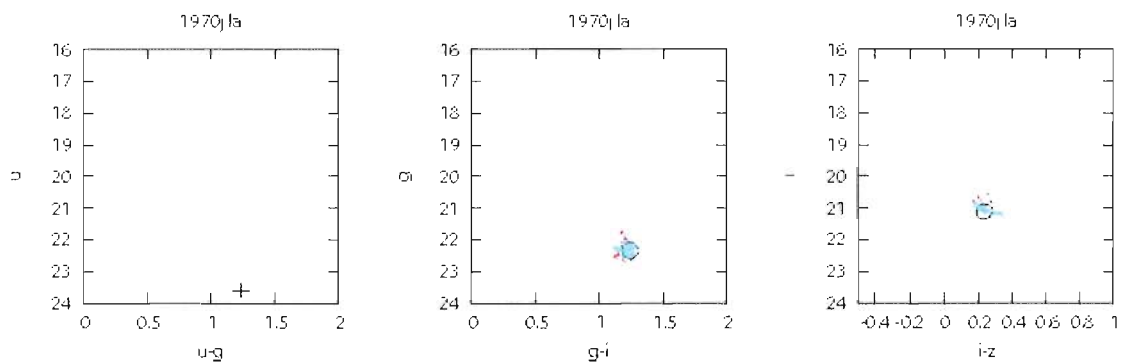


Figure 5.308. SN 1970j  $u,u-g$ ,  $g,g-i$ , and  $i,i-z$  pseudo color-magnitude plots.

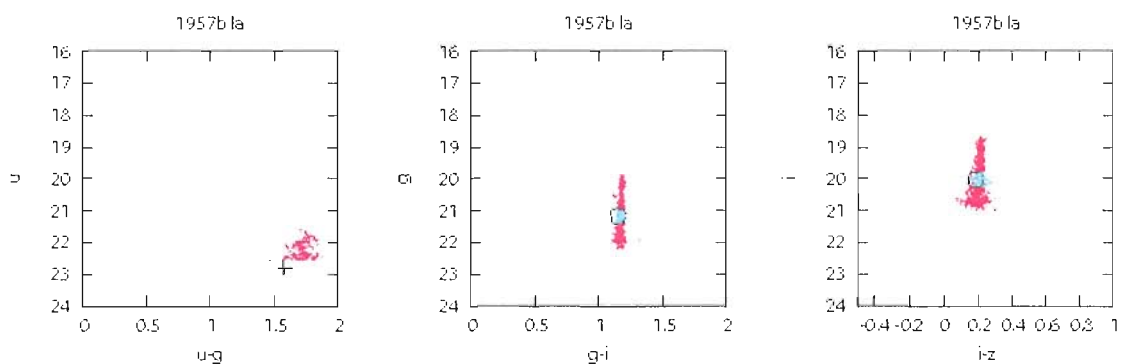


Figure 5.309. SN 1957b  $u,u-g$ ,  $g,g-i$ , and  $i,i-z$  pseudo color-magnitude plots.

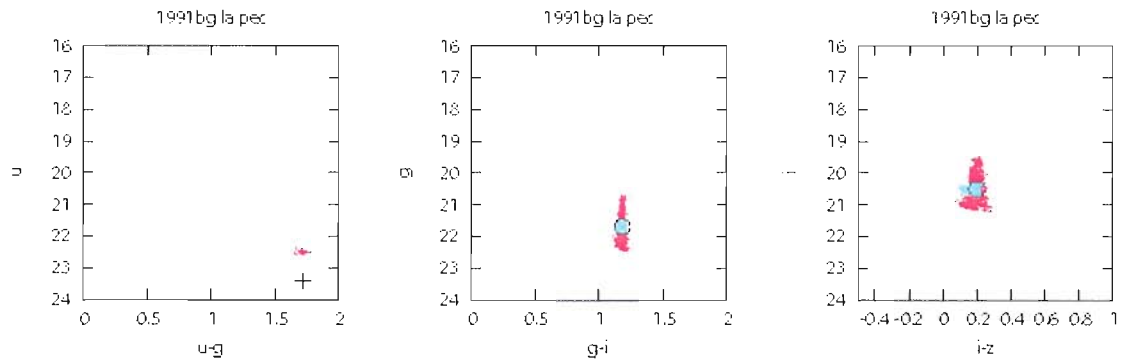


Figure 5.310. SN 1991bg  $u,u-g$ ,  $g,g-i$ , and  $i,i-z$  pseudo color-magnitude plots.

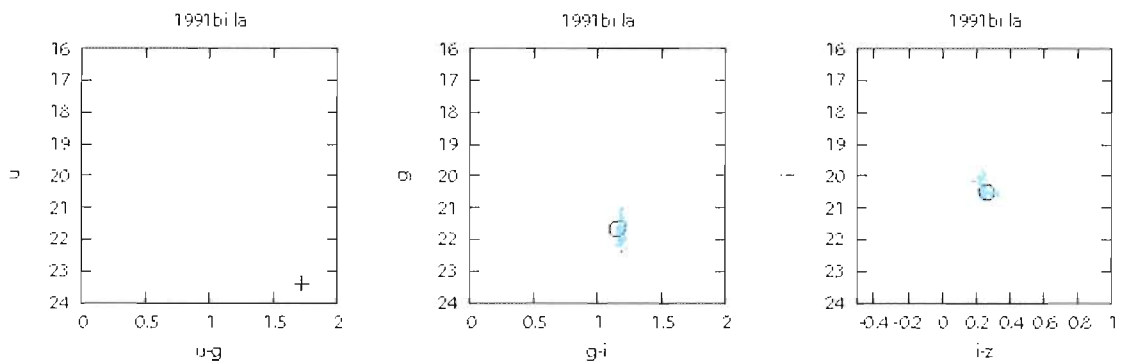


Figure 5.311. SN 1991bi  $u,u-g$ ,  $g,g-i$ , and  $i,i-z$  pseudo color-magnitude plots.

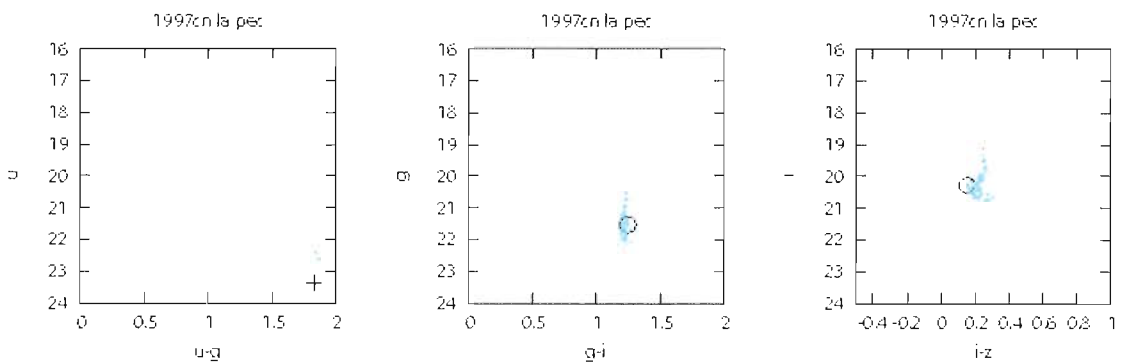


Figure 5.312. SN 1997cn  $u,u-g$ ,  $g,g-i$ , and  $i,i-z$  pseudo color-magnitude plots.

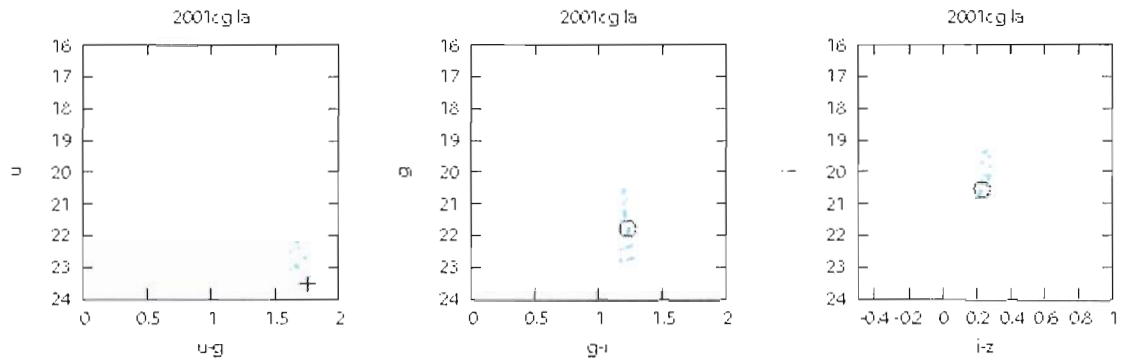


Figure 5.313. SN 2001cg  $u,u-g$ ,  $g,g-i$ , and  $i,i-z$  pseudo color-magnitude plots.

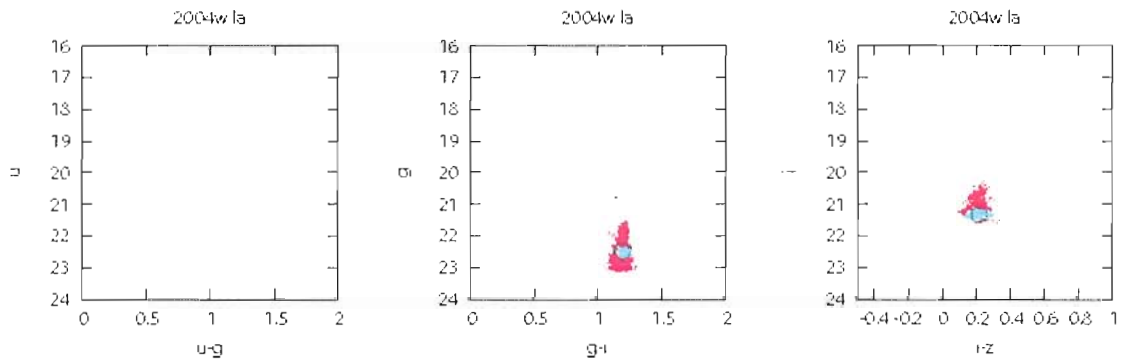


Figure 5.314. SN 2004w  $u,u-g$ ,  $g,g-i$ , and  $i,i-z$  pseudo color-magnitude plots.

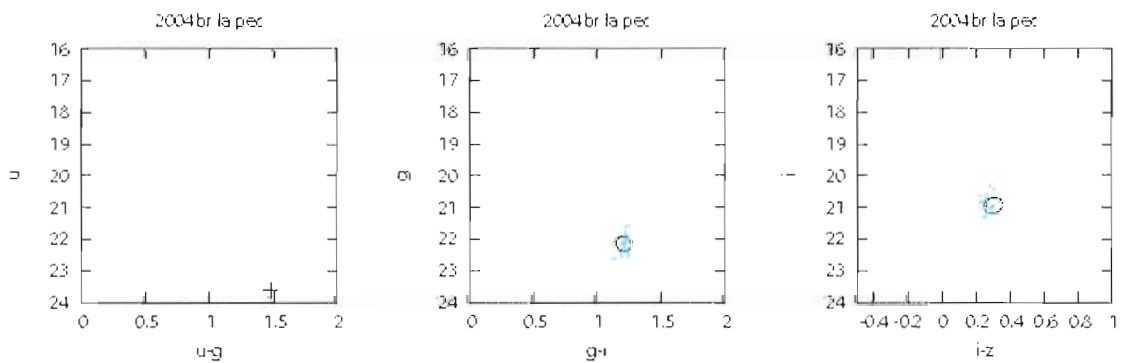


Figure 5.315. SN 2004br  $u,u-g$ ,  $g,g-i$ , and  $i,i-z$  pseudo color-magnitude plots.

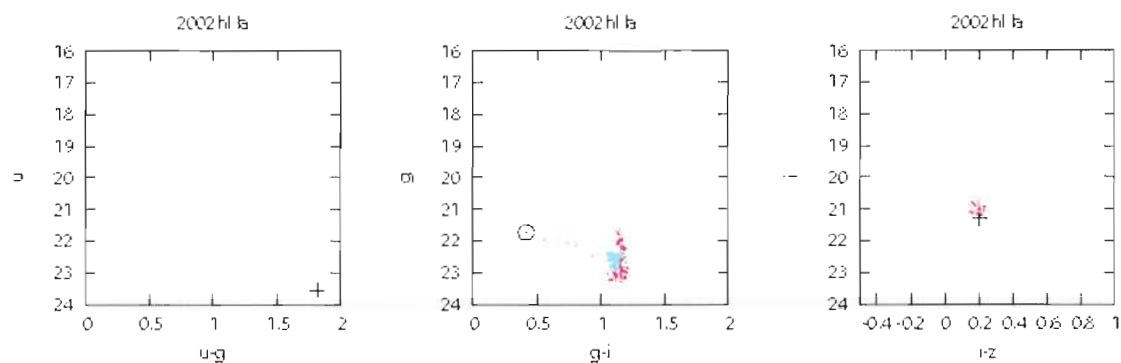


Figure 5.316. SN 2002hl  $u,u-g$ ,  $g,g-i$ , and  $i,i-z$  pseudo color-magnitude plots.

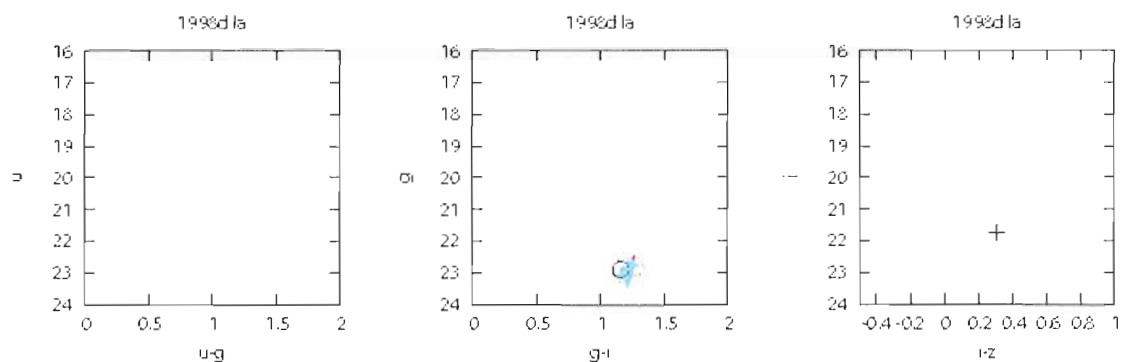


Figure 5.317. SN 1998d  $u,u-g$ ,  $g,g-i$ , and  $i,i-z$  pseudo color-magnitude plots.

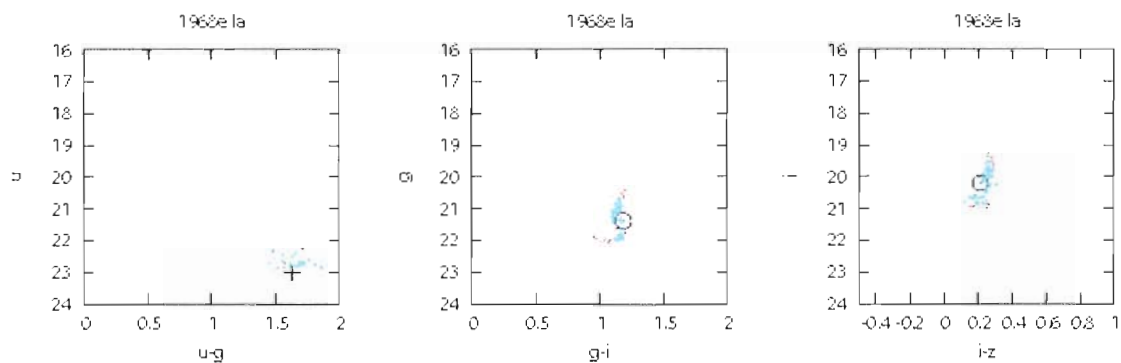


Figure 5.318. SN 1968e  $u,u-g$ ,  $g,g-i$ , and  $i,i-z$  pseudo color-magnitude plots.

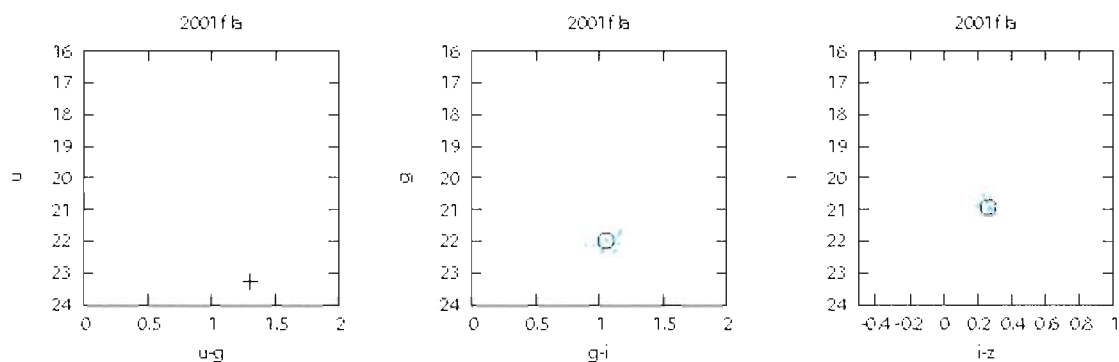


Figure 5.319. SN 2001f  $u,u-g$ ,  $g,g-i$ , and  $i,i-z$  pseudo color-magnitude plots.

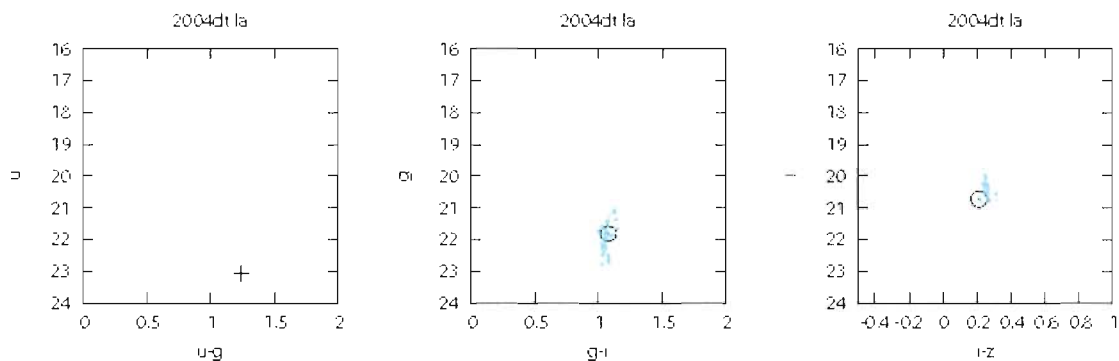


Figure 5.320. SN 2004dt  $u,u-g$ ,  $g,g-i$ , and  $i,i-z$  pseudo color-magnitude plots.

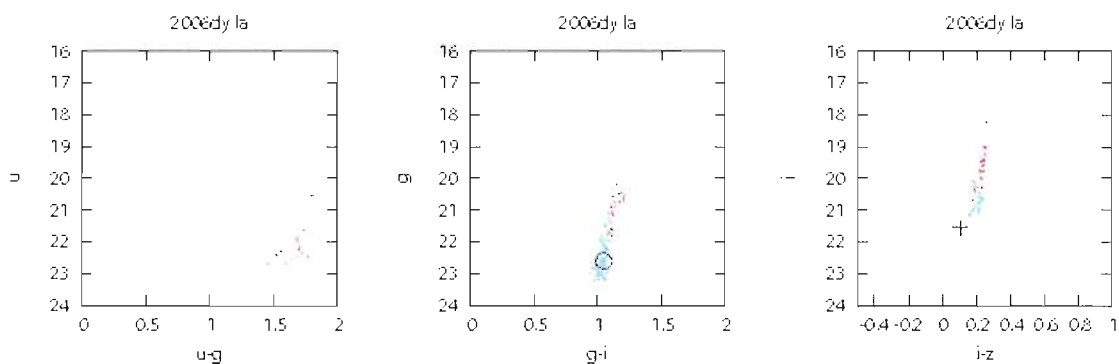


Figure 5.321. SN 2006dy  $u,u-g$ ,  $g,g-i$ , and  $i,i-z$  pseudo color-magnitude plots.

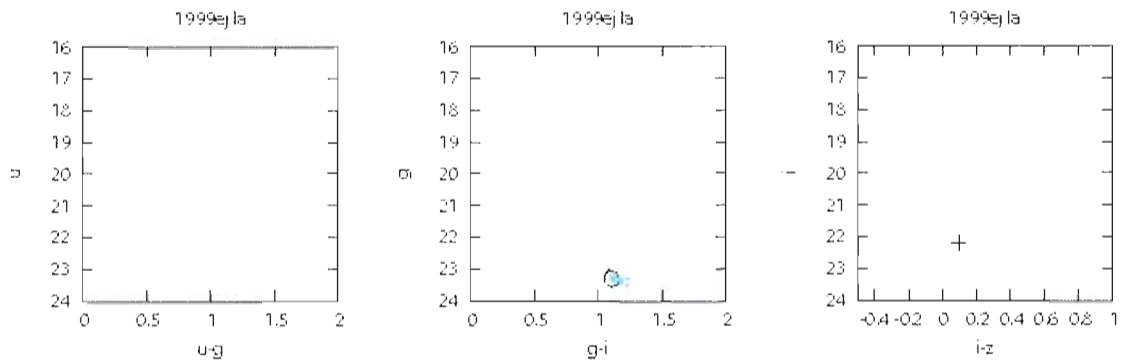


Figure 5.322. SN 1999ej  $u,u-g$ ,  $g,g-i$ , and  $i,i-z$  pseudo color-magnitude plots.

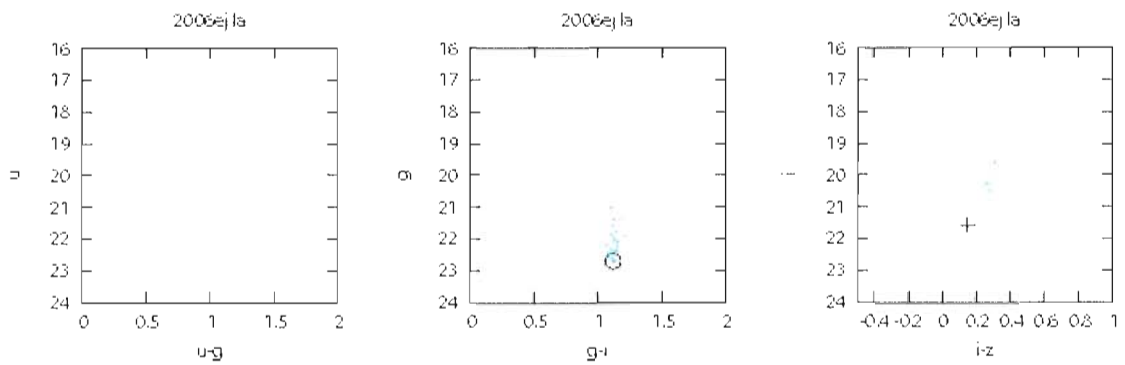


Figure 5.323. SN 2006ej  $u,u-g$ ,  $g,g-i$ , and  $i,i-z$  pseudo color-magnitude plots.

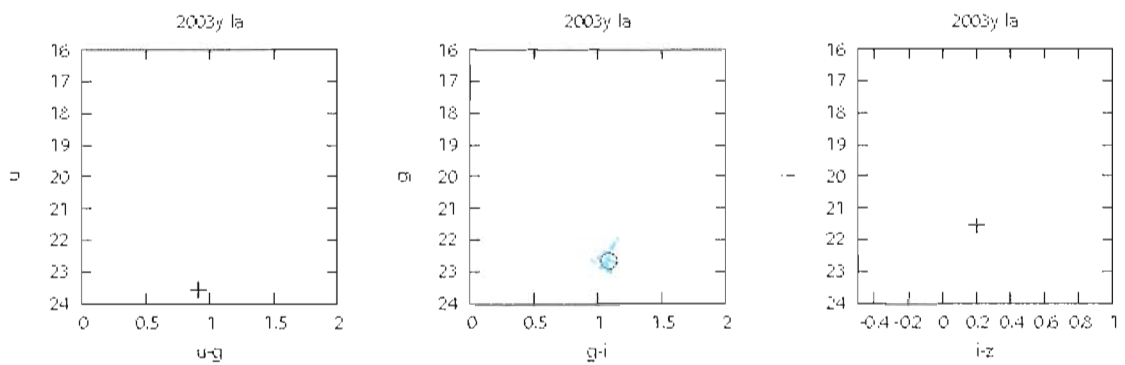


Figure 5.324. SN 2003y  $u,u-g$ ,  $g,g-i$ , and  $i,i-z$  pseudo color-magnitude plots.

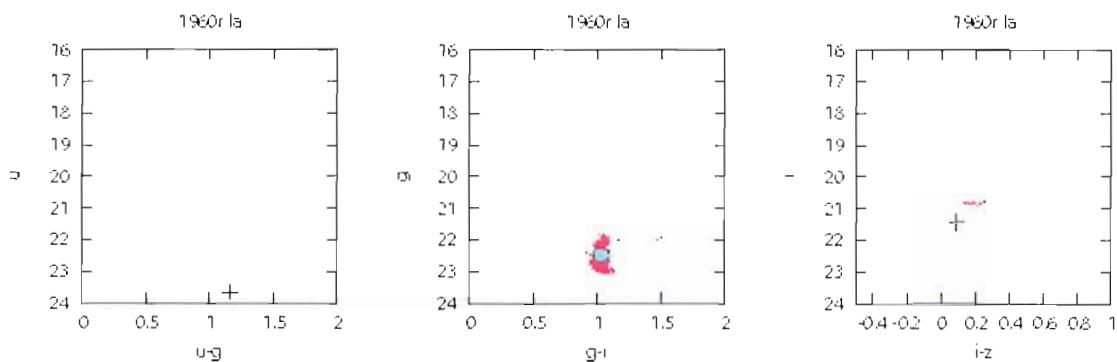


Figure 5.325. SN 1960r  $u,u-g$ ,  $g,g-i$ , and  $i,i-z$  pseudo color-magnitude plots.

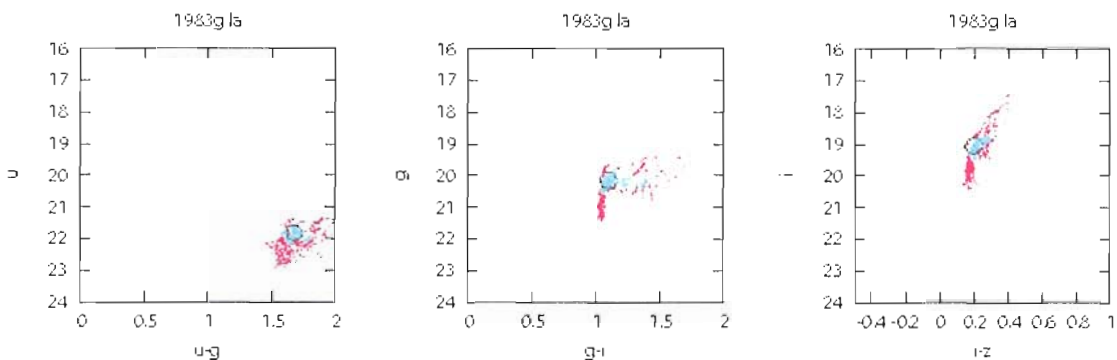


Figure 5.326. SN 1983g  $u,u-g$ ,  $g,g-i$ , and  $i,i-z$  pseudo color-magnitude plots.

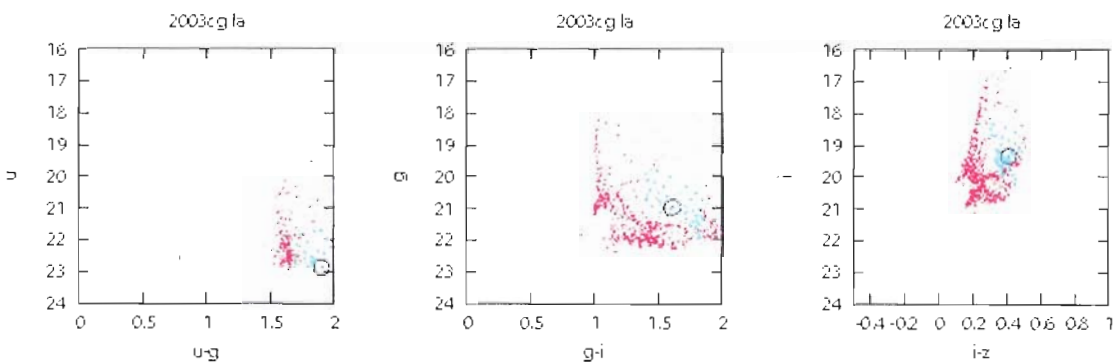


Figure 5.327. SN 2003cg  $u,u-g$ ,  $g,g-i$ , and  $i,i-z$  pseudo color-magnitude plots.

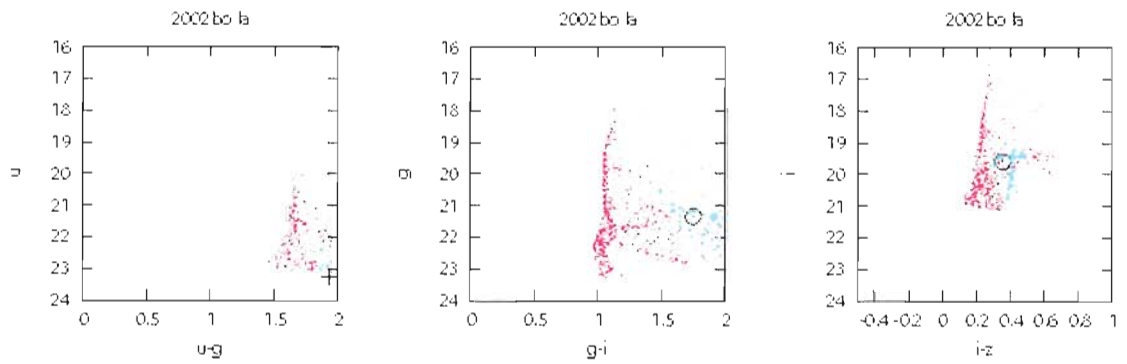


Figure 5.328. SN 2002bo  $u,u-g$ ,  $g,g-i$ , and  $i,i-z$  pseudo color-magnitude plots.

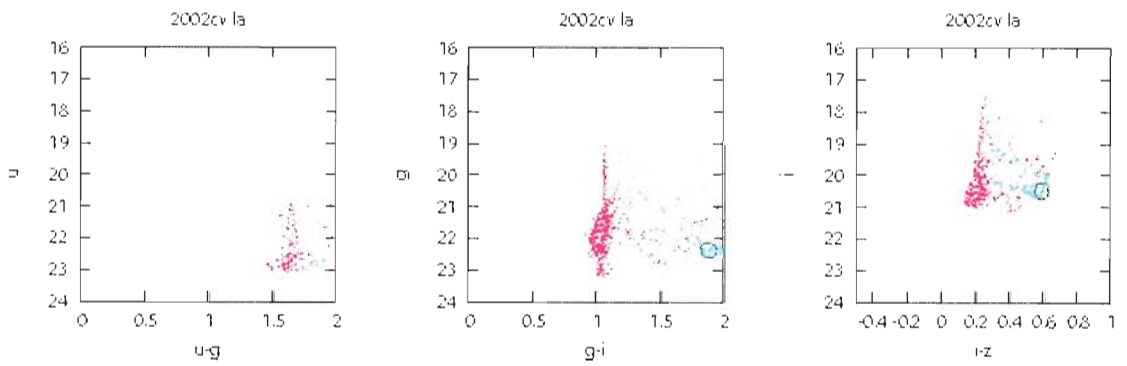


Figure 5.329. SN 2002cv  $u,u-g$ ,  $g,g-i$ , and  $i,i-z$  pseudo color-magnitude plots.

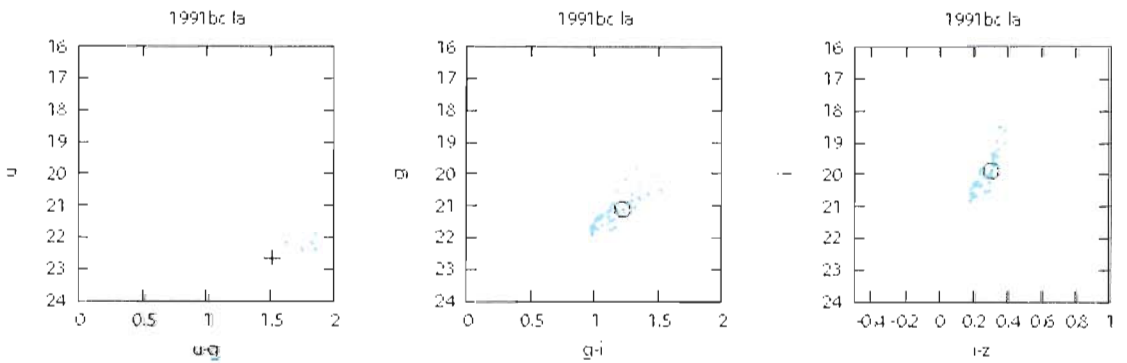


Figure 5.330. SN 1991bc  $u,u-g$ ,  $g,g-i$ , and  $i,i-z$  pseudo color-magnitude plots.



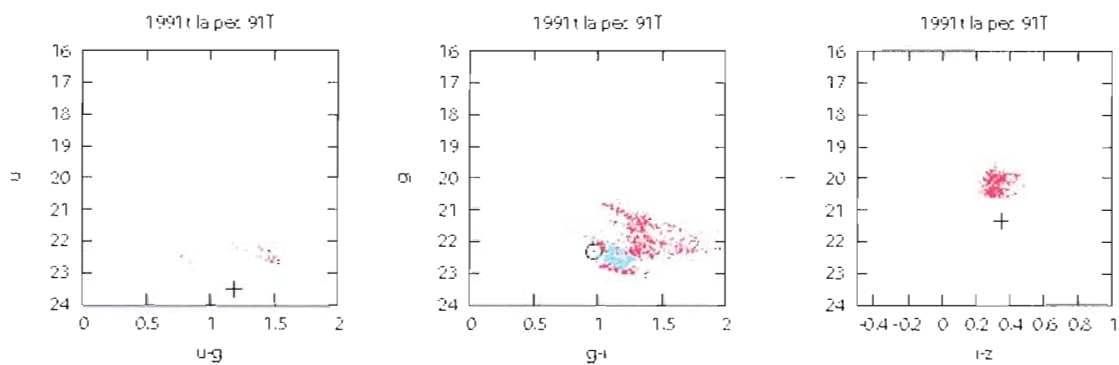


Figure 5.331. SN 1991t  $u,u-g$ ,  $g,g-i$ , and  $i,i-z$  pseudo color-magnitude plots.

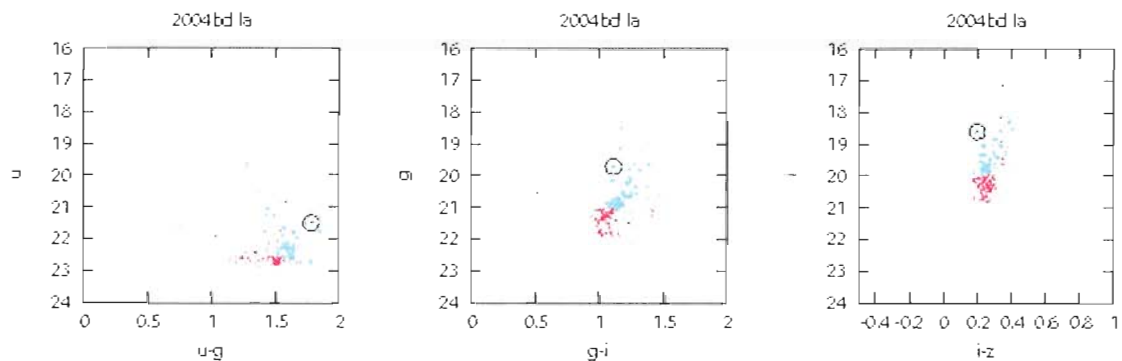


Figure 5.332. SN 2004bd  $u,u-g$ ,  $g,g-i$ , and  $i,i-z$  pseudo color-magnitude plots.

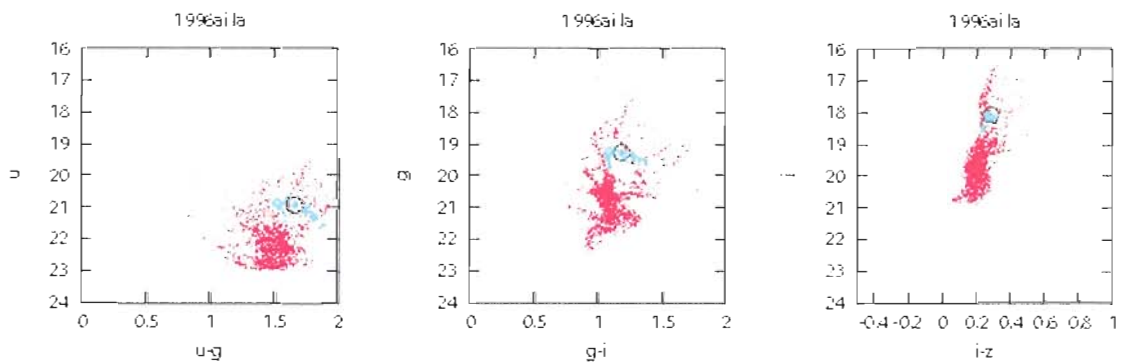


Figure 5.333. SN 1996ai  $u,u-g$ ,  $g,g-i$ , and  $i,i-z$  pseudo color-magnitude plots.

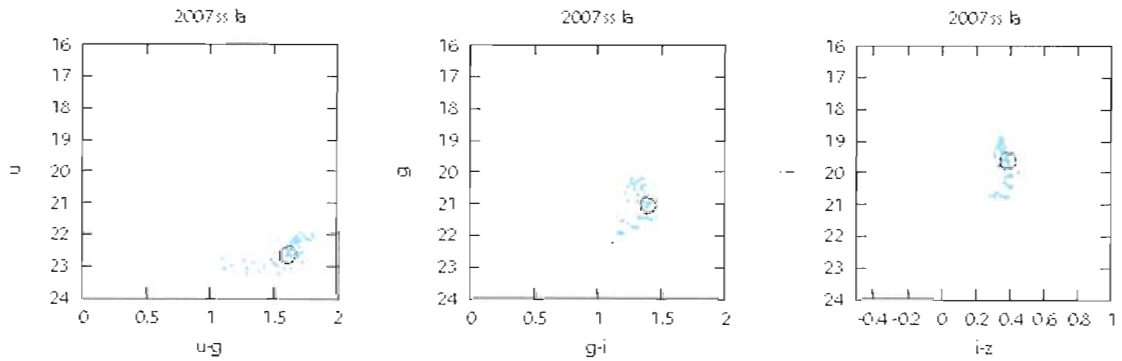


Figure 5.334. SN 2007ss  $u,u-g$ ,  $g,g-i$ , and  $i,i-z$  pseudo color-magnitude plots.

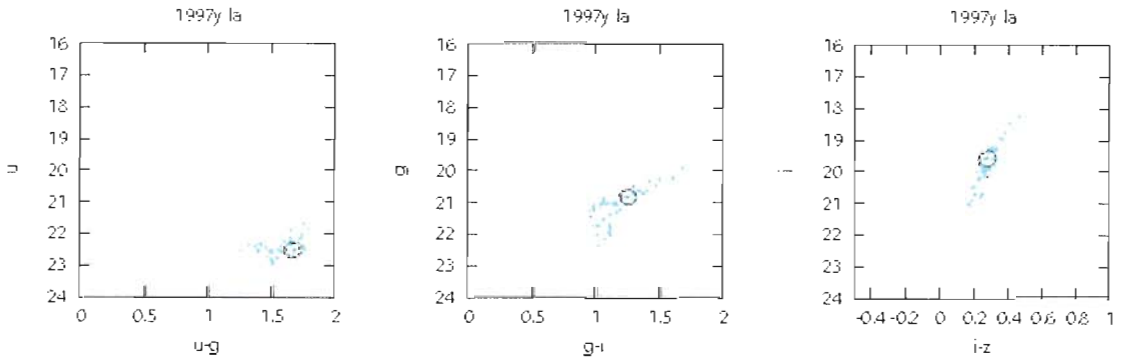


Figure 5.335. SN 1997y  $u,u-g$ ,  $g,g-i$ , and  $i,i-z$  pseudo color-magnitude plots.

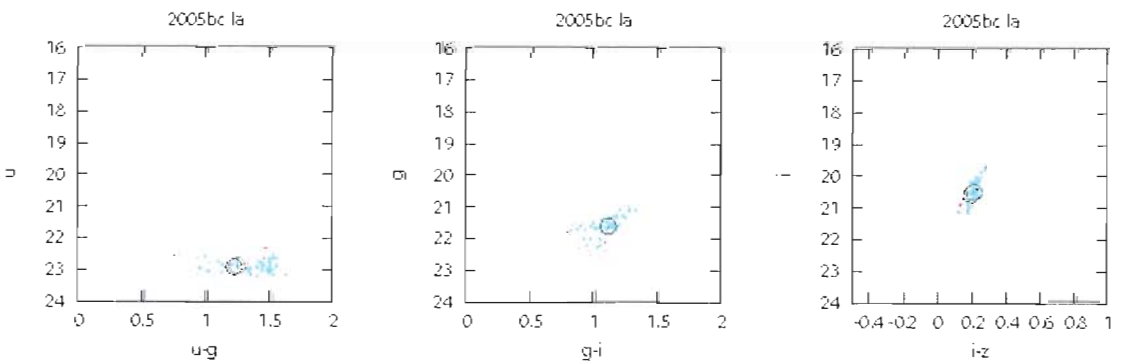


Figure 5.336. SN 2005bc  $u,u-g$ ,  $g,g-i$ , and  $i,i-z$  pseudo color-magnitude plots.

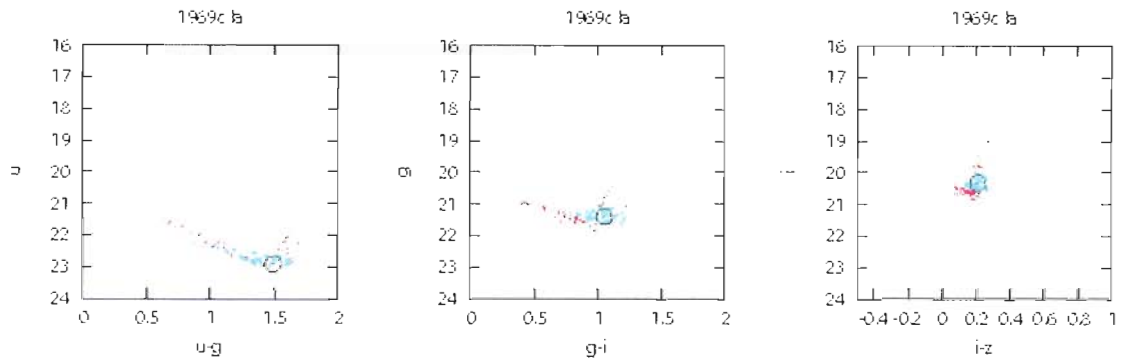


Figure 5.337. SN 1969c  $u,u-g$ ,  $g,g-i$ , and  $i,i-z$  pseudo color-magnitude plots.

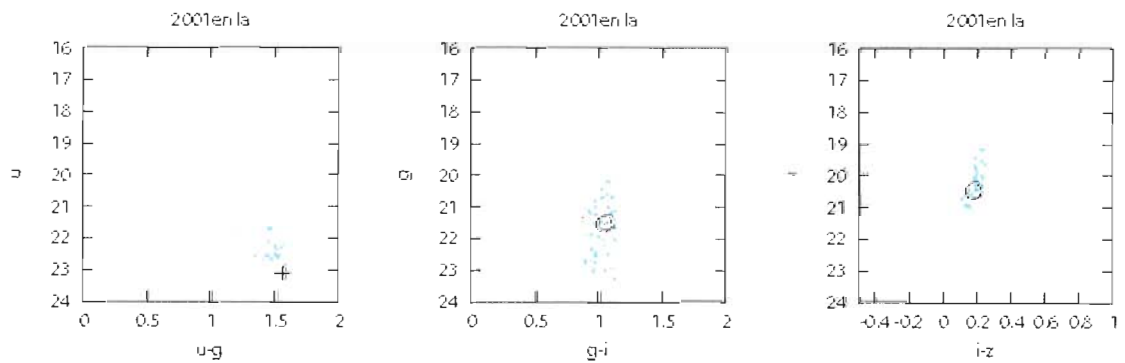


Figure 5.338. SN 2001en  $u,u-g$ ,  $g,g-i$ , and  $i,i-z$  pseudo color-magnitude plots.

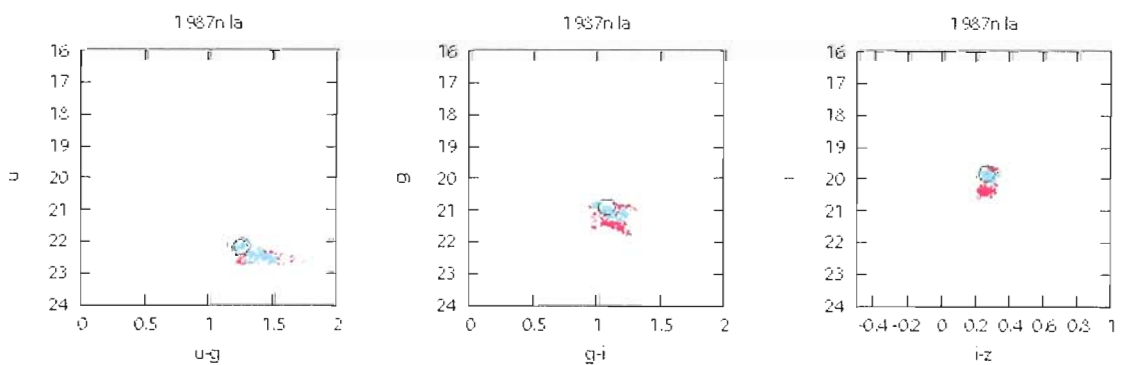


Figure 5.339. SN 1987n  $u,u-g$ ,  $g,g-i$ , and  $i,i-z$  pseudo color-magnitude plots.

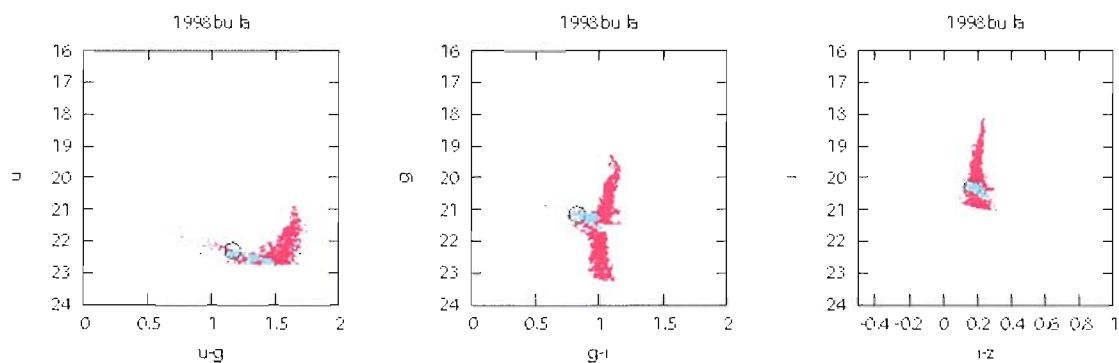


Figure 5.340. SN 1998bu  $u,u-g$ ,  $g,g-i$ , and  $i,i-z$  pseudo color-magnitude plots.

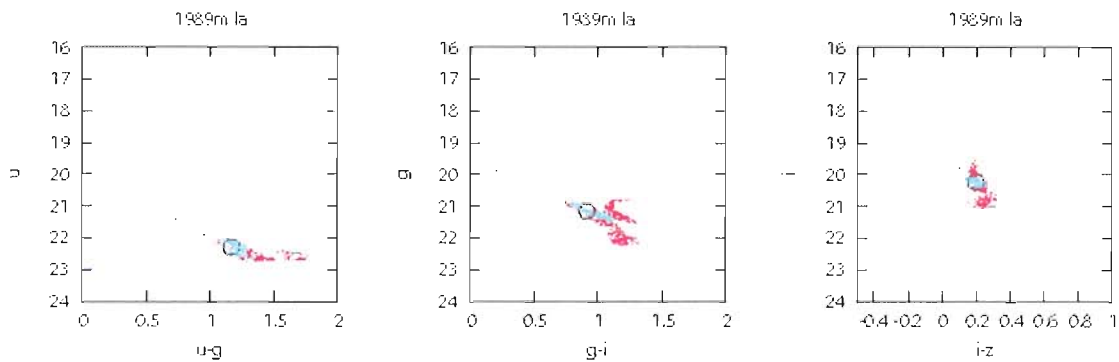


Figure 5.341. SN 1989m  $u,u-g$ ,  $g,g-i$ , and  $i,i-z$  pseudo color-magnitude plots.

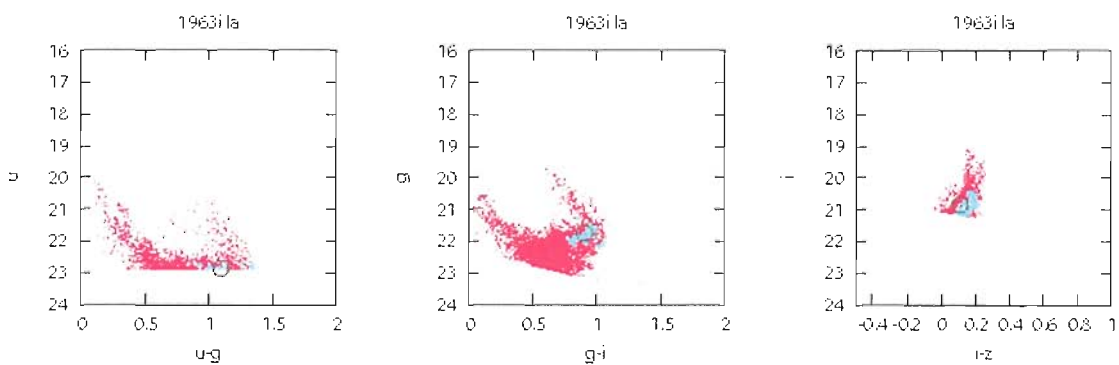


Figure 5.342. SN 1963i  $u,u-g$ ,  $g,g-i$ , and  $i,i-z$  pseudo color-magnitude plots.

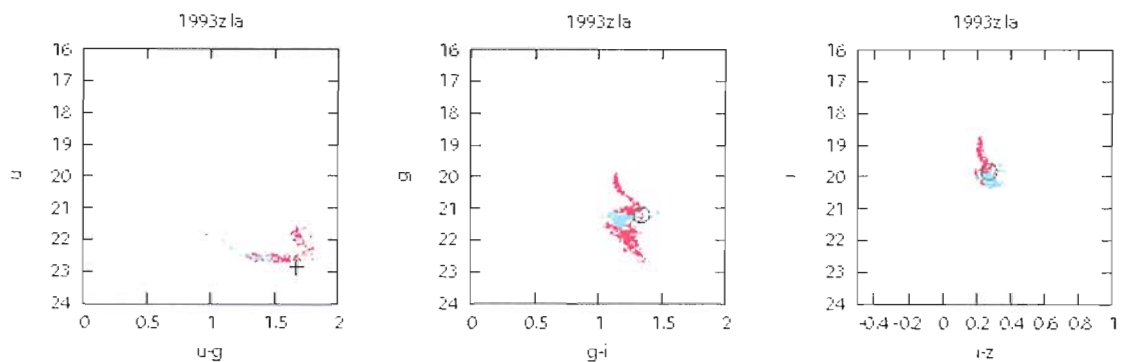


Figure 5.343. SN 1993z  $u,u-g$ ,  $g,g-i$ , and  $i,i-z$  pseudo color-magnitude plots.

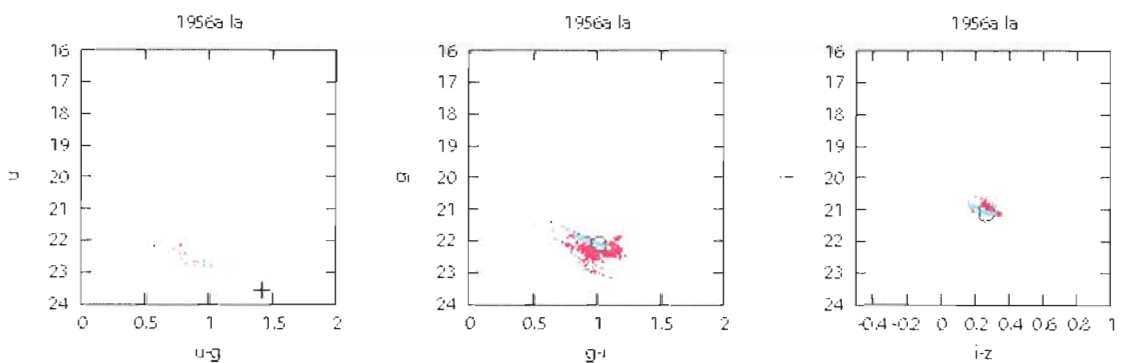


Figure 5.344. SN 1956a  $u,u-g$ ,  $g,g-i$ , and  $i,i-z$  pseudo color-magnitude plots.

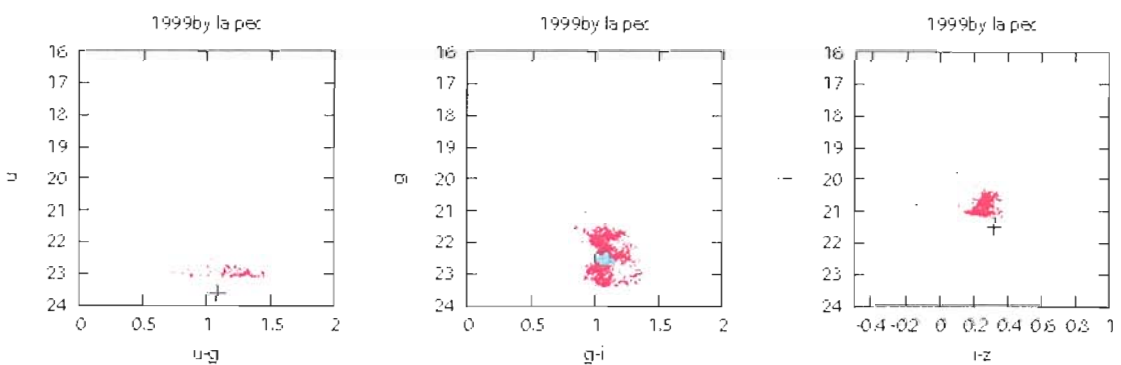


Figure 5.345. SN 1999by  $u,u-g$ ,  $g,g-i$ , and  $i,i-z$  pseudo color-magnitude plots.

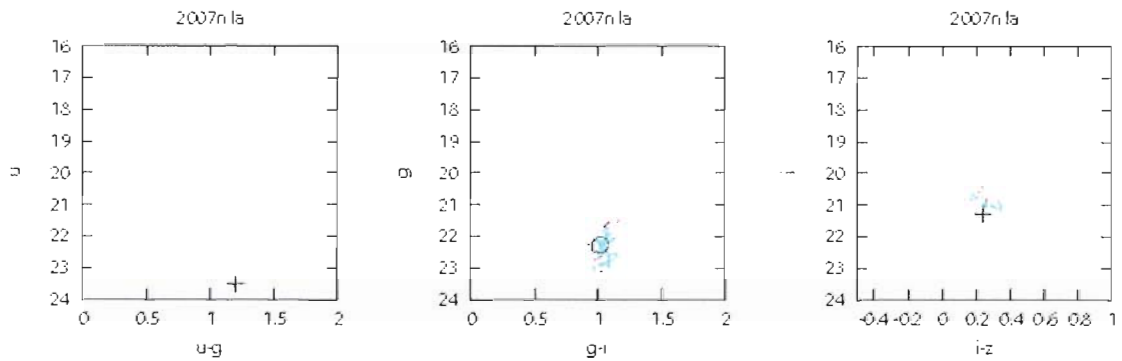


Figure 5.346. SN 2007n  $u, u-g, g, g-i,$  and  $i, i-z$  pseudo color-magnitude plots.

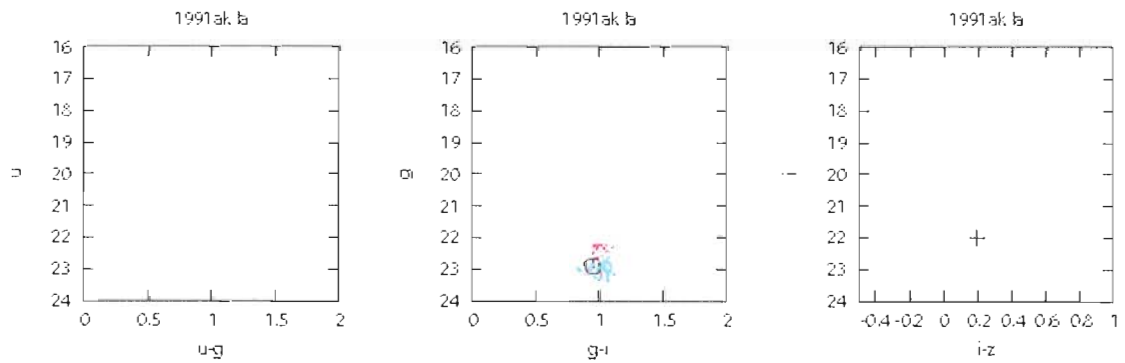


Figure 5.347. SN 1991ak  $u, u-g, g, g-i,$  and  $i, i-z$  pseudo color-magnitude plots.

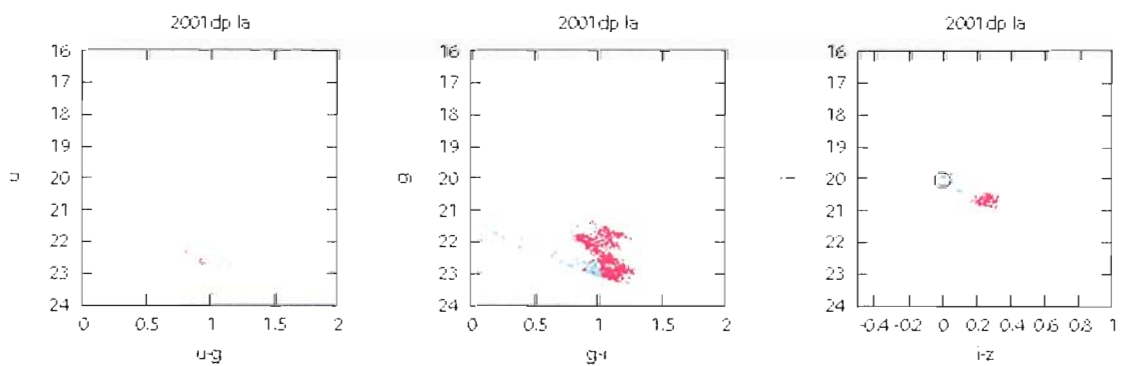


Figure 5.348. SN 2001dp  $u, u-g, g, g-i,$  and  $i, i-z$  pseudo color-magnitude plots.

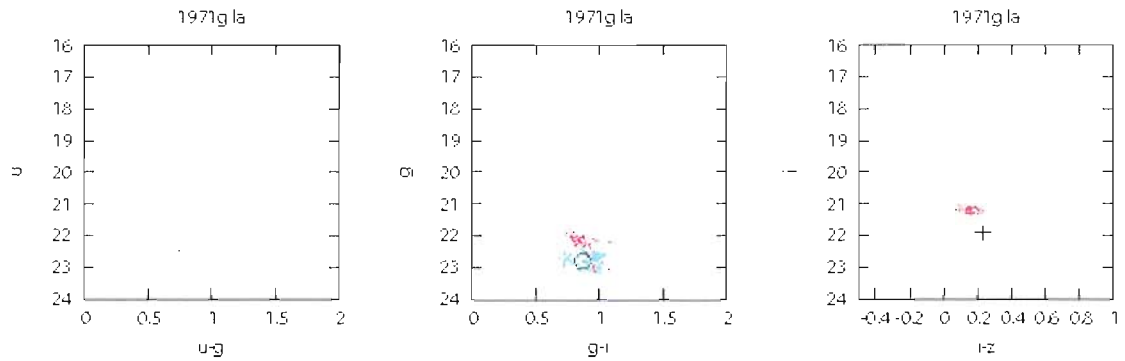


Figure 5.349. SN 1971g  $u,u-g$ ,  $g,g-i$ , and  $i,i-z$  pseudo color-magnitude plots.

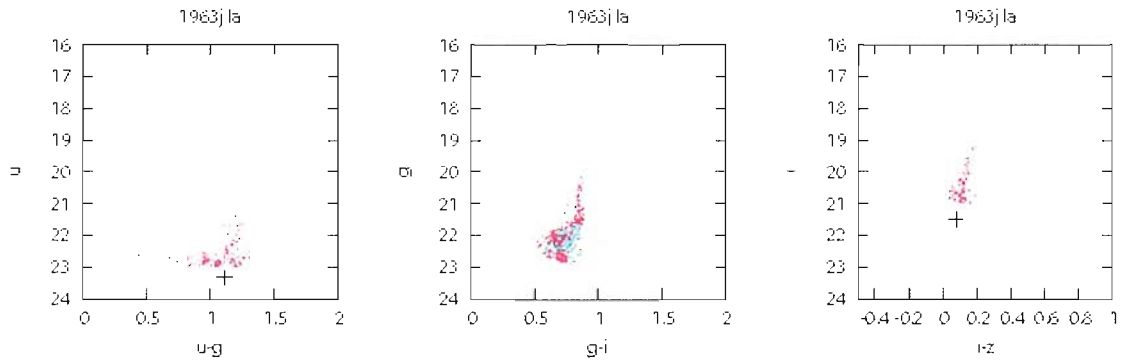


Figure 5.350. SN 1963j  $u,u-g$ ,  $g,g-i$ , and  $i,i-z$  pseudo color-magnitude plots.

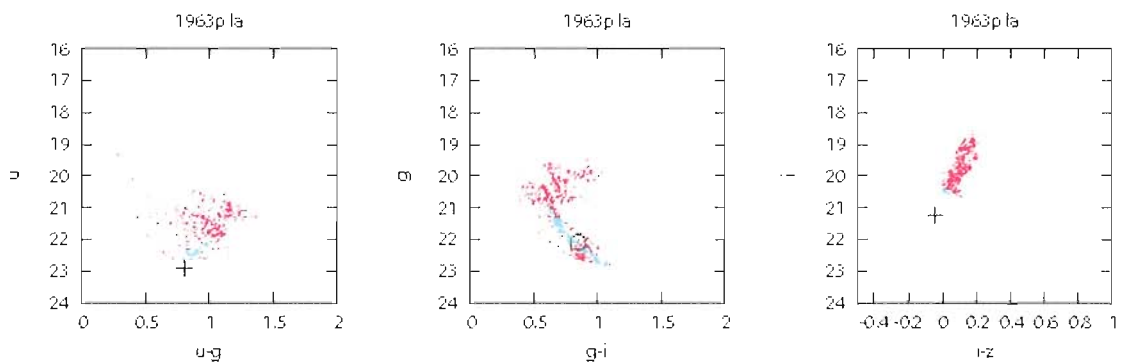


Figure 5.351. SN 1963p  $u,u-g$ ,  $g,g-i$ , and  $i,i-z$  pseudo color-magnitude plots.

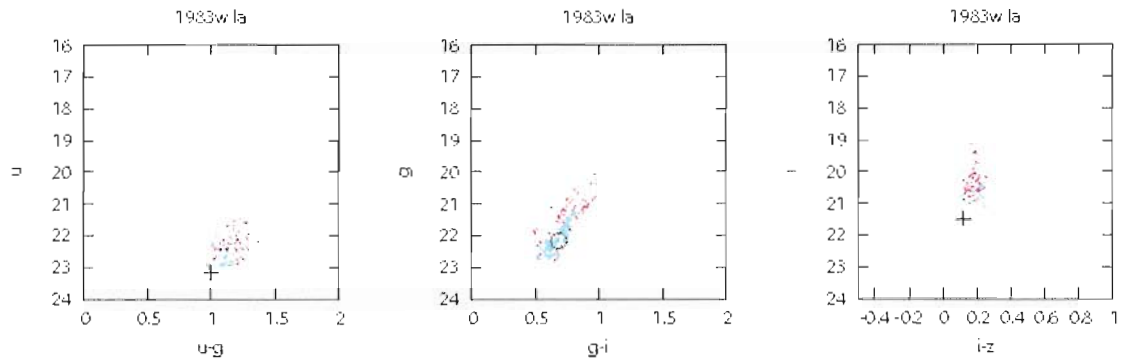


Figure 5.352. SN 1983w  $u,u-g$ ,  $g,g-i$ , and  $i,i-z$  pseudo color-magnitude plots.

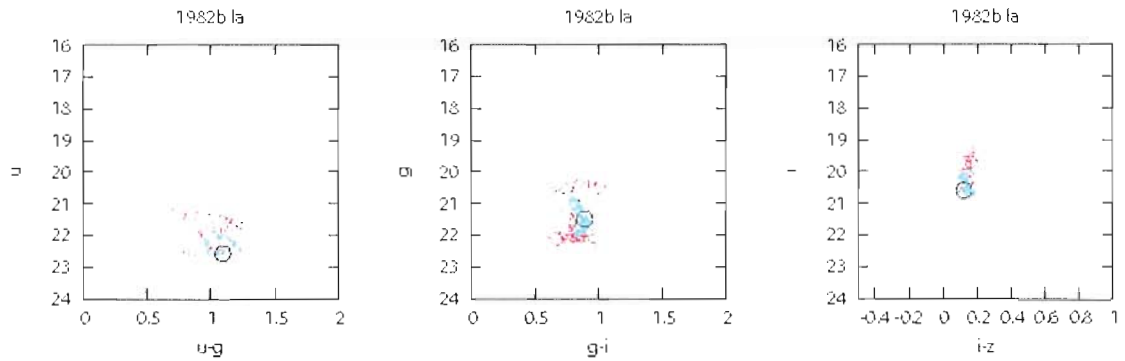


Figure 5.353. SN 1982b  $u,u-g$ ,  $g,g-i$ , and  $i,i-z$  pseudo color-magnitude plots.

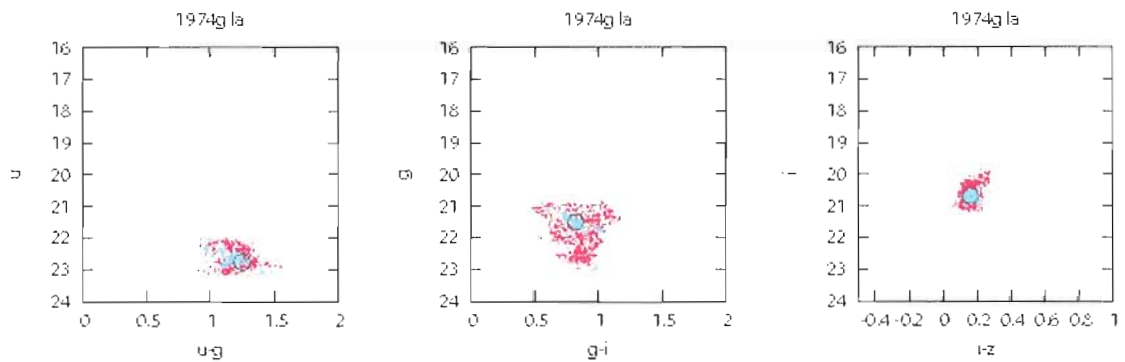


Figure 5.354. SN 1974g  $u,u-g$ ,  $g,g-i$ , and  $i,i-z$  pseudo color-magnitude plots.



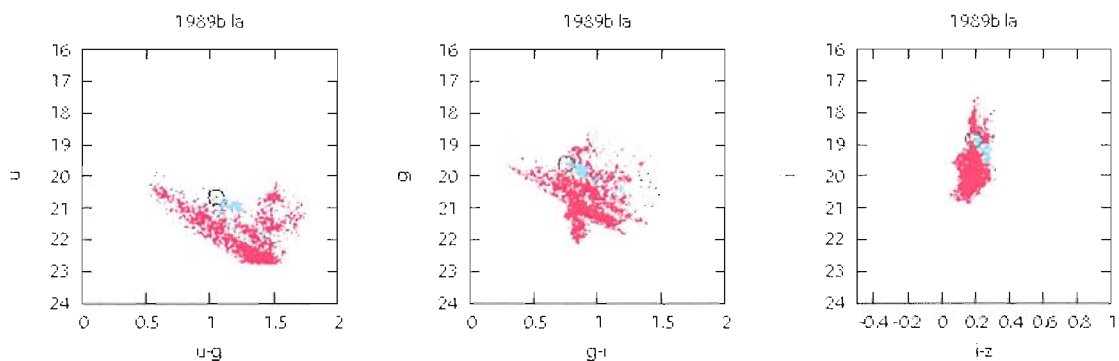


Figure 5.355. SN 1989b  $u,u-g$ ,  $g,g-i$ , and  $i,i-z$  pseudo color-magnitude plots.

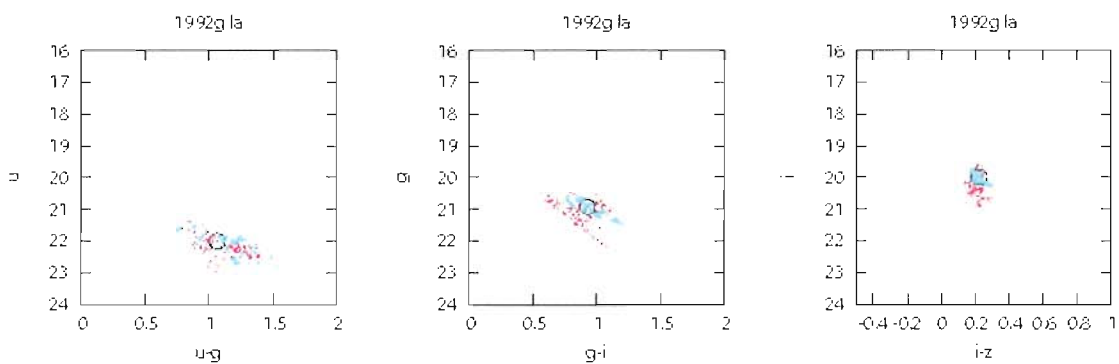


Figure 5.356. SN 1992g  $u,u-g$ ,  $g,g-i$ , and  $i,i-z$  pseudo color-magnitude plots.

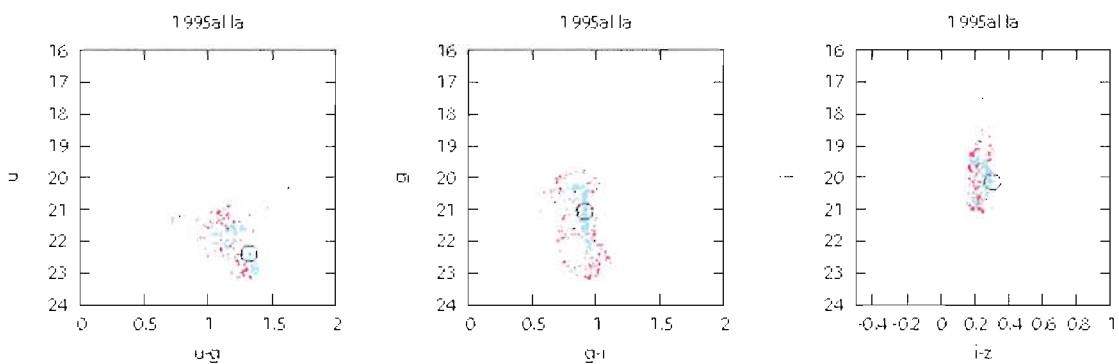


Figure 5.357. SN 1995al  $u,u-g$ ,  $g,g-i$ , and  $i,i-z$  pseudo color-magnitude plots.

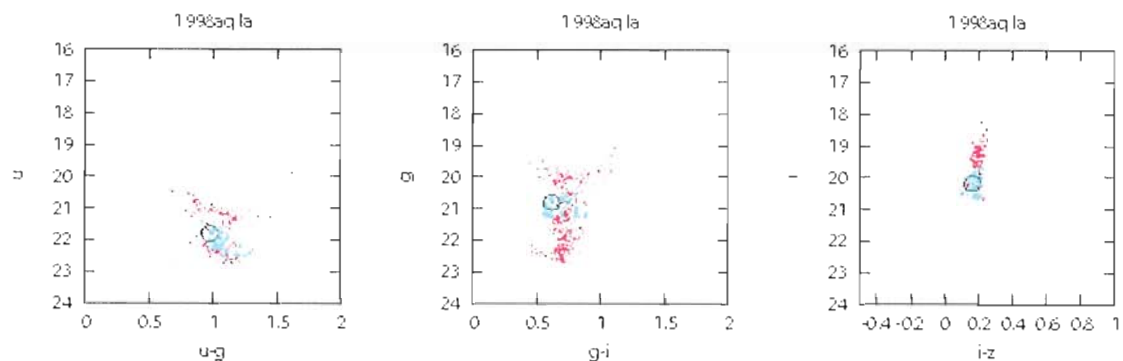


Figure 5.358. SN 1998aq  $u,u-g$ ,  $g,g-i$ , and  $i,i-z$  pseudo color-magnitude plots.

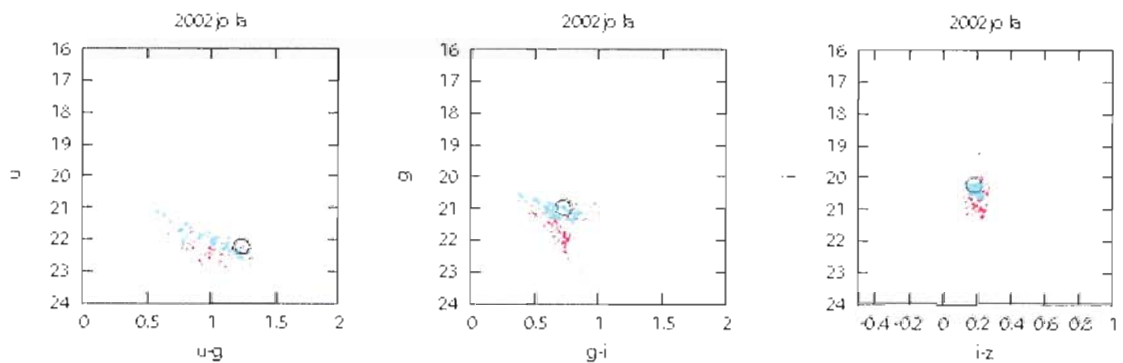


Figure 5.359. SN 2002jo  $u,u-g$ ,  $g,g-i$ , and  $i,i-z$  pseudo color-magnitude plots.

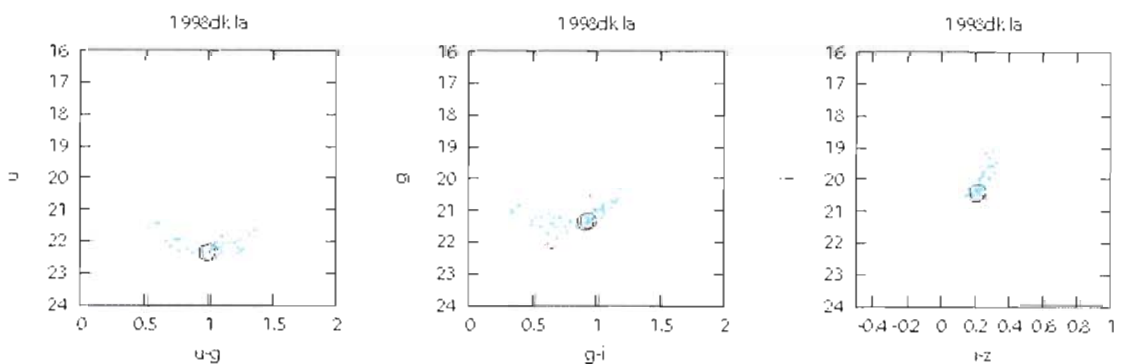


Figure 5.360. SN 1998dk  $u,u-g$ ,  $g,g-i$ , and  $i,i-z$  pseudo color-magnitude plots.

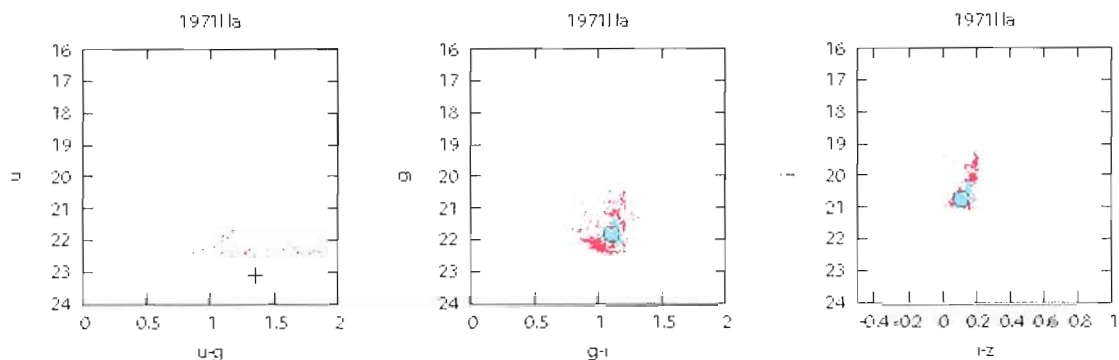


Figure 5.361. SN 1971l  $u,u-g$ ,  $g,g-i$ , and  $i,i-z$  pseudo color-magnitude plots.

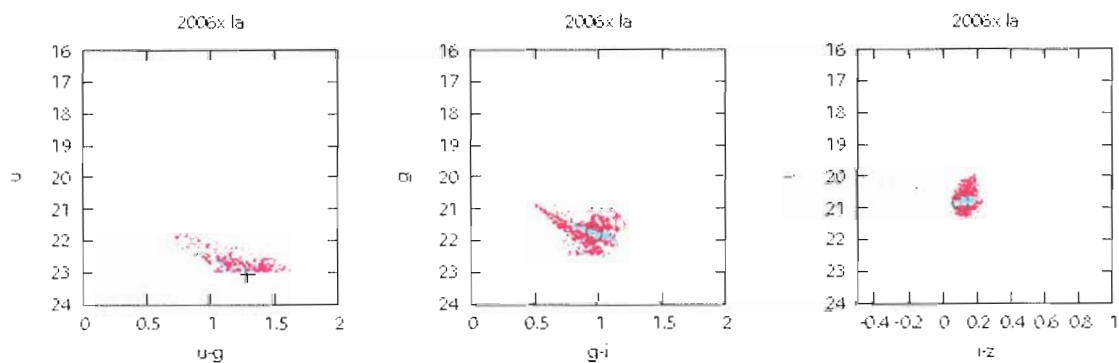


Figure 5.362. SN 2006x  $u,u-g$ ,  $g,g-i$ , and  $i,i-z$  pseudo color-magnitude plots.

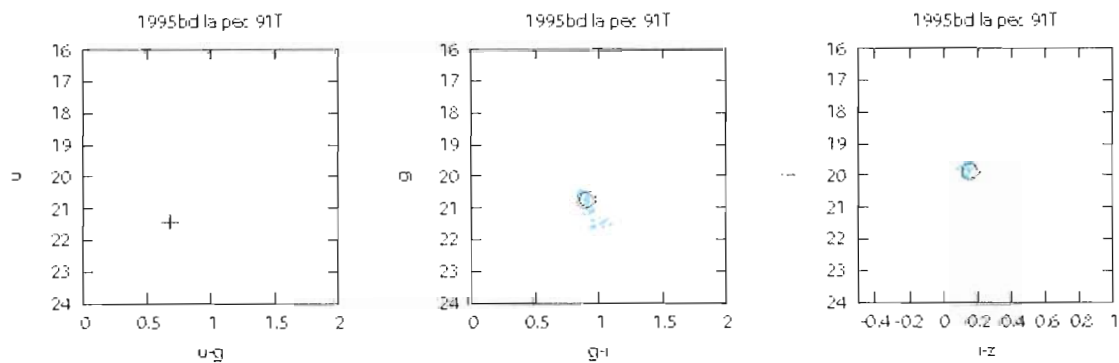


Figure 5.363. SN 1995bd  $u,u-g$ ,  $g,g-i$ , and  $i,i-z$  pseudo color-magnitude plots.

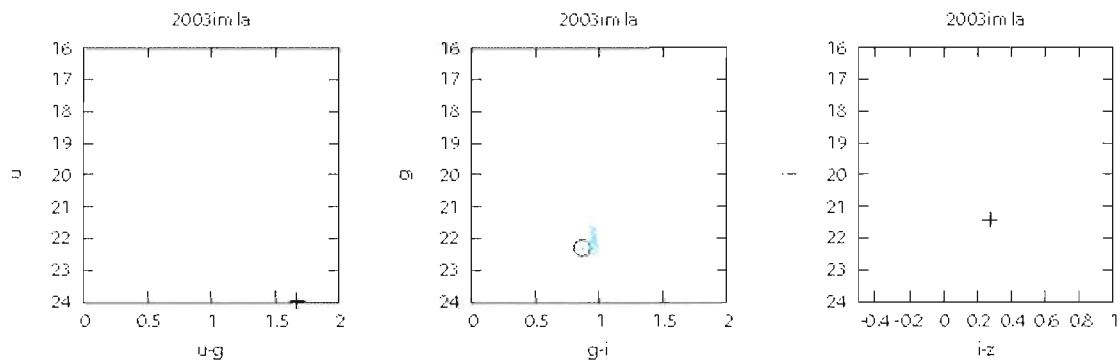


Figure 5.364. SN 2003im  $u,u-g$ ,  $g,g-i$ , and  $i,i-z$  pseudo color-magnitude plots.

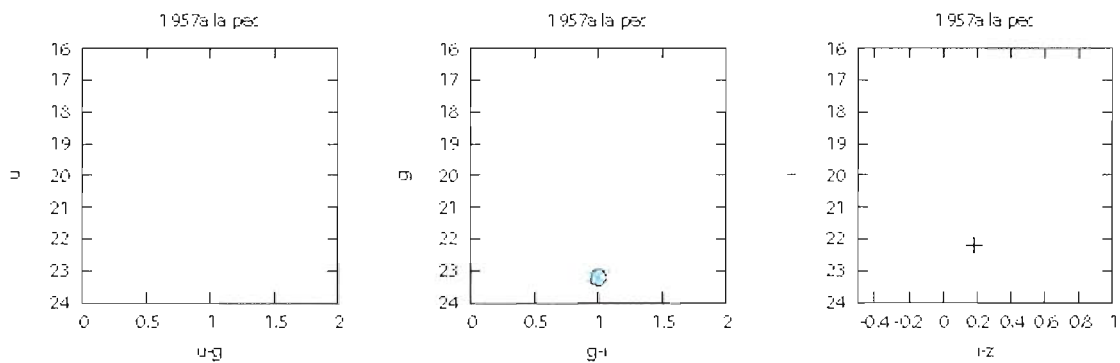


Figure 5.365. SN 1957a  $u,u-g$ ,  $g,g-i$ , and  $i,i-z$  pseudo color-magnitude plots.

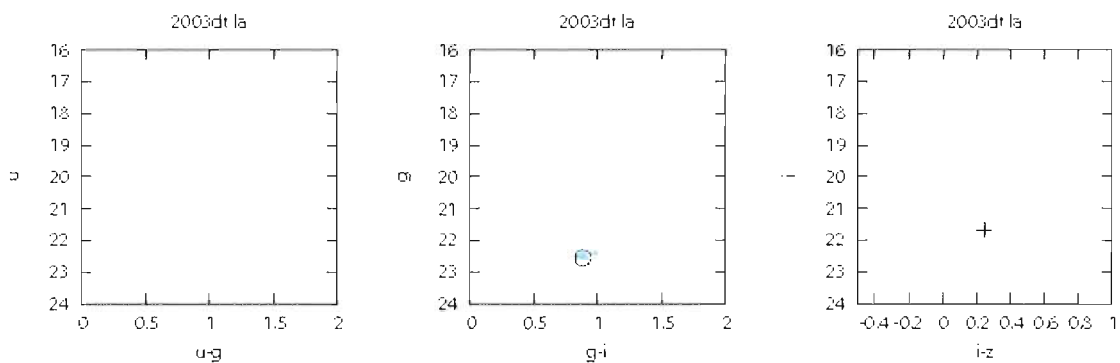


Figure 5.366. SN 2003dt  $u,u-g$ ,  $g,g-i$ , and  $i,i-z$  pseudo color-magnitude plots.

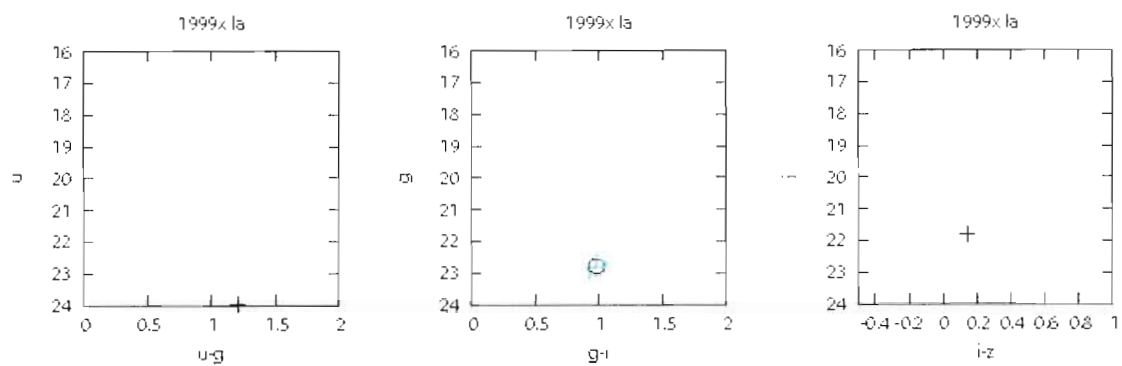


Figure 5.367. SN 1999x  $u,u-g$ ,  $g,g-i$ , and  $i,i-z$  pseudo color-magnitude plots.

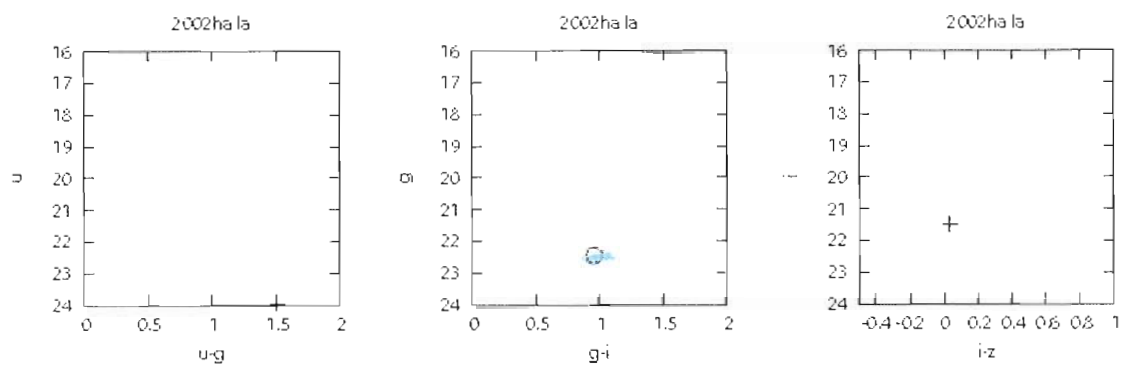


Figure 5.368. SN 2002ha  $u,u-g$ ,  $g,g-i$ , and  $i,i-z$  pseudo color-magnitude plots.

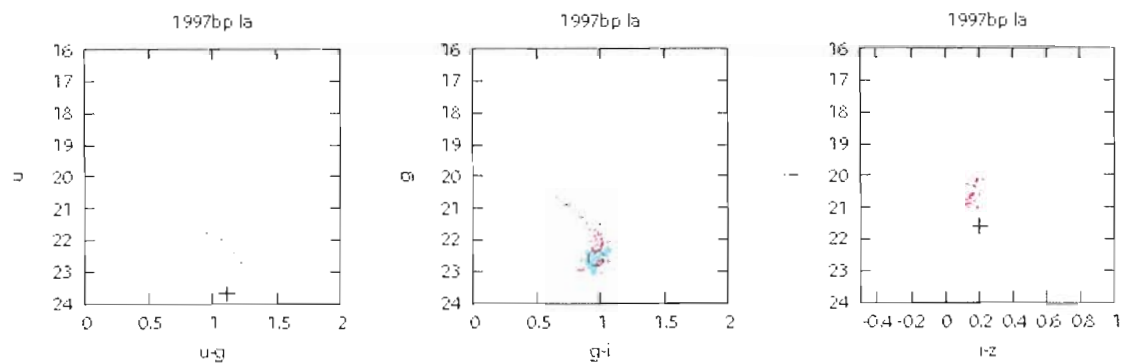


Figure 5.369. SN 1997bp  $u,u-g$ ,  $g,g-i$ , and  $i,i-z$  pseudo color-magnitude plots.

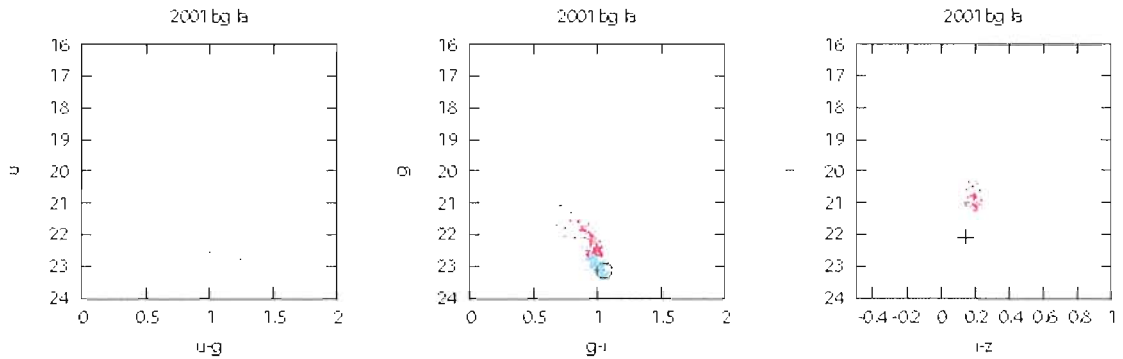


Figure 5.370. SN 2001bg  $u,u-g$ ,  $g,g-i$ , and  $i,i-z$  pseudo color-magnitude plots.

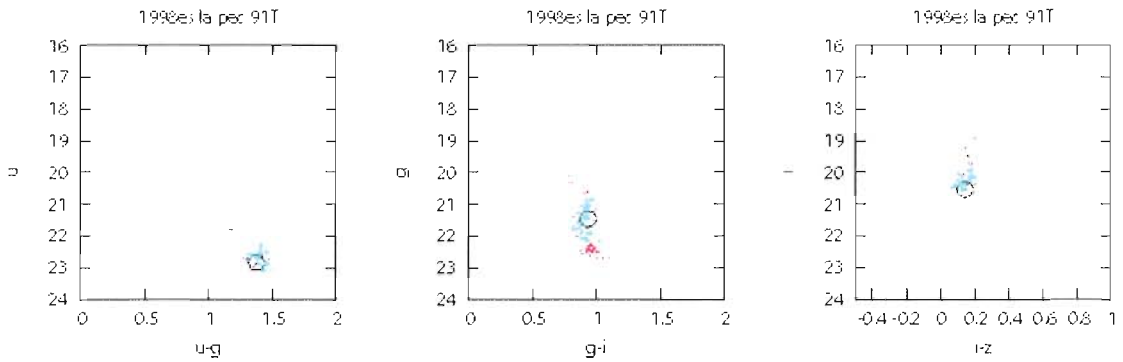


Figure 5.371. SN 1998es  $u,u-g$ ,  $g,g-i$ , and  $i,i-z$  pseudo color-magnitude plots.

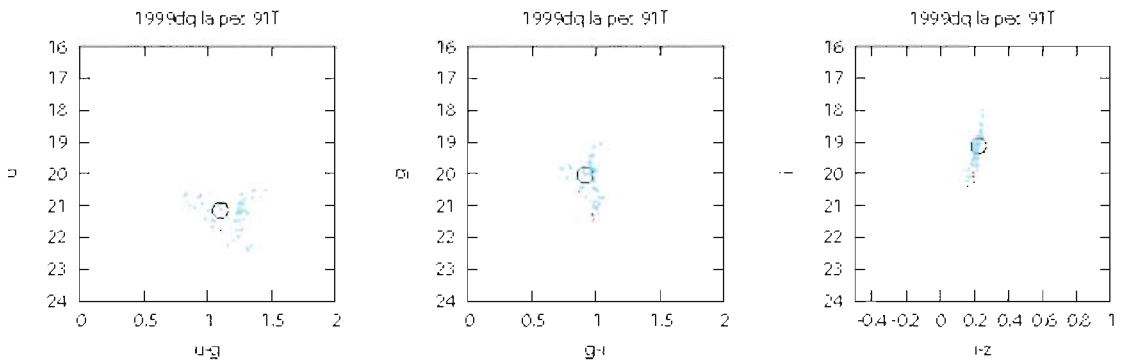


Figure 5.372. SN 1999dq  $u,u-g$ ,  $g,g-i$ , and  $i,i-z$  pseudo color-magnitude plots.

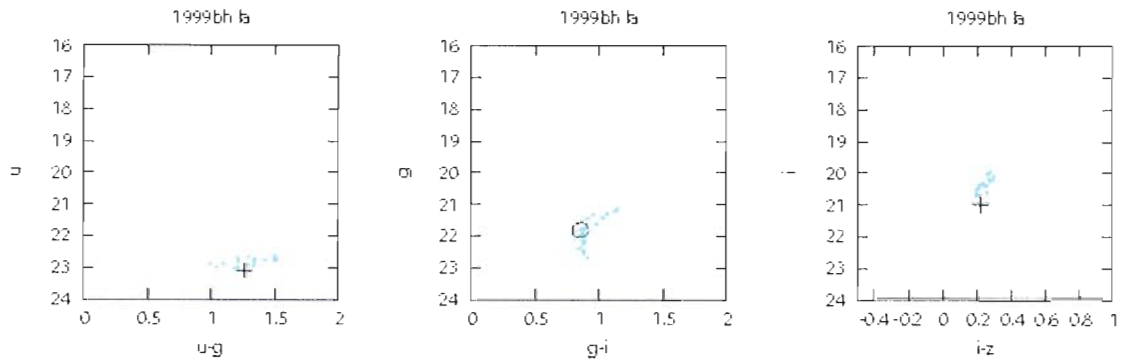


Figure 5.373. SN 1999bh  $u,u-g$ ,  $g,g-i$ , and  $i,i-z$  pseudo color-magnitude plots.

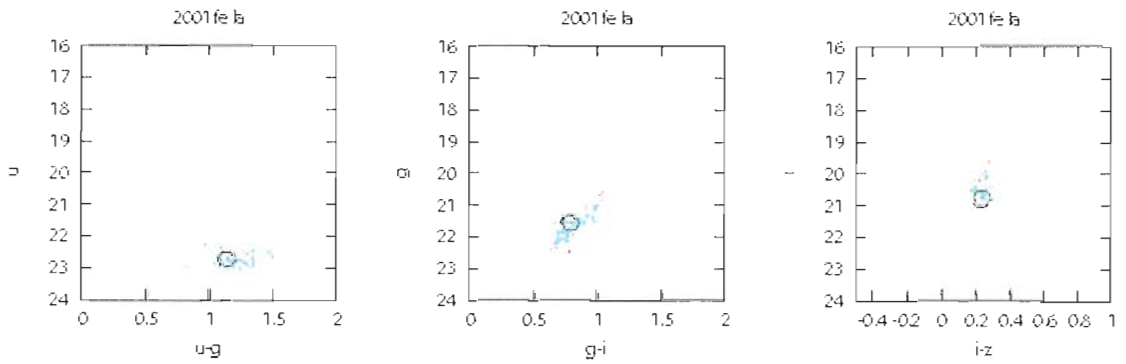


Figure 5.374. SN 2001fe  $u,u-g$ ,  $g,g-i$ , and  $i,i-z$  pseudo color-magnitude plots.

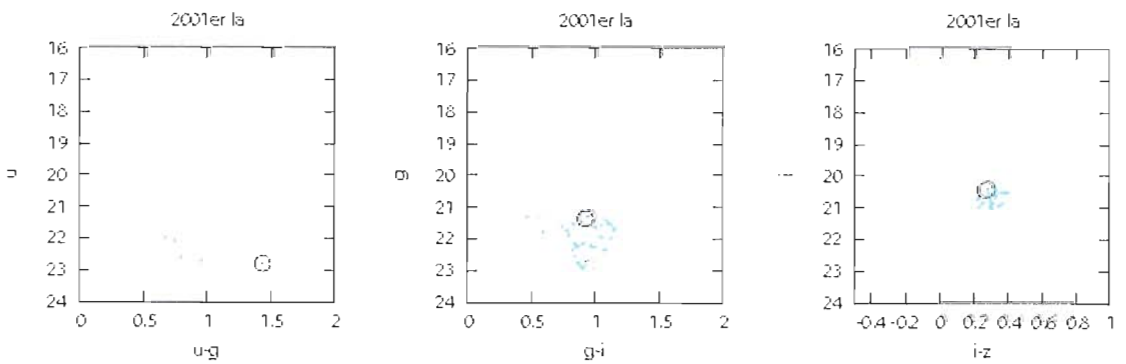


Figure 5.375. SN 2001er  $u,u-g$ ,  $g,g-i$ , and  $i,i-z$  pseudo color-magnitude plots.

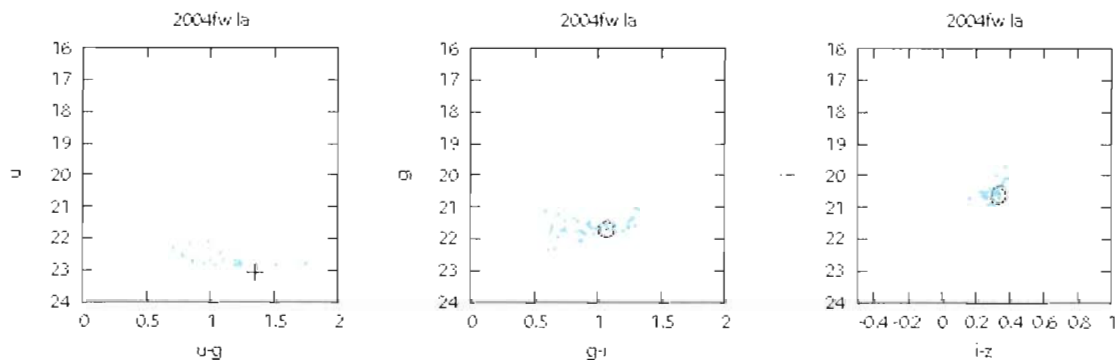


Figure 5.376. SN 2004fw  $u,u-g$ ,  $g,g-i$ , and  $i,i-z$  pseudo color-magnitude plots.

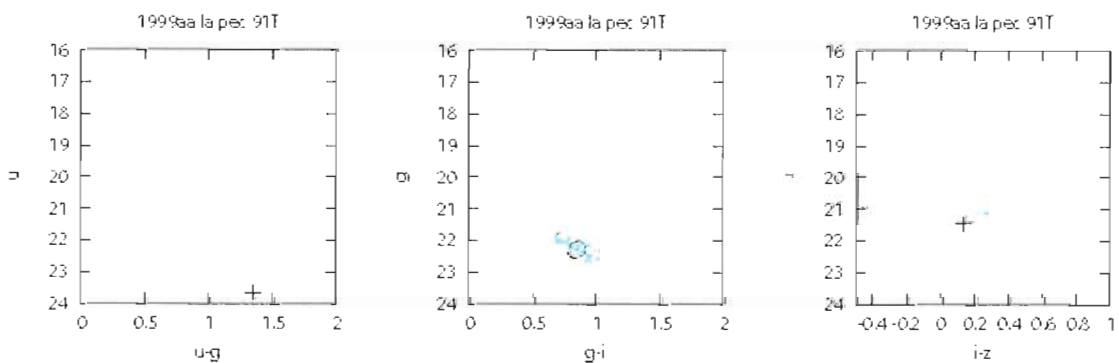


Figure 5.377. SN 1999aa  $u,u-g$ ,  $g,g-i$ , and  $i,i-z$  pseudo color-magnitude plots.

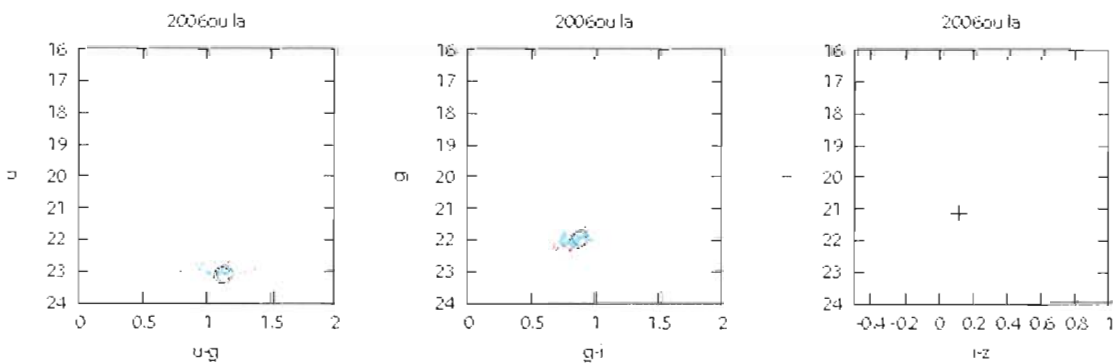


Figure 5.378. SN 2006ou  $u,u-g$ ,  $g,g-i$ , and  $i,i-z$  pseudo color-magnitude plots.



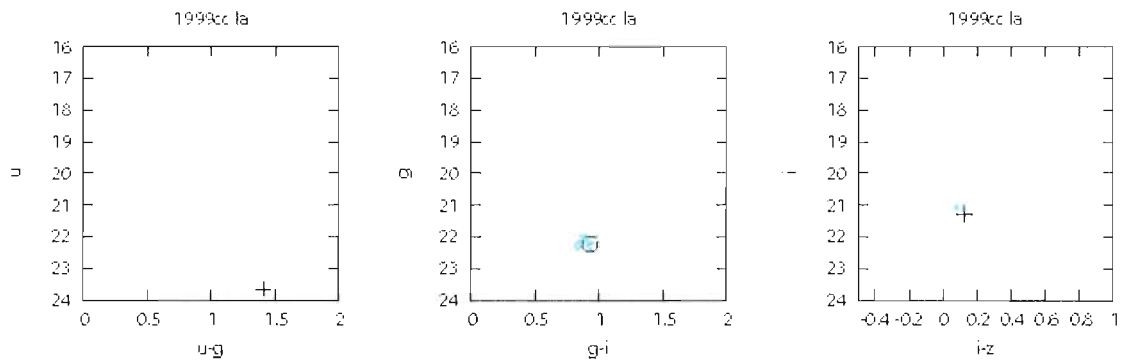


Figure 5.379. SN 1999cc  $u,u-g$ ,  $g,g-i$ , and  $i,i-z$  pseudo color-magnitude plots.

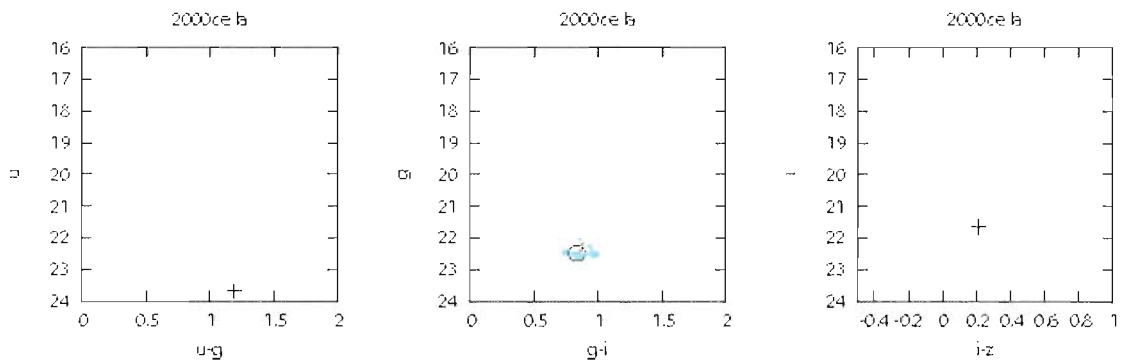


Figure 5.380. SN 2000ce  $u,u-g$ ,  $g,g-i$ , and  $i,i-z$  pseudo color-magnitude plots.

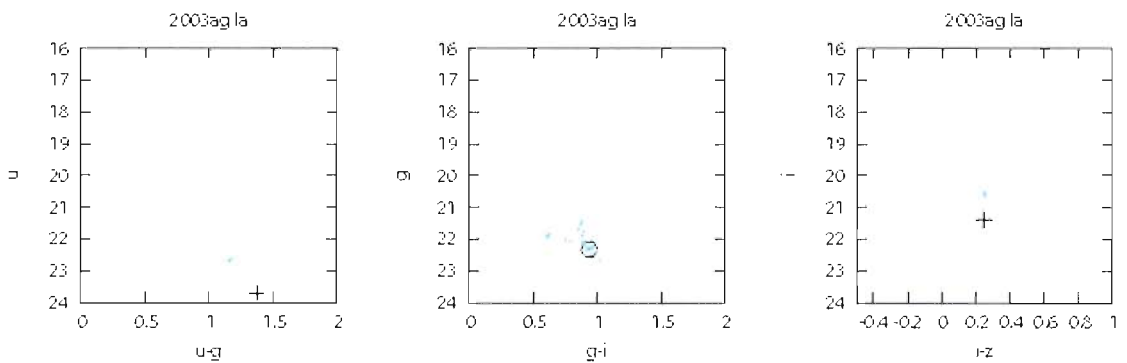


Figure 5.381. SN 2003ag  $u,u-g$ ,  $g,g-i$ , and  $i,i-z$  pseudo color-magnitude plots.

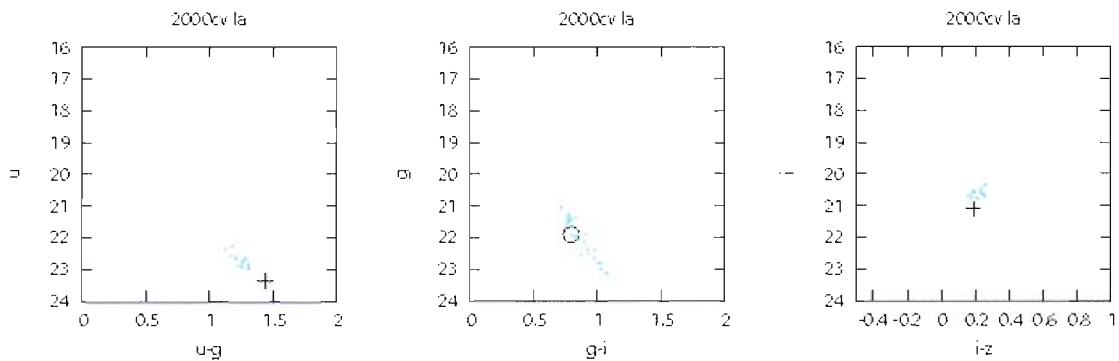


Figure 5.382. SN 2000cv  $u,u-g$ ,  $g,g-i$ , and  $i,i-z$  pseudo color-magnitude plots.

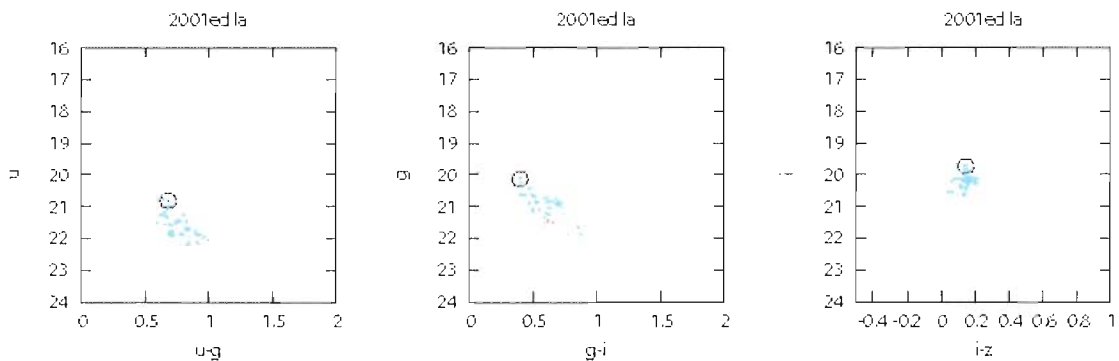


Figure 5.383. SN 2001ed  $u,u-g$ ,  $g,g-i$ , and  $i,i-z$  pseudo color-magnitude plots.

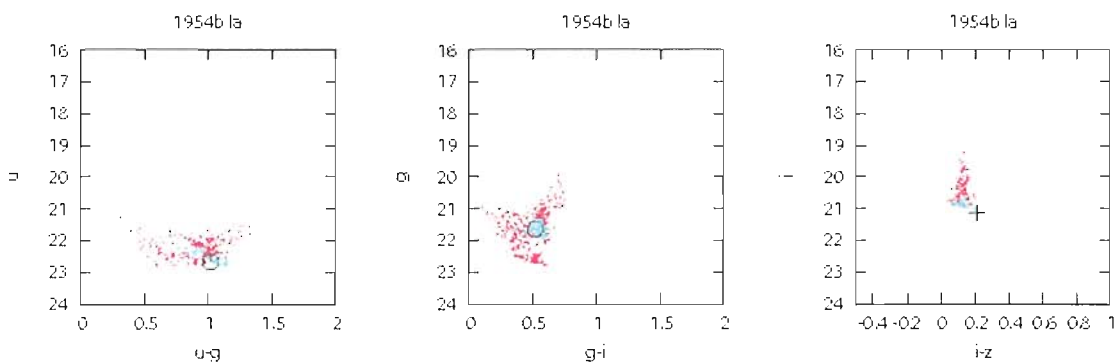


Figure 5.384. SN 1954b  $u,u-g$ ,  $g,g-i$ , and  $i,i-z$  pseudo color-magnitude plots.

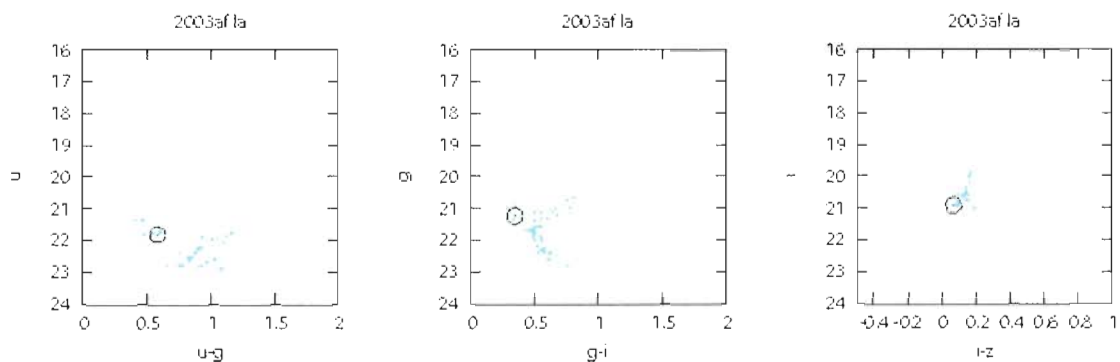


Figure 5.385. SN 2003af  $u,u-g$ ,  $g,g-i$ , and  $i,i-z$  pseudo color-magnitude plots.

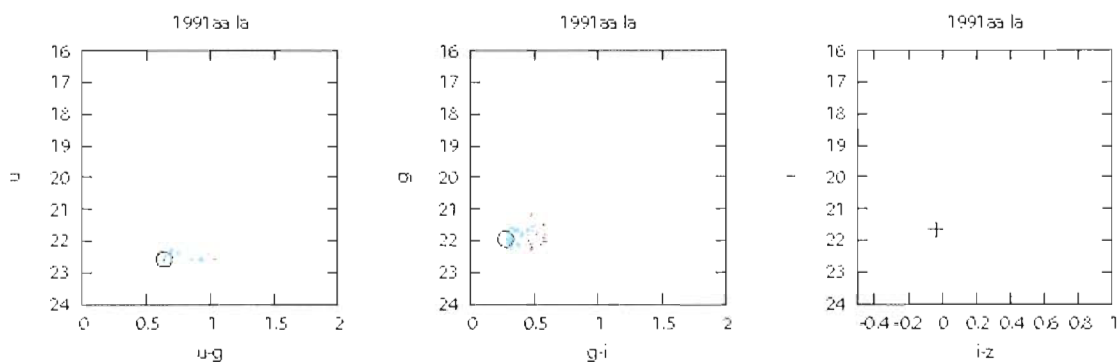


Figure 5.386. SN 1991aa  $u,u-g$ ,  $g,g-i$ , and  $i,i-z$  pseudo color-magnitude plots.

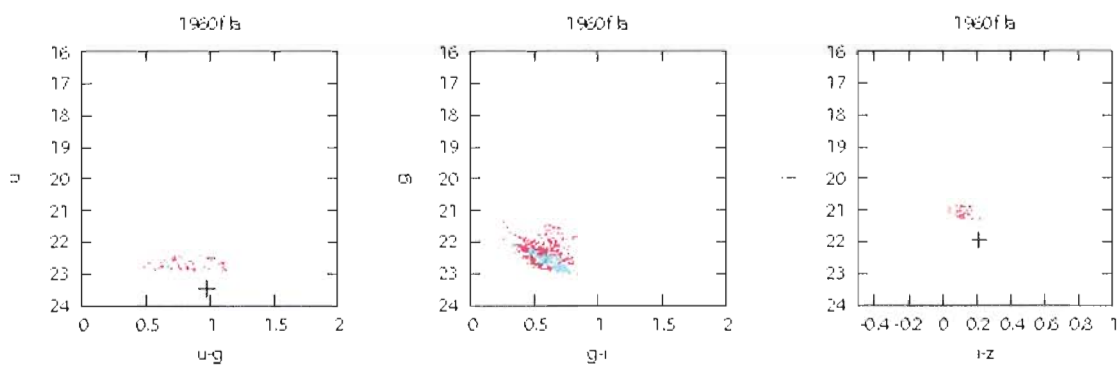


Figure 5.387. SN 1960f  $u,u-g$ ,  $g,g-i$ , and  $i,i-z$  pseudo color-magnitude plots.

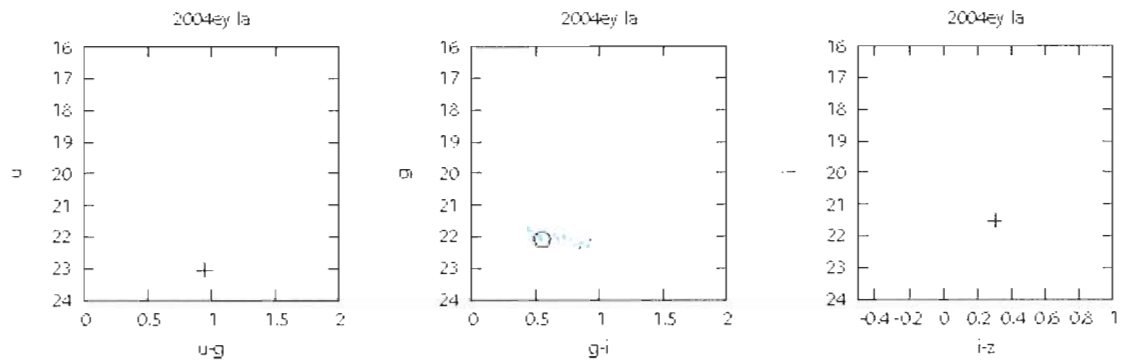


Figure 5.388. SN 2004ey  $u,u-g$ ,  $g,g-i$ , and  $i,i-z$  pseudo color-magnitude plots.

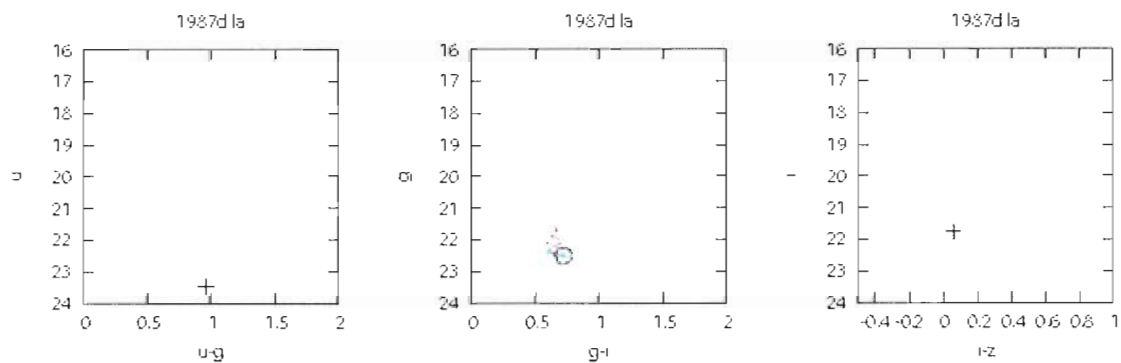


Figure 5.389. SN 1987d  $u,u-g$ ,  $g,g-i$ , and  $i,i-z$  pseudo color-magnitude plots.

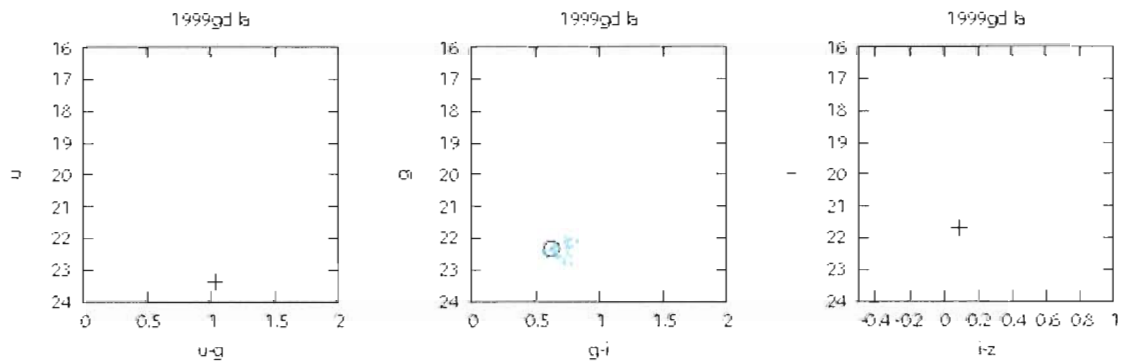


Figure 5.390. SN 1999gd  $u,u-g$ ,  $g,g-i$ , and  $i,i-z$  pseudo color-magnitude plots.

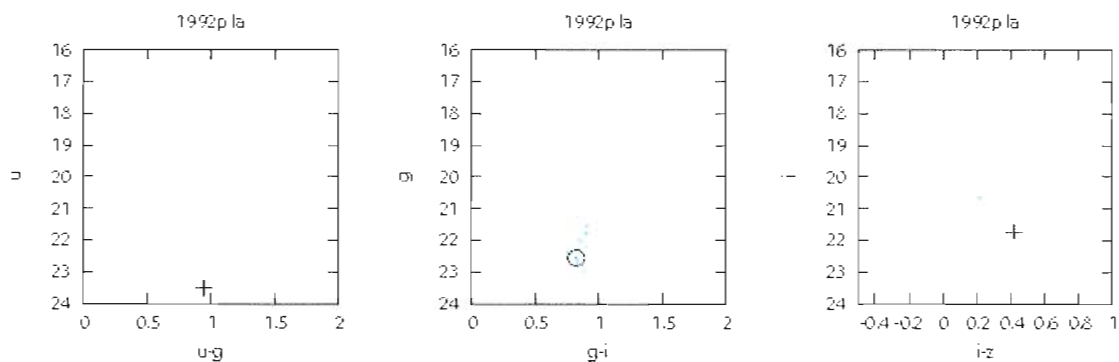


Figure 5.391. SN 1992p  $u,u-g$ ,  $g,g-i$ , and  $i,i-z$  pseudo color-magnitude plots.

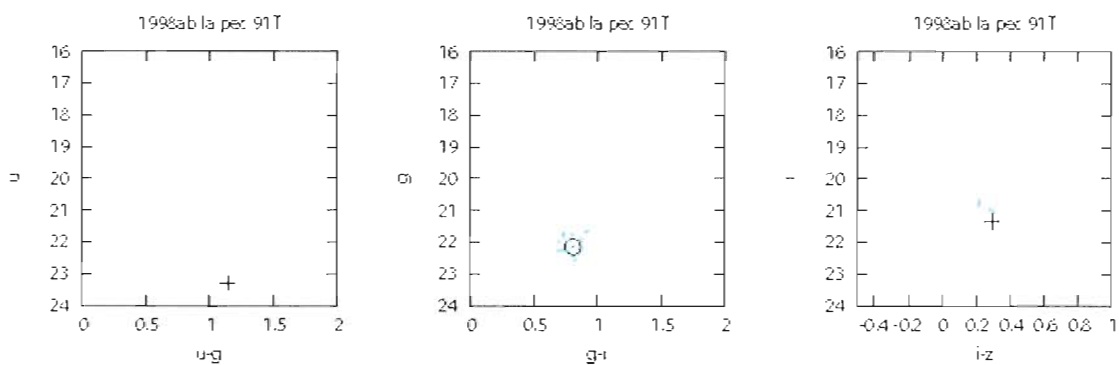


Figure 5.392. SN 1998ab  $u,u-g$ ,  $g,g-i$ , and  $i,i-z$  pseudo color-magnitude plots.

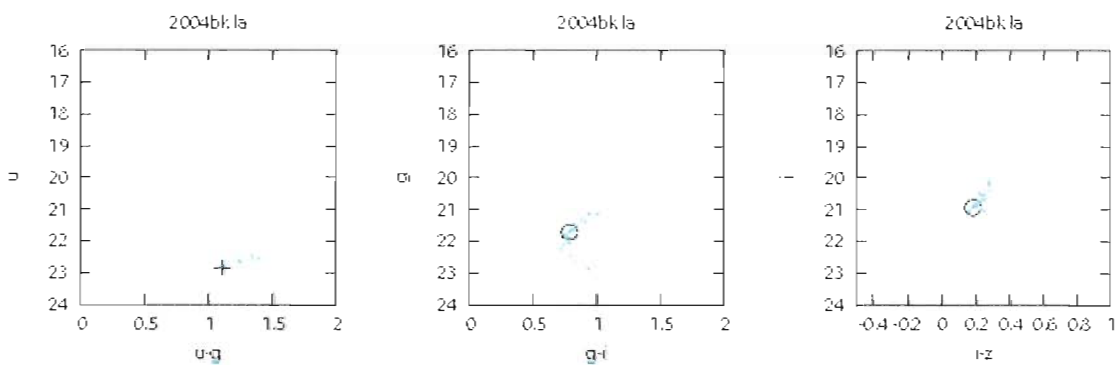


Figure 5.393. SN 2004bk  $u,u-g$ ,  $g,g-i$ , and  $i,i-z$  pseudo color-magnitude plots.

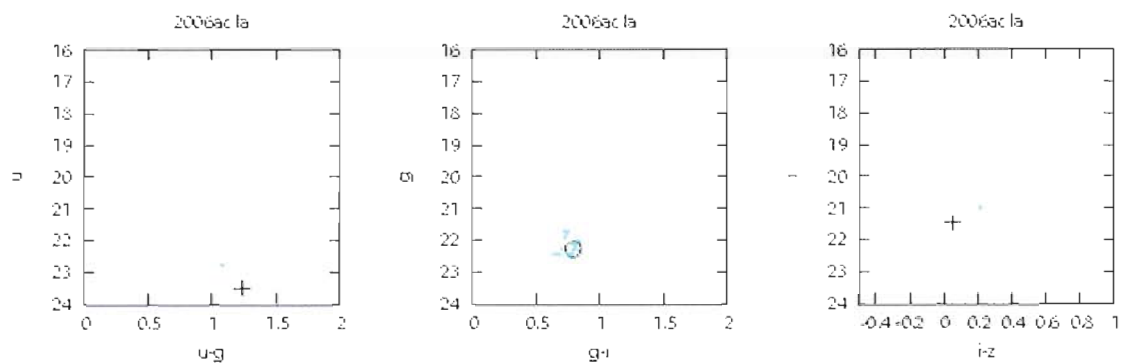


Figure 5.394. SN 2006ac  $u,u-g$ ,  $g,g-i$ , and  $i,i-z$  pseudo color-magnitude plots.

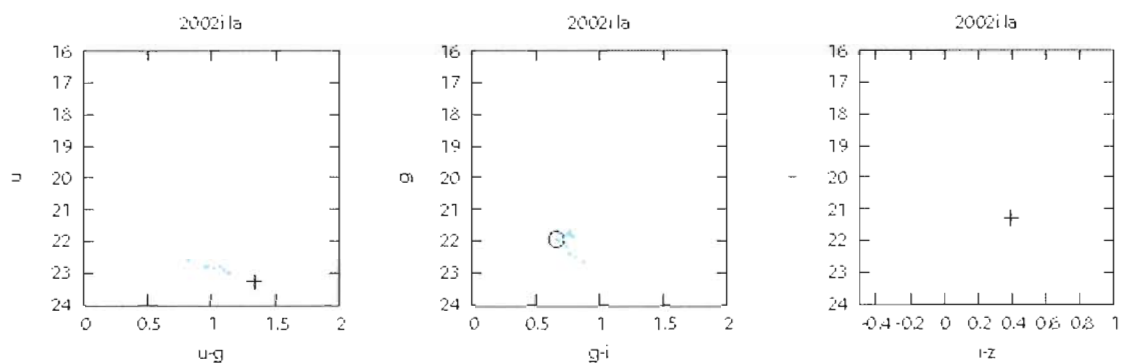


Figure 5.395. SN 2002i  $u,u-g$ ,  $g,g-i$ , and  $i,i-z$  pseudo color-magnitude plots.

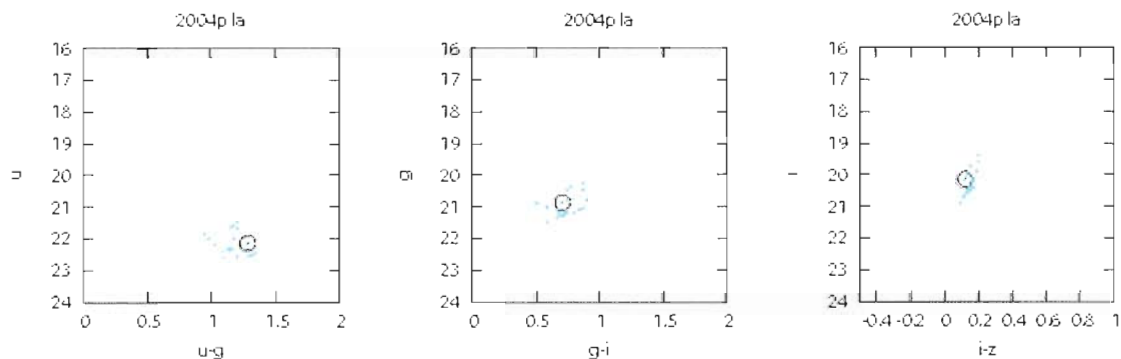


Figure 5.396. SN 2004p  $u,u-g$ ,  $g,g-i$ , and  $i,i-z$  pseudo color-magnitude plots.

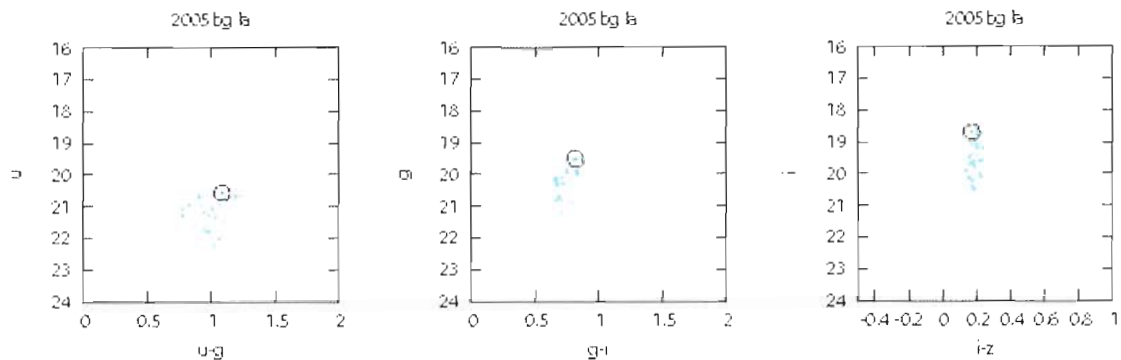


Figure 5.397. SN 2005bg  $u,u-g$ ,  $g,g-i$ , and  $i,i-z$  pseudo color-magnitude plots.

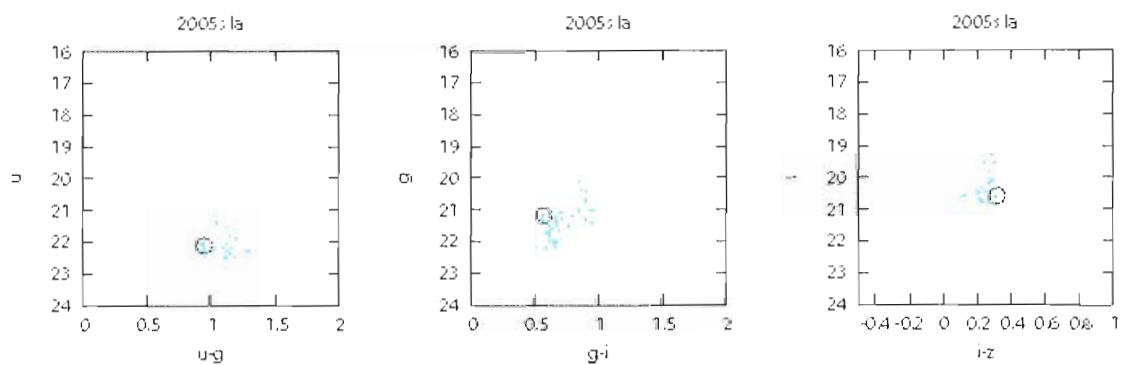


Figure 5.398. SN 2005s  $u,u-g$ ,  $g,g-i$ , and  $i,i-z$  pseudo color-magnitude plots.

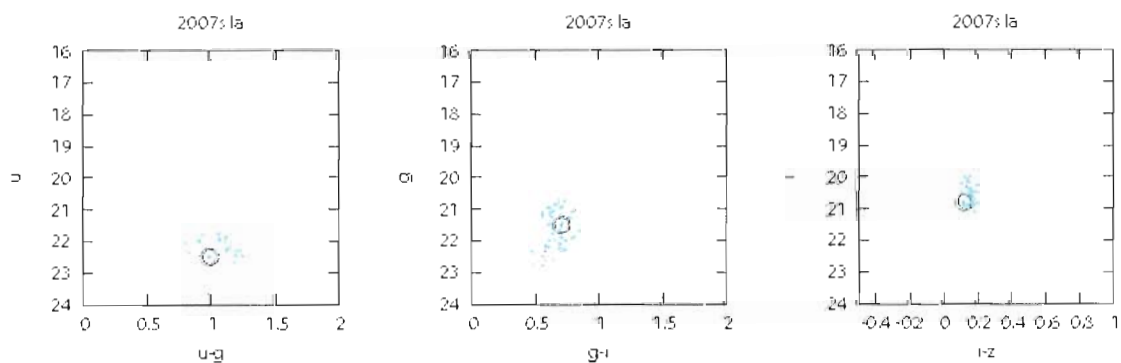


Figure 5.399. SN 2007s  $u,u-g$ ,  $g,g-i$ , and  $i,i-z$  pseudo color-magnitude plots.

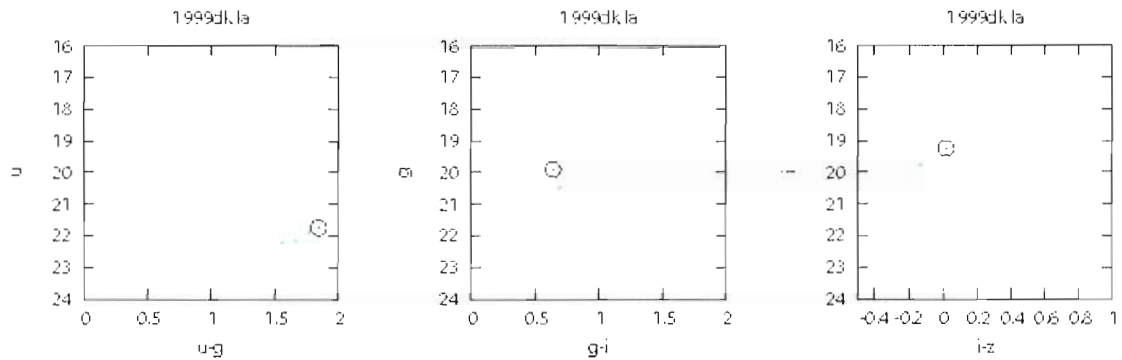


Figure 5.400. SN 1999dk  $u,u-g$ ,  $g,g-i$ , and  $i,i-z$  pseudo color-magnitude plots.

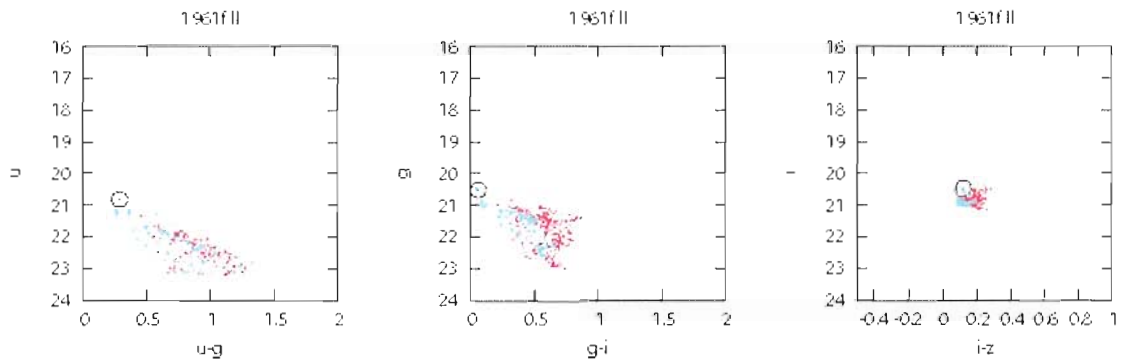


Figure 5.401. SN 1961f  $u,u-g$ ,  $g,g-i$ , and  $i,i-z$  pseudo color-magnitude plots.

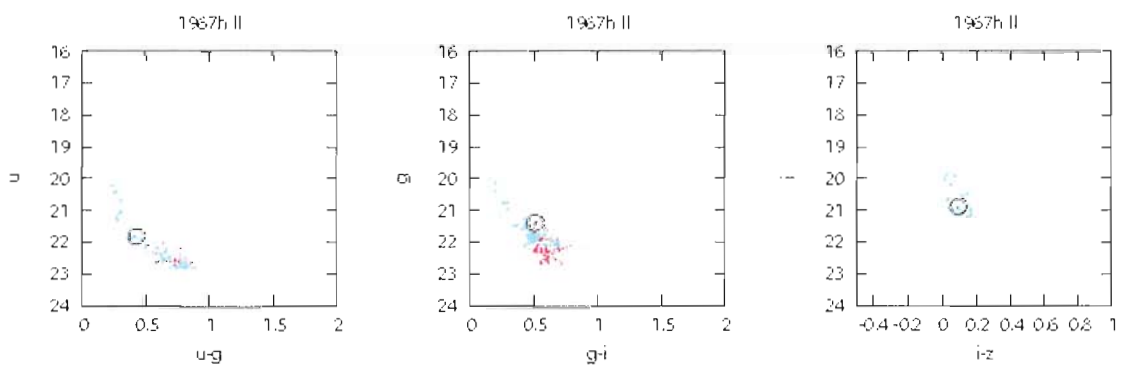


Figure 5.402. SN 1967h  $u,u-g$ ,  $g,g-i$ , and  $i,i-z$  pseudo color-magnitude plots.



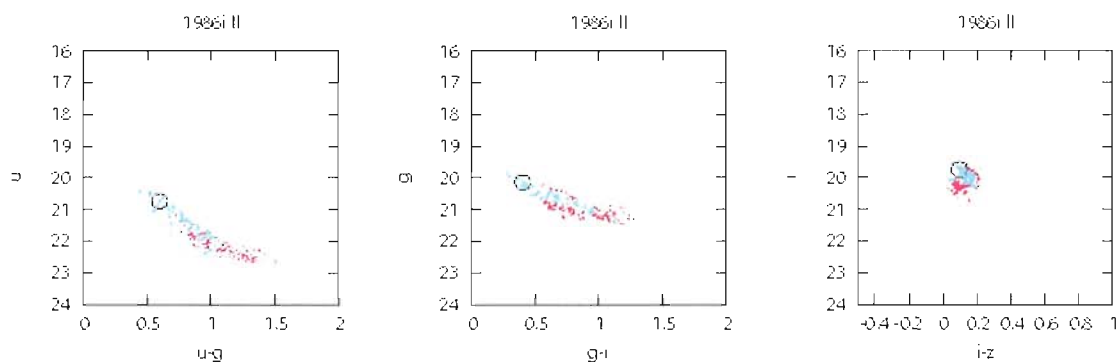


Figure 5.403. SN 1986i  $u,u-g$ ,  $g,g-i$ , and  $i,i-z$  pseudo color-magnitude plots.

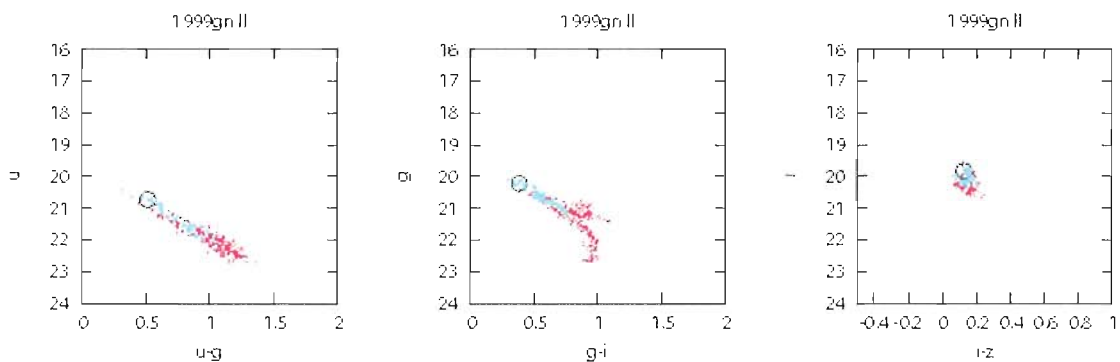


Figure 5.404. SN 1999gn  $u,u-g$ ,  $g,g-i$ , and  $i,i-z$  pseudo color-magnitude plots.

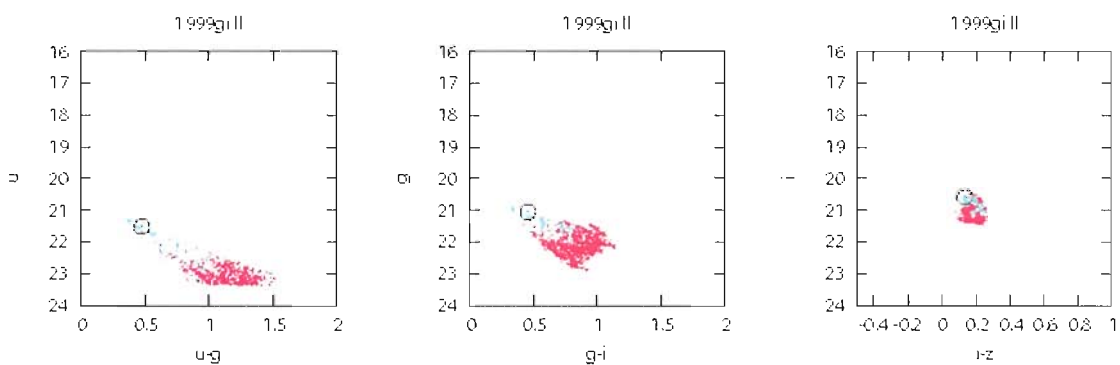


Figure 5.405. SN 1999gi  $u,u-g$ ,  $g,g-i$ , and  $i,i-z$  pseudo color-magnitude plots.

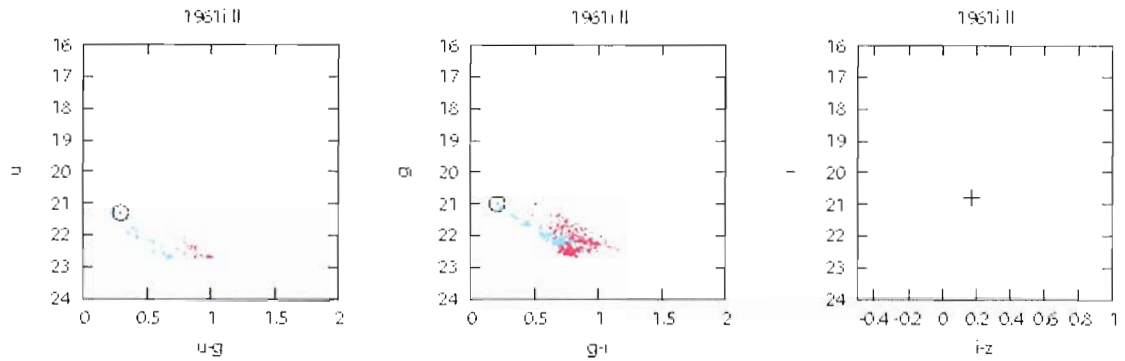


Figure 5.406. SN 1961i  $u,u-g$ ,  $g,g-i$ , and  $i,i-z$  pseudo color-magnitude plots.

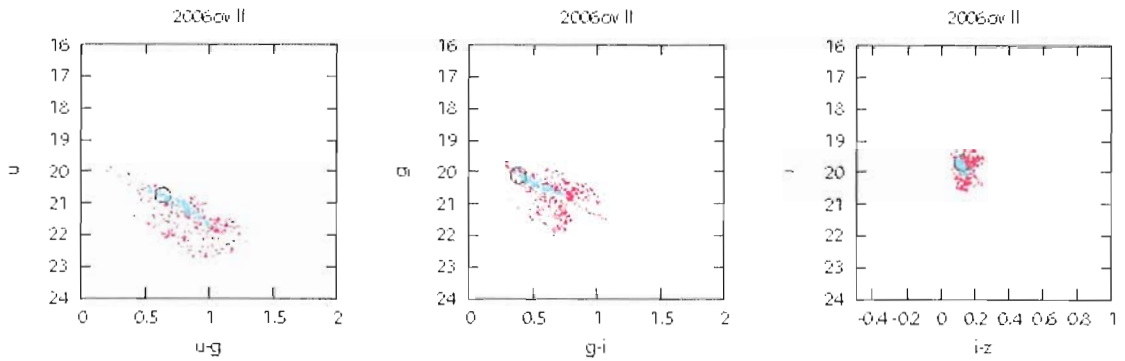


Figure 5.407. SN 2006ov  $u,u-g$ ,  $g,g-i$ , and  $i,i-z$  pseudo color-magnitude plots.

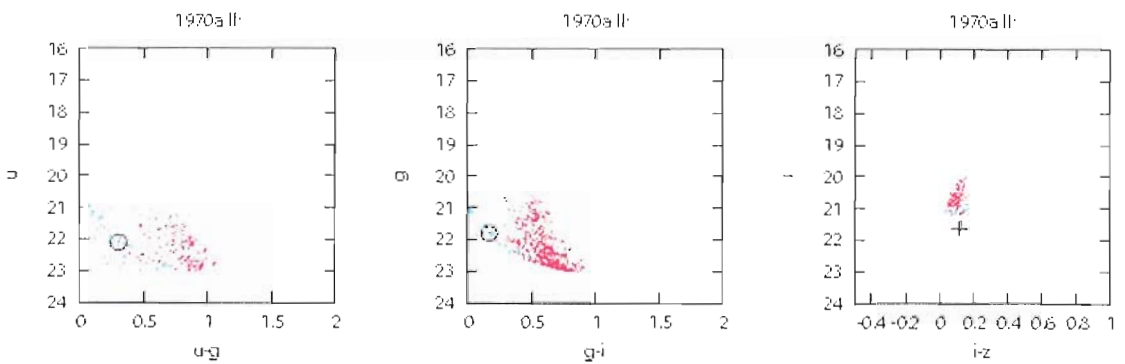


Figure 5.408. SN 1970a  $u,u-g$ ,  $g,g-i$ , and  $i,i-z$  pseudo color-magnitude plots.

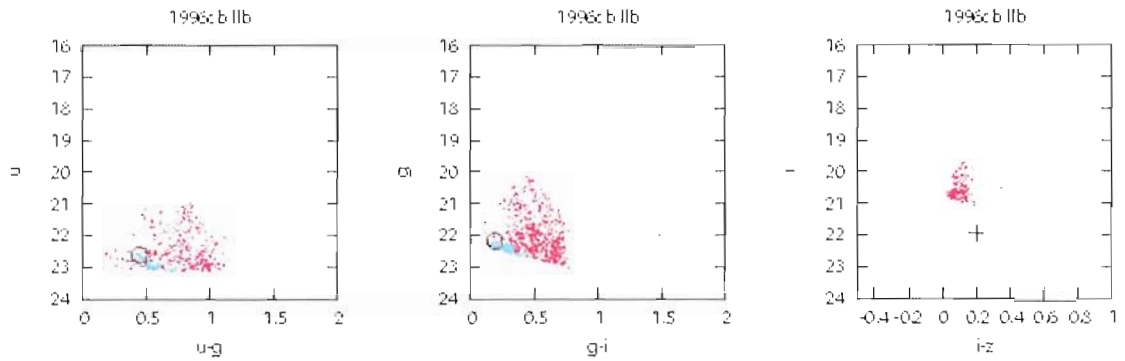


Figure 5.409. SN 1996cb  $u,u-g$ ,  $g,g-i$ , and  $i,i-z$  pseudo color-magnitude plots.

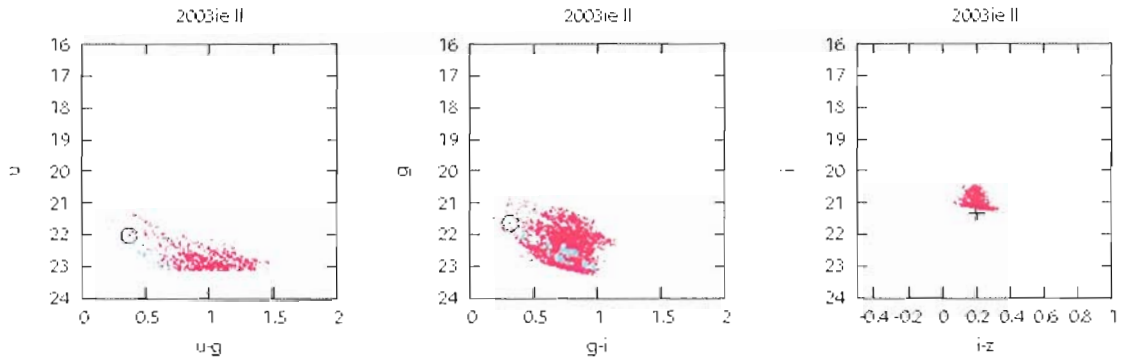


Figure 5.410. SN 2003ie  $u,u-g$ ,  $g,g-i$ , and  $i,i-z$  pseudo color-magnitude plots.

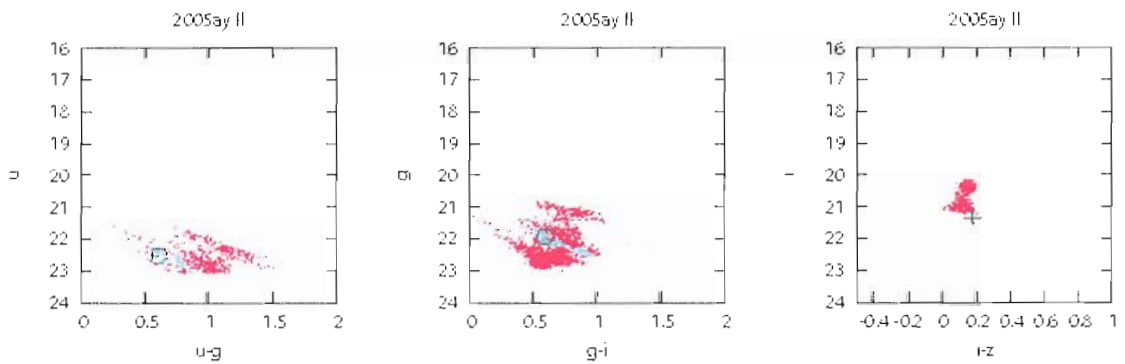


Figure 5.411. SN 2005ay  $u,u-g$ ,  $g,g-i$ , and  $i,i-z$  pseudo color-magnitude plots.

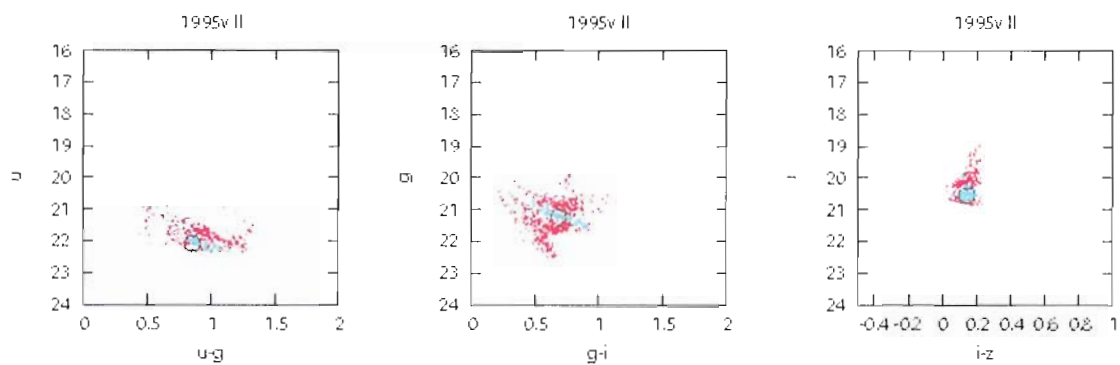


Figure 5.412. SN 1995v  $u, u-g, g, g-i,$  and  $i, i-z$  pseudo color-magnitude plots.

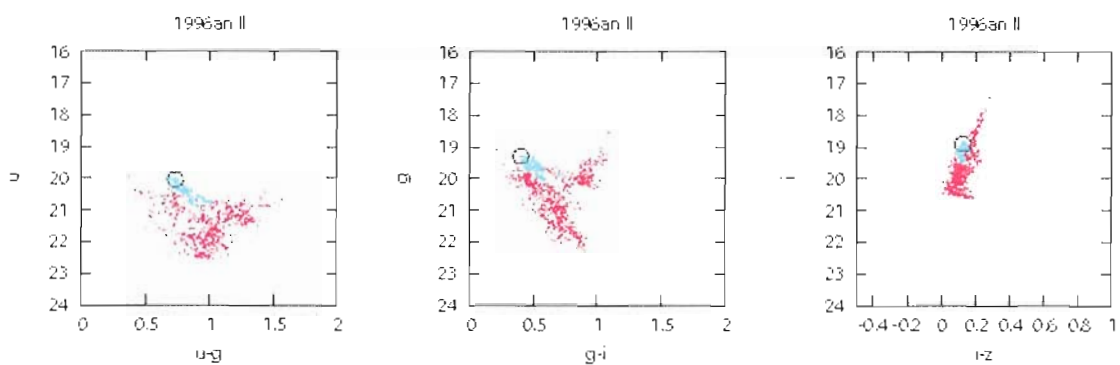


Figure 5.413. SN 1996an  $u, u-g, g, g-i,$  and  $i, i-z$  pseudo color-magnitude plots.

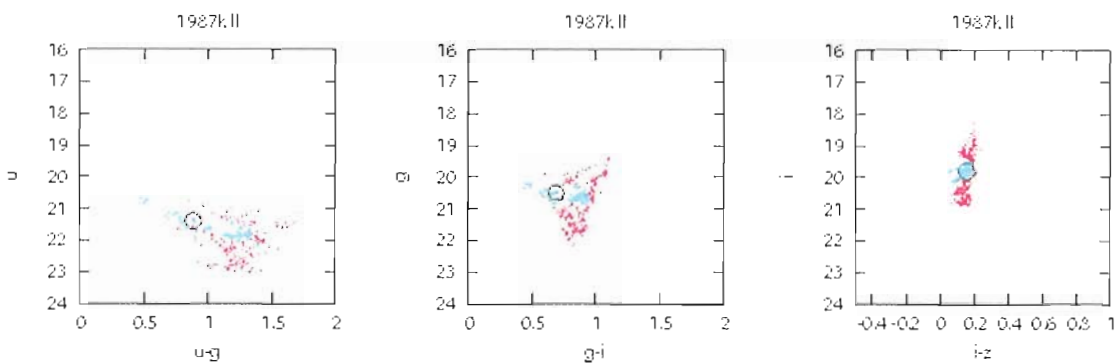


Figure 5.414. SN 1987k  $u, u-g, g, g-i,$  and  $i, i-z$  pseudo color-magnitude plots.

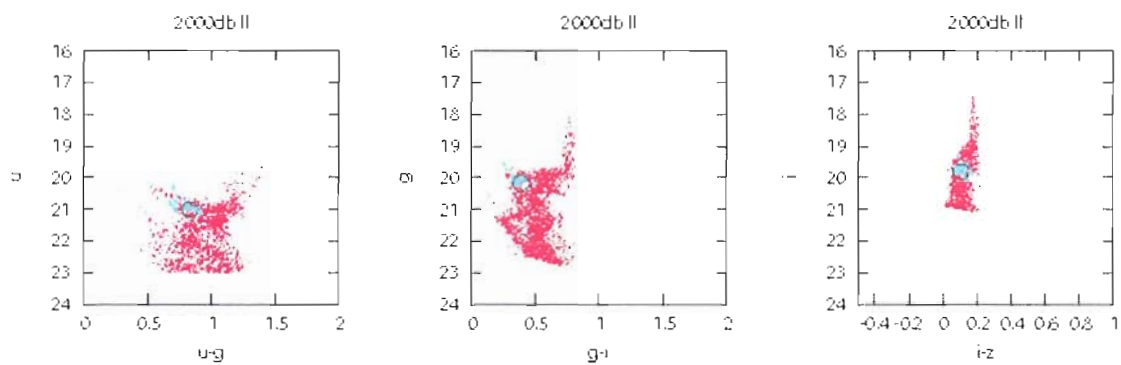


Figure 5.415. SN 2000db  $u,u-g$ ,  $g,g-i$ , and  $i,i-z$  pseudo color-magnitude plots.

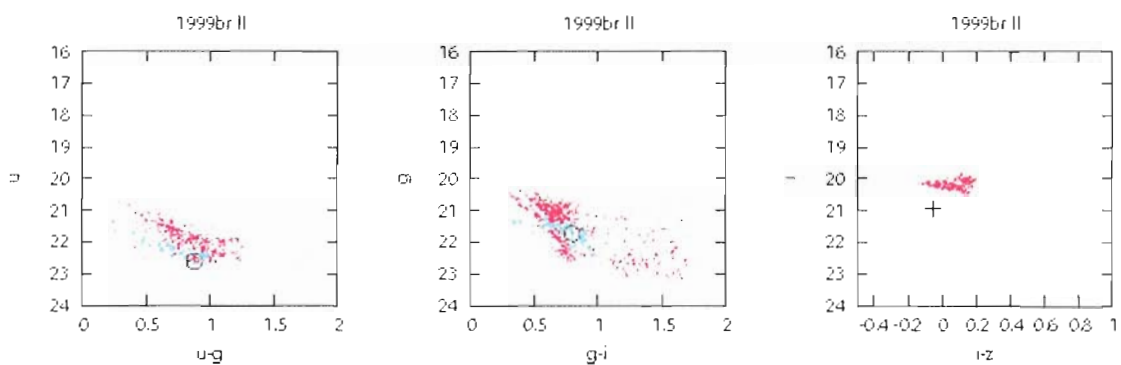


Figure 5.416. SN 1999br  $u,u-g$ ,  $g,g-i$ , and  $i,i-z$  pseudo color-magnitude plots.

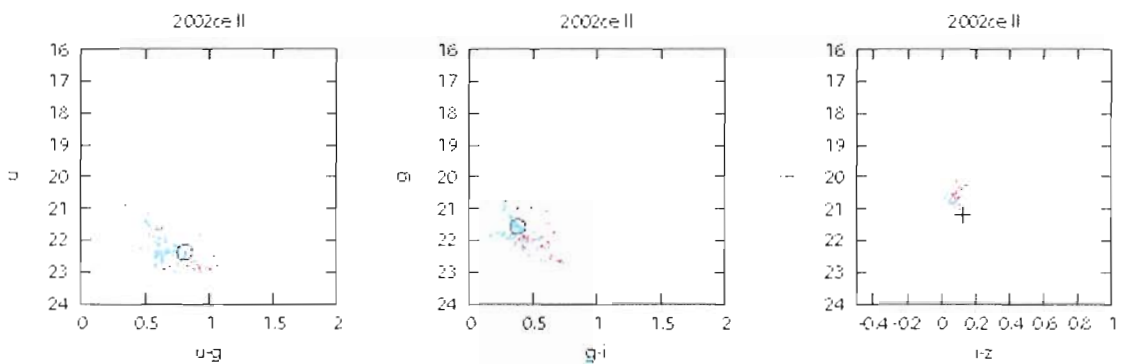


Figure 5.417. SN 2002ce  $u,u-g$ ,  $g,g-i$ , and  $i,i-z$  pseudo color-magnitude plots.

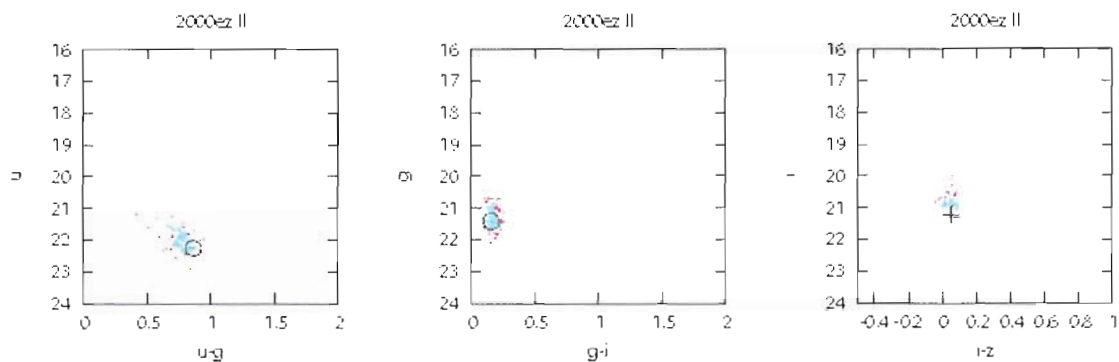


Figure 5.418. SN 2000ez  $u,u-g$ ,  $g,g-i$ , and  $i,i-z$  pseudo color-magnitude plots.

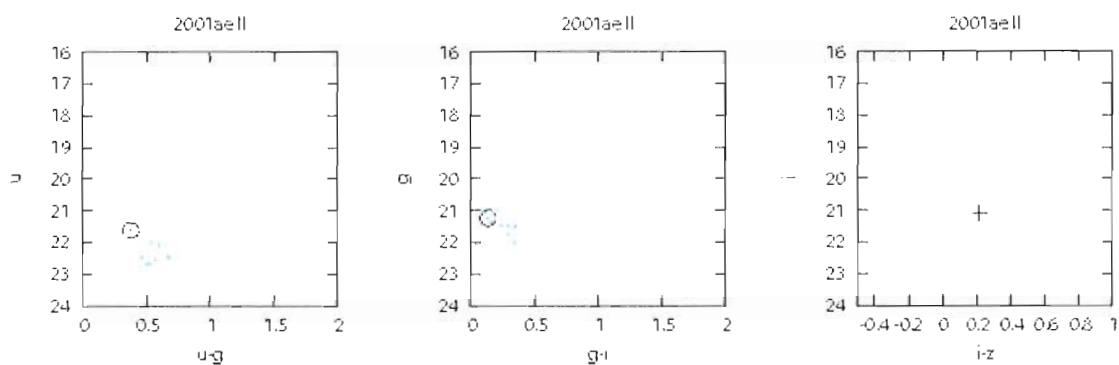


Figure 5.419. SN 2001ae  $u,u-g$ ,  $g,g-i$ , and  $i,i-z$  pseudo color-magnitude plots.

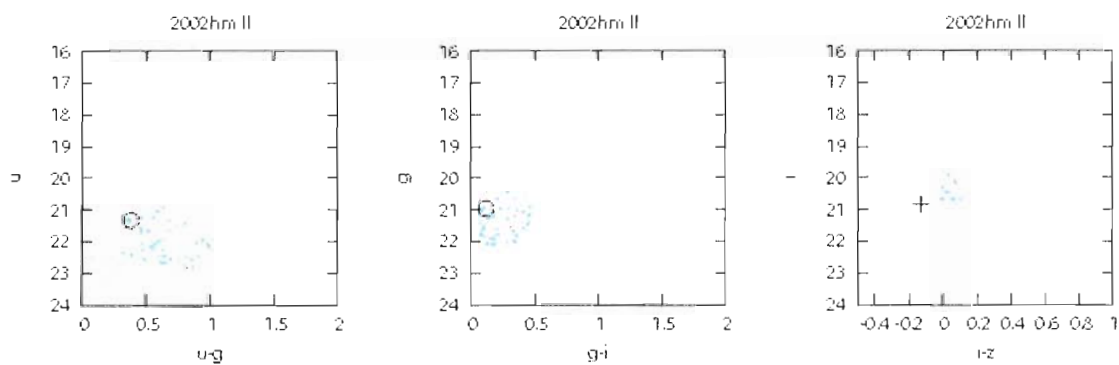


Figure 5.420. SN 2002hm  $u,u-g$ ,  $g,g-i$ , and  $i,i-z$  pseudo color-magnitude plots.

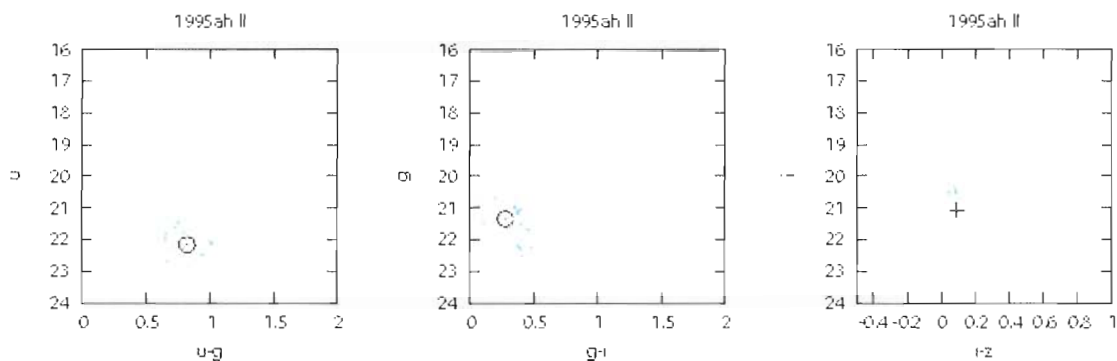


Figure 5.421. SN 1995ah  $u,u-g$ ,  $g,g-i$ , and  $i,i-z$  pseudo color-magnitude plots.

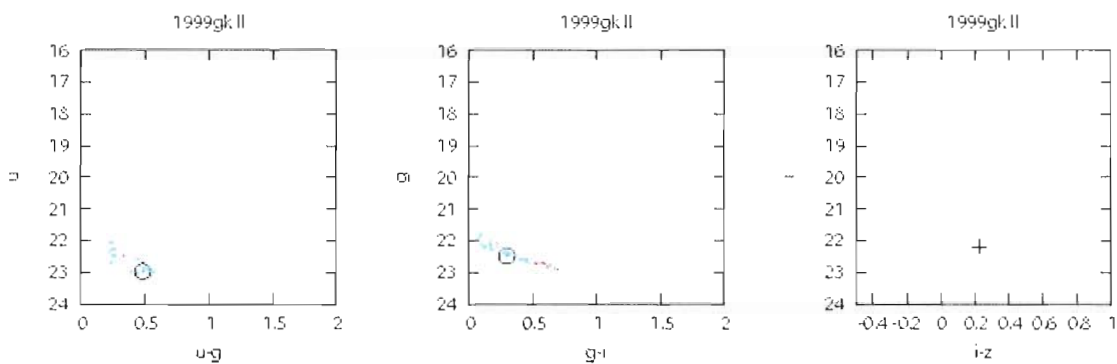


Figure 5.422. SN 1999gk  $u,u-g$ ,  $g,g-i$ , and  $i,i-z$  pseudo color-magnitude plots.

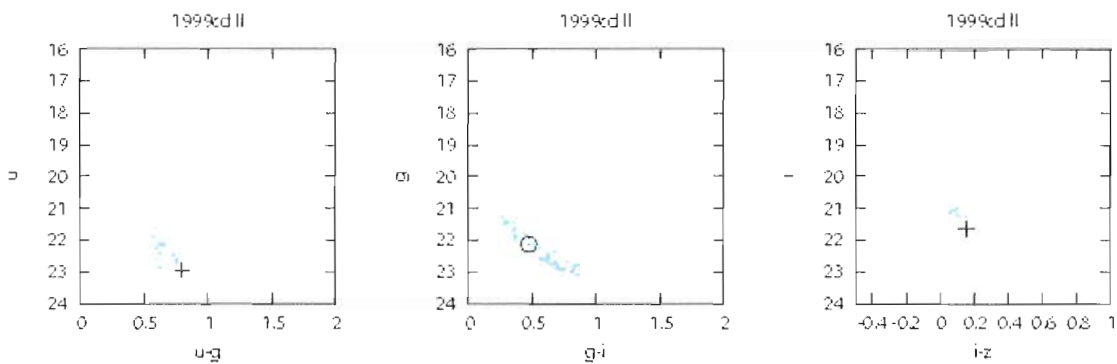


Figure 5.423. SN 1999cd  $u,u-g$ ,  $g,g-i$ , and  $i,i-z$  pseudo color-magnitude plots.

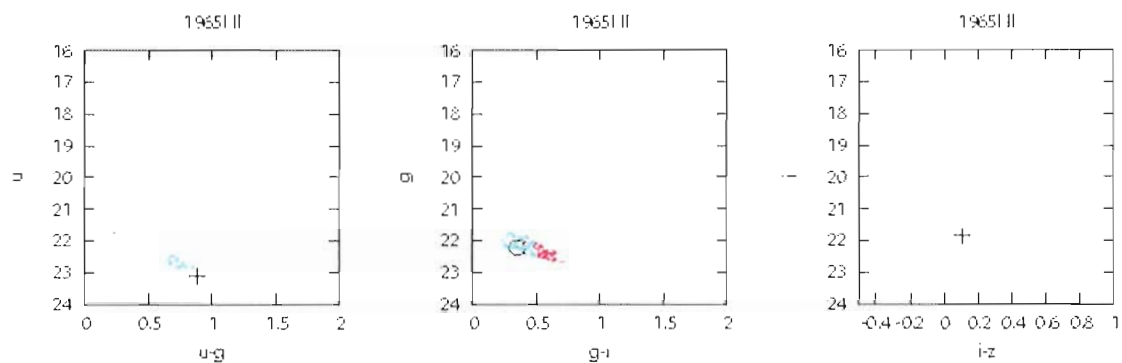


Figure 5.424. SN 1965I  $u,u-g$ ,  $g,g-i$ , and  $i,i-z$  pseudo color-magnitude plots.

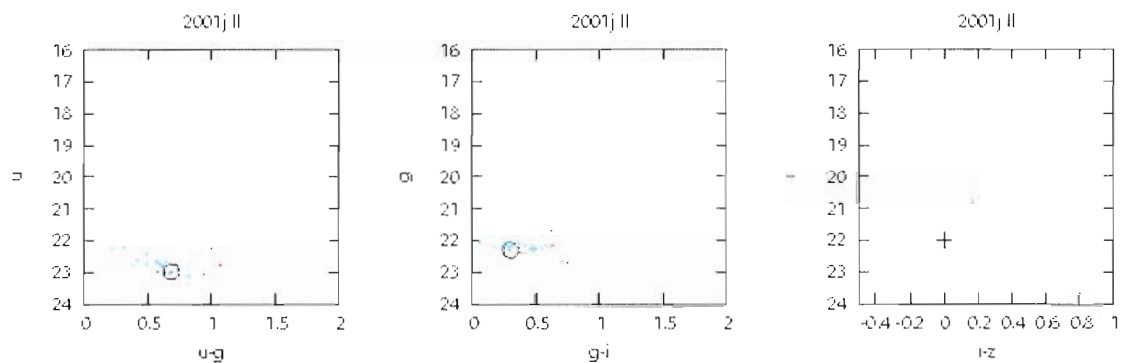


Figure 5.425. SN 2001j  $u,u-g$ ,  $g,g-i$ , and  $i,i-z$  pseudo color-magnitude plots.

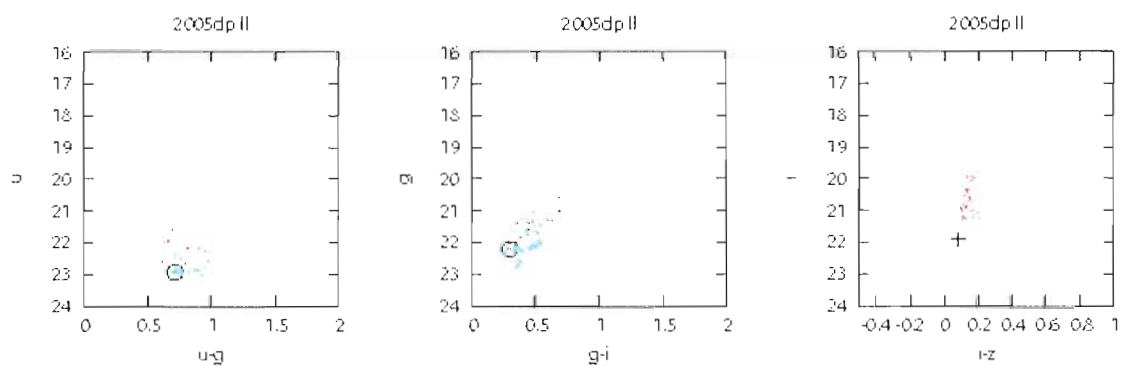


Figure 5.426. SN 2005dp  $u,u-g$ ,  $g,g-i$ , and  $i,i-z$  pseudo color-magnitude plots.



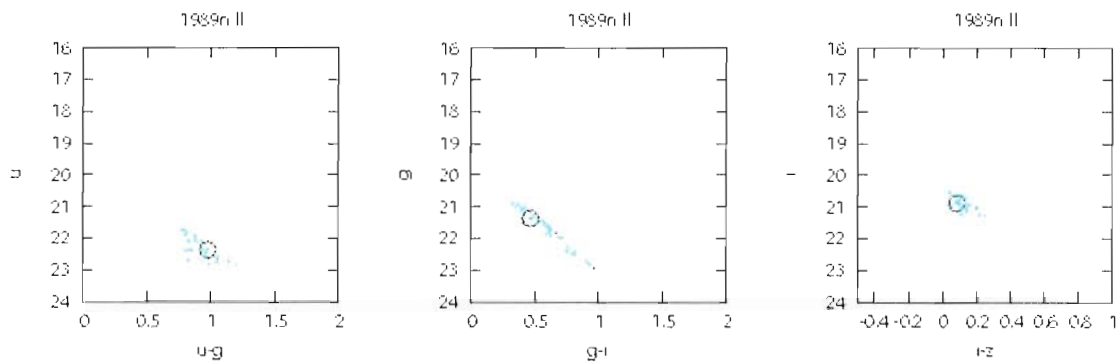


Figure 5.427. SN 1989n  $u,u-g$ ,  $g,g-i$ , and  $i,i-z$  pseudo color-magnitude plots.

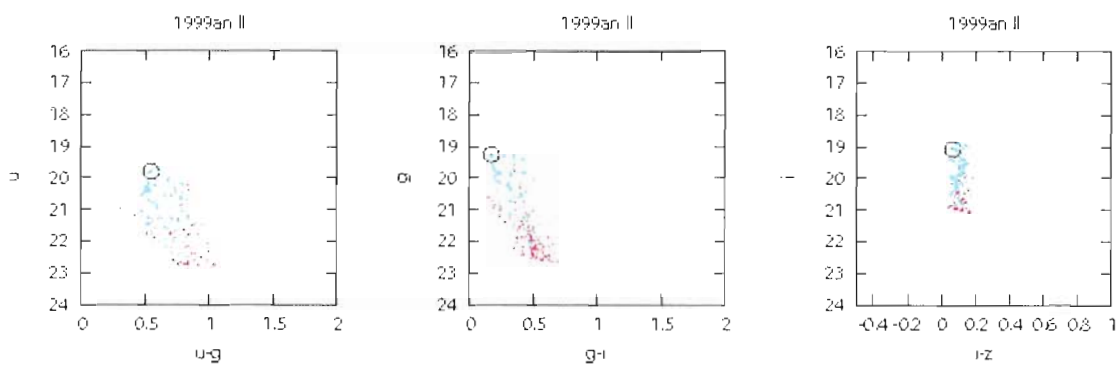


Figure 5.428. SN 1999an  $u,u-g$ ,  $g,g-i$ , and  $i,i-z$  pseudo color-magnitude plots.

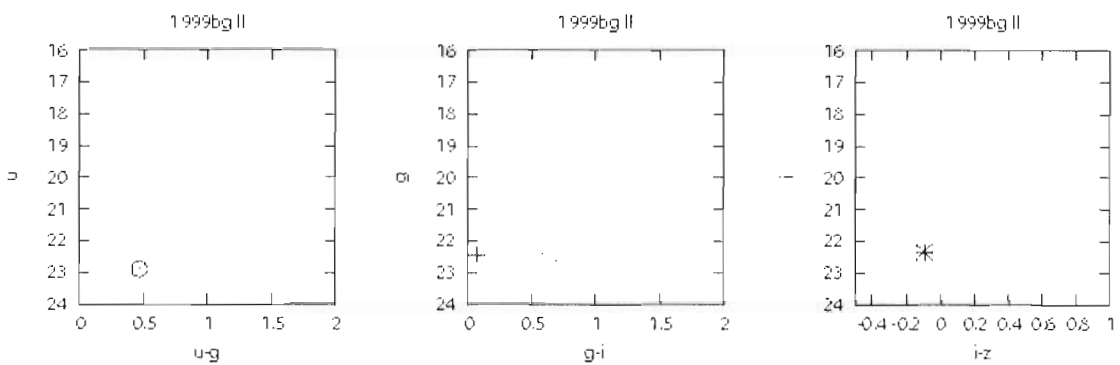


Figure 5.429. SN 1999bg  $u,u-g$ ,  $g,g-i$ , and  $i,i-z$  pseudo color-magnitude plots.

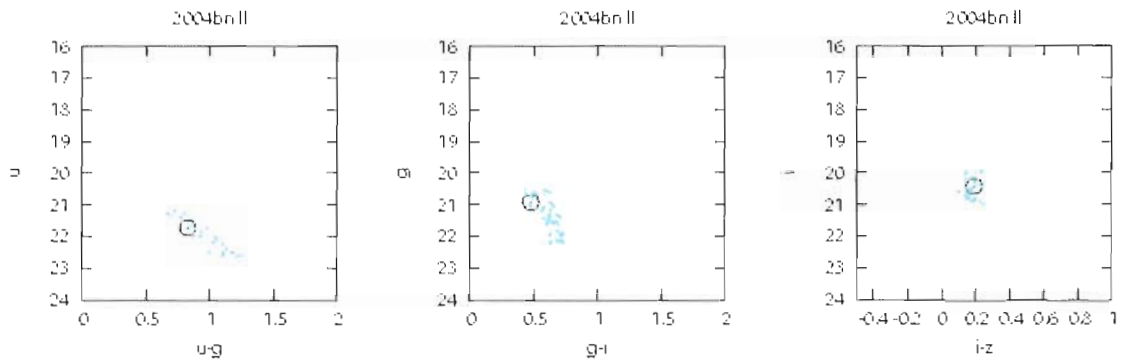


Figure 5.430. SN 2004bn  $u,u-g$ ,  $g,g-i$ , and  $i,i-z$  pseudo color-magnitude plots.

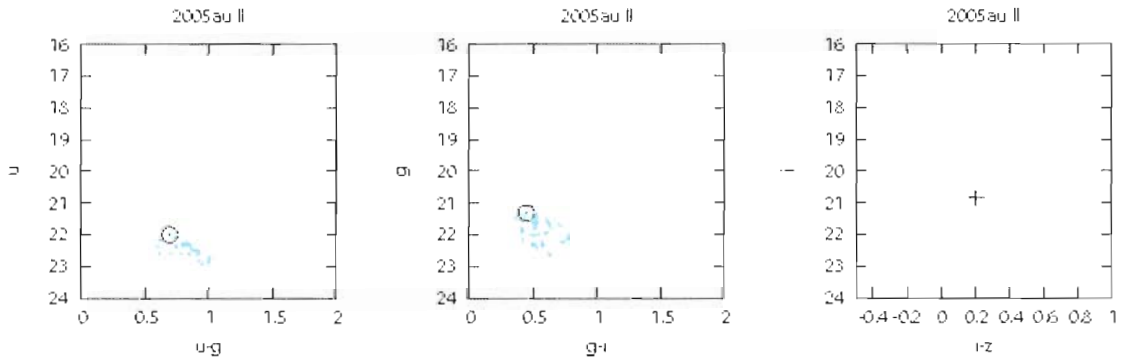


Figure 5.431. SN 2005au  $u,u-g$ ,  $g,g-i$ , and  $i,i-z$  pseudo color-magnitude plots.

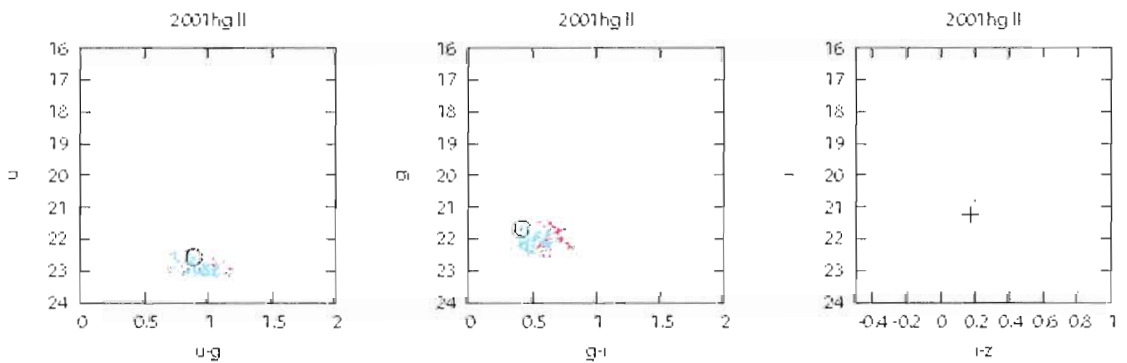


Figure 5.432. SN 2001hg  $u,u-g$ ,  $g,g-i$ , and  $i,i-z$  pseudo color-magnitude plots.

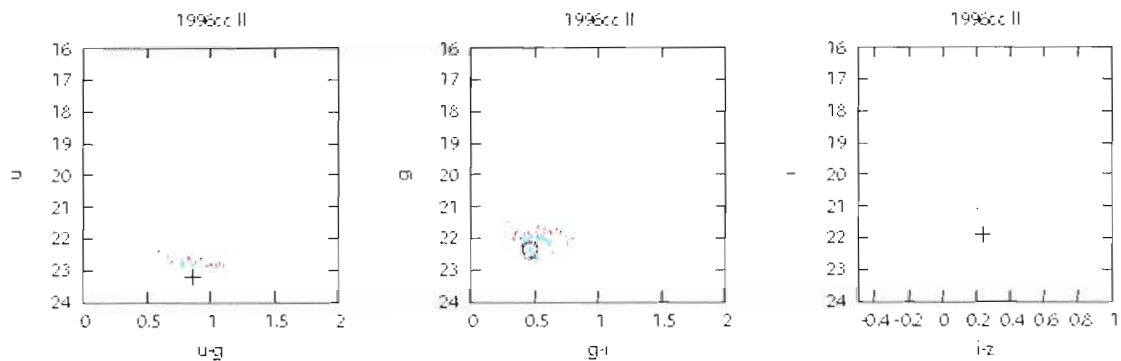


Figure 5.433. SN 1996cc  $u,u-g$ ,  $g,g-i$ , and  $i,i-z$  pseudo color-magnitude plots.

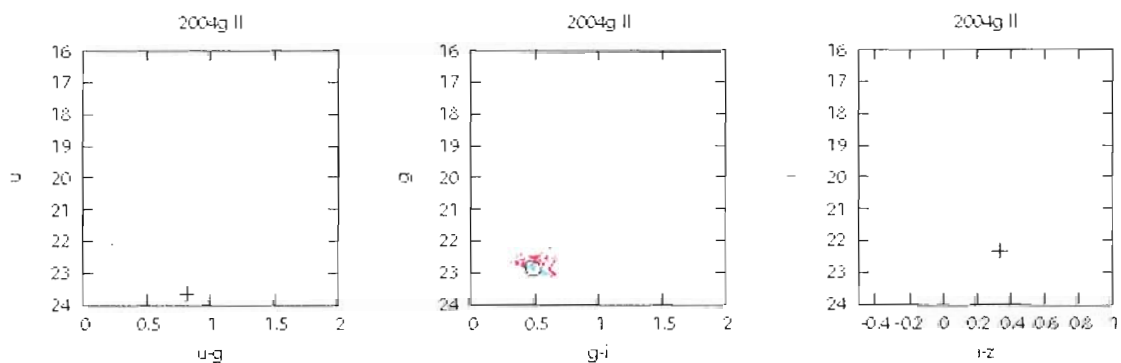


Figure 5.434 SN 2004g  $u,u-g$ ,  $g,g-i$ , and  $i,i-z$  pseudo color-magnitude plots.

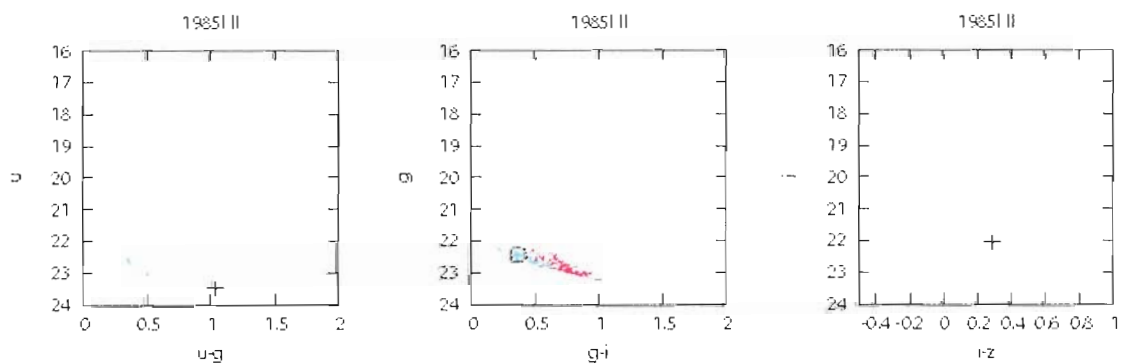


Figure 5.435. SN 1985l  $u,u-g$ ,  $g,g-i$ , and  $i,i-z$  pseudo color-magnitude plots.

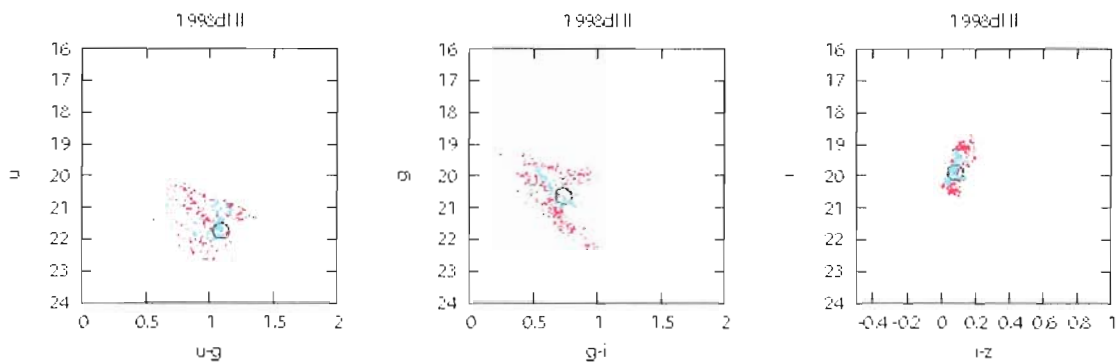


Figure 5.436. SN 1998dl  $u,u-g$ ,  $g,g-i$ , and  $i,i-z$  pseudo color-magnitude plots.

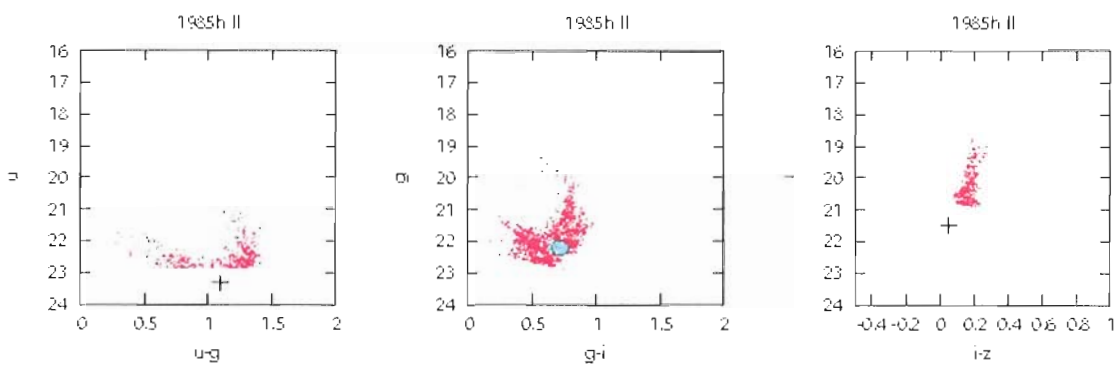


Figure 5.437. SN 1985h  $u,u-g$ ,  $g,g-i$ , and  $i,i-z$  pseudo color-magnitude plots.

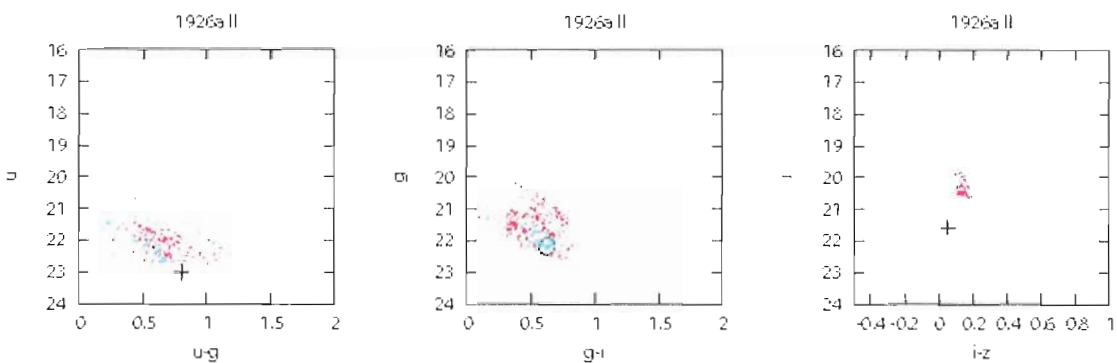


Figure 5.438. SN 1926a  $u,u-g$ ,  $g,g-i$ , and  $i,i-z$  pseudo color-magnitude plots.

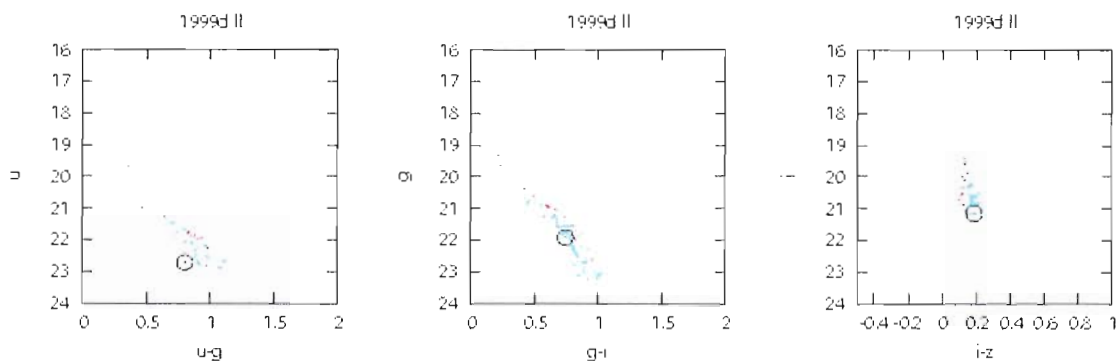


Figure 5.439. SN 1999d  $u,u-g$ ,  $g,g-i$ , and  $i,i-z$  pseudo color-magnitude plots.

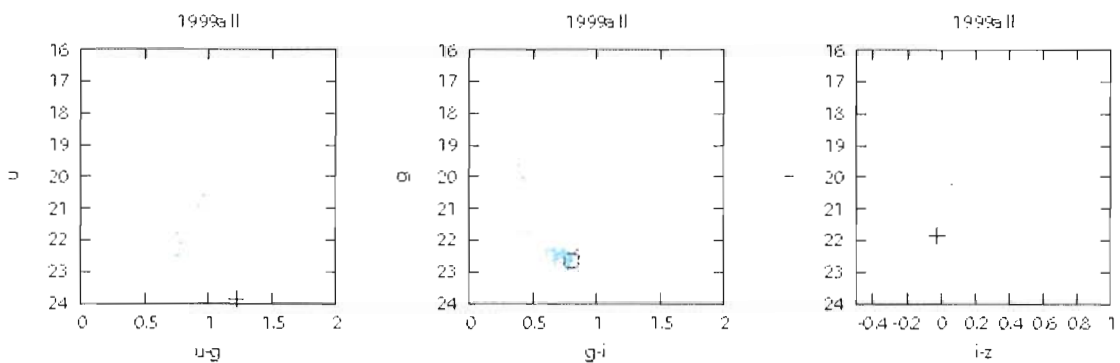


Figure 5.440. SN 1999a  $u,u-g$ ,  $g,g-i$ , and  $i,i-z$  pseudo color-magnitude plots.

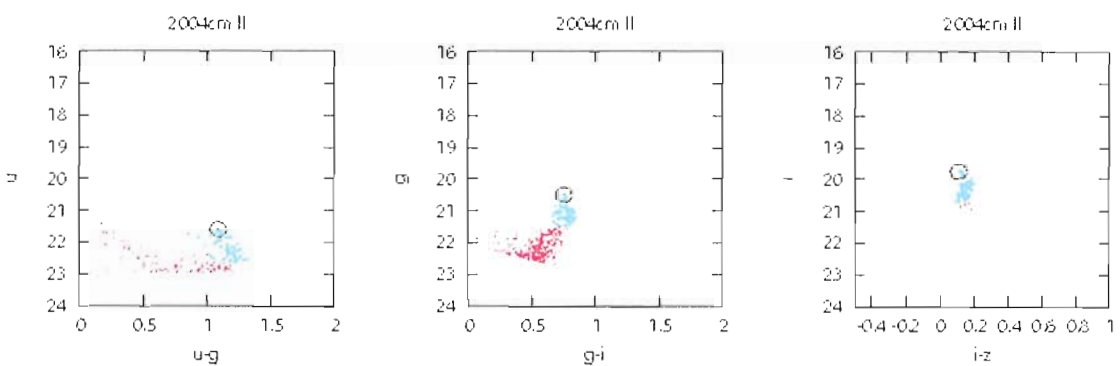


Figure 5.441. SN 2004cm  $u,u-g$ ,  $g,g-i$ , and  $i,i-z$  pseudo color-magnitude plots.

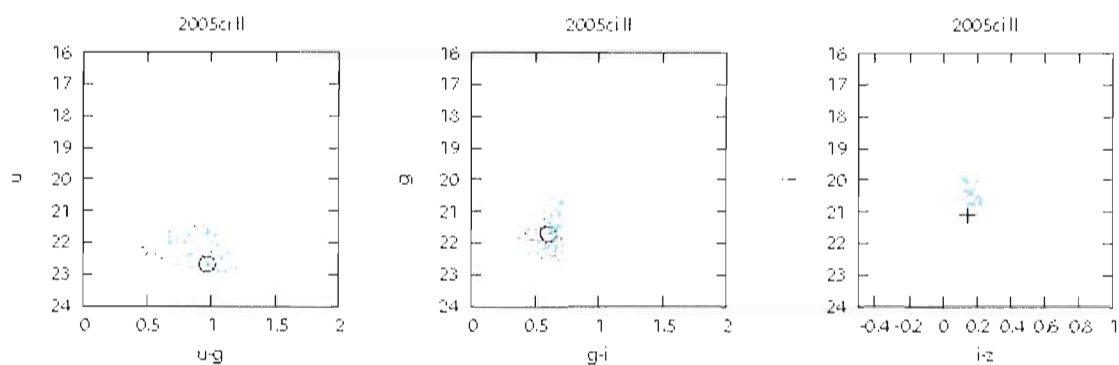


Figure 5.442. SN 2005ci  $u,u-g$ ,  $g,g-i$ , and  $i,i-z$  pseudo color-magnitude plots.

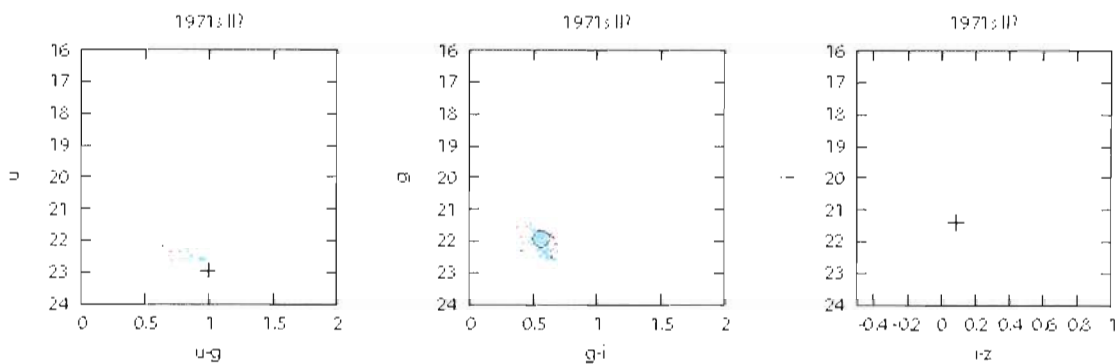


Figure 5.443. SN 1971s  $u,u-g$ ,  $g,g-i$ , and  $i,i-z$  pseudo color-magnitude plots.

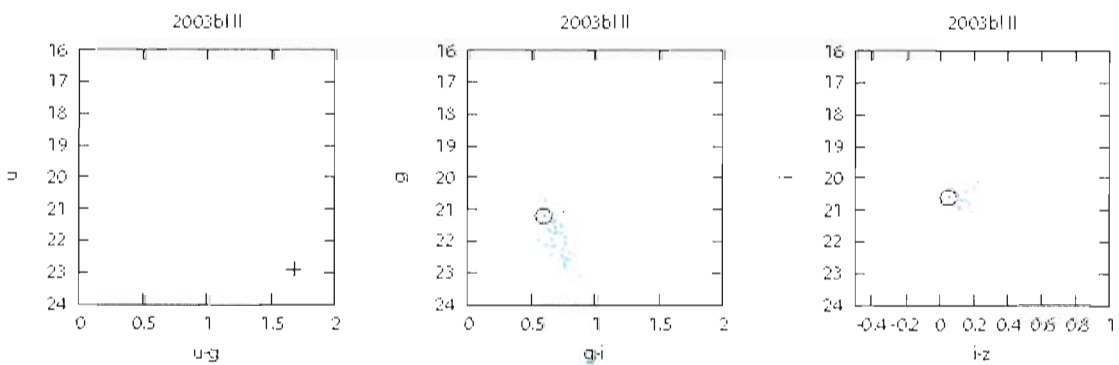


Figure 5.444. SN 2003bl  $u,u-g$ ,  $g,g-i$ , and  $i,i-z$  pseudo color-magnitude plots.

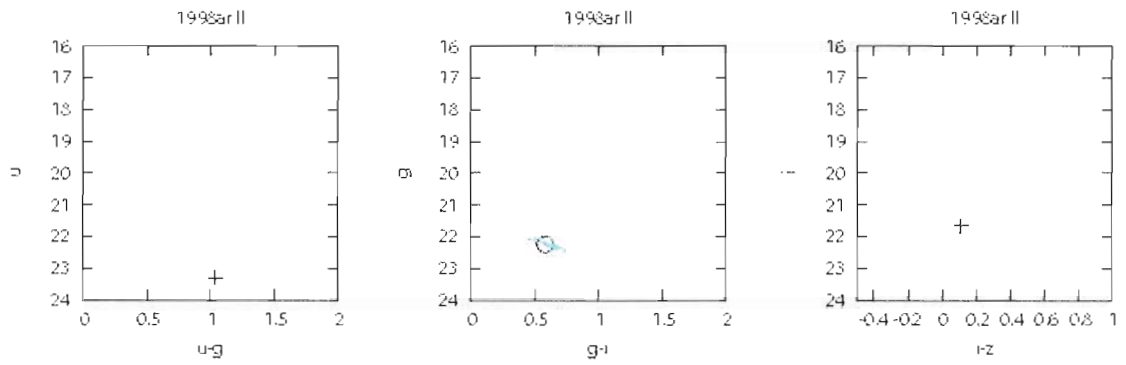


Figure 5.445. SN 1998ar  $u,u-g$ ,  $g,g-i$ , and  $i,i-z$  pseudo color-magnitude plots.

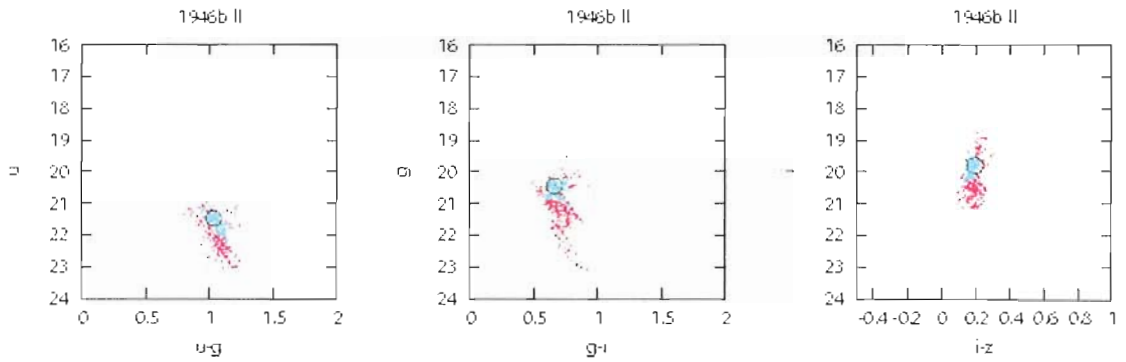


Figure 5.446. SN 1946b  $u,u-g$ ,  $g,g-i$ , and  $i,i-z$  pseudo color-magnitude plots.

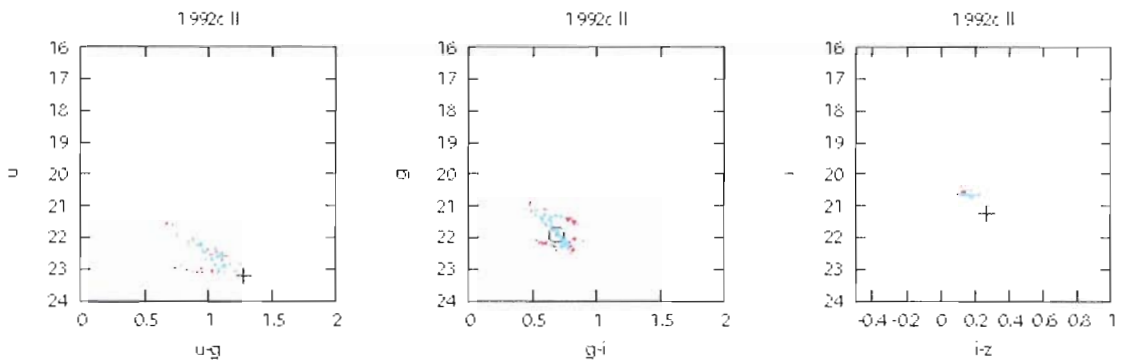


Figure 5.447. SN 1992c  $u,u-g$ ,  $g,g-i$ , and  $i,i-z$  pseudo color-magnitude plots.

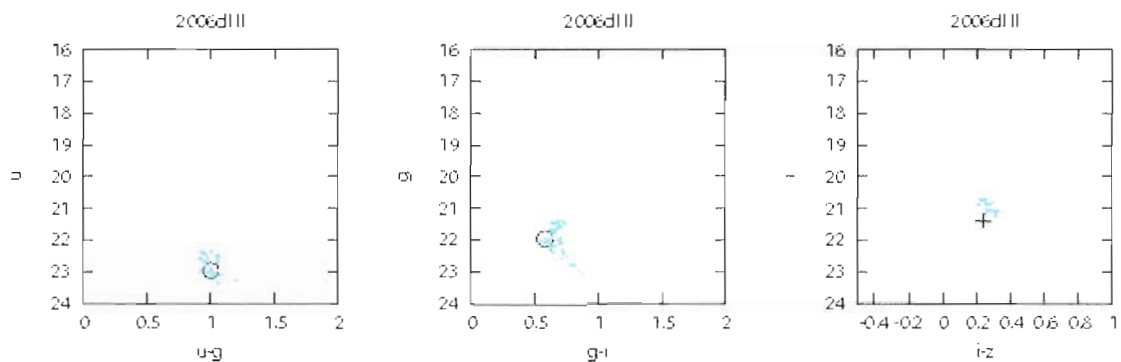


Figure 5.448. SN 2006dl  $u,u-g$ ,  $g,g-i$ , and  $i,i-z$  pseudo color-magnitude plots.

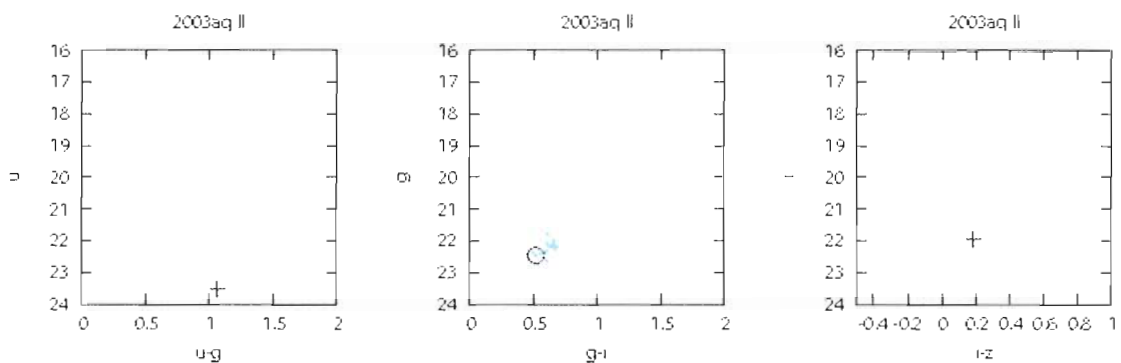


Figure 5.449. SN 2003aq  $u,u-g$ ,  $g,g-i$ , and  $i,i-z$  pseudo color-magnitude plots.

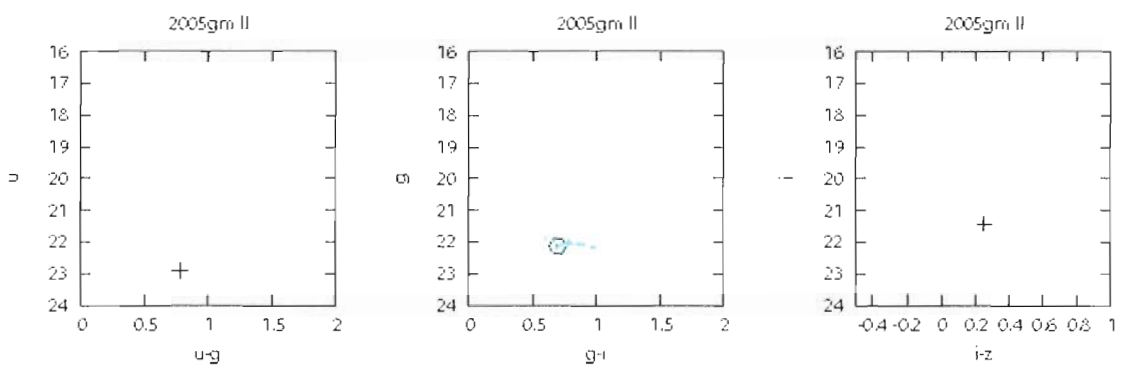


Figure 5.450. SN 2005gm  $u,u-g$ ,  $g,g-i$ , and  $i,i-z$  pseudo color-magnitude plots.



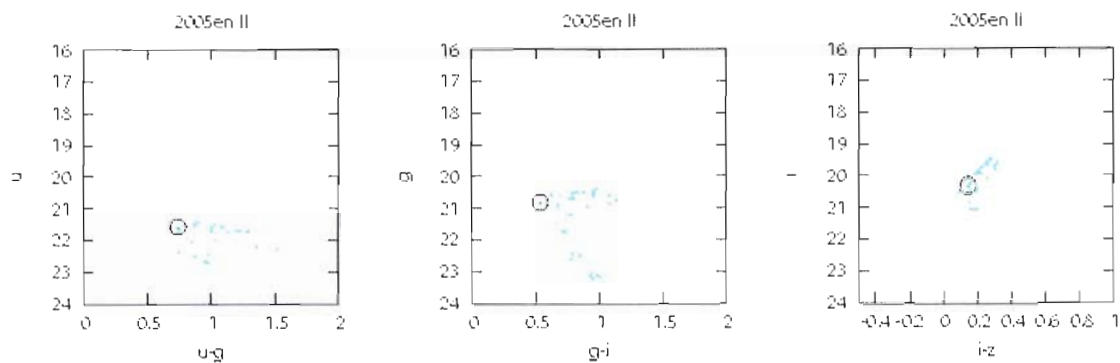


Figure 5.451. SN 2005en  $u,u-g$ ,  $g,g-i$ , and  $i,i-z$  pseudo color-magnitude plots.

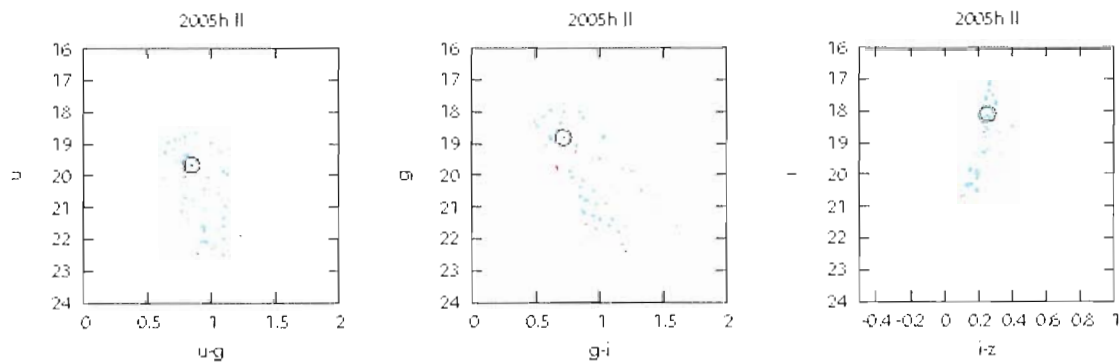


Figure 5.452. SN 2005h  $u,u-g$ ,  $g,g-i$ , and  $i,i-z$  pseudo color-magnitude plots.

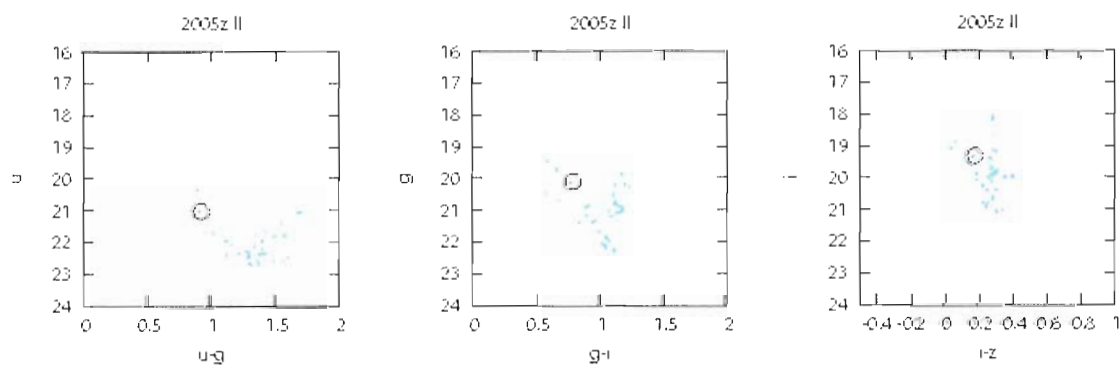


Figure 5.453. SN 2005z  $u,u-g$ ,  $g,g-i$ , and  $i,i-z$  pseudo color-magnitude plots.

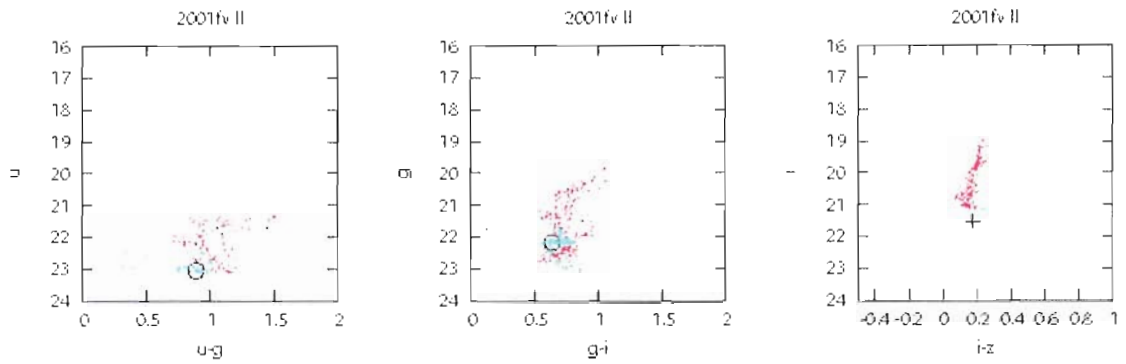


Figure 5.454. SN 2001fv  $u,u-g$ ,  $g,g-i$ , and  $i,i-z$  pseudo color-magnitude plots.

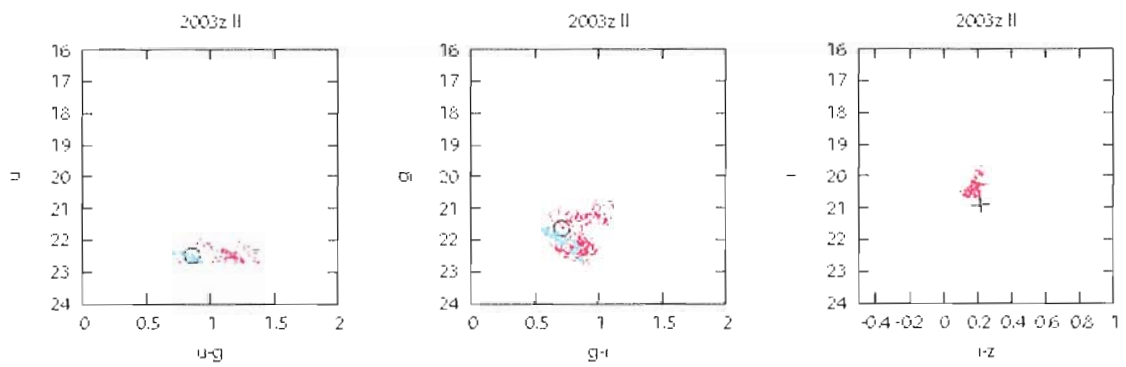


Figure 5.455. SN 2003z  $u,u-g$ ,  $g,g-i$ , and  $i,i-z$  pseudo color-magnitude plots.

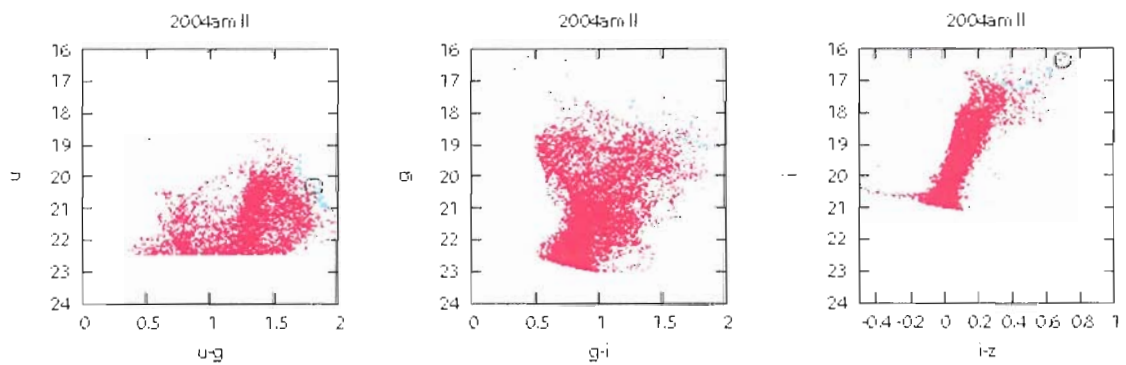


Figure 5.456. SN 2004am  $u,u-g$ ,  $g,g-i$ , and  $i,i-z$  pseudo color-magnitude plots.

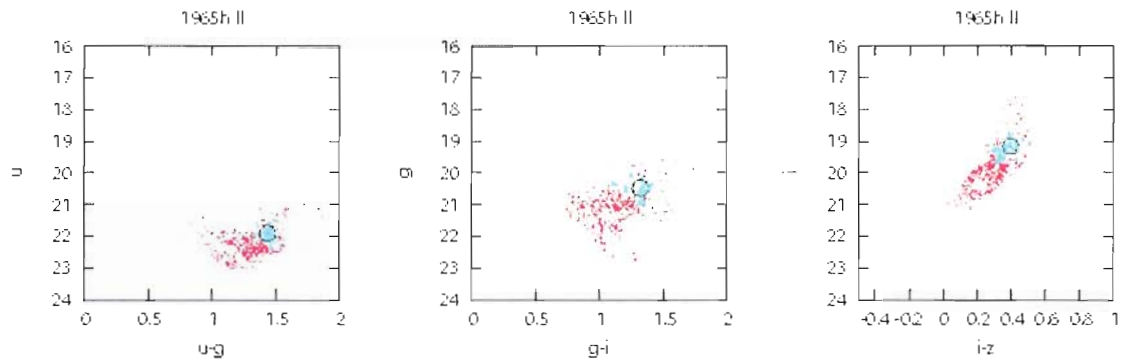


Figure 5.457. SN 1965h  $u,u-g$ ,  $g,g-i$ , and  $i,i-z$  pseudo color-magnitude plots.

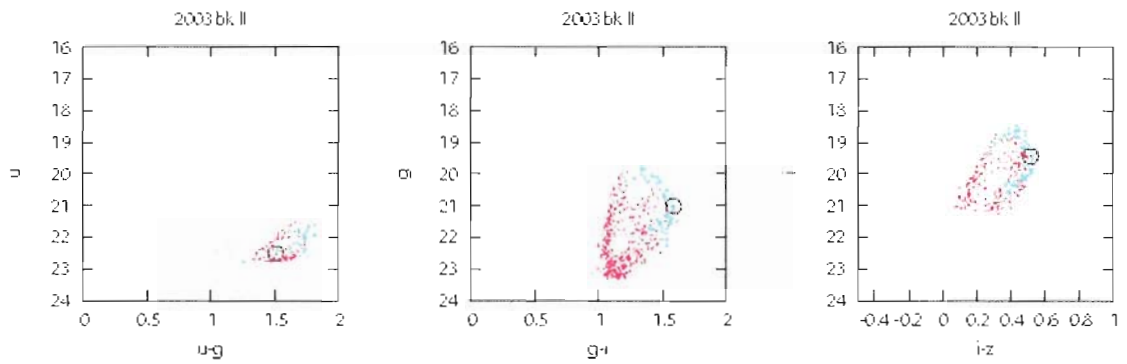


Figure 5.458. SN 2003bk  $u,u-g$ ,  $g,g-i$ , and  $i,i-z$  pseudo color-magnitude plots.

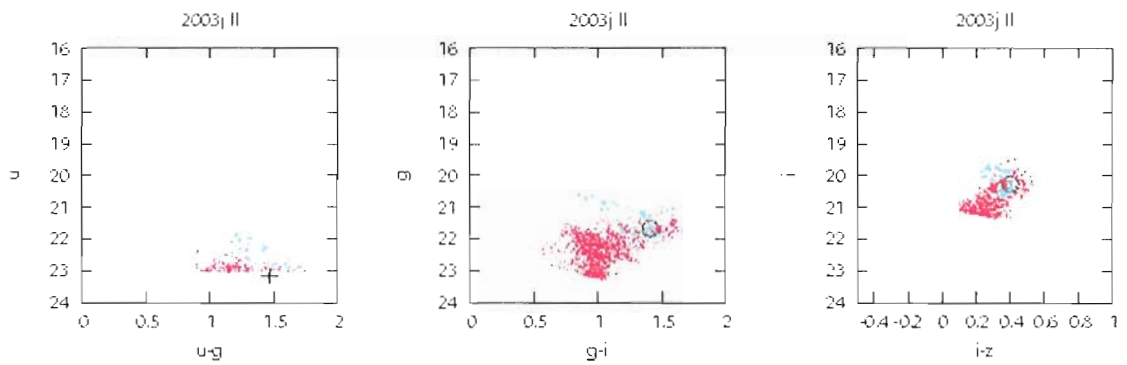


Figure 5.459. SN 2003j  $u,u-g$ ,  $g,g-i$ , and  $i,i-z$  pseudo color-magnitude plots.

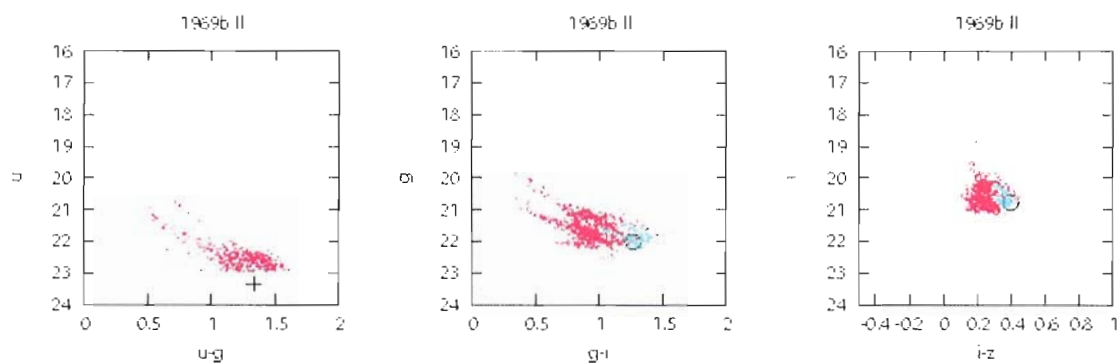


Figure 5.460. SN 1969b  $u,u-g$ ,  $g,g-i$ , and  $i,i-z$  pseudo color-magnitude plots.

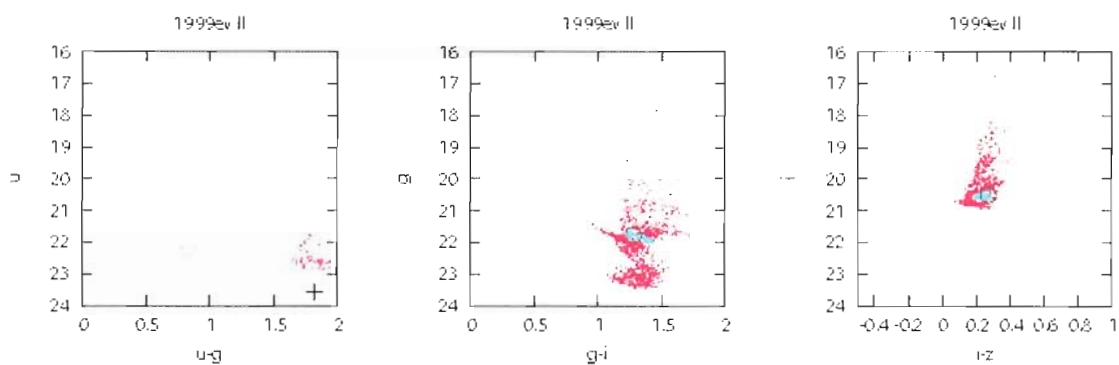


Figure 5.461. SN 1999ev  $u,u-g$ ,  $g,g-i$ , and  $i,i-z$  pseudo color-magnitude plots.

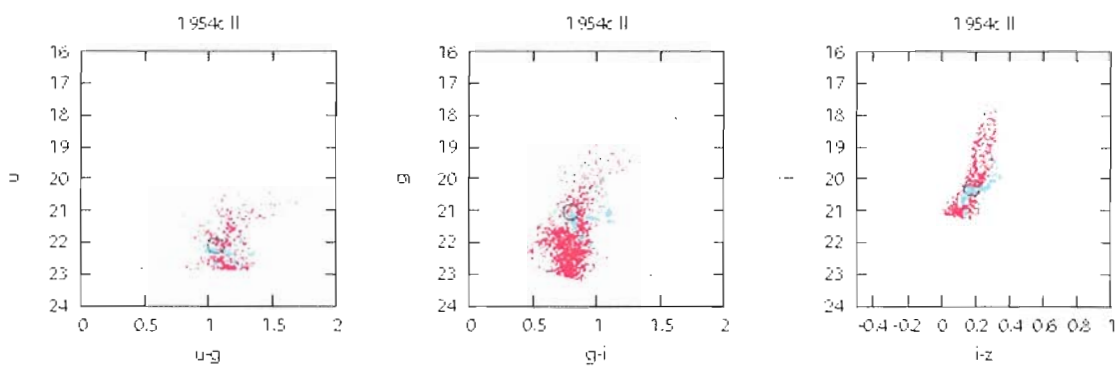


Figure 5.462. SN 1954c  $u,u-g$ ,  $g,g-i$ , and  $i,i-z$  pseudo color-magnitude plots.

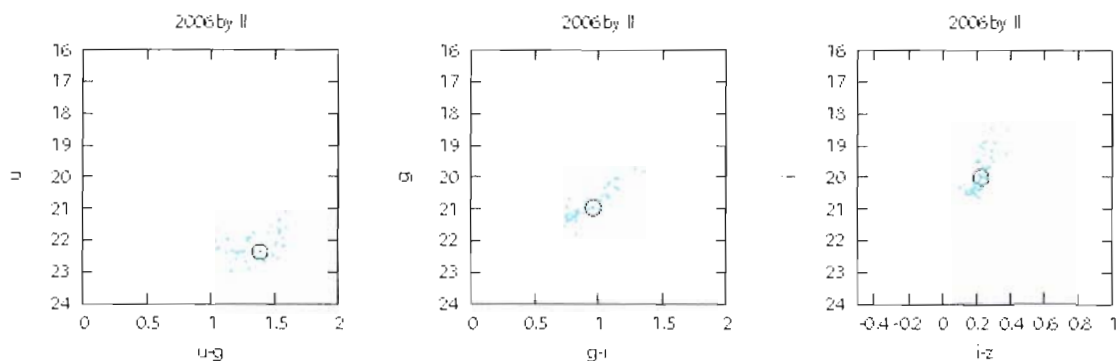


Figure 5.463. SN 2006by  $u,u-g$ ,  $g,g-i$ , and  $i,i-z$  pseudo color-magnitude plots.

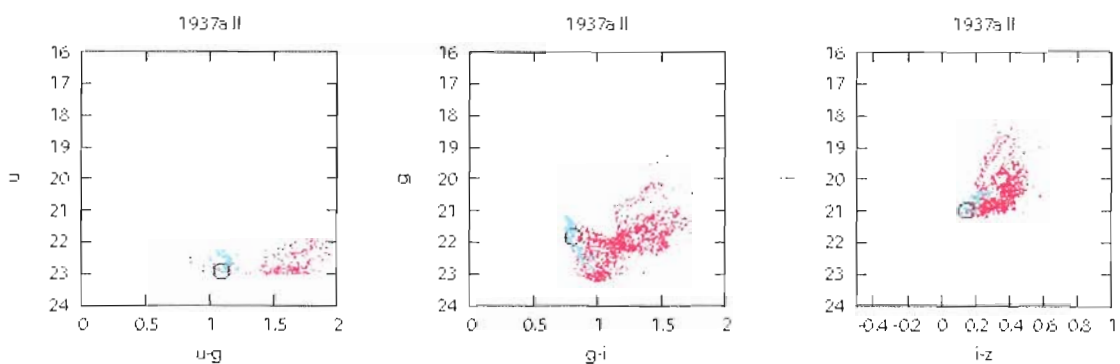


Figure 5.464. SN 1937a  $u,u-g$ ,  $g,g-i$ , and  $i,i-z$  pseudo color-magnitude plots.

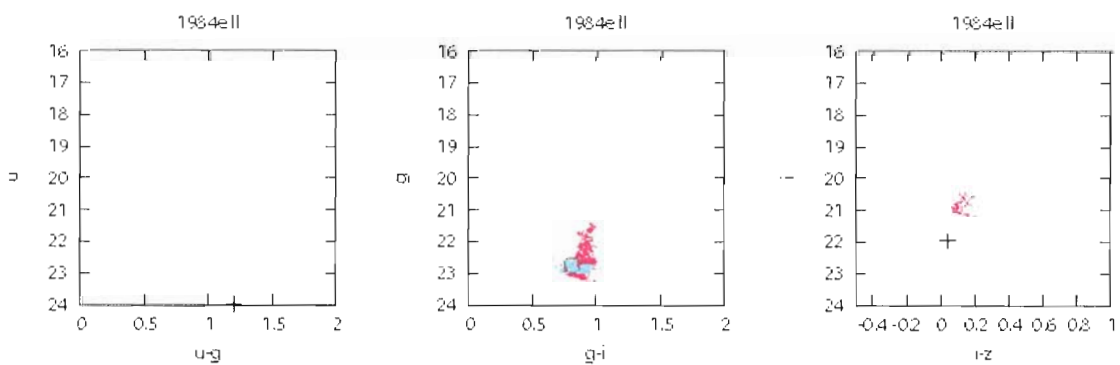


Figure 5.465. SN 1984e  $u,u-g$ ,  $g,g-i$ , and  $i,i-z$  pseudo color-magnitude plots.

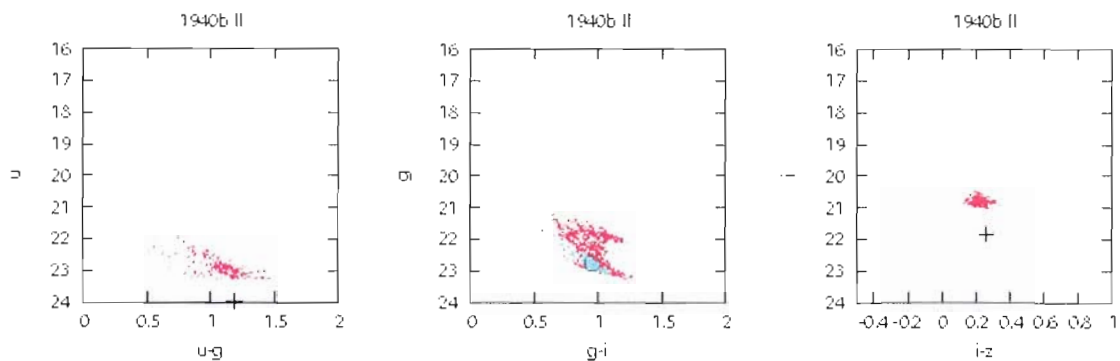


Figure 5.466. SN 1940b  $u,u-g$ ,  $g,g-i$ , and  $i,i-z$  pseudo color-magnitude plots.

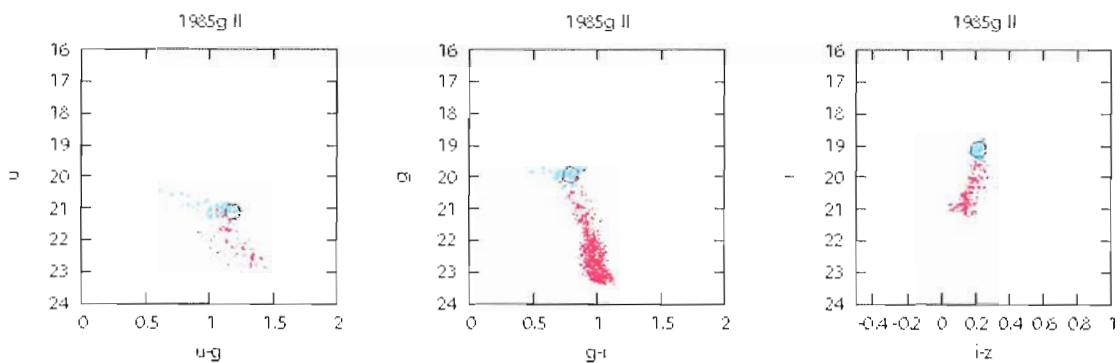


Figure 5.467. SN 1985g  $u,u-g$ ,  $g,g-i$ , and  $i,i-z$  pseudo color-magnitude plots.

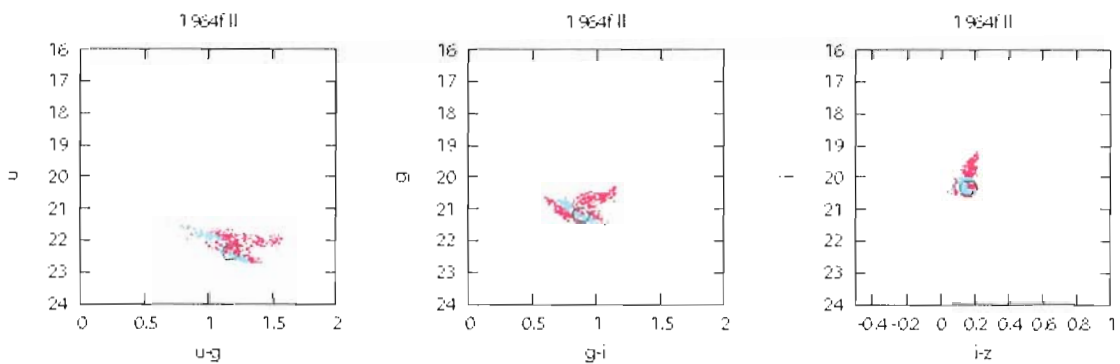


Figure 5.468. SN 1964f  $u,u-g$ ,  $g,g-i$ , and  $i,i-z$  pseudo color-magnitude plots.

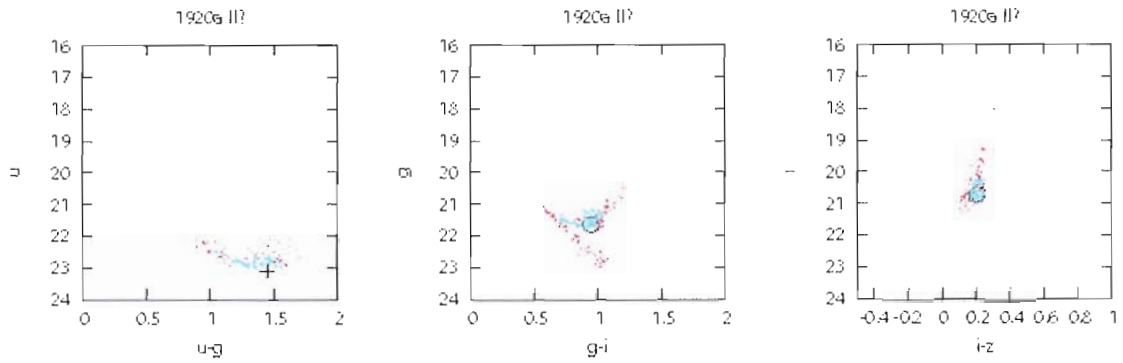


Figure 5.469. SN 1920a  $u,u-g$ ,  $g,g-i$ , and  $i,i-z$  pseudo color-magnitude plots.

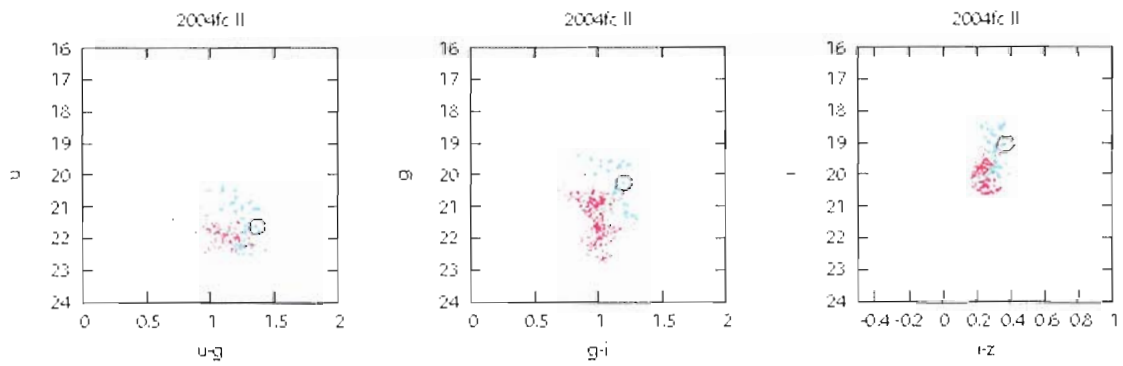


Figure 5.470. SN 2004fc  $u,u-g$ ,  $g,g-i$ , and  $i,i-z$  pseudo color-magnitude plots.

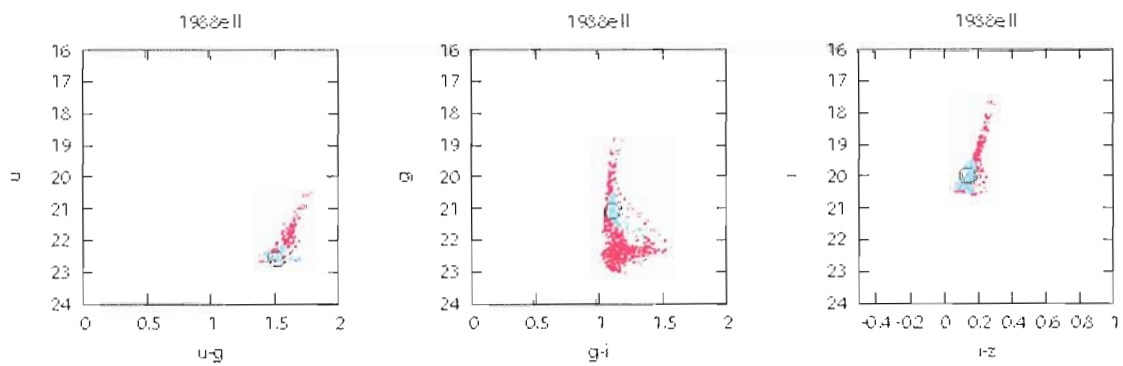


Figure 5.471. SN 1988e  $u,u-g$ ,  $g,g-i$ , and  $i,i-z$  pseudo color-magnitude plots.

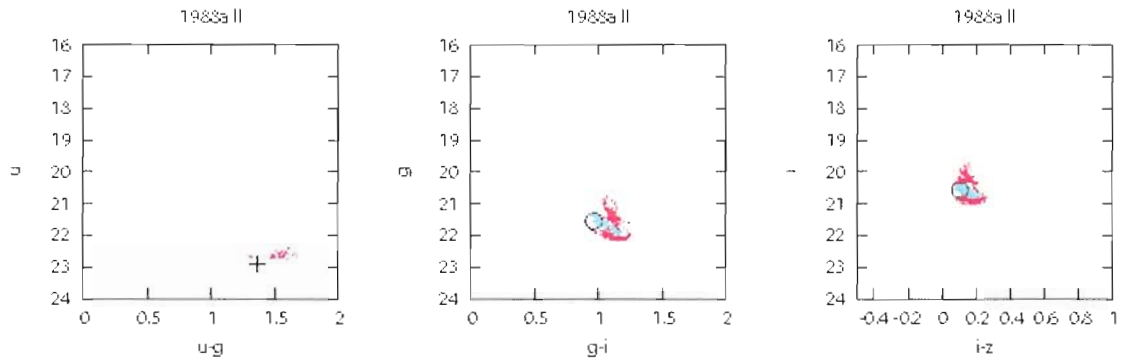


Figure 5.472. SN 1988a  $u,u-g$ ,  $g,g-i$ , and  $i,i-z$  pseudo color-magnitude plots.

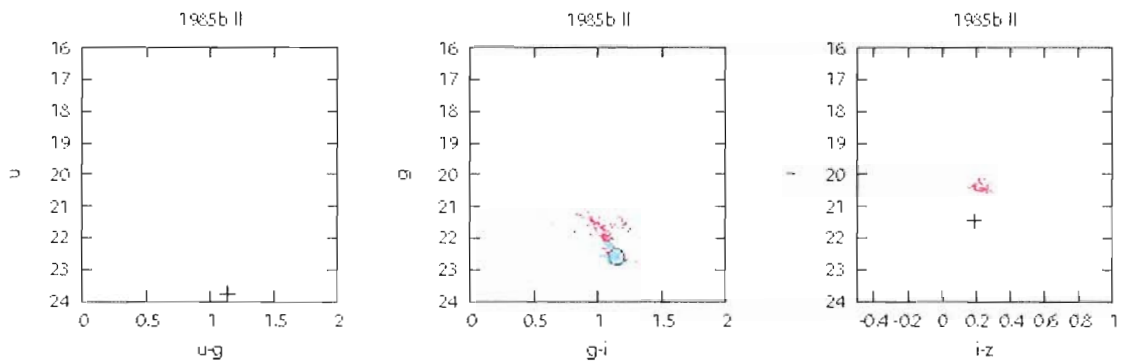


Figure 5.473. SN 1985b  $u,u-g$ ,  $g,g-i$ , and  $i,i-z$  pseudo color-magnitude plots.

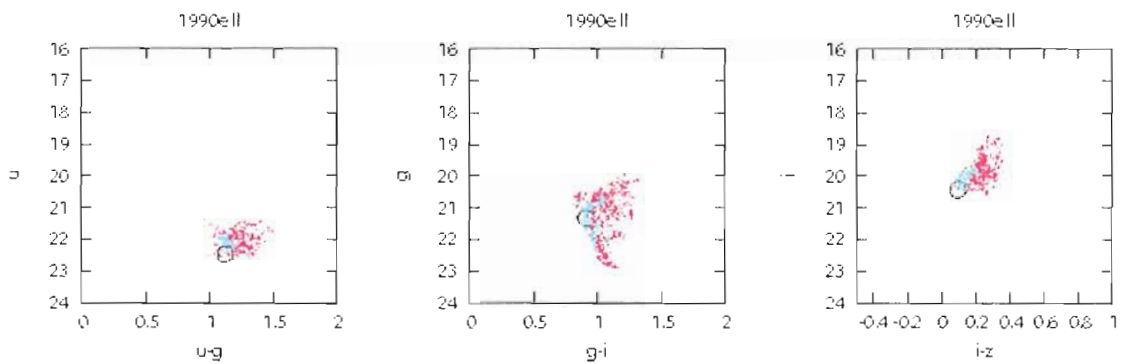


Figure 5.474. SN 1990e  $u,u-g$ ,  $g,g-i$ , and  $i,i-z$  pseudo color-magnitude plots.



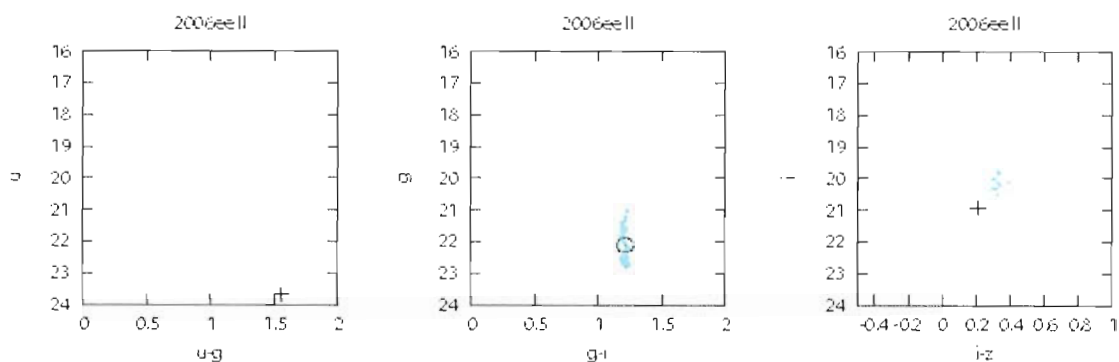


Figure 5.475. SN 2006ee  $u,u-g$ ,  $g,g-i$ , and  $i,i-z$  pseudo color-magnitude plots.

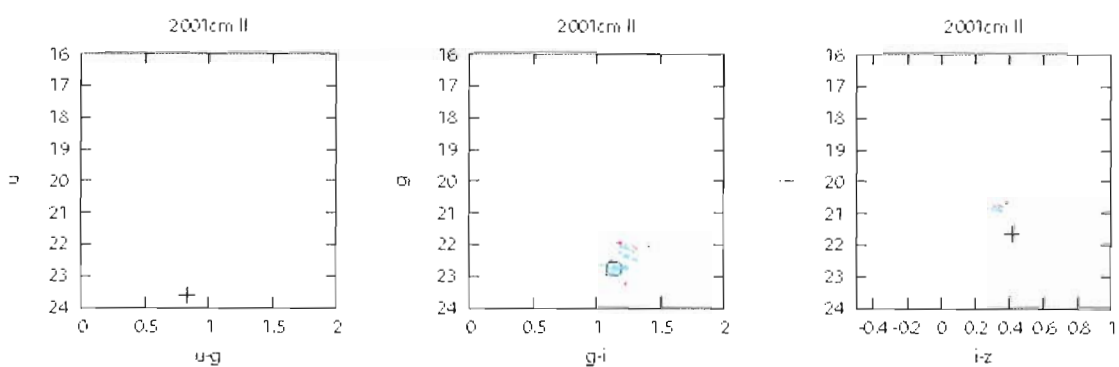


Figure 5.476. SN 2001cm  $u,u-g$ ,  $g,g-i$ , and  $i,i-z$  pseudo color-magnitude plots.

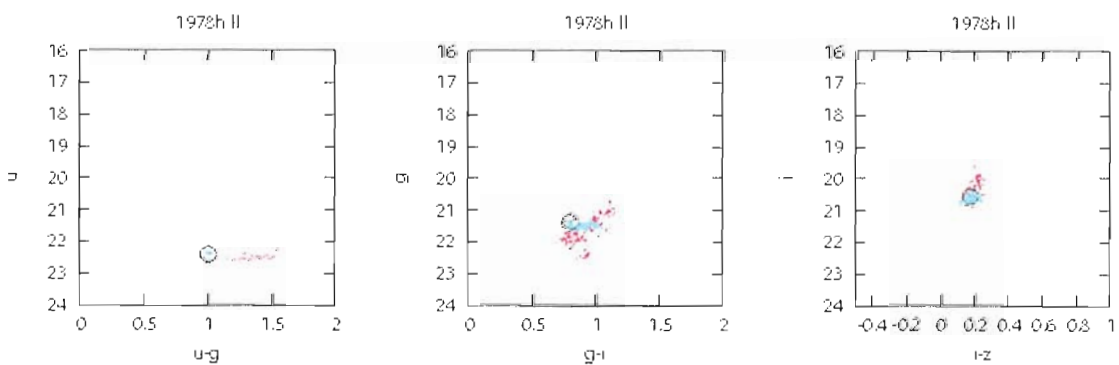


Figure 5.477. SN 1978h  $u,u-g$ ,  $g,g-i$ , and  $i,i-z$  pseudo color-magnitude plots.

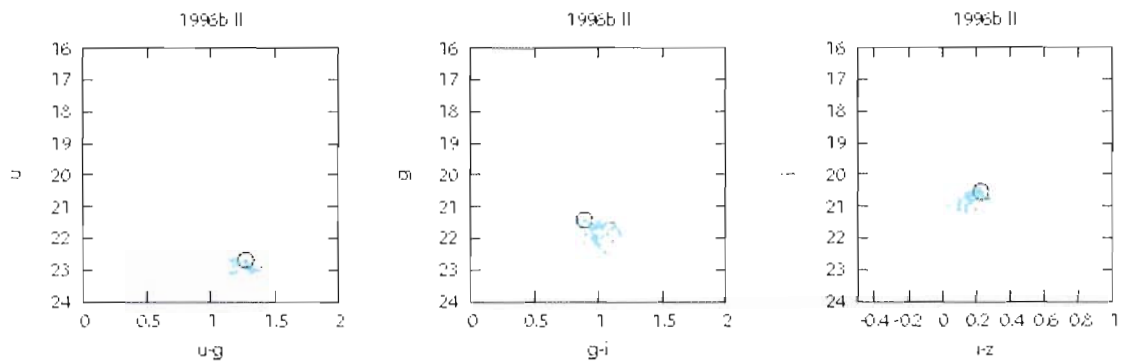


Figure 5.478. SN 1996b  $u,u-g$ ,  $g,g-i$ , and  $i,i-z$  pseudo color-magnitude plots.

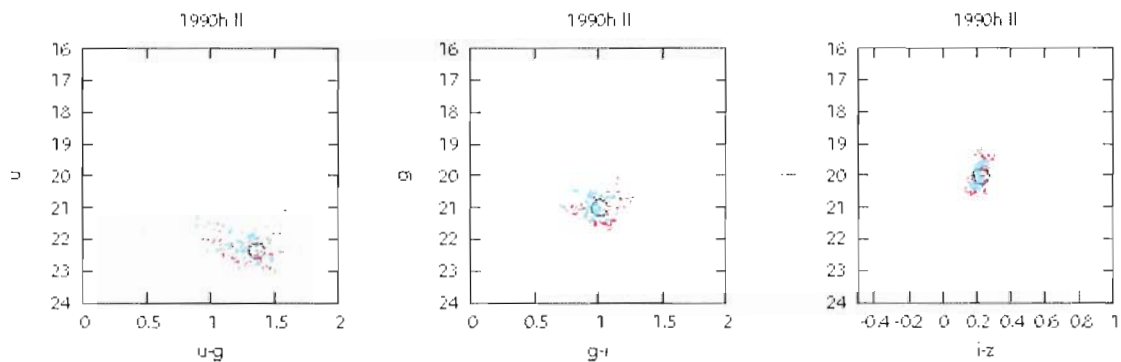


Figure 5.479. SN 1990h  $u,u-g$ ,  $g,g-i$ , and  $i,i-z$  pseudo color-magnitude plots.

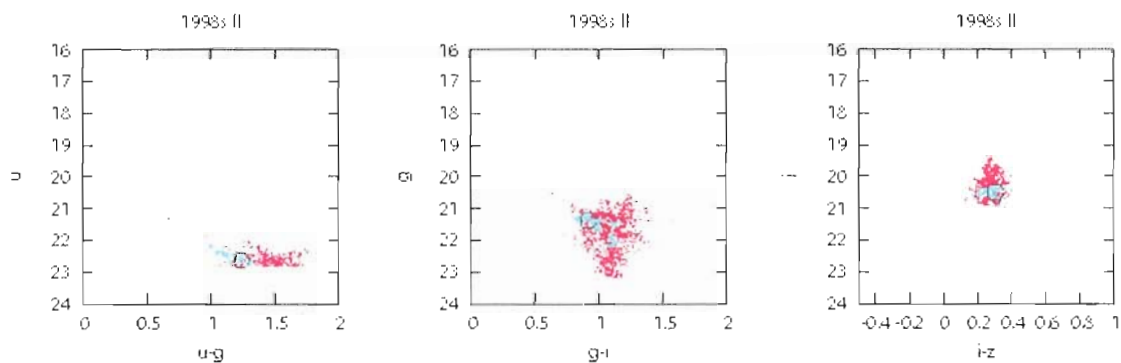


Figure 5.480. SN 1998s  $u,u-g$ ,  $g,g-i$ , and  $i,i-z$  pseudo color-magnitude plots.

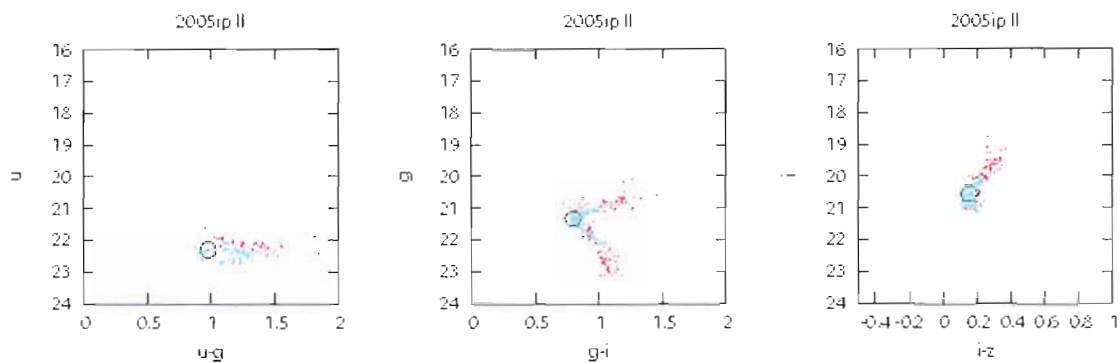


Figure 5.481. SN 2005ip  $u,u-g$ ,  $g,g-i$ , and  $i,i-z$  pseudo color-magnitude plots.

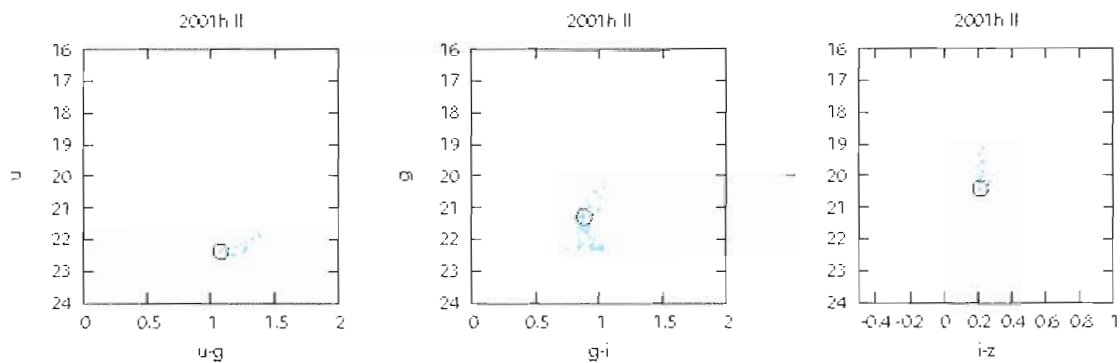


Figure 5.482. SN 2001h  $u,u-g$ ,  $g,g-i$ , and  $i,i-z$  pseudo color-magnitude plots.

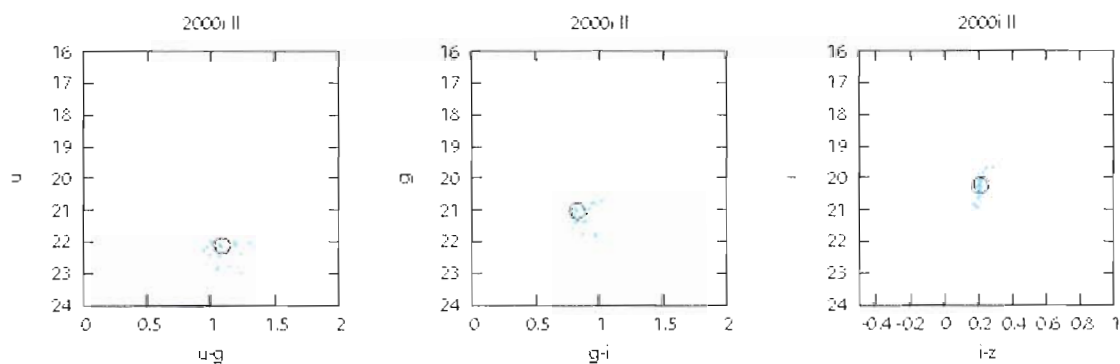


Figure 5.483. SN 2000i  $u,u-g$ ,  $g,g-i$ , and  $i,i-z$  pseudo color-magnitude plots.

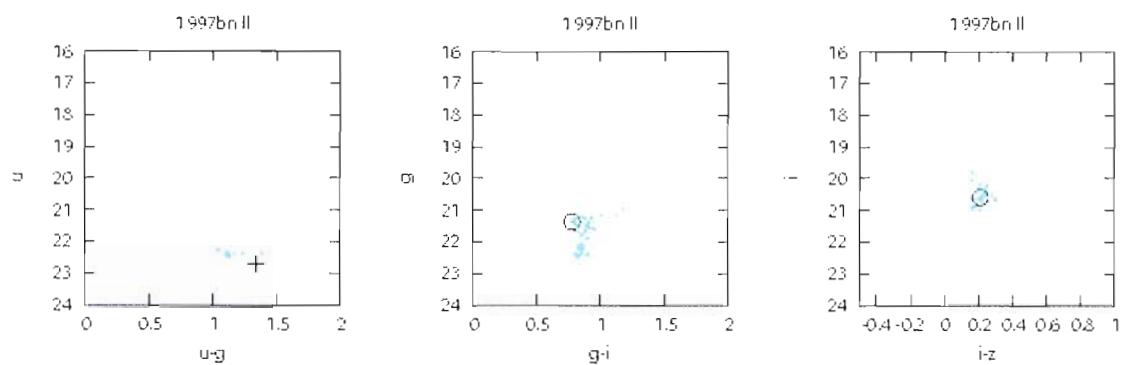


Figure 5.484. SN 1997bn  $u,u-g$ ,  $g,g-i$ , and  $i,i-z$  pseudo color-magnitude plots.

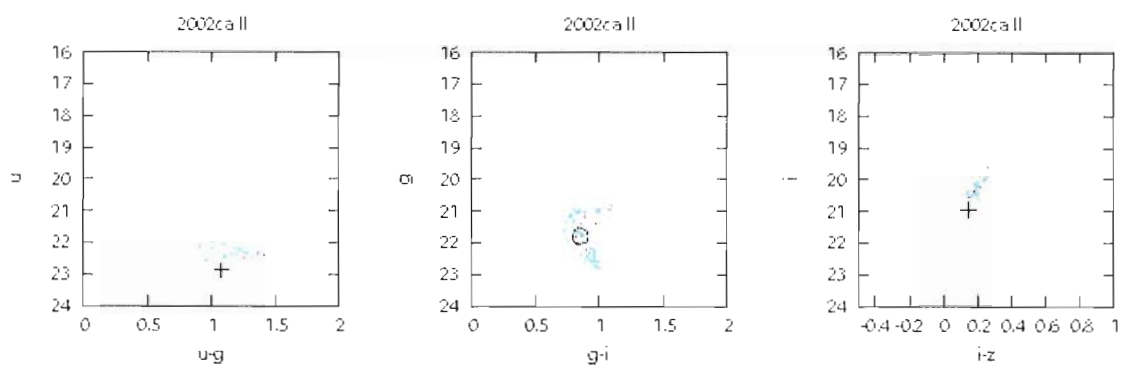


Figure 5.485. SN 2002ca  $u,u-g$ ,  $g,g-i$ , and  $i,i-z$  pseudo color-magnitude plots.

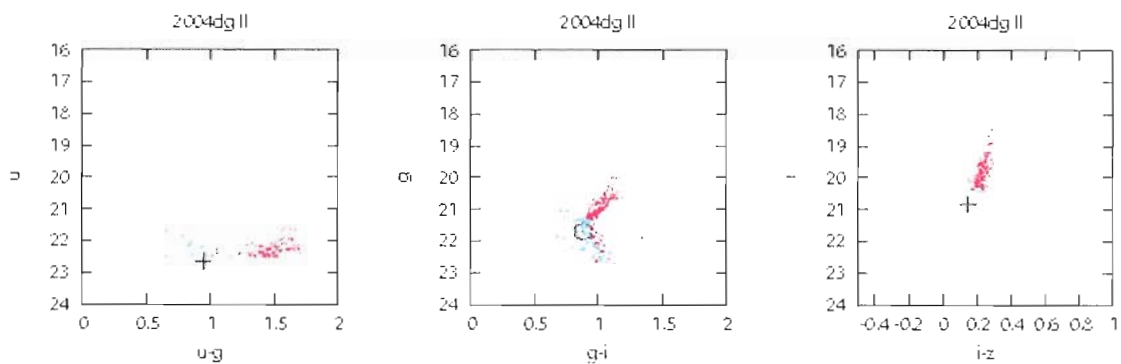


Figure 5.486. SN 2004dg  $u,u-g$ ,  $g,g-i$ , and  $i,i-z$  pseudo color-magnitude plots.

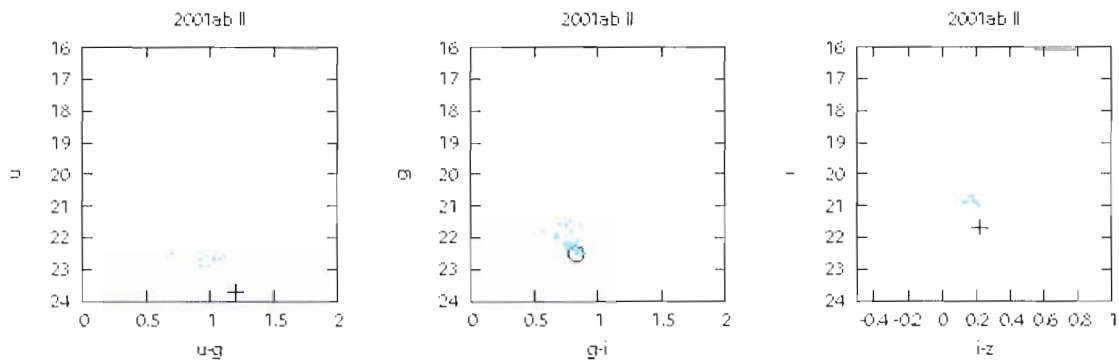


Figure 5.487. SN 2001ab  $u,u-g$ ,  $g,g-i$ , and  $i,i-z$  pseudo color-magnitude plots.

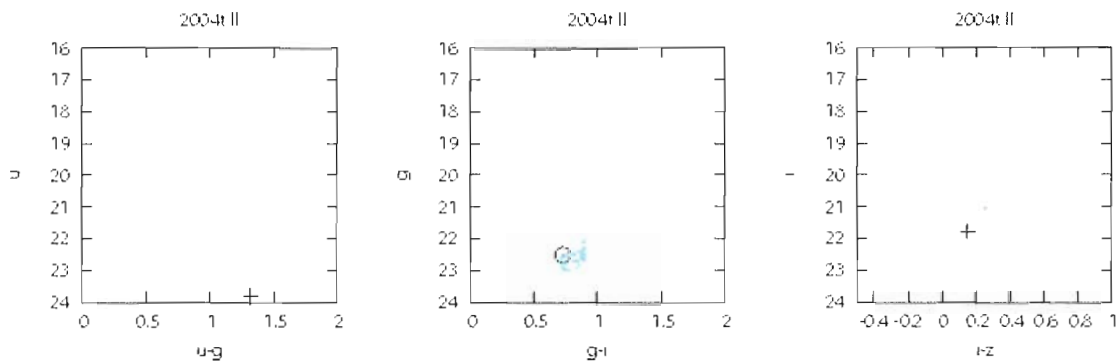


Figure 5.488. SN 2004t  $u,u-g$ ,  $g,g-i$ , and  $i,i-z$  pseudo color-magnitude plots.

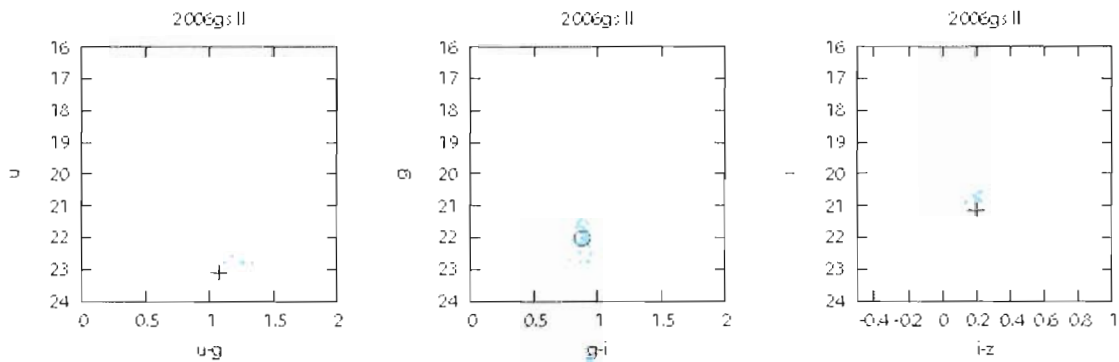


Figure 5.489. SN 2006gs  $u,u-g$ ,  $g,g-i$ , and  $i,i-z$  pseudo color-magnitude plots.

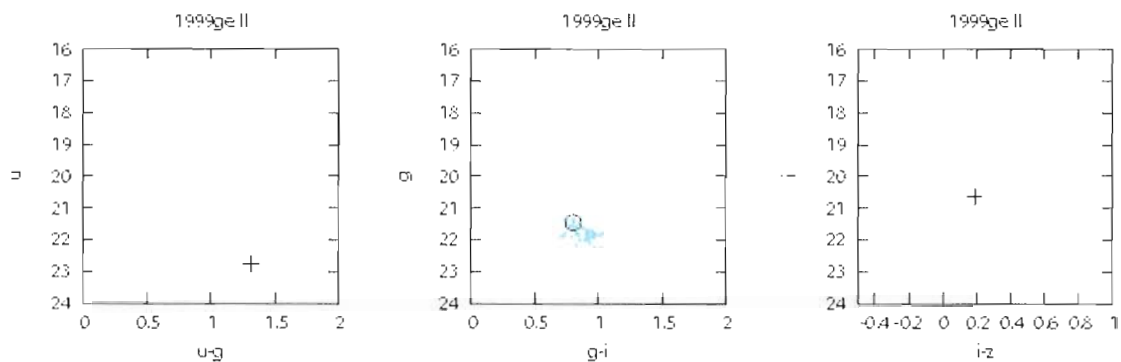


Figure 5.490. SN 1999ge  $u,u-g$ ,  $g,g-i$ , and  $i,i-z$  pseudo color-magnitude plots.

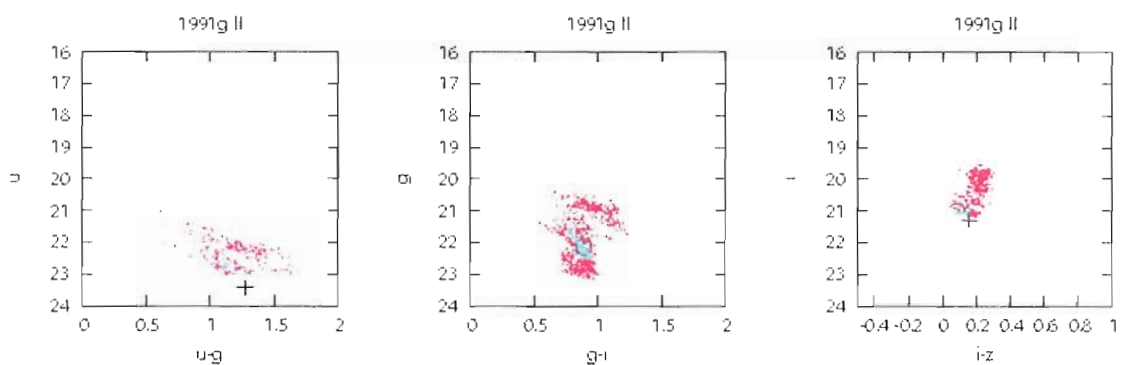


Figure 5.491. SN 1991g  $u,u-g$ ,  $g,g-i$ , and  $i,i-z$  pseudo color-magnitude plots.

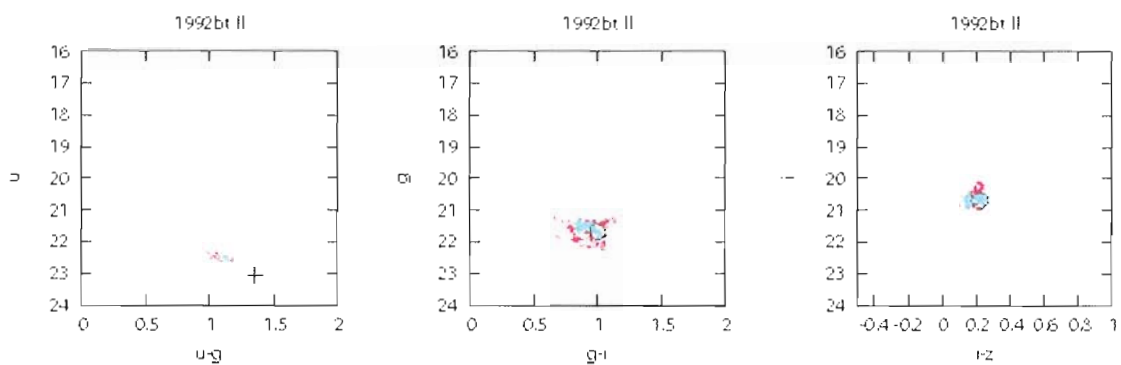


Figure 5.492. SN 1992bt  $u,u-g$ ,  $g,g-i$ , and  $i,i-z$  pseudo color-magnitude plots.

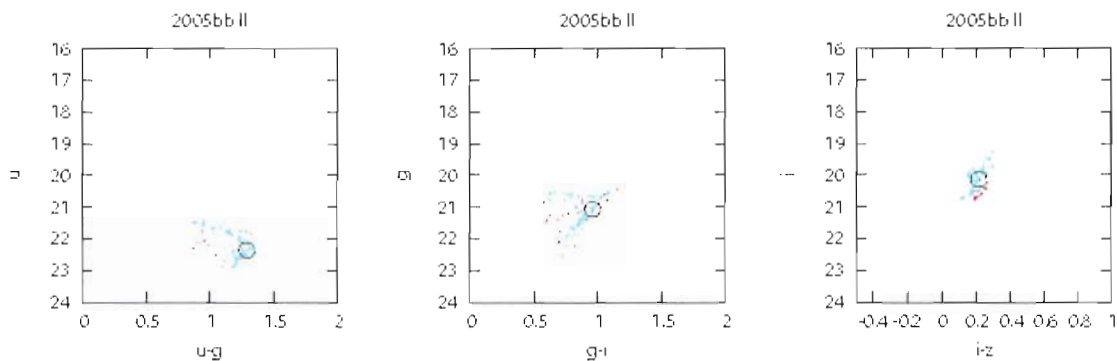


Figure 5.493. SN 2005bb  $u,u-g$ ,  $g,g-i$ , and  $i,i-z$  pseudo color-magnitude plots.

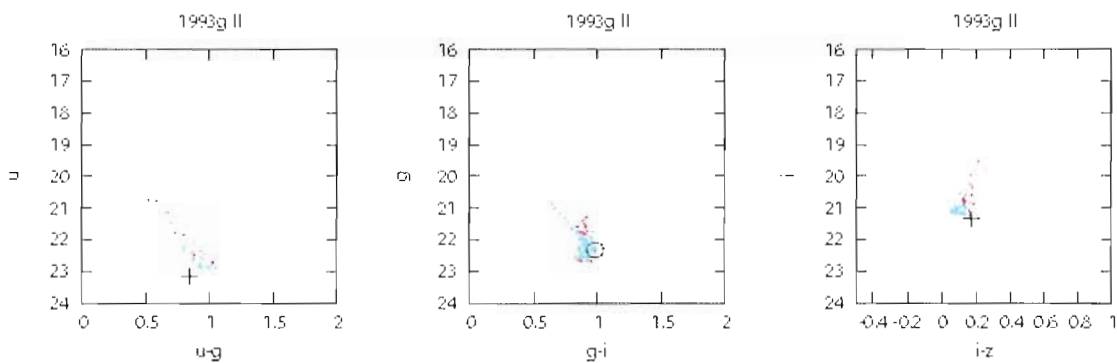


Figure 5.494. SN 1993g  $u,u-g$ ,  $g,g-i$ , and  $i,i-z$  pseudo color-magnitude plots.

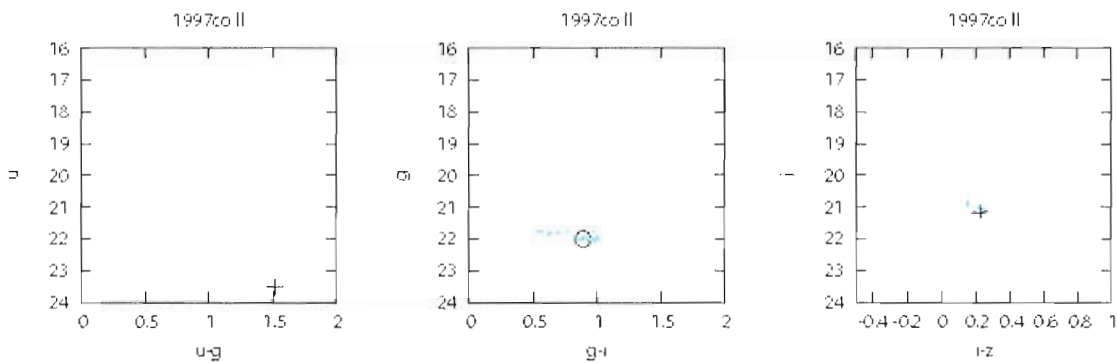


Figure 5.495. SN 1997co  $u,u-g$ ,  $g,g-i$ , and  $i,i-z$  pseudo color-magnitude plots.

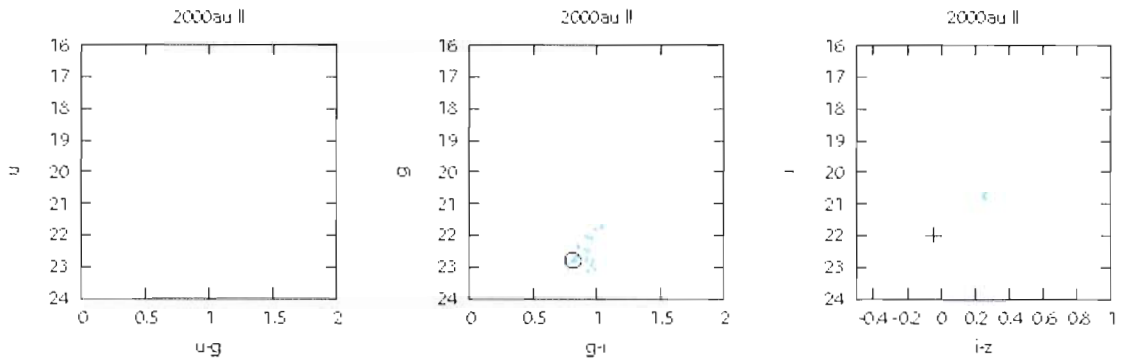


Figure 5.496. SN 2000au  $u,u-g$ ,  $g,g-i$ , and  $i,i-z$  pseudo color-magnitude plots.

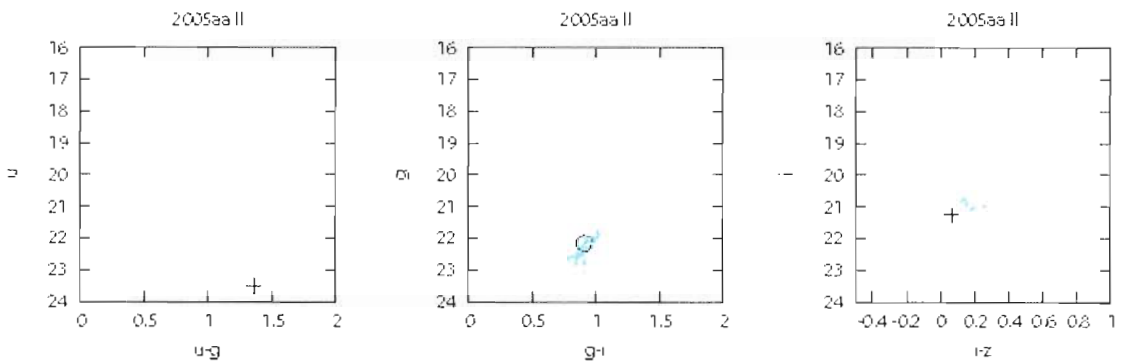


Figure 5.497. SN 2005aa  $u,u-g$ ,  $g,g-i$ , and  $i,i-z$  pseudo color-magnitude plots.

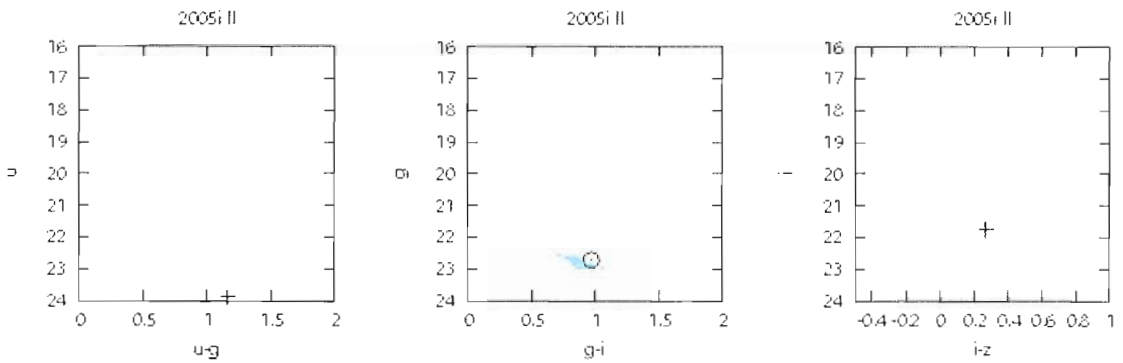


Figure 5.498. SN 2005i  $u,u-g$ ,  $g,g-i$ , and  $i,i-z$  pseudo color-magnitude plots.



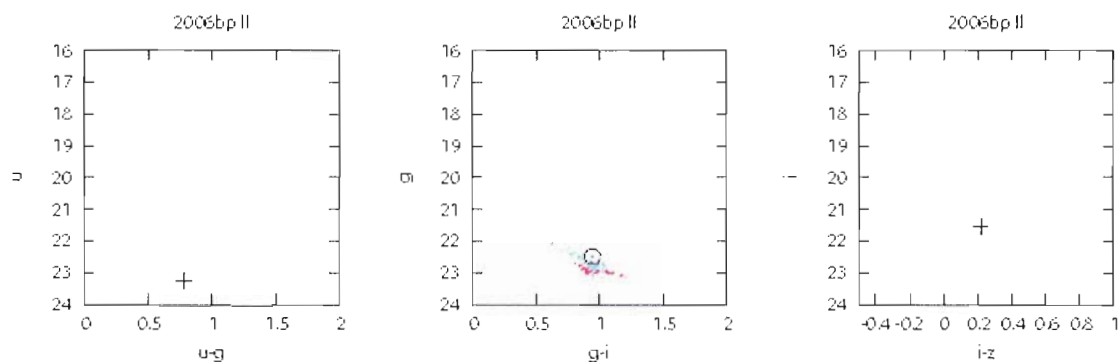


Figure 5.499. SN 2006bp  $u,u-g$ ,  $g,g-i$ , and  $i,i-z$  pseudo color-magnitude plots.

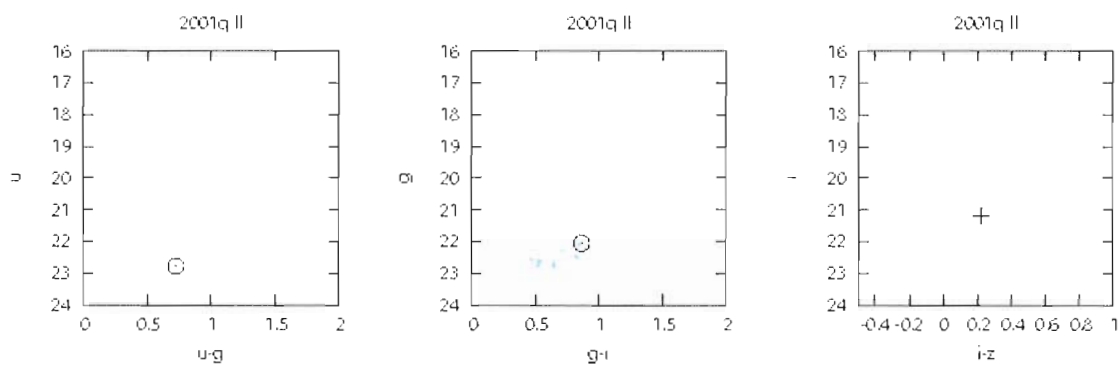


Figure 5.500. SN 2001q  $u,u-g$ ,  $g,g-i$ , and  $i,i-z$  pseudo color-magnitude plots.

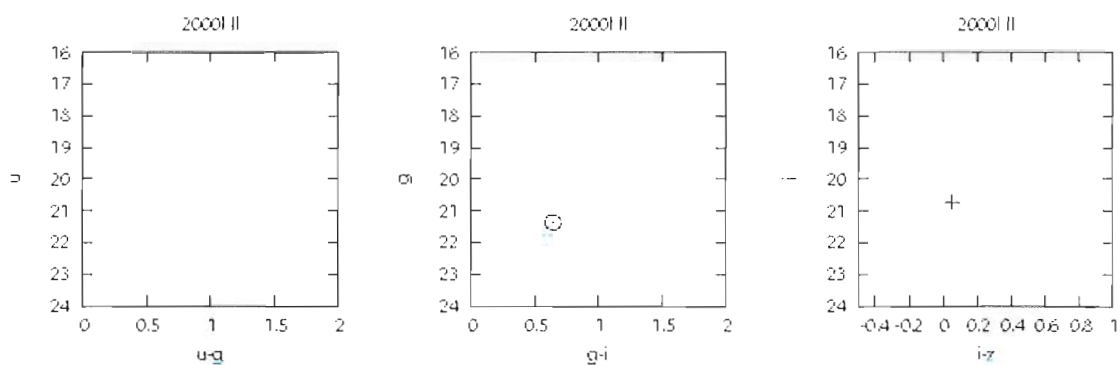


Figure 5.501. SN 2000I  $u,u-g$ ,  $g,g-i$ , and  $i,i-z$  pseudo color-magnitude plots.

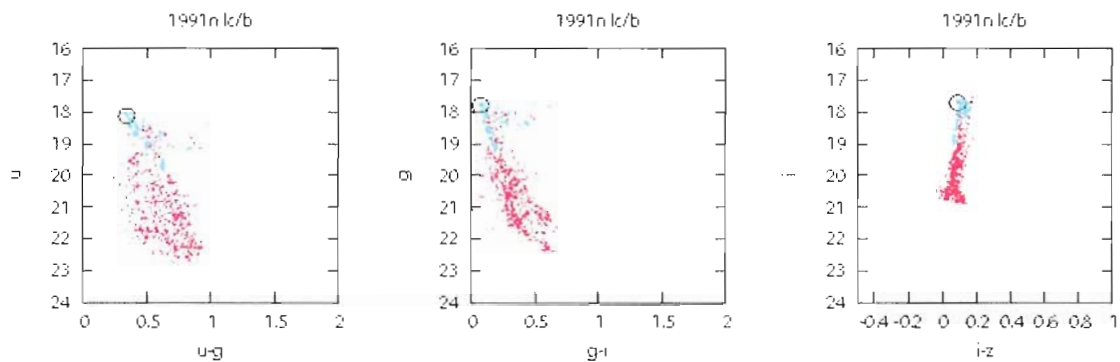


Figure 5.502. SN 1991n  $u,u-g$ ,  $g,g-i$ , and  $i,i-z$  pseudo color-magnitude plots.

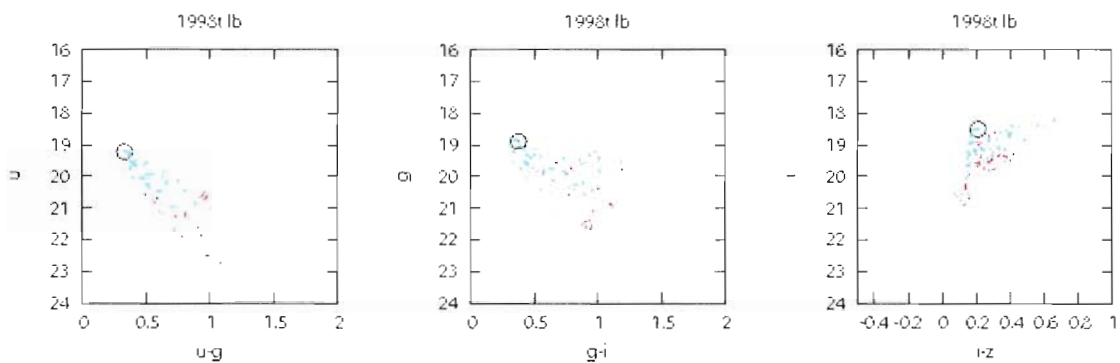


Figure 5.503. SN 1998t  $u,u-g$ ,  $g,g-i$ , and  $i,i-z$  pseudo color-magnitude plots.

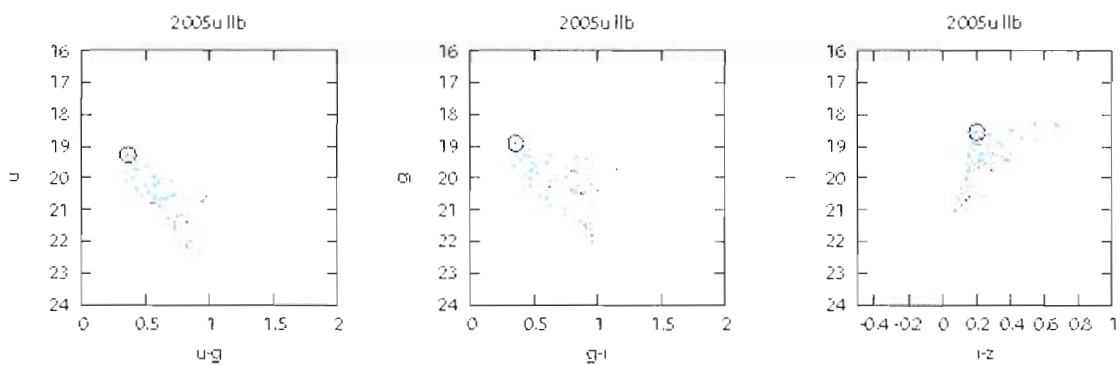


Figure 5.504. SN 2005u  $u,u-g$ ,  $g,g-i$ , and  $i,i-z$  pseudo color-magnitude plots.

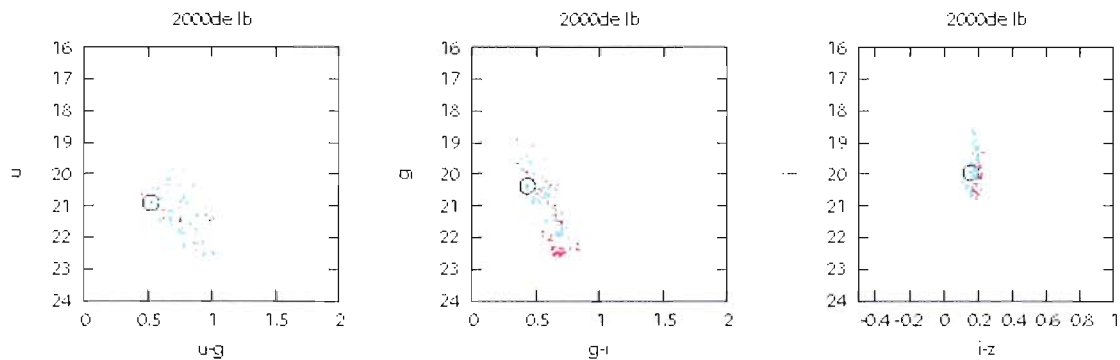


Figure 5.505. SN 2000de  $u,u-g$ ,  $g,g-i$ , and  $i,i-z$  pseudo color-magnitude plots.

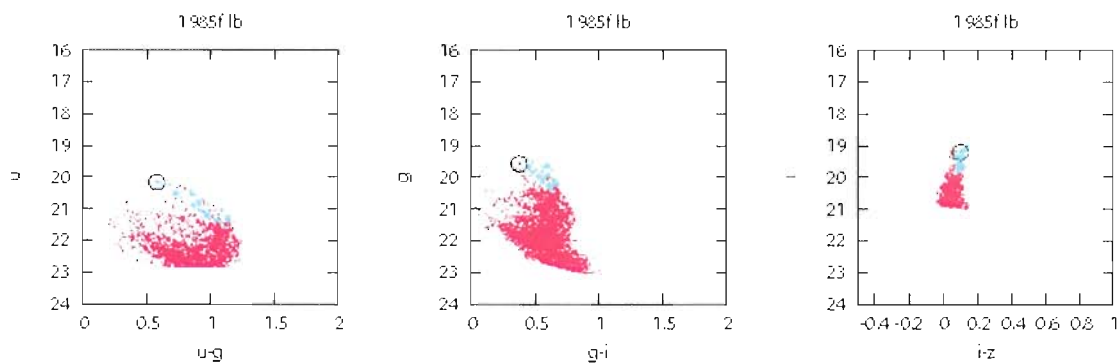


Figure 5.506. SN 1985f  $u,u-g$ ,  $g,g-i$ , and  $i,i-z$  pseudo color-magnitude plots.

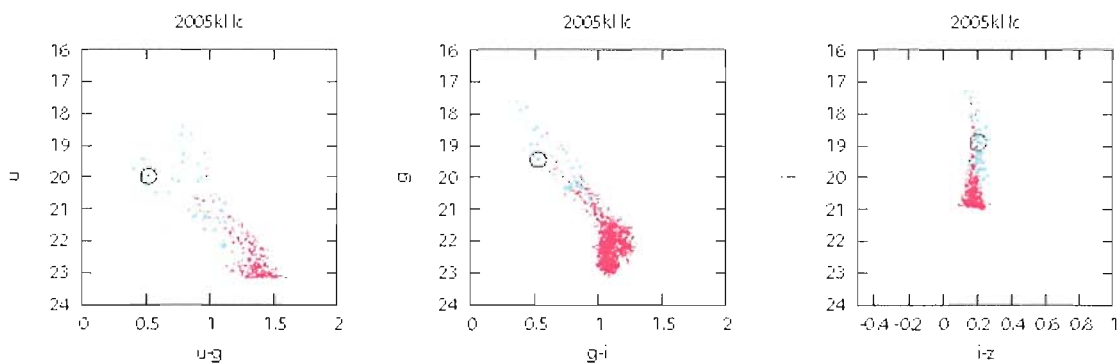


Figure 5.507. SN 2005kl  $u,u-g$ ,  $g,g-i$ , and  $i,i-z$  pseudo color-magnitude plots.

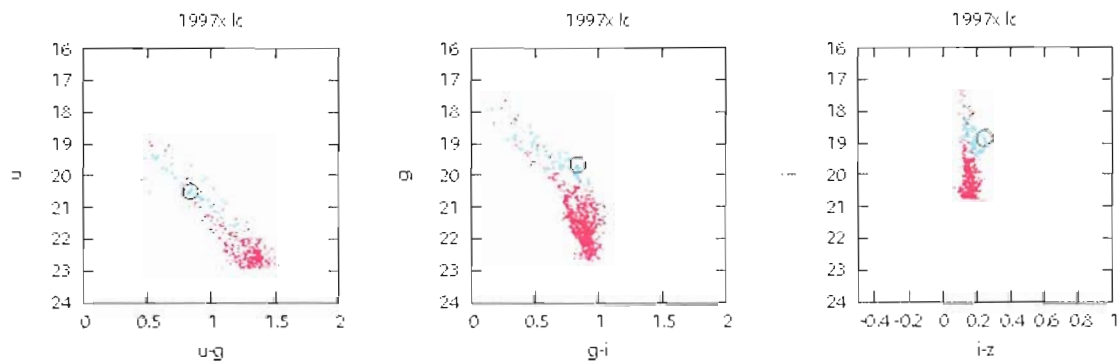


Figure 5.508. SN 1997x  $u,u-g$ ,  $g,g-i$ , and  $i,i-z$  pseudo color-magnitude plots.

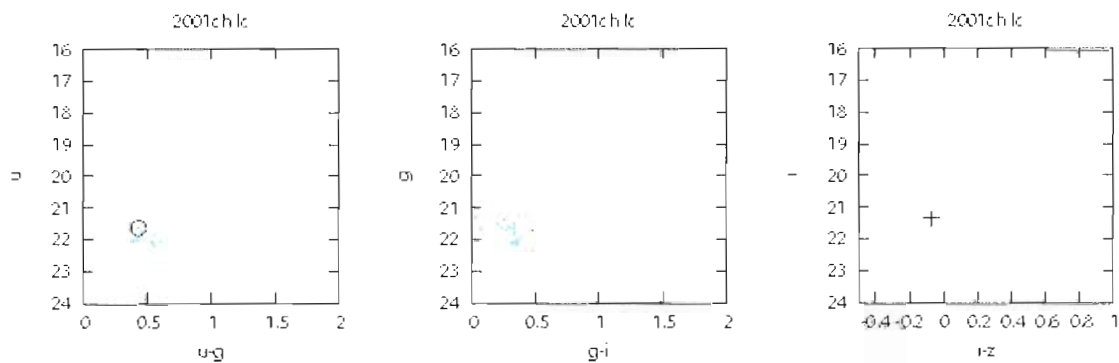


Figure 5.509. SN 2001ch  $u,u-g$ ,  $g,g-i$ , and  $i,i-z$  pseudo color-magnitude plots.

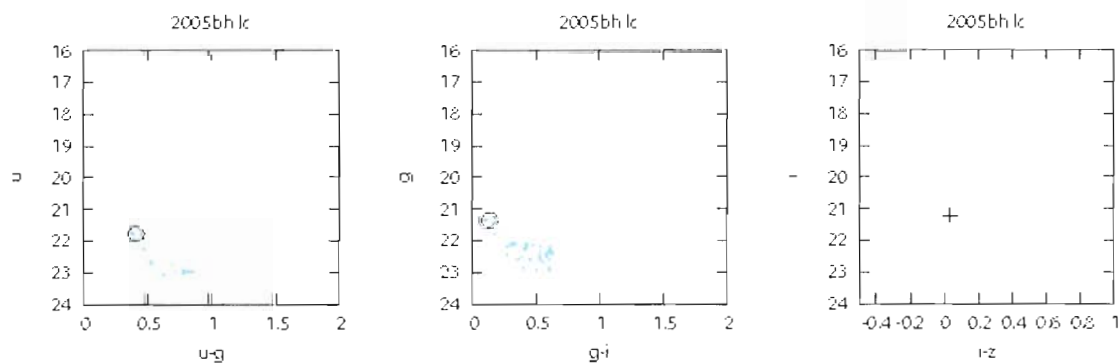


Figure 5.510. SN 2005bh  $u,u-g$ ,  $g,g-i$ , and  $i,i-z$  pseudo color-magnitude plots.

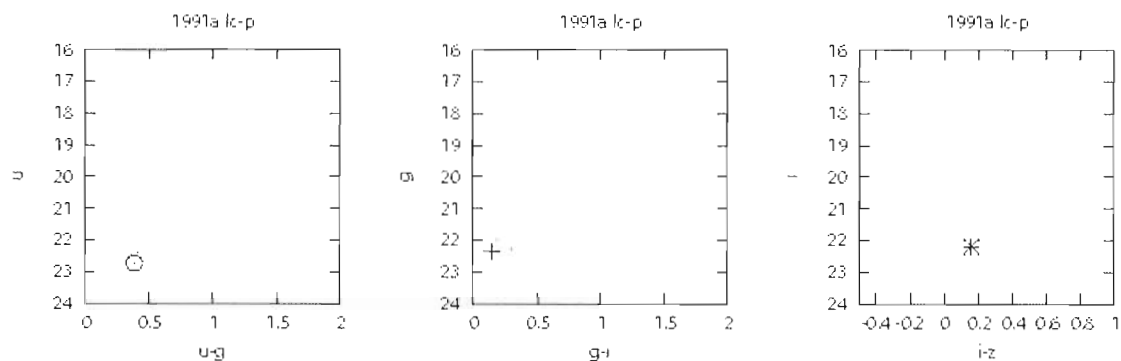


Figure 5.511. SN 1991a  $u,u-g$ ,  $g,g-i$ , and  $i,i-z$  pseudo color-magnitude plots.

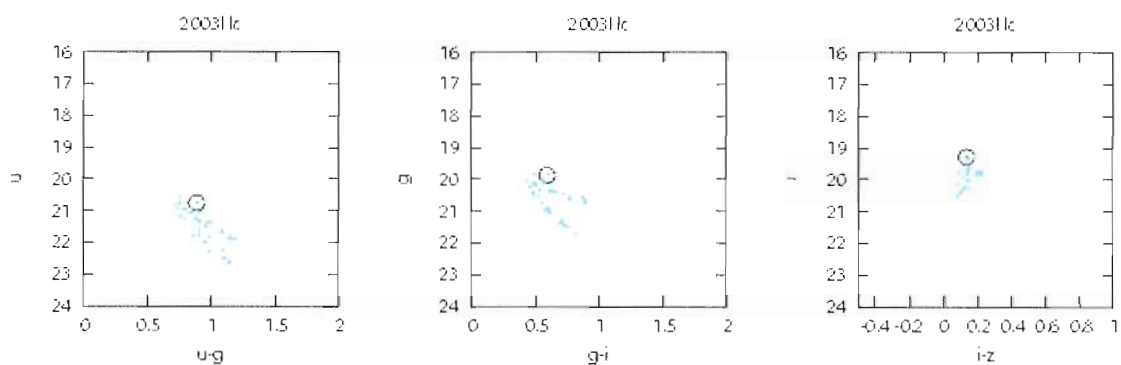


Figure 5.512. SN 2003l  $u,u-g$ ,  $g,g-i$ , and  $i,i-z$  pseudo color-magnitude plots.

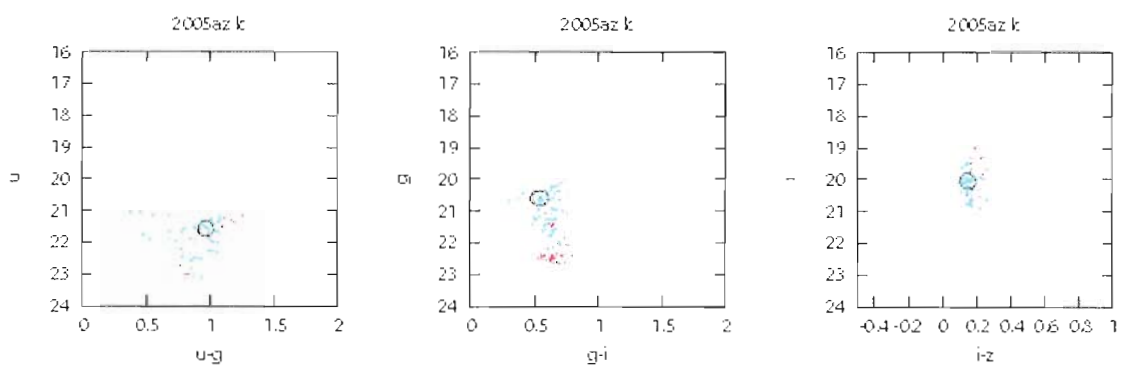


Figure 5.513. SN 2005az  $u,u-g$ ,  $g,g-i$ , and  $i,i-z$  pseudo color-magnitude plots.

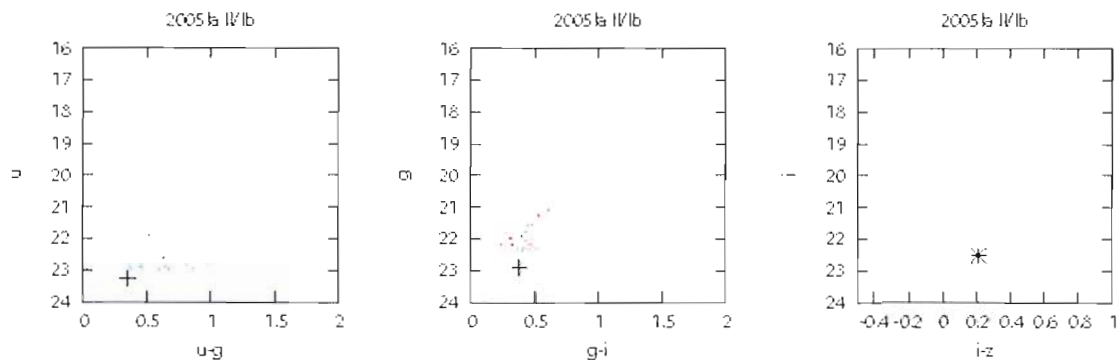


Figure 5.514. SN 2005la  $u,u-g$ ,  $g,g-i$ , and  $i,i-z$  pseudo color-magnitude plots.

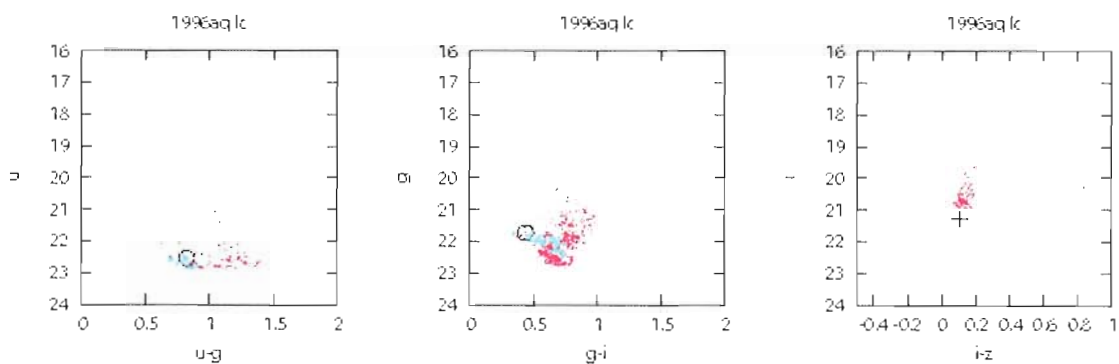


Figure 5.515. SN 1996aq  $u,u-g$ ,  $g,g-i$ , and  $i,i-z$  pseudo color-magnitude plots.

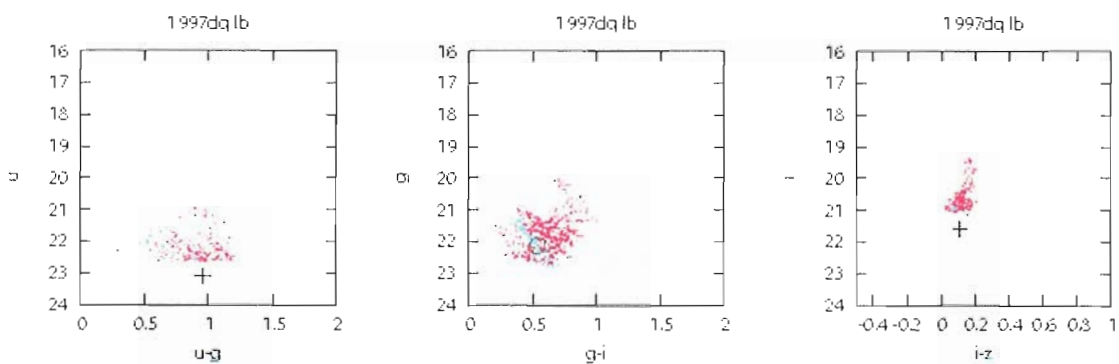


Figure 5.516. SN 1997dq  $u,u-g$ ,  $g,g-i$ , and  $i,i-z$  pseudo color-magnitude plots.

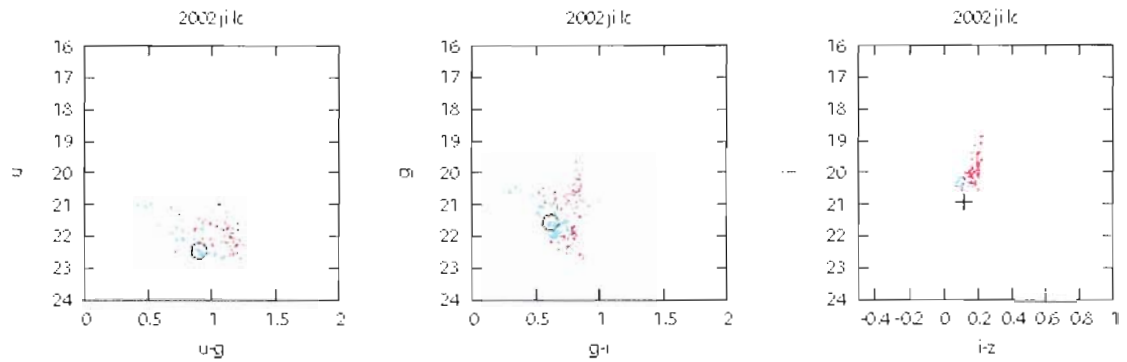


Figure 5.517. SN 2002ji  $u,u-g$ ,  $g,g-i$ , and  $i,i-z$  pseudo color-magnitude plots.

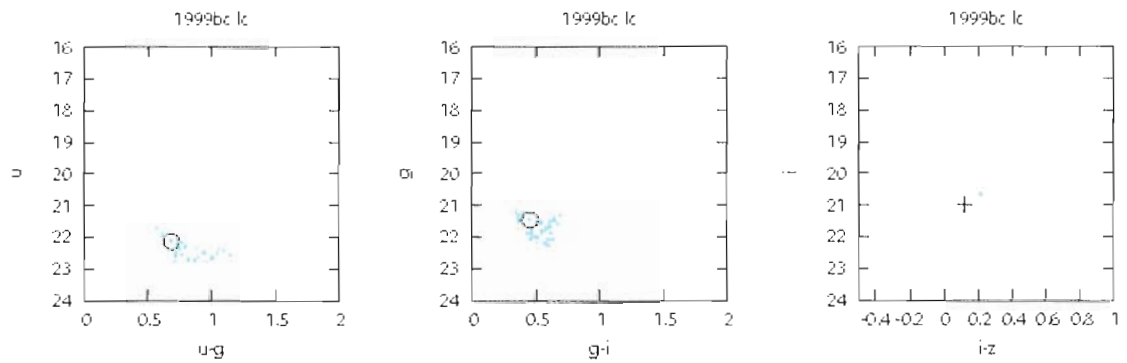


Figure 5.518. SN 1999bc  $u,u-g$ ,  $g,g-i$ , and  $i,i-z$  pseudo color-magnitude plots.

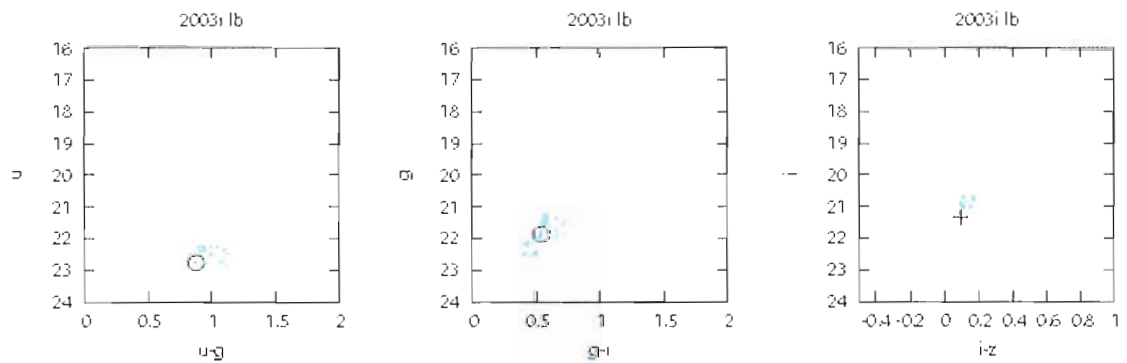


Figure 5.519. SN 2003i  $u,u-g$ ,  $g,g-i$ , and  $i,i-z$  pseudo color-magnitude plots.

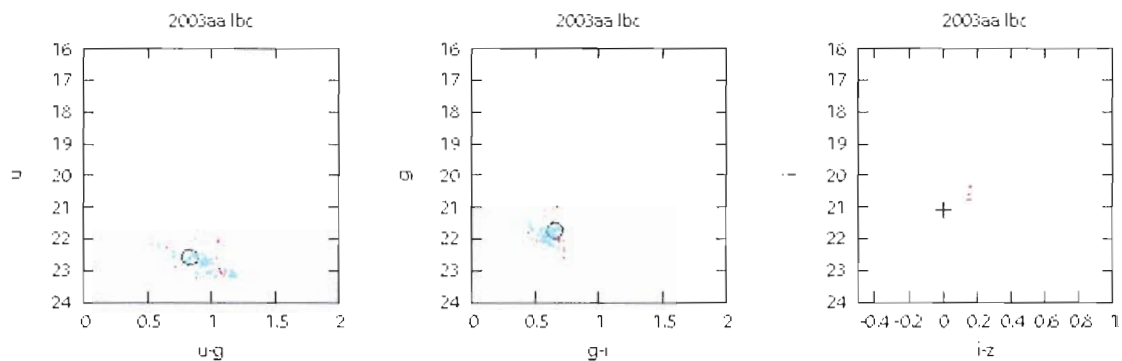


Figure 5.520. SN 2003aa  $u,u-g$ ,  $g,g-i$ , and  $i,i-z$  pseudo color-magnitude plots.

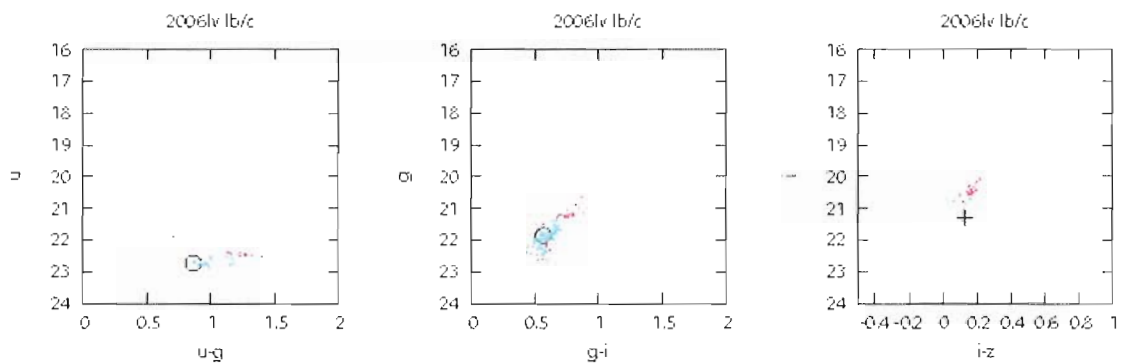


Figure 5.521. SN 2006lv  $u,u-g$ ,  $g,g-i$ , and  $i,i-z$  pseudo color-magnitude plots.

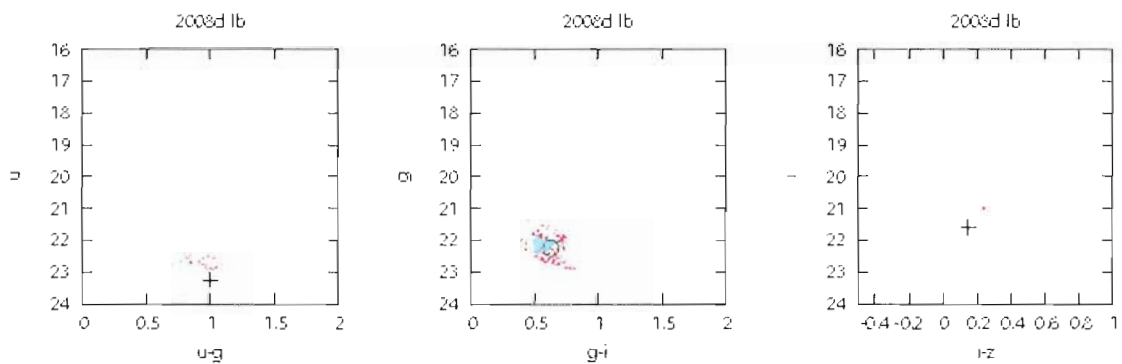


Figure 5.522. SN 2008d  $u,u-g$ ,  $g,g-i$ , and  $i,i-z$  pseudo color-magnitude plots.



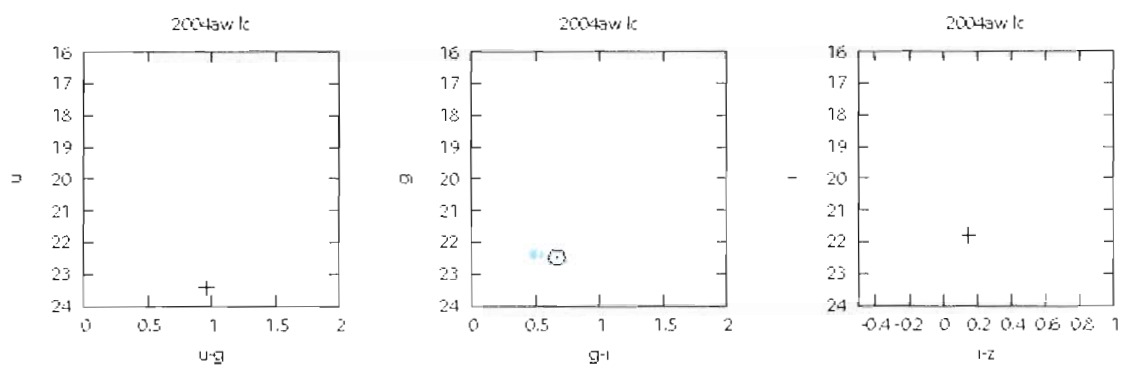


Figure 5.523. SN 2004aw  $u,u-g$ ,  $g,g-i$ , and  $i,i-z$  pseudo color-magnitude plots.

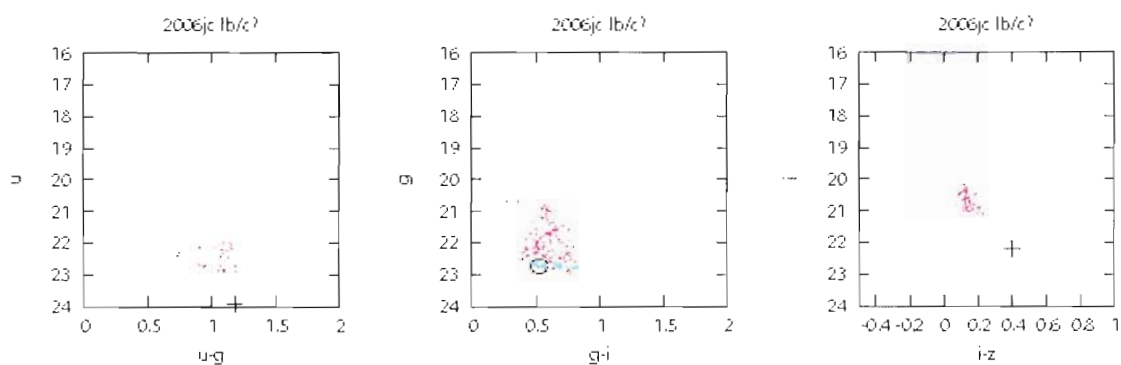


Figure 5.524. SN 2006jc  $u,u-g$ ,  $g,g-i$ , and  $i,i-z$  pseudo color-magnitude plots.

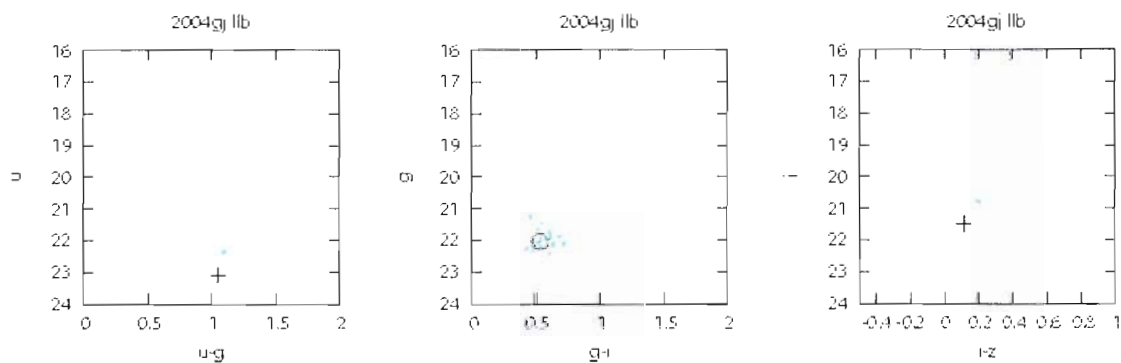


Figure 5.525. SN 2004gj  $u,u-g$ ,  $g,g-i$ , and  $i,i-z$  pseudo color-magnitude plots.

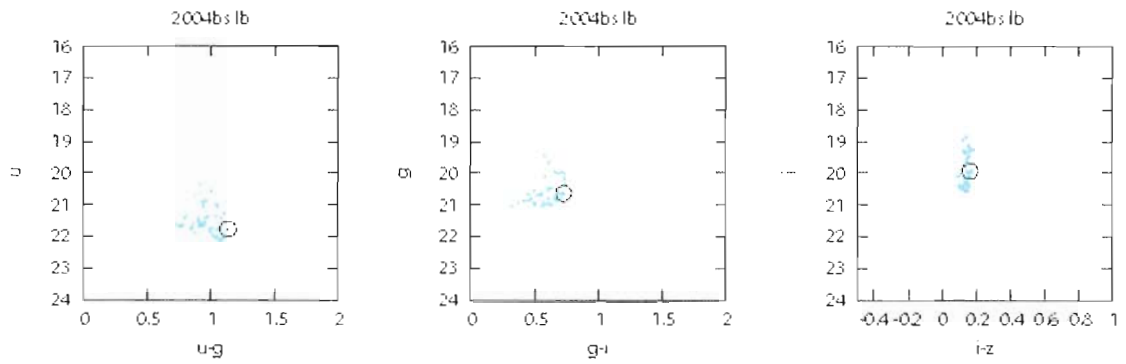


Figure 5.526. SN 2004bs  $u,u-g$ ,  $g,g-i$ , and  $i,i-z$  pseudo color-magnitude plots.

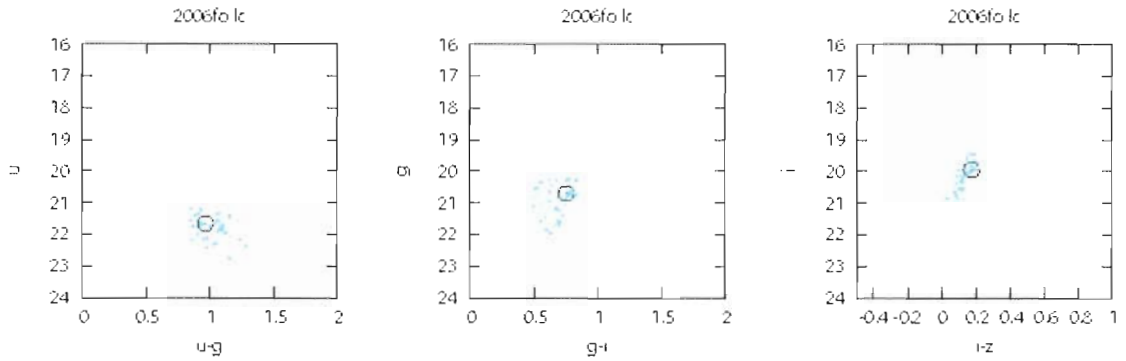


Figure 5.527. SN 2006fo  $u,u-g$ ,  $g,g-i$ , and  $i,i-z$  pseudo color-magnitude plots.

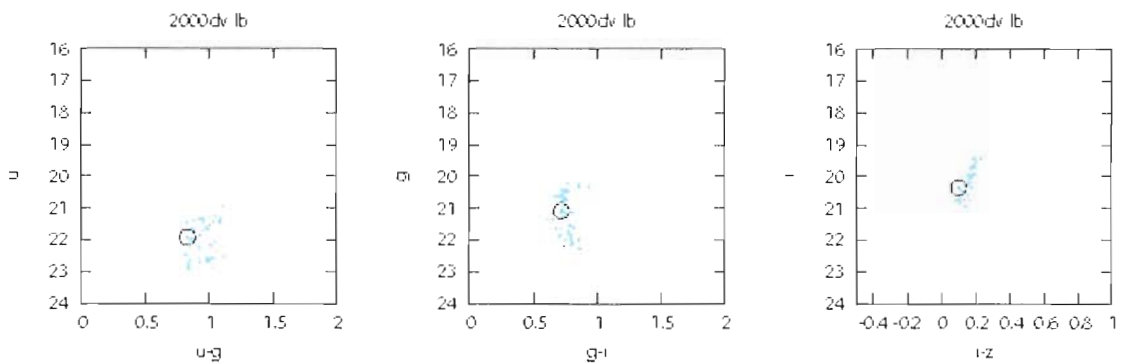


Figure 5.528. SN 2000dv  $u,u-g$ ,  $g,g-i$ , and  $i,i-z$  pseudo color-magnitude plots.

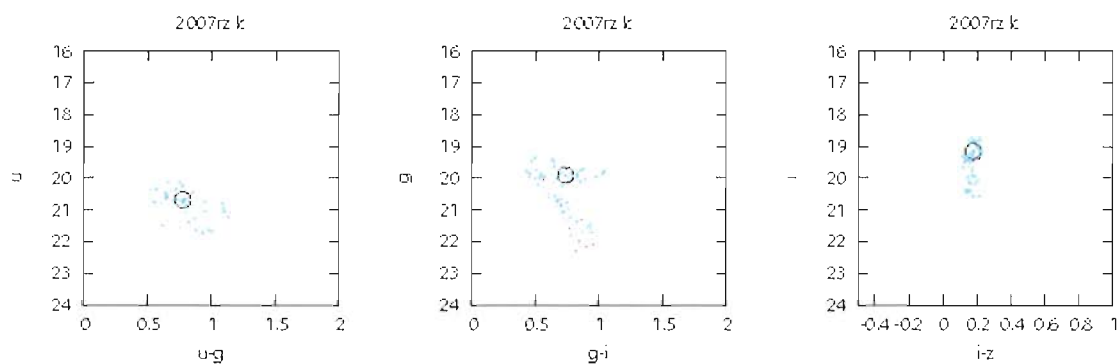


Figure 5.529. SN 2007rz  $u, u-g$ ,  $g, g-i$ , and  $i, i-z$  pseudo color-magnitude plots.

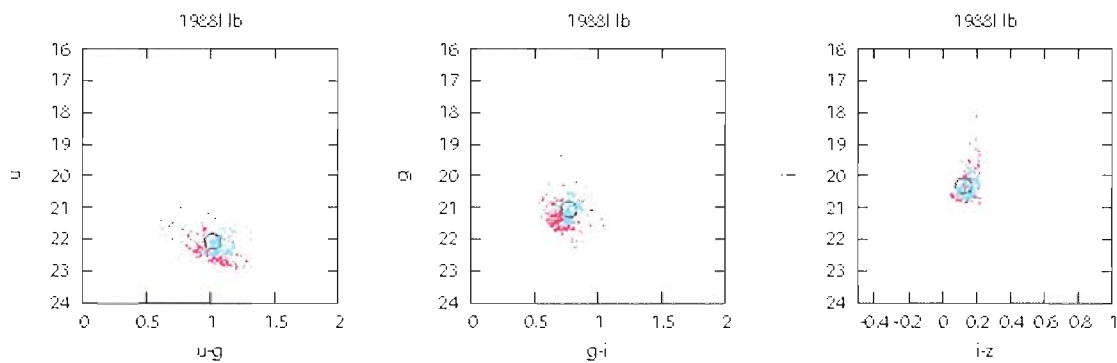


Figure 5.530. SN 1988l  $u, u-g$ ,  $g, g-i$ , and  $i, i-z$  pseudo color-magnitude plots.

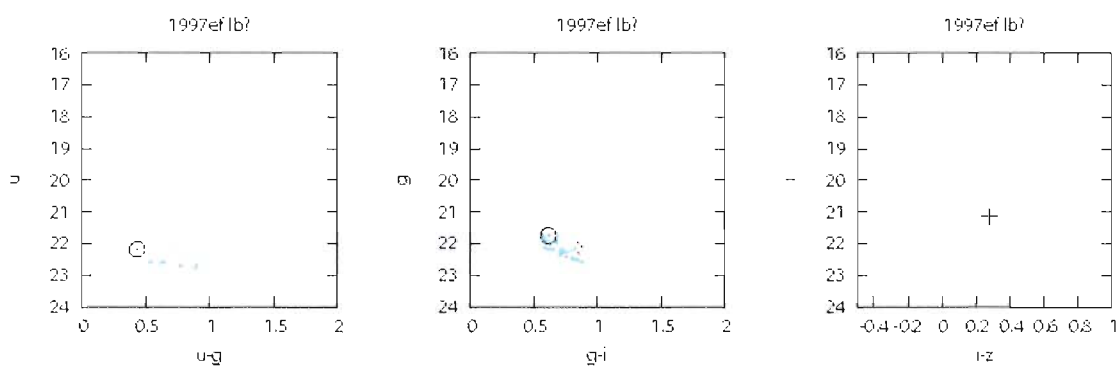


Figure 5.531. SN 1997ef  $u, u-g$ ,  $g, g-i$ , and  $i, i-z$  pseudo color-magnitude plots.

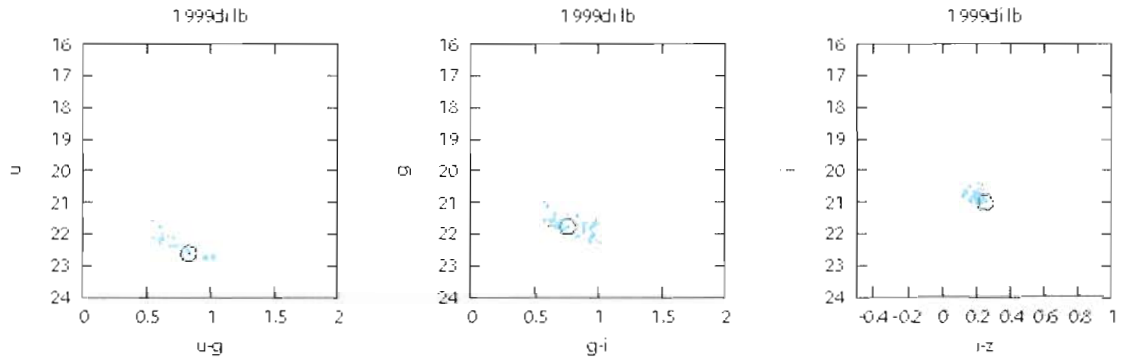


Figure 5.532. SN 1999di  $u,u-g$ ,  $g,g-i$ , and  $i,i-z$  pseudo color-magnitude plots.

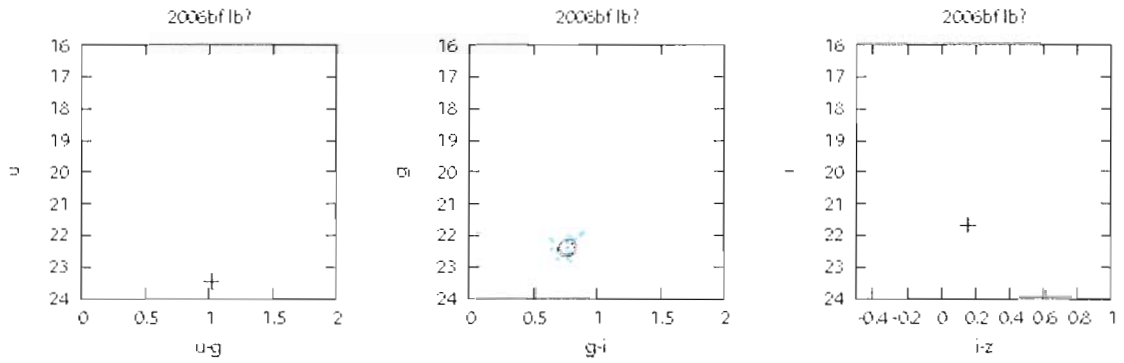


Figure 5.533. SN 2006bf  $u,u-g$ ,  $g,g-i$ , and  $i,i-z$  pseudo color-magnitude plots.

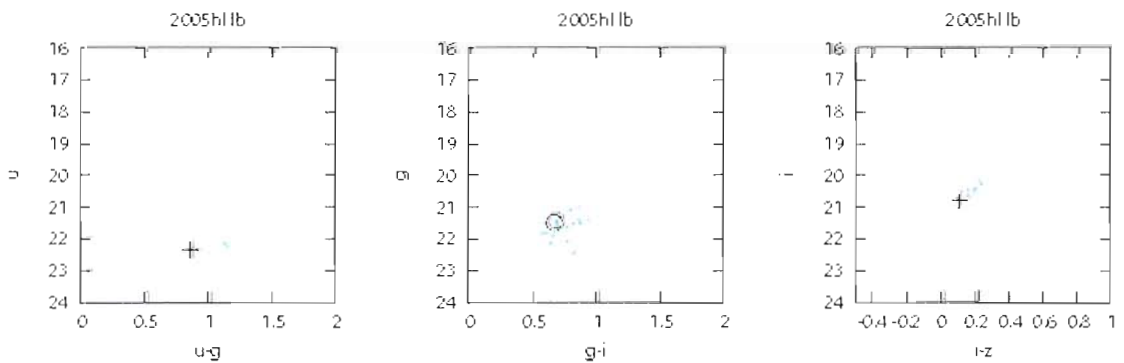


Figure 5.534. SN 2005hl  $u,u-g$ ,  $g,g-i$ , and  $i,i-z$  pseudo color-magnitude plots.

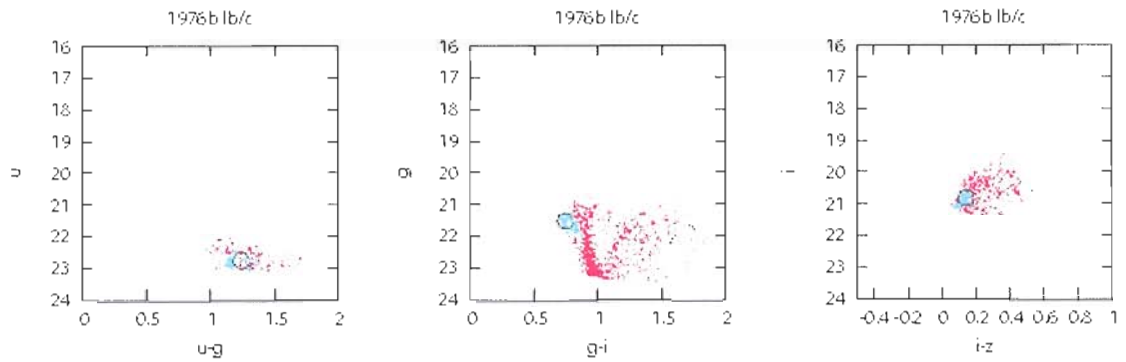


Figure 5.535. SN 1976b  $u,u-g$ ,  $g,g-i$ , and  $i,i-z$  pseudo color-magnitude plots.

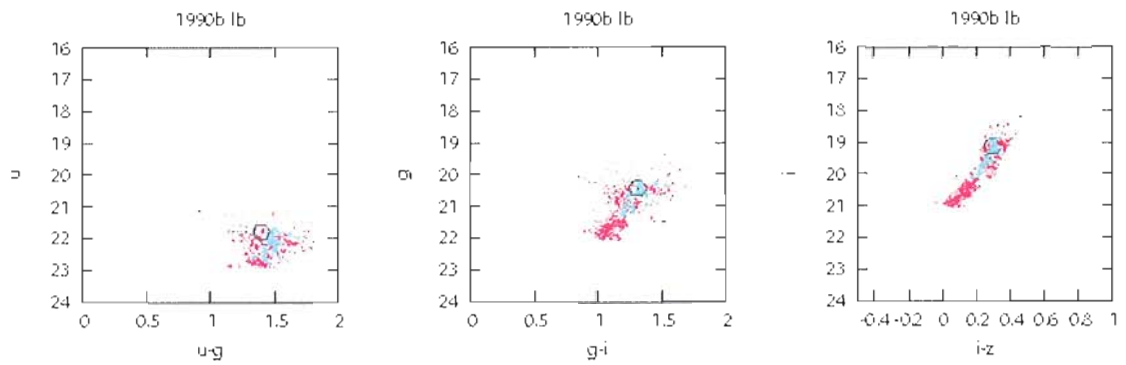


Figure 5.536. SN 1990b  $u,u-g$ ,  $g,g-i$ , and  $i,i-z$  pseudo color-magnitude plots.

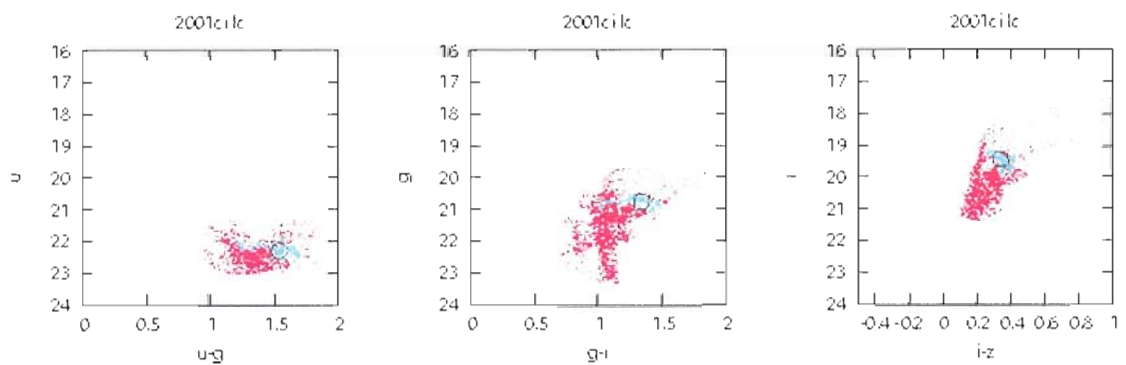


Figure 5.537. SN 2001ci  $u,u-g$ ,  $g,g-i$ , and  $i,i-z$  pseudo color-magnitude plots.

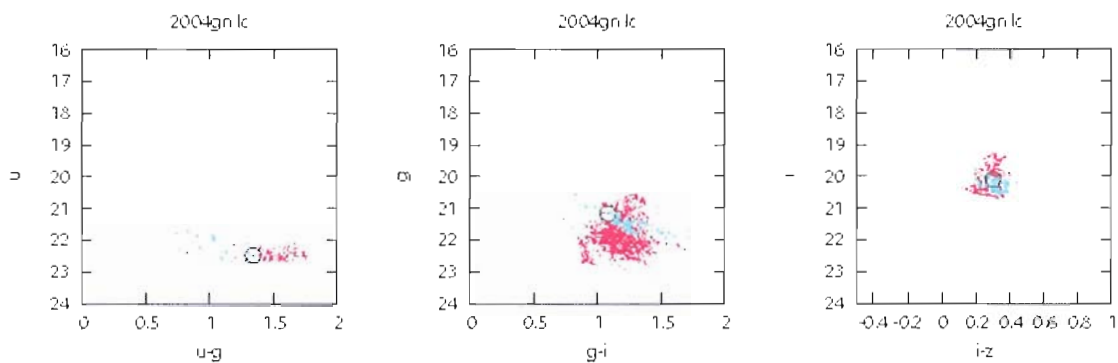


Figure 5.538. SN 2004gn  $u,u-g$ ,  $g,g-i$ , and  $i,i-z$  pseudo color-magnitude plots.

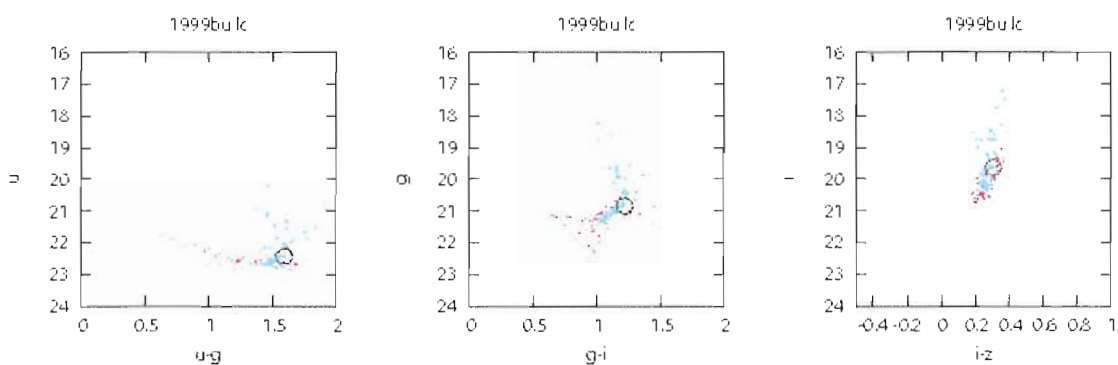


Figure 5.539. SN 1999bu  $u,u-g$ ,  $g,g-i$ , and  $i,i-z$  pseudo color-magnitude plots.

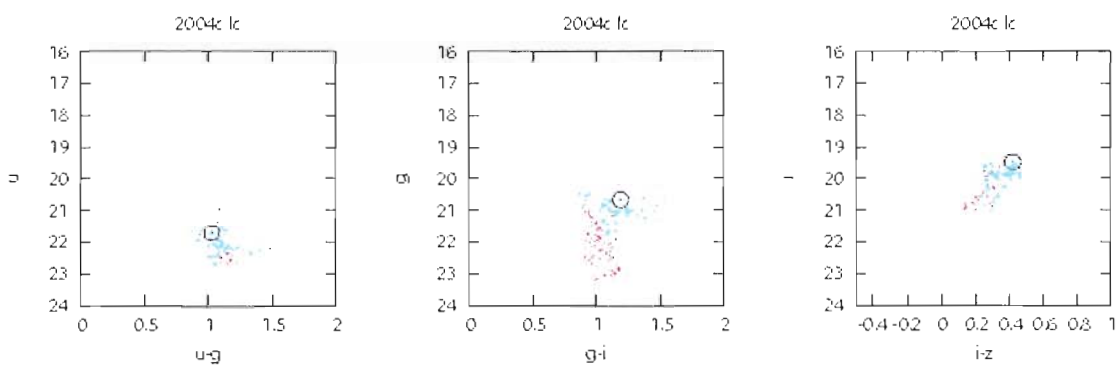


Figure 5.540. SN 2004c  $u,u-g$ ,  $g,g-i$ , and  $i,i-z$  pseudo color-magnitude plots.

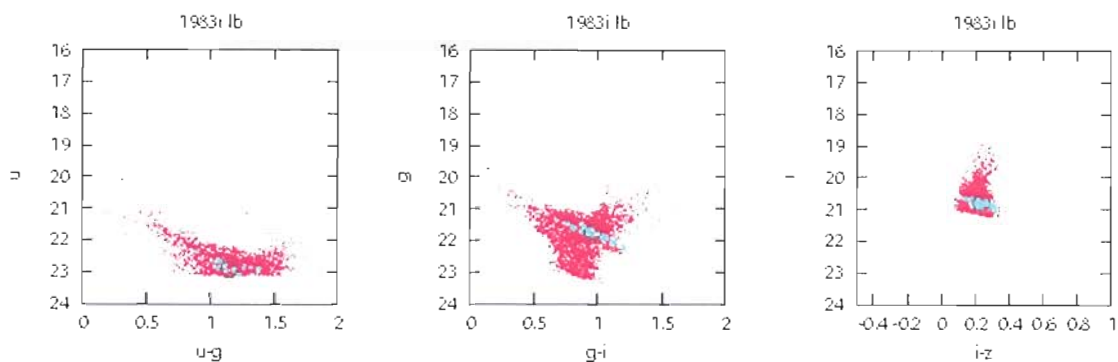


Figure 5.541. SN 1983i  $u,u-g$ ,  $g,g-i$ , and  $i,i-z$  pseudo color-magnitude plots.

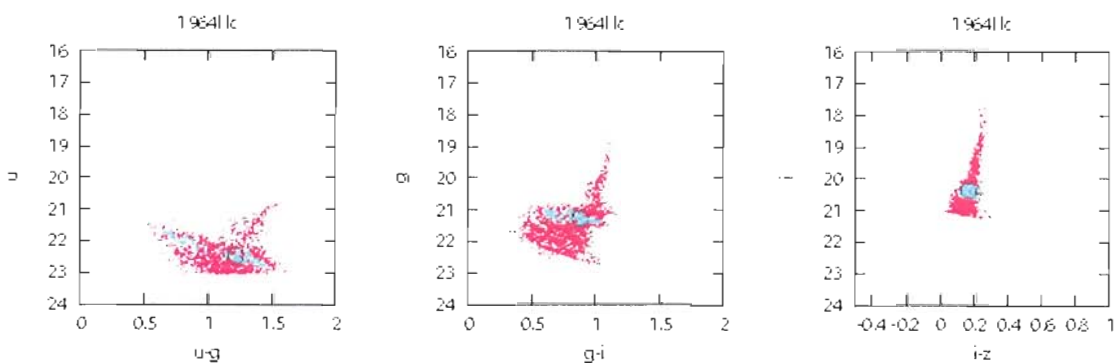


Figure 5.542. SN 1964l  $u,u-g$ ,  $g,g-i$ , and  $i,i-z$  pseudo color-magnitude plots.

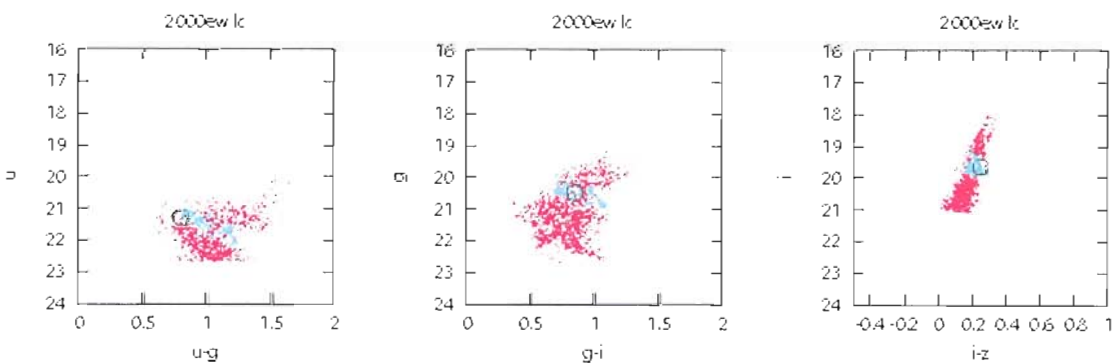


Figure 5.543. SN 2000ew  $u,u-g$ ,  $g,g-i$ , and  $i,i-z$  pseudo color-magnitude plots.

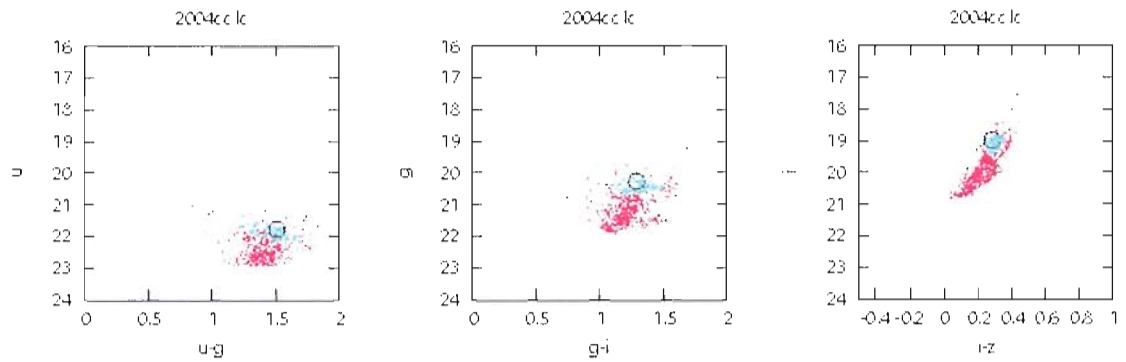


Figure 5.544. SN 2004cc  $u,u-g$ ,  $g,g-i$ , and  $i,i-z$  pseudo color-magnitude plots.

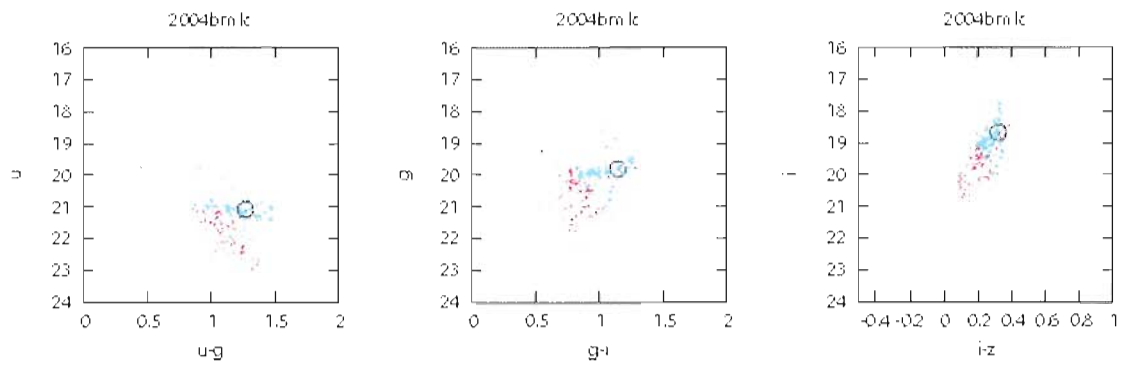


Figure 5.545. SN 2004bm  $u,u-g$ ,  $g,g-i$ , and  $i,i-z$  pseudo color-magnitude plots.

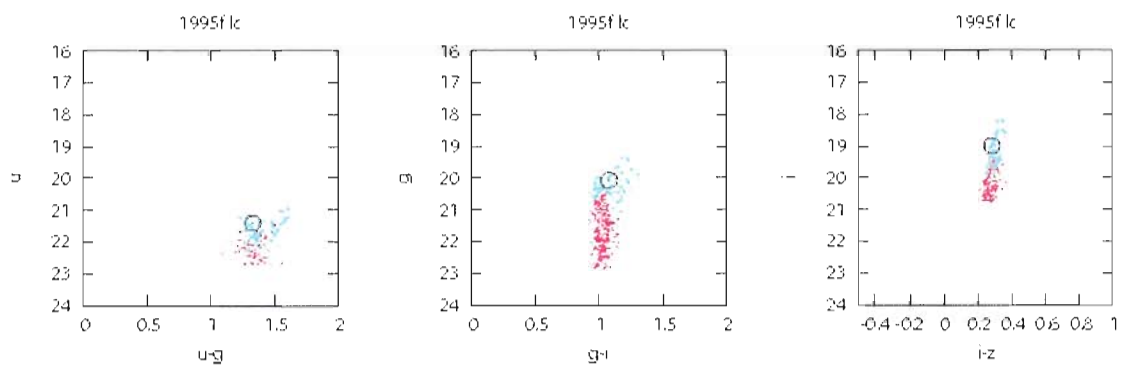


Figure 5.546. SN 1995f  $u,u-g$ ,  $g,g-i$ , and  $i,i-z$  pseudo color-magnitude plots.



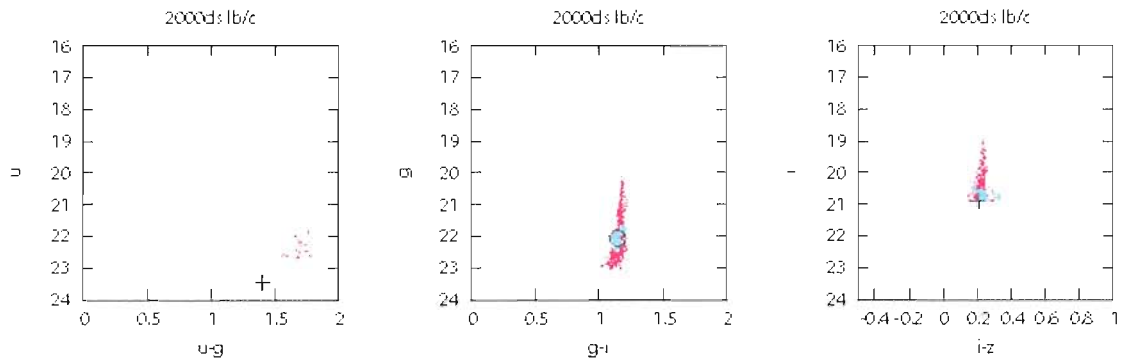


Figure 5.547. SN 2000ds  $u,u-g$ ,  $g,g-i$ , and  $i,i-z$  pseudo color-magnitude plots.

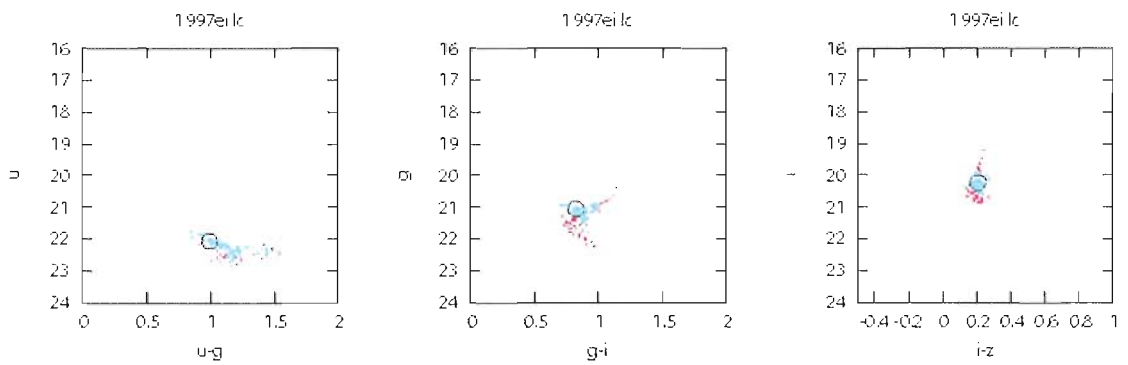


Figure 5.548. SN 1997ei  $u,u-g$ ,  $g,g-i$ , and  $i,i-z$  pseudo color-magnitude plots.

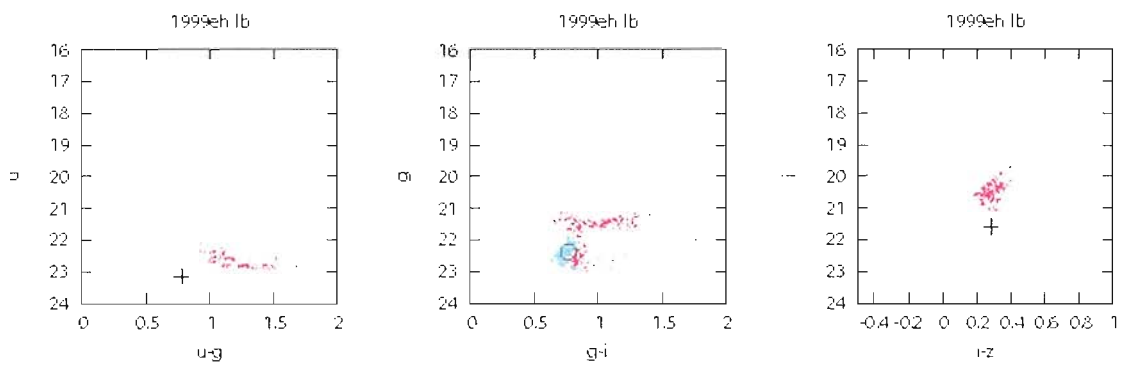


Figure 5.549. SN 1999eh  $u,u-g$ ,  $g,g-i$ , and  $i,i-z$  pseudo color-magnitude plots.

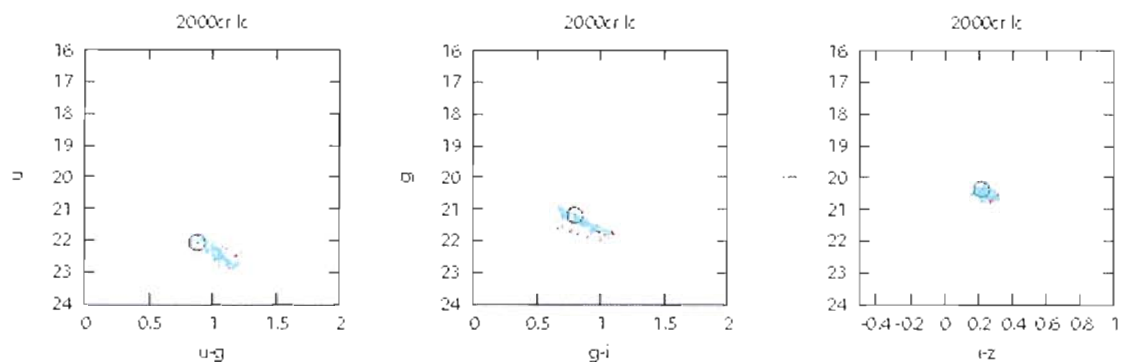


Figure 5.550. SN 2000cr  $u,u-g$ ,  $g,g-i$ , and  $i,i-z$  pseudo color-magnitude plots.

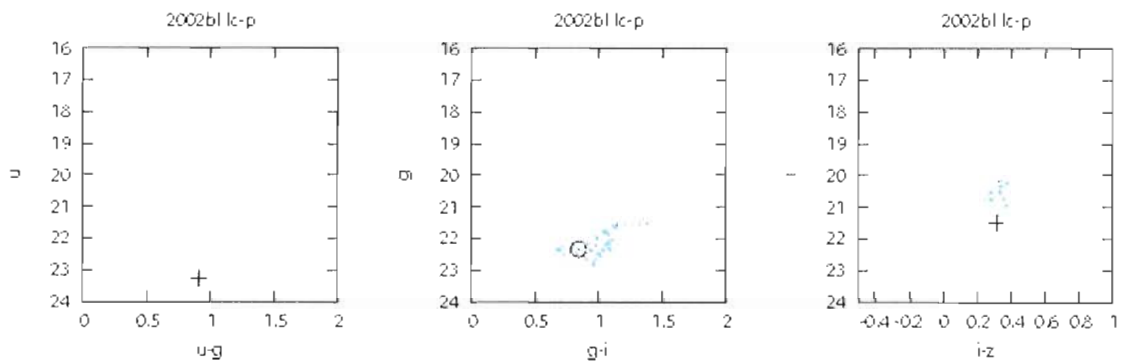


Figure 5.551. SN 2002bl  $u,u-g$ ,  $g,g-i$ , and  $i,i-z$  pseudo color-magnitude plots.

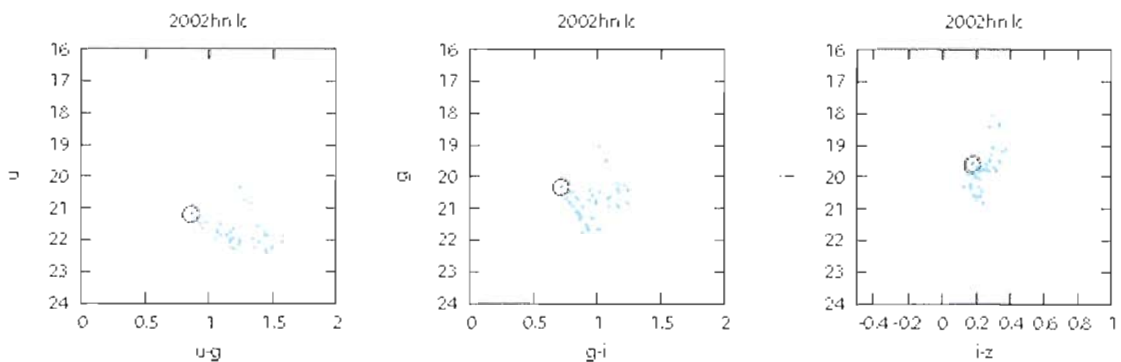


Figure 5.552. SN 2002hn  $u,u-g$ ,  $g,g-i$ , and  $i,i-z$  pseudo color-magnitude plots.

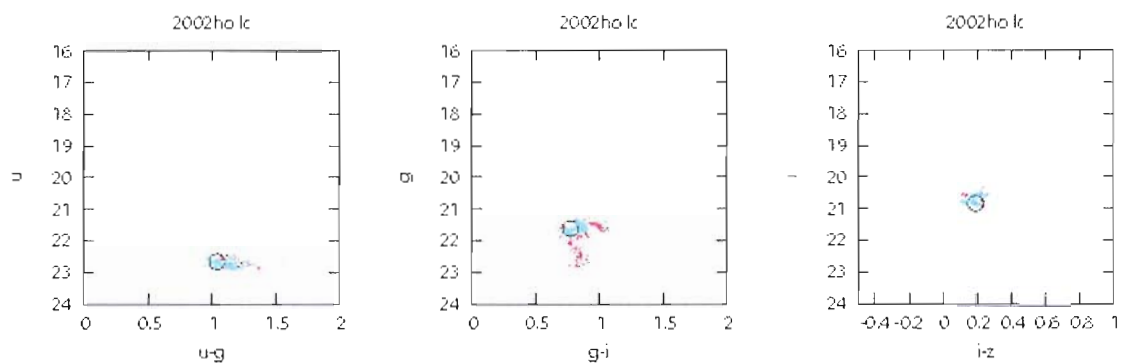


Figure 5.553. SN 2002ho  $u,u-g$ ,  $g,g-i$ , and  $i,i-z$  pseudo color-magnitude plots.

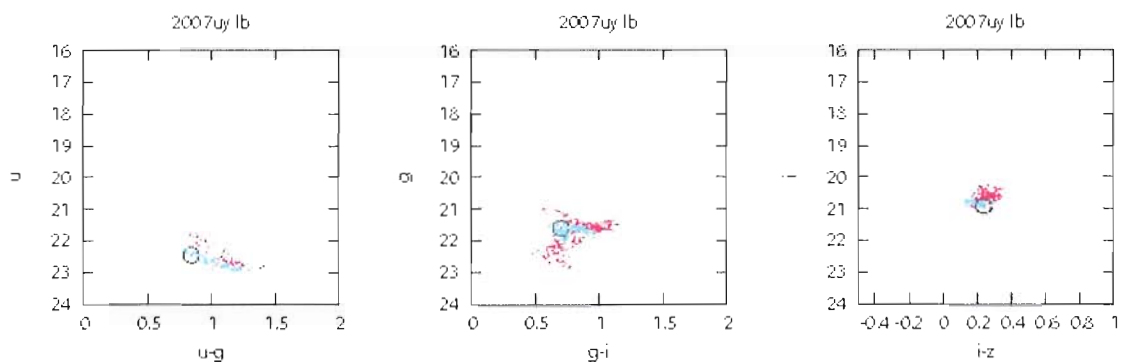


Figure 5.554. SN 2007uy  $u,u-g$ ,  $g,g-i$ , and  $i,i-z$  pseudo color-magnitude plots.

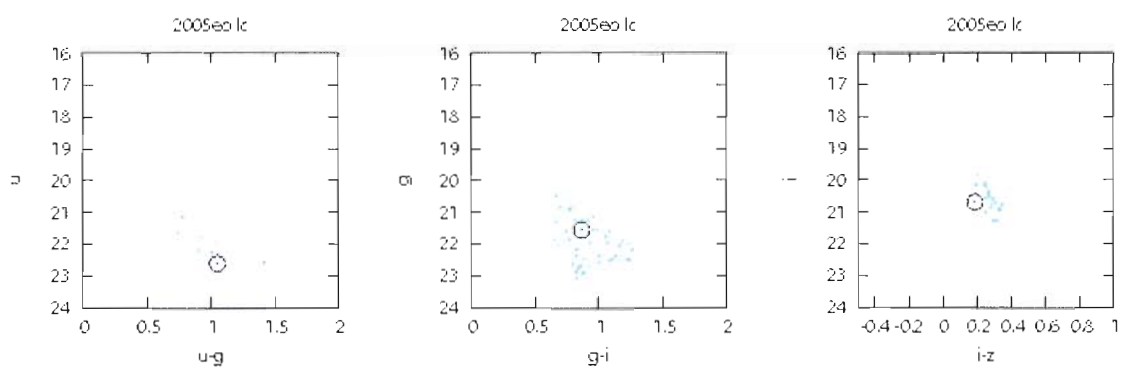


Figure 5.555. SN 2005eo  $u,u-g$ ,  $g,g-i$ , and  $i,i-z$  pseudo color-magnitude plots.

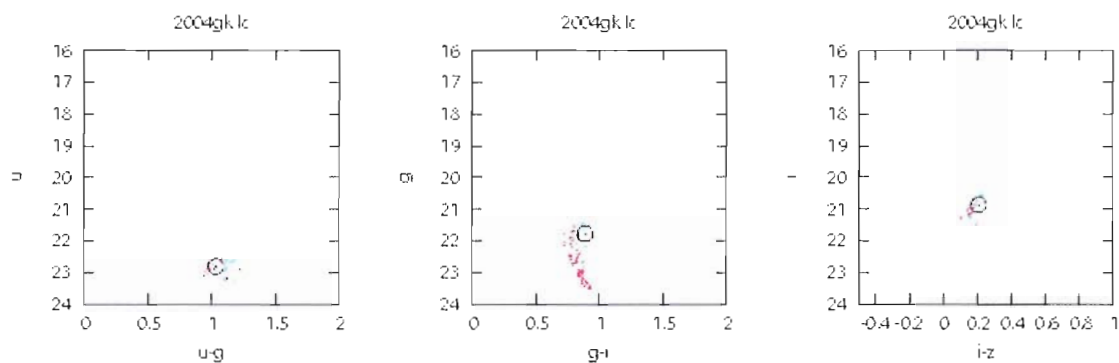


Figure 5.556. SN 2004gk  $u,u-g$ ,  $g,g-i$ , and  $i,i-z$  pseudo color-magnitude plots.

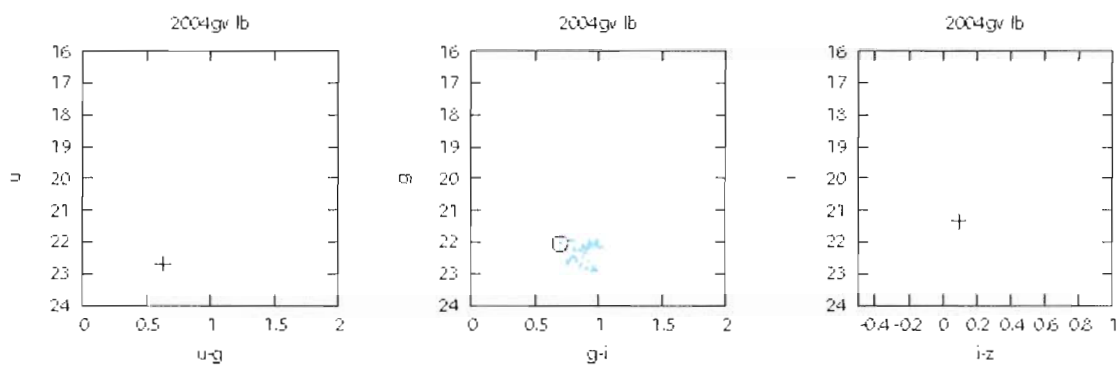


Figure 5.557. SN 2004gv  $u,u-g$ ,  $g,g-i$ , and  $i,i-z$  pseudo color-magnitude plots.

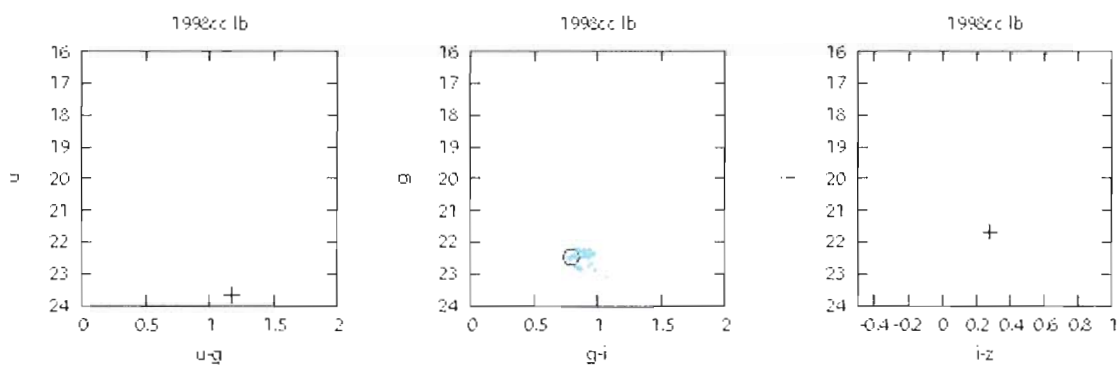


Figure 5.558. SN 1998cc  $u,u-g$ ,  $g,g-i$ , and  $i,i-z$  pseudo color-magnitude plots.

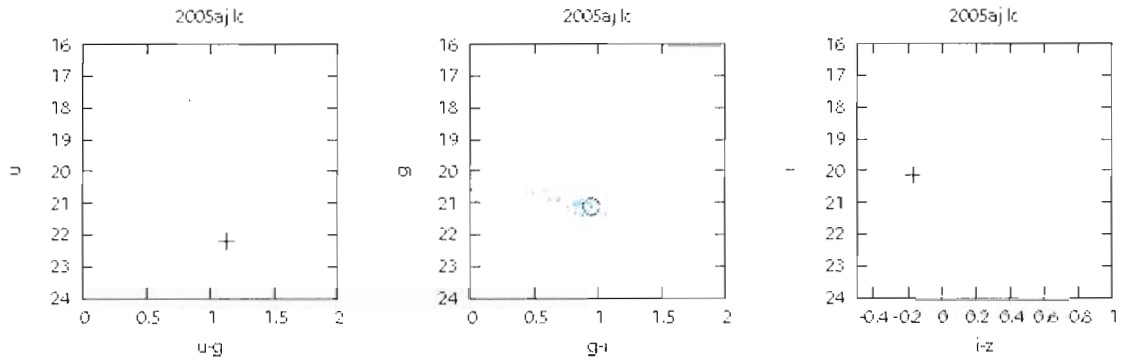


Figure 5.559. SN 2005aj  $u,u-g$ ,  $g,g-i$ , and  $i,i-z$  pseudo color-magnitude plots.

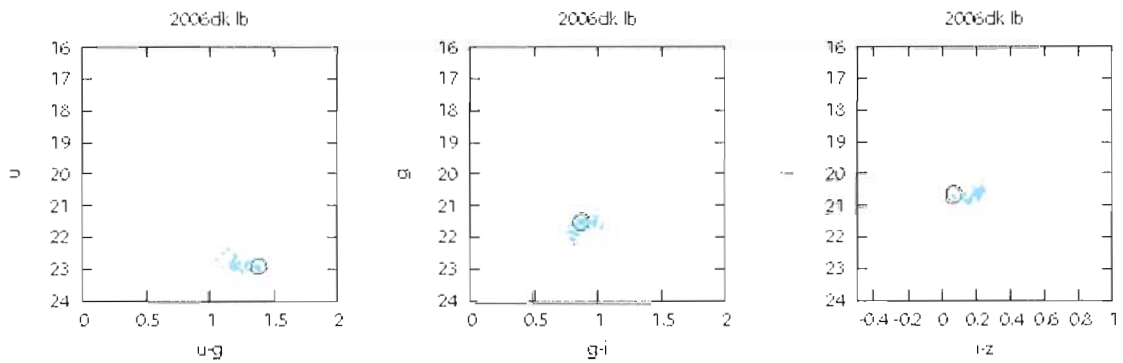


Figure 5.560. SN 2006dk  $u,u-g$ ,  $g,g-i$ , and  $i,i-z$  pseudo color-magnitude plots.

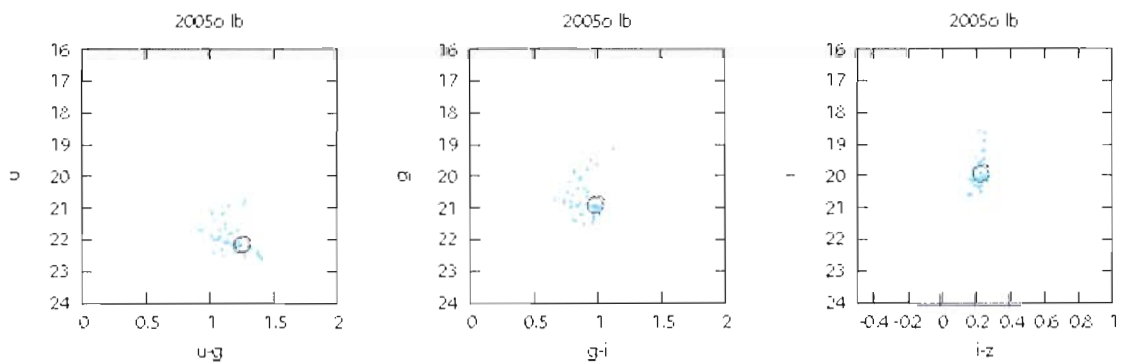


Figure 5.561. SN 2005o  $u,u-g$ ,  $g,g-i$ , and  $i,i-z$  pseudo color-magnitude plots.

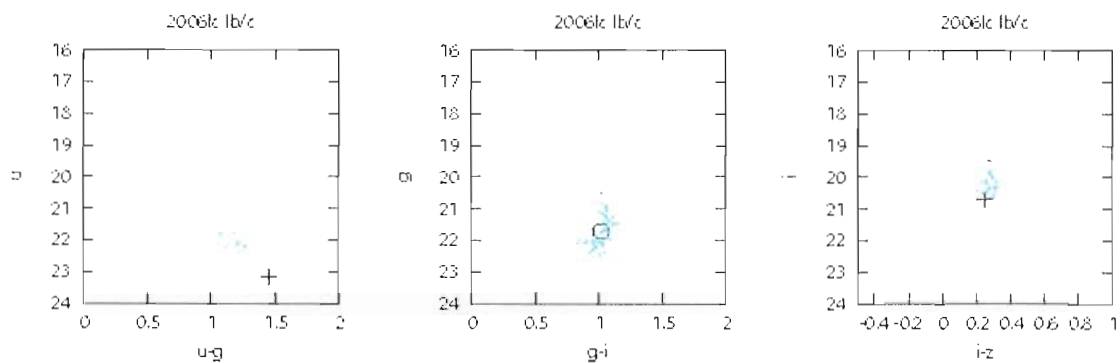


Figure 5.562. SN 2006lc  $u,u-g$ ,  $g,g-i$ , and  $i,i-z$  pseudo color-magnitude plots.

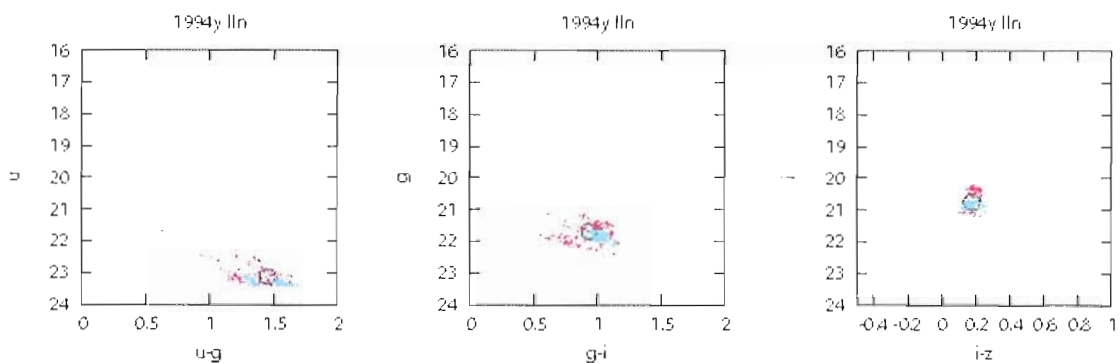


Figure 5.563. SN 1994y  $u,u-g$ ,  $g,g-i$ , and  $i,i-z$  pseudo color-magnitude plots.

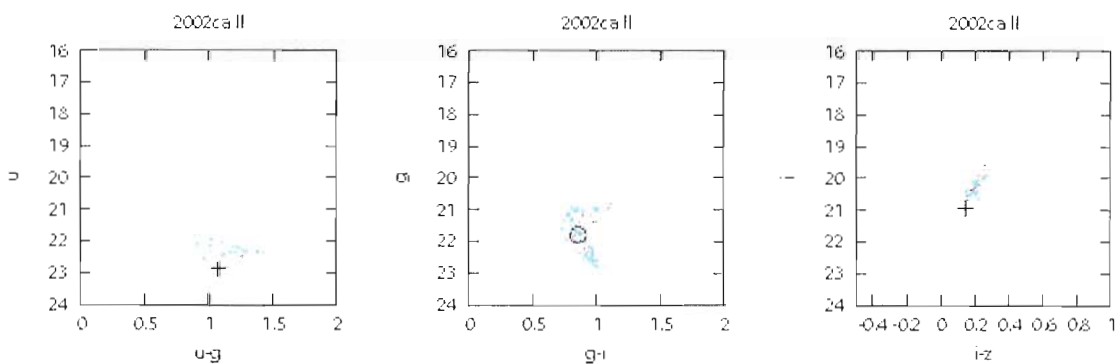


Figure 5.564. SN 2002ca  $u,u-g$ ,  $g,g-i$ , and  $i,i-z$  pseudo color-magnitude plots.

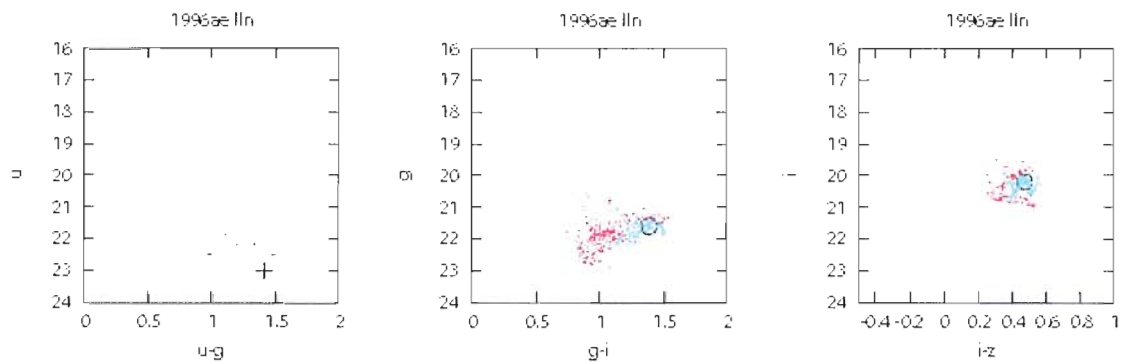


Figure 5.565. SN 1996ae  $u,u-g$ ,  $g,g-i$ , and  $i,i-z$  pseudo color-magnitude plots.

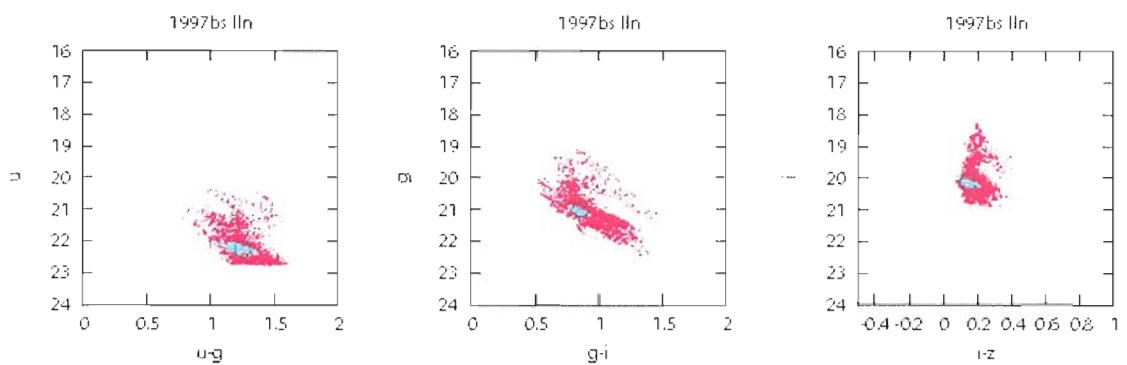


Figure 5.566. SN 1997bs  $u,u-g$ ,  $g,g-i$ , and  $i,i-z$  pseudo color-magnitude plots.

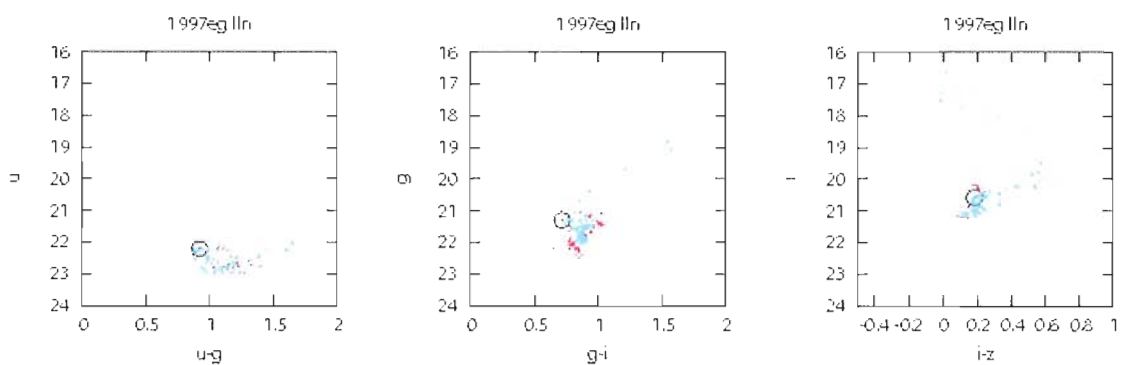


Figure 5.567. SN 1997eg  $u,u-g$ ,  $g,g-i$ , and  $i,i-z$  pseudo color-magnitude plots.

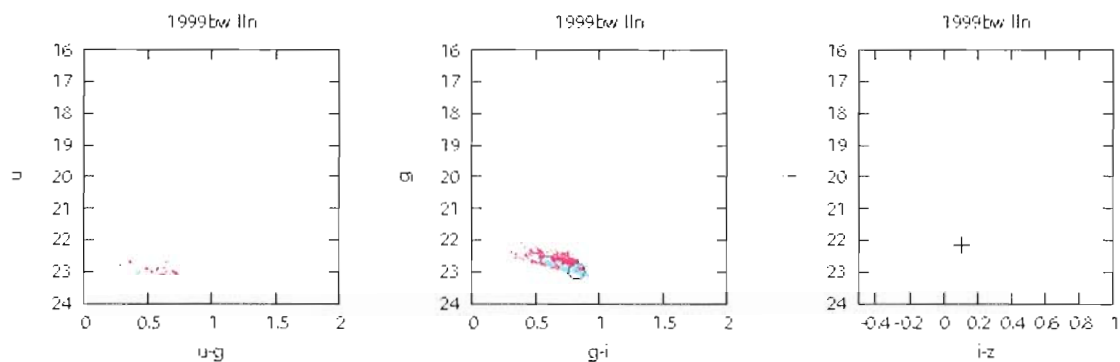


Figure 5.568. SN 1999bw  $u,u-g$ ,  $g,g-i$ , and  $i,i-z$  pseudo color-magnitude plots.

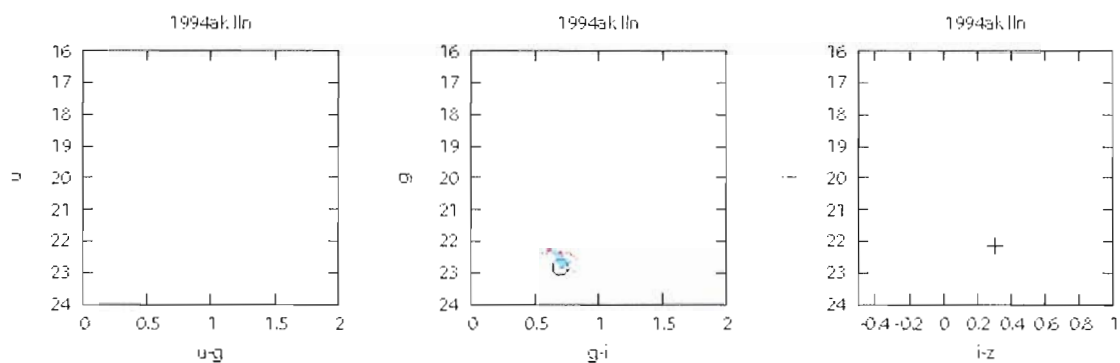


Figure 5.569. SN 1994ak  $u,u-g$ ,  $g,g-i$ , and  $i,i-z$  pseudo color-magnitude plots.

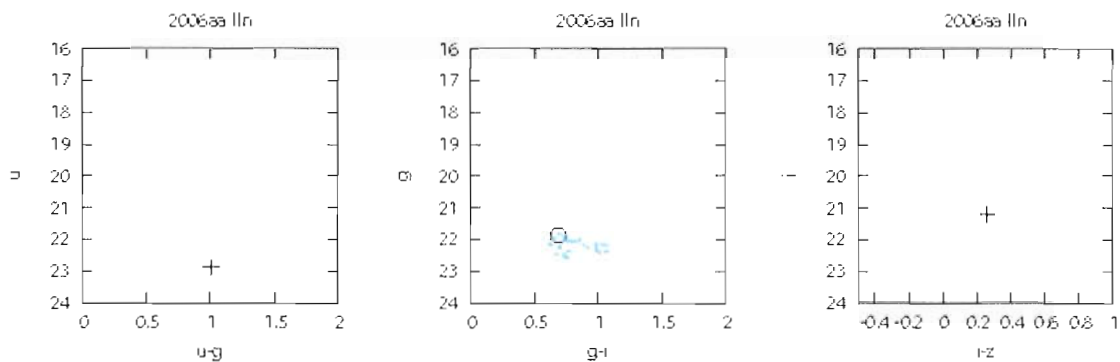


Figure 5.570. SN 2006aa  $u,u-g$ ,  $g,g-i$ , and  $i,i-z$  pseudo color-magnitude plots.



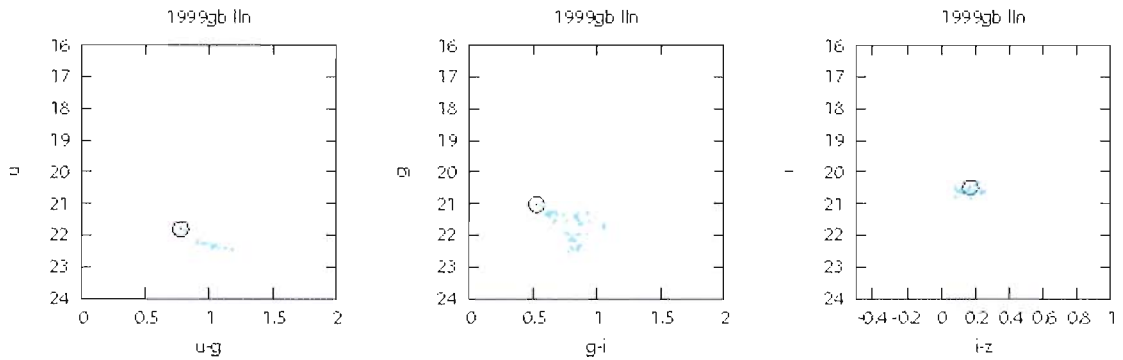


Figure 5.571. SN 1999gb  $u,u-g$ ,  $g,g-i$ , and  $i,i-z$  pseudo color-magnitude plots.

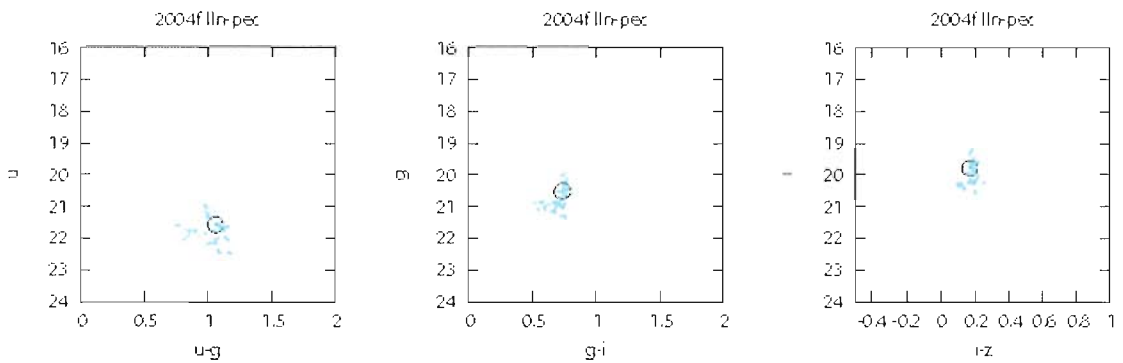


Figure 5.572. SN 2004f  $u,u-g$ ,  $g,g-i$ , and  $i,i-z$  pseudo color-magnitude plots.

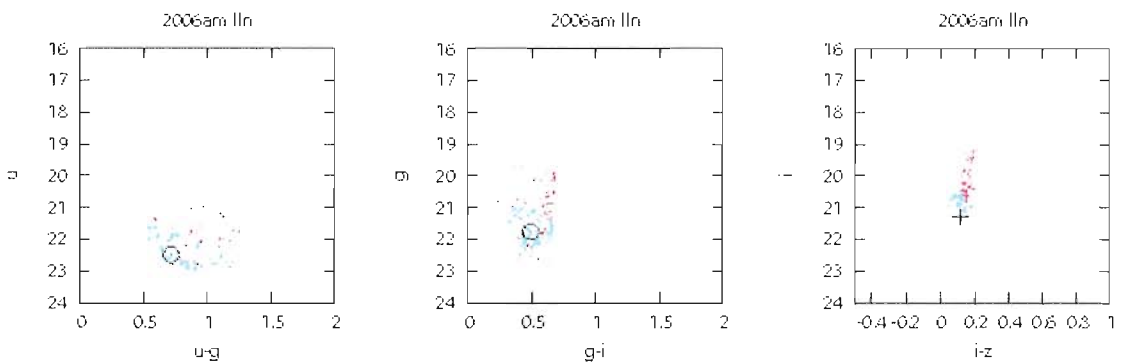


Figure 5.573. SN 2006am  $u,u-g$ ,  $g,g-i$ , and  $i,i-z$  pseudo color-magnitude plots.

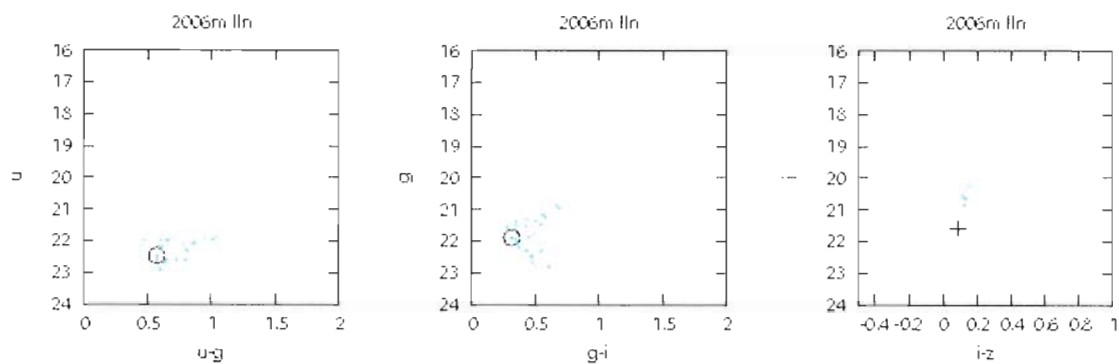


Figure 5.574. SN 2006m  $u,u-g$ ,  $g,g-i$ , and  $i,i-z$  pseudo color-magnitude plots.

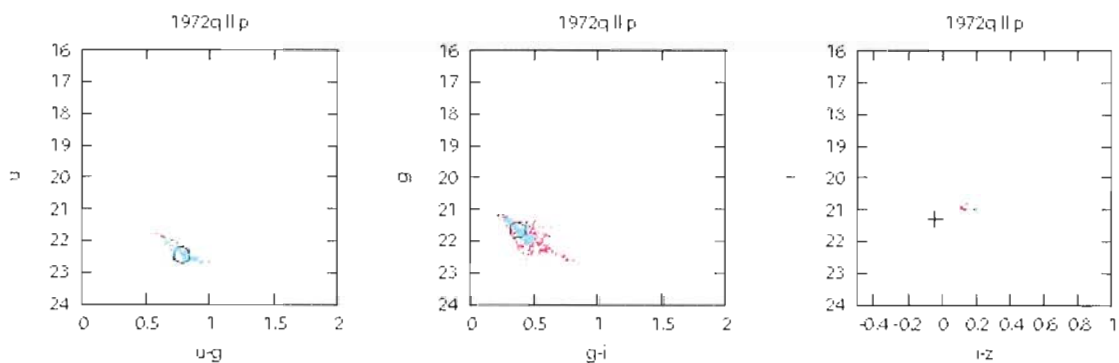


Figure 5.575. SN 1972q  $u,u-g$ ,  $g,g-i$ , and  $i,i-z$  pseudo color-magnitude plots.

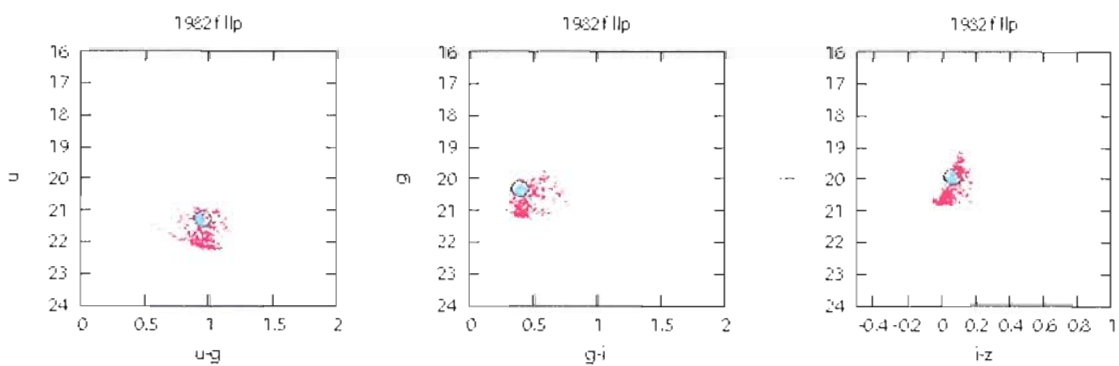


Figure 5.576. SN 1982f  $u,u-g$ ,  $g,g-i$ , and  $i,i-z$  pseudo color-magnitude plots.

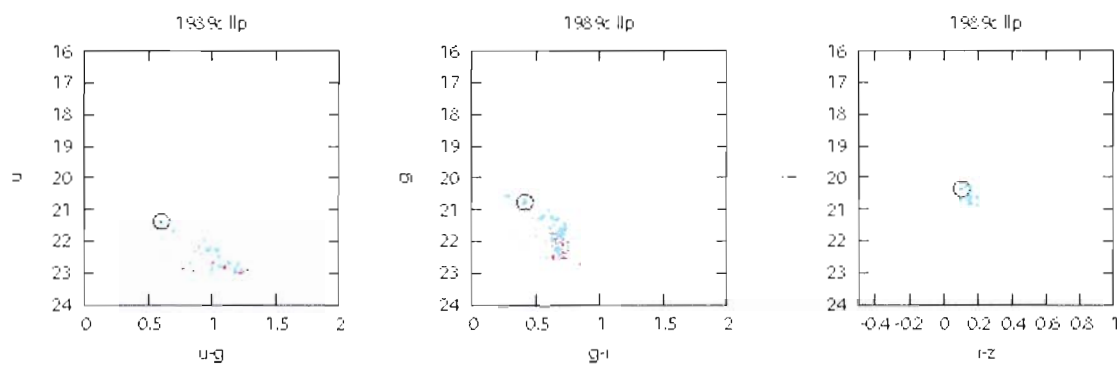


Figure 5.577. SN 1989c  $u,u-g$ ,  $g,g-i$ , and  $i,i-z$  pseudo color-magnitude plots.

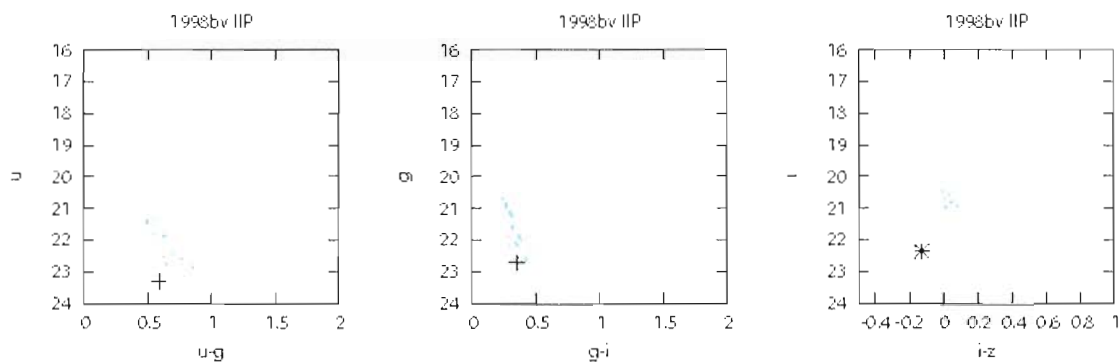


Figure 5.578. SN 1998bv  $u,u-g$ ,  $g,g-i$ , and  $i,i-z$  pseudo color-magnitude plots.

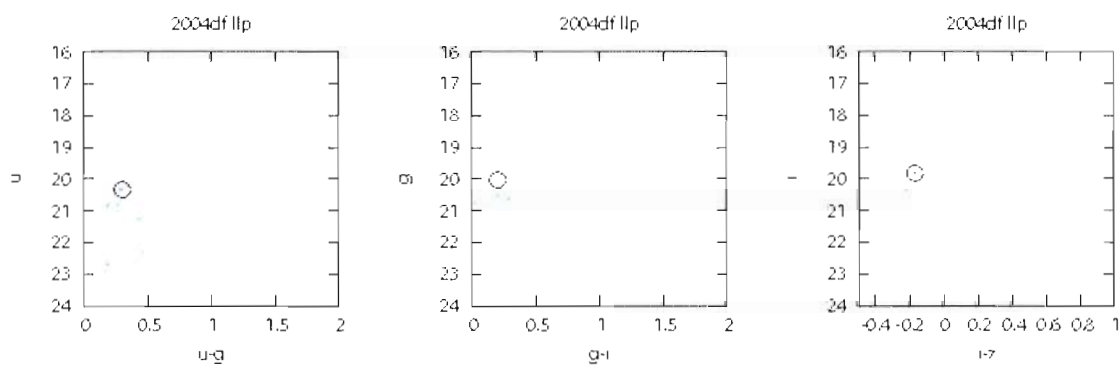


Figure 5.579. SN 2004df  $u,u-g$ ,  $g,g-i$ , and  $i,i-z$  pseudo color-magnitude plots.

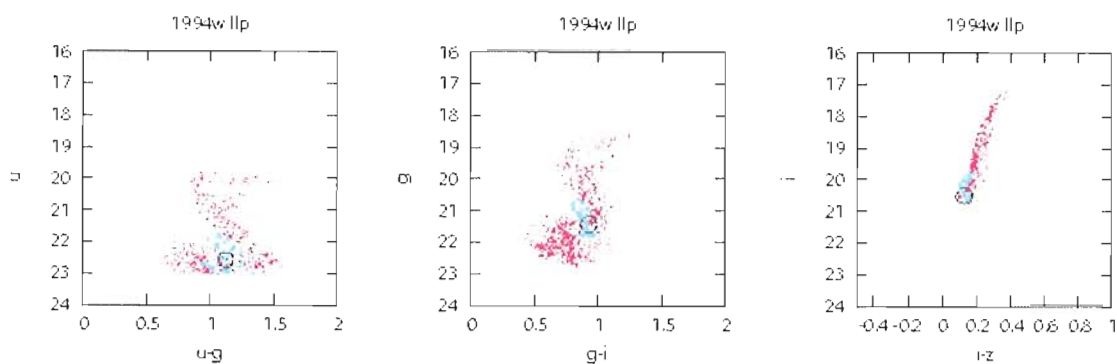


Figure 5.580. SN 1994w  $u,u-g$ ,  $g,g-i$ , and  $i,i-z$  pseudo color-magnitude plots.

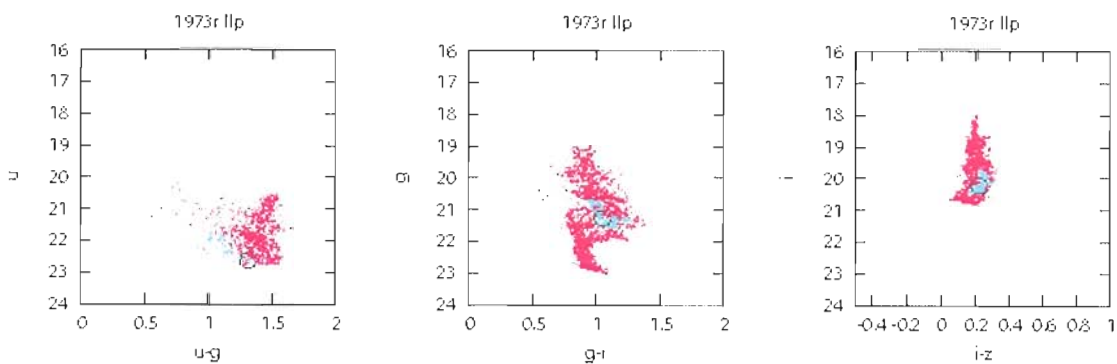


Figure 5.581. SN 1973r  $u,u-g$ ,  $g,g-i$ , and  $i,i-z$  pseudo color-magnitude plots.

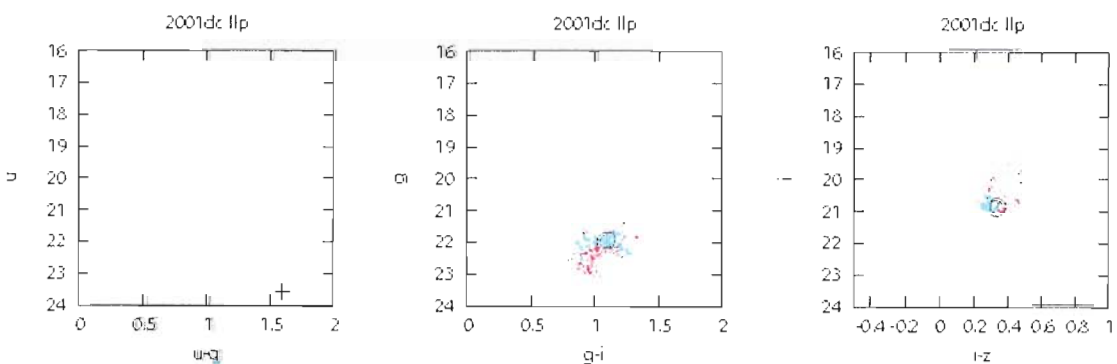


Figure 5.582. SN 2001dc  $u,u-g$ ,  $g,g-i$ , and  $i,i-z$  pseudo color-magnitude plots.

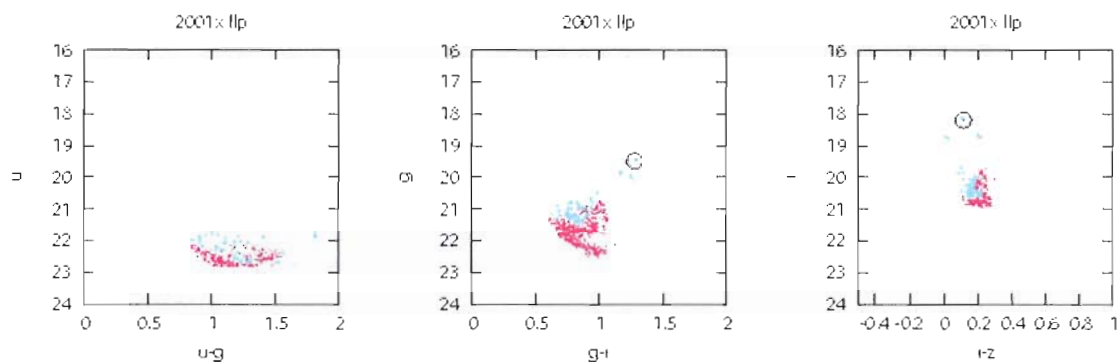


Figure 5.583. SN 2001x  $u,u-g$ ,  $g,g-i$ , and  $i,i-z$  pseudo color-magnitude plots.

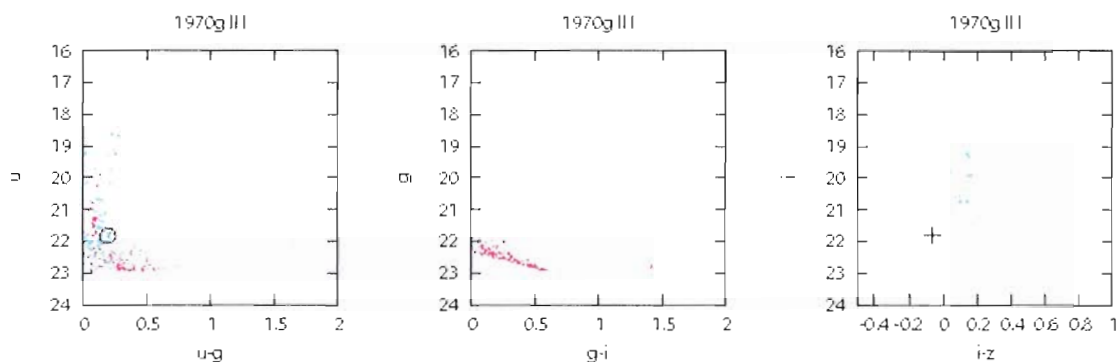


Figure 5.584. SN 1970g  $u,u-g$ ,  $g,g-i$ , and  $i,i-z$  pseudo color-magnitude plots.

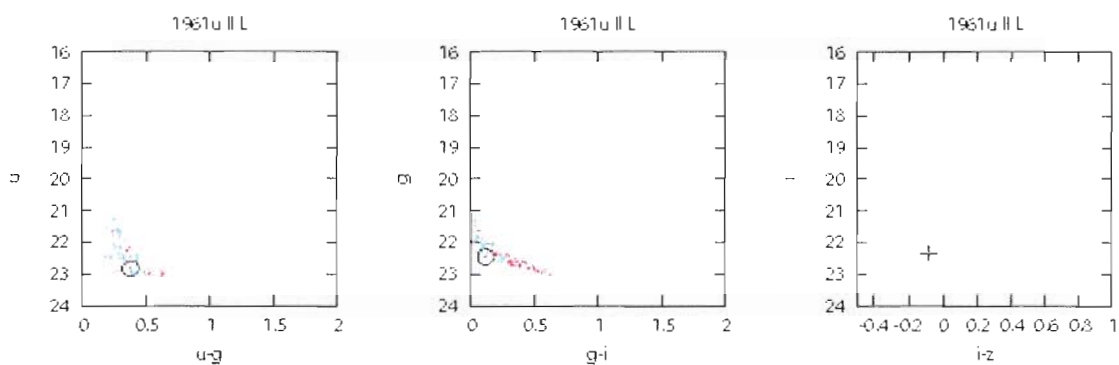


Figure 5.585. SN 1961u  $u,u-g$ ,  $g,g-i$ , and  $i,i-z$  pseudo color-magnitude plots.

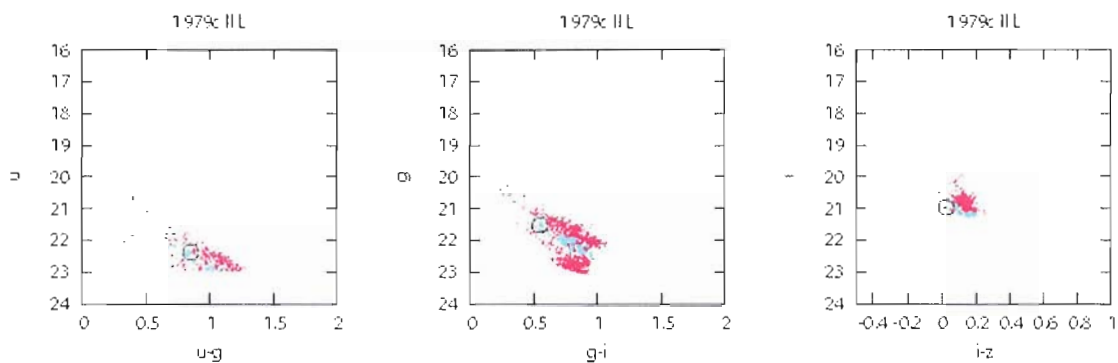


Figure 5.586. SN 1979c  $u,u-g$ ,  $g,g-i$ , and  $i,i-z$  pseudo color-magnitude plots.

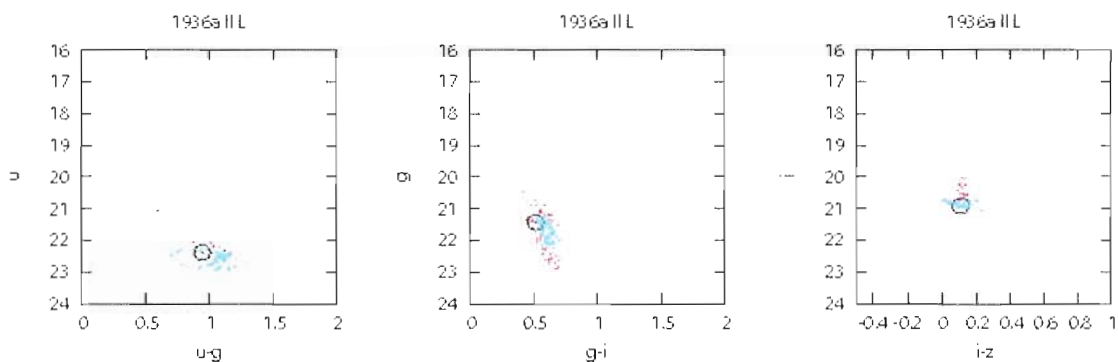


Figure 5.587. SN 1936a  $u,u-g$ ,  $g,g-i$ , and  $i,i-z$  pseudo color-magnitude plots.

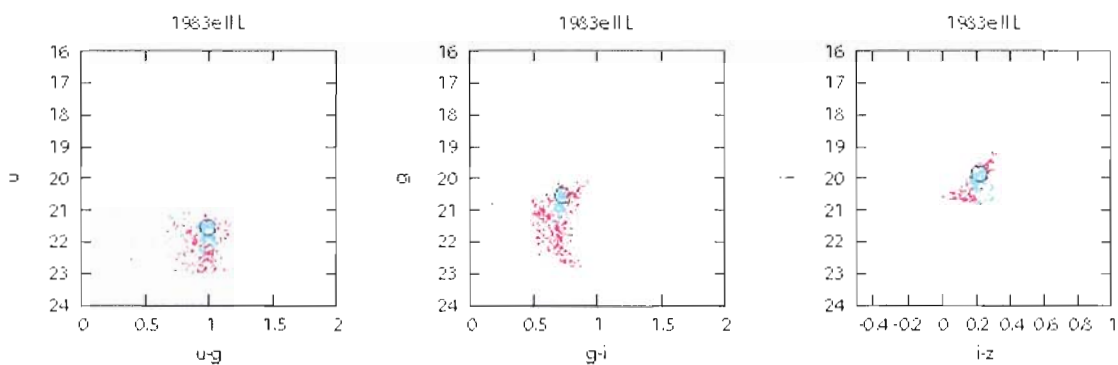


Figure 5.588. SN 1983e  $u,u-g$ ,  $g,g-i$ , and  $i,i-z$  pseudo color-magnitude plots.

Table 5.1. All SNe with at least one color from SDSS. SNe listed have both spatial and pCMD plots. The column ‘cz’ refers to the host galaxy redshift and ‘SN mag.’ is the discovery magnitude of the supernova. The last two columns are the figure numbers for the spatial and pCMD plots, respectively, in this chapter.

SN	Host Galaxy	cz (km/s)	SN Mag.	SN Type	Fig. # Sp.	Fig. # pCMD
1920a	NGC 2608	2135	11.8	II	175	469
1926a	NGC 4303	1566	14.0	II	144	438
1936a	NGC 4273	2378	14.4	II L	293	587
1937a	NGC 4157	774	16.2	II	170	464
1939a	NGC 4636	938	11.9	Ia	3	297
1940b	NGC 4725	1206	12.8	II	172	466
1946b	NGC 4632	1723	15.7	II	152	446
1954b	NGC 5668	1583	12.3	Ia	90	384
1954c	NGC 5879	772	14.9	II	168	462
1956a	NGC 3992	1048	12.3	Ia	50	344
1957a	NGC 2841	638	14.0	Ia 91bg	71	365
1957b	NGC 4374	1060	12.5	Ia	15	309
1960f	NGC 4496A	1730	11.6	Ia	93	387
1960r	NGC 4382	729	12.0	Ia	31	325
1961f	NGC 3003	1478	13.1	II	107	401
1961h	NGC 4564	1142	11.2	Ia	1	295
1961i	NGC 4303	1566	13.0	II	112	406
1961u	NGC 3938	809	13.7	II L	291	585
1963i	NGC 4178	378	14.3	Ia	48	342
1963j	NGC 3913	954	13.7	Ia	56	350
1963p	NGC 1084	1407	14.0	Ia	57	351
1964f	NGC 4303	1566	14.0	II	174	468
1964l	NGC 3938	809	13.3	Ic	248	542
1965h	NGC 4666	1533	14.0	II	163	457
1965l	NGC 3631	1156	16.0	II	130	424
1967h	NGC 4254	2407	14.6	II	108	402
1968e	NGC 2713	3922	14.3	Ia	24	318
1969b	NGC 3556	699	16.0	II	166	460
1969c	NGC 3811	3105	13.8	Ia	43	337
1970a	IC 3476	-169	14.0	II	114	408
1970g	NGC 5457	241	11.5	II L	290	584
1970j	NGC 7619	3762	14.5	Ia	14	308
1971g	NGC 4165	1859	13.6	Ia	55	349
1971l	NGC 6384	1665	12.8	Ia	67	361
1971s	NGC 493	2338	15.5	II	149	443
1972q	NGC 4254	2407	15.8	IIp	281	575
1973r	NGC 3627	727	14.5	IIp	287	581
1974g	NGC 4414	716	13.0	Ia	60	354
1976b	NGC 4402	232	14.7	Ib?	241	535

Table 5.1. (continued).

SN	Host Galaxy	cz (km/s)	SN Mag.	SN Type	Fig. # Sp.	Fig. # pCMD
1978h	NGC 3780	2399	16.5	II	183	477
1982b	NGC 2268	2222	14.0	Ia	59	353
1982f	NGC 4490	565	16.0	IIp	282	576
1983e	NGC 3044	1292	14.0	II L	294	588
1983g	NGC 4753	1239	13.0	Ia	32	326
1983i	NGC 4051	700	13.5	Ib	247	541
1983w	NGC 3625	1940	16.5	Ia	58	352
1984e	NGC 3169	1238	15.0	II	171	465
1985b	NGC 4045	1981	13.0	II	179	473
1985f	NGC 4618	544	12.1	Ib	212	506
1985g	NGC 4451	864	14.5	II	173	467
1985h	NGC 3359	1014	16.4	II	143	437
1985l	NGC 5033	875	12.5	II	141	435
1986i	NGC 4254	2407	14.0	II	109	403
1987d	UGC 7370	2217	14.0	Ia	95	389
1987k	NGC 4651	805	15.0	II	120	414
1987n	NGC 7606	2233	13.8	Ia	45	339
1988a	NGC 4579	1519	13.5	II	178	472
1988e	NGC 4772	1040	17.0	II	177	471
1988l	NGC 5480	1856	16.5	Ib	236	530
1989b	NGC 3627	727	13.0	Ia	61	355
1989c	UGC 5249	1874	14.5	IIp	283	577
1989m	NGC 4579	1519	12.2	Ia	47	341
1989n	NGC 3646	4248	14.5	II	133	427
1990b	NGC 4568	2255	16.0	Ib	242	536
1990e	NGC 1035	1241	16.7	II	180	474
1990h	NGC 3294	1586	16.0	II	185	479
1991a	IC 2973	3206	18.0	Ic-p	217	511
1991aa	PGC158033	3209	16	Ia	92	386
1991ak	NGC 5378	3042	15.5	Ia	53	347
1991bc	UGC 2691	6408	16.0	Ia	36	330
1991bg	NGC 4374	1060	14.0	Ia 91bg	16	310
1991bi	NGC 5127	4782	18.5	Ia	17	311
1991g	NGC 4088	757	17.0	II	197	491
1991n	NGC 3310	993	15.0	Ic/b	208	502
1991t	NGC 4527	1736	13.0	Ia 91t	37	331
1992bt	NGC 3780	2399	16.0	II	198	492
1992c	NGC 3367	3037	16.5	II	153	447
1992g	NGC 3294	1586	14.0	Ia	62	356
1992p	IC 3690	7615	16.2	Ia	97	391
1993g	NGC 3690	3064	16.6	II	200	494
1993z	NGC 2775	1354	13.9	Ia	49	343



Table 5.1. (continued).

SN	Host Galaxy	cz (km/s)	SN Mag.	SN Type	Fig. # Sp.	Fig. # pCMD
1994ak	NGC 2782	2562	16.3	IIn	275	569
1994d	NGC 4526	448	15.2	Ia	4	298
1994w	NGC 4041	1234	13.5	IIp	286	580
1994y	NGC 5371	2558	15.0	IIn	269	563
1995ah	HS 0016+1449	4407	17.6	II	127	421
1995al	NGC 3021	1541	13.0	Ia	63	357
1995bd	UGC 3151	4377	18.8	Ia 91t	69	363
1995f	NGC 2726	1518	14.7	Ic	252	546
1995v	NGC 1087	1517	15.0	II	118	412
1996aa	NGC 5557	3213	17.0	Ia	2	296
1996ae	NGC 5775	1681	16.5	IIn	271	565
1996ai	NGC 5005	946	14.5	Ia	39	333
1996an	NGC 1084	1406	14.0	II	119	413
1996aq	NGC 5584	1638	15.7	Ic	221	515
1996b	NGC 4357	4122	17.5	II	184	478
1996bk	NGC 5308	2041	14.5	Ia	5	299
1996cb	NGC 3510	705	16.5	I Ib	115	409
1996cc	NGC 5673	2082	15.0	II	139	433
1997bn	UGC 4329	4099	16.4	II	190	484
1997bp	NGC 4680	2492	13.8	Ia	75	369
1997bs	NGC 3627	727	17.0	IIn	272	566
1997cn	NGC 5490	4855	15.8	Ia 91bg	18	312
1997co	NGC 5125	6980	18.2	II	201	495
1997dq	NGC 3810	993	15.0	Ib	222	516
1997ef	UGC 4107	3504	16.7	Ib?	237	531
1997eg	NGC 5012	2619	15.6	IIn	273	567
1997ei	NGC 3963	3188	16.5	Ic	254	548
1997x	NGC 4691	1110	13.5	Ic	214	508
1997y	NGC 4675	4757	14.8	Ia	41	335
1998ab	NGC 4704	8134	16.1	Ia 91t	98	392
1998aq	NGC 3982	1109	14.9	Ia	64	358
1998ar	NGC 2916	3730	18.4	II	151	445
1998bu	NGC 3368	897	13.0	Ia	46	340
1998bv	HS 1035+4758	1590	17.1	I Ip	284	578
1998cc	NGC 5172	4030	18.1	Ib	264	558
1998d	NGC 5440	3689	15.6	Ia	23	317
1998dk	UGC 139	3963	17.6	Ia	66	360
1998dl	NGC 1084	1406	16.0	II	142	436
1998es	NGC 632	3168	14.6	Ia 91t	77	371
1998s	NGC 3877	895	15.2	II	186	480
1998t	NGC 3690 ned 2	3121	16.6	Ib	209	503
1999a	NGC 5874	3128	18.3	II	146	440

Table 5.1. (continued).

SN	Host Galaxy	cz (km/s)	SN Mag.	SN Type	Fig. # Sp.	Fig. # pCMD
1999aa	NGC 2595	4330	15.5	Ia 91t	83	377
1999an	IC 755	1524	15.0	II	134	428
1999bc	UGC 4433	6299	18.9	Ic	224	518
1999bg	IC 758	1275	15.5	II	135	429
1999bh	NGC 3435	5158	16.8	Ia	79	373
1999br	NGC 4900	960	17.5	II	122	416
1999bu	NGC 3786	2678	17.5	Ic	245	539
1999bw	NGC 3198	663	17.8	IIIn	274	568
1999by	NGC 2841	638	15.0	Ia 91bg	51	345
1999cc	NGC 6038	9392	16.3	Ia	85	379
1999cd	NGC 3646	4248	17.9	II	129	423
1999d	NGC 3690	3064	16.6	II	145	439
1999dg	UGC 9758	6613	16.7	Ia	6	300
1999di	NGC 776	4921	18.0	Ib	238	532
1999dk	UGC 1087	4485	16.7	Ia	106	400
1999dq	NGC 976	4295	16.3	Ia 91t	78	372
1999eh	NGC 2770	1947	17.5	Ib	255	549
1999ej	NGC 495	4114	18.1	Ia	28	322
1999ev	NGC 4274	930	14.4	II	167	461
1999gb	NGC 2532	5260	16.1	IIIn	277	571
1999gd	NGC 2623	5696	17.8	Ia	96	390
1999ge	NGC 309	5662	17.2	II	196	490
1999gi	NGC 3184	592	14.5	II	111	405
1999gk	NGC 4653	2626	15.7	II	128	422
1999gn	NGC 4303	1566	16.0	II	110	404
1999x	CGCG 180-022	7546	16.1	Ia	73	367
2000au	MCG +08-15-14	5790	17.9	II	202	496
2000ce	UGC 4195	4888	15.0	Ia	86	380
2000cr	NGC 5395	3491	17.0	Ic	256	550
2000cv	PGC 039222	6115	16.1	Ia	88	382
2000db	NGC 3949	800	14.3	II	121	415
2000de	NGC 4384	2513	16.0	Ib	211	505
2000ds	NGC 2768	1373	17.9	Ib/c	253	547
2000dv	UGC 4671	4053	17.5	Ib	234	528
2000ew	NGC 3810	993	14.9	Ic	249	543
2000ez	NGC 3995	3254	16.8	II	124	418
2000i	NGC 2958	6663	18.6	II	189	483
2000l	UGC 5520	3315	17.8	II	207	501
2001a	NGC 4261	2238	18.9	Ia	8	302
2001ab	NGC 6130	5137	17.5	II	193	487
2001ae	IC 4229	6978	17.3	II	125	419
2001bg	NGC 2608	2135	14.0	Ia	76	370

Table 5.1. (continued).

SN	Host Galaxy	cz (km/s)	SN Mag.	SN Type	Fig. # Sp.	Fig. # pCMD
2001cg	IC 3900	7115	17.8	Ia	19	313
2001ch	MCG -01-54-16	2930	16.7	Ic	215	509
2001ci	NGC 3079	1116	18.3	Ic	243	537
2001cm	NGC 5965	3412	17.5	II	182	476
2001dc	NGC 5777	2145	18.5	IIp	288	582
2001dp	NGC 3953	1052	14.5	Ia	54	348
2001ed	NGC 706	4980	14.9	Ia	89	383
2001en	NGC 523	4758	17.5	Ia	44	338
2001er	UGC 5301	4862	17.2	Ia	81	375
2001f	IC 867	6870	16.5	Ia	25	319
2001fe	UGC 5129	4059	16.0	Ia	80	374
2001fv	NGC 3512	1376	16.4	II	160	454
2001h	MCG -01-10-19	5248	17.5	II	188	482
2001hg	NGC 4162	2569	17.4	II	138	432
2001j	UGC 4729	3900	17.5	II	131	425
2001n	NGC 3327	6303	16.3	Ia	13	307
2001q	UGC 6429	3726	18.6	II	206	500
2001x	NGC 5921	1480	17.0	IIp	289	583
2002bl	UGC 5499	4753	17.0	Ic-p	257	551
2002bo	NGC 3190	1271	15.5	Ia	34	328
2002ca	UGC 8521	3277	17.3	II	191	485
2002ce	NGC 2604	2094	16.0	II	123	417
2002cv	NGC 3190	1271	19.0	Ia	35	329
2002ea	NGC 820	4418	17.7	IIIn	270	564
2002ha	NGC 6962	4211	17.3	Ia	74	368
2002hl	NGC 3665	2080	16.3	Ia	22	316
2002hm	NGC 4016	3448	16.9	II	126	420
2002hn	NGC 2532	5260	16.8	Ic	258	552
2002ho	NGC 4210	2732	17.0	Ic	259	553
2002i	IC 4229	6978	17.3	Ia	101	395
2002ji	NGC 3655	1473	15.1	Ic	223	517
2002jo	NGC 5708	2751	16.4	Ia	65	359
2003aa	NGC 3367	3037	17.6	Ibc	226	520
2003af	KUG 1107+236?	5996	15.6	Ia	91	385
2003ag	UGC 6440	6845	16.5	Ia	87	381
2003aq	NGC 5490C	5464	18.5	II	155	449
2003bk	NGC 4316	1252	17.0	II	164	458
2003bl	NGC 5374	4295	18.4	II	150	444
2003cg	NGC 3169	1238	14.4	Ia	33	327
2003dt	NGC 6962	4211	17.5	Ia	72	366
2003gs	NGC 936	1430	14.0	Ia	7	301
2003i	IC 2481	5322	17.6	Ib	225	519

Table 5.1. (continued).

SN	Host Galaxy	cz (km/s)	SN Mag.	SN Type	Fig. # Sp.	Fig. # pCMD
2003ie	NGC 4051	700	15.2	II	116	410
2003im	2MASX J00445922-0853228	5804	17.4	Ia	70	364
2003j	NGC 4157	774	16.7	II	165	459
2003jz	UGC 5225	4906	17.5	Ia	12	306
2003l	NGC 3506	6403	16.9	Ic	218	512
2003y	IC 522	5079	17.4	Ia	30	324
2003z	NGC 2742	1289	16.7	II	161	455
2004am	NGC 3034	203	17.0	II	162	456
2004aw	NGC 3997	4771	17.1	Ic	229	523
2004bd	NGC 3786	2678	14.3	Ia	38	332
2004bk	NGC 5246	6906	16.0	Ia	99	393
2004bm	NGC 3437	1283	17.5	Ic	251	545
2004bn	NGC 3441	6533	18.8	II	136	430
2004br	NGC 4493	6943	16.3	Ia 91bg	21	315
2004bs	NGC 3323	5164	17.0	Ib	232	526
2004c	NGC 3683	1716	14.0	Ic	246	540
2004cc	NGC 4568	2255	17.5	Ic	250	544
2004cm	NGC 5486	1390	18.8	II	147	441
2004df	2MASX J15082139+2152457	6182	18.4	IIp	285	579
2004dg	NGC 5806	1359	17.1	II	192	486
2004dt	NGC 799	5915	16.1	Ia	26	320
2004ey	UGC 11816	4750	16.0	Ia	94	388
2004f	NGC 1285	5239	17.8	IIn-pec	278	572
2004fc	NGC 701	1829	15.5	II	176	470
2004fw	UGC 4633	5777	18.3	Ia	82	376
2004g	NGC 5668	1583	17.2	II	140	434
2004gj	IC 701	6143	18.3	IIb	231	525
2004gk	IC 3311	-122	13.3	Ic	262	556
2004gn	NGC 4527	1736	16.6	Ic	244	538
2004gv	NGC 856	5974	17.6	Ib	263	557
2004p	UGC 8561	7120	16.3	Ia	102	396
2004t	UGC 6038	6446	17.5	II	194	488
2004w	NGC 4649	1117	18.8	Ia	20	314
2005aa	MCG +05-22-8	6381	18.8	II	203	497
2005aj	UGC 2411	2547	18.0	Ic	265	559
2005au	NGC 5056	5592	15.8	II	137	431
2005ay	NGC 3938	809	15.6	II	117	411
2005az	NGC 4961	2535	17.4	Ic	219	513
2005bb	UGC 8067	2839	19.8	II	199	493
2005bc	NGC 5698	3679	16.6	Ia	42	336
2005bg	MCG +03-31-93	6921	16.2	Ia	103	397
2005bh	UGC 6495	6501	17.3	Ic	216	510

Table 5.1. (continued).

SN	Host Galaxy	cz (km/s)	SN Mag.	SN Type	Fig. # Sp.	Fig. # pCMD
2005ci	NGC 5682	2273	18.5	II	148	442
2005dp	NGC 5630	2655	16.0	II	132	426
2005en	UGC 4132	5219	17.5	II	157	451
2005eo	UGC 4132	5219	18.3	Ic	261	555
2005gm	NGC 1423	6356	18	II	156	450
2005h	NGC 838	3851	15.9	II	158	452
2005hl	cgcg 374-027	6945	18.9	Ib	240	534
2005i	IC 983	5443	18.4	II	204	498
2005ip	NGC 2906	2140	15.5	II	187	481
2005kl	NGC 4369	1045	14.6	Ic	213	507
2005la	KUG 1249+278	558	17.6	II/Ib	220	514
2005o	NGC 3340	5432	16.1	Ib	267	561
2005s	UGC 9037	5940	19.1	Ia	104	398
2005u	NGC 3690	3064	16.2	IIb	210	504
2005z	NGC 3363	5766	16.7	II	159	453
2006aa	NGC 3947	6197	18.1	IIIn	276	570
2006ac	NGC 4619	6927	16.0	Ia	100	394
2006am	NGC 5630	2655	18.5	IIIn	279	573
2006bf	UGC 8093	7115	17.7	Ib?	239	533
2006bp	NGC 3953	1052	16.7	II	205	499
2006by	NGC 5149	5652	18.2	II	169	463
2006dk	NGC 4161	4946	16.3	Ib	266	560
2006dl	MCG +04-31-5	6521	18	II	154	448
2006dy	NGC 5587	2303	16.6	Ia	27	321
2006ee	NGC 774	4595	17.6	II	181	475
2006ej	IC 1563	6131	16.4	Ia	29	323
2006fo	UGC 02019	6205	18.2	Ic	233	527
2006gs	NGC 3977	5807	17	II	195	489
2006jc	UGC 4904	1670	13.8	Ib/c?	230	524
2006lc	NGC 7364	4865	18.7	Ib/c	268	562
2006lv	UGC 6517	2491	17	Ib/c	227	521
2006m	CGCG 161-055	4629	18.5	IIIn	280	574
2006n	MCG +11-8-12	4280	15.0	Ia	11	305
2006ou	UGC 6588	4047	16	Ia	84	378
2006ov	NGC 4303	1566	14.9	II	113	407
2006x	NGC 4321	1571	17.0	Ia	68	362
2007ax	NGC 2577	2057	17.2	Ia	10	304
2007gi	NGC 4036	1445	16.3	Ia	9	303
2007n	MCG -01-33-12	3861	17.3	Ia	52	346
2007rz	NGC 1590	3897	16.9	Ic	235	529
2007s	UGC 5378	4161	16.7	Ia	105	399
2007ss	NGC 4617	4655	16.6	Ia	40	334

Table 5.1. (continued).

SN	Host Galaxy	cz (km/s)	SN Mag.	SN Type	Fig. # Sp.	Fig. # pCMD
2007uy	NGC 2770	1947	17.2	Ib	260	554
2008d	NGC 2770	1947	17.5	Ib	228	522

### Location

The SNe regions originate from a wide variety of galaxy types – elliptical to irregular, Sa to barred Sc. SNe can and have occurred on all types of structures of the host galaxies (arms, disk, outside visible disk). Here, the regions are classified by the structure (or nearby structure) of where they appeared –arm, inter arm, disk, inner central arms, etc. Some regions defied classification, usually because the host is an irregular or interacting galaxy with clumps of bright regions not conforming to any specific shape, or the galaxy axis is inclined to the degree that no structural information was apparent. These areas were either labeled “irregular” or “disk”. In other cases, “dust” labeled regions describe any location (arm, center, disk) with copious amounts of dust. Inner disk refers to areas close to the center on spiral galaxies where the arms are tightly wound and indistinguishable from one another. Table 5.2 shows the fraction of SNe that occurred in different structures separated by type. These numbers are based on the entire sample – that is, they include regions of negligible background galaxy flux as well, not plotted in the spatial and pCMD diagrams.

Table 5.2. Fraction of SNe per structure per type.

Structure	Ia	Ia 91bg	Ia 91T	II	Ib/c	II L	II n	II P	All SNe
arm	0.26	-	0.25	0.40	0.46	0.14	0.37	0.21	0.34
E/S0	0.17	0.71	-	0.01	0.01	-	-	-	0.08
inter arm	0.05	-	0.25	0.06	0.04	-	0.11	0.07	0.06
irregular	0.05	-	-	0.09	0.16	0.29	0.05	0.07	0.09
disk	0.07	-	0.25	0.07	0.10	0.29	-	-	0.08
inner disk	0.06	-	-	0.07	0.07	-	0.05	0.07	0.06
dust	0.04	-	-	0.05	0.06	-	0.05	0.07	0.05
no flux	0.31	0.29	0.25	0.25	0.10	0.29	0.37	0.50	0.26
Total SNe	137	7	8	136	69	7	19	14	397

As table 5.2 shows, most events occur on spiral arms for all SNe types except for under luminous Ia 91bg events. The numbers are much less (26%) for the Ia population, whereas 40% of type II and 47% of the Ib/c sample occur on spiral arms. The smaller percentage of SNe Ia on arms is due to the large number of Ia events occurring in E/S0 galaxies, which almost exclusively are host to SNe Ia and accounts for a nearly a fifth of the environments for normal Ia. There are no over luminous Ia 91T types occurring in E/S0. The number of events occurring in between arms is about the same for all types except Ia 91T and II L. Type Ib/c are twice as likely to occur in irregular environments than type II and three times more likely than type Ia. Other than these differences, the relative amounts of SNe per location are roughly the same for the main types (I, II and Ib/c).

A higher percentage (31%) of SNe Ia are in areas of insignificant galaxy background flux than the core collapsed SNe, particularly for the case of type Ib/c where 10% occur in areas of negligible flux. These low flux regions don't necessarily correspond to areas outside the optical radius of the galaxy, defined as  $25\text{mag(B)}/\text{arcsec}^2$ . In fact, only 29 are outside the galactic radius in this sample, of which four were Ib/c and eight type II. It is unclear why any core collapsed SNe appear far from the host galaxy since the lifetime of a massive progenitor is small in comparison to the time it takes for the stellar cluster to dissociate ( $\sim 1/2$  billion years). This points to two possibilities: either some mechanism has flung the star far from the original stellar formation region or there is a significant amount of galactic light not detected – probably in ultraviolet. The first possibility requires a model of galactic and cluster dynamics, which is outside the work of this thesis. The second possibility can be explored using online UV catalogs. The GALEX Ultraviolet Atlas of Nearby Galaxies (Gil de Paz et al., 2007) contains images in far-UV and near-UV for 9 host galaxies, with SNe occurring in low flux regions, in this sample. Six of them, 3 Ia and 3 type II, have far UV light associated with their positions and 3 do not. Only one is outside the galactic radius (2001ad) and amazingly, this event is one of the SNe with associated UV light. A more thorough investigation of SNe in

seemingly empty regions utilizing HST and GALEX data should yield interesting results and will be left for future work.

### Colors

Now that the SNe regions have been categorized by galactic structures, the next items to consider are similarities of the structures across the supernova types. For example, are the spiral arms that produce Ia SNe the same as the ones producing core collapsed SNe? One way to do this is to compare the central grid colors of the spatial maps that contain the location of the supernova and treat them as a proxy for the structure color. By averaging these central colors per type per structure yields the information in tables 5.3-5.5 The  $g-i$  color gives the most robust result because it contains more grids above the signal to noise than the  $u-g$  and  $i-z$  colors.

Table 5.3. The  $u-g$  colors for each structure divided by SN type.

Structure	Ia	Ia 91bg	Ia 91T	II	Ib/c	II L	II n	II P	All SNe
arm	1.07	-	1.20	0.82	0.88	0.85	0.91	1.04	0.90
E/S0	1.76	-	-	1.52	-	-	-	-	1.74
inter arm	0.99	-	-	1.22	1.14	-	1.45	1.12	1.16
irregular	0.90	-	-	0.63	0.65	0.29	0.72	0.95	0.66
disk	-	-	-	0.92	0.91	0.97	-	-	0.93
inner disk	1.38	-	-	1.10	1.22	-	1.18	0.61	1.21
dust	1.72	-	-	1.56	1.28	-	-	-	1.50

Table 5.4. The  $g-i$  colors for each structure divided by SN type.

Structure	Ia	Ia 91bg	Ia 91T	II	Ib/c	II L	II n	II P	All SNe
arm	0.87	-	0.93	0.64	0.69	0.65	0.65	0.71	0.71
E/S0	1.15	1.20	-	1.20	1.15	-	-	-	1.15
inter arm	0.88	-	0.82	0.84	0.91	-	0.87	0.92	0.87
irregular	0.68	-	-	0.39	0.53	-0.02	0.49	0.40	0.47
disk	0.92	-	0.94	0.70	0.72	0.62	-	-	0.79
inner disk	1.02	-	-	0.83	1.06	-	0.98	0.41	0.93
dust	1.56	-	-	1.43	1.17	-	1.38	1.07	1.39



Table 5.5. The  $i-z$  colors for each structure divided by SN type.

Structure	Ia	Ia 91bg	Ia 91T	II	Ib/c	II L	II n	II P	All SNe
arm	0.21	-	0.18	0.16	0.18	0.03	0.17	0.21	0.18
E/S0	0.25	0.22	-	0.15	-	-	-	-	0.25
inter arm	0.15	-	-	0.19	0.20	-	0.17	0.13	0.17
irregular	0.19	-	-	0.14	0.18	-	-	0.06	0.16
disk	-	-	0.17	0.12	0.16	0.16	-	-	0.15
inner disk	0.23	-	-	0.21	0.28	-	0.20	0.11	0.23
dust	0.40	-	-	0.44	0.31	-	0.47	0.33	0.40

### Arm Colors

SN Ia types coming from spiral arms are redder than any core collapsed SNe from the same structure. This is not surprising, because only the more massive stars evolve quickly in young clusters and thus trace the star forming region and HII emission. Core collapse SNe effectively following the brightest areas of galactic light (Kelly et al., 2008). The Ia spiral arms are redder by approximately  $3\sigma_c$  compared to types II, IIL and II n and  $2\sigma_c$  with Ib/c and II P types. The color range of type II and Ib/c arms is  $0.1 < g-i < 1.0$  where as the range in colors for Ia arms spans  $0.4 < g-i < 1.2$ . About 8% of the Ia sample are in extremely blue ( $g-i < 0.6$ ) arms, with colors characteristic of core-collapse SNe. The  $u-g$  colors for all core-collapse SNe are bluer by approximately  $2\sigma_c$ , to SNe Ia, except for IIP, which are similar colored regions to Ia. The Ia 91T subtype regions are slightly redder by about  $1\sigma_c$  in both  $g-i$  and  $u-g$  and bluer in  $i-z$  by a less than significant amount, than normal Ia occurring on spiral arms. There are two data points for 91T events occurring on arms, 1998es and 199dq. The colors for both SNe are fairly close in  $u-g$  and  $g-i$ . In fact, both regions 1998es and 1999dq look remarkably identical.

The  $i-z$  colors for all types ,except II L are not significantly different from one another, but Ia tend to be the reddest. The Type II L colors come from just one data point, 1979c. But 1979c is bluer than any other supernova area by  $3\sigma_c$  in  $i-z$ , and similar in  $u-g$  and  $g-i$  colors to type II and Ib/c regions, meaning that this supernova comes from very young, metal poor region.

### *E/S0 Colors*

Ia and Ia 91bg events dominate this category. The colors span a fairly narrow range of  $1.1 < g-i < 1.5$ ,  $1.5 < u-g < 2.0$  and  $0.15 < i-z < 0.3$ . Normal Ia events occur in both E/S0 regions of large  $u$ ,  $g$  and  $i$  flux and areas of low flux. However, this is not the case with Ia 91bg types. There are five sub-luminous Ia SNe in this sample from regions of average to low flux. Interestingly, none of these five 91bg-type events occur in regions of significant  $u-g$  flux in any type of galaxy. And even more amazing, is that the positions of two of these events are as close as 0.2 fractional radii from the center of the galaxy and still there isn't any  $u-g$  flux.

The lack of  $u-g$  flux in 91bg events could mean that the Ia/Ia91bg ratio is dependent on the white dwarf density of the region or the mass of the progenitor. If most events from elliptical galaxies are truly white dwarf-white dwarf (WD-WD) mergers (Gilfanov and Bogàn 2010), then the difference between the normal Ia and 91bg events is the mass of the combined white dwarfs (see Von Hippel et al., 1997). And perhaps, the reason why 91bg events mostly occur in elliptical hosts is because statistically, there is a larger ratio of white dwarfs to main sequence stars. Unfortunately, other than the luminosity profile of elliptical galaxies, we don't know the distribution of white dwarfs in a galaxy as a function of white dwarf mass and galaxy radius. Another possible explanation for the difference in Ia and 91bg events is that dust dimming the light of the supernova and extinguishing the background UV light. Two of the 91bg events in this sample occur in SA/b galaxies, making the WD-WD merger a less likely scenario for regions with abundant main sequence stars.

Two core collapsed SN 2000ds (type Ib) and 2006ee (type II) are both from S0 type hosts. It is an unusual event for a young core-collapse SNe to occur in an old population of stars. These host galaxies have no other apparent peculiar structure that might indicate a burst of recent star formation or merger in the spatial maps, pCMDs or  $g$  band image. It is suspected that the SNe were misclassified. Unfortunately, not much data exists for 2006ee. However, Maund & Smartt (2005) led a study looking for progenitors for several core-collapse SNe, including 2000ds with null results. Based on the host

galaxy type, it was suggested that 2000ds arose from a helium low mass star in a binary system and not a single progenitor.

### *Irregular Colors*

Irregular regions are the bluest of all structure types because most, if not all, of these areas come from interacting, starburst other peculiar galaxies. Irregular regions for Ia are redder than the core-collapsed SNe, particularly type II with a difference of 0.3 in  $g-i$  and a difference of 0.15 for type Ib/c, meaning that Ib/c are in redder and probably dustier than type II. Type IIL, again are the bluest areas of all by approximately 0.3 in  $u-g$  and 0.4 in  $g-i$  from the other core collapsed SNe. These regions are unique in this sample because they don't contain significant amounts of  $z$  band flux, but they do contain more flux in all the other bands. If the remnants of these supernovae are indeed magnetars (Kasen and Bildsten, 2009) then the flux measured from the region could be dominated by emission from the remnant and not by the underlying stellar population.

### *Disks, Inner Disk and Inter Arm Colors*

Regions labeled as "disk" are either areas where the inclination of the galaxy is too great to determine the exact structure or they are environments near the faint limits of the outer parts of the host galaxy. The latter scenario is more common than the former because a lot of these areas have low to no flux in  $u-g$  and  $i-z$ . This is especially true for Ia and Ia 91T types because they tend to occur in disks of lower flux than II and all other core collapsed SNe. Ia and Ia 91T are also redder in  $g-i$  than all other types. We will return to this when discussing the amount of flux in  $u$ ,  $g$  and  $i$  bands for each type and structure.

Inner disks tend to be redder than the other structures except for dusty regions and E/S0 regions simply because these areas are near the centers of galaxies. Ib/c regions are redder than II, in all three colors. This is usually true of the entire sample, but it is unclear why the inner regions of galaxies producing II SNe are less dusty than their Ib/c counterparts.

Inter arm colors are similar across all types, indicating that the progenitor has probably migrated from the original location. These areas are low to average flux in all three colors. Approximately 25% of the entire sample of inter arm regions has an average amount of UV flux, which probably means there is some amount of star formation going on between spiral arms.

#### *Average Color Comparison*

It is also instructive to see if supernovae come from areas with substantially different colors than the brightest, bluest areas within their local regions. The center grid color can be compared to the average color of the entire 4x4 kpc region. For this study, regions with foreground stars and visible supernovae were not included, as before.

Columns 2-5 in table 5.6 show the percentage of center grids bluer in color than the average color of the 4x4 kpc area and columns 4-7 list out the average colors for these regions per type. The Ia events are distributed evenly between blue and red environments, for all three bands showing no real strong preference for occurring in redder or bluer areas. There isn't a lot of information for Ia sub types, but the 91T events do tend to appear on the bluer areas in  $g-i$  and 91bg are typically in the redder parts of the region.

The core collapsed SNe trace the bright star forming regions showing a preference for occurring in the bluer area of the region in both  $u-g$  and  $g-i$ , but not so in  $i-z$ , where the center grid is not likely to be the bluer than most. Both types have the same average colors for their regions, but Ib/c center grids are redder areas in  $i-z$  than type II, suggesting Ib/c are more likely to occur in more metal rich environments, such as the centers of galaxies, than any other core collapsed supernova (Anderson and James, 2009). Dust is more prevalent in the centers of galaxies and maybe contributing to the colors of the Ib/c regions as well. Type IIP are less likely to occur in the bluer areas of the region (this can also be easily seen in the spatial plots) and II L SNe are just over 50% bluer in the center grid. But both types come from regions substantially bluer in  $u-g$  and  $g-i$  than all other core collapsed SNe, Type IIIn is the largest subtype group. The average colors of

the regions are very similar to II and Ib/c environments and so are the percentages of blue center grids.

Table 5.6. Percentages of center grid bluer than the whole 4x4 kpc region

SNe	<i>u-g</i> % blue	<i>g-i</i> % blue	<i>i-z</i> % blue	<i>u-g</i> tot. ave.	<i>g-i</i> tot. ave.	<i>i-z</i> tot. ave.
Ia	55	48	51	1.38	0.97	0.23
II	72	70	50	1.02	0.80	0.19
Ib/c	68	62	41	1.07	0.81	0.20
Ia 91T	50	67	0	1.24	0.96	0.18
Ia 91bg	-	25	33	-	1.17	0.23
II L	50	67	0	0.60	0.53	0.19
II n	75	70	71	1.10	0.82	0.22
II P	25	50	50	0.94	0.74	0.18

For types Ia, II and Ib/c, the same analysis was done as a function of the galactic structure. The last three columns in tables 5.7-5.9 are the averages of each region that have supernovae occurring on the specific structure. In all three types, the supernova is likely to occur on the brightest portion of the arm, although this is truer in II where approximately 90% or more center grids are on bluer areas in *u-g* and *g-i*. Ib/c types are closer to 75% for similar regions and Ia are 78% and 64% for *u-g* and *g-i*, respectively, for much redder averaged regional colors. The pCMDs indicate dust in some of the arms for all types (e.g. 1998bu, 1999gn, 2000cr), which appear as grids aligned in a sloped band in the *g-i*, *g* plots.

For E/S0 color regions, Ia SNe are more or less evenly divided between bluer and redder areas in both *u-g* and *g-i*. Notice how this different this distribution is than Ia 91bg types in table 5.6, showing that under luminous Ia come from redder parts of older/redder hosts. E/S0 colors for core-collapsed SNe are limited to one data point apiece, so the statistics don't say much other than both occur in bluer regions of E/S0 hosts.

SNe grids occurring in inter arm areas are all dim, which is not surprising since they are flanked by blue spiral arms, but for Ia, the *u-g* and *i-z* are bluer than the region as a whole. Regions where Ia occurred between the arms are bluer than regions where SNe

Ia happened on the arm. The numbers for these two colors are based on only 2 regions apiece which happen to contain very blue arms, so it doesn't necessarily reflect the sample as a whole. Dust is evident in half of the sample for all types.

The distribution of blue center grids in irregular regions is similar for Ia and II, but the average colors are so much bluer in II that it is difficult to compare the two. The irregular Ia regions are some of the bluest for the Ia sample (e.g. 2001ed, 2004ey) yet they are still not as blue as the core-collapsed SNe. Type II and type Ib/c also have different averaged regional colors where Ib/c are redder than II in all three bands, but the center grids for Ib/c tend to be bluer than average in all three bands. It is not clear why type Ib/c is redder than type II because the pCMDs indicate that both types have about the same amount of regions with dust. Or possibly, there is a different reddening law in irregular galaxies/regions.

SNe Ia occurring in disks are typically in regions of low flux near the outer parts of the host galaxies. The same areas for type II and Ib/c have almost the same distribution and average colors except the much bluer  $i-z$  colors for II regions show disk like structures are not as metal rich as Ib/c. The average colors of the inner disks indicate that they are some of the reddest parts of the host galaxy with again, type II having colors not as red as Ia and Ib/c. The most interesting is type Ib/c with 80% of events coming from areas redder in  $i-z$  than the average regional color.

Table 5.7. Percentage of structure bluer than entire 4x4kpc region for type Ia.

Ia structure	$u-g$ % blue	$g-i$ % blue	$i-z$ % blue	$u-g$ tot. ave.	$g-i$ tot. ave.	$i-z$ tot. ave.
Arm	78	64	56	1.17	0.90	0.21
E/S0	45	55	38	1.74	1.16	0.24
inter arm	100	14	100	1.07	0.84	0.19
irregular	50	67	75	1.03	0.75	0.19
Disk	-	83	-	-	0.96	-
inner disk	25	0	67	1.27	0.94	0.23

Table 5.8. Percentage of structure bluer than entire 4x4kpc region for type II.

II structure	<i>u-g</i> % blue	<i>g-i</i> % blue	<i>i-z</i> % blue	<i>u-g</i> tot. ave.	<i>g-i</i> tot. ave.	<i>i-z</i> tot. ave.
Arm	89	97	67	1.02	0.78	0.18
E/S0	100	100	100	1.62	1.18	0.20
inter arm	0	13	33	1.09	0.79	0.17
irregular	50	67	50	0.77	0.50	0.15
Disk	75	60	100	0.96	0.77	0.14
inner disk	57	56	38	1.12	0.86	0.20

Table 5.9. Percentage of structure bluer than entire 4x4kpc region for type Ib/c.

Ibc structure	<i>u-g</i> % blue	<i>g-i</i> % blue	<i>i-z</i> % blue	<i>u-g</i> tot. ave.	<i>g-i</i> tot. ave.	<i>i-z</i> tot. ave.
Arm	76	78	43	1.00	0.74	0.18
E/S0	-	100	-	-	1.15	-
inter arm	0	0	33	1.10	0.84	0.20
irregular	86	75	67	0.91	0.69	0.18
Disk	100	57	100	0.94	0.75	0.24
inner disk	60	20	20	1.31	1.06	0.24

### 5.3.2.2. Surface Brightness Analysis

Much in the same manner as was done for the colors, we now analyze the flux of bands *u*, *g* and *i*, for each structure to determine if there is any correlation between the brightness of the region and the SNe type. Again, we use the center grid values for flux to describe the brightness of the structures for each type. Tables 5.10-5.12 list out the surface brightnesses per SN type, structure and filter band.

With the exception of Ia 91T, II L and II P events, the fluxes for the arms in all three bands are relatively the same (table 5.13). II L and II P fluxes are slightly dimmer by no more than 0.5 in mag/arcsec<sup>2</sup> in *u*, but *g* and *i* are comparatively the same as the rest of the sample. Over luminous 91T regions are brighter than the other regions by about 1 mag/arcsec<sup>2</sup> in *g* and *i*. This corresponds to just two events, 1998es and 1999dq,

but is an interesting trend and with more 91T-like discoveries, should be examined more thoroughly.

S0 and elliptical regions hosting Ia events are the brightest in the entire Ia sample for all three bands. In comparison these regions are brighter by at least  $0.85 \text{ mag/arcsec}^2$  than the under luminous Ia 91bg regions for  $g$  and  $i$  bands. Again, this is restating what was mentioned earlier when discussing the colors of these two areas and that is, not only do 91bg events occur in E/S0 type hosts, but also they never occur in bright regions of these hosts.

Inter arm regions in  $u$  are fairly dim for all types of SNe which makes sense because most of the UV emitting star formation is occurring in the arms and not the dim regions in between the arms. Irregular regions are brightest for Ib/c and II P, but more so for Ib/c with a difference in brightness of  $> 1 \text{ mag/arcsec}^2$  in comparison to the other core collapse SNe. In fact, Ib/c occurring in irregular regions are the brightest in all structures and SN types by at least  $0.6 \text{ mag/arcsec}^2$ . SNe Ia areas are unremarkable, but are brighter in  $u$  than type II, II L and II n. For the  $g$  and  $i$  bands, the relative brightnesses are the same except that IIP is brighter than Ib/c types.

Disk-like structures are fairly dim for most types, but type II L and 91T are slightly brighter than the core collapse and normal Ia types. Inner disks have similar  $u$  band surface brightnesses for all core collapsed SNe, where as Ia are much dimmer. However  $g$  and  $i$  fluxes are brightest for Ib/c and II n, particularly for the Ib/c  $i$  band flux which is the brightest for all types and structures for this filter. Finally, dusty structures are bright emitters in  $g$  and  $i$  for all SNe. Clearly, Ib/c and IIL SNe occur in the brighter parts of galaxies.

Listed in table 5.13 are the percentages of center grids brighter than the total average brightness of the whole region for Ia, II and Ib/c types. The average surface brightness for the  $4 \times 4$  kpc regions is similar for each region with the exception of type II L. The results are the same as for tables 5.7-5.9, offering a more direct comparison to specific types, structure brightness and average regional brightness.



Table 5.10. The average  $u$  surface brightness for each SN type and structure.

Structure	Ia	Ia 91bg	Ia 91T	II	Ib/c	II L	II n	II P	All SNe
arm	22.22	-	22.00	21.95	21.97	22.38	22.07	22.54	22.03
E/S0	21.84	-	-	22.60	-	-	-	-	21.91
inter arm	22.43	-	-	22.05	22.38	-	23.15	22.57	22.43
irregular	21.86	-	-	22.09	20.73	22.33	22.50	21.29	21.63
disk	-	-	-	22.20	22.34	21.98	-	-	22.20
inner									
disk	22.37	-	-	21.52	21.34	-	21.57	21.38	21.76
dust	22.17	-	-	21.49	22.07	-	-	-	21.92

Table 5.11. The average  $g$  surface brightness for each SN type and structure.

Structure	Ia	Ia 91bg	Ia 91T	II	Ib/c	II L	II n	II P	All SNe
arm	21.63	-	20.76	21.43	21.38	21.54	21.50	21.49	21.46
E/S0	20.90	21.79	-	21.60	21.11	-	-	-	21.10
inter arm	22.04	-	22.23	21.85	21.25	-	22.34	21.45	21.89
irregular	21.46	-	-	21.63	20.81	22.04	21.78	20.34	21.32
disk	22.49	-	21.53	21.87	21.61	21.01	-	22.73	21.98
inner disk	21.09	-	-	20.70	20.12	-	20.39	20.78	20.70
dust	21.01	-	-	21.15	20.71	-	21.60	21.98	21.09

Table 5.12. The average  $i$  surface brightness for each SN type and structure.

Structure	Ia		Ia 91T	II	Ib/c	II L	II n	II P	All SNe
	Ia	91bg							
arm	20.76	-	19.84	20.82	20.72	20.99	20.85	20.79	20.76
E/S0	19.75	20.57	-	20.44	20.91	-	-	-	19.94
inter arm	20.96	-	21.40	20.81	20.34	-	21.46	20.53	20.96
irregular	20.78	-	-	21.27	20.28	22.06	21.29	19.95	20.86
disk	21.56	-	20.59	21.17	20.88	20.39	-	22.38	21.20
inner disk	20.07	-	-	19.87	19.07	-	19.41	20.36	19.77
dust	19.45	-	-	19.71	19.49	-	20.22	20.90	19.68

Table 5.13. Percentages of center grid brighter than the whole 4x4 kpc region.

SNe	u % bright	g % bright	i % bright	u tot. ave.	g tot. ave.	i tot. ave.
Ia	42	71	68	22.11	21.75	20.66
II	57	71	60	22.13	21.87	20.91
Ib/c	74	82	73	22.07	21.59	20.70
Ia 91T	50	50	50	21.80	21.57	20.61
Ia 91bg	-	0	50	-	22.16	20.75
II L	75	100	100	22.27	22.33	21.30
II n	50	67	70	22.20	21.73	20.63
II P	50	83	67	22.13	21.66	20.81

The brightness of the structure in comparison to the average brightness shows again, that structures where Ib/c events occur are typically brighter than type II regions except for arms, where they are identical. The average regional colors for Ib/c are also slightly brighter than type II. The average flux in E/S0 regions is the brightest for all regions and types. Tables 5.14-5.16 summarize these results.

Table 5.14. Percentages of Ia center grids brighter than the whole 4x4 kpc region.

Ia structure	u % bright	g % bright	i % bright	u tot. ave.	g tot. ave.	i tot. ave.
arm	44	88	84	22.18	21.87	20.90
E/S0	50	86	79	21.85	21.11	19.93
inter arm	0	29	43	22.15	22.00	21.14
irregular	0	86	67	22.31	21.70	20.78
disk	-	50	0	-	22.38	21.23
inner disk	25	63	100	22.28	21.69	20.59

Table 5.15. Percentages of II center grids brighter than the whole 4x4 kpc region.

II structure	u % bright	g % bright	i % bright	u tot. ave.	g tot. ave.	i tot. ave.
arm	71	86	69	22.21	21.86	20.92
E/S0	0	100	100	21.91	21.73	20.52
inter arm	0	0	13	21.77	21.56	20.72
irregular	50	70	67	22.14	22.00	21.23
disk	25	60	50	-	22.03	21.09
inner disk	43	67	67	21.92	21.36	20.42

Table 5.16. Percentages of Ib/c center grids brighter than the whole 4x4 kpc region.

Ib/c structure	u % bright	g % bright	i % bright	u tot. ave.	g tot. ave.	i tot. ave.
arm	71	85	67	22.08	21.65	20.82
E/S0	-	0	0	-	21.99	20.81
inter arm	33	67	67	22.18	21.27	20.40
irregular	100	89	88	21.88	21.62	20.78
disk	50	57	57	-	21.79	20.98
inner disk	80	100	100	21.98	21.15	20.06

### 5.3.2.3. Dust in pCMDs

In several of the pCMD plots, particularly the core collapse pCMDs, the grids align themselves into linear sloping bands in the direction of increasing surface brightness and blue color. For the most part, these bands correspond to areas that are reddened by dust, which for the  $g, g-i$  pCMDs is a slope of 2.2. Regions such as 1999d and 1999bw are examples of slopes of grids that don't correspond to dust, but are either due to a combination of young and old stellar populations or dust with an extinction law different from the Milk Way. In order to test for dust (similar to the Milky Way), a simple linear regression is performed on the  $g-i$  data in the pCMD plots. Only bands that contain the supernova location center grid are analyzed and regions with too little data or elliptical colors are ignored. For a meaningful fit, only grids within about 15 pixels of either side of the SN center grid were used in the regression.

Table 5.17 shows results of the fits. Only the results of the Ia fits will be discussed, although, the non-Ia types were left to show the results. All SNe regions with linear features within the range  $1.7 < \text{slope} < 2.7$  are considered to have dust similar to the Milky Way.

There are correlations between the calculated slope of the reddening vector and the spatial plots in regions: 1956a and 2001dp; 1974g, 1989b and 1992g; 1989m, 1998bu and 2006x. The 2006x, 1989m and 1998bu regions all resemble one another and have similar slopes, except 2006x which appears slightly off of the main arm in a dustier area with no UV emission. SNe 2006x has very red peak colors for a normal Ia,  $\text{SN (B-V)}_{\text{max}} = 1.31$  (Wang et al. 2006), so does 1998bu ( $\text{B-V}_{\text{max}} = 0.36$ ; Reindl et al., 2005). From light echo analysis of 2006x, the dust surrounding the SN has a reddening law of  $R_V \sim 1.5$  (Wang et al., 2006; Folatelli et al., 2010) and a much smaller distribution of grain sizes. It is unclear whether this is due to circumstellar dust or pre-existing interstellar dust in the environment. The SDSS image for this analysis was taken two years prior to the event, indicating that at least part of this nonstandard dust must be due to interstellar dust.

SN 1974g, 1989b, 1992g, 1956a and 2001dp all indicate dust similar to the Milky Way. The peak SN colors of 1974 and 1989b are redder than average (1974g  $\text{B-V}_{\text{max}} = 0.11$ , 1989b:  $\text{B-V}_{\text{max}} = 0.32$ ; Reindl et al., 2005) and may reflect some amount of contamination of dust in the SN colors. As for the two remaining SNe with measured peak colors, both SN 1999aa and 1960f indicate standard dust but they both have bluer peak colors.

### *Visible Supernovae*

As expected in large sky surveys, some supernovae were captured on the SDSS images as part of the general operational scan of the galactic poles. None of these were actual discovery images, because most were taken about a month after found by a supernova search. But interestingly enough, two were imaged two to four weeks prior to discovery, only to be independently discovered later by other SN searches. The criteria to determine if a bright blob was indeed a supernova was looking at the time stamp of the image, the

Table 5.17. Fitted slopes of linear structures in pCMDs. The slope and error are estimated from linear regression using the grids nearest the supernova event. The column ‘MW Dust’ refers to slopes with dust similar to the Milky Way.

SN	Type	Slope	Error	MW Dust
1926a	II	1.43	0.16	
1940b	II	2.34	0.12	x
1956a	Ia	1.67	0.06	x
1960f	Ia	1.70	0.13	x
1961i	II	2.43	0.10	x
1963p	Ia	3.80	0.09	
1964f	II	2.29	0.06	x
1964l	Ic	0.80	0.09	
1967h	II	4.08	0.30	
1970a	II	2.57	0.09	x
1972q	II P	2.81	0.33	x
1974g	Ia	1.93	0.13	x
1983i	Ib	1.65	0.05	x
1985l	II	1.09	0.10	
1986i	II	1.50	0.06	
1988a	II	2.26	0.12	x
1989b	Ia	2.17	0.13	x
1989c	II P	3.32	0.47	
1989m	Ia	1.57	0.05	
1989n	II	3.28	0.09	
1992g	Ia	1.82	0.11	x
1995v	II	1.98	0.11	x
1996aq	Ic	1.51	0.21	x
1997bs	II n	1.73	0.14	x
1997dq	Ib	4.02	0.27	
1997x	Ic	2.78	0.15	
1998ar	II	1.40	0.09	
1998bu	Ia	1.10	0.17	
1998dl	II	2.34	0.25	x
1999aa	Ia 19T	1.49	0.19	
1999br	II	1.56	0.14	x
1999bw	II n	1.11	0.10	
1999cd	II	2.35	0.14	x
1999d	II	4.35	0.13	
1999di	Ib	1.35	0.19	
1999ev	II	1.64	0.11	x
1999gi	II	2.14	0.13	x
1999gk	II	1.56	0.09	
1999gn	II	2.27	0.08	x
2000cr	Ic	1.88	0.09	x
2001dp	Ia	1.97	0.10	x

Table 5.17. (continued).

SN	Type	Slope	Error	MW Dust
2001ed	Ia	2.48	0.27	x
2003ie	II	2.04	0.14	x
2003j	II	1.97	0.24	x
2003z	II	2.10	0.14	x
2004g	II	1.50	0.11	
2004gn	Ic	1.39	0.12	
2005aj	Ic	1.97	0.09	x
2005ay	II	1.44	0.09	
2005kl	Ic	3.83	0.20	
2006bp	II	1.89	0.12	x
2006ov	II	2.07	0.08	x
2006x	Ia	1.48	0.06	

SN discovery date and then checking NED for any other object in the SN location. In the end, there were 29 regions in this sample that were imaged within 6 months of a supernova event, 17 post discovery and 12 taken a few months before the discovery. Out of these 29 regions, 13 are seen, and summarized in table 5.18. Most of these events are noticeable in the spatial plots and pCMDs (shown as horizontal lines of pixels). Two of these events, 2003bl and 2005bg, are only visible in the *g* band images and not the spatial plots. Most of the events are substantially bluer than the surrounding region except for 2001x and 2001q, which appear red. One event, 2005z, appears one grid off center which is somewhat disconcerting. Clearly, the coordinates for this SN were off by a few arc seconds, but given the number of visible SNe that are on the center grid and poorer resolution of this region, SN positional accuracy in the rest of the images isn't a large concern.

The pre-discovery supernova images bring up the question of how many SNe can be detected in a sky survey and will be addressed in the supernova search simulation portion of this thesis. SDSS does have a supernova search component of the mission, which has discovered hundreds of SNe. However, most of these discoveries are from host galaxies at distances of  $z > 0.1$ , therefore, none of these images are included in this analysis due to the distance or small apparent size of the hosts.

Table 5.18. Visible supernovae on SDSS images in this sample. The discovery date is the date the SNe was reported. The image date is the date of the SDSS image. Two of the SDSS images have SNe visible before the reported discovery.

SN	Type	Discovery Date	Image Date
1999dk	Ia	8/12/99	10/14/99
2000l	II	2/29/00	4/6/00
2001a	Ia	1/1/01	2/20/01
2001dp	Ia	8/12/01	12/20/01
2001q	II	1/31/01	3/19/01
2001x	II P	2/27/01	6/16/01
2002hl	Ia	11/4/02	4/26/03
2003bl	II	3/2/03	4/1/03
2004bd	Ia	4/7/04	5/14/04
2004df*	II P	6/27/04	6/12/04
2005bg	Ia	3/28/05	6/1/05
2005bh*	Ic	4/10/05	3/12/05
2005z	II	1/31/05	2/4/05

\*Indicates pre-discovery SN image.

### 5.3.3. Aperture Photometry

In addition to the grid analysis, photometry was done using circular apertures of 6 and 13 pixels in diameter (2.4" – 5.2") centered about the supernova location. The smaller size is to isolate the progenitor population by better matching to the shape of the SN parent population geometry (as opposed to a square). The larger aperture is for combining the 2MASS photometry data with the SDSS data. There are several quantities to examine here, so it helps if they are listed out.

First we'll examine the colors of each region by averaging various bands as a function of SN type and SN plus galaxy type, also looking at the number of regions with and without significant flux. Then, the color-color diagrams are discussed along with the colors as a function of galactic radius, paying particular attention to specific SNe Ia used in cosmology. SN Ia peak colors from Wang et al. (2006), Hicken et al. (2009) and Folatelli et al. (2010) will be compared to the SDSS environment colors.

## 5.3.3.1. Average Aperture Colors

Table 5.19 shows the averaged color per SN type. There are 15 potential colors for each region, but 14 are listed. The  $z-K_S$  color had the least amount of flux for many regions, and so it was omitted. Next to each value is the standard deviation in tenths of magnitude. For both Ia 91T and Ia 91bg types, the scatter is very small. The colors for 91T are also bluer than the normal Ia types. Across all colors, 91T are bluer than normal Ia and 91bg are redder than normal. The  $K_S$  colors of 91T match those of core collapse SNe and normal Ia are the reddest of these colors. Type II L are the bluest of all and do not occur in any region of substantial IR  $K_S$  flux or dust, followed by II P with significant, but low  $K_S$  band flux. All of these results confirm previous findings in the grid photometry section.

Table 5.19. Average color of each band per SN type.

	Ia	Ia 91bg	Ia 91T	II	Ib/c	II n	IIP	II L
<i>u-g</i>	1.35(38)	-	1.19(17)	0.87(37)	0.90(35)	0.98(31)	0.75(32)	0.67(36)
<i>u-r</i>	1.97(54)	-	1.82(19)	1.32(57)	1.42(53)	1.44(45)	1.10(44)	1.01(46)
<i>u-i</i>	2.30(64)	-	2.12(18)	1.55(75)	1.66(65)	1.67(54)	1.22(56)	1.17(73)
<i>u-z</i>	2.61(59)	-	-	1.95(88)	2.01(64)	2.04(44)	0.97(55)	-
<i>g-r</i>	0.62(18)	0.72(09)	0.56(06)	0.49(24)	0.51(19)	0.49(18)	0.42(21)	0.34(11)
<i>g-i</i>	0.98(27)	1.16(10)	0.90(05)	0.75(36)	0.75(29)	0.75(30)	0.64(36)	0.42(36)
<i>g-z</i>	1.30(33)	1.43(06)	1.12(02)	1.02(54)	1.03(35)	1.07(39)	0.74(56)	-
<i>r-i</i>	0.34(11)	0.43(03)	0.32(03)	0.24(17)	0.23(13)	0.25(10)	0.19(15)	0.06(25)
<i>r-z</i>	0.61(17)	0.64(08)	0.52(00)	0.48(31)	0.45(18)	0.50(21)	0.29(35)	-
<i>i-z</i>	0.23(08)	0.21(07)	0.19(03)	0.21(13)	0.21(08)	0.21(13)	0.11(18)	-
<i>u-K<sub>s</sub></i>	3.15(66)	-	2.85(02)	2.55(94)	2.52(83)	2.51(37)	2.21(94)	-
<i>g-K<sub>s</sub></i>	1.78(47)	2.07(08)	1.54(17)	1.54(70)	1.53(56)	1.57(58)	1.28(73)	-
<i>r-K<sub>s</sub></i>	1.09(33)	1.28(08)	0.93(15)	1.02(56)	0.94(40)	0.98(42)	0.73(52)	-
<i>i-K<sub>s</sub></i>	0.73(25)	0.85(06)	0.62(16)	0.69(40)	0.68(31)	0.68(35)	0.43(44)	-

In order to test if SNe are more of a function of stellar population and independent of galaxy morphological type, the colors of each region are averaged together by SNe and galaxy type. Tables 5.20-5.23 list out the averages for colors *u-g*, *g-r*, *r-i*, and *i-z*. For comparison, the last column contains the average galaxy colors from table 4 of Fukugita



et al. (2007) (F07), who calculated colors for 1000 SDSS galaxies as a function of morphological type. The galaxies averaged in F07 are all brighter than  $r < 16$  and have been visually classified by the authors. Since most of the SNe in this sample come from bright RC3 galaxies, their results should be a fair comparison to the data present here. Unfortunately, Sab galaxies were not considered for the F07 sample, but they are included here since they constitute a large portion of the data.

The color variations per SN type vary dramatically for Sa galaxies, the reddest colors being from the Ia category. Only the Ia population is within the F07 values; the core collapse SNe are much bluer. Sab and Sb galaxies also vary by SN type for the  $u-g$  color, and the other bands to a lesser degree. Note that the 91T types are slightly bluer than normal types, for all kinds of galaxies except the Sab  $r-i$  color. But these differences are less than the error (error was calculated by only morphological type and not subdivided by SN type). Under luminous 91bg types are similar in color to normal Ia for equivalent galaxies, except for the lack of  $u-g$  colors. Values from late type galaxies such as Sd-Irr are based on low numbers and core collapse subtype averages are also based on low numbers. All colors gradually get bluer from E to later types for Ia. This same variation is present in the Ib/c data, but not in the II regions, probably due to low numbers of type II in irregular galaxies.

Table 5.20. The  $u-g$  colors for SNe type and host galaxy type. F07 is data from Fukugita et al., 2007. Errors were calculated for the entire galaxy type and not subdivided by SN type.

	Ia	II	Ib/c	Ia91T	Ia91bg	IIP	IIIn	II L	Errors	F07
E	1.82	-	-	-	-	-	-	-	0.08	1.73(18)
S0	1.73	-	-	-	-	-	-	-	0.04	1.65(21)
Sa	1.27	0.91	0.90	1.07	-	0.96	-	0.37	0.33	1.50(29)
Sab	1.24	0.73	1.00	-	-	-	1.08	0.56	0.45	n/a
Sb	1.24	0.86	0.93	1.32	-	0.78	0.95	0.94	0.39	1.33(28)
Sc	1.14	0.98	0.89	-	-	-	-	-	0.25	1.35(26)
Sd	1.27	0.67	0.43	-	-	-	0.71	-	0.36	1.18(10)
Irr	1.67	1.12	0.58	-	-	-	-	-	0.56	1.15(34)

Table 5.21. The  $g-r$  colors for SNe type and host galaxy type. F07 is data from Fukugita et al., 2007. Errors were calculated for the entire galaxy type.

	Ia	II	Ib/c	Ia91T	Ia91bg	IIP	IIn	II L	Errors	F07
E	0.77	-	-	-	0.79	-	-	-	0.06	0.77(04)
S0	0.75	0.79	0.70	-	-	-	-	-	0.04	0.74(07)
Sa	0.69	0.43	0.57	0.62	0.62	0.43	-	0.29	0.21	0.63(10)
Sab	0.57	0.50	0.52	0.50	-	0.71	0.45	0.29	0.20	n/a
Sb	0.57	0.50	0.52	0.57	-	0.43	0.55	0.41	0.20	0.60(13)
Sc	0.50	0.61	0.49	-	-	-	-	-	0.18	0.54(04)
Sd	0.51	0.23	0.28	-	-	-	0.36	-	0.26	0.47(04)
Irr	0.65	0.92	0.41	-	-	-	-	-	0.33	0.36(04)

Table 5.22. The  $r-i$  colors for SNe type and host galaxy type. F07 is data from Fukugita et al., 2007. Errors were calculated for the entire galaxy type.

	Ia	II	Ib/c	Ia91T	Ia91bg	IIP	IIn	II L	Errors	F07
E	0.41	-	-	-	0.43	-	-	-	0.03	0.39(03)
S0	0.40	0.42	0.39	-	-	-	-	-	0.02	0.38(04)
Sa	0.39	0.22	0.21	0.30	0.38	0.22	-	-	0.14	0.35(05)
Sab	0.34	0.26	0.26	0.42	-	0.33	0.26	-0.07	0.14	n/a
Sb	0.33	0.25	0.23	0.31	-	0.20	0.27	0.20	0.15	0.31(09)
Sc	0.23	0.23	0.22	-	-	-	-	-	0.06	0.26(08)
Sd	0.32	0.04	0.12	-	-	-	0.13	-	0.23	0.16(08)
Irr	0.39	0.45	0.11	-	-	-	-	-	0.26	0.09(11)

Table 5.23. The  $i-z$  colors for SNe type and host galaxy type. F07 is data from Fukugita et al., 2007. Errors were calculated for the entire galaxy type.

	Ia	II	Ib/c	Ia91T	Ia91bg	IIP	IIn	II L	Errors	F07
E	0.25	-	-	-	0.21	-	-	-	0.05	0.18(04)
S0	0.25	-	-	-	-	-	-	-	0.02	0.19(05)
Sa	0.31	0.15	0.22	0.22	-	-	-	-	0.10	0.18(07)
Sab	0.19	0.21	0.23	-	-	0.19	0.15	-	0.08	n/a
Sb	0.22	0.24	0.22	-	-	0.18	0.29	0.25	0.10	0.15(09)
Sc	0.22	0.22	0.13	-	-	-	-	-	0.09	0.06(13)
Sd	0.22	-	-	-	-	-	-	-	0.04	0.01(15)
Irr	0.18	0.79	0.19	-	-	-	-	-	0.23	0.06(21)

### 5.3.3.2. Host Galaxies with Multiple SNe

Over 50 galaxies, with SDSS images, hosted more than one supernova in the last 100 years. This offers the opportunity to compare the colors of different supernova-producing stellar populations to one another within the same galaxy. Table 5.24 lists out the regional color information of these “prolific” galaxies. The first three columns give the name of the host galaxy, the redshift and the ratio of minor to major diameters. The fourth through sixth columns list out the SN name, type, and distance from center of the host galaxy in units of fractional radii and the rest of the columns give the colors. Only the  $r$ - $K_S$  color was included from the 2MASS data because it has a largest signal to noise ratio and provides information on longer wavelengths (as opposed to  $g$ - $K_S$ ).

Scanning through the list shows the diversity of the stellar populations for one galaxy. For example, NGC 4374 hosted both a Ia and under luminous Ia at roughly the same radial distances from the center of the galaxy. Almost all the colors are exactly the same except the under luminous SN region has more flux in  $K_S$ . There are other cases with non Ia types; NGC 4303, a nearly face on spiral, hosted at least 5 type II SNe (a sixth was discovered in 2008) and has two SNe at the same distance from the center with similar regional colors except the area underlying 1999gn is half a magnitude brighter in  $K_S$  and a tenth of a magnitude brighter in  $r$ . There are other interesting cases within this table; however, they will be left to the reader to peruse.

### 5.3.3.3. Amount of Flux

The percentage of SNe coming from areas with flux (or lack of flux) breaks down into very distinct groups. At least 42% of the core collapsed SNe come from regions of significant UV flux and all have more flux than IR ( $z$  band). For completeness, unclassified (uk=unknown) SNe were also included in the sample. Their numbers match the statistics of the Ia sample, which is expected since many of these objects were classified as ‘I’ instead of Ia. SNe Ia also contain the least amount of flux for UV and 23% do not contain any significant flux. Many of these Ia are within the galaxy, only 8 out of the 137 SNe Ia are outside the optical radius.

Table 5.24. The environment colors of all SNe occurring in galaxies with more than one SNe. The first three columns describe the attributes of the host galaxy including redshift and major and minor diameters. The next three columns list the SNe occurring in each galaxy, type and distance from the center of the galaxy in units of fractional radius. The rest of the columns are the colors for each SNe environment.

Host Galaxy	cz	dmn/dmj	SN	Type	r/R	u-g	u-r	u-i	u-z	g-r	g-i	g-z	r-i	r-z	i-z	r-K
IC 4229	6978	0.77	2001ae	II	0.64	0.37	0.55	0.49	0.75	0.18	0.12	-	-0.06	-	-	-
			2002i	Ia	0.38	-	-	-	-	0.41	0.68	-	0.27	-	-	-
NGC 1084	1407	0.56	1963p	Ia	0.34	-	-	-	-	0.49	0.87	-	0.38	-	-	-
			1996an	II	0.28	0.73	0.96	1.13	1.26	0.23	0.40	0.53	0.17	0.29	0.13	0.47
			1998dl	II	0.37	1.11	1.57	1.86	1.94	0.46	0.74	0.83	0.28	0.37	0.09	0.69
NGC 1090	2760	0.43	1962k	-	0.42	-	-	-	-	0.55	0.60	-	0.05	-	-	-
			1971t	-	0.18	-	-	-	-	0.53	0.87	-	0.34	-	-	-
NGC 2532	5260	0.82	1999gb	IIn	0.30	0.72	1.04	1.23	1.36	0.32	0.51	0.64	0.19	0.32	0.13	0.58
			2002hn	Ib/c	0.08	0.82	1.23	1.50	1.66	0.41	0.68	0.85	0.26	0.43	0.17	1.07
NGC 2608	2135	0.61	1920a	II	0.14	-	-	-	-	0.59	0.94	1.14	0.34	0.55	0.21	1.01
			2001bg	Ia	0.61	-	-	-	-	0.74	1.08	-	0.34	-	-	-
NGC 2770	1947	0.21	1999eh	Ib/c	0.11	-	-	-	-	0.50	0.79	-	0.29	-	-	-
			2007uy	Ib/c	0.21	0.81	1.35	1.51	1.75	0.55	0.71	0.95	0.16	0.40	0.24	0.85
			2008d	Ib/c	0.55	-	-	-	-	0.41	0.65	-	0.23	-	-	-

Table 5.24. (continued).

Host Galaxy	cz	dmn/dmj	SN	Type	r/R	<i>u-g</i>	<i>u-r</i>	<i>u-i</i>	<i>u-z</i>	<i>g-r</i>	<i>g-i</i>	<i>g-z</i>	<i>r-i</i>	<i>r-z</i>	<i>i-z</i>	r-K	
NGC 2841	638	0.43	1912a	-	0.25	-	-	-	-	0.70	1.08	1.30	0.38	0.59	0.22	0.93	
			1957a	Ia91bg	0.55	-	-	-	-	0.60	-	-	-	-	-	-	-
			1972r	-	0.38	-	-	-	-	-	-	-	-	-	-	-	-
			1999by	Ia91bg	0.56	-	-	-	-	0.64	1.02	-	0.38	-	-	-	
NGC 3074	5144	0.91	1965n	-	0.17	-	-	-	-	0.68	1.02	-	0.35	-	-	1.35	
			2002cp	Ib/c	0.99	-	-	-	-	-	-	-	-	-	-	-	
NGC 3169	1238	0.64	1984e	II	0.47	-	-	-	-	0.58	0.82	-	0.24	-	-	-	
			2003cg	Ia	0.12	-	-	-	-	1.01	1.59	1.99	0.58	0.98	0.40	1.75	
NGC 3184	592	0.93	1921b	II	0.86	-	-	-	-	-	-	-	-	-	-	-	
			1921c	-	1.24	-	-	-	-	-	-	-	-	-	-	-	
			1937f	II P	0.81	-	-	-	-	-	-	-	-	-	-	-	-
			1999gi	II	0.27	0.45	0.83	0.88	1.03	0.38	0.44	0.58	0.06	0.20	0.14	0.62	
NGC 3190	1271	0.34	2002bo	Ia	0.14	-	-	-	-	1.13	1.71	2.05	0.58	0.92	0.34	1.73	
			2002cv	Ia	0.22	-	-	-	-	1.13	1.92	2.51	0.79	1.38	0.59	2.75	
NGC 3198	663	0.38	1966j	Ia	0.65	-	-	-	-	-	-	-	-	-	-	-	
			1999bw	IIIn	0.40	-	-	-	-	0.54	-	-	-	-	-	-	

Table 5.24. (continued).

Host Galaxy	cz	dmn/dmj	SN	Type	r/R	<i>u-g</i>	<i>u-r</i>	<i>u-i</i>	<i>u-z</i>	<i>g-r</i>	<i>g-i</i>	<i>g-z</i>	<i>r-i</i>	<i>r-z</i>	<i>i-z</i>	r-K
NGC 3294	1586	0.51	1990h	II	0.14	1.37	2.04	2.41	2.63	0.67	1.04	1.26	0.37	0.59	0.22	0.96
			1992g	Ia	0.29	1.05	1.70	1.99	2.21	0.65	0.94	1.15	0.29	0.50	0.21	0.99
NGC 3310	993	0.77	1974c	-	0.10	0.47	0.60	0.60	0.67	0.12	0.12	0.20	0.00	0.08	0.08	0.32
			1991n	Ib/c	0.09	0.33	0.44	0.41	0.49	0.11	0.08	0.16	-0.03	0.05	0.09	0.19
NGC 3367	3037	0.88	1986a	-	0.33	1.11	1.59	1.82	2.07	0.48	0.71	0.96	0.23	0.48	0.25	0.57
			1992c	II	0.39	-	-	-	-	0.43	0.71	-	0.28	-	-	-
			2003aa	Ib/c	0.54	0.75	1.29	1.39	-	0.54	0.64	-	0.10	-	-	-
NGC 3504	1534	0.78	1998cf	-	0.01	0.88	1.42	1.55	1.81	0.55	0.67	0.93	0.13	0.38	0.26	0.92
			2001ac	IIn	0.69	-	-	-	-	-	-	-	-	-	-	-
NGC 3627	727	0.46	1973r	II P	0.20	-	-	-	-	0.71	1.04	1.23	0.33	0.52	0.19	1.10
			1989b	Ia	0.19	1.02	1.50	1.75	1.94	0.47	0.73	0.92	0.26	0.45	0.19	0.98
			1997bs	IIn	0.26	1.23	1.77	2.08	2.20	0.53	0.85	0.97	0.31	0.43	0.12	0.83
NGC 3631	1156	0.96	1964a	II P	0.82	-	-	-	-	-	-	-	-	-	-	-
			19651	II	0.50	-	-	-	-	0.16	-	-	-	-	-	-
			1996bu	IIn	0.81	-	-	-	-	-	-	-	-	-	-	-
NGC 3646	4248	0.56	1989n	II	0.41	0.93	1.27	1.41	1.47	0.34	0.48	0.55	0.14	0.21	0.06	0.85
			1999cd	II	0.39	-	-	-	-	0.33	0.47	-	0.14	-	-	-

Table 5.24. (continued).

Host Galaxy	cz	dmn/dmj	SN	Type	r/R	u-g	u-r	u-i	u-z	g-r	g-i	g-z	r-i	r-z	i-z	r-K
NGC 3656	2869	1.00	1963k	-	0.43	-	-	-	-	0.73	1.08	-	0.36	-	-	-
			1973c	-	0.39	-	-	-	-	0.64	0.94	1.03	0.31	0.40	0.09	0.82
NGC 3690	3064	0.83	1992bu	-	0.14	0.91	1.53	1.78	2.01	0.62	0.87	1.10	0.26	0.48	0.22	1.29
			1993g	II	0.60	-	-	-	-	0.57	0.98	-	0.41	-	-	-
			1999d	II	0.69	0.74	1.17	1.49	1.67	0.44	0.75	0.93	0.32	0.50	0.18	-
			2005u	I Ib	0.74	0.35	0.66	0.70	0.90	0.31	0.35	0.55	0.04	0.24	0.20	0.96
NGC 3780	2399	0.81	1978h	II	0.19	1.03	1.51	1.82	1.96	0.49	0.79	0.94	0.31	0.45	0.14	0.86
			1992bt	II	0.23	-	-	-	-	0.64	1.01	1.26	0.36	0.62	0.25	1.06
NGC 3786	2678	0.59	2004bd*	Ia	0.06	1.81	2.78	2.92	3.11	0.97	1.11	1.31	0.14	0.34	0.20	-
			1999bu	Ib/c	0.06	1.60	2.41	2.82	3.12	0.80	1.22	1.52	0.42	0.71	0.30	1.54
NGC 3810	993	0.89	1997dq	Ib/c	1.01	-	-	-	-	0.36	0.54	-	0.18	-	-	-
			2000ew	Ib/c	0.42	0.73	1.33	1.58	1.80	0.60	0.84	1.07	0.25	0.47	0.23	1.00
NGC 3811	3105	0.77	1969c	Ia	0.21	1.45	2.14	2.50	2.71	0.68	1.04	1.26	0.36	0.58	0.22	1.07
			1971k	II	0.55	-	-	-	-	-	-	-	-	-	-	-
NGC 3913	954	1.00	1963j	Ia	0.18	-	-	-	-	0.50	0.71	-	0.22	-	-	-
			1979b	Ia	0.58	-	-	-	-	-	-	-	-	-	-	-

Table 5.24. (continued).

Host Galaxy	cz	dmn/dmj	SN	Type	r/R	u-g	u-r	u-i	u-z	g-r	g-i	g-z	r-i	r-z	i-z	r-K
NGC 3938	809	0.91	1961u	II L	0.83	0.37	0.66	-	0.37	0.29	-	-	-	-	-	-
			1964l	Ib/c	0.19	1.21	1.74	2.06	2.22	0.53	0.85	1.01	0.32	0.48	0.16	0.88
			2005ay	II	0.36	0.54	0.98	1.11	1.31	0.44	0.57	-	0.13	-	-	-
NGC 3947	6197	0.86	1972c	-	1.12	-	-	-	-	-	-	-	-	-	-	-
			2001p	Ia	0.52	-	-	-	-	-	-	-	-	-	-	-
			2006aa	IIIn	0.32	-	-	-	-	0.42	0.68	-	0.26	-	-	-
NGC 3953	1052	0.51	2001dp*	Ia	0.42	2.57	2.15	2.40	2.41	-0.42	-0.17	-0.17	0.25	0.26	0.01	-
			2006bp	II	0.54	-	-	-	-	0.66	1.02	-	0.36	-	-	-
NGC 3977	5807	0.82	1946a	-	0.30	-	-	-	-	0.66	0.95	-	0.29	-	-	0.68
			2006gs	II	0.35	-	-	-	-	0.60	0.89	-	0.29	-	-	-
NGC 3995	3254	0.36	1988ac	-	0.50	0.27	0.39	0.28	0.37	0.12	0.01	0.10	-0.11	-0.02	0.09	-
			2000ez	II	0.28	0.91	1.04	1.09	1.15	0.13	0.18	-	0.05	-	-	-
NGC 4051	700	0.75	1983i	Ib/c	0.32	1.15	1.81	2.11	2.33	0.66	0.96	1.18	0.30	0.52	0.22	1.04
			2003ie	II	0.60	0.35	0.61	0.64	0.82	0.26	0.29	-	0.03	-	-	-
NGC 4157	774	0.13	1937a	II	0.22	-	-	-	-	0.47	0.82	-	0.35	-	-	1.12
			1955a	-	0.43	-	-	-	-	0.59	0.94	-	0.36	-	-	-
			2003j	II	0.30	-	-	-	-	0.94	1.44	1.84	0.50	0.91	0.41	1.84



Table 5.24. (continued).

Host Galaxy	cz	dmn/dmj	SN	Type	r/R	u-g	u-r	u-i	u-z	g-r	g-i	g-z	r-i	r-z	i-z	r-K
NGC 4162	2569	0.61	1965g	-	0.52	-	-	-	-	0.44	-	-	-	-	-	-
			2001hg	II	0.53	0.85	1.09	1.28	1.45	0.24	0.43	-	0.19	-	-	-
NGC 4246	3720	0.34	1975c	-	0.58	-	-	-	-	0.54	-	-	-	-	-	-
			1984u	-	0.47	-	-	-	-	-	-	-	-	-	-	-
NGC 4254	2407	0.87	1967h	II	0.51	0.43	1.06	0.98	1.05	0.63	0.55	0.62	-0.07	-0.01	0.07	-
			1972q	II P	0.63	0.77	1.02	1.14	1.10	0.25	0.37	-	0.12	-	-	-
			1986i	II	0.24	0.60	0.87	1.02	1.11	0.27	0.42	0.51	0.15	0.24	0.09	0.58
NGC 4303	1566	0.89	1926a	II	0.37	-	-	-	-	0.41	0.64	-	0.24	-	-	-
			1961i	II	0.43	0.26	0.40	0.44	0.58	0.14	0.18	-	0.04	-	-	-
			1999gn	II	0.26	0.55	0.86	0.91	1.05	0.31	0.37	0.50	0.06	0.19	0.14	0.95
			2006ov	II	0.27	0.62	0.84	1.00	1.14	0.22	0.38	0.52	0.16	0.31	0.14	0.55
			1964f	II	0.15	1.14	1.69	2.01	2.18	0.55	0.87	1.04	0.33	0.49	0.17	1.06
NGC 4321	1571	0.85	1901b	-	0.51	-	-	-	-	0.68	1.00	-	0.32	-	-	-
			1914a	-	0.50	-	-	-	-	0.65	-	-	-	-	-	-
			1959e	-	0.27	-	-	-	-	0.72	1.05	1.28	0.33	0.56	0.23	0.95
			1979c	II L	0.47	0.91	1.30	1.47	1.49	0.39	0.56	-	0.17	-	-	-
			2006x	Ia	0.22	-	-	-	-	0.64	0.98	1.11	0.34	0.47	0.12	0.84

Table 5.24. (continued).

Host Galaxy	cz	dmn/dmj	SN	Type	r/R	u-g	u-r	u-i	u-z	g-r	g-i	g-z	r-i	r-z	i-z	r-K
NGC 4374	1060	0.86	1991bg	Ia91bg	0.29	-	-	-	-	0.79	1.19	1.38	0.40	0.59	0.20	1.22
			1957b	Ia	0.24	-	-	-	-	0.75	1.16	1.35	0.41	0.60	0.20	1.01
NGC 4526	448	0.33	1969e	-	0.13	-	-	-	-	0.72	1.21	1.39	0.48	0.67	0.18	1.10
			1994d	Ia	0.05	1.83	2.65	3.10	3.40	0.82	1.27	1.57	0.44	0.75	0.30	1.36
NGC 4527	1736	0.34	1915a	-	0.26	-	-	-	-	0.66	0.97	-	0.32	-	-	-
			1991t	Ia91T	0.27	-	-	-	-	0.52	0.97	-	0.46	-	-	-
			2004gn	Ib/c	0.31	1.28	1.97	2.34	2.61	0.69	1.06	1.33	0.38	0.64	0.27	1.38
NGC 4579	1519	0.80	1988a	II	0.26	-	-	-	-	0.59	0.95	1.07	0.37	0.48	0.12	-
			1989m	Ia	0.22	1.16	1.72	2.08	2.25	0.56	0.92	1.09	0.36	0.53	0.17	1.03
NGC 4617	4655	0.17	2005ab	II	0.45	-	-	-	-	0.31	-	-	-	-	-	-
			2007ss	Ia	0.08	1.58	2.49	2.98	3.37	0.91	1.40	1.80	0.49	0.88	0.40	1.56
NGC 4725	1206	0.71	1940b	II	0.50	-	-	-	-	0.58	0.92	-	0.35	-	-	-
			1969h	-	0.09	1.77	2.64	3.08	3.28	0.87	1.31	1.51	0.44	0.64	0.20	1.09
			1999gs	-	0.33	-	-	-	-	0.50	0.82	-	0.32	-	-	-
NGC 4753	1239	0.47	1965i	Ia	0.67	-	-	-	-	-	-	-	-	-	-	-
			1983g	Ia	0.12	1.67	2.38	2.78	2.97	0.71	1.10	1.30	0.40	0.59	0.19	0.90

Table 5.24. (continued).

Host Galaxy	cz	dmn/dmj	SN	Type	r/R	u-g	u-r	u-i	u-z	g-r	g-i	g-z	r-i	r-z	i-z	r-K
NGC 5033	875	0.47	1950c	-	0.67	-	-	-	-	-	-	-	-	-	-	-
			1985l	II	0.27	-	-	-	-	0.31	0.35	-	0.04	-	-	-
			2001gd	IIb	0.52	-	-	-	-	0.42	-	-	-	-	-	-
NGC 5172	4030	0.52	1998cc	Ib/c	0.25	-	-	-	-	0.51	0.73	-	0.22	-	-	-
			2001r	II	0.43	-	-	-	-	0.47	-	-	-	-	-	-
NGC 5457	241	0.93	1909a	II	0.86	-	-	-	-	-	-	-	-	-	-	-
			1970g	II L	0.46	0.21	0.41	0.10	0.00	0.20	-0.11	-	-0.31	-	-	-
NGC 5584	1638	0.67	1996aq	Ib/c	0.24	0.81	1.04	1.26	1.36	0.23	0.45	-	0.22	-	-	-
			2007af	Ia	0.63	-	-	-	-	0.31	-	-	-	-	-	-
NGC 5630	2655	0.32	2005dp	II	0.21	0.67	0.90	0.94	1.07	0.23	0.27	-	0.04	-	-	-
			2006am	II n	0.17	0.71	1.07	1.20	1.30	0.36	0.49	-	0.13	-	-	-
NGC 5668	1583	0.91	1952g	-	0.29	0.74	0.97	1.14	1.04	0.23	0.40	-	0.17	-	-	-
			1954b	Ia	0.20	-	-	-	-	0.38	0.54	-	0.16	-	-	-
			2004g	II	0.46	-	-	-	-	0.29	-	-	-	-	-	-
NGC 5857	4682	0.50	1950h	-	0.83	-	-	-	-	0.54	-	-	-	-	-	-
			1955m	-	0.86	-	-	-	-	0.62	0.96	-	0.34	-	-	-

Table 5.24. (continued).

Host Galaxy	cz	dmn/dmj	SN	Type	r/R	u-g	u-r	u-i	u-z	g-r	g-i	g-z	r-i	r-z	i-z	r-K
NGC 6962	4211	0.79	2002ha	Ia	0.35	-	-	-	-	0.58	1.00	-	0.42	-	-	-
			2003dt	Ia	0.46	-	-	-	-	-	0.58	-	-	-	-	-
NGC 7606	2233	0.21	1965m	-	0.34	1.10	1.71	2.03	2.33	0.61	0.93	1.23	0.32	0.62	0.30	1.17
			1987n	Ia	0.22	1.27	1.94	2.34	2.59	0.67	1.07	1.32	0.40	0.65	0.25	1.19
UGC 4132	5219	0.26	2005en	II	0.15	0.68	1.02	1.19	1.33	0.34	0.51	0.65	0.17	0.31	0.14	0.82
			2005eo	Ib/c	0.48	-	-	-	-	-	0.58	0.87	1.05	0.29	0.47	0.18
UGC 4433	6299	0.80	1984d	-	1.53	-	-	-	-	-	-	-	-	-	-	-
			1999bc	Ib/c	0.45	0.67	1.03	1.12	1.24	0.36	0.45	-	0.10	-	-	-
UGC 6983	1082	0.69	1964e	Ia	0.83	-	-	-	-	-	-	-	-	-	-	-
			1994p	II	1.07	-	-	-	-	-	-	-	-	-	-	-
UGC 7020	6132	0.90	2001cf	IIb	0.91	-	-	-	-	-	-	-	-	-	-	-
			2006c	II	0.91	-	-	-	-	-	-	-	-	-	-	-

Table 5.25. Percentage of grids with non-zero fluxes by color and percentage of grids with numbers of non-zero flux for SDSS bands.

Type	u %	g %	r %	i %	z %	5 c %	4 c %	3 c %	2 c %	1 c %	0 c %	Total SNe
Ia	29	77	72	66	42	27	16	23	6	6	23	137
II	42	81	79	71	34	27	19	26	7	1	19	136
Ib/c	59	90	87	84	50	49	10	26	1	3	10	68
II n	42	74	63	53	37	32	16	5	11	11	26	19
II L	71	71	71	57	14	14	43	14	0	0	29	7
II P	43	71	64	57	43	29	29	0	7	7	29	14
Ia 91T	25	75	75	75	25	13	25	38	0	0	25	8
Ia 91bg	0	63	63	50	38	0	38	13	13	0	25	8
uk	26	69	66	56	30	20	16	19	10	3	31	99
Total	37	78	74	67	38	28	17	22	7	4	22	496

#### 5.3.3.4. Color vs. Radius

The  $u-g$ ,  $g-i$ ,  $i-z$  and  $r-K_s$  colors are plotted against the fractional or galacto-centric radius in units of scale lengths (using 3 scale lengths  $\sim 1$  galaxy radius) in figures 5.589-5.592. The regions chosen, come from galaxies inclined no more than 38 degrees, where by definition, face-on galaxies have an inclination of zero degrees. Greater inclinations give incorrect radial position information. The  $u-g$  color shows the most obvious radial dependency as UV light is effected heavily by dust extinction, which is concentrated toward the center of galaxies.

The collection of environments between  $1.5 < u-g < 2.0$  are a mixture of both spiral types and elliptical galaxies for normal Ia. The over luminous Ia appear to obey the opposite trend and get redder with increased radius, but the limited number of points. Type II colors are much more concentrated to colors of  $u-g < 1.2$  and Ib/c are in slightly redder centers of galaxies with values of  $u-g < 1.5$ , again confirming what was found in the grid analysis. The  $g-i$  colors for all three types have less of a radial dependence as the  $u-g$  data. Type II has the broadest color range and Ib/c colors are very concentrated towards the center. Ia events are red and 91bg events are constant in color, which is to be expected since E/S0 galaxies have narrow color ranges. The  $g-i$  color for 91T Ia types also spans a narrow range without much scatter like the normal Ia data. The color is

almost constant except for a slight dip toward the outer radii. All three 91T data points are from three different spiral type galaxies. Two of the points, 1998es and 1999dq, come from identical regions on arms and the third point, 1998ab, is located between spiral arms.

### 5.3.3.5. Color-Color Plots

Color diagrams indicate if there is a special population of stars that produce specific SNe, type and if the color differences are large enough, can provide information on age and metal abundances. Here, colors are plotted for pairs,  $u-g$ ,  $g-r$ ;  $g-r$ ,  $r-i$ ;  $r-i$ ,  $i-z$  and  $u-r$ ,  $r-K_s$ , divided by major SN type (figures 5.593-5.596). The error bars were not included for clarity, but the errors are, at most, 0.1 for all of the SDSS bands and 0.2 for  $r-K_s$ . The core collapse subtypes have been placed in a separate plot and the sub Ia types are plotted together with normal Ia. Here, SNe Ia will first be discussed followed by core collapse SNe.

The color plots for SNe Ia show the data deviating away from the reddening vector due to intrinsic differences in the stellar populations. The points clustered towards the top right of all the Ia plots (most visible in either the  $u-g$  or  $u-r$  bands) are regions from E/S0 galaxies and indicate an older stellar population. The Ia  $g-r$ ,  $r-i$  plot also shows data aligned to the reddening vector, meaning that the Ia stellar population colors do contain dust as well as having differences due age or possibly metal abundance. Interestingly, Ia 91T types cluster with similar colors in the  $g-r$ ,  $r-i$  plot, meaning that 91T types come from a very specific, similar environment (other than regions of low or no flux) of the same age and dust content.

The last color pair,  $u-r$ ,  $r-K_s$ , was determined by Li and Han (2008; hereafter LH08) to break the age-metallicity degeneracy based on stellar population synthesis models (Bruzual and Charlot 2003). The  $u-r$  color is sensitive to age and the  $r-K_s$  color is a strong indicator of metals. For example, a very red color for both bands indicates an old, metal-rich stellar population. The color pairs derived in LH08 are based on SDSS filters system and colors similar to 2MASS, so they are very appropriate for this data.

There is a clear separation of SN region colors in the Ia data corresponding to redder galaxies. This separation at  $u-r = 2.2$  was first noted by Ivezić et al. (2002) when characterizing the colors of galaxies in SDSS data. Galaxies with  $u-r > 2.2$  correspond to red ellipticals and S0 types with stellar population ages greater than 4 Gyr. The lower leftmost regions on the Ia plot of figure 5.596 are metal rich and young  $\sim 0.5$  Gyr. The 91T type SNe come from metal rich regions with ages less than 2 Gyr, which contradicts the theory that higher metallicity in progenitors makes dimmer explosions. In fact, all normal and 91T type Ia are in metal rich regions and vary only by age and dust. Points to the far upper right correspond to highly dusty, reddened regions 2003cg and 2002bo.

In contrast to the Ia population, types II and Ib/c show similar ages, but differ only by dust extinction and reddening. Core-collapse types span a larger range of colors than Ia, particularly towards the blue range. Figure 5.596 indicates that type II and Ib/c stellar populations are young ( $\sim 0.5$  Gyr) and have average metal abundance. The core collapse stellar colors are consistent with A and F star light, whereas Ia regions have light similar to G type or cooler stars. Under luminous Ia have colors closest to K stars (Finlator et al., 2000).

### 5.3.4. Environment Colors and Supernova Peak Colors

#### 5.3.4.1. Template Color-Color Plots

The color-color plots (fig. 5.597) of only the SNe Ia used as light curve templates show clumps of points divided between the younger spirals and ellipticals. Two distinct groups of points are evident in the  $u-g$ ,  $g-r$  and  $g-r$ ,  $r-i$  plots, differing by reddening and age. In the  $u-r$ ,  $r-K_S$  plot, four points (2001fe, 1999dq, 1999cc, 1995al) have similar regional and supernova colors (see next section about SN colors). Five out of the six right most points are dusty environments near high flux regions. Only one, 2006n, comes from a galaxy with E/S0 colors. But the rest can be extrapolated back to the similar group of points near  $u-r=1.5-2$  and  $r-K_S=1$ , reaffirming that most of these objects used in SN cosmology come from a similar population of stars with high metal abundance, ages 0.5-2 Gyr and differing amounts of dust.

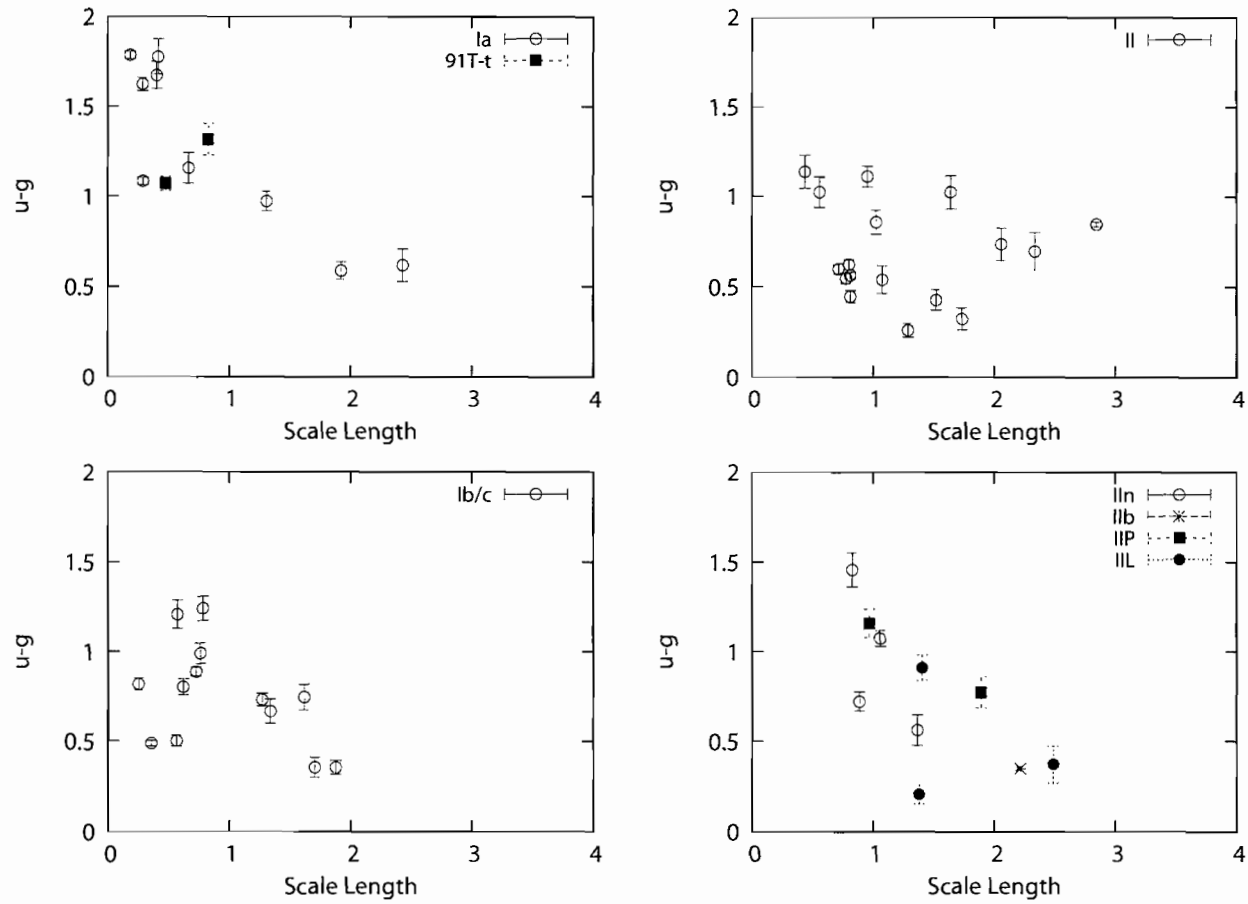


Figure 5.589. The  $u-g$  color plotted as a function of radial distance (in units of scale length) from the host galaxy center. All points are from galaxies with inclinations less than 38 degrees from face on.



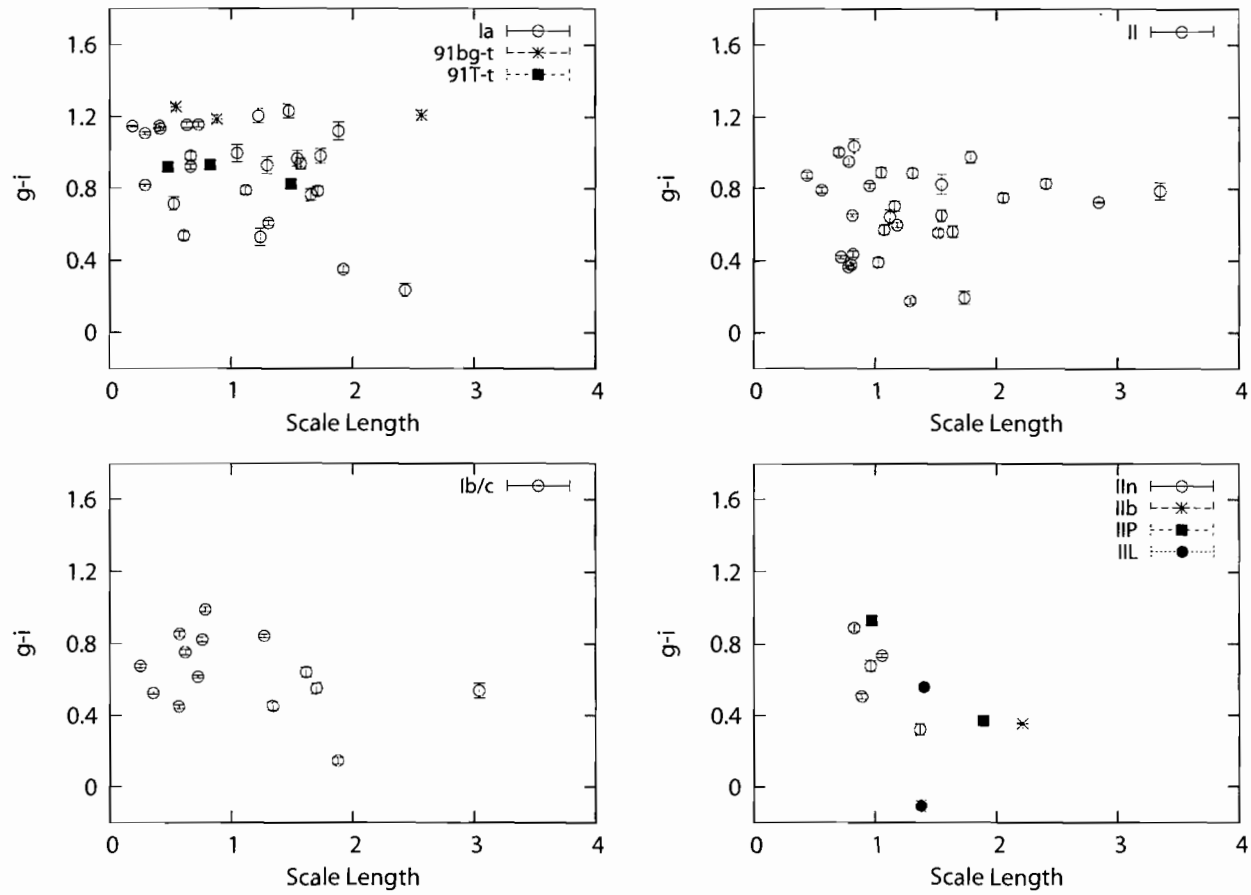


Figure 5.590. The  $g-i$  color plotted as a function of radial distance (in units of scale length) from the host galaxy center. All points are from galaxies with inclinations less than 38 degrees from face on.

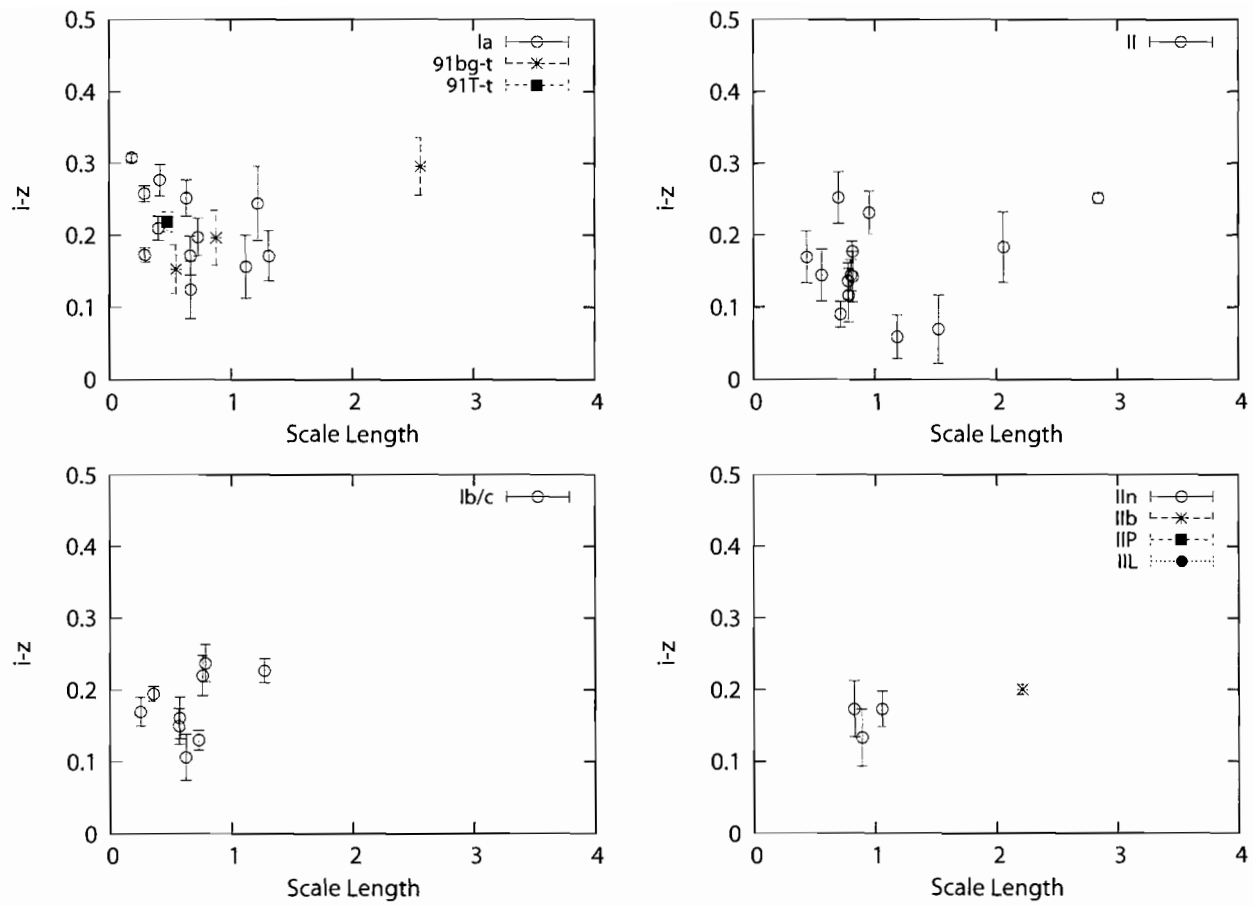


Figure 5.591. The  $i-z$  color plotted as a function of radial distance (in units of scale length) from the host galaxy center. All points are from galaxies with inclinations less than 38 degrees from face on.

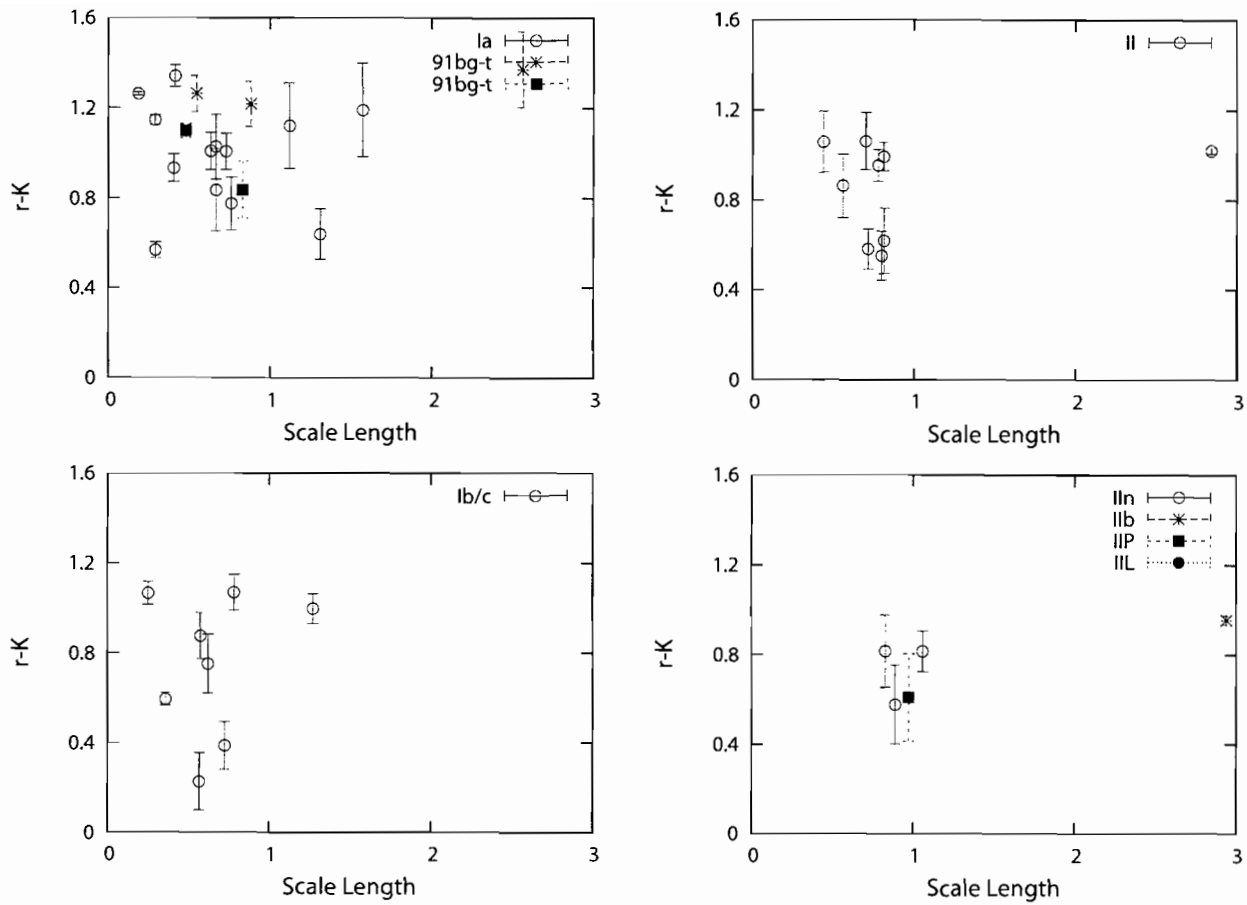


Figure 5.592. The  $u-K_s$  color plotted as a function of radial distance (in units of scale length) from the host galaxy center. All points are from galaxies with inclinations less than 38 degrees from face on.

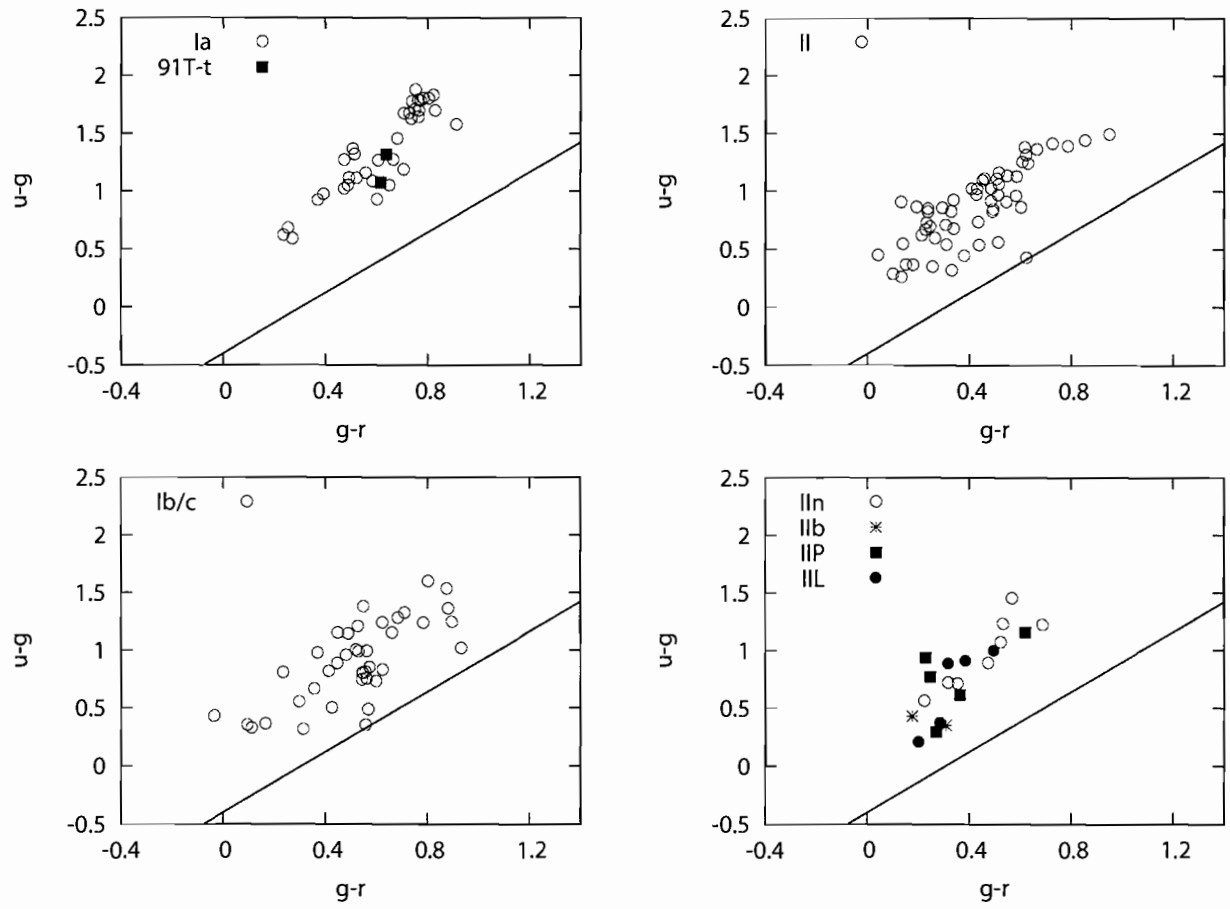


Figure 5.593. The  $u-g$ ;  $g-r$  color-color plots for type Ia and subtypes, II, Ib/c and all other core collapse SNe. The diagonal line in each plot indicates the reddening vector.

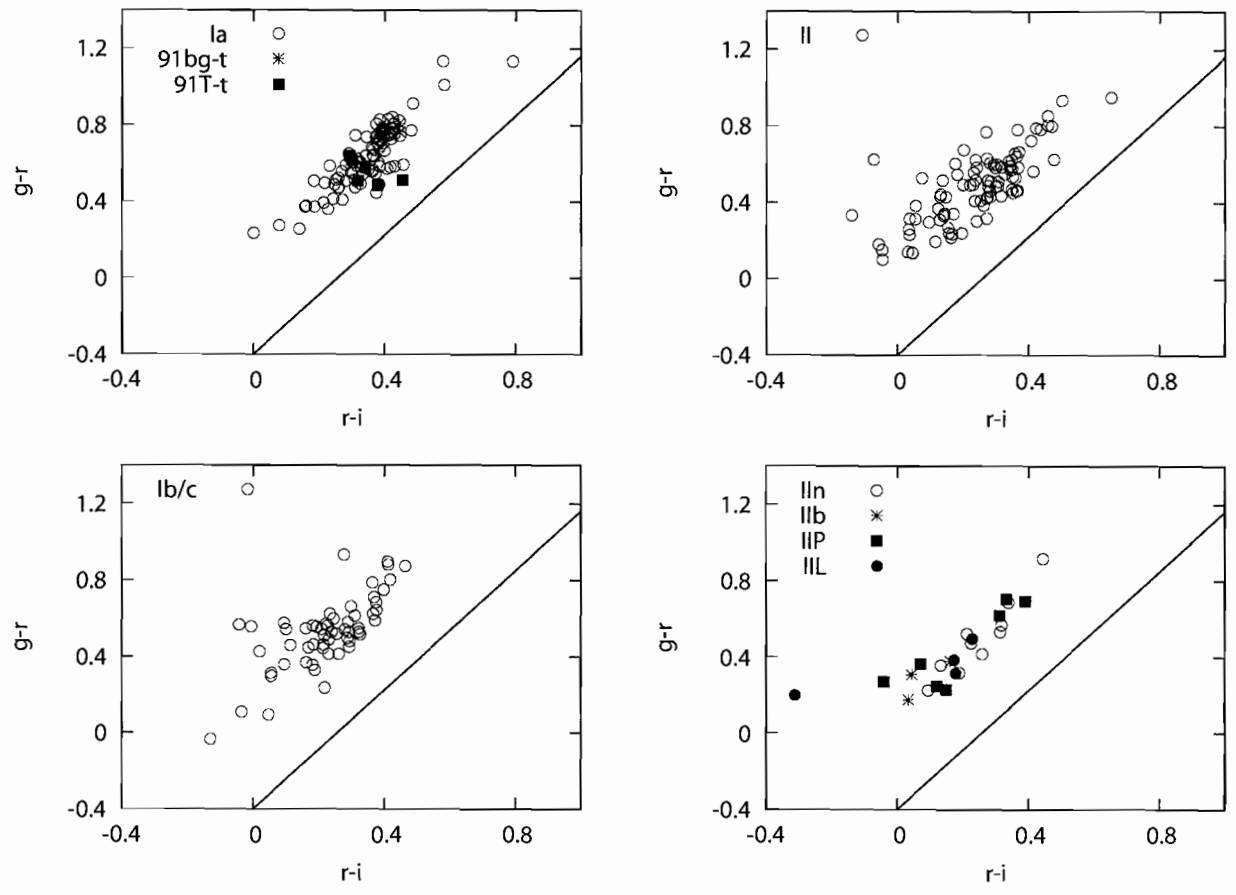


Figure 5.594. The  $g-r$ ;  $r-i$  color-color plots for type Ia and subtypes, II, Ib/c and all other core collapse SNe. The diagonal line in each plot indicates the reddening vector.

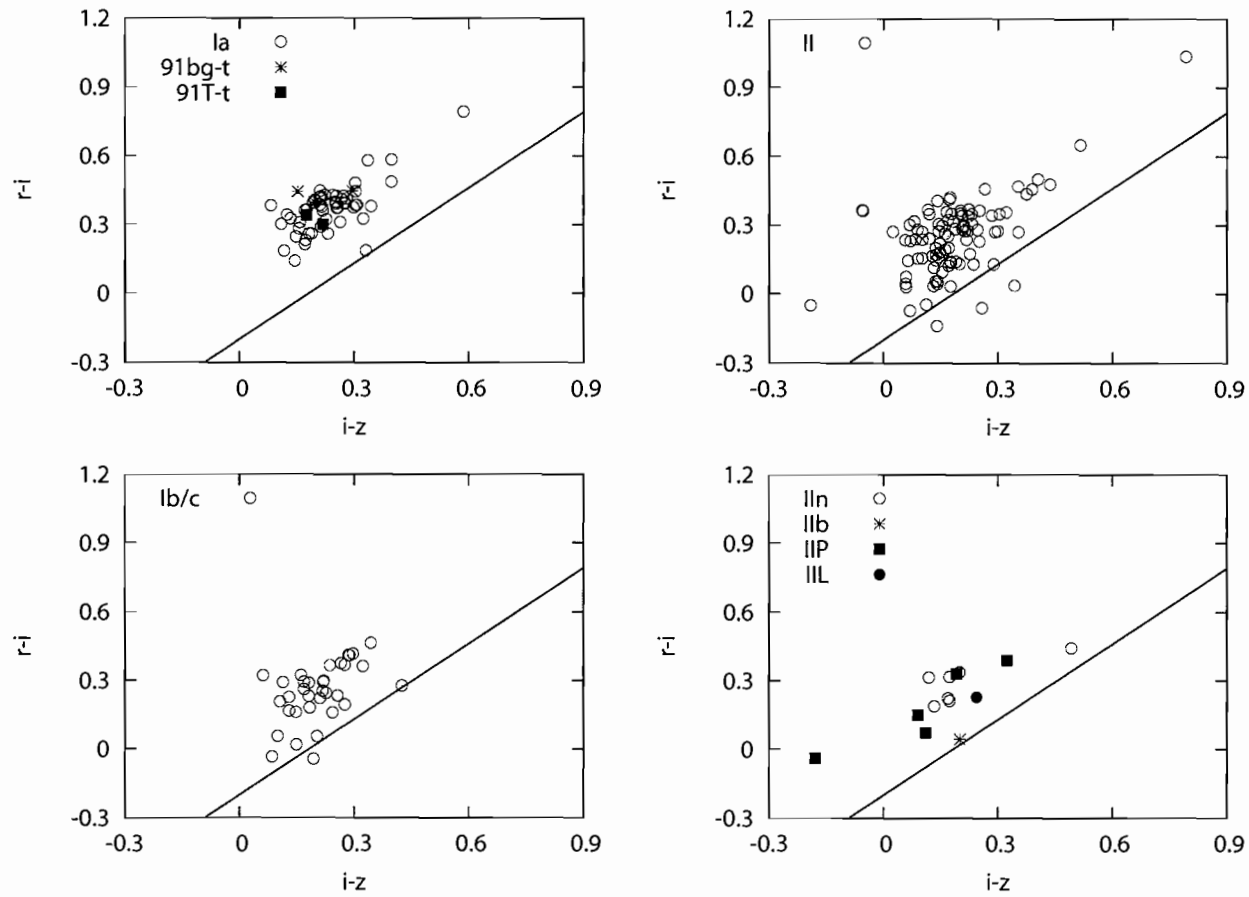


Figure 5.595. The  $r-i$ ;  $i-z$  color-color plots for type Ia and subtypes, II, Ib/c and all other core collapse SNe. The diagonal line in each plot indicates the reddening vector.

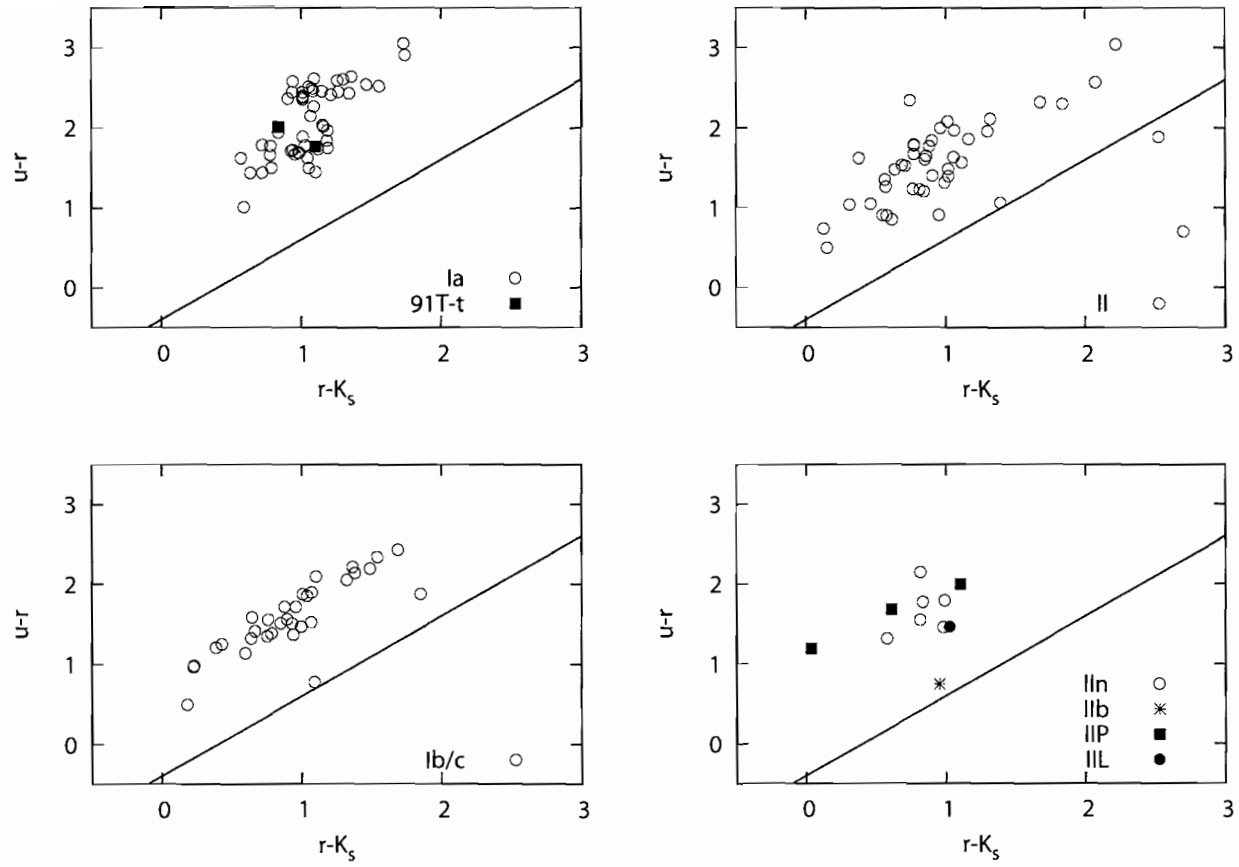


Figure 5.596. The  $u-r$ ;  $r-K_s$  color-color plots for type Ia and subtypes, II, Ib/c and all other core collapse SNe. The diagonal line in each plot indicates the reddening vector.

Unfortunately, 91bg types cannot be plotted in the Ia diagrams in figure 5.593 and 5.596 due to their lack of UV flux. We can, however compare the average  $r-K_S$  colors of 91bg types to normal Ia for similar galaxy types. The average  $r-K_S$  color for under luminous Ia is  $(r-K_S)_{ave} = 1.29(07)$  and for normal Ia from elliptical galaxies this is  $(r-K_S)_{ave} = 1.12(10)$ , where the error is indicated in parenthesis. Clearly, there is a difference in the  $K_S$  flux for 91bg type regions in comparison to normal Ia environments. The fluxes from all bands are less in under luminous Ia in comparison to Ia, and a larger ratio of  $K_S$  to other colors in 91bg type events.

#### 5.3.4.2. Template Supernova Colors

A true test of any SNe dependence on environment is to compare the environmental colors, against the peak colors of the SNe. This is done using again the three pixel radii aperture measurements and published SNe peak magnitudes taken from Wang et al. (2006), supplemented by Hicken et al. (2009) and Folatelli et al. (2010). In all there are 48 peak  $B_{max}$  and  $V_{max}$  found in the literature corresponding to the SDSS regions with thirty seven from Wang et al. (2006), eleven from Hicken et al. (2009) and two from Folatelli et al. (2010). All three data sets have been corrected for Galactic extinction and K-corrected, but no other correction has been applied. Some supernovae are duplicated in both papers, but only differ by from 0.0 to 0.05 in B-V color. The sample is reduced to 34 data points that have environmental colors brighter than the cutoff in  $g$  and  $r$ .

Comparing the peak  $B_{max}-V_{max}$  supernova colors against the environmental colors (using the same cutoff criteria as the grid data) indicates a correlation between increasing red B-V colors and regional  $g-r$  colors (figure 5.598). In order to determine if this is a significant trend, the environment colors are divided into two groups, ones that had peak supernova colors of  $B_{max}-V_{max} < 0.24$  and one that had colors  $B_{max}-V_{max} > 0.24$ . The average  $g-r$  color for these two bins are  $(g-r)_{<0.24} = 0.57$  and  $(g-r)_{>0.24} = 0.68$  respectively, with a total population average of 0.61. A z test on these points indicates that the  $B_{max}-V_{max} < 0.24$  population is significantly bluer and the  $B_{max}-V_{max} > 0.24$  is significantly redder than the total population average. If we eliminate edge on galaxies, the averages



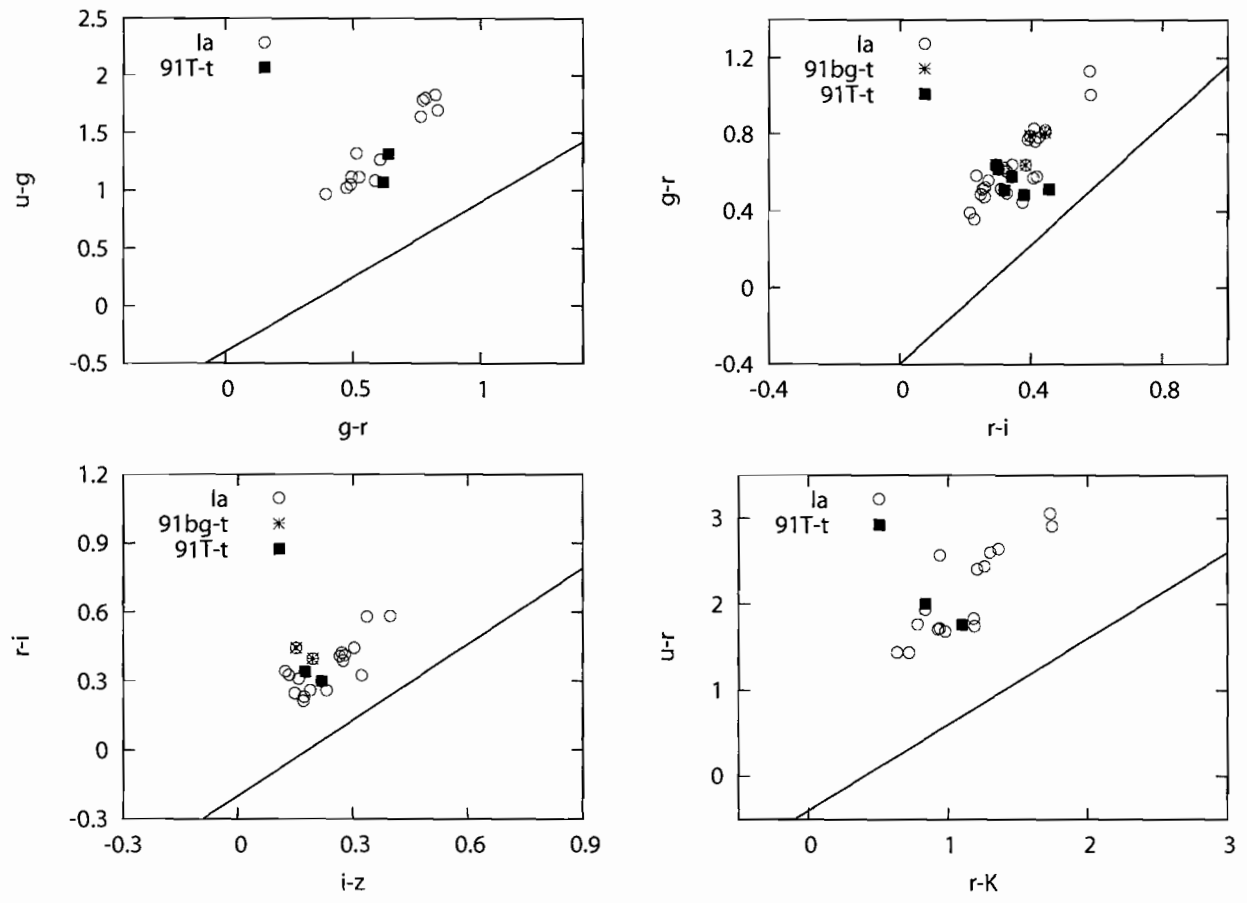


Figure 5.597. The color-color plots for all Ia and Ia subtypes used as light curve templates in supernova cosmology. The diagonal line in each plot indicates the reddening vector.

become  $g-r = 0.55, 0.67$  and  $0.61$ , respectively. The difference in reddening between the two groups is still significant, but not as much when considering the entire sample. Of this smaller group, three are under luminous 91bg-type events (1991bg, 1997cn, 1999by), four are over luminous 91T-type events (1998ab, 1998es, 1999aa, 1999dq). Or separating by galaxy type, three SNe come from E/S0 galaxies (1991bg, 1997cn, 2006n) and 25 regions are from spiral galaxies. One could argue that most of the redder  $B_{\max}-V_{\max}$  colors in the  $B_{\max}-V_{\max} > 0.24$  bin are dominated by 91bg events coming from elliptical galaxies because this type of galaxy has consistent colors of roughly  $g-r \sim 0.8$ . However, this is not the case as figure 5.599 shows the same plot, but divided by galaxy type. Regions from elliptical galaxies account for only points in the middle of the diagram and not the reddest points. SN 2006N is the only normal Ia that comes from an elliptical galaxy where the peak B-V color is substantially blue  $-0.01$ . The other two SNe from elliptical galaxies are indeed 91bg events, and their peak colors are between  $0.5 - 1$ , but again, they aren't the reddest of this sample. All of the 91T events have blue SN  $B_{\max}-V_{\max}$  peak values as well as come from bluer  $g-r$  regions and 91bg events are all from redder regions relative to the 91T type events.

It is difficult to tell if there is a similar trend in other bands. Both the  $u-g$  and  $r-K_S$  colors are missing several data points (figure 5.600) at redder B-V values and the errors are large in the  $r-K_S$  plot. The red and infrared colors,  $r-i$  and  $i-z$ , do not indicate any correlation with increased B-V either. The  $r-i$  plot may show a slight increase in red color with larger B-V, but for the most part, the environment colors are between  $0.2 < r-i < 0.4$ . Both Ia template  $r-i$  and  $i-z$  plots span a much narrower range in color than the entire Ia sample supporting the idea that most of these SNe came from similar parent stellar populations and vary in color due to dust.

## 5.4. Discussion

There were several results in the data presented here. The most relevant to supernova Ia cosmology will be discussed and the rest of the results will be outlined.

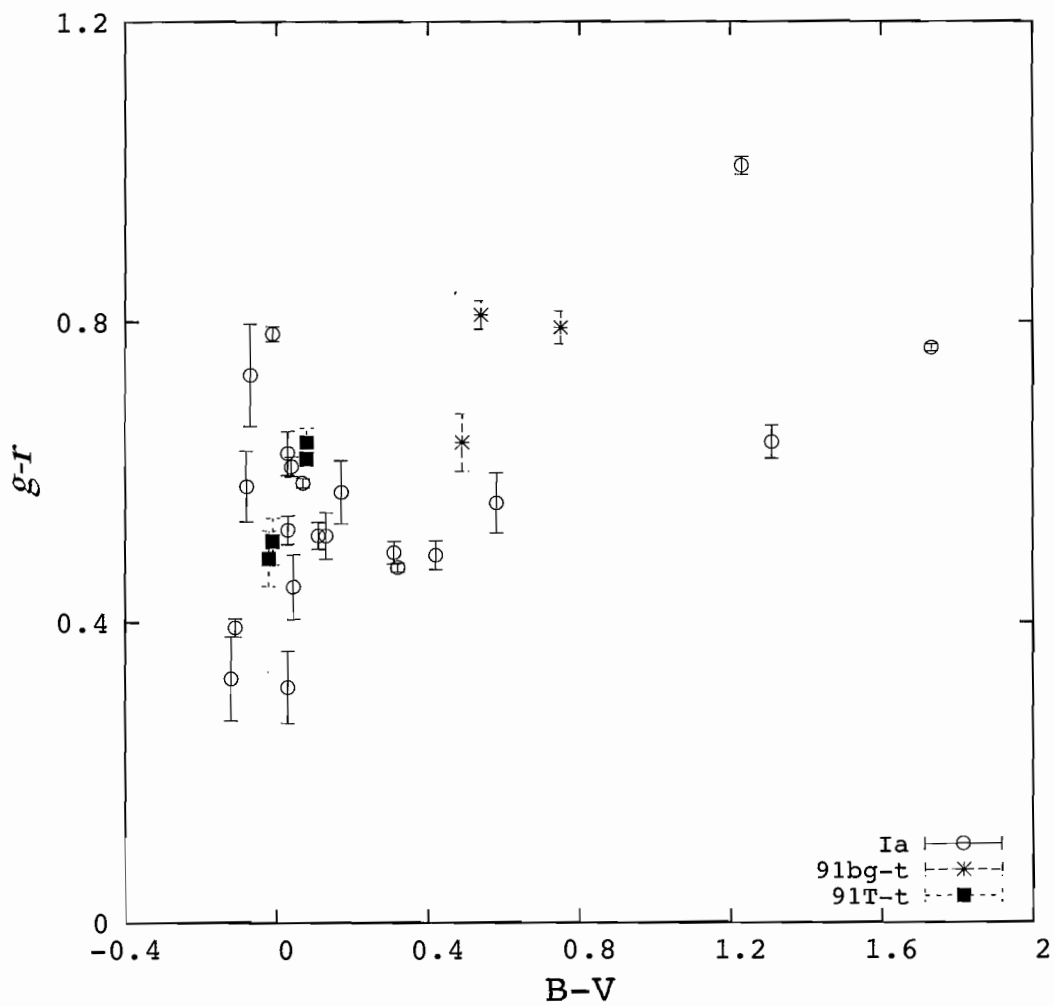


Figure 5.598. The environment  $g-r$  color vs. supernova peak color for template Ia SNe.

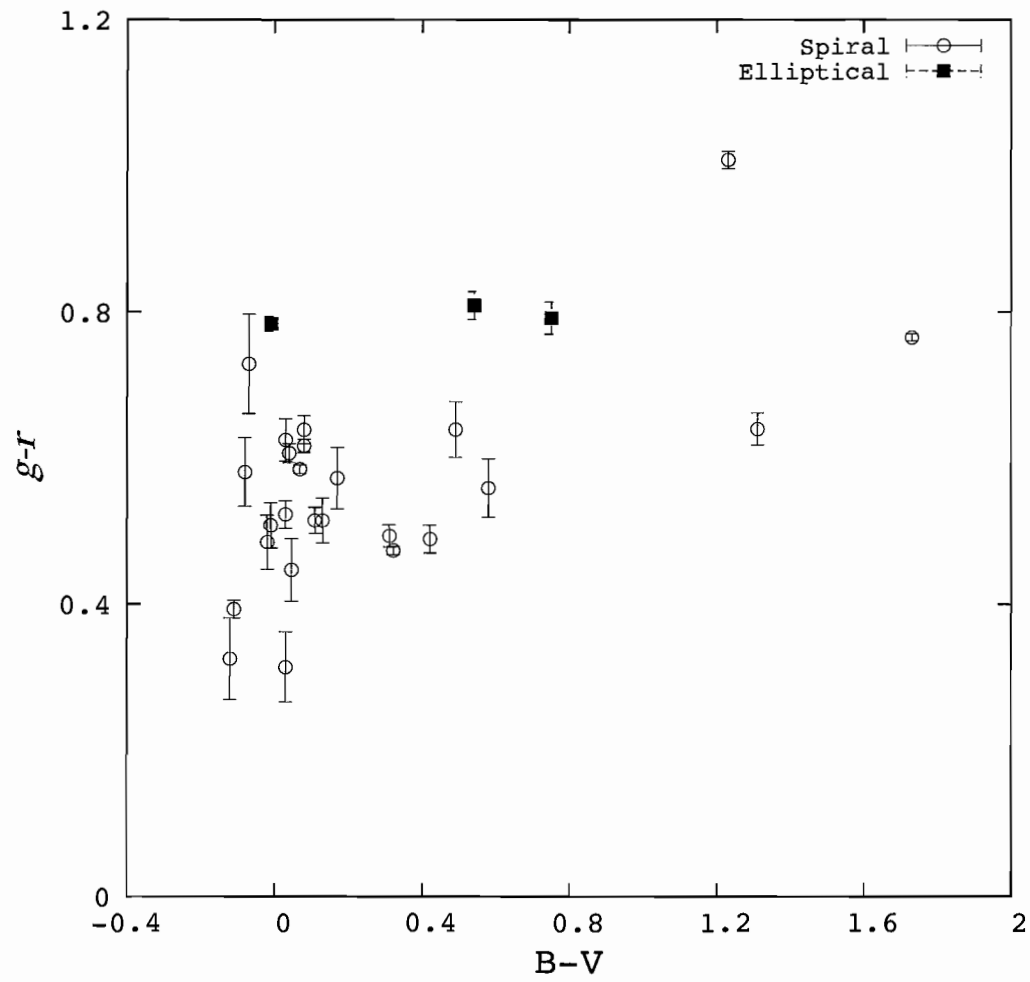


Figure 5.599. The environment  $g-r$  color vs. supernova peak color for template Ia SNe. Here the elliptical galaxies are distinguished from the spiral galaxies.

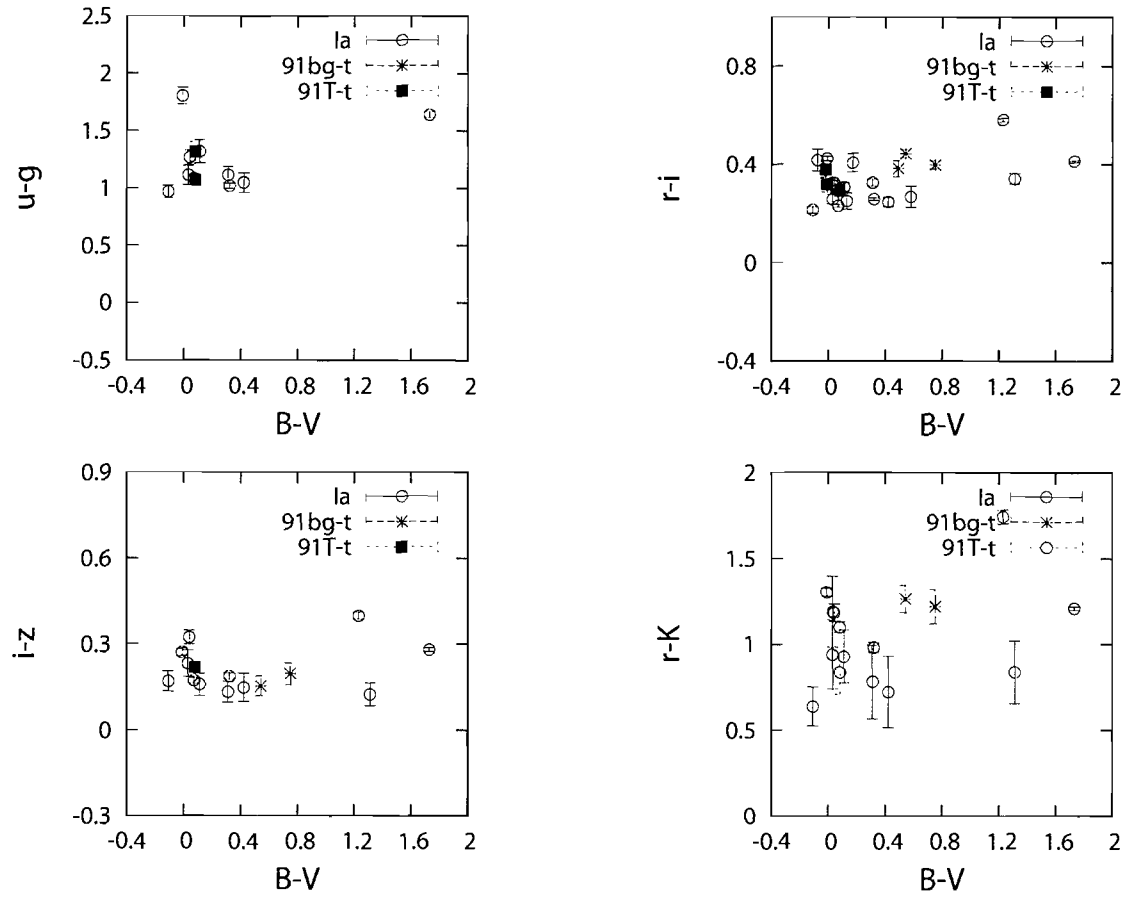


Figure 5.600. The environment color-SN peak color plots for template SNe Ia.

### *Template SN Ia Environment Colors*

Perhaps the most interesting result from this work is the correlation of peak supernova Ia colors with the environmental backgrounds. The color-color plots indicate that all SNe Ia come from similar metal rich regions, but differ in dust and age. Ages range from 0.5-2 Gyr for SNe in spiral galaxies and over 4 Gyr for the elliptical galaxies. Evidence of dust similar to the Milky Way in template Ia regions from the pCMD maps corresponds to redder peak colors in some of the SNe. Wood-Vasey et al., 2008 and Nobili et al., 2009 have suggested measuring the rest frame I band light curves for all distances of SNe to remove the problem of dust and reddening. In fact, efforts to prove that SNe are good standard candles in near infrared (NIR) (Freedman et al., 2009) have increased because of better CCD sensitivity and the interest in distant, redshifted optical light curves.

However, the problem with using I band light curves is that the flux is much smaller in comparison to the optical colors. The apparent brightness is about 1.5 magnitudes dimmer than it is in blue, which may exacerbate selection effects at high redshifts. If IR light curves do eliminate the dust problem, then it is possible to disentangle the effects due to age and to see if SNe Ia are capable of being standard candles.

### *91bg Environments*

The unique environment for Ia 91bg events is cause for concern. None of these events occur in significant  $u$  band flux regions, independent of radial distance to the center of the host galaxy, whereas normal Ia appearing in similar E/S0a galaxies, have no correlation of the kind. Type 91bg Ia also occur in the redder, low-flux portions of these regions whereas Ia do not, containing more far infrared flux than other colors. There are two possible reasons for this result. The first reason might be that the stellar population consists of the oldest and smallest (sub-Chandrasekhar) mass stars, hence low amount of UV flux. If these events are created from double degenerate mergers, then the combined mass of each dim, old star must not equal  $1.4M_{\odot}$ , creating sub-luminous events. The other possible reason is dust. Dust effects UV light more than optical colors, however, it does redden optical colors. From the pCMD diagrams, dust is not readily apparent in two

of the 91bg type events and plots, and the other 91bg regions are inconclusive. But this doesn't mean dust is not present. There are few grids for these regions and it would be worth pursuing further with higher resolution images.

### *Ia Structure Colors*

On average, colors of SNe Ia regions are redder than any core-collapse SNe region independent of structure type. The redder colors simply reflect that Ia come from older environments, with higher metal abundances than the core-collapse SNe, as demonstrated by the average structural colors and by the  $ur-rK_S$  color-color plots. SNe Ia have no preference for brighter, bluer, dimmer or redder regions. They occur in any region unlike type II and Ib/c, which map out the brightest areas on arms and structures of galaxies.

### *91T Type Environmental Colors*

SN Ia 91T regions show similar environmental colors, yet the pCMD plots of these objects all vary. Visually, some of these objects come from very similar regions (arms) on different galaxies. It could mean that the companion stars are all from similar age populations or simply that these regions are less dusty than normal Ia. Like the 91bg regions, this needs to be pursued further with more data and higher resolution images.

### *Other results*

- Type Ib/c do occur in redder environments than type II indicating that Ib/c are more frequent in metal rich environments as shown by the average regional  $i-z$  colors.
- SNe IIL are from the bluest regions in galaxies. It is unclear if the blue flux from these areas is from x-ray emission from a stellar remnant or a population of very young massive stars.
- Core collapse SNe do come from the brighter regions of galaxies, confirming Kelly et al. (2008) findings.

## CHAPTER VI

### SELECTION FUNCTION

#### 6.1. Monte Carlo Simulations

The second portion of this thesis research was estimating the true rate of SNe Ia in the local ( $z < 0.1$ ) Universe based on the Earth's observational selection function for the past 70 years. Determining the local supernova rate has been an ongoing, unresolved problem in supernova cosmology because of the limited number of galaxies searched by a supernova group – as the calculated rates vary based on different searches and galaxy samples. For cosmologists, the SNe Ia rate can provide clues to the progenitor which enables better models (Mannucci, 2009) and light curve simulations. The rate can indicate the age of the progenitor system using the delay time distribution (DTD). A well-modeled DTD describes the span of time between formation of the stellar population and the supernova explosion. If the rate is best characterized by a short time DTD  $< 1$  Gyr, this means that most white dwarf progenitors come from massive main sequence stars and are more than likely a single degenerate system, that is the companion is not a white dwarf. Longer DTDs mean that the SNe Ia arise from white dwarfs evolved from smaller main sequence stars and potentially double degenerate systems. The two-component model was a solution to the discrepancy of a large SNe Ia rate in spiral galaxies and smaller rate in elliptical galaxies.

Perhaps not as obvious, but very important, is that the rate provides information about the variability in the white dwarf progenitor, based on the observer bias. If for example, von Hippel et al. (1997) and Kasen et al. (2009) models are accurate physical descriptions of the peak luminosity scatter, then there will be a much higher rate of SNe



Ia at  $z < 0.1$  than at  $z > 1$ , simply because observers can see both the brighter and dimmer events occurring nearby. Therefore in order to test if intrinsic variability will decrease the number of distant SNe detected, the local rate needs to be determined. But before a rate is calculated, there needs to be an understanding of the observational biases and how they effect the extrapolated SN rate. Firstly, the rate must be based on data from within a limited redshift range so that results are meaningful and not averaged out. The range must be small enough so that most observers can detect dim events without requiring a large observatory telescope, but large enough to contain a significant number of ( $>50000$ ) galaxies. A small range also guarantees that cosmological effects won't be a factor in the calculation. Modern SNe Ia search efforts have moved to further redshifts ( $z > 0.2$ ), where the number of galaxies in one image increases by  $z^3$ . Searching at greater distances is a much more efficient way to find SNe, as it allows for more galaxies in one image and increases the probability of detection. But measuring the SNe Ia rate in the high redshift regime introduces a new set of systematic errors into the data set. Cosmological and selection effects like the Malmquist bias can alter the data along with more common dispersive effects such as dust.

If, on the other hand supernova rates increase with redshift, then this means that the average star formation rate at  $z > 1$  is much larger than nearby populations, implying that most of these distant progenitors are younger (and brighter) than the nearby population of SNe. If distant rates decrease, then most SNe are missed and only the overly luminous events or SNe in a particular environment are detected. For example, if normal Ia are selected against and brighter events are over-selected in comparison to the nearby ratio of normal to bright Ia, then these over-luminous events mimic a cosmology where the Universe appears to decelerate at higher redshifts. In other words, the distance modulus is underestimated when confusing the over-luminous and normal types.

The more subtle effect of the Malmquist bias is that selection effects alter the randomness of the distant sample by skewing the distribution to only brighter events. Therefore the error in dispersion doesn't decrease due to higher sample numbers as  $(1/N)^{1/2}$  because the distant SNe are not necessarily from a random sample. The

dispersion will undoubtedly decrease with more measurements of overly bright and distant SNe, but will be an erroneous description of the dispersion in the entire, unbiased sample of SNe. With a better understanding of how many SNe Ia to expect at far distances based on the local sample, observers will be able to determine if SNe are capable of measuring an accurate cosmology.

### 6.1.1. Target Galaxy Selection

An accurate determination of the local Ia rate requires a representative sample of all types of galaxies within a predefined volume. The most unbiased search is a blind, random pointing in the sky, and outside the plane of the Milky Way where each type of galaxy is observed, from the largest elliptical and brightest spiral to the dimmest dwarf and low surface brightness galaxy. Usually a search like this is primarily observing some other phenomenon such as near Earth objects or surveying the sky instead of looking for SNe. If it is a dedicated SN search, targets are galaxy clusters or small patches within particular RA and Dec. There might be a bias searching only clusters. A galaxy with an elevated SNe production can dominate and skew the interpreted rate. The same might be true for selecting too small a region. Most observers generate a target list of galaxies from the RC3 (see chapter IV) catalog. Amateurs with CCD cameras, are typically limited to 19<sup>th</sup> magnitude objects, so it makes sense to observe the nearest and brightest galaxies. Traditionally, the RC3 was also the choice for professional SN observers, (e.g. BAO Survey, Qiu, Hu & Li, 2001; LOSS, Li et al., 2000; Filippenko et al., 2000) but now bigger groups are pushing the limits of detection and no longer rely on the RC3 catalog.

As discussed in chapter IV, the RC3 collection consists of 23,000 bright galaxies within a volume of  $z = 0.1$ , in comparison to over 500,000 galaxies catalogued to date for the same volume. If the majority of local events detected come from the RC3 galaxies and not the larger collection of galaxies within the same volume, then how do we know that properties of these events adequately represent all SNe if we're only observing 5% of the galaxies? The findings of Sullivan et al. (2010) state a correlation between host galaxy luminosity (or mass) and the supernova peak brightness. Brighter and more

massive galaxies produce brighter SNe Ia by an average of 0.08 magnitudes. If the RC3 catalog contains the brightest and nearest galaxies, then the observed SN Ia population is skewed and biased because most discoveries come from RC3 galaxies. In fact, Sullivan et al. (2010) further conclude that galaxies decrease in mass with distance, introducing a systematic error into the data set for galaxies at large distances. Therefore it is crucial to observe SNe Ia in all types of galaxies within a volume to ensure fewer biases. Figure 4.10 in chapter IV puts perspective on comparing the number of RC3 galaxies to the larger sample of galaxies at the same distance. About 99% of RC3 galaxies have redshifts less than 15,000 km/s. At this same distance, there are over 160,000 galaxies listed in all catalogs. And it is not unreasonable to think that this present count of galaxies is a lower limit. There is a decrease in the number of galaxies catalogued past 25,000 km/s compared to the 22,500 to 25,000 km/s redshift bin, indicating that selection effects are very much present in all catalogs.

### 6.1.2. Selection Functions

In this work, selection functions are considered a mathematical description of the observational conditions for supernova detections. Selection functions contain information about the detection capabilities of the telescope and the amount of time spent observing each candidate host galaxy. Selection functions are a necessary prior step to determine supernova rates because rates depend on the observational times of each target galaxy. A complete model of the observing conditions will also eliminate errors in the data set due to observer bias.

Observational selection functions are modeled for individual data sets (e.g. Dilday et al., 2010), but not for all SNe Ia discovered from different searches. The inhomogeneity of the data sets is daunting and observational details are usually lacking. Ideally, to reduce the dependence of the rate on the selection function, all galaxies within a defined volume should be observed in a world wide collaborative effort to measure the most accurate rate. For practical reasons, this is impossible, not only for coordinating the data and observations, but for the reason that most galaxies aren't visible the entire year.

However, at mid latitudes, a large area consisting of circumpolar galaxies could be watched by several observers throughout the year. This would be a representative sample of all galaxies provided that every square arc second is monitored each night. Such an effort would eliminate most selection effects, and allow for the most honest rate calculation.

The first attempt at a collaborative rate measurement was a combination of five SNe searches (Cappellaro et al., 1997). Data was from four photographic and one visual search. Unfortunately, there were only 7700 galaxies observed, and by today's standards, this isn't a large sample. Presently, there are cross collaborations, such as the Supernova Cosmology Project (SCP; Perlmutter et al., 1997), that combines the data from 10 or more independent data sets encompassing distances out to  $z \sim 1$ . This is too large a volume to determine a rate. In fact, most SCP data is used to measure light curves and add high redshift data to the Hubble diagram. Rate considerations from the SCP are only for the distant samples (Kuznetsova et al., 2008; Pain et al., 2002). Rate estimates from other groups span 0.125 to 0.26 SNU (Blanc et al., 2004; Yasuda et al., 2009) for  $z < 0.3$ . But again, all modern searches use data from their observations and do not combine data with other supernova searches.

### 6.1.3. Host Galaxy Dust

The previous discussion highlights the need for consistent observations of SNe for an accurate rate. However, even with consistent observation, there are intrinsic qualities to supernovae that can effect the selection function. Unlike the consideration for completeness in target lists, dust of some form, has been explored as a mechanism causing either the dispersion in peak Ia magnitudes in the same redshift range or an alternate explanation for the appearance of an accelerating Universe. The later is referred to as a grey dust model and for now, hasn't proved as a possible explanation for the dim, distant SNe Ia data (e.g. Nobili et al., 2005; Corasaniti et al., 2005; Robaina et al., 2007). The former refers to dust from the host galaxy or supernova explosion. It is estimated from spectra or from the deviation of the peak brightness from the template SNe. For

details on a selection of dust estimation techniques, see chapter V. Dust has the opposite effect of the Malmquist bias. Objects appear dimmer, which can either lead to overestimating the distance modulus (for distant galaxies) or can give the impression of an under luminous SN. Usually the degree of reddened peak SN colors indicate dust or an under luminous event for nearby SNe and therefore eliminate these data from the sample. However, this is where grey dust can still be a factor in the supernova picture. Grey dust is independent of wavelength and its effects are seen as dimmer magnitudes, not redder colors. The dust grains are large ( $\sim 0.1 \mu\text{m}$ ) due to an elimination of smaller dust particles from some expulsion mechanism, such as star formation or supernova explosions. Grey dust may not be prevalent enough to sufficiently model the observed cosmology, but its presence hasn't been completely ruled from all galaxies. Therefore, it becomes difficult to distinguish between intrinsically dimmer SNe, distant SNe and dusty SNe and increases the scatter in the cosmological data. To make matters worse, it is unclear how much extinction and reddening is due to dust in the host and dust from the supernova explosion and whether dust from either of these sources is similar.

Regardless of the source, it is crucial to determine how dust alters the perceived SNe Ia rate and magnitude distribution, accurately. Dust is visible at low redshifts (e.g. 2004am, 2003cg) and presumed present at high redshifts (Nobili et al., 2009; Freeman et al., 2009). The reddening law of SN host galaxies is estimated between  $R_V \sim 1-2$  (Lampeitl et al., 2010; Folatelli et al., 2010; Nobili and Goobar, 2008) in comparison to the Milky Way,  $R_V \sim 3$ . Although Folatelli et al. (2010) eliminate two SNe from their data set and retrieve the standard law of  $R_V = 3.2$ , demonstrating that conclusions about the host galaxy dust from SN Ia data are not only based on a priori assumptions (see section 5.2.1), but are not robust. Truly, the extent of the effects of dust is unknown, but no model is complete without considering some type of dust extinction.

## 6.2. Simulations

### 6.2.1. Prior Work

Previously, Li et al. (2001) examined the effects of the Malmquist bias, dust extinction, age of SNe and light curve shape on the ability to detect supernovae for two kinds of searches, magnitude and distance limited. Magnitude limited searches define a search based on the faintest object detected with the search telescope. Only large observatories are capable of doing this type of search, because their telescopes can peer into further distances. The data from a magnitude-limited search tends to span a large range in redshift. Distance-limited searches are focused on specific galaxies within a set volume. Most, if not all, distance-limited searches are of nearby catalogued galaxies and clusters. Li et al. (2001) concluded that under luminous SNe are selected against and over luminous Ia are overrepresented in magnitude limited surveys. Distance limited surveys will select all SNe Ia, of all subtypes if the limiting magnitude of each survey is sufficiently dim, reaching a maximum detection efficiency of 84%. Dust extinction will only effect the rate of peculiar types by decreasing the number of events at the distance limits of the survey. Results from Li et al. (2001) are based on a one-observatory model, where all galaxies in the target sample are viewed every night of the year and visible above the horizon. The generated supernova events are evenly distributed in the sky. Thus, under the most ideal of circumstances, not all SNe will be detected.

The work here will improve upon the Li et al. (2001) model by simulating several real observatories, dust extinctions and search techniques. The simulations will attempt to replicate and retrieve the number of Ia events detected by 28 historical and ongoing searches by testing various rates against the known local galaxy population. These searches account for approximately 780 SNe Ia discovered in 70 years from host galaxies with redshifts less than  $z = 0.1$ , which is approximately the limiting distance for most supernova searches.

The size of the rate is a reflection of the progenitor population. A fit with a small rate would indicate that most SNe Ia come from an older population of stars where as a

high rate shows that they emerge from young, star forming regions. Presently, published rates are defined in terms of volume ( $\text{Mpc}^{-3}$  per yr per mass) or SNu (1 SN event per century per  $10^{10} L(B)_{\odot}$ ) where  $L(B)_{\odot}$  is the solar blue luminosity. For this study, rates will be expressed in units of SNu and based on a one-component model dependent solely on the stellar mass with the intention that it is a lower limit to a two-component rate.

There are four parts to the simulations, beginning with assembling a list of all known galaxies within the  $z < 0.1$  range. Events are generated from this list, sorted and run through all 28 search models. Results of these individual simulations are combined and compared to the actual observed sample. Each step in this process is described in more detail below. All routines were written specifically for this research. Following this is a description of each observatory and their observing statistics. A discussion of the results concludes this section.

### 6.2.2. Galaxy List

Galaxies were extracted from the HyperLeda<sup>16</sup> (Paturel et al., 2003) online database, which recently (as of 2008) assimilated several galaxy catalogs such as 2MASS and SDSS. HyperLeda is effectively the Catalog of Principle Galaxies (PGC), therefore, objects must be certified galaxies before they are entered into the database. Like NED, this database contains information on the characteristics of all types of extragalactic objects such as magnitude, redshift, apparent diameter, etc. However, HyperLeda has greater consistency with attributes such as magnitudes. NED gives the magnitudes published in various bands, but HyperLeda calculates the absolute blue band magnitude for each galaxy (if redshift information is available). Initially, over 500,000 galaxies were gathered fitting the  $z < 0.1$  criteria, for all areas of the sky. This also included galaxies with no redshift information as well. These galaxies were removed from the sample leaving approximately 460,000 objects. Data was downloaded on more than one occasion to ensure the latest updates to the database. Further cuts were made based on unphysical

---

<sup>16</sup> <http://leda.univ-lyon1.fr>

magnitudes, usually corresponding to overly bright galaxies. Any unknown small errors of  $\sim 0.5$  in absolute magnitude are assumed to average out and be of small significance.

Besides absolute magnitude, other attributes taken from the database were semi major and minor apparent diameters, redshift, galaxy type, extinction due to Milky Way and correction to the blue magnitude due to galaxy inclination. The absolute blue band magnitude listed in the database includes the correction for Galactic extinction and the inclination of the galaxy. In other words, the value given is extrapolated to be the absolute magnitude of the entire galaxy, not just the measured portion seen from Earth. This was corrected back to the original perceived blue band luminosity in the simulation since it is assumed that observers are not going to detect SNe from portions of galaxies not visible from Earth's point of view.

The blue band magnitudes were converted into units of  $10^{10}L(B)_{\odot}$  by

$$10^{0.4(M(B)_{\text{sun}} - M(B)_{\text{gal}})} \quad 6.1$$

where  $M(B)_{\text{sun}}$  (not to be confused with  $M_{\odot}$ , the solar mass) is the absolute blue magnitude of the sun,  $M(B)_{\text{sun}}=5.45$  and  $M(B)_{\text{gal}}$  is the total absolute blue magnitude of the galaxy. These galaxies were then placed into the event generator that creates random<sup>17</sup> supernova Ia events based on the user's input for any span of years, and SNe rate. Galaxies were meticulously divided into groups according to their blue band magnitude and events were chosen randomly from each group. This ensures that the frequency of events from one galaxy was appropriate for its amount of blue light emission. For example, assume 50000 galaxies in this sample have luminosities near  $0.1 * 10^{10}L(B)_{\odot}$  and the supernova rate is 0.2 SNe. Therefore in 10 years,

$$50000_{\text{gal}} \times 0.1_{\text{centuries}} \times 0.2 \text{ SNe} \times 0.1 \cdot 10^{10}L(B)_{\odot} = 100 \text{ SNe} \quad 6.2$$

---

<sup>17</sup> All random numbers in these simulations are generated from the routine RAN3 from Numerical Recipes for Fortran77 (Press et al., 1992)



will have occurred in this group of galaxies. Or for a similarly sized sample of galaxies each with a luminosity of  $1 \cdot 10^{10} L(B)_{\odot}$ , this becomes 1000 SNe in 10 years. Thus it's important to bin these galaxies into appropriately sized groups. If the number of galaxies in the groups is too small, there won't be enough galaxies to select. If the groups are too large, meaning that the range of blue luminosity is too large, smaller galaxies run the risk of being over selected.

Once a host galaxy is picked, the event generator then randomly chooses a day, month and year for each SNe Ia, accounting for leap years. Five different rates (0.1, 0.15, 0.2, 0.25, 0.3 SNU) were tested with each observatory. The same rate was applied to all types of galaxies for the main analysis, including elliptical galaxies, which traditionally have had lower SN rate estimates than spirals. Truly, this doesn't matter significantly because the number of galaxies with a listed morphological type is small in comparison to the entire sample.

Event lists for each rate started at January 1936 and ended January 2007. The beginning date was chosen to encompass the first organized supernova search by Fritz Zwicky on the 18" Schmidt telescope at Palomar.

The apparent peak blue magnitude of the supernova is calculated based on the galaxy redshift. An absolute B band magnitude of -19.5 is assumed for each supernova.

The apparent magnitudes are calculated by:

$$m = M + 5 \log(D_L) + 25 \quad 6.3$$

where  $D_L$  is the luminosity distance given by

$$D_L = \frac{c}{H_0} \left[ z + \frac{1 - q_0}{2} z^2 \right] \quad 6.4$$

This is an approximation of a more formal distance modulus equation and is sufficient for the range in distances here. However, comparing this to the approximation,

$$D_L = \frac{cz}{H_0}$$

for a universe with a Hubble constant of  $H_0 = 73 \text{ km s}^{-1}\text{Mpc}^{-1}$ ,  $\Omega_M = 0.3$  and  $\Omega_\Lambda = 0.7$ , gives an acceleration of  $q_0 = -0.775$  resulting in a difference of approximately 0.18 mag for galaxies at  $z=0.1$  and less for smaller distances. That is, the apparent magnitudes of supernovae at  $z=0.1$  are 0.18 mag dimmer than ones calculated with eq. (6.5). This is rather small. However, for our purposes, especially at the higher end of the range in redshifts, it is better to assume that we can detect less SNe at these distances. This will become apparent when discussing the simulation results.

At smaller redshifts ( $z < 0.003$ ) eq. (6.5) becomes questionable because the velocities due to galaxy gravitational interaction within the Virgo cluster are on the same order as the recessional velocities of the Hubble flow. Therefore the redshift becomes an inaccurate tool for measuring distance. In some cases, the actual distance can't be computed from the redshift (e.g. M 31 has a redshift of  $cz = -300 \text{ km/s}$ ). But this is not a concern because firstly, these nearby host galaxies comprise an insignificant 0.04% of the entire galaxy sample and secondly, even if the calculated apparent magnitude is dimmer than what the actual magnitude would be, the supernova is still always detectable because of the proximity of the host. Therefore, SNe from galaxies at these close distances shouldn't alter the results.

### 6.2.3. Light Curves

After the event list is created, light curves are generated for each supernova. Since the events span 70 years, the list is filtered for each particular observatories search dates and potential sky coverage. The routine loops through the list of supernovae and expands each event into 16 days, -2 days before and +13 days after peak brightness. At this point, the generated "curves" are only lines that correspond to a constant apparent peak magnitude. The shape of the light curve and correction to the magnitudes is applied in the observatory simulation. In reality, supernovae can remain detectable (and undiscovered)

months after peak brightness and even weeks prior to peak brightness. But, for SN cosmology purposes, events several months past peak brightness are not useful and tend to go unreported. Once the light curves are generated, they are sorted<sup>18</sup> chronologically and put into the observatory simulation routine.

## 6.2.4. Supernova Search Routines

### 6.2.4.1. Magnitude and Distance Limited Surveys

The decision to model specific searches was based on the total number of nearby SNe (including unknown types) discovered by the observer(s), yearly rate of discoveries and the amount of information available for the search. A lower limit of discoveries was set to 10, however in some cases, such as WOOTS (Gal-Yam et al., 2008), this was ignored because these discoveries were found within a period of one year. There were supernovae groups that had discovered several SNe, such as the search at Zimmerwald (Wild, 1974), but this search spanned 35 years and found approximately 50 objects of which 15 were type Ia. Clearly, for practical reasons, this telescope was not dedicated to only searching for supernovae all those years. Therefore, it was decided not to model this search and searches with such a low yearly discovery rate. Almost all groups with a large number of discoveries had information published in either IAUC notices or on group websites about their telescopes and target galaxy requirements. Some amateur collaborations, such as CROSS<sup>19</sup>, utilized different locations, observers and telescopes. Considering the number of supernova found by the CROSS group (20 SNe as of January 2007), the simulation would have to be unnecessarily complicated for so few discoveries.

The simulation encompasses both magnitude and distance limited searches, and both photographic and CCD detectors. Magnitude limited searches and photographic surveys are done only near new moon. Distance limited surveys are not as stringent about moon brightness, especially for amateurs. For these searches, the moon must be 30

---

<sup>18</sup> Sort routine was taken from SORT3 in Numerical Recipes for Fortran77 (Press et al., 1992)

<sup>19</sup> <http://www.cortinastelle.it/cross/scoperte.htm>

degrees (regardless of phase) below the horizon in order for observations to take place. Each search has nontrivial differences, therefore separate routines were written for each. The amount of information for each survey varies. Surveys, such as SDSS (Frieman et al., 2008) and POSSII (Reid et al., 1991) provide date and coordinate information for regions scanned, and others like Cerro Tololo, (Tammann & Sandage, 1995) give coordinates with no specific dates of observation.

Catalog searches are the most common type of search whether amateur or professional, astronomers generate a search list of target galaxies before embarking on the observations. Each group appears to have a cadence to their search such that the same galaxy is checked once every few days. The galaxy list is more than likely taken from the RC3 catalog, or individual NGC, UGC or IC catalogs. Like the magnitude limited surveys, a few SN campaigns, such as the first supernova search at Palomar, provide a list of galaxies. However for most, this wasn't the case and target galaxies for these searches were considered any galaxy in the RC3 above the declination limit for the observatory. They were randomly generated based on any information provided by the observer such as the minimum magnitude of target, number of galaxies, apparent size or distance. If no target information was specified, then only the declination limit was taken into consideration.

#### 6.2.5. Sky Coverage Algorithm

The first part of the telescope simulation runs through each day of the search calculating the total amount of dark time available for that night. The times of sunrise and sunset were derived from algorithms in Meeus (1989). The dark time is measured by taking the difference between these two times for each night of the survey period. For all professional observatory simulations this begins and ends at astronomical twilight where the sun is 18 degrees below the horizon. For amateurs, especially ones higher latitudes, this was reduced to nautical twilight (sun is 12 degrees below horizon) because during the summer the sun never dips below the astronomical twilight limit.

Since objects rise and set at various times at night, each dark time is divided into five intervals and within each time interval a number of galaxies are observed based on the exposure and slew time of the telescope. The target list for the particular observatory is read in and depending on the length of the list, either galaxies are selected sequentially or randomly picked. The routine checks to see if the galaxy is above the horizon or telescope horizon limit because not all galaxies are visible at all times of the year. If the target galaxy passes this test, then it is sent to a subroutine that checks the sky brightness based on the moon and galaxy position. This is to check if the galaxy is worth observing because it might be too close to the moon. The subroutine estimates the moon's phase and position based on an algorithm also from Meeus (1989). The routine also randomly assigns a value for the seeing between 1"-2.5". The moon and seeing information are then passed to the sky brightness routine using the moon brightness model from Krisciunas and Schaefer (1991). Assuming a central galaxy brightness of 21.6 mag/arcsec<sup>2</sup> in V band, the galaxy is considered "viewable" if it is detected with a signal-to-noise of at least S/N~3. The signal to noise is determined from a basic program from Schaefer (Sky and Telescope, 1998) called CCDLIMI2.BAS. This routine was adapted to each observatory and their particular CCD characteristics. Unfortunately, a lot of information wasn't available on each aspect of every CCD, so the S/N ratio became more of an estimate rather than an exact value. If the galaxy is viewable, then it is flagged as being observed and cannot be re-examined until at least all the days in the particular search cadence have passed. If the moon is above the horizon, the program bypasses the time interval or entire night until the moon sets. For surveys with listed coordinates and dates of observation, this step was skipped.

Next, placing the target galaxy coordinates at the center of the CCD detector, RA and Dec limits are set based on the detector field of view (FOV). For most single CCD telescopes, this ranges from 5'-20'. Lines of constant RA are not parallel and so a projected square on the sky surface has different values of RA for different Dec and these are calculated by,

$$RA_{\text{limit}} = RA \pm \frac{FOV}{(2 * \cos(\text{Dec}))} \quad 6.6$$

Therefore, galaxies hosting a supernova that are not on an observatory target list have the potential of being imaged provided they are within the field of view of the target galaxy. Once the detector limits are established, the routine scrolls through the list of supernovae visible on that day to see if any are within the field of view. If so, then the supernova is passed to a similar sky brightness routine to see if it is bright enough for the CCD to detect it. In this routine, the SN magnitude is now adjusted to the appropriate value based on the day relative to the peak brightness. The light curves are modeled after SN 2005cf (Puckett and Langoussis, 2005) from Pastorello et al. (2007) in UBVRI bands. Data coverage spans from -2 to +13 days around the peak magnitude and is considered a “normal” type Ia supernova. If the supernova search filters are based in another system, such as SDSS *ugriz* filters, the light curves are first computed in UBVRI and then are transformed to the appropriate filter system. Typically, filters are not used for most nearby searches since they decrease the magnitude limit. In this case, the unfiltered magnitude approximates the R band. At this point, the user has the option of adding host galaxy dust to the supernova. Here, dust was added in amounts  $A_v = 0, 1, 2$ . The dust obeyed the same reddening law as the Milky Way of  $R_v = 3.3$ . The same amount of extinction is applied to all SNe for the entire run of the observatory simulation.

The final part of the telescope routine is comparing the SN magnitude against the sky brightness plus the background host galaxy light using an aperture equal to 1.5 times the seeing (generated from before). The host galaxy light is created randomly by selecting a position within the galaxy with a central surface brightness of  $21.6m(V)/\text{arcsec}^2$  where  $m(V)$  is the V band apparent magnitude. Assuming an exponential galaxy brightness profile, the galactic light decreases with increasing radius. This was applied to all morphological types. Extinction due to the atmosphere and Galaxy (Schlegel et al. 1991) is also added to the resulting supernova magnitude. Supernovae are detected if they are

within the limiting magnitude of the telescope and have a sufficiently high signal to noise ratio.

The CCDLIMI2 routine also allows for parameters such as temperature and humidity. But these were not used and a fixed temperature and humidity was assumed for all simulations. K corrections and evolution of type with redshift were also not added into the simulation since these effects are only noticeable at large distances. Bad weather and other factors, such as the operational time of the telescope were applied in the form of 50% and 100% (ideal) operating conditions. This was only added to groups who didn't have lists of coordinate times and dates. If the search group specified that their telescope wasn't a dedicated instrument for hunting supernovae, then a reduced amount of observational time, was folded into the individual simulation as well along with 50% operating conditions.

In the end, there are six different variations for each rate, making 30 simulations for almost each observatory and 15 for searches that provided lists of coordinates and search dates. The searches simulated here account for 82% of Ia in sample B (see chapter IV, table 4.3). The individual supernova searches will now be described in greater detail, grouped by CCD, amateur and photographic search.

## 6.2.6. Observatory Details

### 6.2.6.1. Professional CCD Searches

#### *LOSS*

The Lick Observatory Supernova Search (Li et al., 2000) was a very successful program that ran from 1998 to the beginning of 2009 and discovered the most nearby SNe as of 2007. Approximately 250 SNe Ia were discovered or co-discovered corresponding to the dates of the simulation. KAIT or the Katzman Automatic Imaging Telescope was dedicated solely to the purpose of discovering SNe. This was a very successful search because as the name implies, the telescope was automated and took images the entire night. KAIT is a 76cm telescope with a 6.7' x 6.7' field of view and pixel resolution of 0.8"/pixel. LOSS also provided two lists of target galaxies. One contained 14,000

galaxies and the other contained ~8000. It was unclear as to which list was used at different times in the history of the search, so the larger list of 14,000 was selected for the simulation. The exposure time was 30 seconds and it was assumed to take another 20 seconds for the telescope to slew to the next target, giving a range of 400-1000 images per night depending on the year. These numbers are consistent with the LOSS website<sup>20</sup> numbers. The limiting magnitude of the search was set to 19.5, even though dimmer supernovae have been discovered by this search. Days and intervals in the night were avoided near full moon, and where the moon was less than 120 degrees from zenith. Seeing was randomly generated from 1-3" and the CCD was unfiltered. Galaxy targets were randomly picked from the list and the search cadence was set to 3 days. In reality, this varied from 3 to 14 days but considering the number of images taken each night and number of targets visible throughout 1 week, it was easier to simplify this to the shortest time possible.

### *WOOTS*

Wise Observatory Optical Transient Search (Gal-Yam et al., 2008) focused on 163 Abell clusters with redshifts ranging from  $z = 0.06 - 0.2$ . The 1 meter telescope has a limiting magnitude of 22 in R band (unfiltered) with a 12'x12' field of view and resolution of 0.7"/pixel. Some of the clusters exceed the field of view in size, however for this search it is assumed that the images are focused only on the center of the cluster and not the entire cluster. This was guessed to be the method of search because it takes approximately 10 minutes to image one cluster (combination of 3 200 second images) making approximately ~50 images per night, depending on the year. Telescope time is limited to 3-5 days per month, which was assumed to occur around new moon in the simulation. The search detected 7 SNe Ia brighter than 20<sup>th</sup> magnitude.

---

<sup>20</sup> [http://astro.berkeley.edu/bait/public\\_html/kait.html](http://astro.berkeley.edu/bait/public_html/kait.html)



### *Nearby Galaxies Supernova Search*

NGSS was a doctoral research project from Strolger (2003), conducted in 1999 and 2000 at the 0.9m Kitt Peak telescope. Viewing times varied from 4 to 16 days in six different months, therefore observational time was very limited as were Ia discoveries (6) brighter than 20<sup>th</sup> magnitude. However it's worth mentioning that the team found 42 SNe of all types and redshifts. Even though this wasn't a prolific search for these simulations, it was worth modeling because the coordinates and dates were provided on the project's website<sup>21</sup>. Images were sometimes taken in less than optimal conditions. However, cloudy weather was ignored for the simulation, and modeled in the standard manner with two runs of 50% and 100% operational time. The field of view is listed as approximately 1 sq. degree, however stars listed in the data files indicate something closer to 1.3x1.3 degree field of view, which is what this simulation uses. The limiting magnitude is unfiltered (R band) 21 and the pixel resolution was set to 1"/pix.

### *Beijing Astronomical Observatory Supernova Survey (BAOSS)*

Based at Xinglong Station, the BAO survey (Qiu, Hu & Li, 2001) ran from 1996-2001 and focused on NGC and UGC high latitude galaxy targets from the RC3 catalog. The 60cm telescope has a 17' x 17' field of view with 1"/pix resolution. The search had the capability of taking 500 images per night with a cadence of 7 days. Their main goal was to discover as many Ia before peak brightness as possible. As a result, twelve SNe Ia were discovered, the dimmest having a magnitude of 18.2. On this basis, the limiting magnitude for this search was set at 18.

### *Texas Supernova Search<sup>22</sup>*

The TSS at McDonald Observatory in Texas, was a wide field search for SNe in nearby clusters such as Virgo, Ursa Major and Coma. This is only a partial list of clusters, as a complete search list was never published. Therefore a list of clusters was generated based

---

<sup>21</sup> <http://www.ctio.noao.edu/~ngss/Data/data.html>

<sup>22</sup> <http://grad40.as.utexas.edu/~quimby/tss/index.html>

on the location of supernova discoveries. This yielded 10 clusters in all. Unlike WOOTS, the entire cluster was imaged. This was simplified by applying large square fields of view on each cluster. The field of view for the telescope is  $1.85 \times 1.85$  degrees giving a pixel resolution of  $3.25''/\text{pixel}$ . The limiting magnitude was set to 18.5 degrees, even though some of their discoveries were as dim as 19<sup>th</sup> magnitude. TSS discovered 15 SNe Ia as of 2007.

#### *Mount Stromlo Supernova Search*

The Mount Stromlo Supernova Search (Reiss et al., 1998) ran from 1997 to 1999 observing 74 southern Abell clusters using a 1.3m telescope with CCD ( $.628''/\text{pixel}$ ) and a  $45'$  field of view. This search had 5% of the telescope time, yet found 48 SNe of which 23 were confirmed SNe Ia. Roughly 12 clusters were searched per week and only clusters with hour angles less than 2 hours at evening twilight and greater than -4 hours at morning twilight are considered for the search (Reiss et al., 1998). Images are taken in special blue and red filters specific to the observatory, but this simulation approximates these filters with standard B and R bands. The limiting magnitude is set to 20. The entire cluster is assumed to be imaged, therefore the fields of view is set to the diameter of each cluster published in Reiss et al. (1998).

#### *BAIT*

The Berkeley Automatic Imaging Telescope (BAIT) was the predecessor to LOSS and the first known automated sky search for SNe (Richmond et al., 1993). Located at the Leuschner Observatory, the 0.5 meter telescope had a  $5.33' \times 5.33'$  field of view and  $0.63''/\text{pixel}$  resolution. The search went from 1992 until 1994 and made 24 SNe discoveries of which 8 were type Ia. The galaxy search list consisted of 700 targets, however it was never published. Therefore one was randomly generated from RC3 based on the latitude of the observatory. The sky brightness was estimated  $18\text{mag}/\text{arcsec}^2$  and probably due to this bright location, the dimmest Ia event seen was 17mag. Therefore, this was the limiting magnitude of this survey.

### *SDSS II*

Sloan Digital Sky Survey conducted a supernova search for part of their sky survey routines. Regions of the sky between  $\pm 2.5$  deg in declination were searched in the fall of 2005, 2006 and 2007. The right ascension and declination limits were recorded for each night of the supernova run. SDSS discovered 28 SNe Ia with magnitudes less than 20. The details of the telescope are described in the photometry data section.

### *SDSS Data*

As a test of the simulation, fields and image dates from the SDSS photometry section of this thesis were placed in the model. The simulation discovered at most 1 SNe in over 500 images, which matches the actual data. Even though 6 SNe Ia were visible in the data, none of these images were taken near the discovery date, which were near or past maximum brightness. All were imaged at least one month after the discovery.

### *Nearby Supernova Factory/NEAT*

The Near Earth Asteroid Tracking (NEAT) group, based at Palomar, scanned regions between  $\pm 40$  degrees in declination looking for asteroids and other Near-Earth transient phenomena. The Nearby Supernova Factory utilized these images to look for supernovae, particularly type Ia. The 1.2m Palomar Samuel Oschin telescope was mounted with a 3 square degree field of view camera with a  $1''$ /pixel resolution. Each night, fields were imaged three times in one hour to look for moving objects in the region. This was adapted in the simulation by reducing the number of possible exposures by  $1/3^{\text{rd}}$ . Regions for observation were randomly generated between  $\pm 40$  degrees in declination and away from the galactic plane. Exposure times were set to 2 minutes and the limiting magnitude was placed at 19.5. The dates of this project ran from 2002-2003 until a new camera was added (see QUESTII). A total of 30 Ia were discovered with magnitudes of 20 or less.

*Nearby Supernova Factory/QUEST II*

The 9 deg<sup>2</sup>, 112-chip array QUESTII camera replaced the NEAT camera on Palomar in 2003. There were two modes to this search, (1) point and track, which was the same technique as NEAT, and (2) drift scan. The drift scan mode points the telescope at a fixed altitude and azimuth all night and allows the rotation of the Earth move stars into the field of view, covering a large sky strip of constant declination. This was replicated by randomly selecting a position between +/- 25 degrees in declination (limits of the search) at the beginning of astronomical twilight and computing region of sky covered until morning. Each mode took 50% of the time on the telescope. The dates of operation were listed beginning in Aug 2003, but discoveries didn't occur until March 2005, so that became the starting date of the simulation. The runs go through the end of 2006. There were filters on each CCD, but this was ignored for the simulation. The only reason to model filtered data is to account for the reduction of flux and the possibility of not detecting a supernova that would normally be detected by an unfiltered camera. Since each filtered CCD had a dimmer limiting magnitude than the simulation, it was unnecessary to account for this. QUESTII discovered 38 Ia, and most of these discoveries were found in the point and track mode.

*EROS*

EROS (Hardin et al., 2000) was part of the larger Supernova Cosmology Project (SCP, Perlmutter et al., 1997) and Supernova Cosmology Consortium (Blanc et al., 2004) designed to look for SNe Ia near  $z \sim 0.1$ . EROS was fairly successful in that it discovered 11 SNe Ia within  $z < 0.1$ . Using an array of CCD detectors with a total field of view of 1 deg<sup>2</sup>, this was a dedicated search for SNe Ia that lasted for 2 months during 1999 and 1 month in 2000 in La Silla, Chile on the 1m telescope. Searches consisted of moonless nights within -12 and -4.5 degrees declination and 150 to 217 degrees in right ascension. The search fields were never published, however, the observation dates were. Given the long exposure times (~600sec) and the anonymity of the host galaxies, it was assumed

that this was not an RC3 catalog search. In order to replicate this, regions were randomly selected from patches of sky within the quoted RA and Dec coordinates. Images were taken in V, I and R filters, but it was considered unnecessary for the same reasons given for the QUESTII camera.

#### 6.2.6.2. Amateur Observers

Amateur hunters have significantly contributed the number of SNe discovered since the CCD was invented. Several of these discoverers have found more SNe than professional searches and so they were included in the simulations. Their “backyard observatories” are quite sophisticated and the only difference with their search techniques and a group like LOSS is that they don’t have a software processing pipeline to extract potential SNe candidates. Instead they visually scan images for SNe.

However, there are shortcomings to the amateur simulations. Most are fairly limited in the details of their search; particularly concerning the number of days per year and hours per night they spend observing their targets. This may be the largest source of error in the simulations. Unless they provided detailed logs of their observations, all amateurs are assumed to observe half of the night. Galaxy targets come from the RC3 and the start date of the simulation was set at the date of their first discovery. The search cadence was also set to 5 days unless otherwise stated. In some cases, observers used more than one telescope at a time. For these, only one telescope was modeled because it was unclear when they started incorporating more telescopes into their search.

#### *Tom Boles*

Three amateurs are based in England. Tom Boles<sup>23</sup> is the most prolific amateur supernova hunter in Europe. At the time of this writing he has discovered over 125 SNe. His observatory consists of three, 35 cm telescopes all mounted with 512x512 CCDs. Based on the telescope manufacturer and CCD size, each telescope was estimated to have a 10’ x10’ field of view with a 1.2”/pixel resolution. Boles searches a total of 12,000 galaxies

---

<sup>23</sup> <http://coddenhamobservatories.org/>

throughout the year and the dimmest object he has detected approaches 19<sup>th</sup> magnitude. For time period of this simulation, he had discovered 36 SNe Ia.

#### *Mark Armstrong*

Based in Kent, England, Mark Armstrong has discovered 35 SNe Ia from mid 1995 to December 2006. Armstrong has provided some documentation on his observations. He patrols UGC and NGC galaxies once every 3 days and averages 4.4 hours for each night. All galaxies are at least 15<sup>th</sup> magnitude. Armstrong has used four different telescopes and CCD during this period, varying from 0.26-0.36 meters in size and 9' to 14' in field of view width. The average telescope diameter (0.3m) and field of view (11.5 x11.5) were placed in the simulation. Pixel resolution was set to 1"/pix and the limiting magnitude was 19m.

#### *Ron Arbour*

Ron Arbour is the last of the British trio of amateur astronomers. Not much information other than latitude and longitude was available for Arbour. His 10 Ia discoveries span 1998 to the end simulation date. Target galaxies were pulled from the RC3 and the limiting magnitude of the search was set to 17m, which was based on the dimmest discovery. Arbour also has gone through several telescopes, however he used a 0.3m Schmidt Cassegrain for most of his patrols with a 15.4' x11.8' field of view. This was simplified to a detector with the same area, but dimensions of 13.5'x13.5'.

#### *Tim Puckett*

The Puckett Observatory<sup>24</sup> is the most successful amateur SN group in the world. Tim Puckett, based in Georgia, USA, built 0.5m and 0.61m telescopes for comet and supernovae studies. He enlists the help of several colleagues and volunteers to scan the images for transient objects. This is a full time observatory and the telescopes run all night averaging about 1000 galaxies each. Puckett Observatory has now grown to

---

<sup>24</sup> <http://www.cometwatch.com/>

incorporate telescopes in Arizona, British Columbia and South Africa. However, only the 0.50m telescope in Georgia was modeled. The target list was pulled from the RC3 and the limiting magnitude was set to 20m. The field of view is 20' x20' with a resolution of 2.4"/pixel. The Puckett Observatory discovered 66 SNe Ia (in Georgia, only) for the relevant dates of the simulation.

*Berto Monard*

Berto Monard is based in Pretoria, South Africa and is one of two amateurs in this simulation based in the southern hemisphere. His first discovery was in May 2003 and since 2007, he has found 19 SN Ia. He uses a 30cm telescope with a 21'x21' field of view. Observations are unfiltered and assumed to have one image every 2 minutes.

*Michael Schwartz*

Michael Schwartz originally started his supernova search in Oregon and then moved to Arizona. The simulations here, model one of his telescopes in Arizona, with a 0.5 telescope and 15'x15' field of view, 1"/pixel resolution and limiting magnitude of 19. His runs from Jun 1999 to 2007 and Schwartz is responsible for discovering 29 Ia. He collaborated at one point with LOSS and formed LOTOSS. Due to this collaboration, the LOSS galaxy list was used in this simulation.

*Rev. Robert Evans*

Rev. Robert Evans has the most unique search out of all observers. All of his discoveries have been visual. In other words, instead of taking images, he scanned nearby galaxies with a small telescope for any new SNe. He had a very successful run from 1981-2005 and found 16 SNe Ia within this time, until SN hunting became increasingly popular. However, he is the other amateur from the southern hemisphere, and searches in the southern hemisphere weren't as plentiful as SN searches in the northern hemisphere. Clearly, the telescope details weren't important in this simulation. The limiting magnitude was set to 15. The rate of discovery is fairly small, however, it was interesting

to see how many SNe could be discovered at this latitude and a low limiting brightness. It was assumed that he observed once every eight days throughout the entire year. Galaxies were chosen from the RC3 by brightest and largest apparent diameters.

#### 6.2.6.3. Photographic Searches/Surveys

##### *POSSII*

The Second Palomar Sky Survey (Reid et al., 1991) took photographs of all areas of sky, north of  $-20$  in declination from 1985 to 2000. Images were taken on  $6.5 \times 6.5$  degree photographic plates in B,R and I bands with limiting magnitudes of 22.5, 20.8 and 19.5 respectively on specific dates. Detection was based on SNe magnitudes brighter than these limits. Shaw (1979) noticed that no supernova had been detected within the inner  $4''$  of the galaxy. This was simulated by comparing the radial position of the number of supernovae discovered on photographic plates to those discovered on CCDs. No detected supernovae occur near the galaxy center for photographs due to the overexposed bulge. For the CCD images, this constitutes approximately 3% of all detected SNe Ia . Therefore, the simulation randomly eliminates 3% of the detected SNe to mimic this effect. This is done for all photographic searches.

##### *POSSI*

The Palomar Observatory Sky Survey was the first all sky survey of the Northern skies that took  $6.5$  degree images from 1949-1965. There were no Ia discovered but 69 unknown types. POSSI was placed in the search to test the possible number of Ia events and get an upper limit of SNe Ia typed as unknown events.

##### *Cerro el Roble*

Originally, the SN search at Cerro el Roble ran from 1979 to May 1984 in Chile. Unfortunately, only one SNe Ia was discovered in this search. Then this search was repeated from 1997 to 1999. Nothing has been published on this search other than the supernova findings from the IAUC. However, Maza et al. (1981) provides a list of fields



and months searched in 1979. The same fields were applied to the 1997-1999 search as well. The field of view is 5x5 degrees on unfiltered blue photographic plates. The limiting magnitude was set to 18.5, although dimmer objects were detected (Hamuy et al., 2001). The later search discovered 15 SNe Ia. For this search and all other photographic searches without specific dates, images were assumed to be taken on moonless nights, near new moon.

### *Fritz Zwicky*

Fritz Zwicky was responsible for several searches at Palomar. His first organized search was on 18" Schmidt telescope at Palomar that ran from 1936-1941. This is the first known supernova search anywhere in the world. He searched galaxies brighter than  $m=15$ , with a search cadence of about a month. The dimmest supernova detected was 16.5. He found 3 Ia and 12 of either unknown or type I. Images were 30 minute exposures covering 70 deg<sup>2</sup> (Zwicky, 1938).

### *Palomar Supernova Search*

Palomar supernova searches ran from 1957 to 1974 under the direction of Zwicky. In fact, the search ended because of Zwicky's death in February 1974. The search utilized the 48" Oschin telescope at Palomar, which was also doing the POSSI survey around the same time. The 48" telescope has a much deeper limiting magnitude as SNe were discovered up to 20.5. For this simulation, the cut off was set at 19m, even though several objects were detected fainter than this. Zwicky also published set of specific search fields. This probably varied for the 11 years of the search, but all were used. Most of the SNe uncovered from this search were unknown types and only 1 type Ia was confirmed.

### *UKST/AANEAS*

The Anglo-Australian Near-Earth Asteroid Survey (Steel et al. 1997) was a photographic search for Near-Earth objects (NEOs) at the Anglo-Australian Observatory from 1990 to

1996. The program utilized the 1.2m U.K Schmidt telescope with its large, 6.5 degree field of view. The center coordinates, dates and filters (B, V, R, I) were provided in the UKST plate archive<sup>25</sup>. There was some confusion as to which plates were used for the AANEAS survey and which were used for the UKST sky survey and for other purposes. Since the search did use other plates for validation of NEOs, all plates from this time period were included in the simulation. During the length of this program 63 SNe were found of which 22 were Ia. The dimmest Ia found was 20<sup>th</sup> magnitude. All discoveries were credited to Robert McNaught as the discoverer.

#### *Calan/CTIO Search*

One of the more famous supernova Ia searches intended to examine SNe Ia for cosmological purposes. This search ran from June 1990-Nov 1993. Fields and information on the telescope are listed in Hamuy et al. (1993). The fields searched each month were taken from Hamuy et al. (1999). Only fields above the horizon and on moonless nights were searched. The images have a 5 degree field of view and a 19.5 limiting magnitude.

#### *Pollas*

Christian Pollas at the Cote D'Azur scanned several photographic plates used for various purposes, for supernovae. Based in France, images were taken on film 0.9m telescope with a 5 degree field of view. Because photographic film takes at least an hour to prepare and image (exposure times are on the order of a ½ hour) it was assumed that 5 images were taken per night from 1985-1996. Since plates were used for various purposes, the coordinates were randomly selected a galaxy from the RC3.

---

<sup>25</sup> <http://www.roe.ac.uk/ifa/wfau/ukstu/ukscat.html>

## 6.3. Results

### 6.3.1. Preliminaries

The data are divided into three sets, photographic, CCD magnitude limited and CCD distance or catalog searches. Figures 6.1-6.7 show the redshift distribution for all 3 sets and combinations of dust extinction and duty cycle, plotted with the observed distribution of the same observers for each group for the closest fitting rates.

The CCD catalog search group (figures 6.1-6.3) has the best fit to the observed population, whereas both photographic and CCD magnitude limited are much worse. Clearly each search type has a different distribution of target galaxies. For the CCD catalog group, the simulation was changed to only find events occurring within the target galaxies, even if another galaxy within the field of view of the telescope had an event. If the detections are not limited to the target galaxy for the catalog group, then the redshift distribution appears more like the magnitude limited search.

The photographic search is not well replicated by the simulation in for any distance. The photographic simulation was also changed to select galaxies within  $z < 13,000 \text{ km/s}$  and brighter magnitudes depending on the search. Still this did not match the observed distribution. Near events are under selected and far events are over selected.

The magnitude limited CCD searched worked with a lower supernova rate of 0.1-0.15 SNU as opposed to 0.25-0.3 SNU for the other searches. One possibility is that the simulation over estimated the amount of time on the telescope. For all of the magnitude limited searches, observations were kept to days around new moon.

Since the fit to the CCD catalog searches appears to fit best to the observed distribution, the focus of the rest of the work will be on this subgroup of the population. Almost all of these galaxies are from the RC3. The completeness of the sample for rates  $R=0.2, 0.25$  and  $0.3$  can be found by taking the ratio of the observed population to the simulation (Yasuda et al., 2009). Figures 6.8-6.10 show the results for all three rates, extinctions and operational cycles. The redshift range is confined to  $cz < 20,000$  because data is sparse ( $< 10$  SNe Ia) past this point. For all rates, redshifts of  $cz < 5000 \text{ km/s}$  are

difficult to replicate, even with no extinction and operation at 100% efficiency. For  $cz > 5000 \text{ km/s}$ , the best fitting models are for rates  $R = 0.25$  and  $0.3$  with an extinction of  $A_v = 2 \text{ mag}$  and 100% efficiency.

### 6.3.2. Magnitudes

The distribution of the magnitudes are shown in figures 6.11 and 6.12 for rates  $R = 0.25$  and  $0.3$ . Clearly, models with  $A_v = 2 \text{ mag}$  extinction fit the number distributions better than models with no extinction. More than likely, dust in the model is mimicking SNe magnitudes well past peak brightness. Our model simulates events two weeks around peak brightness and they decrease at most 0.8 magnitudes from peak brightness in this time span. The fact that only SNe modeled with dust can fit the observed distribution may imply that observers are not detecting most events at peak brightness. In order to determine if observers are missing peak times and to distinguish this effect from dust extinction, the simulation is tested on a 100-day light curve. For simplicity, the simulation is limited to the LOSS search. LOSS has discovered the most Ia out of any of the searches, therefore the statistics are more representative of the entire sample. Figure 6.13 compares the LOSS sample to the simulation with the longer light curve for 100% efficiency and  $A_v = 0, 1, \text{ and } 2$ . The model with dust is still the best fit to the distribution, even when SNe are discovered well past maximum.

### 6.3.3. Discussion

From the above results, the rate is between  $0.25 < R < 0.3 \text{ SNU}$  for the local universe. The rate is almost entirely based on RC3 galaxies and is complete to  $z = 0.05$ . If the rate was based solely on magnitude limited searches, or all galaxies visible within  $z < 0.1$ , it would be much lower,  $R = 0.1 - 0.15 \text{ SNU}$ , illustrating the difference of target selection. In order to replicate the magnitude distribution, there must be 2 magnitudes of extinction in front of every Ia event. The difference between the two rate results is evident in the literature. Blanc et al. (2004) estimated a rate of 0.125 for redshifts out to  $z = 0.13$ , and

Dilday et al. (2008) determined a similar rate,  $R = 0.246$  SNU at  $z = 0.1$  from SDSS II Supernova Survey data, agreeing with the results here. The SDSS II survey was modeled in these simulations and it can be checked to see if the results agree with their search fields. For  $R = 0.25$  SNU and  $0.3$  SNU, the recovered number of SNe from SDSS was 21 and 25, respectively, in comparison to the actual observed number of 28 Ia. The simulation for the SDSS supernova survey was accurate because date and coordinate information was provided for each search area, making the results robust. If extinction is included, the number of detected SNe drops to 11 and 15 for magnitudes brighter than 20. These results are puzzling because it is suggesting that we are detecting the expected number of SNe, but all Ia are dust free at  $z \sim 0.1$ . The rate at  $z < 0.017$  was not modeled successfully, in that there were more events observed than detected, possibly due to using a one component rate instead of a two component rate that is dependent on stellar formation rate. It could be that the rate is much larger than  $R = 0.3$ , and we are only detecting the dust-free events at  $z \sim 0.1$  and at distances of  $z < 0.017$  we are detecting all events.

#### 6.3.4. Improvements

Modeling the photographic searches is challenging. The field of view is very large ( $\sim 5$  degrees) and allows for many galaxies to be observed in one image. Within the volume of  $15,000 \text{ km/s}$ , there are 160,000 galaxies, but only nearby galaxies were supposedly targeted for SN inspection. Added to this difficulty is that most SNe from these early searches are unclassified (denoted in literature as “?”) because most were discovered several years after the image was taken and at dimmer magnitudes in non catalogue galaxies than most discovered at the time of the image date. A better model would eliminate all galaxies except for RC3 and possibly reduce the efficiency cycle. A better model would have to mimic the film response to the light and human efforts to scan the image.

Modeling the magnitude limited searches requires exact date and coordinates. From the SDSS example above, the simulation works, but only if complete search details are provided.

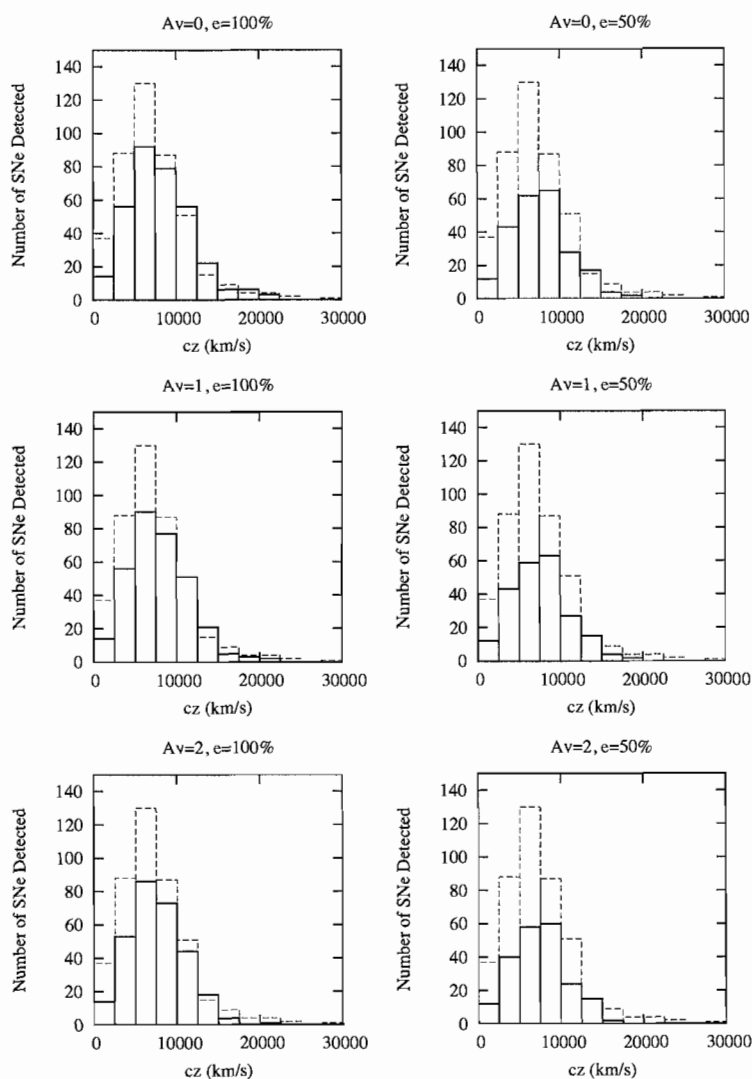


Figure 6.1. Redshift distributions for all simulated CCD catalog/distance limited searches (solid line) for a rate of  $R=0.2$  SNU. The plots on the left are for 100% duty cycle ( $e$ ) and the plot on the right correspond to 50% duty cycle. The rows correspond to  $A_v = 0, 1, 2$  amounts of extinction from top to bottom. The dashed line is the observed Ia from the same observers.

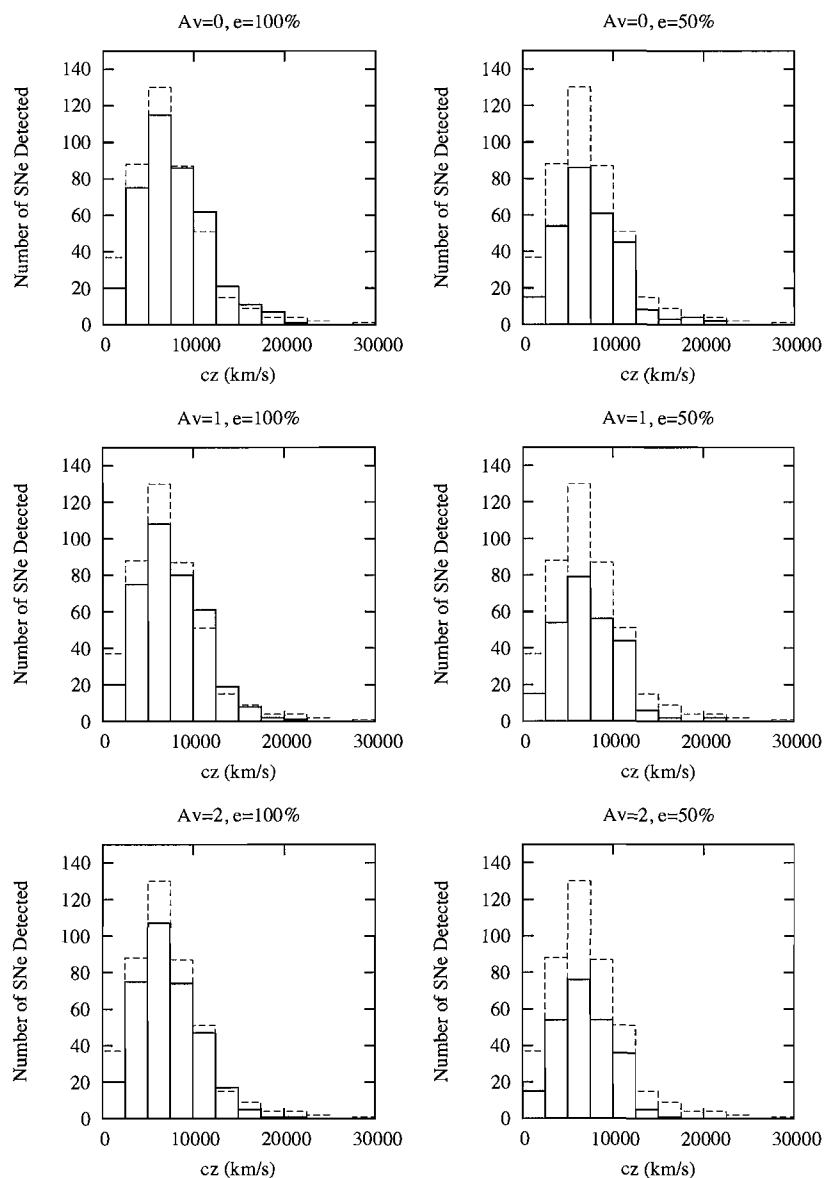


Figure 6.2. Redshift distributions for all simulated CCD catalog/distance limited searches (solid line) for a rate of  $R=0.25$  SNU. The plots on the left are for 100% duty cycle ( $e$ ) and the plot on the right correspond to 50% duty cycle. The rows correspond to  $A_v = 0, 1, 2$  amounts of extinction from top to bottom. The dashed line is the observed Ia from the same observers.

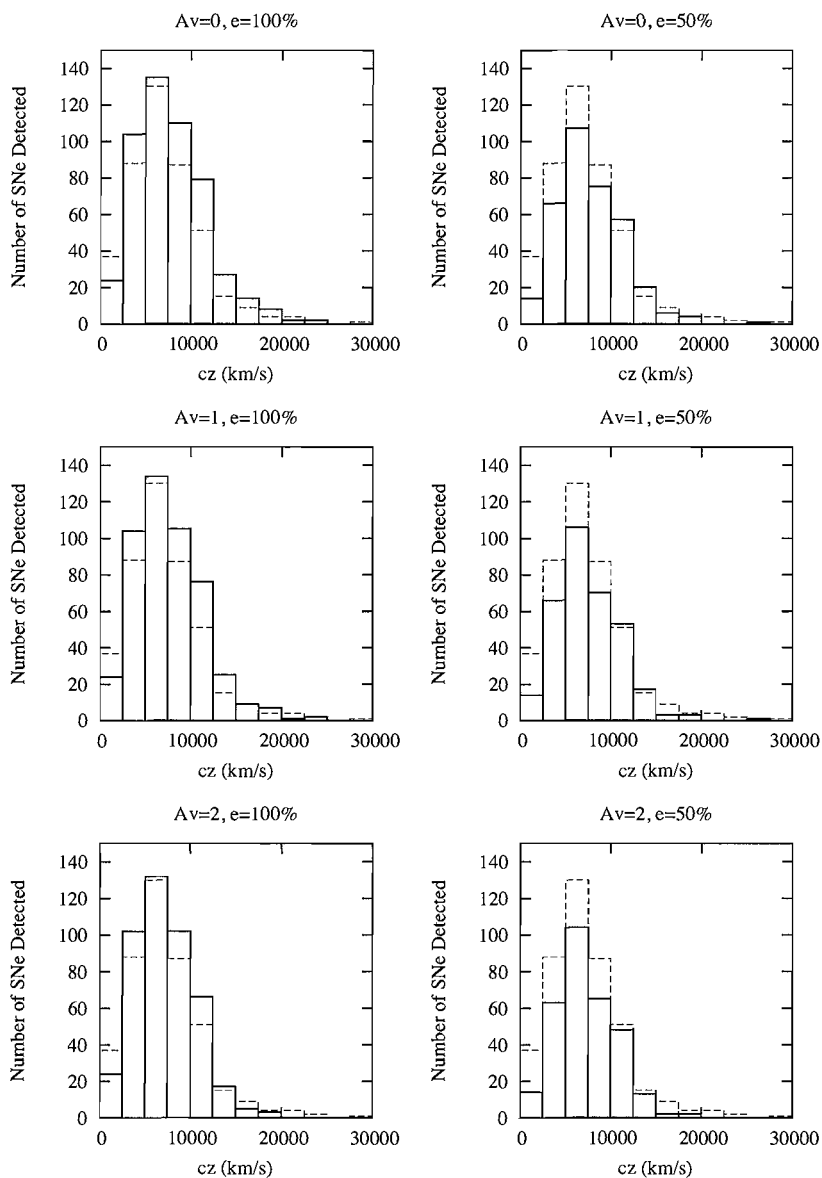


Figure 6.3. Redshift distributions for all simulated CCD catalog/distance limited searches (solid line) for a rate of  $R=0.3$  SNU. The plots on the left are for 100% duty cycle ( $e$ ) and the plot on the right correspond to 50% duty cycle. The rows correspond to  $A_v = 0, 1, 2$  amounts of extinction from top to bottom. The dashed line is the observed Ia from the same observers.



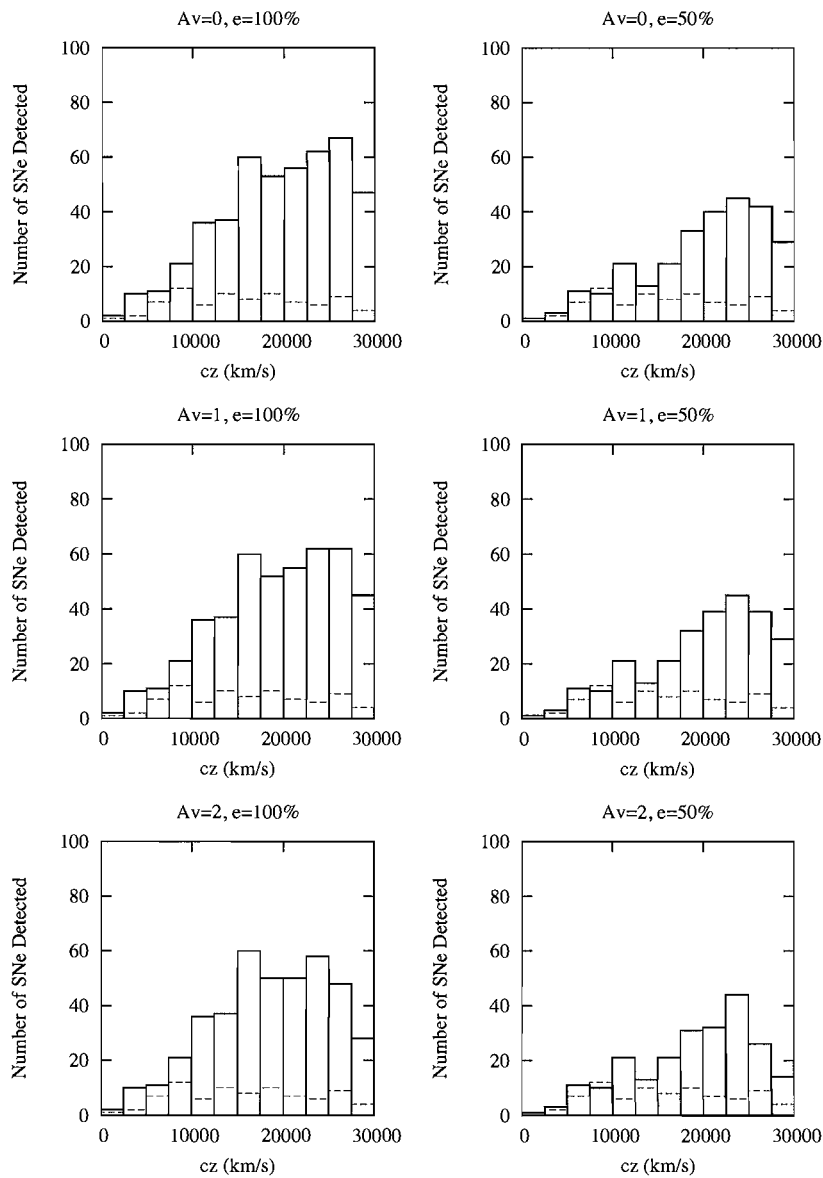


Figure 6.4. Redshift distributions for all simulated CCD magnitude limited searches (solid line). The plots on the left are 100% duty cycle and the plot on the right correspond to 50% duty cycle. The rows correspond to  $A_v = 0, 1, 2$  amounts of extinction from top to bottom for a rate  $R=0.1$  SNU. The dashed line is the observed Ia from the same observer.

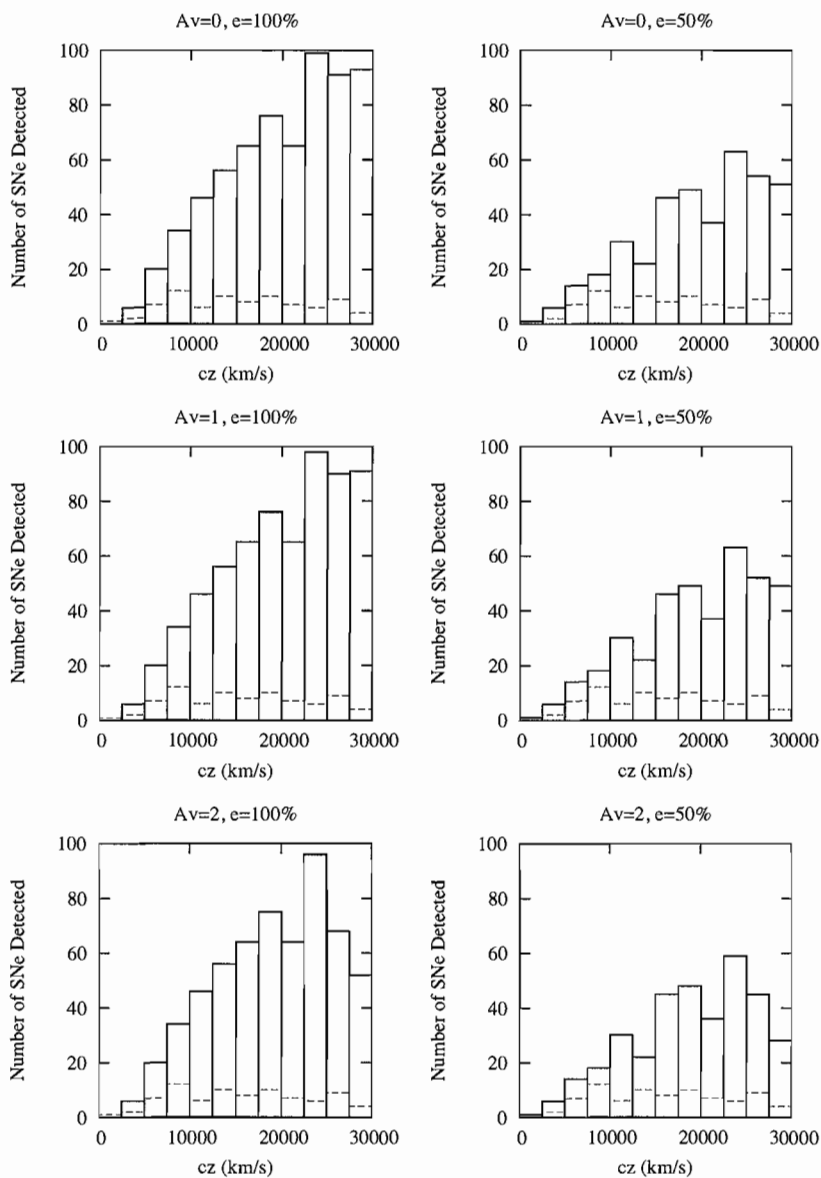


Figure 6.5. Redshift distributions for all simulated CCD magnitude limited searches (solid line). The plots on the left are 100% duty cycle and the plot on the right correspond to 50% duty cycle. The rows correspond to  $A_v=0,1,2$  amounts of extinction from top to bottom for a rate  $R=0.15$  SNU. The dashed line is the observed Ia from the same observer.

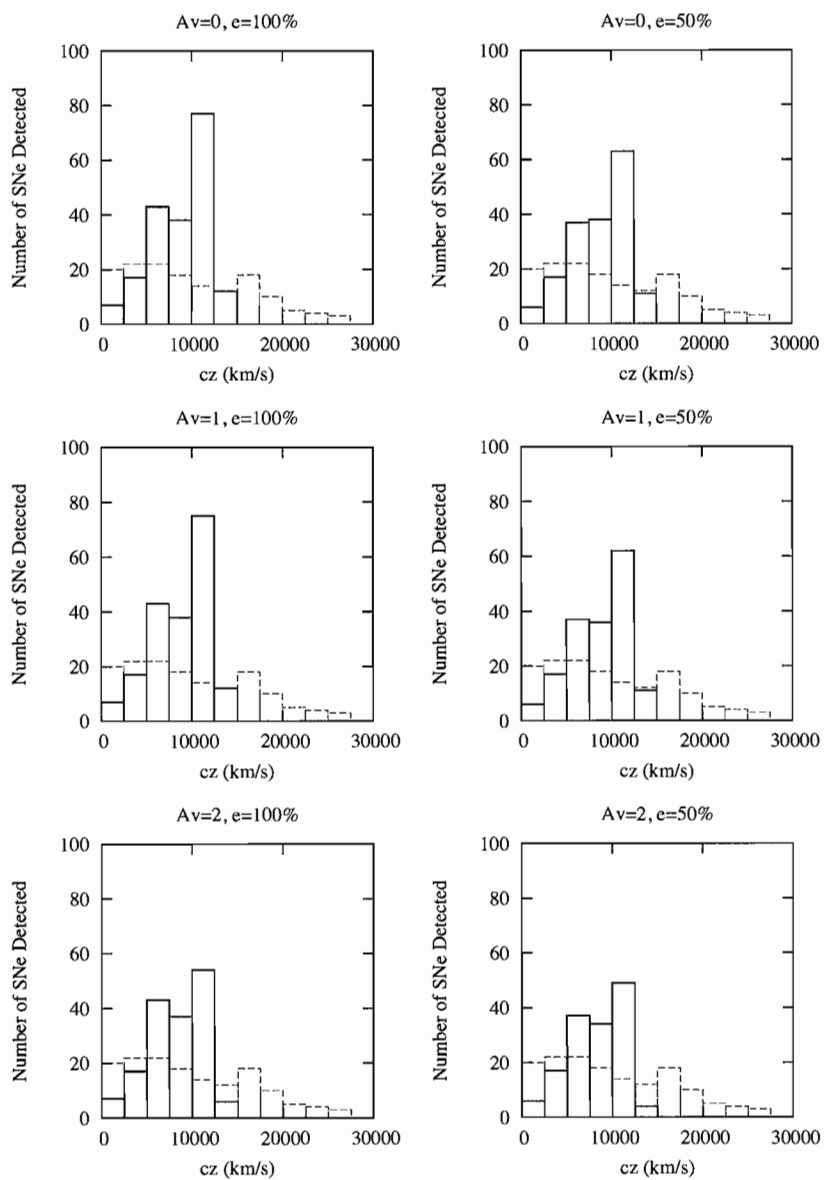


Figure 6.6. Redshift distributions for all simulated photographic searches (solid line). The plots on the left are 100% duty cycle and the plot on the right correspond to 50% duty cycle. The rows correspond to  $A_v = 0, 1, 2$  amounts of extinction from top to bottom for a rate  $R = 0.25$  SNu. The dashed line is the observed Ia from the same observer.

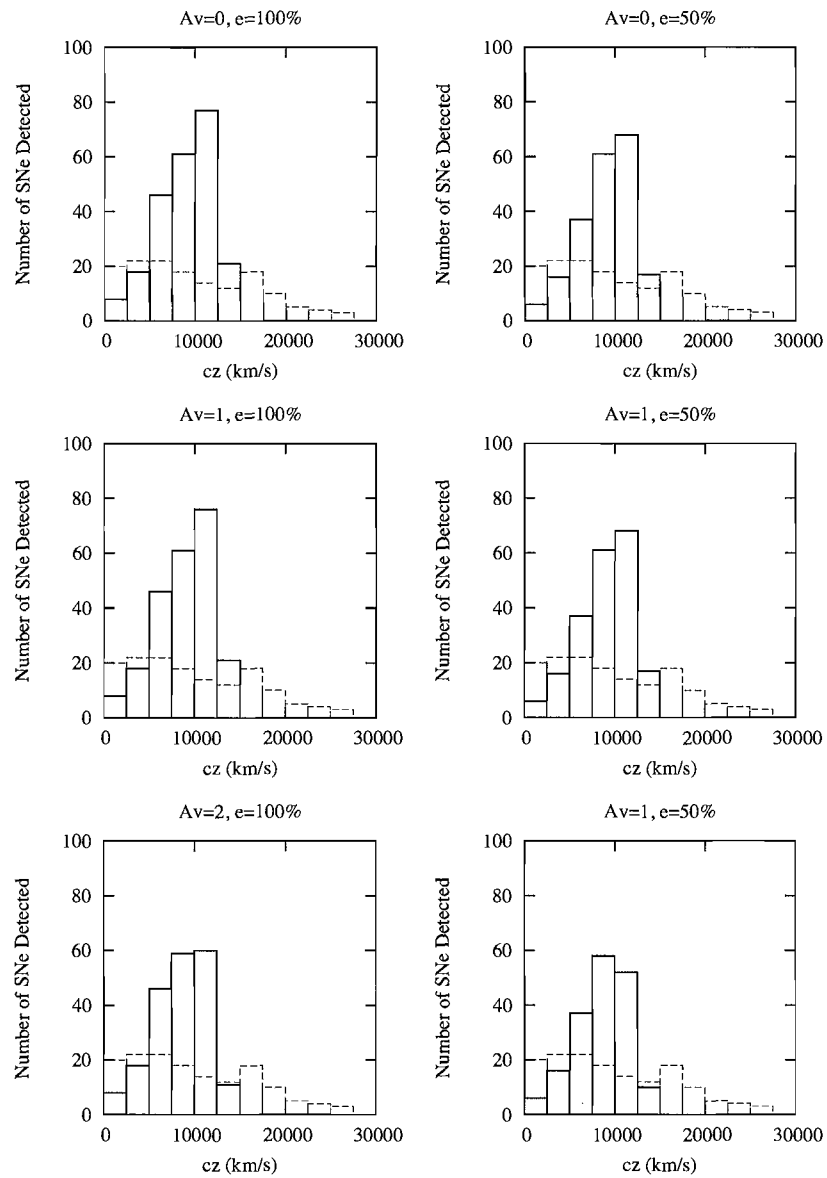


Figure 6.7. Redshift distributions for all simulated photographic searches (solid line). The plots on the left are 100% duty cycle and the plot on the right correspond to 50% duty cycle. The rows correspond to  $A_v=0,1,2$  amounts of extinction from top to bottom for a rate  $R=0.30$  SNU. The dashed line is the observed Ia from the same observer.

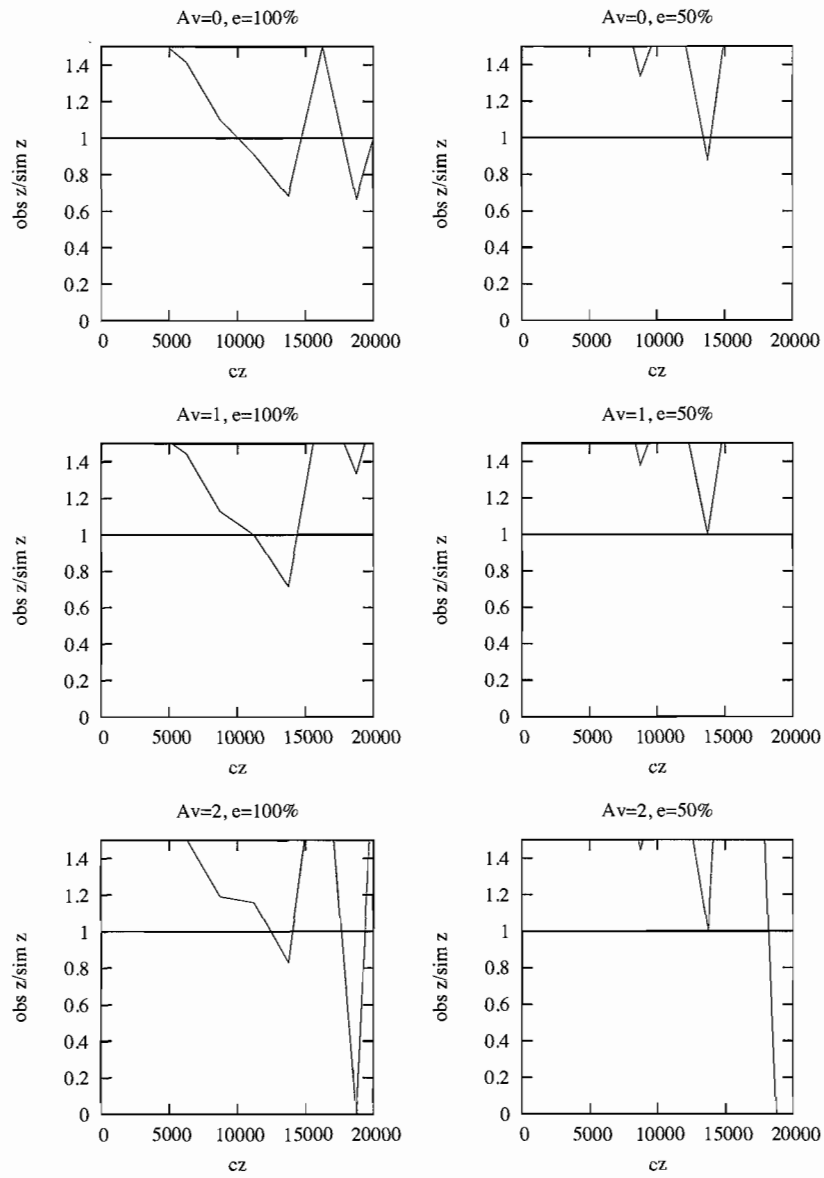


Figure 6.8. The ratio of the observed number of SNe Ia to the simulated SNe for the CCD catalog group for a rate of  $R=0.2$ .

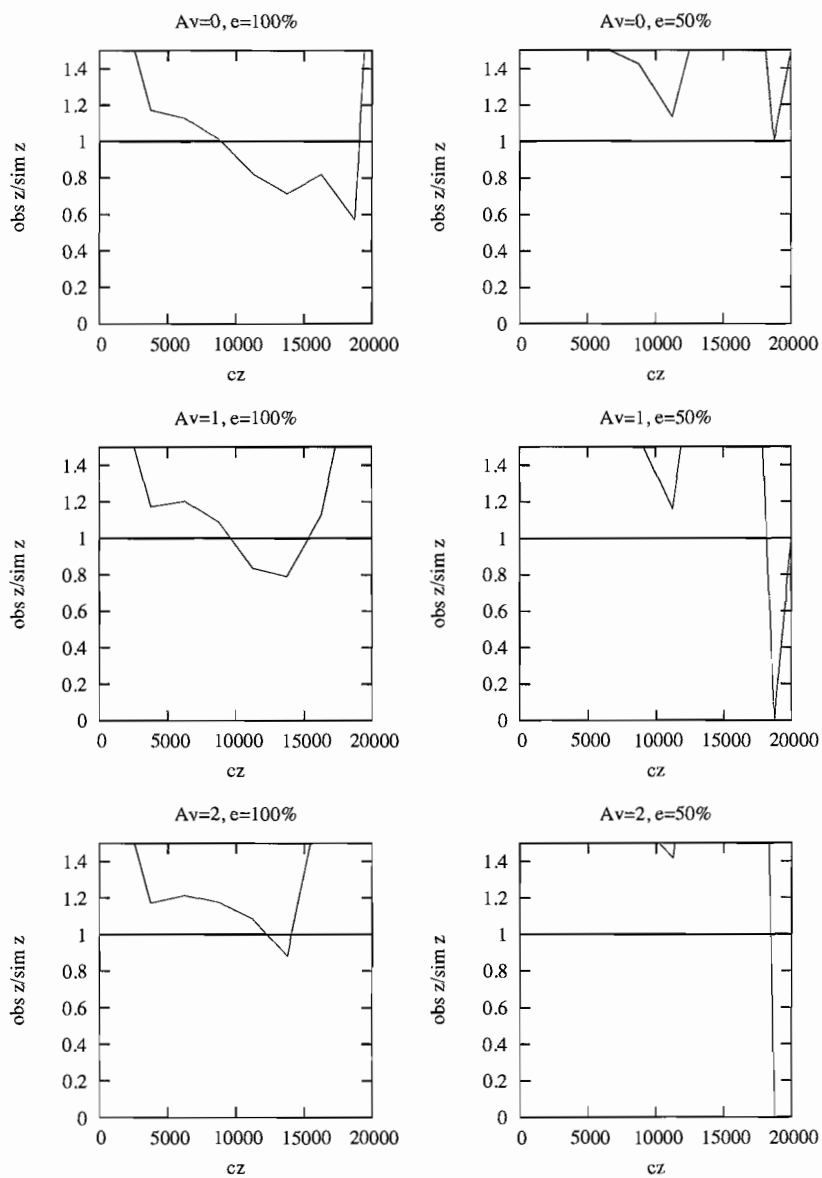


Figure 6.9. The ratio of the observed number of SNe Ia to the simulated SNe for the CCD catalog group for a rate of  $R=0.25$ .

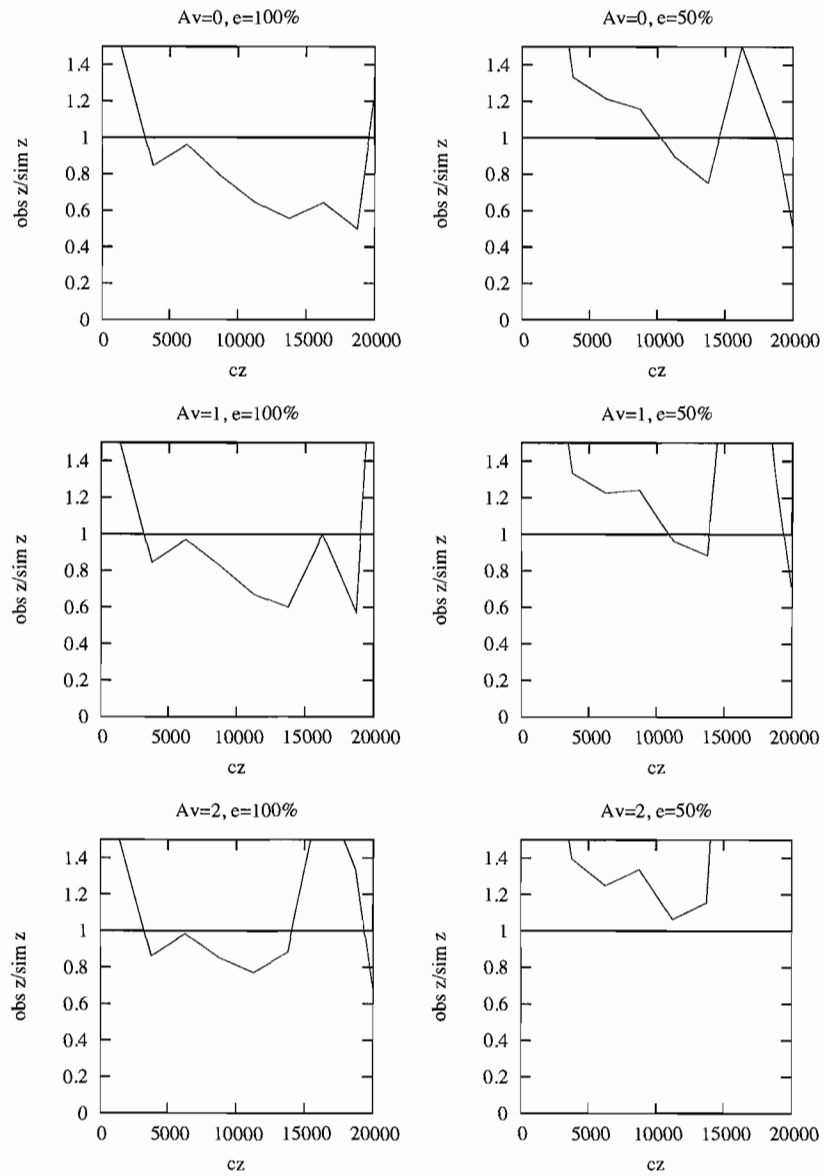


Figure 6.10. The ratio of the observed number of SNe Ia to the simulated SNe for the CCD catalog group for a rate of  $R=0.30$ .

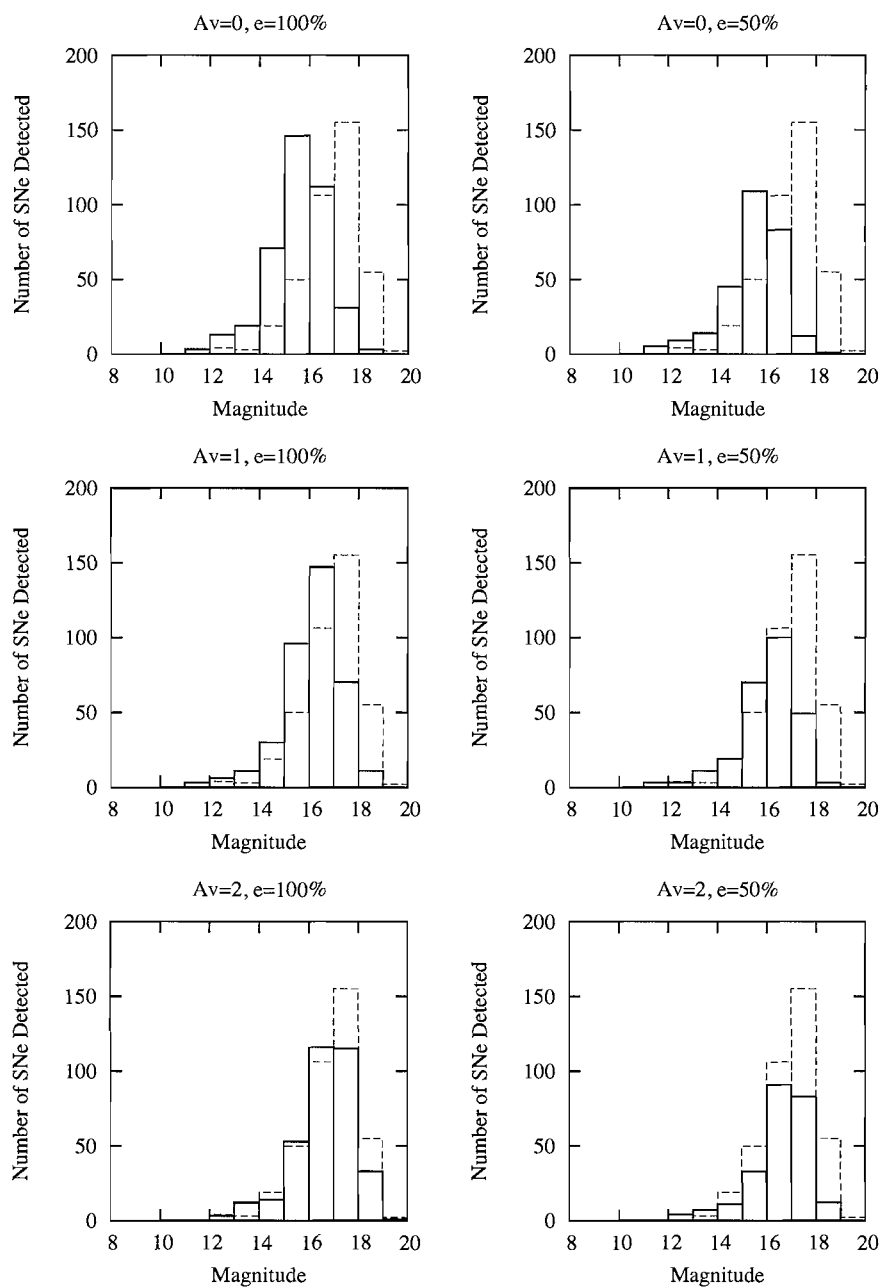


Figure 6.11. The magnitude distribution of the observed (dashed line) and simulated (solid) Ia population for  $R=0.25$ .



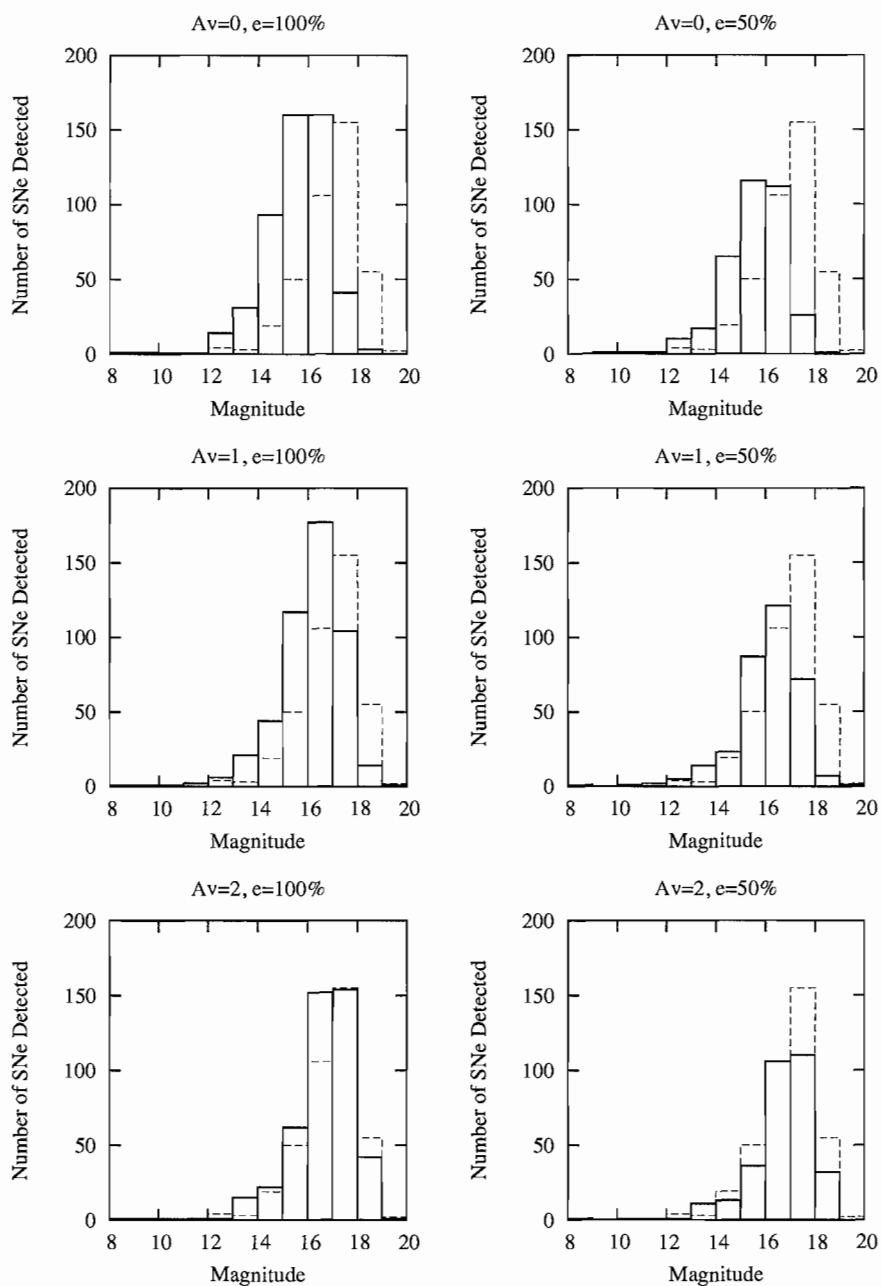


Figure 6.12. The magnitude distribution of the observed (dashed line) and simulated (solid) Ia population for  $R=0.30$ .

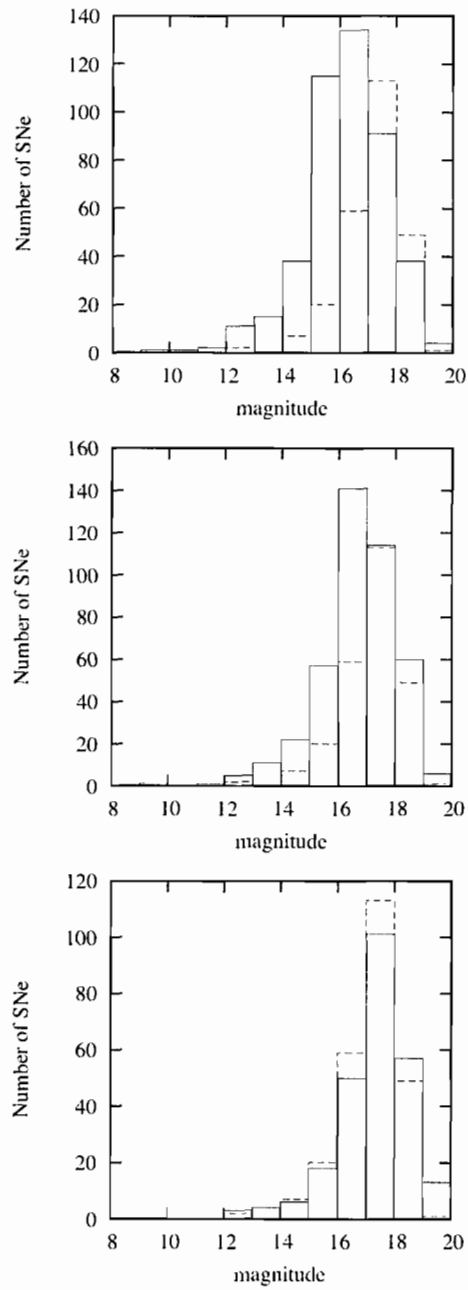


Figure 6.13. Distribution of simulated (solid line) LOSS magnitudes and observed magnitudes for  $A_v=0,1,2$  (top to bottom plots) for 100% efficiencies.

## CHAPTER VII

### DISCUSSION AND FUTURE WORK

#### 7.1. Implications of Supernova Ia Dependency on Stellar Environment

Data presented in chapter V shows a distinct relationship between Ia events and their environments. The correlation of the local stellar population colors with the supernova Ia peak colors means that there is an environment-dependent systematic effect in the data set, which is proportional to the span of colors in figure 5.598. Wang et al. (2006) does attribute some of these redder colors to dust in their estimation of host galaxy reddening and extinction. 91bg environments are assumed to be dustless, but as figure 5.598 shows, these environments also correlate in the same manner as the normal and 91T SN types. The fact that 91bg and 91T types were demonstrated to have distinctly similar environments within their type shows a strong dependence of peak color and possibly absolute magnitude on the progenitor stellar population. 91T Ia regions have very similar colors in all bands regardless of their radial location in the host galaxy and contain dust similar to the Milky Way. All 91bg events occur in regions of insignificant UV flux unlike normal Ia, which can appear in either high or low UV flux environments in similar hosts.

What does this mean for supernova cosmology? Until there is more SN environment data in IR and UV with corresponding SN light curve information, it will be difficult to determine whether these effects are due to age or dust. If the correlation in figure 5.598 is due exclusively to dust then this increases the error in the individual data points in the Hubble plot from 0.2 - 0.8 mag. The colors can be adjusted due to the reddening  $E(B-V)$ , but to determine the extinction  $A_V$ , one needs to know the reddening

law  $R_V$  for the particular stellar environment. As mentioned previously,  $R_V$  isn't necessarily the same elsewhere as for the Milky Way. Current estimates range from  $R_V = 1.5$ -3 depending on the particular SN sample. Therefore errors and scatter in the data can vary 1 to 2 times the color. For example, a region with  $E(B-V) = 0.3$  can vary from 0.5 to 0.9 magnitudes in extinction or an error of 0.4 in peak magnitude. Determining  $R_V$  accurately requires a color magnitude diagram of stellar populations in the host and therefore the capability of imaging the host galaxy. At cosmological distances this is impossible with the current technology.

If the progenitor age and dust are a factor in SN color, it will be much harder to disentangle the two effects. A distant ( $z > 1$ ) and younger population of SNe needs only to average a tenth of a magnitude brighter than nearby SNe to give the incorrect cosmology. Figure 3.1 showed that at  $z > 1$  the scatter in absolute magnitude is at least 0.5 magnitudes and the average errors in the binned data (figures 3.2 and 3.3) exceed 0.2 magnitudes. In published plots (e.g. Amanullah et al., 2010), errors and averages of redshift binned data are weighted giving much smaller errors (0.1 mag) and scatter (0.2 mag), but these are based on few data points at  $z > 1$ . Regardless of the number of distant data points, if there is a proven supernova luminosity dependence on age it will be impossible to distinguish age from cosmological effects and dust. A method to determine age-luminosity dependence is to calculate the absolute peak magnitudes of SNe occurring galaxies with known distances estimated from other techniques (e.g. Cepheid Variables). The data sample is extremely limited, but it can offer an accurate estimate of SN brightness dependence on progenitor age.

## 7.2. Supernova Ia Rate

This work determines a rate of 0.25 to 0.3 SNU within a volume of  $z < 0.1$  based on CCD distance-limited/catalog searches. Given the current methods of reporting SNe, it is difficult to improve upon this simulation. As less SNe are reported to the IAUC, the observed SNe numbers are smaller than many SN field search coverages would indicate. Only distance limited searches reliably report SNe. Interestingly, the rate calculation also

demonstrated that if galaxies other than the target galaxy are imaged together on a CCD, then only the target galaxy is scanned for SNe. Therefore, observers are probably missing several nearby SNe because they aren't looking in these less conspicuous galaxies unless the events are unusually bright. This is more of an amateur problem because they usually don't have the software to subtract images and usually rely on scanning several images by eye. More modern professional searches (similar to QUEST and NEAT) are now scanning the skies at nearby distances such that a random selection of galaxies within  $z < 0.1$  are observed instead of just the big, bright objects.

But more importantly, what does this rate mean in the context of the characteristics of supernovae Ia and their reliability as standard candles? In order to really answer this question, we need to discuss the observed white dwarf mass function (WDMF). Koester et al. (2009) measured the masses of several nearby white dwarfs and observed the distribution of masses as shown in figure 7.1. The first thing to notice in figure 7.1 is that the most probable mass is  $0.55M_{\odot}$ , less than half the Chandrasekhar limit. If SNe Ia only explode at  $1.4M_{\odot}$  and SNe progenitors are predominately white dwarf-white dwarf mergers, then the tail of the distribution where  $M > 0.7M_{\odot}$  and therefore younger stellar population, must be driving the supernova Ia rate. If this is true then we should be able to measure a distant rate that is similar to the nearby rate, provided that effects due to observational bias and dust extinction are accurately estimated, because this means both distant and nearby populations of SNe are similar. But, if SNe Ia occur at masses above and below this limit, creating a continuum of bright and dim events, then only the bright events will be visible at large distances whereas all nearby SNe, both bright, and dim are visible to observers. The result is that the nearby rate will be much larger than the distant rate, demonstrating a mass/age-luminosity dependence and calling into question the plausibility of SNe Ia as standard candles and the ability to calibrate these objects.

As stated before in this work, proving the accuracy of SNe Ia as standard candles is very difficult with so many entangled effects altering the peak output of light. Statistically, it's been estimated (Genovese et al., 2009) that SNe are unlikely to ever

have small enough errors to measure dark energy. If you ask an SN cosmologist if this is true, they will tell you that more data will reduce errors. But if the data have offsets due to an evolving population of SNe or dust or observational bias because the progenitor characteristics vary, then no amount of data will give you the correct answer. Recalling the results of Kasen et al. (2009), they state that variability due to the asymmetries in the explosion causes an offset in distant SNe, meaning that distances will be over estimated by 2%. In terms of the distance modulus,  $m-M$ , a  $z \sim 1.5$  SNe with  $m-M = 45$  mag will have an error of 0.9 mag.

In order to put perspective on these errors, figure 7.2 indicates the current status of supernova cosmology. Similar to figures 3.2 and 3.3, the binned data are plotted with the accepted values for the matter and energy density  $\{\Omega_M = 0.25; \Omega_E = 0.75\}$  for four different equations of state:  $\omega = -0.9, -1, -1.1, -1/3$ . The first three values of  $\omega$  were chosen because the current consensus for the equation of state is approximately  $\omega \sim -1$  and the present objective for cosmology is to measure  $\omega$  within 10%. The resolution between the first three models is much smaller than the errors and scatter in the SN peak magnitudes. At a redshift of  $z=1.5$ , the maximum difference between  $\omega = -0.9$  and  $\omega = -1.1$  cosmologies is 0.1 magnitudes and less for smaller redshifts. Even if these data are weighted and binned (e.g. Amanullah, 2010; Riess et al., 2007) the errors are still 0.1 magnitude for  $z > 0.9$ , with a scatter of at least 0.2 magnitudes (see fig 9 in Amanullah 2010). SN cosmology relies heavily on measurements past  $z > 0.9$  to pin down an accurate value of  $\omega$  because of the larger differences between models. Data must be well sampled such that any error from the Malmquist bias is reduced to less than 0.1 magnitudes, otherwise a misinterpretation of the data will result in a different cosmology.

Also included in figure 7.2 is the special case of  $\omega = -1/3$  corresponding to the threshold between an accelerating ( $\omega < -1/3$ ) and non-accelerating ( $\omega > -1/3$ ) universe. Bothun et al. (2008) proved that  $\omega < -1/3$  using only values of  $H_0$  and  $\Omega_M$  derived independently from techniques other than SN cosmology. Effectively, cosmologists could have arrived at this conclusion whether or not SNe were standard candles. Furthermore, figure 7.2 is demonstrative of the fact that the SN data show an accelerating Universe, but

other than confirming the existence of dark energy (Riess et al., 1998; Perlmutter et al., 1999), SNe data haven't estimated any robust values for  $\omega$ .

The problems in SN Ia cosmology are documented in the literature, yet the hope persists that such wildly varying unknowns in these standard candles can precisely and accurately determine the equation of state parameter  $\omega$ . Concluding this document is an example of current SN cosmology efforts. The SDSS Supernova Survey collaboration (Frieman et al., 2008) has determined  $\omega$  within an uncertainty of 10%. However the value for  $\omega$  is different depending on the light curve fitter. Kessler et al. (2009) demonstrates that using both the SALT2 and MLCS2k2 techniques on SDSS supernova data, two different values of  $\omega$  (-0.99 and -0.76) emerge. Only by using about 60% of the data sample, do both techniques results agree with a value of  $\omega = -0.92$ , showing that it is a lot easier (albeit circular and erroneous) to fit data to a model if you know the answer ahead of time.

### 7.3. Future Work

Clearly, improvements to both the SN environmental study and rate calculation demand lots of data. Figure 5.598 could be further supplemented with more high resolution data of SN Ia regions within  $z < 0.01$  and published SN light curve information including peak colors in B and V. At last count, Hubble Space Telescope WFPC2 has archival images of 19 SN Ia regions in V and I bands. These colors are different than the  $g-r$  SDSS colors, but should indicate a similar trend as the SDSS data. GALEX UV image data is also another resource for determining ages of stellar populations. There are SNe occurring in galactic regions with no detectable flux in SDSS colors, but measurable flux in GALEX. High resolution NIR image data could determine if the redder colors are red due to dust or age.

Refinements to the professional magnitude limited searches need to be made in order to confirm the rate. The photographic searches are too difficult to model because

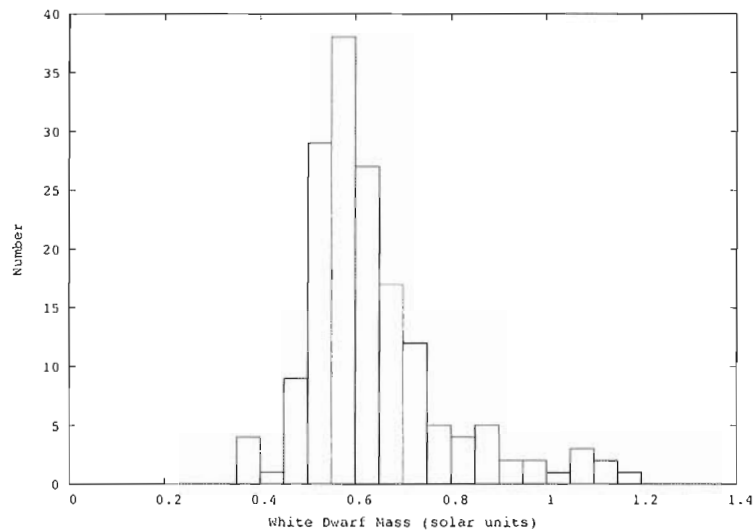


Figure 7.1. The observational white dwarf mass distribution function adapted from Koester et al. (2009). Mass is in units of solar mass.

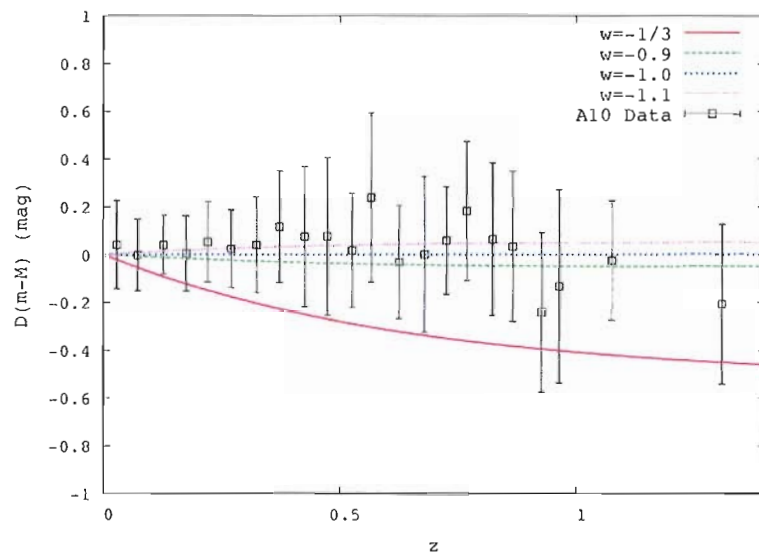


Figure 7.2. A Hubble residual diagram of unweighted data adapted from Amanullah et al. (2010) subtracted from the  $\Lambda$ CDM model plotted with  $\omega = -1/3, -0.9, -1, -1.1$  cosmologies. Data and corresponding errors are averaged in bins of  $\Delta z = 0.05$  for  $z < 1$  and  $\Delta z = 0.2$  for  $z > 1$ .



they rely heavily on human detection capability and the exposure qualities of the photograph.

## BIBLIOGRAPHY

- Abazajian, K.N.; Adelman-McCarthy, J.K.; Agüeros, M.A.; Allam, S.S.; Allende Prieto, C.; An, D.; Anderson, K.S.J.; Anderson, S.F.; Annis, J.; Bahcall, N.A.; et al. *The Astrophysical Journal Supplement Series* **2009**, *182*, 543-558.
- Abell, G.O. *Leaflet of the Astronomical Society of the Pacific* **1959**, *8*, 121-126.
- Amanullah, R.; Lidman, C.; Rubin, D.; Aldering, G.; Astier, P.; Barbary, K.; Burns, M.S.; Conley, A.; Dawson, K.S.; Deustua, S.E.; et al. *The Astrophysical Journal* **2010**, *716*, 712-738.
- Anderson, J.P.; & James, P.A. *Monthly Notices of the Royal Astronomical Society* **2009**, *399*, 559-573.
- Bailey, S.; Aldering, G.; Antilogus, P.; Aragon, C.; Baltay, C.; Bongard, S.; Buton, C.; Childress, M.; Chotard, N.; Copin, Y.; et al. *Astronomy and Astrophysics* **2009**, *500*, L17-L20.
- Bartunov, O.S.; Makarova, I.N.; & Tsvetkov, D.I. *Astronomy and Astrophysics* **1992**, *264*, 428-432.
- Bennett, C.L.; Bay, M.; Halpern, M.; Hinshaw, G.; Jackson, C.; Jarosik, N.; Kogut, A.; Limon, M.; Meyer, S.S.; Page, L.; et al. *The Astrophysical Journal* **2003**, *583*, 1-23.
- Blanc, G.; Afonso, C.; Alard, C.; Albert, J.N.; Aldering, G.; Amadon, A.; Andersen, J.; Ansari, R.; Aubourg, E.; Balland, C.; et al. *Astronomy and Astrophysics* **2004**, *423*, 881-894.
- Blondin, S.; Prieto, J.L.; Patat, F.; Challis, P.; Hicken, M.; Kirshner, R.P.; Matheson, T.; & Modjaz, M. *The Astrophysical Journal* **2009**, *693*, 207-215.
- Bonnarel, F.; Fernique, P.; Bienaymé, O.; Egret, D.; Genova, F.; Louys, M.; Ochsenbein, F.; Wenger, M.; Bartlett, J.G. *Astronomy and Astrophysics Supplement Series* **2000**, *143*, 33-40.

- Borkowski, K.J.; Williams, B.J.; Reynolds, S.P.; Blair, W.P.; Ghavamian, P.; Sankrit, R.; Hendrick, S.P.; Long, K.S.; Raymond, J.C.; Smith, R.C.; et al. *The Astrophysical Journal* **2006**, *642*, L141-L144.
- Bothun, G. *The Astronomical Journal* **1986**, *91*, 507-516.
- Bothun, G. University of Oregon, Eugene, OR. Personal Communication, 2003.
- Bothun, G., Hsu, S.D.H., & Murray, B., *Physics Letters B* **2008**, *660*, 133-137.
- Bouchet, P.; Lequeux, J.; Maurice, E.; Prevot, L.; & Prevot-Burnichon, M.L. *Astronomy and Astrophysics* **1985**, *149*, 330-336.
- Branch, D. *Monthly Notices of the Royal Astronomical Society* **1977**, *179*, 401-408.
- Branch, D.; Baron, E.; Thomas, R.C.; Kasen, D.; Li, W.; & Filippenko, A.V. *Publications of the Astronomical Society of the Pacific* **2004**, *116*, 903-908.
- Bruzual, G.; & Charlot, S. *Monthly Notices of the Royal Astronomical Society* **2003**, *344*, 1000-1028.
- Cappellaro, E.; Evans, R.; & Turatto, M. *Astronomy and Astrophysics* **1999**, *351*, 459-466.
- Cappellaro, E.; Turatto, M.; Tsvetkov, D.Y.; Bartunov, O.S.; Pollas, C.; Evans, R.; & Hamuy, M. *Astronomy and Astrophysics* **1997**, *322*, 431-441.
- Cardelli, J.A.; Clayton, G.C.; & Mathis, J.S. *The Astrophysical Journal* **1989**, *345*, 245-256.
- Chandrasekhar, S. *The Astrophysical Journal* **1931**, *74*, 81-82.
- Colless, M.; Dalton, G.; Maddox, S.; Sutherland, W.; Norberg, P.; Cole, S.; Bland-Hawthorn, J.; Bridges, T.; Cannon, R.; Collins, C.; et al. *Monthly Notices of the Royal Astronomical Society* **2001**, *329*, 1039-1063.
- Corasaniti, P.-S.; Giannantonio, T.; & Melchiorri, A. *Physical Review D* **2005**, *71*, 123521.
- D'Andrea, C.B.; Sako, M.; Dilday, B.; Frieman, J.A.; Holtzman, J.; Kessler, R.; Konishi, K.; Schneider, D.P.; Sollerman, J.; Wheeler, J.C.; et al. *The Astrophysical Journal* **2010**, *708*, 661-674.

- de Vaucouleurs, G.; de Vaucouleurs, A.; Corwin, H.G.; Buta, R.J.; Paturel, G.; & Fouque, P. *Third Reference Catalogue of Bright Galaxies (RC3)*; Springer-Verlag: New York, 1995.
- Dilday, B.; Bassett, B.; Becker, A.; Bender, R.; Castander, F.; Cinabro, D.; Frieman, J.A.; Galbany, L.; Garnavich, P.; Goobar, A.; et al. *The Astrophysical Journal* **2010**, *715*, 1021-1035.
- Dilday, B.; Kessler, R.; Frieman, J.A.; Holtzman, J.; Marriner, J.; Miknaitis, G.; Nichol, R.C.; Romani, R.; Sako, M.; Bassett, B.; et al. *The Astrophysical Journal* **2008**, *682*, 262-282.
- Drake, A.J.; Djorgovski, S.G.; Mahabal, A.; Beshore, E.; Larson, S.; Graham, M.J.; Williams, R.; Christensen, E.; Catelan, M.; Boattini, A.; et al. *The Astrophysical Journal* **2009**, *696*, 870-884.
- Eisenstein, D.J.; Zehavi, I.; Hogg, D.W.; Scoccimarro, R.; Blanton, M.R.; Nichol, R.C.; Scranton, R.; Seo, H.-J.; Tegmark, M.; Zheng, Z.; et al. *The Astrophysical Journal* **2005**, *633*, 560-574.
- Eldridge, J.J.; & Tout, C.A. *Monthly Notices of the Royal Astronomical Society* **2004**, *353*, 87-97.
- Eskridge, P.B.; Frogel, J.A.; Taylor, V.A.; Windhorst, R.A.; Odewahn, S.C.; Chiarenza, C.A.T.C.; Conselice, C.J.; de Grijs, R.; Matthews, L.D.; O'Connell, R.W.; et al. *The Astrophysical Journal* **2003**, *586*, 923-938.
- Finlator, K.; Ivezić, Z.; Fan, X.; Strauss, M.A.; Knapp, G.R.; Lupton, R.H.; Gunn, J.E.; Rockosi, C.M.; Anderson, J.E.; Csabai, I.; et al. *The Astronomical Journal* **2000**, *120*, 2615-2626.
- Folatelli, G.; Phillips, M.M.; Burns, C.R.; Contreras, C.; Hamuy, M.; Freedman, W.L.; Persson, S.E.; Stritzinger, M.; Suntzeff, N.B.; Krisciunas, K.; et al. *The Astronomical Journal* **2010**, *139*, 120-144.
- Foley, R.J.; Matheson, T.; Blondin, S.; Chornock, R.; Silverman, J.M.; Challis, P.; Clocchiatti, A.; Filippenko, A.V.; Kirshner, R.P.; Leibundgut, B.; et al. *The Astronomical Journal* **2009**, *137*, 3731-3742.
- Freedman, W.L.; Burns, C.R.; Phillips, M.M.; Wyatt, P.; Persson, S.E.; Madore, B.F.; Contreras, C.; Folatelli, G.; Gonzalez, E.S.; Hamuy, M.; et al. *The Astrophysical Journal* **2009**, *704*, 1036-1058.

- Frieman, J.A.; Bassett, B.; Becker, A.; Choi, C.; Cinabro, D.; DeJongh, F.; Depoy, D.L.; Dilday, B.; Doi, M.; Garnavich, P.M.; et al. *The Astronomical Journal* **2008**, *135*, 338-347.
- Fukugita, M.; Nakamura, O.; Okamura, S.; Yasuda, N.; Barentine, J.C.; Brinkmann, J.; Gunn, J.E.; Harvanek, M.; Ichikawa, T.; Lupton, R.H.; et al. *The Astronomical Journal* **2007**, *134*, 579-593.
- Gal-Yam, A.; Maoz, D.; Guhathakurta, P.; & Filippenko, A.V. *The Astrophysical Journal* **2008**, *680*, 550-567.
- Gallagher, J.S.; Garnavich, P.M.; Caldwell, N.; Kirshner, R.P.; Jha, S.W.; Li, W.; Ganeshalingam, M.; & Filippenko, A.V. *The Astrophysical Journal* **2008**, *685*, 752-766.
- Gaskell, C.M.; Cappellaro, E.; Dinerstein, H.L.; Garnett, D.R.; Harkness, R.P.; & Wheeler, J.C. *The Astrophysical Journal* **1986**, *306*, L77-L80.
- Genovese, C.; Freeman, P.; Wasserman, L.; Nichol, R.; & Miller, C. *Annals of Applied Statistics* **2009**, *3*, 144-178.
- Gil de Paz, A.; Boissier, S.; Madore, B.F.; Seibert, M.; Joe, Y.H.; Boselli, A.; Wyder, T.K.; Thilker, D.; Bianchi, L.; Rey, S.-C.; et al. *The Astrophysical Journal Supplement Series* **2007**, *173*, 185-255.
- Gilfanov, M.; Bogdán, Á. *Nature* **2010**, *463*, 924-925.
- Gunn, J.E.; Carr, M.; Rockosi, C.; Sekiguchi, M.; Berry, K.; Elms, B.; de Haas, E.; Ivezić, Z.; Knapp, G.; Lupton, R.; et al. *The Astronomical Journal* **1998**, *116*, 3040-3081.
- Gunn, J.E.; Siegmund, W.A.; Mannery, E.J.; Owen, R.E.; Hull, C.L.; Leger, R.F.; Carey, L.N.; Knapp, G.R.; York, D.G.; Boroski, W.N.; et al. *The Astronomical Journal* **2006**, *131*, 2332-2359.
- Guy, J.; Astier, P.; Baumont, S.; Hardin, D.; Pain, R.; Regnault, N.; Basa, S.; Carlberg, R.G.; Conley, A.; Fabbro, S.; et al. *Astronomy and Astrophysics* **2007**, *466*, 11-21.
- Guy, J.; Astier, P.; Nobili, S.; Regnault, N.; & Pain, R. *Astronomy and Astrophysics* **2005**, *443*, 781-791.
- Hakobyan, A.A. *Astrophysics* **2008**, *51*, 69-76.

- Hakobyan, A.A.; Petrosian, A.R.; McLean, B.; Kunth, D.; Allen, R.J.; Turatto, M.; & Barbon, R. *Astronomy and Astrophysics* **2008**, *488*, 523-531.
- Hamuy, M.; Phillips, M.M.; Suntzeff, N.B.; Aviles, R.; & Maza, J. *Bulletin of the American Astronomical Society* **1993**, *25*, 1340.
- Hamuy, M.; Phillips, M.M.; Suntzeff, N.B.; Schommer, R.A.; Maza, J.; Antezan, A.R.; Wischnjewsky, M.; Valladares, G.; Muena, C.; Gonzales, L.E.; et al. *The Astronomical Journal* **1996**, *112*, 2408-2437.
- Hamuy, M.; Phillips, M.M.; Suntzeff, N.B.; Maza, J.; González, L.E.; Roth, M.; Krisciunas, K.; Morrell, N.; Green, E.M.; Persson, S.E.; et al. *Nature* **2003**, *424*, 651-654.
- Hamuy, M.; & Pinto, P.A. *The Astrophysical Journal* **2002**, *566*, L63-L65.
- Hamuy, M.; & Pinto, P.A. *The Astronomical Journal* **1999**, *117*, 1185-1205.
- Hamuy, M.; Pinto, P.A.; Maza, J.; Suntzeff, N.B.; Phillips, M.M.; Eastman, R.G.; Smith, R.C.; Corbally, C.J.; Burstein, D.; Li, Y.; et al. *The Astrophysical Journal* **2001**, *558*, 615-642.
- Hardin, D.; Afonso, C.; Alard, C.; Albert, J.N.; Amadon, A.; Andersen, J.; Ansari, R.; Aubourg, E.; Bareyre, P.; Bauer, F.; et al. *Astronomy and Astrophysics* **2000**, *362*, 419-425.
- Hicken, M.; Challis, P.; Jha, S.; Kirshner, R.P.; Matheson, T.; Modjaz, M.; Rest, A.; Michael Wood-Vasey, W.; Bakos, G.; Barton, E.J.; et al. *The Astrophysical Journal* **2009**, *700*, 331-357.
- Hicken, M.; Wood-Vasey, W.M.; Blondin, S.; Challis, P.; Jha, S.; Kelly, P.L.; Rest, A.; & Kirshner, R.P. *The Astrophysical Journal* **2009**, *700*, 1097-1140.
- Hoffman, J.L. *Supernova 1987A: 20 Years After: Supernovae and Gamma-Ray Bursters AIP Conference Proceedings* Aspen, CO, February 19-23, 2007; Immler, S.; Weiler, K.; McCray, R., Eds; American Institute of Physics: Melville, NY, 2007.
- Howell, D.A.; Sullivan, M.; Brown, E.F.; Conley, A.; Le Borgne, D.; Hsiao, E.Y.; Astier, P.; Balam, D.; Balland, C.; Basa, S.; et al. *The Astrophysical Journal* **2009**, *691*, 661-671.
- Howell, D.A.; Sullivan, M.; Nugent, P.E.; Ellis, R.S.; Conley, A.J.; Le Borgne, D.; Carlberg, R.G.; Guy, J.; Balam, D.; Basa, S.; et al. *Nature* **2006**, *443*, 308-311.

- Ivanov, V.D.; Hamuy, M.; & Pinto, P.A.; *The Astrophysical Journal* **2000**, *542*, 588-596.
- Ivezic, Z.; Becker, R.H.; Blanton, M.; Fan, X.; Finlator, K.; Gunn, J.E.; Hall, P.; Kim, R.S.J.; Knapp, G.R.; Loveday, J.; et al. *Proceedings of IAU Colloquium 184* Byurakan, Armenia, June 18-22, 2001; Green, R.; Khachikian, E.; Sanders, D., Eds; ASP: San Francisco, CA, 2001
- Jha, S.; Riess, A.G.; & Kirshner, R.P. *The Astrophysical Journal* **2007**, *659*, 122-148.
- Kasen, D., Röpke, F.K., & Woosley, S.E., *Nature* **2009**, *460*, 869-872.
- Kasen, D.; & Bildsten, L. *The Astrophysical Journal* **2010**, *717*, 245-249.
- Kelly, P.L.; Hicken, M.; Burke, D.L.; Mandel, K.S.; & Kirshner, R.P. *The Astrophysical Journal* **2010**, *715*, 743-756.
- Kelly, P.L.; Kirshner, R.P.; & Pahre, M. *The Astrophysical Journal* **2008**, *687*, 1201-1207.
- Kessler, R.; Becker, A.C.; Cinabro, D.; Vanderplas, J.; Frieman, J.A.; Marriner, J.; Davis, T.M.; Dilday, B.; Holtzman, J.; Jha, S.W.; et al. *The Astrophysical Journal Supplement Series* **2009**, *185*, 32-84.
- Khokhlov, A.M. *Astronomy and Astrophysics* **1991**, *245*, 114-128.
- Koester, D., Voss, B., Napiwotzki, R., Christlieb, N., Homeier, D., Lisker, T., Reimers, D., & Heber, U., *Astronomy and Astrophysics* **2009**, *505*, 441-462.
- Krisciunas, K.; & Schaefer, B.E. *Publications of the Astronomical Society of the Pacific* **1991**, *103*, 1033-1039.
- Kuznetsova, N.; Barbary, K.; Connolly, B.; Kim, A.G.; Pain, R.; Roe, N.A.; Aldering, G.; Amanullah, R.; Dawson, K.; Doi, M.; et al. *The Astrophysical Journal* **2008**, *673*, 981-998.
- Lanyon-Foster, M.M.; Conselice, C.J.; & Merrifield, M.R. *Monthly Notices of the Royal Astronomical Society* **2007**, *380*, 571-584.
- Li, W.D.; Filippenko, A.V.; Treffers, R.R.; Friedman, A.; Halderson, E.; Johnson, R.A.; King, J.Y.; Modjaz, M.; Papenkova, M.; Sato, Y.; et al. *American Institute of Physics Conference Proceedings* College Park, MD, October 11-13 1999; Holt, S.; Olin, F., Eds; American Institute of Physics: Melville, NY, 2000.

- Li, W.; Filippenko, A.V.; Chornock, R.; Berger, E.; Berlind, P.; Calkins, M.L.; Challis, P.; Fassnacht, C.; Jha, S.; Kirshner, R.P.; et al. *Publications of the Astronomical Society of the Pacific* **2003**, *115*, 453-473.
- Li, W.; Filippenko, A.V.; & Riess, A.G. *The Astrophysical Journal* **2001**, *546*, 719-733.
- Li, Z.; & Han, Z. *Monthly Notices of the Royal Astronomical Society* **2008**, *385*, 1270-1278.
- Lintott, C.J.; Schawinski, K.; Slosar, A.; Land, K.; Bamford, S.; Thomas, D.; Raddick, M.J.; Nichol, R.C.; Szalay, A.; Andreescu, D.; et al. *Monthly Notices of the Royal Astronomical Society* **2008**, *389*, 1179-1189.
- Lira, P. MS. Thesis, University of Chile, 1996.
- Lupton, R.H.; Gunn, J.E.; & Szalay, A.S. *The Astronomical Journal* **1999**, *118*, 1406-1410.
- Mannucci, F.; Della Valle, M.; & Panagia, N. *Monthly Notices of the Royal Astronomical Society* **2006**, *370*, 773-783.
- Mannucci, F. American Institute of Physics Conference Series 2009, 1111, 467-476.
- Maund, J.R.; & Smartt, S.J. *Monthly Notices of the Royal Astronomical Society* **2005**, *360*, 288-304.
- Maza, J. *Proceedings of the Texas Workshop on Type I Supernovae* Austin, TX, March 17-19, 1980; Wheeler, J., Ed; University of Texas: Austin, TX
- Meeus, J. *Astronomical Algorithms* Willmann-Bell: Richmond, VA, 1998.
- Meng, X.; & Yang, W. *Monthly Notices of the Royal Astronomical Society* **2010**, *401*, 1118-1130.
- Neill, J.D.; Sullivan, M.; Howell, D.A.; Conley, A.; Seibert, M.; Martin, D.C.; Barlow, T.A.; Foster, K.; Friedman, P.G.; Morrissey, P.; et al. *The Astrophysical Journal* **2009**, *707*, 1449-1465.
- Nobili, S.; Amanullah, R.; Garavini, G.; Goobar, A.; Lidman, C.; Stanishev, V.; Aldering, G.; Antilogus, P.; Astier, P.; Burns, M.S.; et al. *Astronomy and Astrophysics* **2005**, *437*, 789-804.



- Nobili, S.; Fadeyev, V.; Aldering, G.; Amanullah, R.; Barbary, K.; Burns, M.S.; Dawson, K.S.; Deustua, S.E.; Faccioli, L.; Fruchter, A.S.; et al. *The Astrophysical Journal* **2009**, *700*, 1415-1427.
- Nobili, S.; & Goobar, A. *Astronomy and Astrophysics* **2008**, *487*, 19-31.
- Oke, J.B.; & Gunn, J.E. *The Astrophysical Journal* **1983**, *266*, 713-717.
- Pain, R.; Fabbro, S.; Sullivan, M.; Ellis, R.S.; Aldering, G.; Astier, P.; Deustua, S.E.; Fruchter, A.S.; Goldhaber, G.; Goobar, A.; et al. *The Astrophysical Journal* **2002**, *577*, 120-132.
- Pakmor, R.; Kromer, M.; Röpke, F.K.; Sim, S.A.; Ruiter, A.J.; & Hillebrandt, W. *Nature* **2010**, *463*, 61-64.
- Panagia, N. *American Institute of Physics Conference Series* Cefalu, Sicily, Italy, September 7-19, 2008; Giobbi, G.; Tornambe, A.; Raimondo, G.; Limongi, M.; Antonelli, L.A.; Menci, N.; Brocato, E., Eds; American Institute of Physics: Melville, NY, 2009.
- Pastorello, A. *American Institute of Physics Conference Series* Cefalu, Sicily, Italy, September 7-19, 2008; Giobbi, G.; Tornambe, A.; Raimondo, G.; Limongi, M.; Antonelli, L.A.; Menci, N.; Brocato, E., Eds; American Institute of Physics: Melville, NY, 2009.
- Pastorello, A.; Taubenberger, S.; Elias-Rosa, N.; Mazzali, P.A.; Pignata, G.; Cappellaro, E.; Garavini, G.; Nobili, S.; Anupama, G.C.; Bayliss, D.D.R.; et al. *Monthly Notices of the Royal Astronomical Society* **2007**, *376*, 1301-1316.
- Paturel, G.; Petit, C.; Prugniel, P.; Theureau, G.; Rousseau, J.; Brouty, M.; Dubois, P.; Cambresy, L. *Astronomy and Astrophysics* **2003**, *412*, 45-55.
- Perlmutter, S.; Aldering, G.; Goldhaber, G.; Knop, R.A.; Nugent, P.; Castro, P.G.; Deustua, S.; Fabbro, S.; Goobar, A.; Groom, D.E.; et al. *The Astrophysical Journal* **1999**, *517*, 565-586.
- Perlmutter, S.; Gabi, S.; Goldhaber, G.; Goobar, A.; Groom, D.E.; Hook, I.M.; Kim, A.G.; Kim, M.Y.; Lee, J.C.; Pain, R.; et al. *The Astrophysical Journal* **1997**, *483*, 565-581.

- Petrosian, A.; Navasardyan, H.; Turatto, M.; Cappellaro, E.; McLean, B.; Allen, R.; Panagia, N.; Leitherer, C.; & MacKenty, J. *1604-2004: Supernovae as Cosmological Lighthouses ASP Conference Series* Padua, Italy, June 15-19, 2005; Turatto, M.; Benetti, S.; Zampieri, L.; Shea, W., Eds; ASP: San Francisco, CA, 2005.
- Phillips, M.M. *The Astrophysical Journal* **1993**, *413*, L105-L108.
- Phillips, M.M.; Lira, P.; Suntzeff, N.B.; Schommer, R.A.; Hamuy, M.; & Maza, J. *The Astronomical Journal* **1999**, *118*, 1766-1776.
- Pier, J.R.; Munn, J.A.; Hindsley, R.B.; Hennessy, G.S.; Kent, S.M.; Lupton, R.H.; Ivezić, Z. *The Astronomical Journal* **2003**, *125*, 1559-1579.
- Press, W.; Flannery, B.; Teukolsky, S.; Vetterling, W. *Numerical Recipes in Fortran 77*; Cambridge University Press: New York, 1996.
- Prevot, M.L.; Lequeux, J.; Prevot, L.; Maurice, E.; & Rocca-Volmerange, B. *Astronomy and Astrophysics* **1984**, *132*, 389-392.
- Puckett, T.; Langoussis, A.; Chen, Y.T.; Hu, C.P.; Pugh, H.; Li, W.; & Harris, B. *International Astronomical Union Circular* **2005**, *8534*, 1.
- Puckett, T.; Moore, C.; Newton, J.; & Orff, T. *Central Bureau Electronic Telegrams* **2008**, *1567*, 1.
- Puckett, T.; Moore, R.; Newton, J.; & Orff, T. *Central Bureau Electronic Telegrams* **2009**, *1762*, 1.
- Qiu, Y.; Hu, J.; & Li, W. *Small Telescope Astronomy on Global Scales, ASP Conference Series* Kenting National Park, China, January 4-8, 2001; Paczynsky, B.; Chen, W.; Lemme, C., Eds; ASP: San Francisco, CA, 2001
- Reid, I.N.; Brewer, C.; Brucato, R.J.; McKinley, W.R.; Maury, A.; Mendenhall, D.; Mould, J.R.; Mueller, J.; Neugebauer, G.; Phinney, J.; et al. *Publications of the Astronomical Society of the Pacific* **1991**, *103*, 661-674.
- Reindl, B.; Tammann, G.A.; Sandage, A.; & Saha, A. *The Astrophysical Journal* **2005**, *624*, 532-554.
- Reiss, D.J.; Germany, L.M.; Schmidt, B.P.; & Stubbs, C.W. *The Astronomical Journal* **1998**, *115*, 26-36.

- Richmond, M.; Treffers, R.R.; & Filippenko, A.V. *Publications of the Astronomical Society of the Pacific* **1993**, *105*, 1164-1174.
- Riess, A.G. *Publications of the Astronomical Society of the Pacific* **2000**, *112*, 1284-1299.
- Riess, A.G.; Filippenko, A.V.; Challis, P.; Clocchiatti, A.; Diercks, A.; Garnavich, P.M.; Gilliland, R.L.; Hogan, C.J.; Jha, S.; Kirshner, R.P.; et al. *The Astronomical Journal* **1998**, *116*, 1009-1038.
- Riess, A.G.; Press, W.H.; & Kirshner, R.P. *The Astrophysical Journal* **1995**, *445*, L91-L94.
- Riess, A.G.; Strolger, L.-G.; Casertano, S.; Ferguson, H.C.; Mobasher, B.; Gold, B.; Challis, P.J.; Filippenko, A.V.; Jha, S.; Li, W.; et al. *The Astrophysical Journal* **2007**, *659*, 98-121.
- Robaina, A.R.; & Cepa, J. *Astronomy and Astrophysics* **2007**, *464*, 465-470.
- Scalzo, R.A.; Aldering, G.; Antilogus, P.; Aragon, C.; Bailey, S.; Baltay, C.; Bongard, S.; Buton, C.; Childress, M.; Chotard, N.; et al. *The Astrophysical Journal* **2010**, *713*, 1073-1094.
- Schlegel, D.J.; Finkbeiner, D.P.; & Davis, M. *The Astrophysical Journal* **1998**, *500*, 525-553.
- Schmidt, B.P.; Kirshner, R.P.; & Eastman, R.G. *The Astrophysical Journal* **1992**, *395*, 366-386.
- Shaw, R.L. *Astronomy and Astrophysics* **1979**, *76*, 188-191.
- Silvia, D.W.; Smith, B.D.; & Shull, J.M. *The Astrophysical Journal* **2010**, *715*, 1575-1590.
- Skrutskie, M.F.; Cutri, R.M.; Stiening, R.; Weinberg, M.D.; Schneider, S.; Carpenter, J.M.; Beichman, C.; Capps, R.; Chester, T.; Elias, J.; et al. *The Astronomical Journal* **2006**, *131*, 1163-1183.
- Smartt, S.J.; Eldridge, J.J.; Crockett, R.M.; & Maund, J.R. *Monthly Notices of the Royal Astronomical Society* **2009**, *395*, 1409-1437.
- Smartt, S.J. *Annual Review of Astronomy and Astrophysics* **2009**, *47*, 63-106.
- Smith, N.; Hinkle, K.H.; & Ryde, N. *The Astronomical Journal* **2009**, *137*, 3558-3573.

- Steel, D.I.; McNaught, R.H.; Garradd, G.J.; Asher, D.J.; & Russell, K.S. *Australian Journal of Astronomy* **1997**, *7*, 67-77.
- Strolger, L.-G. Ph.D. Thesis, University of Michigan, 2003.
- Sullivan, M.; Conley, A.; Howell, D.A.; Neill, J.D.; Astier, P.; Balland, C.; Basa, S.; Carlberg, R.G.; Fouchez, D.; Guy, J.; et al. *Monthly Notices of the Royal Astronomical Society* **2010**, *406*, 782-802.
- Tammann, G.A.; & Sandage, A. *The Astrophysical Journal* **1995**, *452*, 16-24.
- Tanaka, M.; Kawabata, K.S.; Yamanaka, M.; Maeda, K.; Hattori, T.; Aoki, K.; Nomoto, K.; Iye, M.; Sasaki, T.; Mazzali, P.A.; et al. *The Astrophysical Journal* **2010**, *714*, 1209-1216.
- Timmes, F.X.; Brown, E.F.; & Truran, J.W. *The Astrophysical Journal* **2003**, *590*, L83-L86.
- Tsvetkov, D.Y.; Pavlyuk, N.N.; & Bartunov, O.S. *Astronomy Letters* **2004**, *30*, 729-736.
- Valenti, S.; Pastorello, A.; Cappellaro, E.; Benetti, S.; Mazzali, P.A.; Manteca, J.; Taubenberger, S.; Elias-Rosa, N.; Ferrando, R.; Harutyunyan, A.; et al. *Nature* **2009**, *459*, 674-677.
- van den Bergh, S. *The Astronomical Journal* **1997**, *113*, 197-200.
- van den Bergh, S.; Li, W.; & Filippenko, A.V. *Publications of the Astronomical Society of the Pacific* **2005**, *117*, 773-782.
- van den Bergh, S.; Li, W.; & Filippenko, A.V. *Publications of the Astronomical Society of the Pacific* **2003**, *115*, 1280-1288.
- van den Bergh, S.; Li, W.; & Filippenko, A.V. *Publications of the Astronomical Society of the Pacific* **2002**, *114*, 820-825.
- Van Dyk, S.D.; Peng, C.Y.; Barth, A.J.; & Filippenko, A.V. *The Astronomical Journal* **1999**, *118*, 2331-2349.
- von Hippel, T.; Bothun, G.D.; & Schommer, R.A. *The Astronomical Journal* **1997**, *114*, 1154-1164.
- Wang, L.; Goldhaber, G.; Aldering, G.; & Perlmutter, S. *Bulletin of the American Astronomical Society* **2002**, *34*, 1305.

- Wang, L. *The Astrophysical Journal* **2005**, *635*, L33-L36.
- Wang, X.; Filippenko, A.V.; Ganeshalingam, M.; Li, W.; Silverman, J.M.; Wang, L.; Chornock, R.; Foley, R.J.; Gates, E.L.; Macomber, B.; et al. *The Astrophysical Journal* **2009**, *699*, L139-L143.
- Wang, X.; Wang, L.; Pain, R.; Zhou, X.; & Li, Z. *The Astrophysical Journal* **2006**, *645*, 488-505.
- Wild, P. *Proceedings of the International Conference on Supernovae* Lecce, Italy, May 7-11, 1973; Cosmovici, C., Ed; D. Reidel: Dordrecht, Netherlands, 1974.
- Williams, B.F.; Hogan, C.J.; Barris, B.; Candia, P.; Challis, P.; Clocchiatti, A.; Coil, A.L.; Filippenko, A.V.; Garnavich, P.; Kirshner, R.P.; et al. *The Astronomical Journal* **2003**, *126*, 2608-2621.
- Wilson, O.C. *The Astrophysical Journal* **1939**, *90*, 634.
- Wright, E.L. *Publications of the Astronomical Society of the Pacific* **2006**, *118*, 1711-1715.
- Yasuda, N.; & Fukugita, M. *The Astronomical Journal* **2010**, *139*, 39-52.
- York, D.G.; Adelman, J.; Anderson, J.E.; Jr.; Anderson, S.F.; Annis, J.; Bahcall, N.A.; Bakken, J.A.; Barkhouser, R.; Bastian, S.; Berman, E.; et al. *The Astronomical Journal* **2000**, *120*, 1579-1587.
- Yuan, F.; Quimby, R.M.; Wheeler, J.C.; Vinko, J.; Chatzopoulos, E.; Akerlof, C.W.; Kulkarni, S.; Miller, J.M.; McKay, T.A.; Aharonian, F. *The Astrophysical Journal* **2010**, *715*, 1338-1343.
- Zwicky, F. *Physical Review* **1939**, *55*, 726-743.
- Zwicky, F. *The Astrophysical Journal* **1938**, *88*, 529.
- Zwicky, F.; Humason, M.L.; Gomes, A.M.; & Gates, H.S. *Publications of the Astronomical Society of the Pacific* 1961, *73*, 351-354.